Vol. 66 February, 1962 No. 2

THE JOURNAL OF PHYSICAL CHEMISTRY

CONTENTS

Contents continued on inside front cover

THE JOURNAL OF PHYSICAL CHEMISTRY

(Registered in U. S. Patent Office)

Published monthly by the American Chemical Society at 20th and Northampton Sts., Easton, Pa.

Second-class mail privileges authorized at Easton, Pa. This publication is authorized to be mailed at the special rates of postage prescribed by Section 131.122.

The *Journal of Physical Chemistry* is devoted to the publication of selected symposia in the broad field of physical chemistry and to other contributed papers.

Manuscripts originating in the British Isles, Europe and Africa should be sent to F. C. Tompkins, The Faraday Society, 6 Gray's Inn Square, London W. C. 1, England.

Manuscripts originating elsewhere should be sent to W. Albert Noyes, Jr., Department of Chemistry, University of Rochester, Rochester 20, N. Y.

Correspondence regarding accepted copy, proofs and reprints should be directed to Assistant Editor, Allen D. Bliss, Department of Chemistry, Simmons College, 300 The Fenway, Boston 15, Mass.

Advertising Office: Reinhold Publishing Corporation, 430 Park Avenue, New York 22, N. Y.

Articles must be submitted in duplicate, typed and double spaced. They should have at the beginning a brief Abstract, in no case exceeding 300 words. Original drawings should accompany the manuscript. Lettering at the sides of graphs (black on white or blue) may be pencilled in and will be typeset. Figures and tables should be held to a minimum consistent with adequate presentation of information. Photographs will not be printed on glossy paper except by special arrangement. All footnotes and references to the literature should be numbered consecutively and placed in the manuscript at the proper places. Initials of authors referred to in citations should be given. Nomenclature should conform to that used in *Chemical Abstracts*, mathematical characters be marked for italic, Greek letters carefully made or annotated, and subscripts and superscripts clearly shown. Articles should be written as briefly as possible consistent with clarity and should avoid historical background unnecessary for specialists.

Remittances and orders for subscriptions and for single copies, notices of changes of address and new professional connections, and claims for missing numbers should be sent to the Subscription Service Department, American Chemical Society, 1155 Sixteenth St., N. W., Washington 6, D. C. Changes of address for the *Journal of Physical Chemistry* must be received on or before the 30th of the preceding month. Please include an old address label with the notification.

Claims for missing numbers will not be allowed (1) if received more than sixty days from date of issue (because of delivery hazards, no claims can be honored from subscribers in Central Europe, Asia, or Pacific Islands other than Hawaii), (2) if loss was due to failure of notice of change of address to be received before the date specified in the preceding paragraph, or (3) if the reason for the claim is "missing from files."

Subscription rates (1962): members of American Chemical Society, $12.00 for 1 year; to non-members, $24.00 for 1 year. Postage to countries in the Pan American Union $0.80; Canada, $0.40; all other countries, $1.20. Single copies, current volume, $2.50; foreign postage, $0.15; Canadian postage $0.10; Pan-American Union, $0.10. Back volumes (Vol. 56–65) $30.00 per volume; foreign postage, per volume $1.20, Canadian, $0.40; Pan-American Union, $0.80. Single copies: back issues, $3.00; for current year, $2.50; postage, single copies: foreign, $0.15; Canadian, $0.10; Pan American Union, $0.10.

The American Chemical Society and the Editors of the *Journal of Physical Chemistry* assume no responsibility for the statements and opinions advanced by contributors to THIS JOURNAL.

The American Chemical Society also publishes *Journal of the American Chemical Society, Chemical Abstracts, Industrial and Engineering Chemistry*, International Edition of *Industrial and Engineering Chemistry, Chemical and Engineering News, Analytical Chemistry, Journal of Agricultural and Food Chemistry, Journal of Organic Chemistry, Journal of Chemical and Engineering Data, Chemical Reviews, Chemical Titles, Journal of Chemical Documentation, Journal of Medicinal and Pharmaceutical Chemistry, Inorganic Chemistry, Biochemistry*, and *CA — Biochemical Sections*. Rates on request.

THE JOURNAL OF
PHYSICAL CHEMISTRY

(Registered in U. S. Patent Office)

VOLUME 66 FEBRUARY 16, 1962 NUMBER 2

RADIATION CHEMISTRY OF POLYETHYLENE. V. HYDROGEN ISOTOPE EXCHANGE STUDIES

BY MALCOLM DOLE AND FRANCIS CRACCO

Chemical Laboratory of Northwestern University, Evanston, Illinois

Received May 12, 1961

After irradiation *in vacuo* with Co-60 γ-rays at liquid nitrogen temperature, Marlex-50 polyethylene was exposed to deuterium gas at room temperature. Considerable D–H exchange occurred, and the exchange was studied as a function of deuterium pressure, exchange cell volume, irradiation dose, and time of initiating the exchange after irradiation. Kinetic equations have been derived for three cases: constant free radical concentration, first-order free radical decay and second-order free radical decay. The data agree best with the first-order decay equations; the decay constant and duration of exchange agree to an order of magnitude with estimates from the e.s.r. work of Lawton, Balwit and Powell. The D_2-free radical reaction rate constant is about 1000-fold faster than calculated for a gas phase reaction between D_2 and RĊHR′, but close to that for the D_2 and $CH_3\dot{C}H_2$ reaction. The exchange, as expected, does not continue until isotopic exchange equilibrium has been established. The total observable number of D–H exchanges was estimated to be between 1 and 2-fold the number of free radical sites initially present. For reasons given in the paper the exchange probably involves hydrogen atoms close to the free radical or on the nearest neighbor sites, and provides a new mechanism for free radical migration in the solid polyethylene.

I. Introduction

The mechanism by which free radicals produced by high energy radiation in solid polyethylene decay is an interesting problem in radiation chemistry. Not only do free radicals disappear on standing at room temperature, but they can spontaneously change from one type to another, such as alkyl free radicals in the presence of vinylene double bonds changing into probably allyl free radicals as suggested by the work of Voevodskii, *et al.*,[1] and demonstrated by Charlesby, Libby and Ormerod[2] in their study of 17-pentatriacontene. In the highly crystalline Marlex-50 polyethylene the alkyl free radical decays at room temperature in the presence of nitrogen for the most part according to a first-order law.[3] On the other hand Charlesby, Libby and Ormerod[2] found the decay to be second order in the presence of hydrogen. In 1954 we[4] postulated that free radicals produced in solid polyethylene by ionizing radiations decayed by reaction following a random walk migration of the free radical centers. A jumping of hydrogen atoms along or across molecular chains from a saturated $-CH_2-$ group to a free radical center $-\dot{C}H-$ was postulated. Lawton, Balwit and Powell[3] explain two rates of decay of the alkyl free radicals as being due to one group of free radical pairs close to each other and the other group with the free radicals farther apart. Voevodskii, *et al.*,[1] tentatively adopted the hydrogen migration concept described above. The latter authors suggested that free valency migration by the jumping of hydrogen atoms may not be the only mechanism of free radical migration. Free radical migration may be classified into two types according to whether the free radical center moves spatially as a whole or whether the free radical center moves by virtue of a chemical mechanism in which the free valency migrates from one carbon atom to another. It is the second type, free radical migration *via* a chemical process, with which we are concerned here. Lawton, Balwit and Powell's explanation of free radical decay was based on the first type, *i.e.*, spatial free radical migration, although a mechanism for such spatial migration was not given.

In this paper we wish to present a new mechanism of free radical migration based on evidence from deuterium–hydrogen exchange experiments. Var-

(1) A. T. Koritskii, Yu. N. Molin, V. N. Shamshev, N. Ya. Bulen and V. V. Voevodskii, *Acad. Nauk S.S.S.R.* (High Molecular Compounds), **1**, 1182 (1959).

(2) A. Charlesby, D. Libby and M. G. Ormerod, *Proc. Roy. Soc.* (London), **262A**, 207 (1961).

(3) E. J. Lawton, J. S. Balwit and R. S. Powell, *J. Chem. Phys.*, **33**, 395 (1960).

(4) M. Dole, C. D. Keeling and D. G. Rose, *J. Am. Chem. Soc.*, **76**, 4304 (1954). This is the first paper of this series. Others are: II, *ibid.*, **80**, 1580 (1958); III, **81**, 2919 (1959); IV, *J. Phys. Chem.*, **63**, 837 (1959).

shavskii, *et al.*,[5] irradiated polyethylene in the presence of deuterium gas at 60° in a nuclear reactor, and found 0.18 mole % D in the polymer after a dose of 400 Mrad. They suggested that the exchange was the result of the chain reaction

$$R\cdot + D_2 \longrightarrow RD + D\cdot \quad (1)$$

$$D\cdot + RH \longrightarrow R\cdot + HD \quad (2)$$

However, during the irradiation there must have existed ionic species, electronically excited methylene groups and excited free radicals, all of which might have been responsible for the deuterium exchange reaction. Furthermore, reaction 1 is endothermic and might be expected to have a rather high activation energy, and consequently a low rate. In order to clarify these uncertainties we have carried out deuterium–hydrogen exchange experiments subsequent to the irradiation when presumably excited states and ionic species would have died out, at least on warming to room temperature. Any post-irradiation isotope exchange under these conditions is assumed to involve only thermalized free radicals.

If reactions 1 and 2 are correct, then the hydrogen exchange chain reaction provides a mechanism by which free radical centers can migrate from site to site in the solid polyethylene, inasmuch as the probability of the free radical of (2) being at the same location as the free radical of (1) must be rather small. In this connection it should be noted that Voevodskii, *et al.*,[6] concluded that D–H exchange between deuterium gas and ethyl free radicals proceeded *via* a one step process, and that the exchange involved only the hydrogen in the free radical group, namely

$$CH_3CH_2\cdot + D_2 \longrightarrow CH_3CHD\cdot + HD \quad (3)$$

If this were exclusively the case, then there would be no migration of free radical sites during the exchange and, in the case of polyethylene, the exchange would be limited at the maximum to one exchange per free radical center except for exchanges with radicals such as $RCH_2\cdot$, where the exchange would be limited to two per free radical. Wijnen and Steacie,[7] however, studied the kinetics of the reaction of ethyl radicals with deuterium and found 13.3 kcal./mole for the activation energy of (1). If the Voevodskii mechanism had prevailed to a significant extent, $C_2H_4D_2$ should have been found as a reaction product, but Wijnen and Steacie detected no trace of it.

II. Plan of the Experiment

In brief the experimental procedure involved irradiating the polyethylene *in vacuo* at liquid nitrogen temperature, then warming the sample to room temperature subsequent to the irradiation, pumping off the evolved hydrogen and then admitting deuterium gas to the irradiation cell. After contact of the deuterium with the polyethylene lasting from 5 to 100 or more hours the gas was analyzed mass spectrometrically for the HD/D_2 and H_2/D_2 mole ratios. Let

$$y = \frac{HD/D_2}{1 + HD/D_2 + H_2/D_2} \quad (4)$$

If there is no change in the total gas pressure, and no significant change was observed, then

$$y = \frac{c_3}{c_4^0}$$

where c_3 is the concentration in moles/cc. of the mass 3 molecule (HD) in the gas phase after an irradiation of t hours, and c_4^0 is the initial concentration in moles/cc. of the mass 4 molecule (D_2) in the gas phase. We now derive an expression for y as a function of time assuming (1) the validity of Henry's law for the solubility of D_2, HD and H_2 in the polyethylene; (2) that the solubility equilibrium is established rapidly with respect to reaction 1 (solubility studies[8] demonstrated the validity of this assumption); and (3) that the reactions 5, 6 and 7 are negligible. Because of the constancy of the total pressure, (5) and (6) were negligible and because of the fact that the ratio of moles of D_2 in the gas phase to moles of $-CH_2-$ in the polyethylene was about 6×10^{-4} reaction 7 initially was considered to be negligible. We also assume steady-state kinetics and a uniform distribution of free radicals and dissolved gas in the solid. Let V be the free volume of the gas in the irradiation cell, w the weight of polyethylene, c_2, c_3 and c_4 concentrations in moles/cc. of H_2, HD and D_2 in the gas phase; m_2, m_3 and m_4 concentrations in moles per gram solid of dissolved H_2, HD and D_2 in the polyethylene phase, then by Henry's law

$$D\cdot + R\cdot \longrightarrow RD \quad (5)$$

$$D\cdot + D\cdot \longrightarrow D_2 \quad (6)$$

$$RD + D\cdot \longrightarrow R\cdot + D_2 \quad (7)$$

$$m_4 = k_h c_4 \quad (8)$$

where k_h is the solubility of deuterium in cc. measured at one atm. pressure and 20° per gram of polyethylene. By material balance

$$\text{moles } D_2 \text{ reacted} = -w \int_0^t \frac{dm_4'}{dt}\, dt = V(c_4^0 - c_4) + w(m_4^0 - m_4) \quad (9)$$

where the superscript zero indicates the value at zero time and dm_4' represents the change in concentration of D_2 in the solid phase due to reaction 1; dm_4 represents the total change of D_2 in the solid phase due both to the reaction and to D_2 dissolving into the solid phase from the gas phase. If k_1 is the reaction rate constant of reaction 1, we have

$$\frac{dm_4'}{dt} = -k_1 [R\cdot] m_4 = -k_1 k_h [R\cdot] c_4 \quad (10)$$

and

$$\frac{dm_4}{dt} = k_h \frac{dc_4}{dt} \quad (11)$$

Equation 9 now becomes

$$V \frac{dc_4}{dt} + wk_h \frac{dc_4}{dt} = -wk_1 k_h [R\cdot] c_4 \quad (12)$$

or

(5) Ya. M. Varshavskii, G. Ya. Vasil'ev, V. L. Karpov, Yu. S. Lazurkin and I. Ya. Petrov, *Doklady Akad. Nauk S.S.S.R.*, **118**, 315 (1958).

(6) V. V. Voevodskii, G. K. Lavrovskaya and R. E. Mardaleishvili, *ibid.*, **81**, 215 (1951).

(7) M. H. J. Wijnen and E. W. R. Steacie, *J. Chem. Phys.*, **20**, 205 (1952).

(8) M. Dole and M. Fallgatter, unpublished.

$$\frac{dc_4}{dt} = -ac_4 \qquad (13)$$

where

$$a = \frac{\frac{w}{V} k_1 k_h}{1 + \frac{w}{V} k_h} [R\cdot] \qquad (14)$$

Assuming [R·], the concentration of the free radicals in the solid state, to be constant (treatments are given below for different mechanisms of R· decay), we have on integrating (13)

$$c_4 = c_4^0 \exp(-at) \qquad (15)$$

For the molecule HD in addition to (2) we assume the reactions

$$R\cdot + HD \longrightarrow RD + H\cdot \qquad (16a)$$

$$R\cdot + HD \longrightarrow RH + D\cdot \qquad (16b)$$

where k_{2a} and k_{2b} are the reaction rate constants of (16a) and (16b). We now can write that the total increase in moles of HD in time dt

$$V\, dc_3 + w\, dm_3$$

is equal to moles of HD formed in reaction 2 less moles of HD consumed in reactions 16. Hence remembering that d[D·]/dt equals zero because of the steady-state approximation

$$V\, dc_3 + wk_h dc_3 = wk_h[R\cdot](k_1 c_4 - k_{2a} c_3)dt \qquad (17)$$

Assuming [R·] to be constant and equal to $[R\cdot]_0$, we obtain

$$\frac{dc_3}{dt} + a\frac{k_{2a}}{k_1} c_3 = ac_4 \qquad (18)$$

Letting

$$b = ak_{2a}/k_1$$

and introducing (15) for c_4

$$\frac{dc_3}{dt} + bc_3 = ac_4^0 \exp(-at) \qquad (19)$$

or

$$\frac{dy}{dt} + by = a \exp(-at) \qquad (20)$$

Integrating (20), we find

$$y = \frac{1}{\frac{b}{a} - 1} [\exp(-at) - \exp(-bt)] \qquad (21)$$

If reactions 16a and 16b were equally probable, and if $k_{2a} + k_{2b}$ equaled k_1, then $2b/a$ would be unity. Any deviation of $2b/a$ from unity demonstrates the fractionation of D and H in the exchange reaction and in the gas solution and diffusion in the polyethylene. We define $2b/a$ as the fractionation factor of the whole process.

From eq. 21, y should be independent of the initial D_2 pressure, but should depend on the volume to weight ratio, and should increase with decrease of volume at constant weight of polyethylene. Furthermore, by equation 21 y should rise to a maximum at a time t given by the equation

$$t_{y-\max} = \frac{1}{b - a} \ln \frac{b}{a} \qquad (22)$$

and at infinite time decrease to zero. The maximum value of y should be independent of the volume, pressure, weight of polyethylene and initial $[R\cdot]_0$ concentration but should depend on the ratio b/a

$$y_{\max} = \left[\frac{b}{a}\right]^{b/(a-b)} \qquad (23)$$

Unfortunately, failure of the free radical concentration [R·] to remain constant with time prevented us from determining the fractionation factor $2b/a$ through (23) from y_{max}. At very short times

$$y \simeq at \qquad (24)$$

Figure 1 illustrates the theoretical variation of y for constant [R·] and for two different volumes as a function of time. The length of the irradiation period affects a through $[R\cdot]_0$, the initial concentration of free radicals. A blank experiment performed without polyethylene in the radiation cell demonstrated no H–D exchange, and, indeed, none would have been expected unless water had been present. Many e.s.r. studies have shown that no atomic hydrogen exists in irradiated polyethylene, so that any D–H exchange initiated by it would not have been possible. Deuterium in contact with unirradiated polyethylene showed no exchange after two months.

The above treatment assumes that k_h is the same for HD as for D_2. A more nearly correct treatment would give for the b and c constants of eq. 21

$$b = \frac{\frac{w}{V} k_h' k_{2a} [R\cdot]_0}{1 + \frac{w}{V} k_h'} \qquad (25)$$

$$a \text{ (eq. 18)} = a \text{ (eq. 14)} \frac{1 + \frac{w}{V} k_h}{1 + \frac{w}{V} k'_h} \qquad (26)$$

where k_h' is the k_h constant for HD. Calculations show that (wk_h/V) was about 0.0086 at the smallest volume used, and experiments on the solubility of D_2 in polyethylene demonstrated that k_h for D_2 was twice k_h for H_2. Hence within the experimental uncertainties, a (eq. 18) can be set equal to a (eq.14), and any change in b caused by a difference between k_h and k_h' can be included in the fractionation factor, $2b/a$.

It is interesting to consider the ratio of the molecular gas concentrations

$$f = \frac{y^2}{x \cdot z} \qquad (27)$$

where x, y and z are c_4/c_4^0, c_3/c_4^0 and c_2/c_4^0, respectively. At zero time f is given by the expression

$$f_0 = 2a/b \qquad (28)$$

and decreases slowly with increasing time (Fig. 1). Equation 28 is useful because it enables an estimate of the ratio of a/b to be made from the data as well as an estimate of the fractionation factor $2b/a$.

III. Experimental Procedures and Results

Materials and Irradiation Procedures.—Linear polyethylene, Marlex-6000, type 9, anti-oxidant free, in the form of a rolled-up cylinder of 0.05 mm. thick film was used. The irradiations were conducted *in vacuo* at liquid nitrogen temperature in the Co-60 γ-ray source[9] for a long enough period, about 50 hr., to produce usually a dose of 4.0×10^{20} e.v.g.$^{-1}$. In all of the experiments the weight of the polyethylene was kept constant at 3.6 g., but the free cell volume was either 20 or 35 ml., approximately. After each experiment, the cell volume was determined to ± 0.5 ml., but

(9) M. Dole, D. C. Milner and T. F. Williams, *J. Am. Chem. Soc.*, **80**, 1580 (1958).

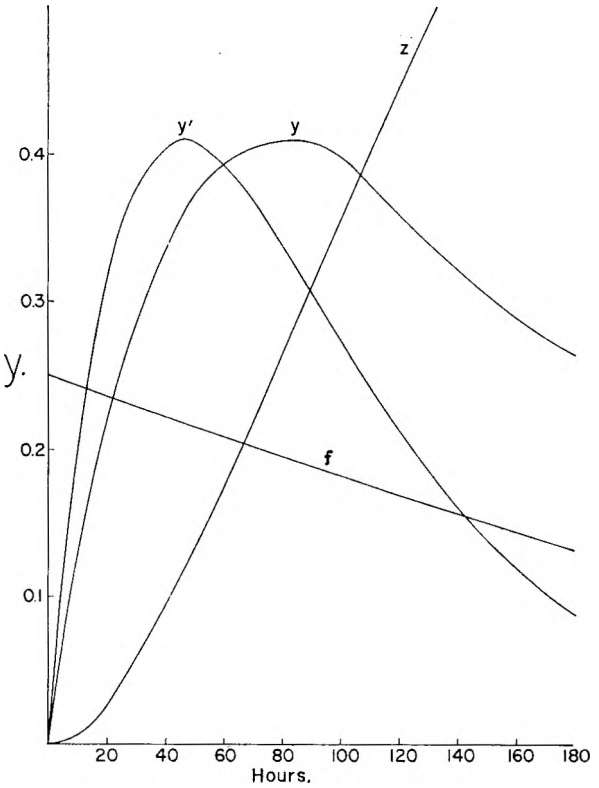

Fig. 1.—Theoretical variation of y, z and f with time assuming no free radical decay. Curves y, z and f calculated for the 35 ml. volume case using a and b equal to 0.014 and 0.0112 hr.$^{-1}$, respectively. Curve y' calculated for the case of the volume equal to 20 ml. The ordinate should be multiplied by 10 to give the f scale.

because of the exponential relationship between y and V no attempt was made to reduce y to a standard volume.

Isotope Ratio Determinations.—The deuterium gas which initially contained 1.3 mole % HD and 0.6 mole % H_2 was analyzed isotopically, both before and after exposure to the irradiated polyethylene, in a Consolidated Electrodynamics Nier-type mass spectrometer model 21-201. Standard mixtures of H_2 and D_2 were prepared and stored over a platinized asbestos catalyst. After isotopic exchange equilibrium had been attained, and the H_2/D_2 and HD/D_2 ratios calculated, the mixtures were used to calibrate the mass spectrometer readings. Correction factors amounted to 3%.

Experimental Procedure.—After the irradiation, the cell was connected to a vacuum line, opened using a magnetic hammer while still at liquid nitrogen temperature and warmed to room temperature as quickly as possible with continual pumping to remove hydrogen as fast as it was evolved. It was found necessary to admit D_2-gas to a pressure of about 5–8 cm. and re-evacuate in order to remove the last trace of free hydrogen in the polyethylene. Deuterium then was admitted to a pressure of about 8 cm. and the cell placed in a constant temperature bath at 20.3°. After a certain number of hours a gas sample was removed and analyzed on the mass spectrometer. Because the removal of this sample lowered the deuterium pressure in the irradiation cell and so increased slightly the extent of H–D exchange, only the isotope ratios of the first sample withdrawn are considered to be significant, and are given in this paper. Practically all of the gas was taken and mixed in a reservoir of the mass spectrometer inlet system. Thus, the gas analyzed was a representative sample of the whole. During the exchange, however, we have to assume that the gas mixed itself fast enough in the exchange cell so that the composition of the gas in the cell was uniform at all times.

It should be noted that on warming up the polyethylene to room temperature, the dark color of the sample was bleached. This indicated that any color centers disappeared rapidly at room temperature and that presumably only trapped free radicals remained. The period from the end of the irradiation to the removal of the liquid nitrogen trap was usually about 45 minutes, and the period from the removal of the liquid nitrogen trap to the final introduction of the D_2- gas at roomt emperature about 12–15 minutes.

In this work we have attempted to determine y as a function of radiation dose, cell volume, initial deuterium gas pressure and time. The data plotted in Figs. 2 and 3 show these relationships and indicate the order of accuracy of y. Some experiments also were done in which the irradiated polyethylene was held at 20° *in vacuo* for 89 and 264 hours before admitting the deuterium. Even after 264 hours some exchange occurred. These results are discussed below.

The y-values were calculated after subtracting the HD/D_2 and H_2/D_2 ratios at zero time from the observed ratios. The scatter in the y-values could have been due (1) to small variations in the free gas volume in the cell from the 35 and 20 ml. standards selected, (2) to accidental contamination of the gas with H_2 or by exchange with traces of water. The irradiation cell containing the polyethylene was evacuated for 24 hours or more before beginning the irradiation. The greatest difficulty was that of removing completely the last traces of H_2 before introducing D_2 into the cell. It was found necessary as mentioned above to introduce D_2 to a pressure of about 4 cm., and after about 30 seconds to pump it out in order to sweep out traces of H_2 before the final introduction of the D_2. The ratios H_2/D_2 were always small, 0.01 to 0.08, and were known much less accurately than the HD/D_2 ratios.

Another source of variation in the y-values was the difficulty of initiating the exchange with deuterium always at the same initial free radical concentration. Inasmuch as the free radical decay is most rapid during the heating of the irradiated polyethylene to room temperature, there must have been variations in $[R\cdot]_0$ due to variations in the heating rate and in the exact moment of final introduction of the deuterium gas.

IV. Discussion of Results[10]

A comparison of the curves of Fig. 2 with those of Fig. 1 demonstrates immediately that the free radical concentration $[R\cdot]$ did not remain constant with time, but decreased so that after about 100 hours no further exchange could be detected. If the free radicals with which the deuterium reacted decayed by a second-order process

$$\frac{d[R\cdot]}{dt} = -k_3[R\cdot]^2 \qquad (29)$$

as would normally be expected, the theoretical treatment given above should be modified. Integrating (29), we obtain

$$[R\cdot] = \frac{[R\cdot]_0}{1 + k_3[R\cdot]_0 t} \qquad (30)$$

Substituting (30) for $[R\cdot]$ in eq. 12, the differential equation for dc_4/dt becomes

$$\frac{dc_4}{dt} = \frac{a}{1 + Bt} c_4 \qquad (31)$$

where

$$B = k_3[R\cdot]_0$$

Integration of (31) yields

$$x = \frac{c_4}{c_4^0} = \frac{1}{(1 + Bt)^{a/B}} \qquad (32)$$

On similarly modifying (17) and introducing (32) for c_4 in eq. 17 the differential equation for dy/dt now has to be written

$$\frac{dy}{dt} + \frac{b}{1 + Bt} y = \frac{a}{(1 + Bt)^{(a/B+1)}} \qquad (33)$$

Integration of (33) yields

(10) A preliminary announcement of these results already has been made, M. Dole and F. Cracco, *J. Am. Chem. Soc.*, **83**, 2584 (1961).

$$y = \frac{1}{\frac{b}{a} - 1}\left\{\exp\left[-\frac{a}{B}\ln(1 + Bt)\right] - \exp\left[-\frac{b}{B}\ln(1 + Bt)\right]\right\} \quad (34)$$

Equation 34 is to be compared with (21).

If the free radicals decayed according to a first-order law, then we find by similar procedures the equation

$$[\mathrm{R}\cdot] = [\mathrm{R}\cdot]_0 \exp(-k_3 t) \quad (35)$$

where k_3 is the first-order decay constant. Letting

$$q = \exp(-k_3 t) \quad (36)$$

the analog of (15) and (32) becomes

$$x = \exp\left[-\frac{a}{k_3}(1 - q)\right] \quad (37)$$

the analog of (20) and (33)

$$\frac{dy}{dt} + bqy = aq \exp\left[\frac{a}{k_3}(q - 1)\right] \quad (38)$$

and the analog of (21) and (34)

$$y = \frac{1}{b/a - 1}\left\{\exp\left[-\frac{a}{k_3}(1 - q)\right] - \exp\left[-\frac{b}{k_3}(1 - q)\right]\right\} \quad (39)$$

At infinite time from (37)

$$\ln x_\infty = -\frac{a}{k_3} \quad (40)$$

At zero time (24) is valid for all three mechanisms as is (28). Equations 24, 28 and 40 enable an initial estimate to be made of the constants a, b and k_3. The constants then can be further adjusted slightly to bring about a more exact fit between the y-values calculated and observed.

From (24) it can be seen that at short times no distinction exists between the three kinetic equations 21, 34 and 39 based on the three postulates, [R·] constant with time or decreasing according to a second- or first-order law. At long times, however, there is a distinct difference between (21), (34) and (39), and the data indicate that eq. 39 resulting from the first-order free radical decay mechanism is the best description of the exchange process. In Fig. 2 the experimental values of y are plotted for free volumes of approximately 20 and 35 ml. in the D–H exchange cell. The solid lines were calculated by means of eq. 39. The constants, a, b and k_3 were chosen to bring about agreement between the calculated and observed values of y for the 35 ml. experiments, and then the a and b constants were increased by the factor 1.744 for the 20 ml. experiments. The factor 1.744 came

$$\frac{a_{20\ \mathrm{ml.}}}{a_{35\ \mathrm{ml.}}} = \frac{35}{20} \times \frac{1 + (3.598/35)(0.048)}{1 + (3.598/20)(0.048)}$$

from the ratio where 3.598 g. is the weight of polyethylene used in all of the experiments and 0.048 is the value of k_h in ml. g.$^{-1}$. Satisfactory agreement exists between the observed values and calculated curves. The scatter of points is due partly to the fact that the exchange cell volume deviated somewhat from the desired 20 and 35 ml. Table I lists the constants of eq. 39. The fractionation factor, $2b/a$, was taken to be equal to 2.22 for all of the calculations.

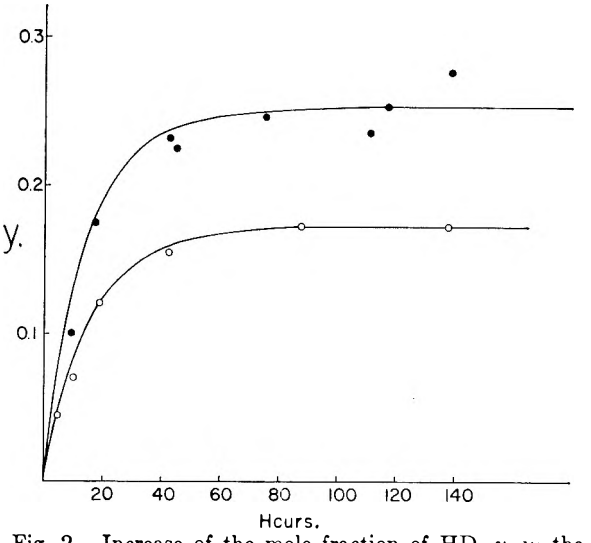

Fig. 2.—Increase of the mole fraction of HD, y, in the gas phase as a function of time of exposure of deuterium to the irradiated polyethylene: open circles, 35-ml. cell volume; solid circles, 20-ml. cell volume; pressure 8 cm.; solid lines, y-values calculated from eq. 39.

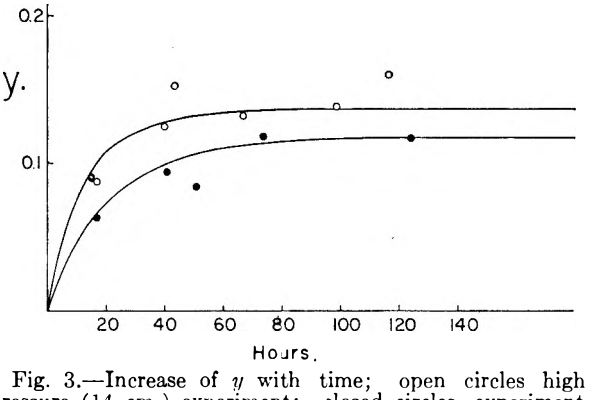

Fig. 3.—Increase of y with time; open circles high pressure (14 cm.) experiment; closed circles, experiment with polyethylene irradiated to half the γ-ray dose; solid lines, y-values calculated from eq. 39.

TABLE I

CONSTANTS OF EQUATION 39

Experimental conditions Radiation dose, e.v.g.$^{-1}$	V, ml.	P, cm.	y_∞, calcd.	a, hr.$^{-1}$	b, hr.$^{-1}$	k_3, hr.$^{-1}$
3.98×10^{20}	~35	~8	0.172	0.0120	0.0133	0.0555
3.98×10^{20}	~20	~8	.254	.0209	.0310	.0555
3.98×10^{20}	~35	~14	.137	.0120	.0133	.0740
1.99×10^{20}	~35	~8	.117	.0060	.0067	.0444

In Fig. 3 are plotted the data for the experiments run at a higher pressure, and at one-half the radiation dose. According to (39), increase of deuterium gas pressure should not change the observed y-values although it would increase the rate of the exchange reaction in the solid. However, if increasing the rate of H–D exchange in the solid increased the rate of free radical migration, then the rate of free radical decay should have increased. Such an increase in this rate can be taken care of mathematically by an increase of k_3. From Table I it can be seen that k_3 had to be increased from 0.0555 to 0.0740 to bring about agreement between theory and observation. (Another possible reason for a decrease in exchange rate at the higher pres-

sure might have been an increase in the rate of reactions 7 and 42, see below.)

An estimate of k_3 can be made from the electron spin resonance studies of Lawton, Balwit and Powell[3] on irradiated polyethylene, although the comparison cannot be completely valid because their studies were made with the radiation cell being flushed continually with nitrogen. They found that the first-order decay of the alkyl radical occurred with four different rate constants, the first rate constant lasting for about 10 seconds, the second for about 20 minutes, the third for about 10 hours and the fourth for an additional 90 or more hours. For the 10-hour period, k_3, estimated from the slope of the straight lines of Fig. 9 of Lawton, *et al.*,[3] was about 0.094 hr.$^{-1}$ and for the 90 hour period, 0.028 hr.$^{-1}$. These values are in the range of the k_3 values of Table I. It is interesting to note that the relative e.s.r. intensity of the alkyl radical was not measurable after about 100 hours; from the curves of Figs. 2 and 3 of the present paper it is evident that D–H exchange had come to an end also after about 100 hours. Thus, this good correlation between our results and those of Lawton, Balwit and Powell[3] indicates a high probability that our exchange was produced by the alkyl radical. However, in the work of Charlesby, Libby and Ormerod[2] the alkyl radical as measured by them disappeared in about 20 to 25 hours. Furthermore, they found that the alkyl radical decayed roughly according to a second-order law. Hydrogen must have been present in their experiments, but the exact pressure is unknown. A high hydrogen pressure could have been responsible for the more rapid rate of alkyl radical decay observed by Charlesby, *et al.*

In a research based on e.s.r. studies and as yet incomplete we have determined the first-order decay constant of the transient free radical in Marlex-50 polyethylene and in the presence of H_2 gas at 8 cm. pressure over the period 2.5 to 60 hours and obtained the value 0.050 hr.$^{-1}$. This value agrees well with those of Table I for k_3.

Turning now to the series of experiments at half the radiation dose, in this case it would be expected that the a and b constants would be halved in value, without any other constants changing, provided that the production of free radicals was linear with dose. The linearity of $[R\cdot]_0$ with dose has been observed by Voevodskii, *et al.*,[1] at these relatively low doses. Actually, it was found that the best agreement with the data, Fig. 3, was obtained not only by halving a and b, but also by decreasing k_3 from 0.0555 to 0.0444, Table I. It is reasonable for k_3 to be smaller for a lower initial free radical concentration. Lawton, *et al.*,[3] as mentioned above, found a lower rate constant of free radical decay with time as the free radical concentration decreased (at constant initial total dose). Almost as good an agreement could have been obtained by keeping k_3 constant and lowering a and b in the ratio 1.6 to 1.0 instead of 2.0 to 1.0.

It is interesting to consider the variation of the gas concentration ratio, f of eq. 27, with time. It is difficult to determine f experimentally because of the necessity of knowing H_2/D_2 accurately. The most accurate data for this ratio were obtained in the series of experiments at the 20 ml. volume, Fig. 2. Table II contains these data along with f-values calculated using the constants of Table I. In Table II expts. 12, 15, 17 and 25 were less reliable than the others because these experiments were carried out before the technique was adopted of flushing the cell with D_2 gas before beginning the exchange experiment. A low value of f would have resulted from a too high measured H_2/D_2 ratio. At 25° the equilibrium constant[11] for the reaction

$$H_2(g) + D_2(g) \rightleftharpoons 2HD(g) \qquad (41)$$

is 3.27.

TABLE II

f-VALUES ($f = y^2/xz$)

Expt. no.	t, hr.	f, obsd.	f, calcd.
	0		1.80
33	9.17	1.79	1.69
12	17.25	1.50	1.64
15	42.73	1.38	1.57
25	44.72	1.41	1.56
32	75.57	2.01	1.54
17	111.0	2.11	1.54
34	116.9	2.17	1.54
31	138.7	2.23	1.54

The data definitely prove that the equilibrium value was not obtained, but they do show that f observed for the longer times is greater than f calculated. This is undoubtedly the result of neglect of reactions of the type

$$RD + H\cdot \longrightarrow R\cdot + HD \qquad (42)$$
$$RD + D\cdot \longrightarrow R\cdot + D_2 \qquad (7)$$

That reactions 42 and 7 may have been significant was shown by a "reverse exchange" experiment in which H_2 was introduced into the radiation cell 77 hours after the first introduction of deuterium.

At the end of the first 75.6 hours with deuterium in the cell (exp. 32, Table II), the deuterium was pumped out, the cell flushed with H_2, hydrogen introduced and allowed to remain in the cell 47 hours. At the end of this time the D_2/H_2 ratio was practically negligible, 0.00025, but the HD/H_2 ratio was 0.006, thus indicating a small amount of reverse exchange. The low D_2/H_2 ratio demonstrated the completeness of the deuterium removal before introducing the hydrogen. Not much exchange would have been expected in any case, because after 75 hours most of the free radicals would have decayed; calculations indicate that, at the maximum, the HD/H_2 ratio could have grown to 0.012. Thus, an estimated 50% of the possible exchanges involved deuterium rather than hydrogen.

If the mechanism of Voevodskii, *et al.*,[6] exclusively prevailed, and if the free radicals did not decay with time, cessation of D–H exchange would have occurred when the ratio of $\overset{|}{\underset{|}{DC\cdot}}$ to $\overset{|}{\underset{|}{HC\cdot}}$ in the solid was such that the free energy of the exchange reactions

$$\overset{|}{\underset{|}{HC\cdot}}(s) + D_2(g) \longrightarrow \overset{|}{\underset{|}{DC\cdot}}(s) + HD(g) \qquad (43)$$

(11) I. Kirshenbaum, "Physical Properties and Analysis of Heavy Water," McGraw-Hill Book Co., New York, N. Y., 1951, p. 54.

and

$$\text{HC}\cdot(s) + HD(g) \longrightarrow \text{DC}\cdot(s) + H_2(g) \qquad (44)$$

had become zero, or in other words when the gaseous equilibrium 41 had become established. But the data of Table II prove that the isotopic exchange equilibrium was not attained. Furthermore, the small amount of reverse exchange mentioned above proves that the observed cessation of exchange, Figs. 2 and 3, was not due to a "saturation" of the alkyl free radical groups with deuterium. By "saturation" we mean an almost complete conversion of the HC· groups to DC· groups.

Unfortunately, it is not possible to derive explicit equations for x, y and z as a function of time for the kinetic scheme which includes reactions 7 and 42 as well as reactions 1, 2, 16a and 16b.

It is instructive to consider the total number of observed D–H exchanges. By "observed exchanges" we mean those calculated from changes in the gas composition. In moles per gram of polyethylene this number is $(y + 2z)PV/wRT$. Table III contains the results estimated at infinite time.

TABLE III

ESTIMATED TOTAL OBSERVED D–H EXCHANGES

Exptl. cond. Radiation dose, e.v.g.$^{-1}$ $\times 10^{-20}$	V, ml.	P, cm.	Y_∞	z_∞	$(Y_\infty + 2z_\infty)PV/wRT$, moles g.$^{-1}$ $\times 10^5$
3.98	~35	~8	0.172	0.030	0.99
3.98	~20	~8	.254	.045	0.84
3.98	~35	~14	.140	.015	1.27
1.99	~35	~8	.118	.013	0.61

Lawton, Balwit and Powell[3] found G (total radicals) = 3.0 for a dose of 40 megaroentgens. At the end of 15 minutes at room temperature the alkyl radical concentration in the work of these authors had dropped to 0.4 of its initial value. The alkyl radical concentration was 0.73 of the total radical concentration. Hence at the start of our D–H exchange experiment (zero time in this work) we estimate on consideration of our total dose of 7.6 megaroentgen that the alkyl radical concentration was 0.6×10^{-5} mole g.$^{-1}$. There is some uncertainty in this figure because of the larger dose used by Lawton, Balwit and Powell, but if our estimate is correct, then there were between 1 and 2 observable exchanges per free radical center in our experiments before the exchange ceased. In addition to the observable exchanges there must have been some exchanges of the type

$$R\cdot + HD \longrightarrow RH + D\cdot \qquad (16a)$$
$$RH + D\cdot \longrightarrow R\cdot + HD \qquad (2)$$
$$R\cdot + H_2 \longrightarrow RH + H\cdot \qquad (45)$$
$$RH + H\cdot \longrightarrow R\cdot + H_2 \qquad (46)$$

which produced no observable change in the gas or solid composition. These non-observable exchanges probably were less than 20% of the total, however. It should be pointed out that m_4^0, the initial concentration of D_2 dissolved in the solid was only 2.0×10^{-7} mole g.$^{-1}$ or about 1/30 as large as the estimated initial free radical concentration. This fact suggests that many free radicals may have decayed without experiencing any D–H exchange. If this is true, then there must have been multiple exchanges involving the free radicals that did undergo D–H exchange. If the mechanism of Voevodskii, *et al.*,[6] were exclusively and strictly valid, the number of exchanges should have been less than the number of alkyl free radicals initially present (unless the free radicals were predominantly $RCH_2\cdot$ rather than RĊHR').

In this paper we have assumed the "B" radical of Lawton, Balwit and Powell[3] to be the

$$-CH_2\dot{C}HCH_2-$$

radical as they and others[1,2] have concluded. With respect to the free radical that persists after the decay of the above radical, Lawton, Balwit and Powell suggest that it is the $RCH_2\cdot$ radical whereas Charlesby, Libby and Ormerod[2] as well as Voevodskii, *et al.*,[2] think that it is the allyl free radical, $-\dot{C}HCH{=}CH-$. Assuming that D_2 would exchange with $RCH_2\cdot$, but not with the allyl-free radical, we attempted to distinguish between these two possible types by carrying out experiments in which the introduction of D_2 into the exchange cell was delayed until 89 or 264 hours had elapsed after removing the H_2 and warming the polyethylene to 20°. An exchange sequence of the type

$$-CH_2\dot{C}H_2\cdot + D_2 \longrightarrow -CH_2CH_2D + D\cdot \qquad (47)$$
$$D\cdot + -CH_2- \longrightarrow -\dot{C}H- + HD \qquad (48)$$

would eliminate the $RCH_2\cdot$ radical and produce one of the $-CH_2\dot{C}HCH_2-$ type. The latter could then decay as has been demonstrated. From eq. 40 and 14, $V \log x_\infty$ should be proportional to the free radical concentration at the start of the exchange providing that k_3 is independent of initial free radical concentration. Results obtained are given in Table IV.

TABLE IV

D–H EXCHANGE AFTER ROOM TEMPERATURE DELAY[a]

Exp. no.	Delay time, hr.	$-V \log x_\infty$, ml.	$[R\cdot]_0$ (Total) relative values L.B.P.[3]	C.L.O.[2]
34	0.25	3.14 (1.00)	1.71 (1.00)	49 (1.00)
41	89	1.27 (0.40)	0.68 (0.40)	11 (0.22)
46	89	1.10 (.35)	.68 (.40)	11 (.22)
45	264	0.52 (.17)	.49 (.29)	9 (.18)

[a] The numbers in parentheses are the ratios of the value at the delay time indicated to the value at the 15 minute delay.

The data of Table IV indicate that even after a room temperature delay *in vacuo* of 264 hours, some exchange still occurred (if there had been no exchange, $\log x_\infty$ would have been zero). In the case of the 89-hour delay experiments the decrease in $V \log x_\infty$ was almost exactly that expected on the basis of Lawton, Balwit and Powell's results assuming that the persistent radical is the $RCH_2\cdot$ radical. However, from the 89-hour to the 264 hour delay, the total exchange decreased more than would have been expected either on the basis of Lawton, *et al.*'s, results[3] or of those of Charlesby, *et al.*[2] If a possible decrease of k_3 in going to the lower free radical concentration also occurred, the discrepancy would be even greater. On the basis of the work reported

here it is not possible to deduce unambiguously the type or types of free radicals with which the D–H exchanges occurred.

Turning now to the question of the migration of free radicals by means of reactions 1 and 2, it should first be pointed out that the presence of hydrogen gas is not essential for free radical decay. For example, Lawton, Balwit and Powell[3] continually swept nitrogen through their radiation cell during the e.s.r. measurements and yet observed a considerable decay. Furthermore, the distance the free radical migrates because of each D–H exchange may be only to the next nearest neighbor site. The fact that reactions 42 and 7 seemed to occur to small extent as indicated by higher f values than calculated and by a detectable reverse exchange proves that the free radical center produced in reaction 2 must be close to the –CHD– group produced in reaction 1.

It is interesting to compute k_1 from the value of a, see eq. 14. Taking k_h to be 0.048 cc. g.$^{-1}$, $[R\cdot]_0$, 5.8×10^{-6} mole cc.$^{-1}$ and a, 0.012 hr.$^{-1}$ or 3.33×10^{-6} sec.$^{-1}$ we find

$$k_1 = 1.1 \times 10^2 \text{ cc. sec.}^{-1} \text{ mole}^{-1}$$

From Trotman-Dickenson's[12] table of the E and A factors of the Arrhenius equation

$$k = A \exp(-E/RT)$$

it is possible to calculate the rate constant of the gaseous reaction

$$C_2H_5\cdot + D_2 \longrightarrow C_2H_5D + D\cdot \qquad (49)$$

With E equal to 13.3 kcal. mole^{-1} and A equal to $10^{11.9}$ cc. sec.$^{-1}$ mole^{-1}, we find

$$k_1 = 1 \times 10^2 \text{ cc. sec.}^{-1} \text{ mole}^{-1}$$

The close agreement of the rate constant of the gaseous reaction at 20° with that calculated for the reaction occurring in the solid is completely unexpected. In this connection it should be pointed out that the activation energy for reaction 1 is probably about 3.8 kcal./mole greater than that of reaction 49 because the C–H bond energy in the methylene group is 93.1 as compared to 96.9 kcal./mole for the C–H bond in ethane.[13] Adding 3.8 to 13.3 kcal./mole and assuming the A-factor to be unchanged, k_1 is calculated to be 0.16, about 1/1000 as large as the observed k_1. This makes the high observed k_1-value even more surprising. Probably in the solid, the endothermicity of reaction 1 is considerably reduced because of the heat of adsorption of atomic deuterium on the solid polyethylene.

The D–H fractionation factor for the entire process, defined here as $2b/a$ or 2.22, probably is largely the result of twice the ratio of the rates of the reactions

$$R\cdot + D_2 \xrightarrow{k_1} RD + D\cdot \qquad (1)$$

$$R\cdot + HD \xrightarrow{k_{2a}} RD + H\cdot \qquad (16a)$$

namely, $2k_{2a}/k_1$. Trotman-Dickenson[12] has tabulated reaction rate constants at 182° for the reactions

$$CH_3\cdot + D_2 \longrightarrow CH_3D + D\cdot \qquad (50)$$

$$CH_3\cdot + H_2 \longrightarrow CH_4 + H\cdot \qquad (51)$$

The ratios of the rate constant of (50) to that of (51) vary from 3.33 to 7, depending on the authors and experimental conditions, with the latter value probably the most reliable. The square root of 7 is 2.64, which is not far from the observed fractionation factor 2.22. The difference in the solubility of D_2 and HD in polyethylene would act to lower the fractionation factor.

Finally, the mechanism of free radical decay should be discussed. For an initially random distribution of free radicals, the decay should be second order in the free radical concentration. The observed first-order dependence is probably the result of a non-random distribution of the free radicals. If the free radicals were formed in pairs with the pairs distributed randomly, and if a free radical in one pair reacted only with the other free radical of the pair, then the decay of the pairs would be first order. Lawton, Balwit and Powell[3] suggested that the free radicals were formed very close to each other. The elimination of the $RCH_2\cdot$ radical and production of $-CH_2\dot{C}HCH_2-$ according to reactions 47 and 48 would be first order in the $RCH_2\cdot$ radical concentration.

V. Applications and Conclusions

The higher rate of decay of the alkyl free radical observed by Charlesby, Libby and Ormerod[2] as compared to the rates estimated from the data of Lawton, *et al.*,[3] and our own unpublished results possibly may be explained by the presence of hydrogen in Charlesby, *et al.*'s, experiments and the higher dose used by them (as compared to our own). Voevodskii, *et al.*,[1] noted the curious fact that free radical decay was more rapid in a sample of polyethylene that had been compressed before the irradiation under a pressure of 30 atm. into a semi-transparent plastic mass than in a sample in the form of a curdy mass. This difference may possibly be explained in part by the longer residence time of the evolved hydrogen in the plastic sample as compared to the fluffy one, the latter having a much larger surface area through which the hydrogen could have escaped. The observations of Charlesby, *et al.*,[2] regarding the greater rate of free radical decay in less crystalline polyethylenes may be partly explained by a possible greater solubility of the hydrogen in low density polyethylenes. Inasmuch as Voevodskii, *et al.*, noted an effect of technical stabilizer in the polyethylene in reducing the rate of free radical decay, part of the discrepancies in the quantitative data mentioned above may be due to different amounts and types of stabilizers present in the samples of polyethylene used by the different authors.

In conclusion, it would appear that the data given in this paper indicate an exchange with free radicals rather than exchange initiated by other active species such as ions. Reasons on which this conclusion are based are (1) the fairly good correlation between the free radical decay rates observed by Lawton, *et al.*,[3] and us and the decay rates estimated above; (2) the order of magnitude agreement between the calculated rate constant of

(12) A. F. Trotman-Dickenson, "Gas Kinetics," Academic Press, New York, N. Y., 1955, p. 208.

(13) G. C. Fettis and A. F. Trotman-Dickenson, *J. Am. Chem. Soc.*, **81**, 5261 (1959).

reaction 49 and the observed rate constant; and (3) the fact that the observed D–H fractionation factor was the expected order of magnitude. Although we cannot deduce unambiguously from our studies the type of free radical with which the D_2-molecule reacts, the evidence indicates reactions with both the RCHR′ and RCH_2· free radicals.

The results of the delayed-exchange experiments definitely prove a higher rate of free radical decay in the presence of 8 cm. pressure of deuterium than *in vacuo*. Thus, there are strong indications that free radical migration occurs as a result of the exchange reactions 1 and 2. Since the D–H exchange did not proceed until isotopic equilibrium had become established, the cessation of exchange was not the result of saturation of the free radical centers with deuterium (as would have occurred without free radical migration).

Finally, we conclude that the exchange probably involved a nearest neighbor H-atom or one close to the initial free radical center. In other words we postulate that the D-atom of reaction 1 did not migrate far through the solid polyethylene before reacting. Evidence for this concept of "nearest neighbor migration" comes from the fact that "*f*" did not decline continually with dose and that some reverse exchange was detected in the special reverse exchange experiment.

This work was supported by the U. S. Atomic Energy Commission. The use of the mass spectrometer was made possible by a grant from the National Science Foundation. Grateful acknowledgment is made for a Fulbright travel grant (to F. C.). This research also was supported by the Advanced Research Project Agency of the U. S. Department of Defense.

PHOTOCHEMICAL ISOMERIZATION OF CINNAMIC ACID IN AQUEOUS SOLUTIONS

BY BERT H. CLAMPITT[1] AND JAMES W. CALLIS

Applied Physics Staff, Boeing Airplane Company, Wichita Division, Wichita, Kansas

Received May 20, 1961

The photochemical isomerization of *cis–trans* organic acids in aqueous solutions is complicated by the ionization of the acids. This gives rise to a number of absorbing species possessing different photochemical properties all of which are related by the ionization constants. A theoretical treatment of the process is presented and the particular case where the ions do not isomerize is solved. The resulting equation is tested for *cis–trans*-cinnamic acid, and shows good agreement with the experimental data.

Introduction

A method of conversion of solar to electrical energy employing the geometrical inversion of stereoisomers recently was proposed by this Laboratory.[2] In this connection, a study of the rate of isomerization of various *cis-trans* organic acids under the influence of ultraviolet light in aqueous solution was undertaken. While Vaidya[3] and Olson[4] investigated several aspects of the photochemical isomerization, a detailed analysis of the kinetics of this process have not been reported previously, and it is the purpose of this paper to present a theoretical approach to the problem together with some experimental data which may be used to compare to the theory.

Previous investigators have failed to take into account that aqueous organic acid solutions are ionized and indeed the amount of ionization is changed as the photochemical reactions proceed. This is equivalent to assuming that the ions and undissociated acids have identical photochemical properties, which in the general case appears to be invalid. When the *trans*-(HB) and *cis*-(HA) forms of the stereoisomers of an organic acid are added to water, they dissociate to some extent to give the respective *trans*-(B) and *cis*-(A) ions. When a cell containing these species is irradiated with monochromatic light, the following photochemical reactions are possible

$$HB + h\nu \longrightarrow HA \quad (1)$$

$$HA + h\nu \longrightarrow HB \quad (2)$$

$$B + h\nu \longrightarrow A \quad (3)$$

$$A + h\nu \longrightarrow B \quad (4)$$

The quantum efficiencies for each process are defined as the number of isomerizations of a given specie per photon absorbed by that species, and are denoted in subsequent discussion by ϕ_{HB}, ϕ_{HA}, ϕ_B, ϕ_A, respectively. Under certain circumstances the individual reactions may be investigated, but for a practical system all of the reactions occur in the photochemical cell and a complex equilibrium is established as denoted in Fig. 1, where in addition to the various stereoisomer species, (H) represents the hydrogen ion concentration, Γ and η are the net rates of conversion of the undissociated *trans* acid and *trans* ion, respectively, while R_A is the net rate of ionization of HA, and R_B is the net rate of recombination of hydrogen and *trans* ions. Initial experimental investigation of this type of system has been limited to cinnamic acids; however, the discussion section should be applicable to a large number of *cis–trans* systems.

Experimental

Materials.—The *trans*-cinnamic acid was obtained from Eastman Organic Chemical Company and was recrystallized from hot water prior to use. The *cis*-cinnamic acid was

(1) Spencer Chemical Company, Merriam, Kansas.

(2) B. H. Clampitt and D. E. German, *S.A.E. Journal*, **68**, 52 (1960).

(3) B. K. Vaidya, *Proc. Roy. Soc.* (London), **129A**, 299 (1930).

(4) A. R. Olson and F. L. Hudson, *J. Am. Chem. Soc.*, **55**, 1410 (1933).

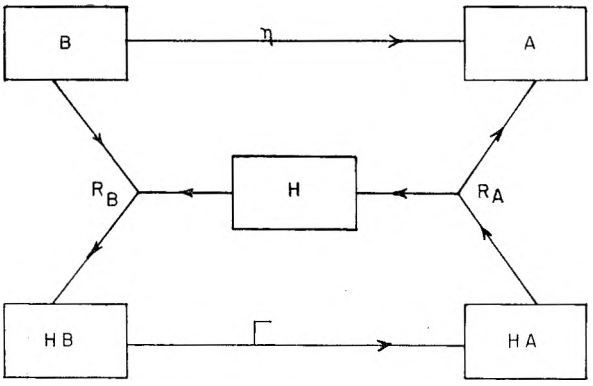

Fig. 1.—Flow diagram.

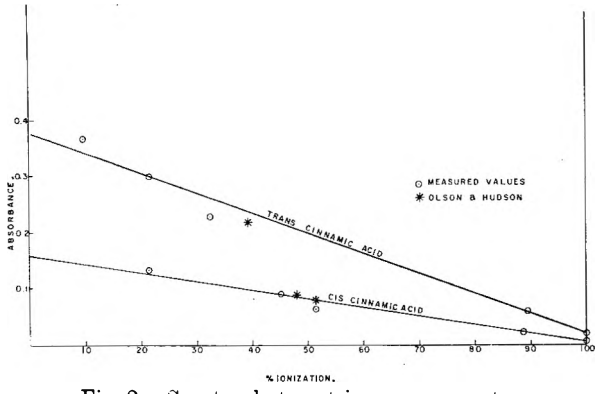

Fig. 2.—Spectrophotometric measurements.

prepared by the hydrogenation of phenylpropiolic acid, obtained from Aldrich Chemical Company, in a Parr hydrogenation apparatus using methanol as a solvent and a palladium–asbestos catalysis as originally described by Taal and Schwarz.[5] The products had melting points of 132° for the *trans* acid, and 68° for the *cis* acid.

Ultraviolet Spectra.—In order to determine the extinction coefficients of the various species of interest, potassium hydroxide and hydrochloric acid were added to solutions of the organic acid in order that the absorbance of the organic acid under various degrees of ionization could be measured. The solutions were made so that the total concentration of ion plus undissociated acid was 2.4×10^{-4} *M* in all cases. The absorbances at 3130 Å. were determined with a Beckman Model DU Spectrophotometer equipped with a 2960 Ultraviolet Accessory Set. The slit width was 0.02 mm. and distilled water was the reference solution. Rectangular silica absorbance cells were used with the reference cell having a path length of 0.999 cm. and the sample cell having a path length of 1.000 cm.

Photochemical.—The actual photochemical experiments were carried out in a rectangular cell having quartz windows with a 2.5-cm. square face and being 4.1 cm. deep. On the sides, the cell was surrounded by water from a constant temperature-bath in order to maintain a reaction temperature of 20°. The source of illumination was a Hanovia lamp equipped with a number 7910 heat deflecting filter and used in conjunction with a one-cm. quartz cell containing 0.001 *N* potassium chromate in order to obtain monochromatic light at 3130 A.[3]

The flux of the incoming radiation was determined by placing uranyl oxalate in the reaction cell and measuring the decomposition at various times. The procedure is very completely described by Leighton and Forbes,[6] and the results were identical for exposure times from 0.5 to 8 hr., with a value of 3.64×10^{14} photons per cm.^{2} per sec. being obtained.

*p*H measurements were made on a Beckman Model GS *p*H meter. The general procedure followed in the kinetic experiments was to measure the *p*H of the solution after a given period of exposure, relative to the unexposed solution. The experiments were run in duplicate and the reproducibility was 0.005 *p*H unit. The original solutions were measured relative to a *p*H 4 buffer and the results were: 3.500 for 0.003 *N trans*-cinnamic acid, 3.595 for 0.002 *N trans*-cinnamic acid, and 3.250 for 0.003 *N cis*-cinnamic acid. This procedure proved very satisfactory in the case where the starting acid was in the *trans* configuration as the *p*H changes were large (*e.g.*, after one hr. exposure the 0.003 *N* solution gave a *p*H change of 0.038). If the starting acid was in the *cis* configuration the *p*H changes relative to the original *cis* acid were small and only after 24 hr. was a change of 0.040 observed for a 0.003 *N* solution. Because of the small *p*H changes and accuracy of the instrument, data obtained at shorter times of exposure are not considered reliable and therefore are not recorded. In addition to the pure acids, potassium salts of both *trans* and *cis*-cinnamic acid were irradiated, and after 48 hr. the 0.003 *N* solutions showed no detectable *p*H change in either case.

Results

The results of the spectrophotometric measurements are shown in Fig. 2. The data of Olson and Hudson[4] showing the extent of ionization of their solutions are indicated on the figure and they are in good agreement with the measured values. From the intercepts the various molar extinction coefficients are calculated as: *trans*-cinnamic acid 1560, *trans*-cinnamate ion 92, *cis*-cinnamic acid 655 and *cis*-cinnamate ion 33. Because of the low extinction coefficients of both of the ions, it is not surprising that detectable *p*H changes were not observed on irradiation of the potassium salts of the cinnamic acids.

The results of the measurements of the hydrogen ion concentration as a function of time starting with pure *trans*-cinnamic acid are shown in Figs. 3 and 4, with the final values of the hydrogen ion concentration measured after 99 hr. of irradiation being shown at the extreme right of the figures. These data are in good agreement with the results of Vaidya[3] obtained by conductivity measurements which are shown in the same figures with the time scale corrected for differences in flux density and cell length.

As the cinnamate ions do not undergo isomerization, the quantum efficiency, ϕ_{HB}, of the *trans*-cinnamic acid may be determined from the initial slope of the rate curve starting with pure *trans*-cinnamic acid. It should be pointed out, however, that the initial slope of a general acid system will not give a unique ϕ_{HB}, but rather is a function of both ϕ_{HB} and ϕ_B. Similarly the quantum efficiency, ϕ_{HA}, of *cis*-cinnamic acid could be determined from the initial slope of a rate curve starting with pure *cis*-cinnamic acid; however, in the present investigation it was not possible to obtain such data. From the theoretical rate curve which is derived later, ϕ_{HA} may be determined from the middle portion of the experimental curves starting with *trans*-cinnamic acid. The sensitivity of the theoretical curve in this region to this parameter is great enough to determine ϕ_{HA} to an accuracy of 10%. As a result of the determinations, these quantum efficiencies were calculated

Normality	Φ_{HA}	Φ_{HB}
0.002	0.21	0.61
0.003	0.30	0.70

The photostationary state values show a somewhat higher amount of *cis*-cinnamic acid than pre-

(5) C. Taal and A. Schwarz, *Ber.*, **51**, 640 (1918).

(6) W. G. Leighton and G. S. Forbes, *J. Am. Chem. Soc.*, **52**, 3139 (1930).

viously reported values. The reason for this is not clear but Vaidya's values may have been taken before the process beginning with excess *trans* acid had reached completion, the results being indicated by the curve beginning with excess *cis* acid on which accurate data are difficult to obtain.

Discussion

Equilibrium State.—When a sample containing a fixed amount of acid in solution is irradiated the concentrations of acid and ions will approach values for which the rates are in equilibrium or, as depicted in Fig. 1, $\Gamma = R_A = R_B = -\eta$. In general these rates will not be zero and thus the system will approach a state of dynamic equilibrium rather than a true photostationary state. In fact, the vanishing of Γ and η fix the ratios HA/HB and A/B but at equilibrium these must be related by the ratio of the ionization constants K_A and K_B. Thus a true photostationary state occurs only when

$$K_A(\alpha_A\phi_A)(\alpha_{HB}\phi_{HB}) = K_B(\alpha_B\phi_B)(\alpha_{HA}\phi_{HA}) \quad (5)$$

where α represents the molar extinction coefficient of the species. It appears in many cases that the ions are only weakly affected by radiation so that equation 5 is approximately satisfied, and a true photostationary state exists in solution.

Rates of Isomerization.—In analyzing the time dependence of the photochemical process the following assumptions are made: (1) The reaction cell is long enough to absorb essentially all of the incoming radiation. (2) The concentration of the various species remains uniform over the volume of the cell. As only direct photochemical isomerizations are considered to contribute to the process, the rate of isomerization of a given species is equal to its quantum efficiency, ϕ_i, times the rate of absorption of light by the species. The relative amount of radiation absorbed by a given species is proportional to the product of its molar extinction coefficient, α_i, and its concentration, x_i. The net rates of isomerization are therefore

$$\Gamma = \frac{1000J_0}{NL} \cdot \frac{\phi_{HB}\alpha_{HB}[HB] - \phi_{HA}\alpha_{HA}[HA]}{\Sigma\alpha_i x_i} \quad (6)$$

$$\eta = \frac{1000J_0}{NL} \cdot \frac{\phi_B\alpha_B[B] - \phi_A\alpha_A[A]}{\Sigma\alpha_i x_i} \quad (7)$$

where in addition to the previously defined symbols, J_0 is the total quanta per cm.^{2} per sec. entering the cell, L is the cell length in cm., N is Avogadro's number, and the 1000 in the numerator allows the concentration terms to be expressed in moles per liter. The total net rate of isomerization of the *trans* form is

$$\frac{d}{dt}(B + HB) = -(\Gamma + \eta) \quad (8)$$

Since the rates of conversion are slow compared to the time required to establish ionization–recombination equilibrium, these restraining equations apply to the system

(a) $[H][A] = K_A[HA]$
(b) $[H][B] = K_B[HB]$
(c) $S = [A] + [HA] + [B] + [HB]$
(d) $[H] = [A] + [B]$ (9)

where S is the solute concentration. It is convenient to integrate equation 8 in terms of the hydrogen ion concentration, which when combined with equations 6, 7 and 9 becomes

$$\frac{1}{K_A - K_B}\left[2H + (K_A + K_B) + \frac{K_AK_BS}{H^2}\right]\frac{dH}{dt} = \Gamma + \eta = \frac{J_0\,1000}{LN} \times \quad (10)$$

$$\frac{(\phi_{HB}\alpha_{HB}H + \phi_B\alpha_BK_B)(H^2 + K_AH - K_AS) + (\phi_{HA}\alpha_{HA}H + \phi_A\alpha_AK_A)(H^2 + K_BH - K_BS)}{(\alpha_{HB}H + \alpha_BK_B)(H^2 + K_AH - K_AS) - (\alpha_{HA}H + \alpha_AK_A)(H^2 + K_BH - K_BS)}$$

which gives the integral

$$t = \frac{LN}{1000\,J_0(K_A - K_B)} \times \int_{H_0}^{H}\left[2H + (K_A + K_B) + \frac{K_AK_BS}{H^2}\right] \times \quad (11)$$

$$\left[\frac{(\alpha_{HB}H + \alpha_BK_B)(H^2 + K_AH - K_AS) - (\alpha_{HA}H + \alpha_AK_A)(H^2 + K_BH - K_BS)}{(\phi_{HB}\alpha_{HB}H + \phi_B\alpha_BK_B)(H^2 + K_AH - K_AS) + (\phi_{HA}\alpha_{HA}H + \phi_A\alpha_AK_A)(H^2 + K_BH - K_BS)}\right] dH$$

where H_0 is the original hydrogen ion concentration.

The polynomial in the denominator has only one zero in the region of realizable hydrogen ion concentration which gives the value of H at the equilibrium state (H_∞). The general form of the integral (11) is

$$\left[E_1H^2 + E_2H + E_3 \ln H + E_4\,1/H + E_5\,1/H^2 \ldots\ldots + \sum_m E_m \ln(H - H_m)\right]_{H_0}^{H} \quad (12)$$

where the H_m's are the zeros of the polynomial in the denominator.

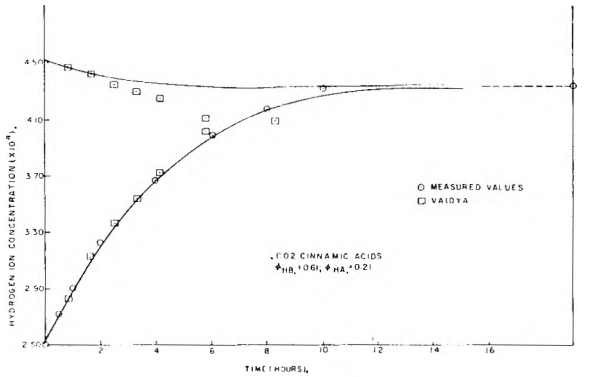

Fig. 3.—Hydrogen ion concentration as a function of exposure time for 0.002 cinnamic acids.

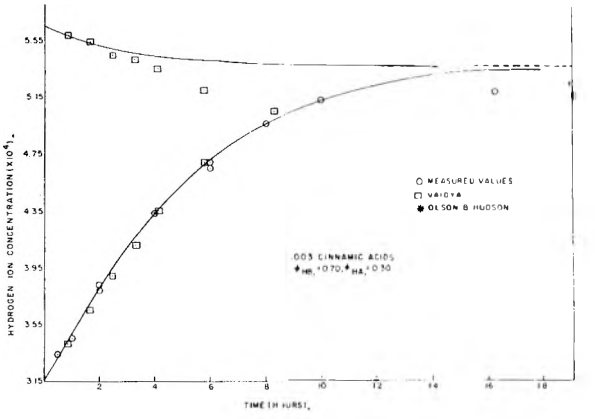

Fig. 4.—Hydrogen ion concentration as a function of exposure time for 0.003 cinnamic acids.

In many systems, for example isomers containing conjugated benzene rings, the ions absorb weakly and do not appear to isomerize. In this case equation 11 integrates in the form

$$t = \frac{LN}{J_0(K_A - K_B)\phi_{HA}1000}\left[E_1H^2 + E_2H + E_3 \ln H + E_4\, 1/H + E_5\, 1/H^2 + E_6 \ln\frac{H - H_1}{H - H_\infty} + E_7 \ln (H - H_1)(H - H_\infty)\right] \quad (13)$$

where

$$H_\infty = \frac{-(qrK_A + K_B) + \sqrt{(qrK_A + K_B)^2 + 4(qr + 1)(qrK_A + K_B)S}}{2(qr + 1)} \quad (14)$$

$$H_1 = \frac{-(qrK_A + K_B) - \sqrt{(qrK_A + K_B)^2 + 4(qr + 1)(qrK_A + K_B)S}}{2(qr + 1)} \quad (15)$$

$$r = \frac{\phi_{HB}}{\phi_{HA}},\ q = \frac{\alpha_{HB}}{\alpha_{HA}},\ m = \frac{\alpha_A}{\alpha_{HA}},\ l = \frac{\alpha_B}{\alpha_{HA}} \quad (16)$$

and the coefficients are

$$E_1 = \frac{q - 1}{qr + 1}$$

$$E_2 = \frac{1}{qr + 1}\left[\frac{(q - 1)(K_A - K_B)(1 - qr)}{1 + qr} - 2\{(m - q)K_A + (1 - l)K_B\}\right]$$

$$E_3 = \frac{K_AK_B}{K_Aqr + K_B}\left[lK_A - mK_B + \frac{(l - m)K_AK_B(1 + qr)}{K_Aqr + K_B}\right]$$

$$E_4 = \frac{K_AK_BS}{K_Aqr + K_B}[K_B - qK_A]$$

$$E_5 = \frac{(m - l)(K_A^2K_B^2S)}{2(qrK_A - K_B)}$$

$$E_6 = \frac{1}{\sqrt{(qrK_A + K_B)^2 + 4(qrK_A + K_B)(qr + 1)S}}\left[\{(qK_A - K_B)S + (m - l)K_AK_B\}\left\{(K_A + K_B) - \frac{(K_Aqr + K_B)}{1 + qr}\right\} + \{(m - q)K_A + (1 - l)K_B\}\left\{2S - \frac{K_A + K_B}{2} + \frac{K_Aqr + K_B}{1 + qr}\right\}\left\{\frac{K_Aqr + K_B}{1 + qr}\right\} + K_AK_B\left\{\frac{(1 + qr)(qK_A - K_B)S}{K_Aqr + K_B} + {}^1/_2\left[lK_A - mK_B + \frac{(1 + qr)(l - m)K_AK_B}{K_Aqr + K_B}\right] + [2(l - m) + (1 - q)]S\right\} + \frac{(K_Aqr + K_B)(1 - q)}{(1 + qr)^2} \times \left\{(K_A - K_B)(1 - qr)(S + {}^1/_2\frac{K_Aqr + K_B}{1 + qr} - S(K_Aqr + K_B)\right\}\right]$$

$$E_7 = \frac{K_AK_B}{2(K_Aqr + K_B)}\left[\frac{(1 + qr)(m - l)K_AK_B}{K_Aqr + K_B} - lK_A + mK_B\right] + \frac{(l - m)K_AK_B}{(1 + qr)} + \frac{K_A - K_B}{2(1 + qr)^2}\left[(qr - 1)(mK_A - lK_B) - q(1 + r)\left\{2S + (K_A - K_B)\frac{(qr - 1)}{qr + 1}\right\}\right]$$

Equation 13 was programed for an IBM 610 computer, and a curve may be computed easily starting from either pure *cis* or pure *trans* acid solutions. The following input information for the system is required: the molar extinction coefficients of the various species; the quantum efficiencies of the undissociated acids; the equilibrium constants; the originial solute concentration; the cell length; and the photon flux entering the cell.

Application to Cinnamic Acid.—Equation 13 was applied specifically to the cinnamic acid system with the following data being determined independently of the photochemistry experiments: $\alpha_{HB} = 1560$, $\alpha_{HA} = 655$, $\alpha_B = 92$, $\alpha_A = 33$, $K_A = 1.32 \times 10^{-4}$, $K_B = 0.37 \times 10^{-4}$, $L = 4.1275$ cm., $J_0 = 3.64 \times 10^{14}$ quanta per cm.^{2} per sec. ϕ_{HB} could be computed easily from the initial slope of the photochemical rate curves starting from pure *trans*-cinnamic acid solutions. As explained previously, ϕ_{HA} was computed from the middle portion of the same curves to give the best fit of the experimental data. These values of the quantum efficiencies then were used to compute the theoretical curves starting from pure *cis* acid solutions. These results starting from both pure *trans* and pure *cis* solutions are shown in Figs. 3 and 4 as the solid curves.

While it is not surprising that the initial and middle portions of the curves starting with pure *trans* acid agree closely, the asymptotic values of equation 13 and the experimental data after 99 hr. are also in reasonable agreement as is indicated in Figs. 3 and 4. As equilibrium state data usually are expressed as the relative amount of *cis* acid, the data are so converted and the results are

Amount of solute, N	% of *cis*-cinnamic acid, Olson and Hudson			
	Measured	Vaidya		Eq. 13
0.002	89.5	75.2	..	89.5
0.003	80.5	71.8	77.0	90.3

The experimental and theoretical values agree perfectly for the 0.002 case; however, the calculated value is somewhat higher than the measured value in the 0.003 case. The reason for this is not, at present, clear.

It also should be noted that the curves starting from pure *cis*-cinnamic acid and using the quantum efficiencies determined from the *trans* data agree with the initial points of Vaidya's results. Considering all of the experimental data on cinnamic acid, it would appear that the theory adequately explains the process; however, it may have to be modified slightly to account for indirect isomerization processes involving reactions by molecules in an excited state.

Acknowledgments.—The authors wish to express their gratitude to Dr. A. Mueller for preparation of the *cis*-cinnamic acid, and to Mr. J. R. Galli for encouragement in this investigation.

ADSORPTION ISOTHERMS OF NITROGEN, BENZENE AND *n*-HEXANE AND THE HEATS OF ADSORPTION OF BENZENE AND *n*-HEXANE ON GRAPHITIZED CARBON BLACKS. II. ADSORPTION ON GRAPHITIZED CHANNEL BLACKS

BY A. A. ISIRIKYAN AND A. V. KISELEV

Adsorption Laboratory, Chemical Department, Moscow State University, and Surface Chemistry Group Institute of Physical Chemistry, U.S.S.R. Academy of Sciences, Moscow, U.S.S.R.

Received May 22, 1961

The adsorption isotherms of nitrogen at −195°, *n*-hexane at 20°, and the differential heats of adsorption of *n*-hexane on graphitized channel black have been measured. The shape of the adsorption isotherms and the heats and entropies of adsorption on graphitized carbon blacks are dependent on the dispersion, particle packing, and mosaic character of the surface. When passing from graphitized thermal blacks to graphitized channel blacks, the adsorption isotherms of both nitrogen and *n*-hexane change from concave to convex in the initial region. Heats of adsorption of helium (measured by other authors) are sensitive indicators of surface inhomogeneity of graphite.

Introduction

In the strict sense of the word, an infinitely large continuous surface with identical arrangement of its constituent atoms, molecules or ions should be regarded as a homogeneous surface of a solid body. For crystalline bodies, this is the surface of a plane of specific index. In practice, we usually encounter substances that are, to one degree or another, dispersed. The adsorption properties of unit total surface of a dispersed substance should differ from the adsorption properties of unit surface of a definite face of the crystal. This difference should increase with increasing degree of dispersion due to greater contribution to the total surface of areas associated with edges and angles of crystals, or of faces of other index. This refers not only to the dispersion of single crystals, but also to the appearance of crystal faces on the surface of initially inhomogeneous bodies as a result of heat treatment. An example of the latter arises in the heat treatment of carbon blacks at temperatures close to 3000°. In this case, the initially spherical particles of carbon blacks rearrange to polyhedra,[1] the faces of which are formed by single crystals of graphite grown inside the particle. In the case of thermal carbon blacks composed of large particles some 5000 Å. in diameter, such treatment leads to the main surface of the polyhedral particles of carbon black being formed by homogeneous basal planes of graphite, and the influence of inhomogeneous sites at edges and angles of polyhedra becomes extremely small.[2,3] In this way, it is possible, from the adsorption isotherms and heats of adsorption obtained on such carbon blacks, to differentiate clearly the role of adsorbate–adsorbent and adsorbate–adsorbate interactions.[3,4]

In the case of channel blacks treated at close to 3000° (Graphon) with particles of considerably smaller size, *i.e.*, 300 Å., that have partially grown together, the role of the inhomogeneous surface is appreciably greater. Here, the inhomogeneous adsorbate–adsorbent interactions interfere in a clear-cut manifestation of adsorbate–adsorbate interactions. Thus, whereas for graphitized thermal blacks of low surface area the adsorption isotherm of nitrogen is at first convex to the pressure axes,[3,5,6] for the finer graphitized channel blacks it is concave in the same pressure range.[6] Characteristic differences likewise are observed in the case of adsorbates that strongly interact with one another. Thus, the adsorption isotherms of alcohols and ammonia on graphitized channel black are satisfactorily described by equations that take into account adsorbate–adsorbate interactions for localized adsorption.[7,8] However, in the case of graphitized thermal blacks which possess the maximum homogeneous surface, the adsorption isotherms of alcohols[9] and ammonia[10] are better described by equations for non-localized adsorption. We also have shown that under pressure an increase in the number of contacts of particles of graphitized channel black increases the inhomogeneity of its surface.[11]

The present paper describes the isotherm and differential heats of adsorption of *n*-hexane vapor as well as the adsorption isotherm of nitrogen on Graphon.[12] It also compares the adsorption isotherms of nitrogen, benzene and hexane, and the heats and entropies of adsorption of benzene, hexane and helium on both graphitized channel and thermal blacks. Possible causes of the inhomogeneity of the surface of graphitized channel black also are considered.

(1) W. D. Schaeffer, W. R. Smith and M. H. Polley, *Ind. Eng. Chem.*, **45**, 1721 (1953); M. H. Polley, W. D. Schaeffer and W. R. Smith, *J. Phys. Chem.*, **57**, 469 (1953); D. Graham and W. S. Kay, *J. Colloid Sci.*, **16**, 182 (1961).

(2) R. A. Beebe, C. H. Amberg and W. B. Spencer, *Can. J. Chem.*, **33**, 305 (1955).

(3) A. A. Isirikyan and A. V. Kiselev, *J. Phys. Chem.*, **65**, 601 (1961).

(4) N. N. Avgul, A. V. Kiselev and I. A. Lygina, *Kolloid. Zhur.*, **23**, N5 (1961); A. V. Kiselev, *Zhur. Fiz. Khim.*, **35**, 233 (1961).

(5) S. Ross and W. Winkler, *J. Colloid Sci.*, **10**, 319 (1955); S. Ross and W. W. Pultz, *ibid.*, **13**, 397 (1958).

(6) A. V. Kiselev and E. V. Khrapova, *Kolloid. Zhur.*, **23**, 163 (1961).

(7) N. N. Avgul, G. I. Berezin, A. V. Kiselev and I. A. Lygina, *Izvest. Akad. Nauk S.S.S.R., Dept. Chem. Sci.*, 205 (1961).

(8) A. V. Kiselev, *Kolloid. Zhur.*, **20**, 338 (1958); A. V. Kiselev, N. V. Kovaleva, V. A. Sinitzin and E. V. Khrapova, *ibid.*, **20**, 444 (1958).

(9) N. N. Avgul, A. V. Kiselev and I. A. Lygina, *ibid.*, **23**, 369 (1961).

(10) R. A. Beebe, J. M. Holmes, A. V. Kiselev and N. V. Kovaleva, *Zhur. Fiz. Khim.*, to be published.

(11) A. A. Isirikyan and A. V. Kiselev, *Kolloid. Zhur.*, **23**, 67 (1961).

(12) The adsorption isotherm of nitrogen on Graphon was published earlier by L. G. Joyner and P. H. Emmett, *J. Am. Chem. Soc.*, **70**, 2353 (1948).

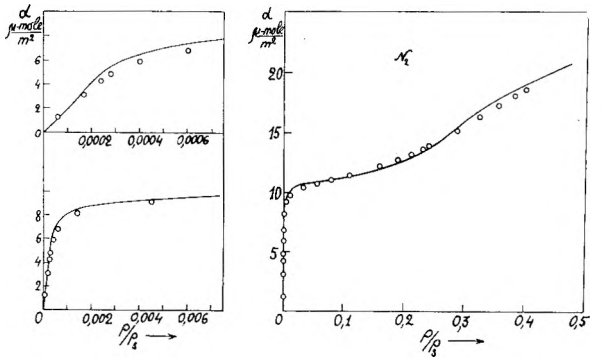

Fig. 1.—Absolute adsorption isotherms of nitrogen at −195° on Graphon (circles), and graphitized thermal carbon black Sterling MT-1 (3100°)[3] (solid line).

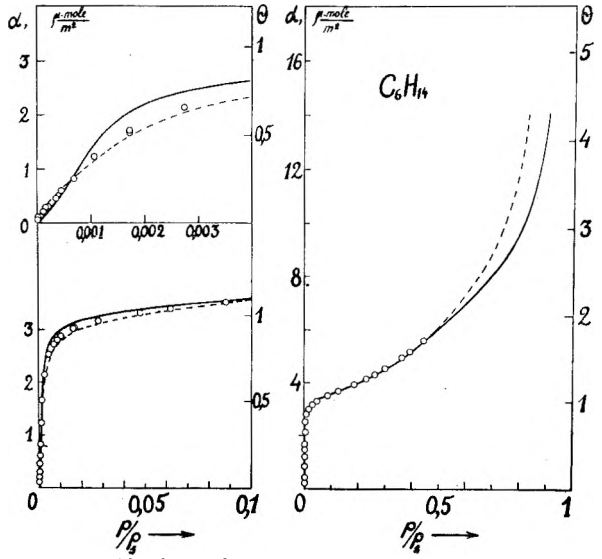

Fig. 2.—Absolute adsorption isotherms of *n*-hexane at 20° on Graphon (circles), Spheron 6 (2800°)[11] (dashed line), and graphitized Sterling MT-1 (3100°)[3] (solid line).

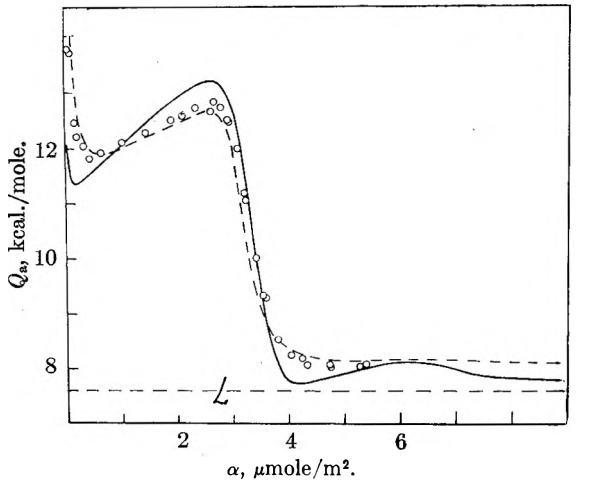

Fig. 3.—The differential heats of adsorption of *n*-hexane at 20° on Graphon (circles), Spheron 6 (2800°)[11] (dashed line) and on Sterling MT-1 (3100°)[3] (solid line).

Experimental

A sample of Graphon obtained by heating of Spheron 6 channel black at 2700° for two hr. was obtained from the Cabot Laboratory. The adsorption calorimetric apparatus and adsorbates were the same as in references 3 and 13. The adsorption isotherms of *n*-hexane and nitrogen were measured only to a relative pressure of 0.4 since surface inhomogeneity is more evident during filling of the first adsorbed layers. The specific surface of this sample of Graphon carbon black (area 82.2 m.²/g.) was determined from the adsorption of nitrogen by the BET method[14] using an area per nitrogen molecule in the dense monolayer of 16.2 Å.². In ref. 3, 5 and 6 it was shown that the adsorption isotherm of nitrogen vapor on graphitized thermal blacks with highly homogeneous surface is wave-shape and convex to the pressure axes in the initial portion (approximately up to filling of the surface $\theta \approx 0.3$). This form of the adsorption isotherm of nitrogen is associated with relatively strong adsorbate–adsorbate interactions.[8] For this reason, the BET equation,[14] which does not assume these interactions, does not describe this isotherm in the initial portion. In our preceding paper,[3] it was shown that the BET equation is, with more reason, applicable to the adsorption isotherm of benzene on graphitized thermal black, for which the adsorbate–adsorbate interaction is very weak. This same paper[3] shows, however, that a formal application of the BET method to the nitrogen isotherm on graphitized thermal blacks in the interval θ from 0.5 to 1.1 (that is, after the first point of inflection) leads to values of surface area S that are close to those obtained in a more acceptable application of the BET method to the adsorption isotherm of benzene vapor. For this reason, we also considered it possible to apply the standard BET method to the adsorption isotherm of nitrogen to determine the specific surface of Graphon carbon black. In this case, the BET equation is applicable from $\theta \approx 0$ to $\theta \approx 1.2$, that is, over a broader interval of surface coverage. However, this is associated only with the influence of the greater inhomogeneity of Graphon which leads to such higher adsorption in the region of low relative pressure that the adsorption isotherm of nitrogen becomes concave to the pressure axes.[6]

The results of measurements of isotherms and heats of adsorption are given in Figs. 1–3. They are compared with results obtained earlier for Graphon (Spheron 6–2800°),[11] and with absolute isotherms and heats of adsorption obtained in an earlier work[3] with graphitized thermal blacks.

Discussion of Results

The Effect of Residual Inhomogeneity of Graphitized Channel Blacks.—As we know,[1,15–17] calcination of a channel black such as Spheron 6 at high temperature removes oxygen- and hydrogen-containing groups from the surface and tends to eliminate surface roughness and partially reduces the area. For different samples of channel black these features must be common, and the properties of a unit surface of heat treated channel black likewise should be similar. As may be seen from Figs. 2 and 3, the adsorption isotherms and the heats of adsorption of *n*-hexane vapor on Graphon are very close to those for a similar sample of carbon black[18] investigated earlier.[11] The somewhat greater homogeneity of the Graphon sample possibly is associated with a greater heating time of the carbon black at 2700° (2 hr.). The sample investigated earlier was heated for only 10 min. at 2800°.[18] In addition, the slight difference in the adsorption isotherms may be due to a difference in the area of these samples (82 *vs.* 90 m.²/g.),

(13) A. A. Isirikyan and A. V. Kiselev, *Zhur. Fiz. Khim.*, **32**, 679 (1958).

(14) S. Brunauer, P. H. Emmett and E. Teller, *J. Am. Chem. Soc.*, **60**, 306 (1938).

(15) R. A. Beebe, J. Biscoe, W. R. Smith and C. B. Wendell, *ibid.*, **69**, 95 (1947).

(16) R. B. Anderson and P. H. Emmett, *J. Phys. Chem.*, **56**, 753, 756 (1952).

(17) A. V. Kiselev and N. V. Kovaleva, *Izvest. Akad. Nauk S.S.S.R., Dept. Chem. Sci.*, 989 (1959).

(18) N. N. Avgul, G. I. Berezin, A. V. Kiselev and A. I. Korolev, *Kolloid. Zhur.*, **20**, 298 (1958).

which likewise suggests a possible greater inhomogeneity of the sample investigated in ref. 11.

From Figs. 1 and 2 we clearly see the difference in the shape of the nitrogen and *n*-hexane isotherms on Graphon as compared with the corresponding absolute adsorption of these vapors on the most homogeneous thermal blacks.[3] As in ref. 6, here also the nitrogen isotherm on graphitized channel black at first rises more steeply and is concave to the pressure axis. In the case of *n*-hexane, the isotherm on Graphon at first also is concave, whereas on graphitized thermal black, with a more homogeneous surface, it definitely is convex. The greater inhomogeneity of Graphon black is clearly seen from the curves of the differential heats (Fig. 3) as well as from entropies (Fig. 4) of adsorption of *n*-hexane. The inhomogeneity of the surface of heat treated channel blacks, particularly when heated at a lower temperature of 1700°,[19,20] increases the initial heats of adsorption. This hampers clear-cut manifestation of adsorbate–adsorbate interactions. At low coverages the entropy of adsorption is reduced. Near completion of the monolayer the maximum in the heat of adsorption and the depth of minimum entropy of adsorption both are diminished.[20]

Figure 5 provides comparison of the isotherms, differential heats and entropies of adsorption of benzene on Spheron 6 black calcinated at 900, 1700[19] and 2800°[18] and on thermal blacks with the most homogeneous surface.[3] In these figures we also see an analogous influence of surface inhomogeneity of the carbon blacks on the adsorption properties of benzene. The nature of the reduction of heat of adsorption in the initial region on the channel blacks is close to that reported by Beebe and Young[21] for adsorption of argon vapor.

Let us now examine the probable causes of this influence. These samples differ first of all in their dispersion. The specific surfaces of the thermal graphitized blacks, Sterling MT (3100°),[22] Sterling MT-1 (3100°)[3] and Sterling FT (2800°),[3,22a] are 6.51, 7.65 and 12.22 m.²/g., respectively, while the specific surfaces of Graphon channel blacks are approximately an order of magnitude greater. The isotherm and heat of adsorption of *n*-hexane on thermal black T-1 (3000°)[3,20] of area 29.1 m.²/g. occupy positions intermediate between the thermal blacks of smaller area and the Graphon blacks with greater area. Thus, homogeneity of the surface is higher the smaller the specific surface; that is, the lower the degree of their dispersion. A similar effect on surface homogeneity is produced by contacts between particles of carbon black, the number of which per unit weight of the sample increases with increasing dispersion. At points of contact, the energy of adsorption of the first portions of adsorbate is elevated and the normal type of surface coverage is distorted.[11]

In addition, there is the effect of peculiarities in the structure of the particles of graphitized blacks themselves. These particles consist of small crystallites of graphite that extend to the surface chiefly through basal planes. As a result, there should appear an additional inhomogeneity (associated with the mosaic-like structure of the surface of a graphitized particle), leading to still greater disintegration of the basal plane of graphite.[23] When only a few adsorbed molecules can find a place on the planes of a single crystallite on the surface of a particle of carbon black the adsorbate–adsorbate interactions likewise become inhomogeneous over the entire surface. Further, in the case of highly dispersed graphitized carbon blacks, the size of the crystallites remains so small that large numbers of steps, formed by prismatic faces, come to the surface. These parts of the surface also may easily bind oxygen chemically and introduce chemical inhomogeneity. The smoother nature of the curves of heat of adsorption as a function of coverage for the more inhomogeneous surface of highly dispersed carbon blacks also is emphasized by the more gradual (for different sites occurring at different relative pressure) superposition of polymolecular adsorption of lower heat and higher entropy.

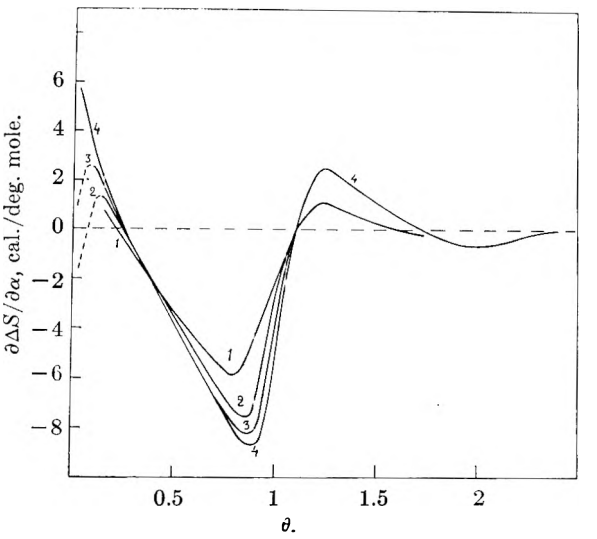

Fig. 4.—Differential entropies of adsorption of *n*-hexane on Spheron 6 (1700°)[19] (1), Spheron 6 (2800°)[11] (2), T (3000°)[20] (3) and Sterling MT-1 (3100°)[3] (4).

Unlike the adsorption of low-molecular weight alcohols at 20°,[7] and ammonia at −79°,[10] the adsorption of nitrogen at −195° and also *n*-hexane and benzene at 20° on the most homogeneous surface of graphitized thermal blacks[3,5,6] is predominantly localized. For this reason, it may be expected that on the Graphon black, at least for small θ, localization of these molecules will be increased. Indeed, in accord with the larger differential heats of adsorption of hexane

(19) N. N. Avgul, G. I. Berezin, A. V. Kiselev and I. A. Lygina, *Zhur. Fiz. Khim.*, **30**, 2106 (1956).

(20) A. A. Isirikyan and A. V. Kiselev, *Kolloid. Zhur.*, **23**, 281 (1961).

(21) R. A. Beebe and D. M. Young, *J. Phys. Chem.*, **58**, 93 (1954).

(22) (a) W. B. Spencer, C. H. Amberg and R. A. Beebe, *ibid.*, **62**, 719 (1958); (b) R. A. Beebe and J. M. Holmes, *ibid.*, **61**, 1684 (1957).

(23) The somewhat greater (as compared with graphite) azimuthal disorder of the carbon platelets in the case of graphitized thermal blacks and the greater distances between these platelets do not, apparently, lead to significant complications in adsorption properties, since the adsorption potential is determined mainly by the outer carbon atoms of the basal plane of the graphite.[19,24]

(24) N. N. Avgul, A. A. Isirikyan, A. V. Kiselev, I. A. Lygina and D. P. Poshkus, *Izvest. Akad. Nauk S.S.S.R., Dept. Chem. Sci.*, 1314 (1957); 1196 (1959).

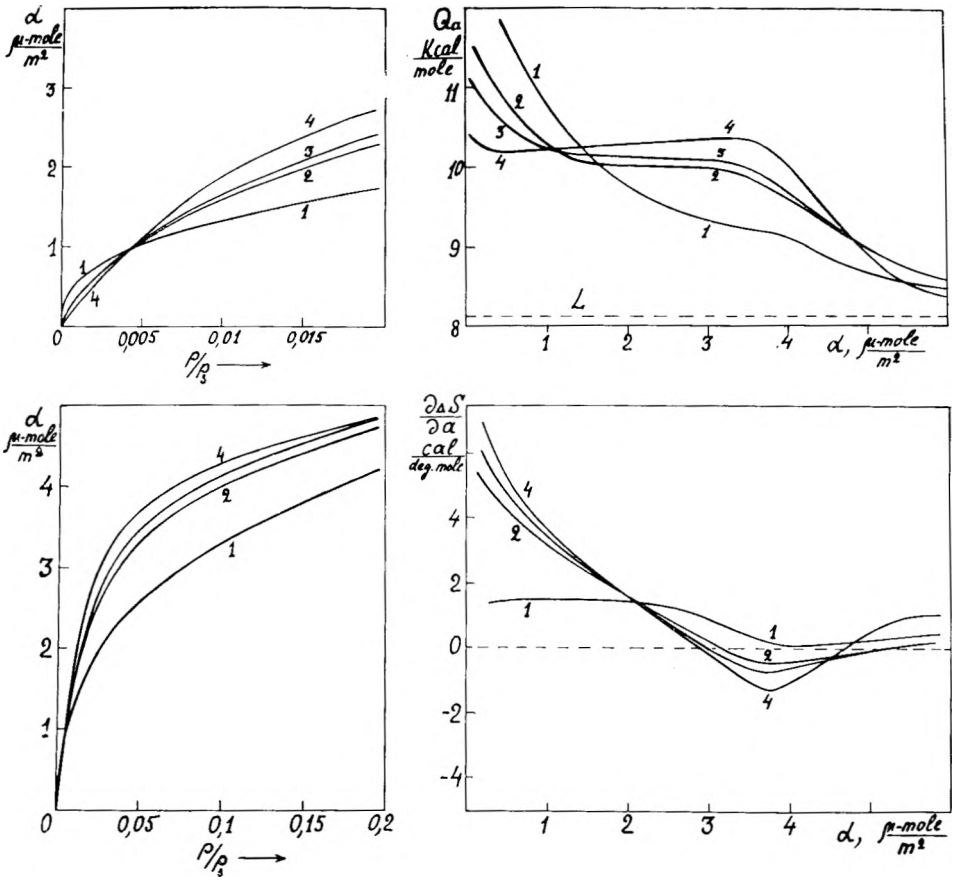

Fig. 5.—Isotherms (left), differential heats (top right) and differential entropies (lower right) of adsorption of benzene on Spheron 6 blacks heated at 900°[18] (1), 1700°[19] (2), and 2800°[18] (3), and on graphitized thermal carbon, Sterling MT-1 (3100°)[3] (4).

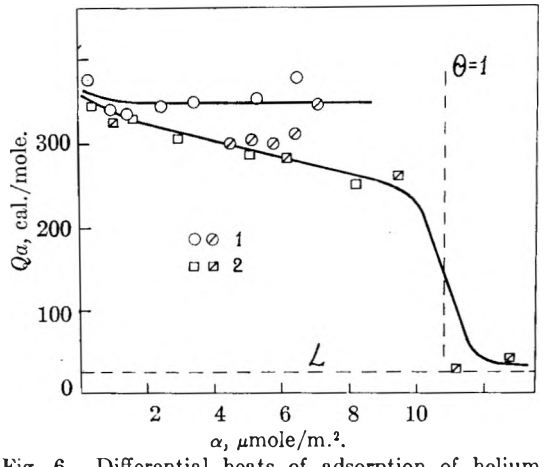

Fig. 6.—Differential heats of adsorption of helium at 15°K.: (1) on Sterling FT (2700°)[26]; (2) on Graphon black.[27] The crossed circles are isosteric heats of adsorption.

and benzene (Figs. 3 and 5) the entropy of adsorption in the region of small coverages on Graphon black is lower than on thermal black MT-1 (3100°) (Figs. 4 and 5).

The influence of surface inhomogeneity usually is superimposed on the effect of adsorbate–adsorbate interactions.[25] For this reason, adsorbates with low interaction are of interest. These include benzene.[3,18] However, the heat of condensation of benzene makes up about 80% of the heat of adsorption in the monolayer. Thus, adsorbates with extremely small heats of condensation are of special interest. The limiting case is helium, the heat of adsorption of which on graphitized carbon black is about 350 cal./mole,[26,27] while the heat of condensation is only 25 cal./mole. Thus the energy of adsorbate–adsorbate interaction probably cannot exceed 10 cal./mole. Thus in the case of helium adsorption on a fully homogeneous basal plane of graphite, the heat of adsorption should not pass through a perceptible maximum. The heats of adsorption of helium on graphitized carbon blacks of the Sterling FT (2700°) type[26] and Graphon[27] have been studied. Figure 6 compares the relationships obtained in these studies of the heats of adsorption of helium as a function of coverage on Sterling FT (2700°)[26] black and Graphon.[27] We have reduced the values given in these papers to a unit surface basis from surface areas determined by the BET method, using nitrogen as the adsorbate.[28]

(25) For example, see T. L. Hill, P. H. Emmett and L. G. Joyner, *J. Am. Chem. Soc.*, **73**, 5102 (1951).

(26) J. G. Aston and J. Greyson, *J. Phys. Chem.*, **61**, 610, 613 (1957).

(27) E. L. Pace and A. R. Siebert, *ibid.*, **63**, 1398 (1959); **64**, 961 (1960).

(28) In ref. 26 and 27 it was pointed out that application of the BET method[14] to adsorption isotherms of very low-boiling substances leads to anomalously high values of the area of graphitized blacks. The cross-sectional areas per molecule of adsorbate in a dense monolayer were determined here in the conventional manner from the density of the appropriate liquid. Thus, in the case of the adsorption of helium, with the value of $\omega_{mHe} = 15.4$ Å.², determined from the density of the

Despite the rather large spread of experimental points in Fig. 6, we clearly see the difference in the trend of the heats of adsorption on these two samples. On graphitized thermal carbon black, Sterling FT (2700°), the heat of adsorption of helium is approximately constant; therefore, its surface already is sufficiently homogeneous. However, the heat of adsorption of helium on Graphon declines with increase in adsorption. This is definite indication of residual inhomogeneity of the surface. In the case of adsorbates that display a more substantial adsorbate–adsorbate attraction on graphitized thermal carbon black, the heat of adsorption must pass through a maximum. On Graphon manifestation of this attraction is, at least partially, compensated by the effect of surface inhomogeneity, which reduces the heat of adsorption with increasing coverage. In the case of adsorption of hydrogen and deuterium, such compensation results in heats of adsorption on Graphon black nearly independent of coverage.[27]

Thus, for adsorption studies on the surface of the basal plane of graphite, which is of great theoretical interest,[24,29–33] one should apply thermal blacks graphitized at about 3000° and of the smallest possible area. However, with the exception of the initial portion (up to $\theta \approx 0.2$), the adsorption properties of channel blacks, graphitized at about 3000° (Graphon), are rather similar to the corresponding properties of graphitized thermal blacks. In the case of the adsorption of *n*-hexane (Fig. 3) and benzene (Fig. 5), the curves of the differential heats of adsorption, close to $\theta \approx 0.3$, converge and intersect, so that in this region the heats of adsorption of these substances on the various graphitized blacks are practically the same. This makes possible the solution of many problems involving comparisons of adsorption properties of different adsorbates with theoretical computations and the utilization in experimental work of graphitized channel blacks of greater surface, thus greatly simplifying measurements.

Acknowledgment.—The authors wish to thank Dr. W. R. Smith for his interest and for his assistance in preparing our manuscript for publication, and the Cabot Laboratories for the samples of Graphon black. We also thank Professor K. V. Chmutov for supporting this study.

liquid, the BET method yielded approximately an area three times greater than from adsorption of nitrogen at $\omega_{mN_2} = 16.2$ Å.^{2}. Despite the fact that in the case of helium the heat of adsorption on graphitized black exceeds the heat of condensation by more than an order of magnitude, it is hard to expect a very large compacting of the monolayer. In this case it is worth applying the method we suggested earlier (*Zhur. Fiz. Khim.*, **34**, 2817 (1960)) for evaluating the capacity of the monolayer from the mean portion of sharp decline in the curve of differential heat of adsorption in the transition from preferential filling of the first layer to preferential filling of the second. From Fig. 6 it will be seen that this decline for helium on graphitized black occurs at about $a_m = 10$–11 μmole/m.^{2}, which corresponds to $\omega_{mHe} = 16$ Å.^{2}, which is a value close to that determined from the density of the liquid. Thus, the sharp fall in the curve of differential heat of adsorption in the case of helium yields a correct indication of the magnitude of the capacity of the monolayer.

Of great interest in this case is to ascertain why the BET method does not apply. The reasons may be associated both with inaccuracy in determination of the shape of the adsorption isotherm and, possibly, with peculiarities in the state of the helium under these conditions, which may radically affect the adsorption equilibrium.

(29) R. M. Barrer, *Proc. Roy. Soc.* (London), **A161**, 476 (1937).

(30) A. D. Crowell, *J. Chem. Phys.*, **22**, 1397 (1954); **26**, 1407 (1957); A. D. Crowell and R. B. Steele, *ibid.*, **34**, 1347 (1961).

(31) A. V. Kiselev, *Vestnik Akad. Nauk S.S.S.R.*, **N 10**, 43 (1957); *Quart. Revs.* (London), **15**, 99 (1961).

(32) E. L. Pace, *J. Chem. Phys.*, **27**, 1341 (1957).

(33) A. V. Kiselev and D. P. Poshkus, *Doklady Akad. Nauk S.S.S.R.*, **132**, 876 (1960); **139**, 1145 (1961).

ADSORPTION ISOTHERMS OF NITROGEN, BENZENE AND *n*-HEXANE AND THE HEATS OF ADSORPTION OF BENZENE AND *n*-HEXANE ON GRAPHITIZED CARBON BLACKS. III. THE THERMODYNAMIC CHARACTERISTICS OF ADSORPTION EQUILIBRIA

BY A. A. ISIRIKYAN AND A. V. KISELEV

Adsorption Laboratory, Chemical Department, Moscow State University, Moscow, U.S.S.R.

Received May 22, 1961

From experimental quantities for graphitized thermal carbon blacks we have obtained and compared the isotherms of the absolute magnitudes of adsorption, and differential heats and entropies of adsorption of *n*-hexane and benzene on the "basal plane of graphite," and also the corresponding standard differential quantities of free and total energy, heat and entropy of adsorption and the extremal values of the differential heats and entropies of adsorption. All these properties are determined solely by the nature of the adsorbate–adsorbent system and practically are free from the influence of surface inhomogeneity of the solid. During filling of a monolayer, the heat of adsorption of *n*-hexane increases by 2, and benzene by 0.3 kcal./mole. The latter value is associated with the considerably weaker adsorbate–adsorbate attractions of benzene. Accordingly, the adsorption isotherm of benzene is at first concave, and of hexane, convex to the pressure axes. A description of the adsorption isotherms of benzene, hexane and nitrogen is discussed in terms of various equations. The BET equation is only a first approximation. Equations taking into account adsorbate–adsorbate attractions yield better agreement. A relationship is established between the constants of these equations and the constant of the BET equation. The adsorption of benzene and *n*-hexane at 20° and of nitrogen at −195° on the "basal plane of graphite" is predominantly localized.

Introduction

In our previous studies on the adsorption and heats of adsorption of benzene and *n*-hexane on graphitized carbon blacks,[1–5] as well as in a series of researches on the adsorption of the vapors of various low-boiling substances[6–10] including ethyl chloride,[11] alcohols,[12] acetone and ether,[13] it has been shown that adsorption on carbon blacks graphitized near 3000°, in particular on thermal blacks with small specific surface, one is dealing with adsorption on a fully homogeneous surface, *i.e.*, on the basal plane of graphite. Investigations of the adsorption isotherms of nitrogen on various samples of graphitized thermal carbon blacks carried on in a number of laboratories[4,7,9] have shown good agreement of the absolute values of adsorption (referred to unit surface).[4] Thus, these absolute quantities represent physico-chemical constants that characterize the system: adsorbate–basal plane of graphite. For some of these constants, such as the heats of adsorption at low surface coverage, it has been possible to find good agreement between theoretically derived and experimental values.[10,13–17]

There also is hope of complete theoretical computation of adsorption equilibria.[13,18,19] A reduction in the influence of surface inhomogeneity of thermal blacks on graphitization[5] permits treating the adsorption properties of such systems by semi-empirical methods on the basis of adsorption isotherm equations on a homogeneous surface, the form of which is derived theoretically, and the constants found from comparison with experiment.[7,13,20–22]

Reference 4 gives absolute adsorption isotherms of nitrogen at −195° and of benzene and *n*-hexane at 20°, as well as the differential heats of adsorption of benzene and *n*-hexane on graphitized thermal carbon black. The present paper compares the thermodynamic properties of the adsorption systems graphite–benzene and graphite–hexane and attempts to describe the isotherms for these systems by approximate semi-empirical methods. We also shall derive a relationship between the constants of equilibrium of the BET equation[23] and the isotherm equation, taking into account adsorbate–adsorbate interaction.

(1) N. N. Avgul, G. I. Berezin, A. V. Kiselev and I. A. Lygina, *Zhur. Fiz. Khim.*, **30**, 2106 (1956); *Izvest. Akad. Nauk S.S.S.R. Dept. Chem. Sci.*, 1304 (1956).

(2) N. N. Avgul, A. V. Kiselev, A. J. Korolev and I. A. Lygina, *Kolloid. Zhur.*, **20**, 298 (1958).

(3) A. A. Isirikyan and A. V. Kiselev, *ibid.*, **23**, 281 (1961).

(4) A. A. Isirikyan and A. V. Kiselev, *J. Phys. Chem.*, **65**, 601 (1961).

(5) A. A. Isirikyan and A. V. Kiselev, *ibid.*, **66**, 205 (1962).

(6) R. A. Beebe and D. M. Young, *ibid.*, **58**, 93 (1954); R. A. Beebe, C. H. Amberg and W. B. Spencer, *Can. J. Chem.*, **33**, 305 (1955).

(7) S. Ross and W. Winkler, *J. Colloid Sci.*, **10**, 319, 330 (1955); S. Ross and W. W. Pultz, *ibid.*, **13**, 397 (1958).

(8) R. A. Beebe and R. M. Dell, *J. Phys. Chem.*, **59**, 746, 754 (1955).

(9) R. A. Beebe and J. M. Holmes, *ibid.*, **61**, 1684 (1957).

(10) E. L. Pace and A. R. Siebert, *ibid.*, **63**, 1398 (1959); **64**, 961 (1960).

(11) J. Mooi, C. Pierce and R. N. Smith, *ibid.*, **57**, 657 (1953).

(12) N. N. Avgul, G. I. Berezin, A. V. Kiselev and I. A. Lygina, *Izvest. Akad. Nauk S.S.S.R., Dept. Chem. Sci.*, 205 (1961); N. N. Avgul, A. V. Kiselev and I. A. Lygina, *Kolloid. Zhur.*, **23**, 369 (1961); **23**, N5 (1961).

(13) A. V. Kiselev, *Zhur. Fiz. Khim.*, **35**, 233 (1961); N. N. Avgul, A. V. Kiselev and I. A. Lygina, *Izvest. Akad. Nauk S.S.S.R., Dept. Chem. Sci.* (in press).

(14) R. M. Barrer, *Proc. Roy. Soc.* (London), **A161**, 476 (1937).

(15) A. D. Crowell and D. M. Young, *Trans. Faraday Soc.*, **49**, 1080 (1953); A. D. Crowell, *J. Chem. Phys.*, **22**, 1397 (1954); **26**, 1407 (1957); A. D. Crowell and R. B. Steele, *ibid.*, **34**, 1347 (1961).

(16) N. N. Avgul, A. A. Isirikyan, A. V. Kiselev, I. A. Lygina and D. P. Poshkus, *Izvest. Akad. Nauk S.S.S.R., Dept. Chem. Sci.*, 1314 (1957); N. N. Avgul, A. V. Kiselev, I. A. Lygina and D. P. Poshkus, *ibid.*, 1196 (1959).

(17) N. N. Avgul, A. V. Kiselev and I. A. Lygina, *ibid.*, 1395, 1404 (1961).

(18) A. V. Kiselev and D. P. Poshkus, *Doklady Akad. Nauk S.S.S.R.*, **132**, 876 (1960); D. P. Poshkus and A. V. Kiselev, *Zhur. Fiz. Khim.* (in press); A. V. Kiselev, *Quart. Revs.* (London), **15**, 99 (1961).

(19) A. V. Kiselev and D. P. Poshkus, *Doklady Akad. Nauk S.S.S.R.*, **139**, 1145 (1961).

(20) A. V. Kiselev, *ibid.*, **117**, 1023 (1957); *Kolloid. Zhur.*, **20**, 338 (1958); A. V. Kiselev, N. V. Kovaleva, V. A. Sinizin and E. V. Khrapova, *ibid.*, **20**, 444 (1958).

(21) A. V. Kiselev and E. V. Khrapova, *ibid.*, **23**, 163 (1961).

(22) R. A. Beebe, J. M. Holmes, A. V. Kiselev and N. V. Kovaleva, *Zhur. Fiz. Khim.* (to be published).

(23) S. Brunauer, P. H. Emmett and E. Teller, *J. Am. Chem. Soc.*, **60**, 309 (1938).

A Comparison of the Thermodynamic Adsorption Properties of the Systems: Benzene–Graphite and *n*-Hexane–Graphite.—The results of studies of the adsorption properties of various graphitized carbon blacks permit comparison of the adsorption characteristics for *n*-hexane and benzene on a "limiting homogeneous" surface of graphitized black, *i.e.*, the basal plane of graphite. Figure 1 contains appropriate isotherms of the adsorption itself and also of the differential heats and entropies of adsorption as a function of θ. They are constructed from the data of Tables II–V of a previous publication.[4] To eliminate the effect of inhomogeneity on the isotherms at low coverage, we took advantage of equations (which will be considered below) of adsorption isotherms for a homogeneous surface, which give a good description of experimental isotherms for higher coverage, and extrapolated the computed isotherms to zero coverage. In Fig. 1 the solid lines denote adsorption isotherms constructed on the basis of the best experimental data from reference 4. These calculated isotherms coincide well with the experimental, with the exception of the initial portion indicated by the dashed line. In this range, the experimental values of adsorption, in accord with the enhanced values of the initial heats of adsorption, exceed the computed values for a homogeneous surface due to the residual surface inhomogeneity of carbon-black particles and contacts between them. The corresponding initial portions of enhanced experimental heats of adsorption[4] are disregarded in Fig. 1. In the field of small coverage, the computed (dashed) portions of the adsorption isotherms are closer to the true values of a homogeneous surface.

From Fig. 1 we see a sharp difference in the form of the isotherms, differential heats and entropies of adsorption for *n*-hexane and benzene. This is due both to the greater energy of adsorbate–adsorbent interaction in the case of *n*-hexane (at $\theta = 0.5$, the net heat of adsorption of *n*-hexane exceeds by a factor of 2.3 the net heat of adsorption of benzene) and, in particular, to the considerable (in the case of *n*-hexane) and slight (in the case of benzene) adsorbate–adsorbate interaction. With increasing θ, the heat of adsorption of *n*-hexane increases by about 2 kcal./mole, and that of benzene by only 0.3 cal./mole. Thus the adsorption isotherm of *n*-hexane at first is convex while benzene is concave to the pressure axis. Accordingly, the magnitudes of the entropies of adsorption indicate a far greater (when compared with liquid) localization of *n*-hexane molecules

The adsorption characteristics given in Fig. 1 are dependent only on the nature of the adsorbate–adsorbent system and are practically free from the effects of geometrical and chemical inhomogeneity of the adsorbent. For this reason, they quantitatively express the physico-chemical properties of the systems: basal plane of graphite–appropriate adsorbate. Of interest in this connection are the values of these physico-chemical characteristics at definite surface coverages. Table I gives the standard values (at $\theta = 0.5$) of the following characteristics of the systems "basal plane of graphite"—*n*-hexane and benzene—the differential

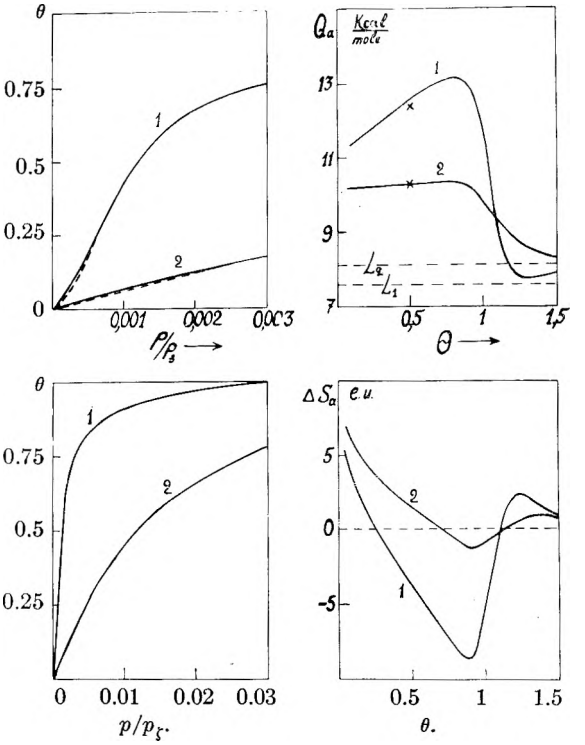

Fig. 1.—Adsorption isotherms (left), differential heats (top right) and differential entropies of adsorption (bottom right) for *n*-hexane (1) and benzene (2) on graphitized thermal carbon black, MT-1 (3100°). The dashed portions of the curves in the region of small θ are extrapolated on the basis of equation 2. L is the heat of condensation.

quantities of free energy of adsorption $\Delta\mu$, the total energy of adsorption, equal to the net heat of adsorption, $\Delta U_a^0 = (\partial\Delta U/\partial a)^0 = -(Q_a^0 - L)$, the heats of adsorption Q_a^0 and the entropies of adsorption $\Delta S_a^0 = (\partial\Delta S/\partial a)^0$, and also the extremal values of the differential magnitudes of heat $Q_{a(max)}$ and of the entropy of adsorption $\Delta S_{a(min)}$ near $\theta = 1$, and the mean molar values of the entropy of adsorption of a monolayer $\overline{\Delta S_m}$ of these vapors. The standard quantities are close to those obtained earlier for graphitized carbon blacks with a less homogeneous surface.[1,3,5] On the other hand, the extreme magnitudes of the differential heats of adsorption are greater, while the differential entropies of adsorption are lower. These extreme values are more sensitive to the degree of surface homogeneity.

As full a theoretical interpretation of these properties as possible is desirable. From Fig. 1 it is seen that the values of heats of adsorption at $\theta = 0.5$ (for *n*-hexane 12.6 and for benzene 10.3 kcal./mole) are close to the theoretically computed values[24] of the potential energy of adsorption as shown by the crosses in Fig. 1. On the basis of these computations of the potential energy, methods of statistical thermodynamics were invoked to carry out a complete theoretical calculation of the benzene isotherm. This calculation likewise led to satisfactory results.[19]

Application, to Experimental Adsorption Isotherms, of Equations Approximately Taking into Account Adsorbate–Adsorbate Interaction.—In ad-

(24) A. V. Kiselev, *Vestnik Akad. Nauk S.S.S.R.*, **N.10**, 43 (1957).

TABLE I

THERMODYNAMIC CHARACTERISTICS OF THE ADSORPTION SYSTEMS GRAPHITE–*n*-HEXANE AND GRAPHITE–BENZENE AT 20°

Adsorbate	$\Delta\mu$, kcal./mole	ΔU_a^0, kcal./mole	Q_{a}^0, kcal./mole	ΔS_a^0, e.u.	$Q_{a(max)}$, kcal./mole	$\Delta S_{a(min)}$, e.u.	$\overline{\Delta S_m}$, e.u.
n-Hexane	−3.90	−5.00	12.60	−3.8	13.2	−8.7	−3.1
Benzene	−2.59	−2.15	10.30	−1.5	10.4	−1.2	1.9

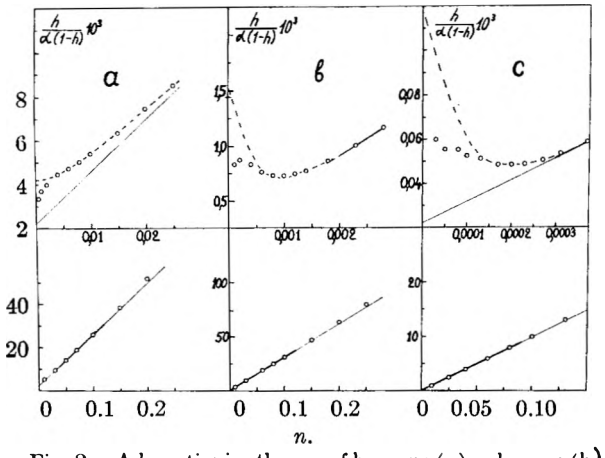

Fig. 2.—Adsorptioni sotherms of benzene (a), *n*-hexane (b) and nitrogen (c) on graphitized thermal carbon black, MT-1 (3100°) (points) in BET equation coördinates. The heavy lines are regions in which the BET equation is fulfilled; the fine lines represent extrapolation of these regions of fulfillment of the BET equation; the dashed lines are isotherms computed from equation 2 and constructed in BET coördinates.

dition to the theoretical computation, semi-empirical descriptions of adsorption equilibria are of interest in which only the general form of the equation of the isotherm is theoretically derived.[20-23] Let us consider some of these equations.

The isotherm equations which take into account adsorbate–adsorbate interactions include the degree of surface coverage $\theta = a/a_m = \alpha/\alpha_m$, where a is the measured (relative) adsorption (per unit weight) and $\alpha = a/s$ is the absolute adsorption quantity computed per unit area, while a_m and α_m are the corresponding quantities of a dense monolayer capacity. Since $\alpha_m = 1/\omega_m$, to find θ from a we must know the specific surface s and the area ω_m occupied by an adsorbate molecule in a dense monolayer.

Usually, to determine the area, s, use is made of the BET equation[23] derived for polymolecular localized adsorption on a homogeneous surface

$$h = \frac{\theta(1-h)^2}{C[1-\theta(1-h)]} = \frac{Z(1-h)}{C(1-Z)} \text{ or } \frac{h}{Z} = \frac{1}{C} + \frac{C-1}{C}h \quad (1)$$

in which $h = P/P_s$ is the relative vapor pressure and C is a constant of equilibrium for adsorbate–adsorbent interactions. To simplify notation Z denotes $\theta(1-h)$. Adsorbate–adsorbate interactions on the surface were disregarded in the derivation of this equation.

Approximate account of interactions in the first layer for localized adsorption on a homogeneous surface leads to the equation[20,25]

$$h = \frac{\theta(1-h)^2}{K_1[1-\theta(1-h)][1+K_n\theta(1-h)]} = \frac{Z(1-h)}{K_1(1-Z)(1+K_nZ)} \text{ or } \frac{Z(1-h)}{h(1-Z)} = K_1 + K_1K_nZ \quad (2)$$

in which K_1 is the constant of the equilibrium for adsorbate–adsorbent interaction, and K_n characterizes the relative role of adsorbate–adsorbate interactions. Equation 2 converts to (1) at $K_n = 0$. The appropriate equation for localized monomolecular adsorption[20]

$$h = \frac{\theta}{K_1(1-\theta)(1+K_n\theta)} \text{ or } \frac{\theta}{h(1-\theta)} = K_1 + K_1K_n\theta \quad (3)$$

at $K_n = 0$ converts to the Langmuir equation. Hence, strictly speaking, application of the BET method for determination of a_m and S is possible only for very strong adsorption (large K_1, small K_n) on a homogeneous surface. In a previous publication,[4] we showed that these conditions, in the case of graphitized thermal carbon black, are most closely satisfied by adsorption of benzene. In addition, a very probable value for the cross-section area of a benzene molecule is 40 Å.^{2}. This value is determined both from the density of the liquid with account taken of the van der Waals thickness of the molecule, and from the van der Waals atomic radii with account taken of flat orientation of benzene at the surface.[4,26]

In Fig. 2a (bottom) the adsorption isotherm of benzene vapor on graphitized thermal carbon black (from the data of Table 3 in ref. 4) is shown in coördinates of the linear form of the BET equation. This equation describes this isotherm only in the interval from $\theta \approx 0.8$, $h \approx 0.04$ to $\theta \approx 1.1$, $h \approx 0.12$; and, as may be seen from the upper part of Fig. 2a, in the region of small h the experimental points deviate from the straight line, as h diminishes, first *upward* and then *downward*. The constant of equilibrium $C_{BET} = 108$ is obtained from the position of the straight line on this graph. In the same way, Fig. 2b gives the adsorption isotherm of *n*-hexane (from data of Table V of ref. 4). The BET equation describes this isotherm, which has a convex initial portion, from $\theta \approx 0.7$, $h \approx 0.002$ to $\theta \approx 1.1$, $h \approx 0.12$; as θ decreases from 0.7 to 0.1, the experimental points deviate sharply upward and then downward. Finally, Fig. 2c gives the same construction for the adsorption isotherm of nitrogen (from data of Table II, reference 4). The BET equation describes this isotherm, which has a convex initial portion, from $\theta \approx 0.4$, $h \approx 0.0003$ to $\theta \approx 1.1$, $h \approx 0.09$; as θ diminishes from 0.4, the experimental isotherm deviates upward even more sharply than in the other cases.

Deviation of experimental points from the BET straight line in the region of $\theta > 1.1$ is associated

(25) A. V. Kiselev and D. P. Poshkus, *Izvest. Akad. Nauk S.S.S.R., Dept. Chem. Soc.*, 590 (1958).

(26) A. A. Isirikyan and A. V. Kiselev, *Kolloid. Zhur.*, **23**, 281 (1961).

with the approximate nature of assumptions in the BET theory[23] associated with the equality of the constants of equilibrium during formation of multiple polymolecular complexes. Deviations downward of experimental points in the field of small θ are due to the influence of residual inhomogeneity, which increases the initial heats of adsorption. This leads to enhanced values of adsorption at small h (as compared with adsorption on a smooth surface of a basal plane of graphite for the same values of h). The reason for upward deviations of experimental isotherms from the straight BET line for diminishing θ from 0.7–0.1 and below is adsorbate–adsorbate interactions in the first layer which are not taken into account in the BET theory. These deviations increase as we pass from an isotherm initially concave to the pressure axes, *i.e.*, benzene, to isotherms initially convex, as with *n*-hexane and nitrogen, and are due to an increase in adsorbate–adsorbate attraction.

For this reason, in the case of adsorption on graphitized carbon blacks of less homogeneous surface, such as graphitized channel blacks (Graphon), an increase in θ (and z) in a broader range of small h leads to a better coincidence of experimental points on the straight BET line. The isotherm for nitrogen on Graphon blacks of more heterogeneous surface is at first concave[21,5] and for this reason is better described by the BET equation (from $h \approx 0$ to $h \approx 0.15$). This equation gives an even better description of the adsorption isotherm of nitrogen on the even more heterogeneous surface of non-graphitized blacks and active carbons.[21,27] However, in these cases, the mechanism of formation of the adsorption layer still is different from the assumptions of the BET theory, because at the most active sites (in cracks, fine pores, and at points of particle contact) a denser layer is formed, whereas at less active sites this layer is more tenuous. Therefore, to quantities a_m obtained by the BET method for *inhomogeneous* surfaces we cannot, strictly speaking, attribute values of monolayer capacities, and the approach should be cautious to the quantities s, α and θ determined in this manner. The significance of this conclusion[21,28] increases with increasing heterogeneity of the adsorbent surface. It follows from the foregoing that the various equations for adsorption isotherms derived for homogeneous surfaces that still are meaningful in the case of carbon blacks are applicable only for *graphitized thermal blacks with low specific surface.*

We already have pointed out that the deviation, which is evident from the graphs in the upper part of Fig. 2, of experimental isotherms from the BET plot is associated with manifestation of adsorbate–adsorbate attraction and is in accord with increase in differential heat of adsorption with increasing θ (see Fig. 1). For this reason, the BET equation should be regarded only as a first approximation. The next approximation is given by taking account of adsorbate–adsorbate interactions

(27) A. V. Kiselev and E. V. Khrapova, *Izvest. Akad. Nauk S.S.S.R., Dept. Chem. Sci.*, 389 (1958).

(28) A. A. Isirikyan, A. V. Kiselev and V. V. Kulichenko, "Proc. of the Second Intern. Congr. on Surface Activity," Vol. 2, London, 1957, p. 199.

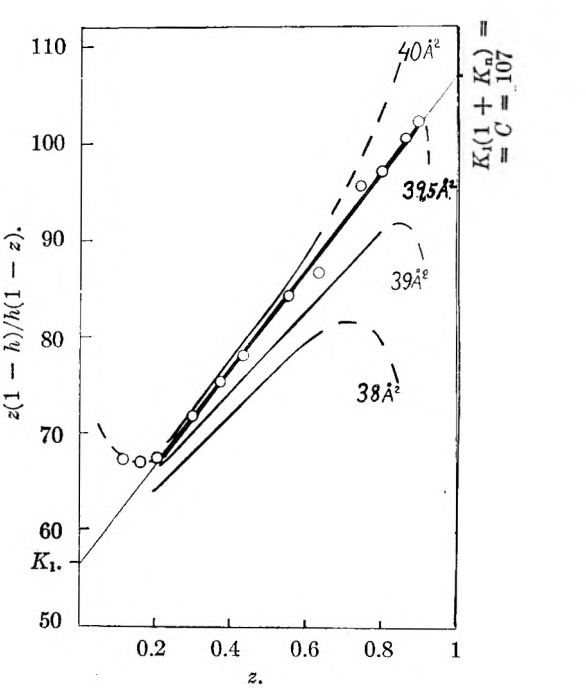

Fig. 3.—Adsorption isotherm of benzene on graphitized thermal carbon black, MT-1 (3100°) in the coördinates of equation 2 for various cross-section areas of benzene.

in the first layer, *i.e.*, equation 2 for localized adsorption. In turn, this equation is approximate, for it does not take into account the differences in the mutual coördination of adsorbate molecules.[20] However, in the region of not too large θ, this assumption is sufficiently justified.

Figure 3 gives the results of construction of an experimental isotherm of benzene in coördinates of linear form of equation 2. This construction requires the choice of a value of $\omega_{mC_6H_6}$ and a determination of the degree of coverage $\theta = \alpha/\alpha_m$ from the values of adsorption α.[29] In Fig. 3, this construction is done for several values of $\omega_{mC_6H_6}$. Equation 2 embraces the largest interval of experimental isotherm (from $\theta \approx 0.2$ to $\theta \approx 1.1$) at $\omega_{mC_6H_6} = 39.5$ Å.², *i.e.*, for the probable value of this quantity.

Deviations of the experimental isotherm from linearity for large z (large h) are connected with inaccuracies of assumptions, the adsorbate–adsorbate interactions being independent of the multiplicity of complexes both perpendicular to the surface (the BET assumption) and along it (assumption of the present theory).[20] For this reason, the linear region of the isotherm is of special interest. The values of the constants of equation 2, $K_1 = 57$ and $K_n = 0.88$ ($K_n/K_1 = 0.0155$) are obtained from Fig. 3 at $\omega_{mC_6H_6} = 39.5$ Å.². In this case, $K_n < 1$, which is due to the concave beginning of the isotherm as a result of relatively weak adsorbate–adsorbate attraction[20] (Fig. 1). Upward deviations of the experimental isotherm

(29) The quantities $\alpha = a/s$ are computed in terms of the values of s determined by the BET method from the isotherm of benzene vapor at 20° and $\omega_{mC_6H_6} = 40$ Å.², which are close to the values of s determined by this method from the portion of the nitrogen isotherm at −195° in the interval h, 0.0003 to 0.09 for $\omega_{mN_2} = 16.2$ Å.². We consider more justified the determination of the magnitude s required for computation of θ by the BET method from the adsorption isotherm of benzene vapor at $\omega_{mC_6H_6} = 40$ Å.².

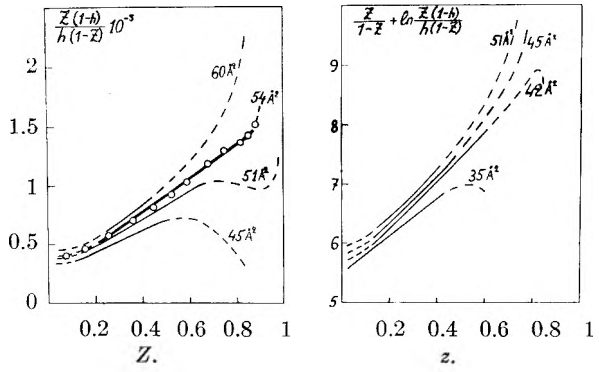

Fig. 4.—The adsorption isotherm of n-hexane on graphitized thermal carbon black, MT-1 (3100°) in coördinates of equation 2 (left) and equation (6¹) (right) for various cross-section areas of n-hexane.

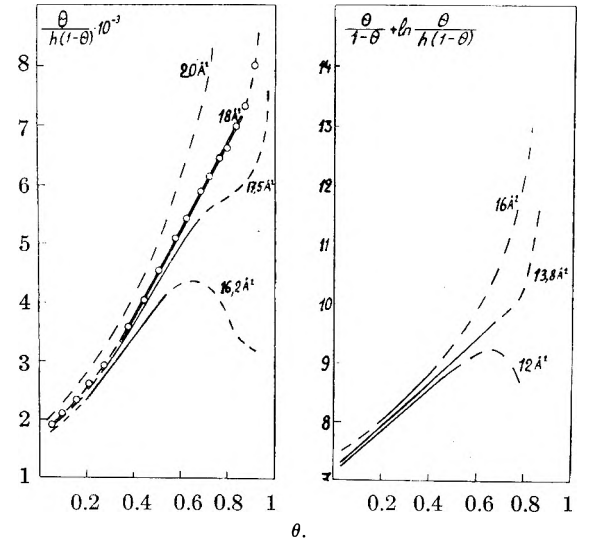

Fig. 5.—The adsorption isotherm of nitrogen on graphitized thermal carbon black, MT-1 (3100°) in coördinates of equation 3 (left) and equation 5 (right) for various cross-sectional areas of nitrogen.

in Fig. 3 for small h (small z) are due to the influence of residual surface inhomogeneity that increases the quantities

$$\left[\frac{z(1-h)}{h(1-z)}\right]_{h\to 0,\ z\to 0} \longrightarrow \frac{\theta}{h}$$

It is interesting to compare equation 2 with the BET equation (1). In the upper part of Fig. 2a, the initial portion of the adsorption isotherm of benzene vapor computed from equation 2 at $K_1 = 57$ and $K_n = 0.88$ (dashed curve) is constructed in linear coördinates of the BET equation. The fine solid line shows the continuation of linearity of the isotherms in these coördinates in the region of lower h (see the lower part of Fig. 2a). From the upper part of Fig. 2a it is seen that even a weak adsorbate–adsorbate attraction in the case of benzene adsorption on a homogeneous surface causes a noticeable upward deviation of the isotherm (2) from the extrapolated BET straight line, *i.e.*, at small h, in the direction of lower θ, which is in good agreement with the experimental isotherm. Isotherm (2) in BET coördinates at $h = 0$ leads to a limiting value

$$\left(\frac{h}{z}\right)_{h\to 0} = \frac{h}{\theta} = 0.0175, \text{ whence } \left(\frac{\theta}{h}\right)_{h\to 0} = k_1 = 57$$

the adsorbate–adsorbent constant of equilibrium in accord with the linear graph of equation 2 in Fig. 3 (at $\omega_{mC_6H_6} = 39.5$ Å.²). From this, as we have seen, it also follows that

$$\left[\frac{z(1-h)}{h(1-z)}\right]_{h\to 0,\ z\to 0} \longrightarrow \left(\frac{z}{h}\right)_{h\to 0,\ z\to 0} \longrightarrow \left(\frac{\theta}{h}\right)_{h\to 0} = K_1 = 57$$

Since in the region of small θ equation 2 gives a better description of the experimental isotherm than the BET equation, so $K_1 = 57$, as compared with $C_{BET} = 108$, is a better approximation to the true adsorbate–adsorbent equilibrium constant (the "Henry constant") in the system benzene–basal plane of graphite.

The relationship between the constant C_{BET} and the constants of equation 2, K_1 and K_n, may be established by taking advantage of the fact that at large θ and h the differences in the adsorption mechanism in the first layer are no longer of importance. Since in the derivation of our equation 2 the same mechanism of *polymolecular* adsorption was taken as in the BET theory, both the BET equation (1) and our equation (2) approach each other in the region of large θ and h. Indeed, from (2) it follows that

$$\frac{h}{z} = \frac{1 + (K_1 - 1)h - K_1K_n(1-z)}{K_1} \qquad (2)$$

approaches a linear dependence on h, since at $h \to 1$, $z \to 1$ and $h/z \to 1$ just as in the case of the BET equation 1. For this reason, we can equate expressions for h from (1) and (2) at the upper limit $h = 1$ and $z = 1$, whence it follows that

$$C_{BET} = K_1(1 + K_n) \qquad (4)$$

In the case of adsorption of benzene on graphite $K_1 = 57$, $K_n = 0.88$, whence from (4) $C_{BET} = 107$ in accordance with the limiting value of the quantity

$$\frac{z(1-h)}{h(1-z)} = K_1 + K_1K_n$$

at $z = 1$ and $h = 1$ in Fig. 3.

In ref. 22 an attempt was made to describe the adsorption isotherms CO_2 and NH_3 at −79° on such carbon blacks with the aid of approximate equations of mono- and polymolecular localized adsorption (3) and (2), and the appropriate Hill equations[30] for non-localized adsorption

$$h = \frac{\theta}{K_1(1-\theta)} \exp\left[\frac{\theta}{1-\theta} - K_2\theta\right] \text{ or}$$

$$\frac{\theta}{1-\theta} + \ln\frac{\theta}{h(1-\theta)} = \ln K_1 + K_2\theta \qquad (5)$$

and

$$h = \frac{\theta(1-h)^2}{K_1[1-\theta(1-h)]} \exp\left[\frac{\theta(1-h)}{1-\theta(1-h)} - K_2\theta(1-h)\right] \qquad (6)$$

or

$$\frac{z}{1-z} + \ln\frac{z(1-h)}{h(1-z)} = \ln K_1 + K_2 z \qquad (6^1)$$

(30) T. L. Hill, *J. Chem. Phys.*, **14**, 441 (1946).

where the constant $K_2 = 2a_2/b_2RT$ characterizes adsorbate–adsorbate interactions and a_2 and b_2 are constants of a two-dimensional equation of state of the van der Waals' type. It was found that the isotherm of CO_2 is better described by equation 3 for localized adsorption, and the isotherm of NH_3 by equation 6 for non-localized adsorption.[13,22] In the case of adsorption of benzene, the fulfillment of equation 6 for non-localized adsorption is worse.

Figure 4 shows the application of approximate equations of the isotherms of localized and non-localized adsorption for describing adsorption on the graphitized thermal black MT-1 (3100°) of *n*-hexane at 20°. The adsorption isotherm of *n*-hexane at 20° is described better by equation 2 for polymolecular localized adsorption than by the appropriate equation of Hill (6) for non-localized adsorption. The range over which equation 2 is fulfilled increases with a slight increase in $\omega_{mC_6H_{14}}$. Thus, at $\omega_{mC_6H_{14}} = 51$ Å.²,[4] equation 2 is fulfilled in the interval θ from 0.2 to 0.7, and at $\omega_{mC_6H_{14}} = 54$ Å.² it is fulfilled in the interval θ from 0.2 to 0.8. At $\omega_{mC_6H_{14}} = 54$ Å.², the constants of equation 2 are: $K_1 = 210$ and $K_n = 6.7$. Here, the adsorbate–adsorbent interaction constant K_1 is exceedingly large and the adsorbate–adsorbate interaction constant K_n relatively small ($K_n/K_1 = 0.032$), yet it still is greater than unity, which determines[25] the convex beginning of the adsorption isotherm of *n*-hexane on graphite.

In ref. 4 and 21 it was pointed out that the first wave of the isotherm of nitrogen at −195° on graphitized thermal black is in good agreement with experiment, as expressed by equation 3 for monomolecular localized adsorption. This equation takes into approximate account the adsorbate–adsorbate interactions. In Fig. 5 the first wave of the adsorption isotherm of nitrogen on the basal plane of graphite is given in linear coördinates of equation 3 for various values of the area occupied by the nitrogen molecule in the dense monolayer. From Fig. 5 it is seen that this equation embraces the broadest isotherm region (up to $h = 0.0025$, $\alpha = 9.3$ μmole/m.² at $\omega_{mN_2} = 18$ Å.², $K_1 = 900$, $K_n = 8$ ($K_n/K_1 = 0.0089$). In the case of $\omega_{mN_2} = 16.2$ Å.², the results are somewhat worse. It is possible that the larger N_2 cross-section conforms better to the form and localization on the basal plane of graphite of the di-atomic nitrogen molecule. (See also ref. 31 and 32). In addition, one must keep in mind the approximate nature of equation 3, which should reflect in the region of large θ, where account is required of the nature of the mutual coördination of adsorbate molecules. From Fig. 5 it also is seen that fulfillment of the Hill equation (5) for monolayer non-localized adsorption[30] is worse. A linear isotherm in the interval up to $\theta \approx 0.8$ is obtained only at $\omega_{mN_2} = 13.8$ Å.², *i.e.*, apparently at too small a value of ω_{mN_2}.

(31) W. C. Walker and A. C. Zettlemoyer, *J. Phys. Chem.*, **57**, 182 (1953).

(32) A. A. Isirikyan and A. V. Kiselev, *Zhur. Fiz. Khim.*, **34**, 2817 (1960).

Thus, the adsorption of *n*-hexane and benzene at 20° and nitrogen at −195° on the "basal plane of graphite" is predominantly localized.[33] We already have pointed out the approximate nature of equations 2 and 3 in the region of large θ. In the future, they must be refined by taking into account the character of mutual coördination of adsorbate molecules on the surface. However, subsequent development apparently will proceed by treating the problem of adsorption equilibrium, taking account of adsorbate–adsorbate interaction by the more general methods of statistical thermodynamics.

For the given values of the constants, equations 2 and 3 are at any rate good interpolation formulas for constructing appropriate adsorption isotherms. The isotherms of *n*-hexane and benzene, which have been computed from equation 2 for the above-mentioned values of the constants ω_m, K_1 and K_n over a broad region of θ, coincide with the experimental values, and only at small θ are they lower (see Fig. 1). Since the residual surface inhomogeneity exerts practically no effect on the quantities computed from (2), the quantities thus computed in the region of small θ are closer to the true values of adsorption on the basal plane of graphite. We therefore list these values in Table II up to the values of θ at which there is no longer a perceptible difference between the values of adsorption computed from (2) and given in Tables II, III and V in ref. 4.

TABLE II

DATA FOR CONSTRUCTION OF ADSORPTION ISOTHERMS OF THE VAPORS OF NITROGEN AT −195°, AND BENZENE AND *n*-HEXANE AT 20° ON THE "BASAL PLANE OF GRAPHITE" FOR SMALL θ

For higher θ, see these data in Tables II, III and V ref. 4

Nitrogen at −195° $\omega_{mN_2} = 18$ Å.², $K_1 = 900$, $K_n = 8$		Benzene at 20° $\omega_{mC_6H_6} = 39.5$ Å.², $K_1 = 57$, $K_n = 0.88$		*n*-Hexane at 20° $\omega_{mC_6H_{14}} = 54$ Å.², $K_1 = 210$, $K_n = 6.7$	
P/P_0	α, μmole/m.²	P/P_0	α, μmole/m.²	P/P_0	α, μmole/m.²
0.0000444	0.50	0.00035	0.084	0.000183	0.15
.0000723	1.00	.00071	.17	.000319	.31
.0000937	1.50	.00178	.42	.000417	.46
.0001124	2.00	.00272	.63	.000512	.62

Acknowledgment.—The authors wish to thank Dr. W. R. Smith and Professor R. A. Beebe for their interest in these studies and Dr. W. R. Smith for his assistance in preparing our manuscript for publication.

CORRECTION.—In paper I of this series (*J. Phys. Chem.*, **65**, 601 (1961)) the first entry in column 4 of Table VI should be 13.18 instead of 13.8.

(33) Localization of a molecule of *n*-hexane on the basal plane of graphite is enhanced by the possibility of the CH_3 and CH_2 groups getting into the energetically most advantageous positions over the centers of carbon hexagons in the basal plane of graphite.[15] There is no such possibility for the flat benzene molecule. In this case, energy barriers along the surface (which contribute to localization) probably arise from the very large energy of adsorption of the entire molecule. The slight retardations of each CH group combine and apparently cause a sufficient retardation of the entire benzene molecule.

THE DISTRIBUTION OF SULFURIC ACID BETWEEN WATER AND KEROSENE SOLUTIONS OF TRI-*n*-OCTYLAMINE AND TRI-*n*-HEXYLAMINE[1]

BY J. M. P. J. VERSTEGEN[2] AND J. A. A. KETELAAR[3]

Laboratory for General and Inorganic Chemistry of the University of Amsterdam, Amsterdam, Holland

Received May 31, 1961

In this paper a description is given of the distribution of sulfuric acid between water and a kerosene solution with tri-*n*-octylamine or tri-*n*-hexylamine. Assuming ideality in the organic phase no evidence could be obtained that the law of mass action underlies the fundamental processes. Assuming aggregation of the amine salt to a micelle of constant activity a qualitative agreement is found and the empirical formula $K_A = a_{H_2SO_4}[\text{amine}]^n$ seems to be of general interest, the power n changing at inflection points in the titration curves of the weak base anion-exchanger. In the range of acidities where no free amine exists a treatment based on mixed crystal equilibrium betweeen amine sulfate and amine bisulfate leads to results which are much the same for both amines. An empirical formula $K_B = (1/a_{H_2SO_4})(X^2/(1 - X))^n$ with X as the mole fraction of the amine bisulfate describes the system.

Introduction

In a previous article[4] it was shown that the distribution of sulfuric acid between water and benzene solutions of tri-*n*-octylamine (TOA) or tri-*n*-hexylamine (THA) could be based on the formation of the sulfates $(TOAH)_2SO_4$ or $(THAH)_2SO_4$.

If it was assumed that the concentrations in the organic phases were equal to the activities the law of mass action gave a satisfactory description of the results, until a certain amine sulfate concentration was reached and deviations occurred. The results were in reasonable agreement with those given by Allen[5] who explained the deviations as being due to aggregation of the amine salt to micelles.[5,6]

In the present study it is shown that the processes underlying the distribution show remarkable differences when the benzene is replaced by kerosene.

Experimental

The commercial products TOA and THA are distilled at 1–2 mm. The boiling points are 182–186° and 118–121°, respectively. During the distillation of TOA the forerun solidifies in the collector. This is probably di-*n*-octylamine. The molecular weight of the main fraction of TOA (boiling range < 2°) is determined by means of potentiometric titration with standard perchloric acid in a benzene–water–alcohol medium. It is found to be 351.6. Assuming that the impurity is di-*n*-octylamine, this value is in agreement with a percentage of 98.6% TOA. The molecular weight of the main fraction of THA is determined as being 278.5. No attempts were made to investigate if the iso-derivatives were present. In all distribution measurements once-distilled amines were used.

Samples of both THA and TOA were exposed to the laboratory atmosphere for three days. No change in weight could be observed and potentiometric titration with standard perchloric acid in a benzene–alcohol–water medium before and after exposure did not show any significant difference.

Ten ml. of a 0.098 *M* amine solution in kerosene,[7] modified with 4 vol. % *n*-octyl alcohol to prevent third phase formation, were brought into contact with the same volume of aqueous phases containing known amounts of sulfuric acid (C_i).

We did not find the anomalous behavior which was reported by Allen and McDowell[8] for the case of uranium extraction. To the aqueous phases, which were brought into contact with the kerosene solution of THA, 0.33 *M* Na_2SO_4 was added to prevent dissolution of the formed $(THAH)_2SO_4$ in the aqueous phase.

Equilibrium was achieved by means of centrifugal stirring for 1 minute. Thirty minutes after equilibration the layers were separated and the acid content of the water layer (C_f) was determined by means of potentiometric titration using either 0.1 *M* or 0.02 *M* NaOH. To verify the material balance in some cases the organic loading C_o was determined by stripping the acid from the kerosene phases with sodium hydroxide and titrating back the excess alkali.

It was found that

$$C_o = C_i - C_f$$

within 1%. From this it might be concluded that the change in volumena is small (unless the changes in the volumena during both extractions compensated each other). Indeed no change in volumena could be detected by measurement after equilibration. From the neutralization curves of the aqueous phases no evidence could be obtained that amine sulfate dissolves in the aqueous phases, if, in the THA case, the salting out agent Na_2SO_4 was added. All experiments were performed at 20 ± 2°.

Results

If it is assumed that the reaction between amine and sulfuric acid taking place at the interface is analogous to the reaction between H_2SO_4 and NH_3, we may write

$$2TOA + H_2SO_4 \rightleftarrows (TOAH)_2SO_4 \qquad (1)$$

and

$$2THA + H_2SO_4 \rightleftarrows (THAH)_2SO_4 \qquad (1a)$$

At higher acidities the equilibria could be represented as

$$(TOAH)_2SO_4 + H_2SO_4 \rightleftarrows 2(TOAH)HSO_4 \qquad (2)$$

$$(THAH)_2SO_4 + H_2SO_4 \rightleftarrows 2(THAH)HSO_4 \qquad (2a)$$

If it is assumed that the concentrations in the organic phases are equal to the activities we could write for the equilibrium constants of eq. 1, 1a

$$K_o = \frac{[(TOAH)_2SO_4]}{[TOA]^2\, a_{H_2SO}} \qquad (3)$$

and

(1) The work, described in this article, forms part of the program of RCN (Reactor Centrum Nederland), The Hague. The experimental results have been obtained in the Laboratory for General and Inorganic Chemistry of the University of Amsterdam.

(2) Institutt for Atomenergi, Postboks 175, Lillestrom, Norway.

(3) Laboratory for Electrochemistry, University of Amsterdam.

(4) J. M. P. J. Verstegen and J. A. A. Ketelaar, *Trans. Faraday Soc.*, **57**, 1527 (1961).

(5) K. A. Allen, *J. Phys. Chem.*, **60**, 239 (1956).

(6) K. A. Allen, *ibid.*, **60**, 943 (1956).

(7) The kerosene used in our experiments was furnished by the Amsterdamsche Chininefabriek. Some physical and chemical properties are: s.w. (at 24°) = 0.778, refractory index $n^{25}D$ 1.431, boiling range 195–240°, aromates <0.5%.

(8) K. A. Allen and W. J. McDowell, *J. Phys. Chem.*, **64**, 877 (1960).

$$K_c^a = \frac{[(THAH)_2SO_4]}{[THA]^2 a_{H_2SO_4}} \qquad (3a)$$

with brackets denoting activities and $a_{H_2SO_4} = 4\gamma_\pm^3 C_f^3$.

The sulfuric acid activity which has to be substituted in equation 3 is the activity of the acid in a pure aqueous solution. Values of the mean ionic molal activity coefficient $\gamma_\pm$ can be found in Harned and Owen.[9] Molarities C_f are obtained from our experiments and as molarities and molalities do not differ very much in our range of concentrations they are combined with $\gamma_\pm$. Consequently all activities $a_{H_2SO_4}$ are expressed in (mole/l.)^3. When logarithms are plotted $\sqrt[3]{a_{H_2SO_4}}$ is used.

$$\sqrt[3]{a_{H_2SO_4}} = 1.59\ \gamma_\pm\ C_f \text{ mole/l.}$$

The sulfuric acid activity in equation 3a is the activity in the presence of 0.33 M sodium sulfate. Harned and several others[10–13] calculated from e.m.f. measurements the activity coefficients of sulfuric acid in the presence of several alkali sulfates M_2SO_4.

The reactions (1, 1a) predominate at low acidities ($C_f < 0.03$ M). Thus the formation of $(THAH)_2SO_4$ according to eq. 1a occurs at about constant ionic strength. The mean ionic molal activity coefficient is taken as $\gamma_\pm = 0.22$. Reaction 2a predominates in a range of acidities where the activity coefficient changes from $\gamma_\pm = 0.21$ to $\gamma_\pm = 0.12$.

ΣTOA is introduced as the total tri-*n*-octylamine content, either in the sulfate, the bisulfate or the free amine form. In our case ΣTOA = 0.098 mole/l. When we plot $\sqrt[3]{a_{H_2SO_4}}$ *vs.* $C_0/\Sigma TOA$ and *vs.* $C_0/\Sigma THA$, respectively, the Figs. 1 and 1a are found.

Allen[5] showed that the curve he obtained when using a 0.1 M solution of TOA in benzene showed resemblance to the titration curve of a weak base anion-exchange resin. In our case, the behavior of TOA is somewhat more complicated (Fig. 1), showing a second neutralization step, which starts at an activity $\sqrt[3]{a_{H_2SO_4}} \backsimeq 1.4 \times 10^{-1}$ mole/l. The first neutralization step starts at an activity $\sqrt[3]{a_{H_2SO_4}} \backsimeq 3.0 \times 10^{-3}$ mole/l. The THA curve (Fig. 1a) shows one neutralization step starting at $\sqrt[3]{a_{H_2SO_4}} \approx 9 \times 10^{-4}$ mole/l.

From our results no evidence could be obtained that K_c and K_c^a given in equations (2,2a) are constants. Thus, the law of mass action is not followed and the processes occurring must be explained on another basis. If it is assumed that the amine sulfates withdraw from the system under formation of a micelle with constant activity we may rearrange (2,2a) as

$$K_1 = [TOA]^2\, a_{H_2SO_4} \qquad (4)$$

and

$$K_1^a = [THA]^2\, a_{H_2SO_4} \qquad (4a)$$

However, when log $a^{1/3}_{H_2SO_4}$ is plotted *vs.* log [TOA] and log [THA], respectively, Figs. 2 and 2a are found. There is a qualitative agreement between both these figures but the straight lines obtained never correspond to a slope

$$\frac{d \log [amine]}{d \log a^{1/3}_{H_2SO_4}} = -3/2 \qquad (5,5a)$$

which might be expected if equations 4 and 4a were followed. In the range of low acidities the slope obtained in Fig. 2 is found as

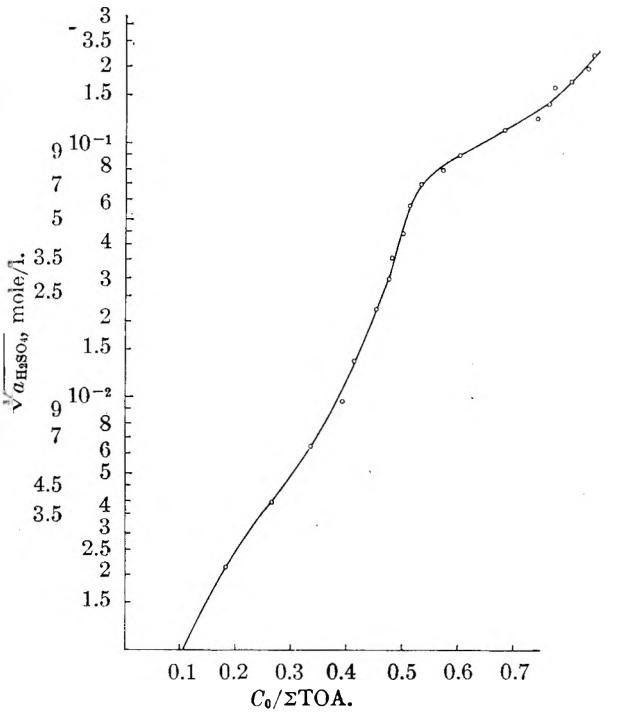

Fig. 1.—Anion-exchange titration curve for TOA.

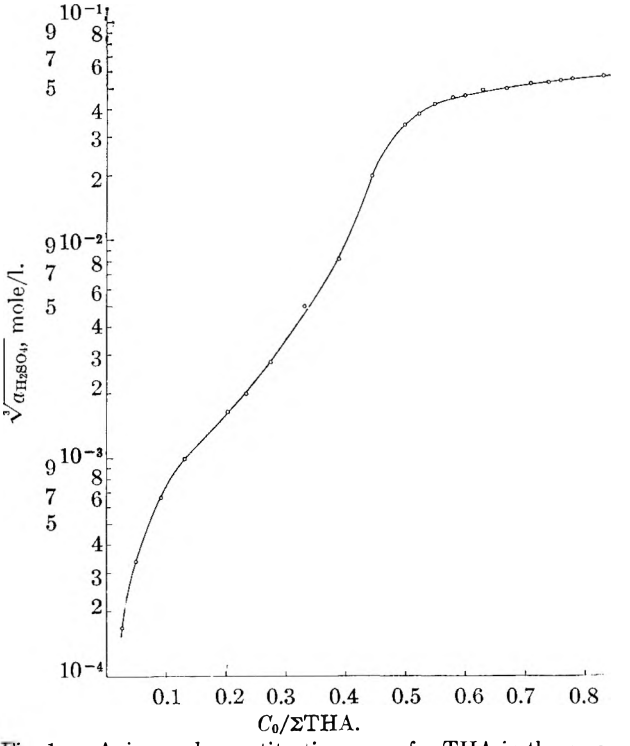

Fig. 1a.—Anion-exchange titration curve for THA in the presence of a salting-out agent (Na_2SO_4).

(9) H. S. Harned and B. B. Owen, "The Physical Chemistry of Electrolytic Solutions," New York, N. Y., 1943.
(10) H. S. Harned and G. Åkerlöf, *Physik. Z.*, **27**, 411 (1926).
(11) H. S. Harned and R. D. Sturgis, *J. Am. Chem. Soc.*, **47**, 945 (1925).
(12) G. Åkerlöf, *ibid.*, **48**, 1160 (1926).
(13) M. Randall and C. T. Langford, *ibid.*, **49**, 1447 (1927).

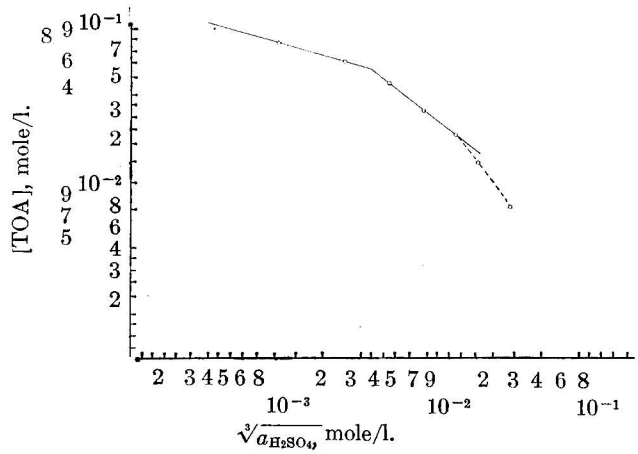

Fig. 2.—Free amine concentration [TOA] *vs.* $\sqrt[3]{a_{H_2SO_4}}$.

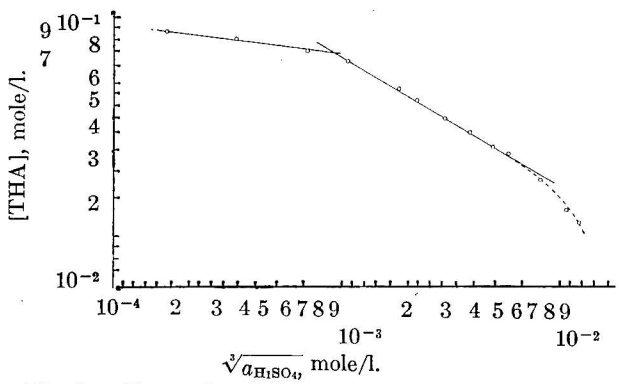

Fig. 2a.—Free amine concentration [THA] *vs.* $\sqrt[3]{a_{H_2SO_4}}$.

$$\frac{\mathrm{d}\log[\mathrm{TOA}]}{\mathrm{d}\log a^{1/3}_{H_2SO_4}} = -1/3 \qquad (6)$$

corresponding to an empirical constant

$$K_2 = a_{H_2SO_4}[\mathrm{TOA}]^9 \qquad (7)$$

with the numerical value

$$K_2 = 75 \times 10^{-21}\ (\mathrm{mole/l.})^{12}$$

In the range of high acidities the slope is found to be equal to $-3/4$, according to an empirical constant

$$K_3 = a_{H_2SO_4}[\mathrm{TOA}]^4 = 24 \times 10^{-14}\ (\mathrm{mole/l.})^7 \qquad (8)$$

In Fig. 2a the slope at low acidities is difficult to estimate and only can be given as

$$|1/12| < \frac{\mathrm{d}\log[\mathrm{THA}]}{\mathrm{d}\log a^{1/3}_{H_2SO_4}} < |1/8| \qquad (6a)$$

or

$$K_2{}^a = a_{H_2SO_4}[\mathrm{THA}]^n \qquad (7a)$$

with $24 < n < 36$.

At high acidities it is found that the slope is equal to $-1/2$, or

$$K_3{}^a = a_{H_2SO_4}[\mathrm{THA}]^6 \qquad (8a)$$

with

$$K_3{}^a = 15 \times 10^{-9}\ (\mathrm{mole/l.})^9$$

The changes in n in the formula $K_A = a_{H_2SO_4}\cdot[\mathrm{amine}]^n$ take place at the activity at which the neutralization step in the titration curves (Fig. 1,1a) starts. The readers attention might be drawn to the fact that the empirical formulas given in 7, 7a, 8 and 8a show a qualitative agreement with the results obtained from the distribution of H_2SO_4 between water and a 0.100 M solution of TOA in benzene at 65°.[4]

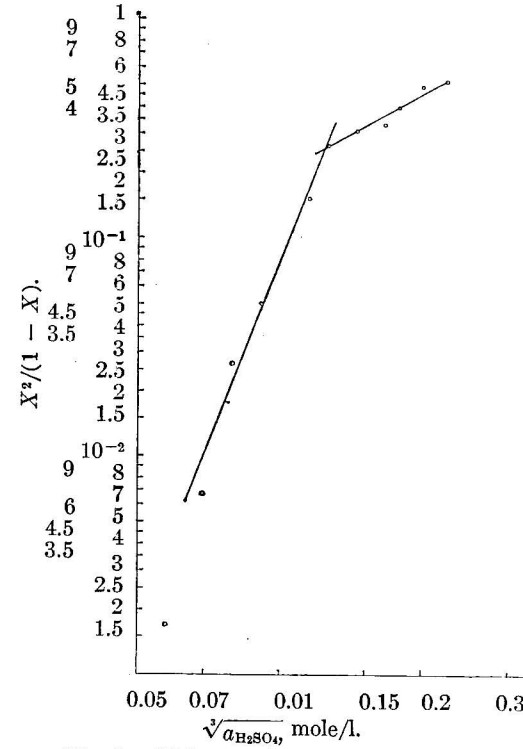

Fig. 3.—$X^2/(1-X)$ *vs.* $\sqrt[3]{a_{H_2SO_4}}$ for TOA.

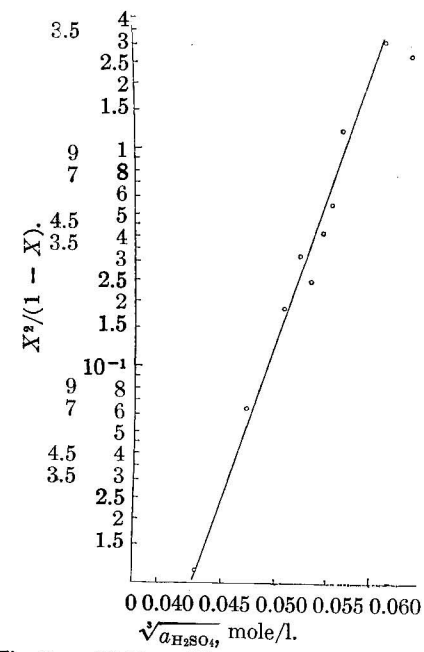

Fig. 3a.—$X^2/(1-X)$ *vs.* $\sqrt[3]{a_{H_2SO_4}}$ for THA.

The deviations from the Figs. 2 and 2a must be ascribed to the first formation of bisulfate. These deviations start at [THA] < 0.030 M and at [TOA] < 0.020 M, in agreement with the greater basicity of THA, which was found previously.[4] In the range of acidities where the equilibria mentioned under 2 and 2a are predominant another treatment must be chosen.

Allen[5] already pointed out that it might be assumed that the normal amine sulfate and the amine bisulfate form a completely miscible ideal solution, which is analogous to the ideal solid solution of the components of a solid ion exchanger. In that case the activities of the resin species can be represented by their mole fraction X.

The equilibrium constants K and K_a of the equilibria 2 and 2a can be given as

$$K_x = \frac{X^2_{(TOAH)HSO_4}}{a_{H_2SO_4} X_{(TOAH)_2SO}} \quad (9)$$

with

$$X_{(TOAH)HSO_4} = X = \frac{(TOAH)HSO_4}{(TOAH)HSO_4 + 2(TOAH)_2SO_4} \quad (10)$$

and

$$X_{(TOAH)_2SO_4} = 1 - X \quad (11)$$

and the same relations exist for THA.

Our K_x can be written now as

$$K_x = \frac{1}{a_{H_2SO_4}} \times \frac{X^2}{1 - X} \quad (9a)$$

Plotting $a^{1/3}_{H_2SO_4}$ *vs.* $X^2/(1 - X)$ for the TOA and the THA system, respectively, we find the Figs. 3 and 3a. There is again a qualitative agreement, but the form of the TOA Fig. 3 is somewhat more complicated, in agreement with the more complicated titration curve (Fig. 1). In Fig. 3 the part at low acidities corresponds to a slope

$$\frac{\mathrm{d} \log \frac{X^2}{1 - X}}{\mathrm{d} \log a^{1/3}_{H_2SO_4}} = 6 \quad (12)$$

in agreement with an empirical constant

$$K_4 = \frac{1}{a_{H_2SO_4}} \left(\frac{X^2}{1 - X}\right)^{1/2} \quad (13)$$

and

$$K_4 = 30.5 \text{ (mole/l.)}^{-3}$$

at high acidities we find a slope

$$\frac{\mathrm{d} \log \frac{X^2}{1 - X}}{\mathrm{d} \log a_{H_2SO_4}} = 1 \quad (14)$$

corresponding to

$$K_5 = \frac{1}{a_{H_2SO_4}} \left(\frac{X^2}{1 - X}\right)^3 \quad (15)$$

with the numerical value

$$K_5 = 11.4 \text{ (mole/l.)}^{-3}$$

In the THA case (Fig. 3a) only the slope 6 is found corresponding to

$$K_4{}^a = \frac{1}{a_{H_2SO_4}} \left(\frac{X^2}{1 - X}\right)^{1/2} \quad (13a)$$

with the numerical value

$$K_4{}^a = 557 \text{ (mole/l.)}^{-3}$$

Discussion

From the experiments and the results described above no quantitative conclusions can be drawn. The relations obtained are only empirical and will certainly have no general thermodynamic validity.

The only conclusion which might be drawn is that the transition points in Fig. 2, 2a and 3 correspond to inflection points in the titration curves 1 and 1a. A surprising point of interest is furthermore the great difference in the processes underlying the distribution when benzene is replaced by kerosene as the solvent.

THE HEAT OF VAPORIZATION AND THE HEAT OF FUSION OF FERRIC CHLORIDE

BY CHARLES M. COOK, JR.

Pigments Department, E. I. du Pont de Nemours & Co., Inc., Wilmington, Delaware

Received June 9, 1961

Pressures of Fe_2Cl_6(g) above solutions of $FeCl_2$ in Fe_2Cl_6(l) were measured in the range 300–470°. These data indicate that above liquid ferric chloride $\log P_{Fe_2Cl_6}$(mm.) = 48.57 − 12.55 log T − 6373/T, where $\Delta H_{580.7}(Fe_2Cl_6$ vap.) = 14.6 ± 0.5 kcal./mole Fe_2Cl_6, $\Delta S_{580.7}(Fe_2Cl_6$ vap.) = 24.8 ± 1.0 e.u./mole Fe_2Cl_6. The boiling point is estimated to be 315°. The heat of fusion was measured by a drop calorimeter and found to be $\Delta H_{580.7}(FeCl_3$ fusion) = 9.0 ± 0.4 kcal./mole $FeCl_3$.

Introduction

The currently accepted[1a,b] value of the heat of vaporization, 12.04 kcal./mole Fe_2Cl_6, at the accepted boiling point of liquid ferric chloride, 319°, derives from measurements by Stirnemann[2] of the total pressure within a closed bulb containing ferric chloride at temperatures up to 493°. This thermodynamic value was calculated without correcting the observed total pressures for the significant partial pressure of Cl_2 present along with the Fe_2Cl_6(g) in the vapor space above the ferric chloride.[3] The magnitude of the chlorine pressure correction to Stirnemann's data is discussed below, and the heat of vaporization of Fe_2Cl_6(l) is recalculated.

Experimental

Vapor Pressure.—Ferric chloride–ferrous chloride mixtures were contained in a *ca.* 13-cc. cylindrical Pyrex sample

(1) (a) "Selected Values of Chemical Thermodynamic Properties," Circular 500, National Bureau of Standards (1952); (b) O. Kubaschewski and E. Evans, "Metallurgical Thermochemistry," 2nd Ed., John Wiley and Sons, New York, N. Y., 1956.

(2) E. Stirnemann, *Neues Jahrb. Mineral. Geol. u. Palaeontol.*, **52A**, 334 (1925).

(3) W. Kangro and E. Peterser, *Z. anorg. Chem.*, **261**, 157 (1950), corrected Stirnemann's pressures for P_{FeCl_3} and for P_{Cl_2}. The latter calculation, however, contained the assumption that a_{FeCl_2} = 1, which is invalid for Stirnemann's experiments above the $FeCl_2$–$FeCl_3$ eutectic temperature because of the solubility of $FeCl_2$ in molten Fe_2Cl_6. See H. Schäfer, *Z. anorg. u. allgem. Chem.*, **266**, 269 (1951).

bulb sealed to a sickle gage. Bulb and gage were placed within a close-fitting 3/4 in. i.d. × 12 in. L brass sleeve closed at the bulb end by a brass plate. That end of the sleeve containing the inlet tube to the outside shell of the sickle gage was packed with Pyrex wool. The bulb-gage-sleeve assembly was inside a vertical pressure tube of 1 in. i.d., 1/4 in. wall stainless steel pipe heated with a uniform external winding of resistance wire covered with 3/4 in. of asbestos insulation. A Chromel–Alumel thermocouple was brought through the brass sleeve endplate to a thermowell in the bulb.

The sickle gage was used as a null-point pressure indicator, external pressure to balance the bulb pressure being supplied from an argon cylinder, and pressure balance being signified by the closing of an electrical circuit through Pt contacts at the pointers of the gage. The pressure within the system was read, in the interval 0-2.4 atm., from a Hg manometer attached to the pressure manifold. Pressures beyond this range were read from a 0–100 p.s.i.g. Ashcroft gage.

Before sample preparation the bulb was baked in Cl_2 at 300°. Ferric chloride, prepared by reacting 1.5 g. of Fe wire with Matheson "oxygen-free" Cl_2, was sublimed in Cl_2 into the bulb. A weighed amount of ferrous chloride, previously prepared by distillation at 950° in HCl of crude $FeCl_2$ from Fe and HCl, was added to the ferric chloride. The bulb was evacuated, heated to 200°, back-filled with approximately 1/2 atm. of argon, sealed off, and assembled in the pressure tube.

Pressures measured during the first heat-up drifted slowly with time, presumably because of reaction of $FeCl_3$ with H_2O in the Pyrex. This effect was limited to the initial few measurements, after which the pressure measured for a given temperature was stable over long periods of time and independent of the direction of approach.

The observed pressures were taken to be the sum of P_{FeCl_3}, $P_{Fe_2Cl_6}$, P_{Cl_2} and P_{inert}. The P_{FeCl_3} was considered to be negligible.[1b] P_{Cl_2}, calculated from equilibrium 2, was small at the $FeCl_2$ concentrations employed. The inert gas contribution was evaluated from measurements at 200–250° where the P_{Cl_2} and $P_{Fe_2Cl_6}$ contributions were small and accurately known. The gas law was employed to estimate P_{inert} at higher temperatures; for the run with initial $X_{FeCl_3} = 0.26$, $P_{inert} = 1.37T$ mm.; for that with initial $X_{FeCl_3} = 0.52$, $P_{inert} = 1.42T$ mm.

Heat of Fusion.—A Vycor ampoule, 1.5 cm. d. × *ca.* 7 cm. l., was sealed to a vertical tube and dried at 300° under vacuum. Ferric chloride, prepared by chlorination of Fe wire (Baker Analyzed, Reagent), was sublimed in Cl_2 into the vertical tube. When this tube was heated in an oven to 310°, the ferric chloride melted and ran into the ampoule. The connection between ampoule and tube then was drawn to about 1 mm. d., and the molten Fe_2Cl_6 cooled to room temperature over a period of about 30 min. under 1 atm. Cl_2. Finally, the system was closed, the Cl_2 pressure reduced to *ca.* 90 mm., and the ampoule sealed off at the constriction.

The sample was suspended by a fine wire within a chamber in a 12 in. furnace constructed of 3/4 in. d. streamline Cu tubing externally wound with Nichrome ribbon and insulated with 3/4 in. of asbestos. The chamber was 5 in. × 5/8 in. d. Cu tubing silver soldered in the middle of the furnace and with removable brass top and bottom end plates. The furnace ends were plugged with asbestos during sample heat-up.

When the sample temperature, measured by a Chromel–Alumel thermocouple in the central well of the ampoule, was constant the lower asbestos plug and the bottom end plate were removed. The furnace was swung over the calorimeter, and the sample dropped. The furnace was quickly removed and the calorimeter closed.

The calorimeter was a one-liter Dewar flask containing 800 cc. of water. A Beckmann thermometer, a stirrer and a test-tube extended through a cork into the water. The sample was caught in the test-tube, which was cushioned on the bottom with Pyrex wool and which contained 20 cc. of silicone oil to assist heat transfer. The water equivalent of this calorimeter assembly was measured by observing the temperature rise per watt-min. passed through a resistor inside the calorimeter.

At the completion of the calorimetric measurements the $FeCl_3$-containing ampoule was weighed, broken and dropped under an inert atmosphere into previously-boiled water. The ferric chloride was titrated for $FeCl_2$ with $KMnO_4$, in the presence of the Zimmermann–Reinhardt reagent. Despite the precaution of maintaining a Cl_2 atmosphere during sample preparation the $FeCl_3$ samples contained 0.005–0.02 atoms Fe(II) per atom Fe(III). The broken ampoule was reweighed to determine the total ferric chloride present.

To obtain the heat content/mole $FeCl_3$, the observed total heat content must be corrected for the heat contained by (a) the Vycor ampoule, (b) the 0.5-2 mole % $FeCl_2$ in the sample and (c) reversal of reaction 2. Correction (c) can be shown to be negligible, while correction (b) comes to about 1%. Correction (a) comes to as much as 50% at the lower temperatures. Five drops of an empty Vycor ampoule in the range 230–380° were fitted to ± 1% by

$$C_p(\text{Vycor}) = 0.10 + 2.39 \times 10^{-4}\, T\ (°\text{K.})\ \text{cal./°C. g. Vycor}$$

The experimentally observed heat contents on any one sample scatter by about ±3%. There is an approximately 5% difference between the heat content measured for $FeCl_3$(c) and the probably more accurate values of Todd and Coughlin.[8] This apparent systematic error may be due to error in the large Vycor correction term; if so it will have little effect upon the measured heat of fusion. The heat contents of Bi in Pyrex determined at two temperatures in an apparatus similar to this were found to agree with the published data[1b] to 1%.

Discussion

Stirnemann's Pressure Temperature Data.—Chlorine pressures generated by the equilibrium

$$2FeCl_3(c) = 2FeCl_2(c) + Cl_2(g) \qquad (1)$$

between 162 and 302°[4–6] fit, with standard deviation $s < 0.19$, the expression

$$\ln P_{Cl_2}(\text{atm.}) = 22.514 - 14327/T - \left[\int_{298.2}^{T} \Delta C_p(1)\, dT - T\int_{298.2}^{T} \Delta C_p(1)\, dT/T\right]/RT$$

where $\Delta C_p(1) = -12.4 - 0.00432T + 920000/T^2$ cal./mole °C.[7] This expression indicates that $\Delta H_{298.2}(1) = 28.46$ kcal., $\Delta S_{298.2}(1) = 44.72$ e.u., in agreement with the values $\Delta H_{298.2}(1) = 27.7$ kcal., $\Delta S_{298.2}(1) = 46.1$ e.u., predicted from the known heats of formation and entropies of the reactants.[1,8–10]

Above solutions of $FeCl_2$ in $Fe_2Cl_6(l)$ P_{Cl_2} is determined by

$$Fe_2Cl_6(l) = 2FeCl_2(l) + Cl_2(g) \qquad (2)$$

The free energy change, and thus the equilibrium constant, of (2) can be calculated as a function of temperature from $\Delta F_T(1)$ and the free energies of fusion of the iron chlorides.

Between 297.5–405° the solubility of $FeCl_2$ in $Fe_2Cl_6(l)$[11] obeys the relation

$$\ln X_{FeCl_2} = 1.288 - 1552T^{-1} \qquad (3)$$

Comparison of this solubility with the ideal solution solubility calculated from $\Delta F_T(FeCl_2$ fusion)

(4) H. Schäfer and E. Oehler, *Z. anorg. u. allgem. Chem.*, **271**, 206 (1953).

(5) O. E. Ringwald, Doctoral Dissertation, Princeton University, 1949.

(6) L. E. Wilson and N. W. Gregory, *J. Phys. Chem.*, **62**, 433 (1958).

(7) C_p values are from K. K. Kelley, "Contributions to the Data on Theoretical Metallurgy. XIII," Bulletin 584, U. S. Bureau of Mines, 1960.

(8) S. S. Todd and J. P. Coughlin, *J. Am. Chem. Soc.*, **73**, 4184 (1951).

(9) M. F. Koehler and J. P. Coughlin, *J. Phys. Chem.*, **63**, 605 (1959).

(10) K. K. Kelley and G. E. Moore, *J. Am. Chem. Soc.*, **65**, 1264 (1943).

(11) H. Schäfer and L. Bayer, *Z. anorg. u. allgem. Chem.*, **271**, 338 (1957).

indicates that the activity coefficient of $FeCl_2$ in its saturated solution in liquid Fe_2Cl_6 is

$$\ln \gamma_{FeCl_2} = 3.297 - 2963T^{-1} \quad (4)$$

with the standard state supercooled $FeCl_2$(l).

A sealed vessel initially charged with $FeCl_3$ will contain $FeCl_2$ in amount proportional to P_{Cl_2}. The proportionality constant, r, depends upon vessel volume and initial $FeCl_3$ content; for Stirnemann's experimental system r can be expected to be in the range $83 \geq r \geq 30$.

P_{Cl_2} corrections to the total pressure data of Stirnemann were calculated for arbitrary r's from the K_{eq} of reaction 2, the γ_{FeCl_2} expression (4), and presuming $\gamma_{Fe_2Cl_6}$ = unity. The resulting net Fe_2Cl_6 vapor pressure equations, given in Table I, show that, although the calculated heat of vaporization varies with the value chosen for r, Stirnemann's data indicate $\Delta H_{vap} \simeq 15$ kcal./mole Fe_2Cl_6.

TABLE I

Fe_2Cl_6 PRESSURES CALCULATED FROM STIRNEMANN'S DATA AND EXPRESSED AS $\ln P_{Fe_2Cl_6}(atm.)/X_{Fe_2Cl_6} = A + BT^{-1}$

Assumed r	Calcd. $X_{Fe_2Cl_6}$	A	B	ΔH_{vap}, kcal.
85	0.90– ..	12.14	−7386	14.7
75	.90–0.64	12.15	−7247	14.8
50	.91– .76	12.62	−7856	15.6
30	.93– .80	14.52	−9372	18.6

Fe_2Cl_6 Pressure above $FeCl_2$ Solutions.—Total pressures were measured above ferric chloride solutions initially containing $X_{Fe_2Cl_6} = 0.26$ and above solutions saturated with $FeCl_2$. Equilibrium (2) indicates P_{Cl_2} above the former solution to be only *ca.* 6% of $P_{Fe_2Cl_6}$ and X_{FeCl_2} to be stabilized at 0.72–0.75; the determination of $P_{Fe_2Cl_6}$ from the total pressure data is correspondingly simplified. Values of $\ln P_{Fe_2Cl_6}/X_{Fe_2Cl_6}$ have been calculated for the X_{FeCl_2} (initial) = 0.26 data and are presented as the open circles in Fig. 1. These values, made linear in T^{-1} by correction for the ΔC_p between gaseous and liquid ferric chloride,[12] are fitted by

$$\ln P_{Fe_2Cl_6}/X_{Fe_2Cl_6} + \left[\int_{580.7}^{T} -25\, dT - T\int_{580.7}^{T} -25\, dT/T\right]/RT = 12.519 - 7365.3/T \quad (5)$$

with standard deviation, $s = 0.024$.[13]

Increasing X_{FeCl_2} from 0.26–0.28 to the saturation concentration brings about a relatively small decrease in the measured $P_{Fe_2Cl_6}/X_{Fe_2Cl_6}$. This insensitivity to X_{FeCl_2} makes it probable that at higher temperatures $\gamma_{Fe_2Cl_6}$ is not strongly concentration dependent and approximates unity.[14]

(12) For liquid ferric chloride C_p = 32 cal./mole $FeCl_3$ °C.[8] For Fe_2Cl_6(g) Kelley[7] has estimated C_p = 34 cal./mole Fe_2Cl_6 °C. However, for many metal chloride vapors the heat capacity at 500°K. approaches the theoretical limit expected with full excitation of the vibrational modes. For Fe_2Cl_6 this limiting $C_p = 22R \simeq 44$ cal./mole °C. A ΔC_p between vapor and liquid ferric chloride of −25 cal./mole Fe_2Cl_6 °C. was used in the heat capacity correction term of Fig. 1 and equation 5.

(13) Those half-shaded data points for which $T^{-1} \geq 0.00168$ were included in this least squares calculation.

(14) For example, at 435° the observed difference in in $P_{Fe_2Cl_6}/X_{Fe_2Cl_6}$ between the data at X_{FeCl_2} = 0.28 and at saturation is ≃0.17. Presuming this difference to result from a concentration dependence of $\gamma_{Fe_2Cl_6}$ in the familiar form $\ln \gamma_{Fe_2Cl_6} = -\beta(X_{FeCl_2})^2/2$, then, since saturation $X_{FeCl_2} \geq 0.42$, $\beta \leq -3.4$ and $\gamma_{Fe_2Cl_6} \simeq 0.9$ for $X_{FeCl_2} = 0.28$.

(15) This b.p. also was found by C. G. Maier, "Vapor Pressures of the Common Metallic Chlorides and a Static Method for High Temperatures," Technical Paper 360, U. S. Bureau of Mines, 1925.

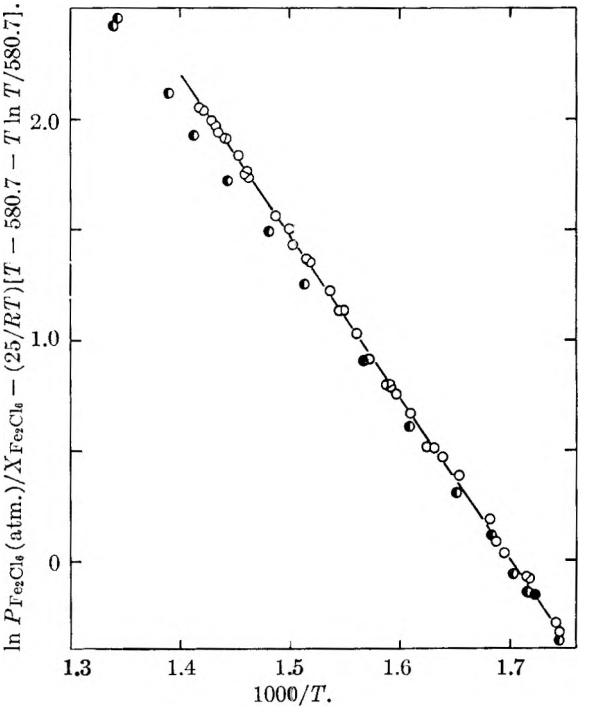

Fig. 1.—Vapor pressures above $Fe_2Cl_{6(l)}$ solutions of $FeCl_2$: ○, X_{FeCl_2} = 0.25–0.28; ◐, X_{FeCl_2} = saturated solution; ● pure solid ferric chloride.

In addition, at the $FeCl_2$ melting point the vapor pressure calculated from the sublimation equation,[6] $\log P^0_{Fe_2Cl_6}(mm.) = 15.111 - 7142/T$, fits closely the experimental $P_{Fe_2Cl_6}/X_{Fe_2Cl_6}$ curve. This implies that at 580.7°K. and $X_{FeCl_2} = 0.25$, $\gamma_{Fe_2Cl_6} \simeq$ unity.

If $\gamma_{Fe_2Cl_6}$ is assumed unity over the experimental temperature range, equation 5 can be rewritten

$$\ln P^0_{Fe_2Cl_6}(atm.) = 12.519 - 7365.3/T + 25[T - 580.7 - T \ln T/580.7]/RT \quad (6)$$

or, alternatively,

$$\log P^0_{Fe_2Cl_6}(mm.) = 48.57 - 12.55 \log T - 6373/T \quad (7)$$

For vaporization of Fe_2Cl_6

$$\Delta H_{580.7} = 14.6 \pm 0.5 \text{ kcal./mole } Fe_2Cl_6$$
$$\Delta S_{580.7} = 24.8 \pm 1.0 \text{ kcal./mole } Fe_2Cl_6$$

with the estimate of error stemming largely from uncertainty in the $\gamma_{Fe_2Cl_6}$ assumption. The indicated boiling point is 315°.[15]

Heat of Fusion.—The measured dependence of the heat content of ferric chloride upon temperature is plotted in Fig. 2. Partial melting of the sample is observed between the $FeCl_2$–$FeCl_3$ eutectic temperature, 297.5°,[11] and the melting point. The heat of fusion of $FeCl_3$ is found to be 9 ± 0.4 kcal./mole $FeCl_3$. The heat content data above the melting point indicate C_p (1/2 Fe_2Cl_6(l)) = 30 cal./mole °C.

The temperature dependence of Fe_2Cl_6 pressure above solid ferric chloride[3,6] indicates ΔH_{sub} = 32.9 ± 0.2 kcal./mole Fe_2Cl_6. If the heat of fusion

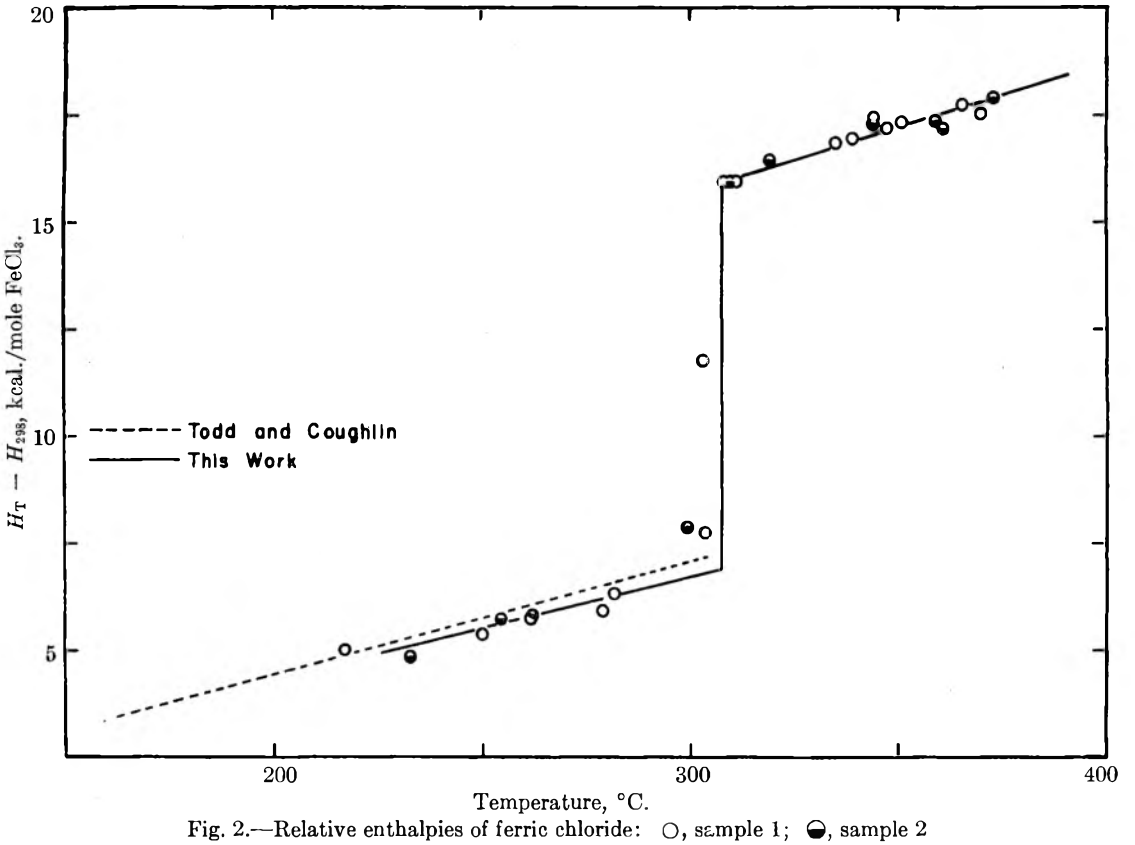

Fig. 2.—Relative enthalpies of ferric chloride: ○, sample 1; ◒, sample 2

is 9 ± 0.4 kcal./mole $FeCl_3$, the heat of vaporization should be ΔH_{vap} = 14.9 ± 0.8 kcal./mole Fe_2Cl_6. This is in agreement with the Table I value derived from Stirnemann's data and with the enthalpy of vaporization calculated from the vapor pressure equation 6.

A SEARCH FOR HYDROGEN–DEUTERIUM EXCHANGE ON CLEAN GERMANIUM SURFACES[1]

BY D. SHOOTER AND H. E. FARNSWORTH

Barus Physics Laboratory, Brown University, Providence, R. I.

Received June 9, 1961

An attempt has been made to measure hydrogen–deuterium exchange on (100) surfaces of a germanium crystal cleaned by outgassing *in vacuo* and by argon ion bombardment. Tests for the reaction also were made on sputtered films. No activity was found for either type of surface. The lower observable limits of the activity were 10^{13} molecules cm.$^{-2}$ sec.$^{-1}$ for the crystal and 5×10^{11} molecules cm.$^{-2}$ sec.$^{-1}$ for the film. It is concluded that the lack of activity cannot be due to contamination of the surface. A comparison is made between this result and other published results for hydrogen–deuterium exchange on germanium.

Introduction

Several workers[2,3] have reported on the activity of germanium for the hydrogen–deuterium exchange reaction. This is of interest because molecular hydrogen does not adsorb to any measurable extent, although atomic hydrogen has been found to adsorb on germanium.[4–6] Since this reaction occurs *via* chemisorption on the surface, it suggests that the reaction may occur on a small number of active centers, possibly defects in the surface. The purpose of this work was to measure the reaction under carefully controlled conditions on surfaces cleaned in high vacuum.

Experimental

Apparatus.—A detailed description of the apparatus is given elsewhere.[7] It consists of a reaction chamber isolated

(1) This work was supported by the U. S. Army Signal Corps.

(2) (a) K. Tamaru and M. Boudart, *Advances in Catalysis*, **9**, 699 (1957); (b) G. K. Boreskov and V. L. Kuchaev, *Doklady Akad. Nauk. S.S.S.R.*, **119**, 302 (1958).

(3) Y. L. Sandler and M. Gazith, *J. Phys. Chem.*, **63**, 1095 (1959).

(4) P. Handler and W. Portnoy, *Phys. Rev.*, **116**, 516 (1959).

(5) M. Green and K. H. Maxwell, *J. Phys. and Chem. Solids*, **11**, 195 (1959).

(6) H. E. Farnsworth, R. E. Schlier and J. A. Dillon, Jr., "Solid State Physics in Electronics and Telecommunications, Academic Press, New York, N. Y., 1960, p. 602.

(7) D. Shooter and H. E. Farnsworth, *J. Phys. and Chem. Solids*, (in press).

from the rest of the system by three metal vacuum valves and liquid nitrogen traps. The three valves connect the reaction chamber to the main pumping line, the gas storage line and to the omegatron mass spectrometer[8] which is used for analysis of gas mixtures. A ground glass valve separates the two compartments of the reaction chamber, as shown in Fig. 1. The crystal is cleaned in the lower compartment, transferred to the upper compartment, and isolated by closing the glass valve with externally operated magnetic controls. The reaction rate then can be measured in the absence of any other materials which might contribute to the activity.

Preparation and Cleaning of the (100) Germanium Crystal.—The single crystal catalyst, with its major surfaces cut parallel to (100) planes, had a resistivity of 56 ohms cm. (p type) at 296°K., and an impurity concentration of 3.3×10^{12} cm.$^{-3}$. It was cut to a "T" shape so that it would hang in the upper crystal support and had a surface area of 4 cm.^{2}. Before placing it in the reaction chamber it was mechanically polished and given a mild etch for 2 min. in a modified CP-4 solution.[9] Instead of initiating the etching action by bromine, the solution was heated to 30°. The crystal then was rinsed with distilled water, washed with 48% hydrofluoric acid and rinsed with distilled water again, before allowing it to come into contact with the atmosphere.

After baking the reaction chamber and outgassing the metal parts, pressures of about 10^{-9} mm. were obtained. To remove contamination, the crystal was subjected to alternate treatments of outgassing at red heat and argon ion bombardment.[10] Standard conditions of ion bombardment were 200 μamp. at 500 volts, for 10 min. on each of the two major faces of the crystal. At the conclusion of the experiments, the crystal had received 170 hr. of outgassing at red heat and 120 min. of ion bombardment.

Preparation of the Sputtered Germanium Film.—A film of germanium was sputtered onto glass in a slightly modified reaction chamber. The crystal, which was fixed in the bottom compartment, was cleaned in the same manner as before. It first was outgassed for 48 hr. at red heat, and given preliminary ion bombardment for 1 hr. which sputtered an extensive film on the walls of the cleaning compartment. A small piece of Pyrex plate, magnetically controlled, then was lowered from the top compartment. The crystal was sputtered under the usual ion bombardment conditions, each side of the glass plate being exposed for 10 min. This Pyrex plate then was raised into the top compartment and the glass valve was closed. A second film later was sputtered on top of the first film. The geometrical area of the sputtered film was about 6 cm.^{2}, and it was opaque.

Results and Discussion

The germanium crystal was examined periodically for activity during the cleaning process. Two experimental runs were carried out with the reaction chamber at a temperature of 170°. Measurements were attempted on the surface immediately after ion bombardment and after annealing, but no activity was found. A sputtered film was prepared because the high activity previously reported was observed on this type of surface. No activity was observed at room temperature on the sputtered film.

Because of the diffusion of the gas mixture through the glass valve a lower limit is placed on the observable activity.[7] This result is given in Table I together with the published results of other workers. The value obtained for polycrystalline nickel in the same apparatus is included for comparison.

Except for the results of Sandler and Gazith, the activities quoted in Table I are too low to observe in the present apparatus and in this sense confirm the negative result of our experiment.[11] It appears that the activity observed by Sandler and Gazith is not an intrinsic property of germanium, nor even of a sputtered germanium film. They suggest that their activity is connected with defects in the surface or possibly with metallic impurities associated with defects such as dislocations. Our results show that suitable active centers are not produced by ion bombardment of germanium. This is in contrast to the results of

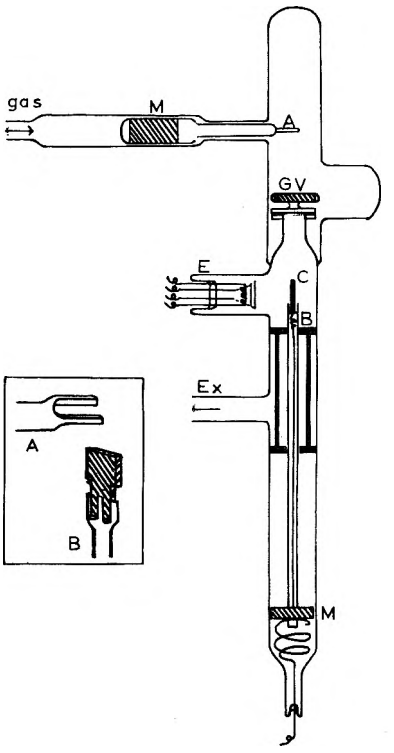

Fig. 1.—Reaction chamber: M, magnetic controls; GV, glass valve C, catalyst E, electron gun; A and B, upper and lower catalyst supports, respectively. Inset shows detail of catalyst support.

TABLE I

ACTIVITY MEASUREMENTS OF HYDROGEN–DEUTERIUM EXCHANGE

	km, molecules, cm.$^{-2}$ sec.$^{-1}$	E, kcal. mole^{-1}
Present work		
(100) single crystal 293°K.	$<1 \times 10^{13}$	
Sputtered film 293°K.[a]	$<5 \times 10^{11}$	
Sandler and Gazith		
Sputtered film 293°K.[b]	1.1×10^{16}	1.6
Boreskov and Kuchaev[2b]		
Crushed sample 573°K.	1.8×10^{14}	17
Above result extrapolated to 293°K.	1.2×10^{8}	17
Tamaru and Boudart[2a]		
Film 575°K.[c]	4.7×10^{11}	..
Solid polycrystalline nickel[7]	8.8×10^{16}	..

[a] Calculated value, assuming a B.E.T. area of twenty times the geometrical area as found by Sandler and Gazith.[3] [b] Calculated value, using B.E.T. area. [c] This film was prepared by decomposition of GeH_4 in reaction chamber filled with glass wool; B.E.T. area was 2.65×10^4 cm.^{2}

(8) D. Alpert and R. S. Buritz, *J. Appl. Phys.*, **25**, 202 (1954).

(9) J. A. Dillon, Jr., and H. E. Farnsworth, *ibid.*, **28**, 174 (1957).

(10) H. E. Farnsworth, R. E. Schlier, T. H. George and R. M. Burger, *ibid.*, **29**, 1150 (1958).

(11) It may be noted that Eley, *et al.*, *Trans. Faraday Soc.*, **54**, 394 (1958) have observed an appreciable reaction on glass at 300° through which we have no evidence to suggest that the results of Boreskov and Kuchaev, Tamaru and Boudart were influenced in this manner.

ethylene hydrogenation on nickel,[12] where ion bombardment of the surface produced large changes of activity. If the activity is associated with impurity atoms, then it is difficult to decide whether the impurities are producing active centers by modification of the electronic properties of germanium or simply because they are active materials on an inert germanium substrate.

A further difficulty is the magnitude of the activity observed by Sandler and Gazith as compared to the activity of nickel. Experiments with a piece of nickel, having the same dimensions as the germanium, in this apparatus[7] gave a very high value for the activity, as was expected. The difference between the activities was at least four orders of magnitude. Sandler and Gazith conclude by comparison with results of Singleton[13] that the activities of germanium and nickel are comparable in magnitude. There is good evidence that for this reaction the number of active centers on nickel is comparable with the number of surface atoms.[7,14] However, on germanium the number of active centers must be much smaller. Since the measured activation energies are about the same one also would expect the rate of conversion to be lower on germanium than on nickel.

In view of the lack of activity, tests were made to check for possible contamination of the surface. The findings are given below.

(a) **Preparation of the Clean Surface.**—The cumulative treatments given to this crystal were 170 hr. of heating and 120 min. of ion bombardment with 500 e.v. ions, at a current density of 100 μamp. cm.$^{-2}$. Electron diffraction[10,15] and electrical measurements[16,17] have proved that such treatments will produce a surface which remains free of contamination in high vacuum for several days. Much shorter cleaning treatments will produce a clean surface initially, but this becomes contaminated by diffusion from the interior of the crystal. After initial ion bombardment, even a surface exposed to oxygen can be regenerated simply by heating to 500°.[15-17] This is ample proof that a clean surface was obtained for the crystal. The films were sputtered from a cleaned crystal, exposing a large area of fresh germanium, so that the amount of initial contamination must have been small.

(b) **Contamination from the Residual Ambient.**—Possible contaminants in a high vacuum system after baking and outgassing are O_2, CO and N_2. The average pressure between reaction runs was 10^{-8} mm., which was due mostly to argon gas. Sputtered germanium on the walls of the reaction chamber also would getter active contaminants and had a much larger area than the crystal. An investigation of the rate of adsorption on a tungsten filament made by the flash filament technique[18] indicated that the pressure of adsorbable gases in the system (O_2 + CO + N_2) was below 10^{-10} mm. Mass 32 has not been observed in the omegatron; this result is consistent with the finding that residual oxygen is converted into CO by the hot filament.[18] The main constituent in the residual ambient is mass 28. This indicates that the partial pressure of oxygen is below 5×10^{-11} mm.

The only one of these gases which adsorbs on germanium to a measureable extent is oxygen.[5] In agreement with the value calculated from kinetic theory, Farnsworth, *et al.*,[10] have found that an exposure (pressure × time) of 2.4×10^{-6} mm. min. is required to form a monolayer on germanium. Even if only a small fraction of the surface is active and this part is covered first, it is not possible to reconcile the lack of activity with contamination from the residual ambient.

(c) **Contamination from the Gases Used.**—The absolute magnitude of impurities in the gases used is higher than that to be found in the residual vacuum. The hydrogen (99.99% H_2) and argon (99.999% A) used in these experiments were mass spectrographically pure. Deuterium was less pure (average 99.66% D_2) and contained HD and D_2O. Analysis of the hydrogen and deuterium in the omegatron showed that both contained an impurity of mass 28. It was concluded that this impurity is nitrogen.[7] No mass 32 was found. It also was concluded in the earlier work[7] that these gases produced no contamination of a nickel surface. Therefore contamination of germanium, which is much less reactive, is extremely unlikely.

Conclusion

The lack of activity found in the present work is not due to contamination, nor to the method of surface preparation. It is concluded that the activity of germanium for hydrogen–deuterium exchange (if any) is too low to measure with the present apparatus. The high activity reported by Sandler and Gazith[3] does not appear to be an intrinsic property of germanium and may be a consequence of the mode of preparation.

NOTE ADDED IN PROOF.—Bennett and Tompkins recently have reported results of hydrogen adsorption on germanium films (paper presented at the 2nd International Vacuum Congress, Washington, D.C., October 1961). They found no measurable adsorption of molecular hydrogen below 195°K. and only about 2% coverage at 273°K., explainable on the basis of activation energy (16.6 kcal. mole^{-1}) required for adsorption. Since hydrogen–deuterium exchange proceeds *via* adsorption and desorption, these results support the work of Boreskov and Kuchaev[2] and the findings of this paper.

(12) J. Tuul and H. E. Farnsworth, *J. Am. Chem. Soc.*, **83**, 2247 (1961).

(13) J. H. Singleton, *J. Phys. Chem.*, **60**, 1606 (1956).

(14) O. Beeck, A. E. Smith and A. Wheeler, *Proc. Roy. Soc.* (London), **A177**, 62 (1940).

(15) R. E. Schlier and H. E. Farnsworth, *J. Chem. Phys.*, **30**, 917 (1959).

(16) J. A. Dillon, Jr., and H. E. Farnsworth, *J. Appl. Phys.*, **28**, 174 (1957).

(17) P. Handler, "Semiconductor Surface Physics," University of Pennsylvania Press, Philadelphia, Pa., 1957, p. 23.

(18) R. E. Schlier, *J. Appl. Phys.*, **29**, 1162 (1958).

DETERMINATION OF THE DISSOCIATION EQUILIBRIA OF WATER BY A CONDUCTANCE METHOD

BY H. C. DUECKER AND W. HALLER

National Bureau of Standards, Washington, D. C.

Received June 21, 1961

Electrical conductivity measurements have been made at various temperatures on electrophoretically purified water with varying impurity content. The temperature coefficients of conduction are determined at 18 and 25° for each fraction. An expression is derived for the activation energy of conduction of very dilute aqueous solutions as a function of electrical conductivity. Upon substitution of the calculated activation energies of conduction into this expression, the theoretical conductivity of pure water is calculated to be 0.0373×10^{-6} ohm^{-1} cm.$^{-1}$ at 18°, a value 3% lower than predicted by Kohlrausch 60 years ago. The dissociation constants for water calculated from this value, the equivalent conductance of the ions and the density, however, agree with those determined from the e.m.f. of galvanic cells.

Introduction

Since postulation of the theory of ionic dissociation by Arrhenius[1] in 1887, many workers have been engaged in the quantitative description of the dissociation equilibria of chemical compounds. Very early efforts were devoted to the study of the substance, water, because of its importance to the physical sciences and its unique role as a mineral and life-supporting liquid, rather than because of experimental convenience.

It appeared rather tempting to exploit the most apparent property of an ion, its capacity to carry electrical charge, for the determination of ionic concentration. Yet, in the case of water, the direct determination of hydrogen and hydroxyl ion concentration by electrical conductivity measurements is complicated by the very small degree of dissociation, which yields approximately one ion pair for each 10^9 water molecules. This means that a reasonable degree of accuracy may be obtained only if impurity ions are reduced to a comparably low level. In 1894, Kohlrausch and Heydweiller[2] reported the electrical conductivity of water which they had purified by 36 vacuum distillations in glass equipment which had been leached with water for ten years. From this data and known values of the equivalent ionic conductances, they estimated the concentration of the hydrogen and hydroxyl ions to be 0.8×10^{-7} equivalent per liter at 18°. The conductivity method for determination of the dissociation constant has not since been used because of the difficulty in preparing and maintaining water of ultra-low-conductivity. Today's best accepted values are from methods which do not necessitate the preparation of ultra pure water, such as the measurement of the electrical potential of cells. This method was used as early as 1893 by Ostwald[3] and Arrhenius,[4] contemporaries of Kohlrausch, but was not perfected until the 1930's by Harned and co-workers.[5]

In a previous publication,[6] the authors of the present paper described an electrophoretic purification procedure capable of producing and maintaining ultra-low-conductivity water having a residual ionic impurity content of only one-third of the minimum previously reported in the literature. Because this more closely approaches the ideal purity, and in view of the fact that better supporting electrochemical data with confirmed accuracy are available today, the authors were convinced that a repetition of the conductance method would help verify the presently accepted values of the fundamental electrochemical properties of the water-substance.

Kohlrausch and Heydweiller measured the electrical conductivity of water fractions of varying purity around 18° and presented their data by the use of a linear equation of the form, $dk/dT = a + bk$, where dk/dT is the temperature dependence of the conductivity and a and b are constants. From the temperature dependence of the equivalent conductivities of the H^+ and OH^- ions and from the heat of neutralization of strong acids and bases, they further predicted a value for the temperature dependence of conductivity for pure water. Substituting this value into the above empirical equation they arrived at a value for the theoretical conductivity of pure water. In evaluating their data the authors of this present paper did not use Kohlrausch and Heydweiller's empirical extrapolation procedure but derived a different method on theoretical grounds.

Theoretical

The conductivity, k, of an ion may be expressed as the product of its equivalent conductance, λ, and its concentration, x. Upon consideration of the temperature coefficients of conductivity and the thermodynamic law for the distribution of energies, one can show that the activation energy for the conduction of the ion, ${}_kE$, is given by the relation

$$ {}_kE = {}_\lambda E + {}_xE \qquad (1) $$

where ${}_\lambda E$ is the minimum thermal energy the ion must have in order to participate in the conductivity process and ${}_xE$ the energy required for dissociation per equivalent ion formed.

Now the total conductivity of the pure substance water is equal to the sum of the conductivities of the H_3O^+ and OH^- ions. By use of similar thermodynamic considerations it can be shown that the total activation energy of conduction for pure water, ${}_kE_w$, is given by the weighted energies of conduction of the ions, *i.e.*

$$ {}_kE_w = \frac{k_{OH}}{k_w} {}_kE_{OH} + \frac{k_H}{k_w} {}_kE_H \qquad (2) $$

(1) S. Arrhenius, *Z. physik. Chem.*, **1**, 631 (1887).

(2) F. Kohlrausch and A. Heydweiller, *Wied. Ann.*, **53**, 209 (1894); *Z. physik. Chem.*, **14**, 317 (1894).

(3) W. Ostwald, *ibid.*, **11**, 521 (1893).

(4) S. Arrhenius, *ibid.*, **11**, 805 (1893).

(5) For a review of this work see H. S. Harned and B. B. Owen, *Chem. Revs.*, **25**, 31 (1939).

(6) W. Haller and H. C. Duecker, *J. Research Natl. Bur. Standards*, **64A**, 527 (1960).

where ${}_kE_{OH}$ is the activation energy for the conduction of the OH^- ion and ${}_kE_H$ is that for the H_3O^+ ion.

Upon adding n impurity ions to the water, the relationship for the total activation energy of conduction is still of the same form, *i.e.*

$$ {}_kE = \frac{k_{OH}}{k} {}_kE_{OH} + \frac{k_H}{k} {}_kE_H + \frac{k_i}{k} {}_kE_i + \frac{k_j}{k} {}_kE_j + \cdots \quad (3) $$

In this general case, k_i, k_j, etc., change with k since $(k - k_w) = k_i + k_j + \cdots$, thus making it difficult to get a simple expression for ${}_kE$ in terms of k or $1/k$.

It can, however, be shown that for a number of special situations the relation of ${}_kE$ is linear with respect to $1/k$, *viz.*, (a) water contaminated with one neutral electrolyte; (b) water contaminated with n ionic impurities where the ratio of the conductivities of the impurity ions remains constant throughout the purification process, *i.e.*, $k_i = ak_j = \ldots$. etc. (This relation might be expected to apply to any of a series of water samples taken from different stages of the purification of any solution if the efficiency of the purification process is the same for all ions present). (c) If the activation energy of conductivity of each of the impurities is equal (or nearly so) as would be expected with fully dissociated substances.[7] In this case the activation energy would increase linearly with $1/k$ regardless of the relative concentrations of the impurities at a given conductivity.

The data obtained in our experiments give a linear relation between $1/k$ and the apparent activation energy of conduction. We do not know which of the discussed situations (if any) exist in our experiments but have treated the data on the merits of its own indicated linearity by use of the relations discussed here.

The derived equations for the above situations are of the form

$$ {}_kE = \frac{k_w}{k} ({}_kE_w - E') + E' \quad (4) $$

where E' is the intercept of the activation energy axis at $1/k = 0$. The conductivity of pure water, k_w, can be evaluated from this equation if we have data for ${}_kE$ as a linear function of $1/k$, since available values for the equivalent conductance of the H_3O^+ and OH^- ions and the temperature dependence of the ionization constant of water can be used to determine ${}_kE_w$, and E' can be determined from the experimental data.

Experimental

An apparatus capable of producing ultra-low-conductivity water by means of electrophoretic ion exclusion has been described by the authors in an earlier paper.[6] In the apparatus, an ion-containing solution is recirculated in a closed system through an electric field of 1000 v./cm. maintained between two ion-selective membranes, the cations of the liquid being attracted to the cathode and separated while the anions are separated at the anode. Conductivity measurements in a carefully calibrated conductivity cell at the exit of the purification cell indicate that the ionic impurity content can be reduced to about 0.001 parts per million, considerably below the ionic content calculated for the best conductivity previously reported. The reader is referred to the earlier paper for details of the design and operation of the apparatus as well as for the calibration of the conductivity cell.

The apparatus is equipped with a cooling jacket in order to control the temperature of the circulating water and measure the conductivity as a function of the temperature. In practice, conductivity measurements are made at 0.5° intervals in the range between 12 and 30°. The probable error in the absolute conductivity values obtained at a given temperature is ±0.7%.

On the basis of equation 4, the theoretical conductivity of purest water, k_w, at a given temperature can be determined if we have values for the total apparent activation energy of conduction as a function of conductivity (ionic impurity content). Therefore, it was necessary to make conductivity *vs.* temperature measurements on samples of water with various constant impurity content.

In order to maintain a given impurity content long enough for the conductivity measurements to be made at various temperatures, it was necessary that the rate of ion removal be identical with the small but measurable influx of impurity ions into the water compartment. Since this contamination rate was not controlled or altered easily, we obtained the impurity balance by varying the efficiency of the apparatus.

It has been pointed out in the earlier paper that the limiting conductivity of the water obtained with the apparatus is independent of the operating voltage above 1000 v./cm. However, the minimum obtainable conductivity is dependent on the operating voltage if less than 1000 v./cm. Thus, by operating the apparatus at voltages less than this value, we were able to produce and maintain water with stable conductivities higher than the apparatus normally produces. Starting with distilled water with a conductivity of about 10^{-6} ohm^{-1} cm.$^{-1}$, we were able to obtain water with stable conductivities between 0.17 and 0.06 (10^{-6} ohm^{-1} cm.$^{-1}$) at 25.0°, by applying voltages between 200 and 1000 v./cm.

In order to make sure the purity of the water did not change during the conductivity measurements, the conductivities were measured during an increase in temperature as well as during the drop to the initial temperature (or *vice versa*). We accepted only those experiments in which the initial and final conductivities agreed within 0.5%. Although it generally was not difficult to get the required agreement, the procedure always was used since it was indicative of a constant ion content at a particular temperature of measurement.

Results and Discussion

Representative plots from which the inverse temperature coefficients, $\mathrm{d} \ln k/\mathrm{d}(1/T)$, were obtained are shown in Fig. 1, along with a typical plot of the same type from the data of Kohlrausch and Heydweiller. It should be pointed out that our data are not linear and that the inverse temperature coefficient is inversely related to the temperature. This is expected since the calculated inverse temperature coefficients for pure water have the same property. The non-linearity of the curves is great enough to be detected on reasonably large plots of the data. Since the variability of the data is reasonably small, and the difference in the slopes between 18 and 25° is almost 5%, the data merited a treatment other than that assuming a linear relation. It was found that the curves fitted a quadratic equation of the type $\ln k = A + BT + CT^2$. The values for A, B and C at each purity level are given in Table I. The slopes of the curves were obtained by differentiation of the quadratic equation for each purity level since, $\mathrm{d} \ln k/\mathrm{d}T = (1/k)(\mathrm{d}k/\mathrm{d}T) = B + 2CT$. The activation energies of conduction for each purity level were obtained by multiplying these slopes by RT^2. These activation energies then were plotted against $1/k$ at 18 and 25° as suggested by equation 4 and shown in Fig. 2. (A comparative plot of the calculated activation energies from the data of Kohlrausch and Heyd-

(7) S. Glasstone "An Introduction to Electrochemistry," D. Van Nostrand Co., Inc., New York, N. Y., 1942, p. 62.

TABLE I

ANALYSIS OF CONDUCTIVITY DATA

Experiment	Constants for equation, $\ln k = A + BT + CT^2$			18°			25°		
	A	B	C	k, 10^{-6} ohm^{-1} cm.$^{-1}$	$1/k$	${}_kE$, cal./equiv.	k, 10^{-6} ohm^{-1} cm.$^{-1}$	$1/k$	${}_kE$, cal./equiv.
B4	−48.26141	25.35728	−3.392861	0.0410	24.39	9431	0.0597	16.75	9051
A2	−46.58938	24.26751	−3.214316	.0415	24.10	9346	.0603	16.58	9006
C2	−46.83571	24.46040	−3.250011	.0421	23.75	9321	.0610	16.39	8971
B5	−46.48676	24.23743	−3.214246	.0422	23.70	9296	.0611	16.37	8954
A1	−45.07485	23.34557	−3.071331	.0433	23.09	9195	.0625	16.00	8883
A3	−44.97743	23.31544	−3.071642	.0437	22.88	9144	.0630	15.87	8830
A4	−41.00420	20.95585	−2.714301	.0498	20.08	8673	.0705	14.18	8424
A5	−36.96784	18.57394	−2.355102	.0577	17.33	8184	.0801	12.48	8000

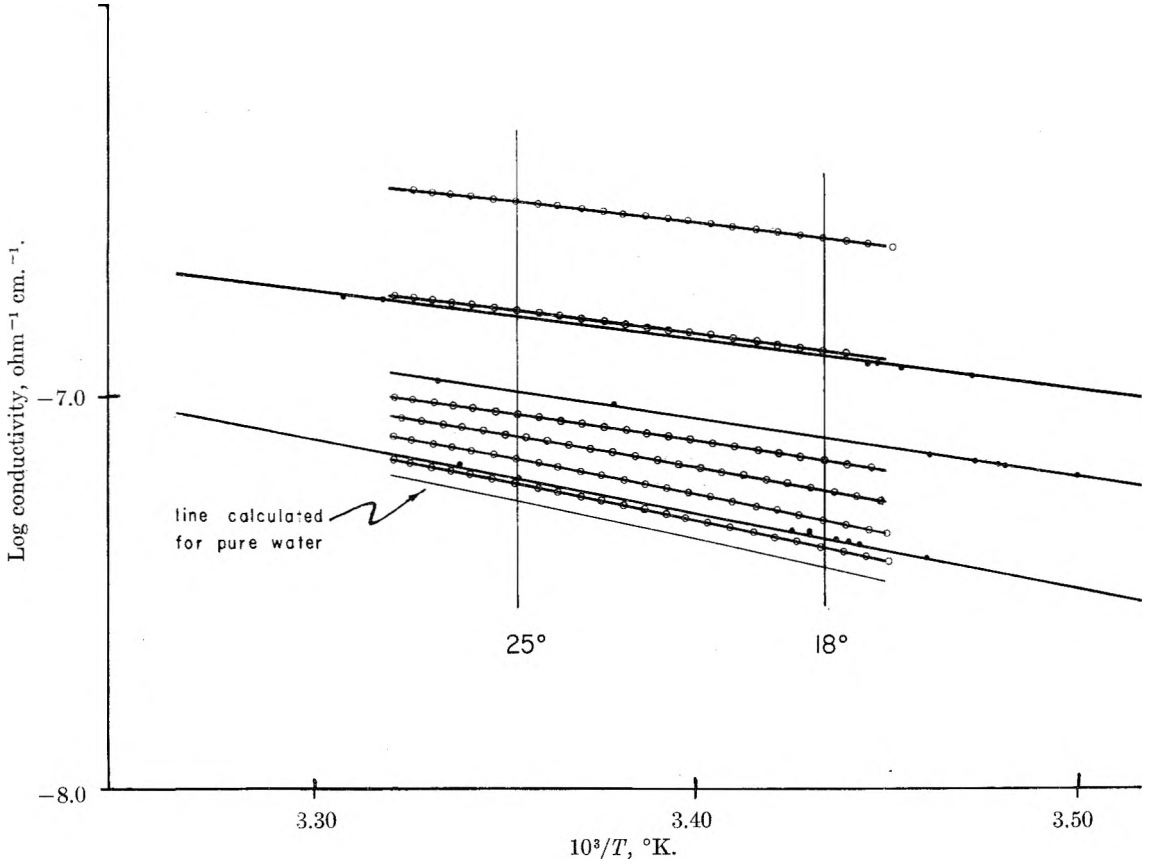

Fig. 1.—Conductivity of water of various purities as a function of $1/T$: ●, data of Kohlrausch and Heydweiller; ○, data from present study.

weiller at 18° also is given). Since the data were linear over the conductivity range tested, the least mean squares line was determined and extrapolated to ${}_kE = {}_kE_w$, the calculated apparent activation energy of conduction for pure water.

The value of ${}_kE_w$ can be calculated from equation 1 if we have values for ${}_xE$ and ${}_\lambda E_w$. Because the dissociation energy of water is a molal energy and the concentration, x, is expressed in equiv./cm.^{3}, a correction must be applied for the expansion of water. If $x = \rho' m$, where m is the molal concentration and ρ' is the weight of 10^{-3} cm.^{3} water, it can be shown that

$$ {}_xE = RT^2 \frac{\mathrm{d} \ln \rho'}{\mathrm{d}T} + RT^2 \frac{\mathrm{d} \ln m}{\mathrm{d}T} = {}_{\rho'}E + {}_mE $$

The molal dissociation energy ${}_mE$ can be obtained from measurements of the molal heat of neutralization of acids and bases. Harned and Owen, however, point out a number of uncertainties inherent in the data on the heats of neutralization.[8] In view of these uncertainties and our above definition of ${}_mE$, we have chosen to use values calculated from the temperature dependence of the dissociation constant, K_w, as given by Harned and Owen.[9] Now $K_w = (m_{H^+})(m_{OH^-})$,

$$ (m_{H^+}) = (m_{OH^-}) = \sqrt{K_w}, \text{ and } RT^2 (\mathrm{d} \ln m/\mathrm{d}T) = RT^2 (\mathrm{d} \ln K_w^{1/2}/\mathrm{d}T) $$

Therefore, since the relation given by Harned and Owen is

(8) H. S. Harned and B. B. Owen, "The Physical Chemistry of Electrolytic Solutions," Reinhold Publ. Corp., New York, N. Y., 1943, pp. 239–241.

(9) Ref. 8, p. 492.

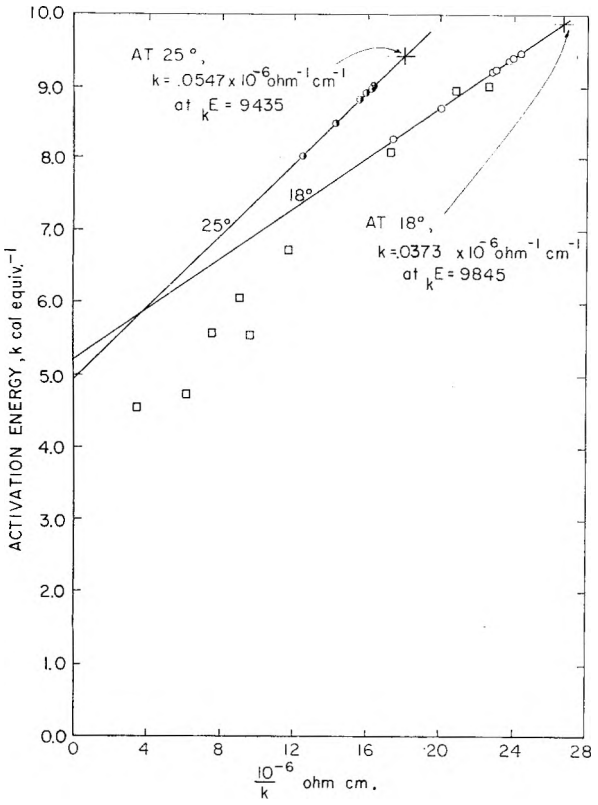

Fig. 2.—Actual dependence of electrolyte concentration (in terms of $1/k$) on the activation energy of conductivity of residual impurities in electrophoretically purified water: ◑, values calculated at 25°; ○, values calculated at 18° (□, values determined from the data of Kohlrausch and Heydweiller at 18°).

$$\log K_w = 35.3944 - 0.0085307T - 11.8261 \log T - \frac{5242.39}{T}$$

$$_mE = RT^2 \frac{d \ln K_w^{1/2}}{dT} = 11994.2 - 11.749T - 0.019516T^2$$

Using this expression we get $_mE$ = 6922 cal./equiv. at 18° and 6755 cal./equiv. at 25°.

The values of $_\rho E$ are determined from tables of density as a function of temperature to be −45 cal./equiv. at 25° and −31 cal./equiv. at 18°. Thus, the resultant values of $_zE$ used in this paper are 6710 cal./equiv. at 25° and 6891 cal./equiv. at 18°.

In order to get the apparent activation energy of mobility, we need accurate data for the equivalent conductance and its temperature dependence since

$$_\lambda E_w = RT^2 \frac{d \ln \lambda_w}{dT} = RT^2 \frac{1}{\lambda_w} \frac{d\lambda_w}{dT}$$

Unfortunately, the values of λ_{OH} (and hence of λ_w) are not known well enough over any sizable temperature range to calculate $d\lambda_w/dT$ accurately. Thus, the energy, $_\lambda E_w$, was determined in two different manners and the average of these values was used to calculate $_kE_w$. In one approximation, it was assumed that λ_w is a linear function of temperature between 18 and 25° and $d\lambda_w/dT$ was determined from the difference of the equivalent conductances at these two temperatures, since the equivalent conductances are known more accurately at these temperatures. Using this value of $d\lambda_w/dT$ and the values of λ_w given in Table II, $_\lambda E_w$ was calculated to be 2935 and 2743 cal. equiv.$^{-1}$ at 18 and 25,° respectively. In another approximation of $_\lambda E_w$, an equation was found to fit the available values of the equivalent conductances from the literature[10] at 10, 18, 25 and 100° (even though there is considerable disagreement on the values for λ_{OH}). The values used were 419, 488.5, 548.1 and 1080 ohm^{-1} cm.^{2} equiv.$^{-1}$ at the respective temperatures. Differentiation of the logarithmic form of the equation gave d ln λ_w/dT from which $_\lambda E_w$ was calculated to be 2972 and 2706 cal. equiv.$^{-1}$ at 18 and 25°, respectively. The average of the above values for $_\lambda E_w$ at 18° is 2954 cal. equiv.$^{-1}$ while at 25° the average is 2725 cal. equiv.$^{-1}$. The uncertainty of these values is not known but is likely to be as large as ± 100 cal.

TABLE II

VALUES USED IN THIS PAPER FOR THE VARIOUS PROPERTIES OF PURE WATER

		Temperature, °C. 18	25	
1	K_w	0.579×10^{-14}	1.008×10^{-14}	
2	$K_w^{1/2}$ (= m)	0.761×10^{-7}	1.004×10^{-7}	equiv. / 1000 g. water
3	$10^3\rho'$ (= ρ)	0.998595	0.997044	g./cm.^{3}
4	λ_H	315.5	349.8	ohm^{-1} cm.^{2} equiv.$^{-1}$
5	λ_{OH}	173	198.3	ohm^{-1} cm.^{2} equiv.$^{-1}$
6	$\lambda_w = \lambda_H + \lambda_{OH}$	488.5	548.1	ohm^{-1} cm.^{2} equiv.$^{-1}$
7	$_\lambda E_w$	2954	2725	cal. equiv.$^{-1}$
8	$_zE$	6891	6710	cal. equiv.$^{-1}$
9	$_kE_w$	9845	9435	cal. equiv.$^{-1}$

The values of k_w determined by the extrapolation in Fig. 2 are subject to the error in the determination of $_kE_w$ as indicated above, and thus make the following determination of the theoretical conductivity subject to an error estimated to be ± 2%. At 25° the least mean squares line through our data has a slope of 246.07 and an ordinate intercept of 4932, as shown in Fig. 2. Using equation 4 we calculate k_w to be 0.0547×10^{-6} ohm^{-1} cm^{-1}. At 18° the slope is 174.47 and the intercept is 5163 so that $k_w = 0.0373 \times 10^{-6}$ ohm^{-1} cm.$^{-1}$. (On the basis of their conductivity values, Kohlrausch and Heydweiller[2] predicted the conductivity of purest water to be 0.0384×10^{-6} ohm^{-1} cm.$^{-1}$ at 18° and 0.0569×10^{-6} ohm^{-1} cm.$^{-1}$ at 25°, values which are about 3% higher than those obtained in this study.

Thus, we have been able to calculate the theoretical conductivity of pure water from the above conductivity data, the temperature dependences of the equivalent conductance of the ions, the density and the dissociation constant. Another method of calculating the conductivity of purest water is to use the absolute values of the equivalent conductances of the H^+ and OH^- ions, the density and the dissociation constant, since

$$k = (\lambda_H + \lambda_{OH})\rho' m$$

where ρ', the weight of 10^{-3} cm.^{3} water, is used to convert the molal concentration, m, (in which the

(10) (a) R. A. Robinson and R. H. Stokes, "Electrolyte Solutions," 2nd Edition, Academic Press, Inc., New York, N. Y., 1959; (b) H. R. Raikes, A. F. Yorke and F. K. Ewart, *J. Chem. Soc.*, 630 (1926); (c) L. S. Darken, H. F. Meier, *J. Am. Chem. Soc.*, **64**, 621 (1942); (d) V. Sivertz, R. E. Reitmeier and H. V. Tartar, *ibid.*, **62**, 1379 (1940); (e) J. Johnston, *ibid.*, **31**, 1010 (1909); (f) F. Kohlrausch, *Wied. Ann.*, **66**, 785 (1898).

dissociation constant generally is given) to units of equivalents/cm.^{3}. Using the values of these parameters given in Table I, we calculate the conductivity of purest water to be 0.0371×10^{-6} ohm^{-1} cm.$^{-1}$ at 18° and 0.0549×10^{-6} ohm^{-1} cm.$^{-1}$ at 25°, subject to the error in the measurement of the parameters used. These values agree very favorably with the values we have obtained in this study.

In view of the above agreement (within the range of experimental error), we conclude that the dissociation equilibrium constant which could be calculated from these conductivity data is not significantly different from the values obtained from e.m.f. measurements given in Table I.

Conclusion

The theoretical conductivity of the pure substance water has been determined from conductivity data to be 0.0373×10^{-6} ohm^{-1} cm.$^{-1}$ at 18° and 0.0547×10^{-6} ohm^{-1} cm.$^{-1}$ at 25°, with an estimated accuracy of 2%. While the values are about 3% lower than predicted by Kohlrausch and Heydweiller 60 years ago, they agree with the theoretical conductivity calculated from the equivalent conductance of the ions, the density and the dissociation constant of water determined by e.m.f. measurements of galvanic cells. The dissociation equilibrium constants calculated from the above determined theoretical conductivities at 18 and 25° thus are in agreement with those determined by e.m.f. measurements. Within the limits imposed by the lack of knowledge on the equivalent conductivities of the OH^- ion, this clears up a discrepancy which has existed in the literature between the values obtained by the conductance and e.m.f. methods.

THE RECOMBINATION OF ATOMIC HYDROGEN IN PROPANE FLAME GASES

BY ROBERT MCANDREW AND ROBERT WHEELER

Department of Chemistry, Queen's University, Kingston, Ontario

Received June 26, 1961

A technique has been devised to allow additions of CO_2, N_2 or SO_2 to be made to a propane–air flame burning at 2080°K. such that the partial pressure of the additive alone was changed in the burnt gases. While small fuel–air adjustments were made, particular attention was directed toward maintaining the temperature and also [OH] = [H] at final equilibrium. Excessively high concentrations of atomic hydrogen were observed by a photometric method in the region just above the hot boundary and the decay of these excesses was followed in the burnt gases. This decay may be attributed to three-body collisions and ternary rate constants were estimated at the single temperature 2080°K. as follows: $k_{(H_2O)} = 4.1 \times 10^{-31}$, $k_{(CO_2)} = 3.2 \times 10^{-31}$, $k_{(SO_2)} = 1.1 \times 10^{-29}$, $k_{(N_2)} \sim 6 \times 10^{-32}$, all units in cm.^{6} molecules^{-2} sec.$^{-1}$.

Introduction

Recently, some measurements in this Laboratory have suggested that hydrogen atoms may be generated in excess concentrations in the burning of certain propane–air mixtures at atmospheric pressure.[1] Bulewicz, James and Sugden[2] and also Kaskan[3] have shown that a system of fast bimolecular exchange reactions between free radicals and the molecules of the burnt gases will quickly transform excesses of any one member of the group OH, H and O into corresponding excesses of the others. Two reactions

$$H + H_2O \rightleftharpoons H_2 + OH \qquad (1)$$

$$H + CO_2 \rightleftharpoons CO + OH \qquad (2)$$

will be important in bringing OH and H to a state of quasi-equilibrium where, at least by the time the burnt gas region is reached

$$\frac{[H]}{[H]_e} = \frac{[OH]}{[OH]_e} \qquad (3)$$

the subscript e denoting the final equilibrium value. A similar ratio will exist for $[O]^{1/2}$. All that the system of bimolecular reactions can do is to exchange unpaired electrons. None can bring an abnormal, or for that matter a subnormal concentration in the free radical gas to its final equilibrium value. Furthermore, as recombination processes at a surface are not available, only infrequent three-body collisions in the thermal zone of the flame can fully equilibrate the free radical concentrations.

Fuel-rich flames tend to have $[OH]_e$ and $[H]_e$ much larger than $[O]_e$ and if equation 3 holds, the decay of excesses on this side of stoichiometry must obtain primarily by the direct removal of OH or H. These reactions may be put down in two forms, one involving an over-all physical (p) and the other chemical (c) third-body activity.

$$H + H + X \longrightarrow H_2 + X \qquad (4p)$$

$$H + H + ZO_n \longrightarrow H_2O + ZO_{n-1} \qquad (4c)$$

$$H + OH + X \longrightarrow H_2O + X \qquad (5p)$$

$$H + OH + ZO_n \longrightarrow H_2 + ZO_{n+1} \qquad (5c)$$

$$OH + OH + ZO_n \longrightarrow H_2O + ZO_{n+1} \qquad (6c)$$

The efficiencies should be in the order 6>5>4, owing to the increase in the collision diameters involved. Hydrogen flames are perhaps the least complex examples and rich mixtures will produce mainly H_2O and H_2 (and N_2 if air is the oxidant) as the important third-bodies. Hydrocarbon–air flames give fairly similar quantities of H_2O, H_2 and N_2, with the addition of moderately large quantities of CO_2 and CO also likely to be important in recombination.

This paper reports some detailed measurements of [H] that have been made in propane–air mix-

(1) R. Reid and R. Wheeler, *J. Phys. Chem.*, **65**, 527 (1961).

(2) E. M. Bulewicz, C. G. James and T. M. Sugden, *Proc. Roy. Soc.* (London), **A235**, 89 (1956).

(3) W. E. Kaskan, *Combustion and Flame*, **3**, 49 (1959).

tures burning to a single temperature of 2080°K. Abnormal [H] have been noted in the burnt gases and our attention has been directed towards following the decay of these excesses in an almost purely thermal zone.

Experimental

The experimental technique was almost identical with that reported by Reid and Wheeler. Here was used a shielded, pre-mixed, propane–air flame on a rather smaller Mèker burner than previously, its diameter being 3.5 cm. To the very central column of gases only, very small but equal amounts of lithium and sodium salts were added by atomization. The flames generally were designed to burn with as little vertical temperature gradient as possible (one reason for the shielding). Temperatures on the central axis of the flame were measured visually by the sodium-D-line reversal method using a tungsten strip filament background source.[4] Comparisons were made at several points on the flame axis of the intensity ratio, lithium red lines/sodium-D-lines, which is sufficient to determine [H] at each point as first shown by Sugden and co-workers.[2] The intensity measurements were made photometrically through a small glass-prismed monochromator constructed in this Laboratory. Attention was confined to the region some millimeters above the burner top where the balance of the reaction

$$Li + H_2O \rightleftharpoons LiOH + H \qquad (7)$$

is assumed to be complete. Reaction 7 accounts for the observed reduction in the line intensity ratio from unity. Knowing the equilibrium constant for the reaction, then [H] $= (K_7[H_2O][Li])/[LiOH]$. The measured intensity ratio is directly related to [Li]/[LiOH] through an instrument factor, and the partial pressure of steam may be calculated from the flame composition. The distance above the burner top was converted to a corresponding time scale by a calculation of the vertical flow rate of the hot expanded gases. A knowledge of the pre-burnt flow rate, initial temperature, final flame temperature and the *measured* flame diameter gives sufficiently accurate results for our purposes.[1]

Results and Discussion

If only reactions 4, 5 and 6 are important in the removal of abnormal concentrations, then the integrated expression for the final equilibration of [H] with time is

$$\ln \left\{ \frac{[H] + [H]_e}{[H] - [H]_e} \right\} = 2at + \text{a constant} \qquad (8)$$

where the parameter a, constant in any one flame is

$$a = \frac{2\{(k_{4p} + k_{4c}) + (k_{5p} + k_{5c})\theta + k_{6c}\theta^2\}}{1 + \theta} \qquad (9)$$

$$\text{and } \theta = \frac{[OH]_e}{[H]_e} = K_1 \frac{[H_2O]}{[H_2]}; \text{ where } K_1 = \frac{[H_2][OH]}{[H_2O][H]} \qquad (10)$$

The apparent second-order constants k_4, k_5 and k_6 include the concentrations of third-bodies.

Taking rich hydrogen–air flames as the simplest case, only H_2O need be considered an important recombination center. In the combination of iodine atoms, Russell and Simons[5] estimate the efficiency of H_2O to be 10 times greater than that of either N_2 or H_2. Furthermore reaction 6 can be ruled out if the over-all efficiency of H_2 is low or if θ is very small (as is the case in fuel-rich flames, both hydrogen and hydrocarbon). Bulewicz and Sugden[6] successfully treated the termolecular scheme by designing a set of hydrogen–air mixtures which burned to the same temperature but different values of the ratio θ. By plotting the numerator of a against θ (neglecting reaction 6 and therefore any θ^2 term in a), they deduced values of k_4 and k_{5p} attributed to steam as the third-body.

In hydrocarbon flames, k_4 and k_{5p} also will include terms involving CO_2 and perhaps CO. CO_2 might be expected to act in much the same manner and with similar efficiency as H_2O. CO, although diatomic, might assist the recombination significantly through chemical action in reactions 6 and 5c. H_2 itself might be important (mainly through 6c) in flames more oxygen-rich where θ is larger and can be greater than unity. This latter effect might be detectable in H_2 flames near stoichiometry as a departure from linearity in the above plot.

There are practical difficulties in making these photometric measurements in the oxygen-rich flames. These burn generally as short, sharply-pointed cones with rather steep vertical temperature gradients. On our small burner, it was impossible to design a set of mixtures which could be burned with the desired isothermicity over a fairly wide range in θ and yet at relatively high values of θ, say unity or greater. This precluded for the present any tests of the influence of CO or H_2. What was possible was to operate with a base flame of mixture (propane/stoichiometric propane) = 1.16 which burned at 2080°K. with the final condition $[OH]_e = [H]_e$ or $\theta = 1$. The parameter a then reduces directly to

$$a = k_{4p} + k_{4c} + k_{5p} + k_{5c} + k_{6c} \qquad (11)$$

Each constant in equation 11 is itself composite and depends on the concentrations of the various third-bodies. Even making reasonable assumptions as to the importance of each (H_2O and CO_2 in reactions 4 and 5p, CO and H_2 in 5c, 6c and perhaps 4c), the complete elucidation of the resulting 11 ternary velocity constants presents a formidable problem. However, in this particular base flame with $\theta = 1$ it was feasible to make small individual additions and hence changes in the concentrations of the product gases while the others remained essentially constant. Only minor fuel–air adjustments were necessary to maintain the composition of the other gases, the temperature and the condition $[OH]_e = [H]_e$. Some terms in equation 11 therefore could be separated at this particular temperature, 2080°K.

Flames with Added SO_2.—Very small quantities of SO_2 were metered into the very center of the flame. This was primarily a test to confirm the existence of abnormal [H]. At any one point on the flame axis, it was evident that even the smallest addition would lower the intensity of the lithium red lines while having no effect on that of the D-lines. Furthermore, the decay of [H] up the flame axis was followed to the same constant steady state value, $[H]_e$, found in the pure base flame. Excessively high concentrations then must flow from the hot boundary into the burnt gas region in these mixtures.

The influence of SO_2 in the subsequent recombination is of interest. For these small excesses in [H], $[H]_e$ also was measured and log $\{([H] + [H]_e)/$

(4) A. G. Gaydon and H. G. Wolfhard, "Flames, Their Structure, Radiation and Temperature," Chapman and Hall, London, 1960.

(5) K. E. Russell and J. Simons, *Proc. Roy. Soc.* (London), **A217**, 271 (1953).

(6) E. M. Bulewicz and T. M. Sugden, *Trans. Faraday Soc.*, **54**, 1855 (1958).

$([H] - [H]_e)\}$ plotted against time after leaving the burner top. This should be a straight line of slope $0.868a[H]_e$. Figure 1 shows the quite good linearity observed for the base flame and 5 others, each with a constant addition of SO_2. The volume additions are indicated as a per cent. on each line. For the base flame, $a = 3.2 \times 10^{-13}$ cm.^{3} molecule^{-1} sec.$^{-1}$ and there is a progressive increase from this as the SO_2 added is raised. Moreover, this increase is quite linear with the quantities of SO_2 added here. Although the measurements were made in the flame gases well past the hot boundary and the SO_2 admixed had ample opportunity to form such radicals as S, SO, etc., it is evident from the linearity in the parameter increase that the acceleration of the recombination rate in the burnt gases is not overduly influenced by dimers such as S_2 or polymeric forms. SO_2 being large and quite stable should be the most important form, acting mainly through reaction 6c. In addition Dooley and Whittingham[7] have shown that the percentage oxidation of SO_2 to SO_3 is lowest in pure hydrocarbon flames. On this basis, a ternary rate constant $k_{6c}(SO_2) = 1.1 \times 10^{29}$ cm.^{6} molecules^{-2} sec.$^{-1}$ at 2080°K. is estimated from the increase in a. This is some 20 times larger than the constant for H_2O measured in H_2 flames at the same temperature[6-8] (also see later).

Flames with Added CO_2.—A calculation of the burnt gas composition of the base flame showed that $[CO_2] = 8.6 \times 10^{-2}$, $[CO] = 4.3 \times 10^{-2}$ atm. expressed as partial pressures. Moreover, calculations showed that it was possible to nearly double the CO_2 pressure by making additions to the burner supply before the pressure of CO increased significantly. These additions were small (up to 4 volume %) and were made to the whole burner area. Adjustments in mixture to maintain θ and the temperature were small, although if continued additions of CO_2 were made both θ and the ratio $[CO]/[CO_2]$ began to rise rapidly (see the upward curvature in Fig. 2). The recombination was followed and a measured, an increase again being noted but of much smaller magnitude. Figure 2 shows the rate of increase in a as the final partial pressure of CO_2 is raised. The elevation of a can be expressed solely in terms of the increase in $[CO]_2$ as

$$\Delta a = \Delta[CO_2]\{k_{4p}(CO_2) + k_{4c}(CO_2) + k_{5p}(CO_2)\} \quad (12)$$

where the constants are now in ternary units. With steam the major third-body in H_2 flames, Bulewicz and Sugden[6] measure a ratio $k_{5p}(H_2O)/k_4(H_2O) \sim 24$ and in addition a value for $k_{5p}(H_2O)$ of 5.3×10^{-31} cm.^{6} molecules^{-2} sec.$^{-1}$ at 2085°K. If the majority increase in a is attributed to reaction 5, then $k_{5p}(CO_2) = 3.2 \times 10^{-31}$ cm.^{6} molecules^{-2} sec.$^{-1}$ from the slope in Fig. 2. This is somewhat lower than Bulewicz's and Sugden's value for H_2O but it is indeed larger than the efficiency CO_2 shows in the low-temperature combination of iodine atoms. For $I + I + X \rightarrow I_2 + X$ at room temperatures, the ternary constants

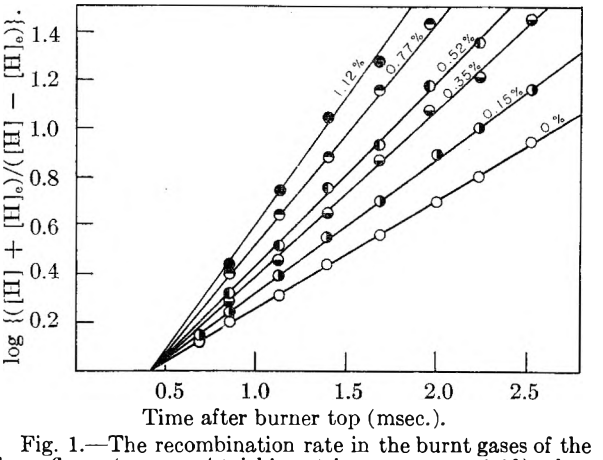

Fig. 1.—The recombination rate in the burnt gases of the base flame (propane/stoichiometric propane = 1.16) when pure and also when additions of SO_2 (indicated as a volume per cent.) have been made. $T = 2080$°K.

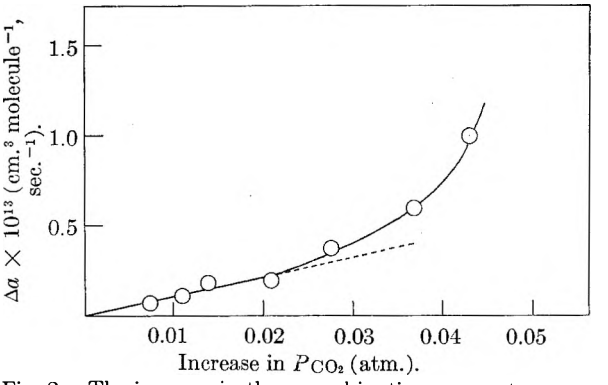

Fig. 2.—The increase in the recombination parameter, a, as the partial pressure of CO_2 is raised, $T = 2080$°K.

measured[5,9] show a ratio $CO_2:N_2$ of only 3 while $H_2O:N_2 = 10$. However, in some studies of the quenching of candoluminescence in H_2 flames, Arthur and Townend[10] have found CO_2 to be more effective. For the third-body removal of H in these flames, they estimate an average volume efficiency of the order $CO_2:N_2 \sim 6$ while $CO_2:CO \sim 2.5$. These temperatures were of course similar to ours and the results are roughly in agreement.

It is possible to make a rather less accurate estimate of the ternary constant for H_2O in this propane flame if the contribution due to CO_2 is subtracted from the value of a measured in the base flame (3.2×10^{-13} cm.^{3} molecules^{-1} sec.$^{-1}$), *i.e.*, attributing all third-body activity to H_2O and CO_2. Using the calculated values, $[CO_2] = 8.6 \times 10^{-2}$ atm., $[H_2O] = 0.156$ atm., this results in $k_{5p}(H_2O) = 4.1 \times 10^{-31}$ cm.^{6} molecule^{-2} sec.$^{-1}$ at 2080°K., this being slightly less than the H_2 flame value above.

Flames with Added N_2.—So far no direct measurements of the ternary rate constants for any of the diatomic gases have been made in these flames. The partial pressure of N_2 in the base flame was high (~0.7 atm.), but using this additive technique we were successful in raising this some 5 to 6%

(7) A. Dooley and G. Whittingham, *Trans. Faraday Soc.*, **42**, 354 (1946).

(8) P. J. Padley and T. M. Sugden, *Proc. Roy. Soc.* (London), **A248**, 248 (1958).

(9) D. L. Bunker and N. Davidson, *J. Am. Chem. Soc.*, **80**, 5090 (1958).

(10) J. R. Arthur and D. T. A. Townend, Natl. Bur. Standards Circular 523, Energy Transfer in Hot Gases, p. 99, 1954.

before it became difficult to compensate the falling temperature and yet maintain a constant θ. When N_2 was added, the base flame did show a barely detectable increase in a. If this is due to an increase in reaction 5 owing to the elevation of $[N_2]$ in the flame, it is estimated $k_{5p(N_2)} \sim 6 \times 10^{-32}$ cm.^{6} molecule^{-2} sec.$^{-1}$ and the ratio $k_{5p(H_2O)}/k_{5p(N_2)}$ is approximately 7, which is of the same order as that measured in the low-temperature iodine atom studies.

This technique shows some promise of at least partial separation of the many ternary constants involved in hydrocarbon flames such as this and more useful information will follow from a study over a reasonable range of temperatures. Flames near stoichiometry where $\theta > 1$ on a properly designed burner are interesting as some measurements might be made for H_2 and CO directly. We are grateful to the National Research Council of Canada for a grant in aid of this research.

THE DOUBLET NATURE OF THE ALDEHYDIC C–H STRETCHING VIBRATION

BY ELEANOR L. SAIER, LAUREN R. COUSINS AND MICHAEL R. BASILA

Gulf Research and Development Co., Pittsburgh, Penna.

Received June 30, 1961

New evidence is reported in support of the hypothesis that the characteristic doublet which occurs in the 2700–2850 cm.$^{-1}$ region for most aldehydes is the result of a Fermi resonance interaction between the aldehydic C–H stretching fundamental and the first overtone of the aldehydic C–H bending vibrations. Part of this evidence was derived from a study of the spectra of a series of chloroacetaldehydes. In this series, it is shown that the occurrence of the characteristic doublet is coincident with a value of the overtone of the aldehydic C–H bending frequency which is in the correct position for interaction with the unperturbed aldehydic C–H stretching frequency. The other evidence is derived from the comparison of the observed aldehydic C–H bending frequencies in a series of *para*-substituted benzaldehydes with values calculated using the experimental frequencies and integrated intensities of the two doublet bands.

Introduction

It is well known that a large number of aldehydes, both aromatic and aliphatic, have two prominent infrared absorption bands in the 2700–2850 cm.$^{-1}$ region. The assignment of these bands has been the subject of several studies in recent years.[1-4]

A single aldehydic C–H stretching vibration is expected, hence a problem exists in choosing one or the other of these bands as this fundamental. Fermi resonance[5] involving the C–H stretching vibration has been suggested as a source of this doublet, presenting the additional problem of the assignment of the proper resonance partner.

Pozefsky and Coggeshall[1] originally suggested that the two infrared bands observed for aldehydes in carbon tetrachloride solution were the result of a Fermi resonance between the aldehydic C–H stretching vibration and an overtone or combination band of the same symmetry. They tentatively chose the overtone of the 1380 cm.$^{-1}$ methyl symmetrical bending vibration as the partner in the resonance. In making the choice, however, they noted that benzaldehyde, which has no methyl group, also exhibited these characteristic bands. Subsequently, Pinchas[2] published a study of twenty-seven aldehydes, all of which exhibited this characteristic doublet. He assigned the lower frequency band, centered at approximately 2720 cm.$^{-1}$, to the aldehydic C–H stretching vibration, and the higher band, at approximately 2820 cm.$^{-1}$, to the first overtone of the aldehydic in-plane C–H bending vibration.

The work of Pinchas[2] was followed by the interesting paper of Eggers and Lingren.[3] They reported a study of four monodeuterated aldehydes with the deuterium atom replacing the aldehydic hydrogen. Upon deuteration, both bands in the 2700–2850 cm.$^{-1}$ region and one in the 1400 cm.$^{-1}$ region disappeared. Two new bands appeared in the C–D stretching region and one in the C–D bending region. Their interpretation was that the two bands in the 2700–2850 cm.$^{-1}$ region were produced by a Fermi resonance between the fundamental aldehydic C–H stretching vibration and the first overtone of the aldehydic C–H bending vibration. They pointed out that the Fermi resonance persists in the monodeuterated aldehydes. These results seem rather conclusive. However, Pinchas[4] has reiterated his view that the lower of the two bands is the aldehydic C–H stretching vibration and has changed his assignment of the higher frequency band to that of a combination between the 1380–1390 and 1455–1470 cm.$^{-1}$ bands.

All of the work cited above has been concerned with the infrared spectra of aldehydes in solution, with carbon tetrachloride the solvent in most cases. Furthermore, these papers were essentially studies of the aldehydic group frequencies in a variety of molecules, rather than the vibrational assignment of a specific molecule. During this period, the vibrational assignment of acetaldehyde had been the subject of several papers.[6-9] These studies were concerned with the infrared spectra in the

(1) A. Pozefsky and N. D. Coggeshall, *Anal. Chem.*, **23**, 1611 (1951).
(2) S. Pinchas, *ibid.*, **27**, 2 (1955).
(3) D. F. Eggers and W. E. Lingren, *ibid.*, **28**, 1328 (1956).
(4) S. Pinchas, *ibid.*, **29**, 334 (1957).
(5) E. Fermi, *Z. Physik*, **71**, 250 (1931).
(6) H. W. Thompson and G. P. Harris, *Trans. Faraday Soc.*, **38**, 37 (1942).
(7) J. C. Morris, *J. Chem. Phys.*, **11**, 230 (1943).
(8) K. S. Pitzer and W. Weltner, *J. Am. Chem. Soc.*, **71**, 2842 (1949).
(9) J. C. Evans and H. J. Bernstein, *Can. J. Chem.*, **34**, 1083 (1956).

vapor and solid states and the Raman spectra in the liquid state of acetaldehyde and its deuterium analogs. The most recent of these studies, that of Evans and Bernstein,[9] contains the most complete assignment of acetaldehyde, and also acetaldehyde-d_1. These authors have shown that both compounds exhibit two strong bands in the respective aldehydic C–H or C–D stretching regions and have interpreted these doublets as due to Fermi resonance involving the fundamental stretching vibration. Their assignment of the other partner in the resonance is uncertain, although they point out that in acetaldehyde the first overtone of the aldehydic in-plane C–H bending vibration is a good possibility. The methyl symmetrical bending vibration also is suggested as a possibility. In acetaldehyde-d_1, however, the situation is more complicated due to the possibility of two alternate assignments. The first would assign the resonance partner as the first overtone of a combination band. The alternate assignment suggests the first overtone of the in-plane aldehydic C–D bending vibration as the resonance partner.

In this Laboratory the problem has been approached from two standpoints. In the first, the spectra of a series of substituted acetaldehydes with the substituent, chlorine, replacing one or more of the methyl hydrogens were obtained. The substitution of heavy, polar, chlorine atoms for the methyl hydrogens produces small changes in the aldehydic C–H stretching and bending force constants through mass and/or inductive effects. The effects of these force constant variations upon the characteristic doublet were studied. In the second approach, the frequencies and integrated absorption coefficients of each of the bands in the characteristic doublet were measured for a series of substituted benzaldehydes. These data were used to calculate the aldehydic C–H in-plane bending frequency (assuming it to be the resonance partner). The calculated values were compared with values which had been assigned previously. The results of these studies support the hypothesis that the characteristic aldehydic doublet is produced by a Fermi resonance involving the aldehydic C–H stretching fundamental and the first overtone of the aldehydic C–H bending vibration.

Experimental

The data were obtained with a Perkin–Elmer Model 21 spectrophotometer. Lithium fluoride and sodium chloride prisms were used in the appropriate spectral regions. The wave length scale was expanded from the normal 5 to 50 cm./μ in order to provide a larger area for the integrated absorption coefficient determinations. The spectral slit widths were approximately 2.0 and 2.5 cm.$^{-1}$ in the 2750 and 1400 cm.$^{-1}$ regions, respectively.

The aldehydes were of the highest purity available and in several cases were redistilled. All the intensity measurements were made in solution. The solvent was Fisher Certified Reagent grade carbon tetrachloride. The cell used for the intensity measurements was fitted with sodium chloride windows and had an optical path length of 14 mm. The aldehyde concentrations varied between 2×10^{-3} and 8×10^{-3} moles/l.

The frequencies in the 1400 cm.$^{-1}$ region were obtained, where possible, from the pure liquid spectrum. Otherwise, carbon tetrachloride solutions supplemented with mineral oil mulls were used. The frequencies quoted are the solution values. The uncertainty in the frequency measurements is of the order of $\pm$ 5 cm.$^{-1}$.

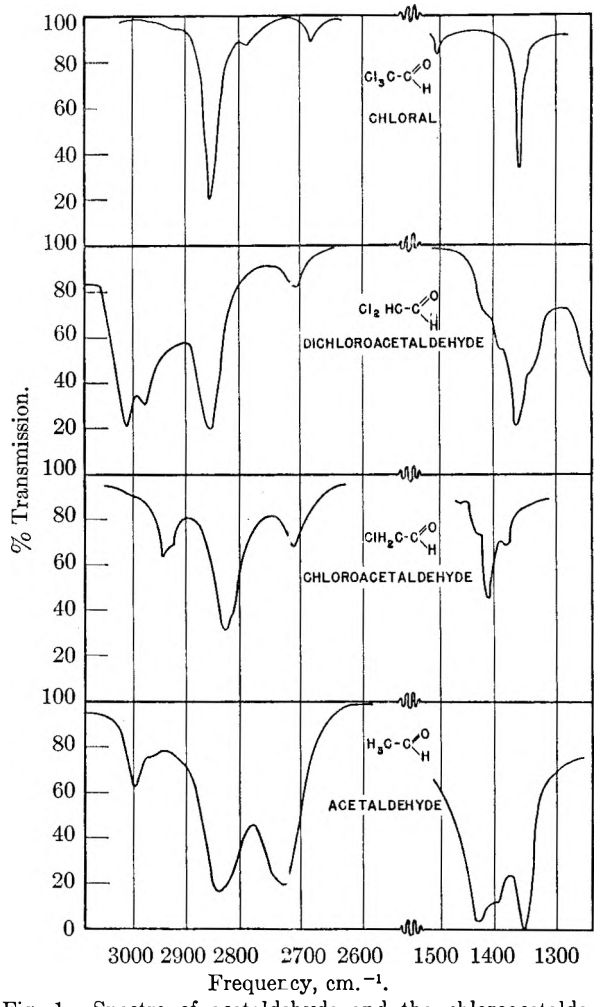

Fig. 1.—Spectra of acetaldehyde and the chloroacetaldehydes in the C–H stretching and bending regions.

The intensities of the characteristic aldehydic doublet were expressed as a ratio of the integrated absorbance of the higher frequency band to that of the lower frequency band. In practically all of the spectra, weak bands due to overtones and combinations also occurred in the region of interest. These necessarily were included in the integration. However, their inclusion should not cause large errors in the estimates of the ratios. In some cases it was necessary to arbitrarily decide where the dividing line between bands should be placed. Again, however we feel that the errors introduced are not excessively large and that the estimates of the relative intensities of the two bands are of suitable accuracy for our purposes.

Results and Discussion

Substituted Acetaldehydes.—The spectra in the C–H stretching and bending regions of acetaldehyde, monochloroacetaldehyde, dichloroacetaldehyde and chloral are given in Fig. 1. The frequencies of the characteristic doublet and the assigned in-plane C–H bending frequencies are given in Table I. Values obtained for bromal, which has essentially the same spectrum as chloral in the regions of interest, also are included in Table I.

Inspection of Fig. 1 and Table 1 reveals that the characteristic aldehydic doublet in the 2700–2850 cm.$^{-1}$ region is missing in the spectra of chloral, bromal and dichloroacetaldehyde, and is present in the spectra of acetaldehyde and monochloroacetaldehyde. This is explained if one assumes that

Table I

Aldehydic C–H Frequencies in Substituted Acetaldehydes[a]

Aldehyde	C–H stretching frequency (cm.$^{-1}$)	C–H bending frequency (cm.$^{-1}$)	Overtone bending frequency (cm.$^{-1}$) Calcd.	Obsd.
Chloral	2850(s)	1358(s)	2716	2681(w)
Bromal	2850(s)	1355(s)	2710	2670(w)
Dichloroacetaldehyde	2850(s)	1375(s)	2750	2706(w)
Monochloroacetaldehyde	2825(s) and 2710(m)	1385(m)	2770	
Acetaldehyde	2839(s) and 2724(m)	1400(m)	2800	

[a] The letters in parentheses indicate the intensity of the band, *viz.*, s = strong; m = medium; w = weak.

the doublet is produced by a Fermi resonance between the aldehydic C–H stretching and the overtone of the aldehydic C–H bending vibrations.

Looking at chloral and bromal first, it is obvious that the separation between the bending overtone and fundamental stretching vibrations (169 cm.$^{-1}$ for chloral) is prohibitively large and no resonance can occur. This is also the case for dichloroacetaldehyde. In monochloroacetaldehyde, on the other hand, the band at 2710 cm.$^{-1}$ is too strong to be a simple overtone and in acetaldehyde the doublet is very prominent, the bands being of almost equal intensity. The unperturbed stretching frequency should fall near the center of the interval defined by the two bands of the doublet, *i.e.*, 2782 and 2768 cm.$^{-1}$ for acetaldehyde and monochloroacetaldehyde, respectively. From the assigned bending fundamentals, the overtones are estimated to appear slightly lower than 2800 and 2770 cm.$^{-1}$, respectively. The overtones of acetaldehyde and monochloroacetaldehyde, therefore, are close enough for the resonance interaction to take place. Thus, in chloral, bromal and dichloroacetaldehyde, where there is apparently no resonance, the bending overtone and stretching fundamental are widely separated. However, in acetaldehyde and monochloroacetaldehyde, where resonance does occur, the bending overtone and unperturbed stretching fundamental are close together. The possibility that one of the other C–H bending modes is the resonance partner in acetaldehyde or monochloroacetaldehyde is ruled out because the overtone would not be close enough to the unperturbed stretching frequency. The fact that the resonance persists after the aldehydic hydrogen is replaced by deuterium[3,9] also rules out other C–H modes and, in addition, combination bands which might fall in the proper frequency range.

Aromatic Aldehydes.—Evidence of a different nature is provided by a study of the frequencies and intensities of the characteristic aldehydic doublet for a series of *para*-substituted benzaldehydes in carbon tetrachloride solution. The purpose of this study was to calculate the aldehydic in-plane C–H bending frequency from the experimental doublet frequencies and intensities. This is done by assuming that the overtone of this bending vibration was the resonance partner which is interacting with the aldehydic C–H stretching fundamental to produce the characteristic doublet. These calculated bending frequencies then are compared with the values assigned by inspection of the spectra.

The frequencies and relative intensities of the characteristic aldehydic doublet for a series of substituted benzaldehydes, measured in carbon tetrachloride solution, are given in Table II.

Table II

Frequencies and Relative Intensities of the Characteristic Doublet in the Aldehydic Stretching Region

Aldehyde	A_H/A_L[a]	ν_H, cm.$^{-1}$	ν_L, cm.$^{-1}$
Benzaldehyde	1.07	2805	2726
p-Nitrobenzaldehyde	1.92	2817	2722
p-Bromobenzaldehyde	1.32	2828	2729
p-Chlorobenzaldehyde	1.35	2825	2723
p-Tolualdehyde	1.27	2817	2729
p-Hydroxybenzaldehyde	1.04	2804	2729
p-Methoxybenzaldehyde	1.21	2840	2732
p-Dimethylaminobenzaldehyde	1.27	2817	2732

[a] The letter A denotes the integrated absorption coefficient and the subscripts H and L denote the high frequency and low frequency bands, respectively.

Spectra of these aldehydes also were obtained in the 1300–1500 cm.$^{-1}$ region. In most cases it was possible to assign, with a fair degree of certainty, the band due to the aldehydic C–H bending vibration. These frequencies are given in Table III. The assignments were made by comparison with the assignments of substituted benzenes in the literature. The principal guides were the work of Jakobsen[10] on the assignments of a series of *para*-substituted phenols, and the work of Eggers and Lingren.[3]

Table III

Observed and Calculated Aldehydic C–H Bending Frequencies

Aldehyde	(Obsd.) (cm.$^{-1}$)	(Calcd.) (cm.$^{-1}$)
Benzaldehyde	1392	1382
p-Nitrobenzaldehyde	1419	1376
p-Bromobenzaldehyde	1411	1386
p-Chlorobenzaldehyde	1412	1383
p-Tolualdehyde	1417	1384
p-Hydroxybenzaldehyde	1400	1383
p-Methoxybenzaldehyde	1429(1393)[a]	1391
p-Dimethylaminobenzaldehyde	1417	1383
Average	1412	1384

[a] Either of these bands could be assigned to the bending frequency.

It can be shown[11] that the zero-order separation, δ, of the two vibrational levels participating in a Fermi resonance interaction can be calculated by the equation

$$\delta = \nu_H^0 - \nu_L^0 = \left(\frac{\gamma - 1}{\gamma + 1}\right)(\nu_H - \nu_L) \qquad (1)$$

(10) R. J. Jakobsen, WADD Technical Report 60-204 (1960).
(11) See, for example, R. N. Dixon, *J. Chem. Phys.*, **31**, 258 (1959).

where ν_H and ν_L are the observed high and low frequencies of the doublet, respectively, the ν_H^0 and ν_L^0 are the corresponding unperturbed vibrational frequencies and γ is the ratio of the integrated absorption coefficients of the two bands, *viz.*

$$\gamma = \frac{A_H}{A_L}$$

In order to derive this equation, it is necessary to make the simplifying assumption that the intensity of the unperturbed overtone is negligible with respect to that of the participating fundamental vibration. Dixon[11] has demonstrated that this assumption does not always hold. However, the spectra of chloral, bromal and dichloroacetaldehyde indicate that the bending overtone is very weak, and we have used this as an indication that the assumption will hold in the cases under consideration. The values of δ were calculated using the data of Table II. The δ values which were calculated subsequently were used to calculate the unperturbed vibrational frequencies.

In order to calculate the fundamental bending frequency, it is necessary to assign the bands of the doublet. The relative intensities of these bands can be used as a guide for this assignment. We already have assumed that the unperturbed overtone intensity is negligible with respect to that of the unperturbed fundamental. If this is the case, the relative intensities of the perturbed bands can be predicted[12] *viz.*

$$A_f/A_o \geq 1$$

where the subscripts f and o designate the fundamental stretching and overtone bending vibrations, respectively. The intensity ratios in Table II indicate that the high frequency band is the most intense in all cases. However, the ratios for benzaldehyde and *p*-hydroxybenzaldehyde are not significantly different from unity. Nevertheless, the data strongly imply that the higher frequency band is the perturbed fundamental and the lower the perturbed bending overtone. We assume this assignment for all of the aldehydes that we have measured.

The fundamental bending frequencies were calculated from the values of the unperturbed bending overtone. These values are given in Table III. Because of the anharmonicity and the means of calculation, the derived values are expected to be low. Taking this into account, the observed and calculated frequencies seem to be in quite good agreement. Anharmonicity probably accounts for most of the discrepancy between the observed and calculated values. This can be demonstrated by comparing these differences with the difference in chloral, bromal or dichloroacetaldehyde between the observed fundamental and the value calculated by halving the observed overtone. The average of these differences is 20 cm.$^{-1}$. The average difference between the observed and calculated values in Table III is 28 cm.$^{-1}$.

(12) G. Herzberg, "Infrared and Raman Spectra of Polyatomic Molecules," D. Van Nostrand Co. New York, N. Y., 1945, p. 266.

Conclusions

Two different approaches have been applied to the problem of establishing whether or not the characteristic aldehydic doublet is the result of a Fermi resonance and if so, which of the vibrations are interacting. The first of these approaches has shown that the characteristic doublet can be disturbed by substitution of heavy, polar atoms in place of the methyl hydrogens in acetaldehyde. The presence or absence of the doublet apparently depends upon the position of the aldehydic C–H bending overtone relative to the aldehydic C–H stretching fundamental. When these two vibrational levels are close together, the doublet occurs; when separated the doublet does not occur, in accordance with the Fermi resonance hypothesis. On the other hand, it has been shown that the unperturbed frequency of the vibration interacting with the stretching fundamental in substituted benzaldehydes, as calculated from the frequencies and intensities of the doublet bands, gives rise (on the assumption that it is an overtone) to a value for the fundamental frequency which is in agreement with the values assigned to the in-plane aldehydic bending vibration. These observations do not, in themselves, prove the case conclusively. However, when taken with the evidence already in the literature, they provide a strong argument supporting the hypothesis that the characteristic aldehydic doublet is due to a Fermi resonance interaction between the aldehydic C–H stretching and overtone C–H bending vibrations.

Acknowledgment.—The authors are indebted to Dr. G. F. Crable for many helpful discussions during the course of the work and to Dr. N. D. Coggeshall for his encouragement and advice.

THE EFFECT OF POLAR–NON-POLAR SOLUTES ON THE WATER WETTABILITY OF SOLID SURFACES SUBMERGED IN OIL[1]

BY WILLARD D. BASCOM AND C. R. SINGLETERRY

U. S. Naval Research Laboratory, Washington 25, D. C.

Received July 5, 1961

A study has been made of the effect of polar–non-polar solutes on the contact angles exhibited by water drops on polytetrafluoroethylene, polyethylene and stainless steel surfaces submerged in decane, isopropylbiphenyl and bis-(2-ethylhexyl)-sebacate. The solutes investigated included the oil-soluble dinonylnaphthalene sulfonates and sodium dodecyl sulfate. A parabolic relation exists between the cosine of the contact angle, cos θ, and the oil-water interfacial tension, γ_{ow}, and this is consistent with the Young–Dupre equation for the oil–water–solid line of intersection. The experimental data also provide a measure of the work required for oils to displace water from the submerged surfaces. This work generally is greater for a polytetrafluoroethylene surface than that necessary to displace water from polyethylene, because the polytetrafluoroethylene has a greater interfacial energy against the oils than does polyethylene. Analytic treatment of the data gave a numerical indication of the various oil–polymer interfacial energies. This treatment suggests that the polar–non-polar solutes are adsorbed at both the water–polymer and oil–water interfaces, but are not significantly adsorbed at the oil–polymer interfaces. The work to displace water from clean steel surfaces submerged in the pure oils is high because of the polar interaction between the water and the metal oxide surface, but in the oil–sulfonate solutions the solute is adsorbed as a monolayer at the metal–oil boundary to expose a non-polar surface so that the work of water displacement is low.

Introduction

The adhesion of a liquid to a solid surface submerged in a second liquid is of technological importance. Advances in this area of surface chemistry would contribute to the understanding of problems such as the detergency process or the recovery of oil from porous subterranean rock by water displacement. The relative wettability of solids is of critical significance to ice adhesion in lubricated systems[2] and to the displacement of oil or water from metal surfaces.[3]

The inherent difficulty in the study of these problems is that the interfacial energy between a solid and a liquid cannot be measured directly. Instead, attention must be given to the directly measurable quantities—the interfacial tension between the two liquids and the contact angle one liquid exhibits on the solid surface submerged in the second liquid.

Earlier investigations have been made of systems of pure liquids on clean metal surfaces.[4] Unfortunately, the high interfacial energies involved favored adsorption of small quantities of polar impurities or the orientation of the liquids themselves at the various interfaces, which makes interpretation of the results difficult without further information about the nature of the adsorbate. The present investigation examines the effect of small changes in the concentration and chemical composition of amphipathic materials on oil–water interfacial tensions and on contact angles at the oil–water–solid intersection. The observed relation between these two experimental quantities permits discussion of the probable magnitude of the solid–liquid interfacial energies and of the way in which they are affected by adsorbed solute.

Experimental Materials and Procedures

The polymer surfaces employed here have been described elsewhere.[5] The stainless steel cylinders used had one face highly polished. Each specimen was cleaned between experiments by washing with hot solvent and then abrading all sides using an alumina–water slurry on a metallographic wheel, followed by thorough rinsing with hot tap water and then distilled water to remove adhering alumina particles. This procedure gave a clean metal oxide surface free of adsorbed organic contamination.

The organic solvents decane, isopropylbiphenyl and bis-(2-ethyl-hexyl)-sebacate were obtained from commercial sources. The decane was washed first with acid and then with water, dried, and finally percolated through Florisil adsorbent. The resulting material did not spread on a clean surface of water made slightly acid or alkaline, which indicated the absence of polar impurities. The isopropylbiphenyl was percolated repeatedly through adsorbent until this liquid also showed no tendency to spread on acid or alkaline water. The diester oil was molecularly distilled and then percolated through Florisil to give a clear, colorless liquid that had physical properties identical with those of a specially synthesized sample of the same ester.[6]

The dinonylnaphthalene sulfonates were of high purity; their properties in non-polar solvents[7] and the methods used for their preparation[8] have been described. The sodium dodecyl sulfate was that used by Bernett and Zisman.[9] It showed no minimum in plots of surface tension or interfacial tension against concentration, indicating no detectable lauryl alcohol contamination.[10]

Contact angle measurements were made on the solid surfaces submerged to a depth of about 2.5 cm. in oil or oil solution in an optical cell. Water drops of approximately 0.03 ml. volume were formed in the oil from a micropipet and allowed to settle under gravity to the surface. The angle of contact through the water drop was measured using a telescope goniometer.[11] The oil and water used previously were equilibrated by shaking with each other and centrifuging. Under these circumstances the initial advancing contact angles, measured through the drop, were constant after ten sec. and were reproducible within less than two degrees. Further advance of the drops on the submerged surfaces by adding water from the micropipet was not found to alter the contact angles. Receding angles were formed by withdrawing water from the drop and were not significantly different from the advancing angles provided that

(1) This work was presented in part at the 136th National Meeting of the American Chemical Society, Atlantic City, N. J., 1959.

(2) H. R. Baker, W. D. Bascom and C. R. Singleterry, accepted for publication in *J. Colloid Sci.*, 1962.

(3) H. R. Baker, P. B. Leach, C. R. Singleterry and W. A. Zisman, "Surface Chemical Methods of Displacing Water and/or Oils and Salvaging Flooded Equipment," Naval Research Laboratory Report No. 5606, February 23, 1961.

(4) (a) F. E. Bartell and P. H. Cardwell, *J. Am. Chem. Soc.*, **64**, 1530 (1942); (b) F. E. Bartell and C. W. Bjorklund, *J. Phys. Chem.*, **56**, 453 (1952).

(5) W. D. Bascom and C. R. Singleterry, *ibid.*, **65**, 1683 (1961).

(6) E. M. Bried, H. F. Kidder, C. M. Murphy and W. A. Zisman, *Ind. Eng. Chem.*, **39**, 484 (1947).

(7) S. Kaufman and C. R. Singleterry, *J. Colloid Sci.*, **12**, 465 (1957).

(8) S. Kaufman and C. R. Singleterry, *ibid.*, **10**, 139 (1955).

(9) M. K. Bernett and W. A. Zisman, *J. Phys. Chem.*, **63**, 1241 (1959).

(10) G. D. Miles and L. Shedlovsky, *ibid.*, **48**, 57 (1944).

(11) H. W. Fox and W. A. Zisman, *J. Colloid Sci.*, **5**, 514 (1950).

the surface was not deliberately roughed and that one min. was allowed for re-equilibration. When the two liquid phases had not been mutually saturated the contact angle was observed to change with time as a result of delayed adsorption of solute at the oil–water interface and of solubilization effects that tended to diminish the drop size. Steel specimens required equilibration with the additive-containing oil for at least 15 hr. to obtain stable contact angles, but the length of time the organic polymers were in contact with the oil solutions had no effect on the contact angle. This behavior suggests that the solutes were not appreciably adsorbed at the oil–polymer interface. The unusual length of time required for the metal oxide surface of the steel specimens to reach adsorption equilibrium with the sulfonate soaps has been shown to be linked to the presence of water in the oil–soap solution.[6] Water appears to effect a slow enhancement of sulfonate adsorption over that observed from anhydrous sulfonate soap solution.

The measurement of contact angles near 180° was extremely difficult. In general, the reproducibility of the contact angles was found to be ±2°, but for drops exhibiting angles greater than 175° the distance of separation between water and the solid surface near the contacting edge of the drop is less than the resolving power of the telescope-goniometer. This error amounts to about 3° for a contact angle measured as 175°, but becomes much less than the reproducibility for angles smaller than this. There is, however, no question that the water drops which exhibit very high contact angles actually make contact with the solid. It is possible to focus the telescope on the flattened area beneath the water drop and observe the water displacing the oil from the solid surface, even when the contact angle is near 180°. The hydrodynamic and surface chemical implications of this displacement are discussed elsewhere.[2] For oils which have densities very close to that of water, such as isopropylbiphenyl, it was found that contact angles between 175 and 140° were difficult to reproduce.

The interfacial tensions between water and the oil solutions of the dinonylnaphthalene sulfonate soaps were determined by the pendent drop method.[12] This technique, which is useful in detecting changes of interfacial tension with time, showed that for the sulfonates 95% of the aging process at the interface took place within the first minute. The interfacial tensions between isopropylbiphenyl and the aqueous solutions of sodium dodecyl sulfate were determined by the drop volume method. The water drops were delivered from microburets as described by Gaddum[13] and the precautions and corrections suggested by Harkins[14] were applied.

Results

The purpose of this study was to investigate the variables that determine the contact angle, θ, a water drop will exhibit on a solid surface submerged in oil. These variables are the three condensed phase interfacial tensions which act at the oil–water–solid line of intersection. The explicit relationship between these quantities and the contact angle, measured through the drop, is given by the Young–Dupre equation

$$\cos\theta = \frac{\gamma_{os} - \gamma_{ws}}{\gamma_{ow}} \qquad (1)$$

Of these quantities only γ_{ow} and the contact angle can be measured experimentally. In order to determine the degree to which changes in each of these interfacial tensions affect the contact angle, each should be altered independently but when γ_{ow} and γ_{os} are specified γ_{ws} cannot be varied arbitrarily.

In this investigation, attention was focused on the relation between γ_{ow} and cos θ for water drops on non-polar surfaces in oil solution. The term "non-polar surface" includes stainless steel surfaces in the oil solutions because the solutes present adsorb on this metal oxide surface to give a monolayer comparable in wetting properties with the non-polar polymer surfaces.

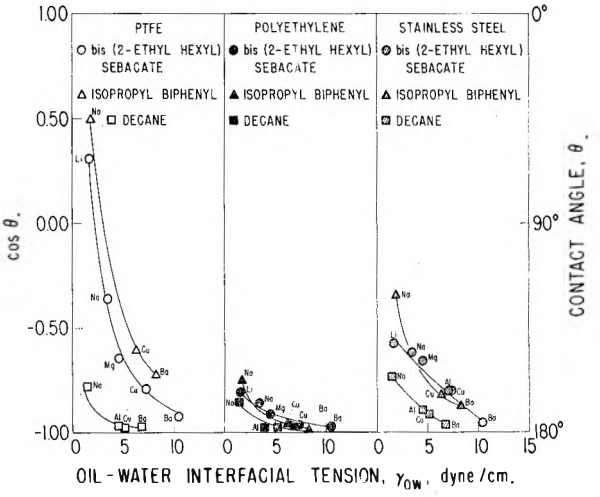

Fig. 1.—Cos θ as a function of γ_{ow} for water drops on solid surfaces submerged in oil solutions of the dinonylnaphthalene sulfonates.

The effect of changes in γ_{ow} on the contact angle for a given oil–polymer pair was determined by using sulfonates having different cations to obtain different oil–water interfacial tensions. These values of γ_{ow} were plotted against the cosine of the observed contact angle.

The effect of a change in the oil–solid interfacial tension on the relationship between cos θ and γ_{ow} was determined by employing different oil–polymer combinations. The polymers chosen were polytetrafluoroethylene and polyethylene; they were studied under solutions of the dinonylnaphthalene sulfonates in decane, bis-(2-ethylhexyl)-sebacate and isopropylbiphenyl.

The results on polytetrafluoroethylene (PTFE) and on polyethylene are plotted in Fig. 1. For both polymeric surfaces there is a systematic decrease in the contact angle, *i.e.*, cos θ becomes less negative, with decreasing oil–water interfacial tension. The decrease in contact angle for a given change in γ_{ow} generally is greater for polytetrafluoroethylene than for polyethylene. That is, the perfluoropolymer is the more readily wet by water when submerged in these oil solutions, which is the reverse of the relative wettability of these polymer surfaces in air.[9]

All of the dinonylnaphthalene sulfonate soap solutions were at a concentration of 1.0 wt. %. It generally was found that greater water solubility of the sulfonate was associated with lower interfacial tension. The values of γ_{ow} were easily reproducible because the soaps were present in amounts well above their critical micelle concentration[7] and small differences in concentration did not produce significant differences in γ_{ow}.

The data obtained for stainless steel surfaces in the sulfonate solutions (Fig. 1) are in many ways similar to data obtained for the polymer surfaces. This is consistent with the fact that the dinonylnaphthalene sulfonates are adsorbed from

(12) J. M. Andreas, E. A. Hauser and W. B. Tucker, *J. Phys. Chem.*, **42**, 1001 (1938).

(13) N. K. Adam, "The Physics and Chemistry of Surfaces," 2nd ed., Oxford Univ. Press, London, p. 379.

(14) W. D. Harkins and F. E. Brown, *J. Am. Chem. Soc.*, **41**, 499 (1919).

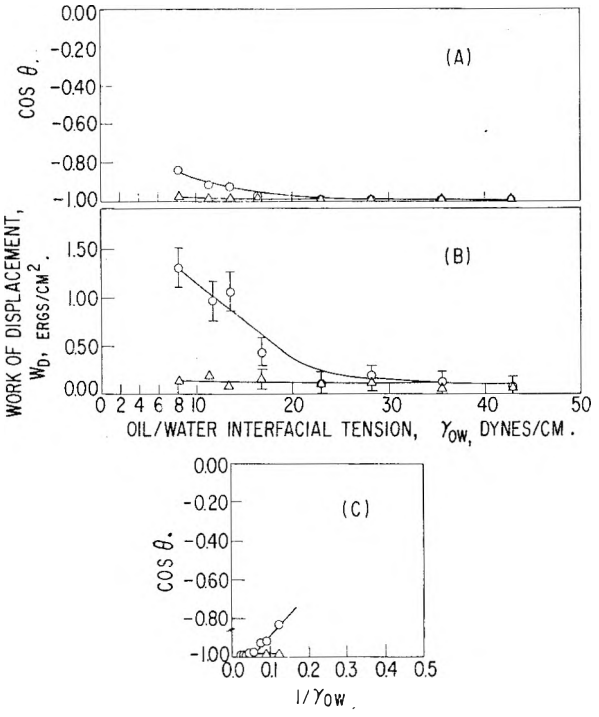

Fig. 2.—Surface chemical behavior of aqueous sodium dodecyl sulfate solutions in isopropylbiphenyl/polymer systems: A, cos θ as a function of γ_{ow}; B, work of displacement as a function of γ_{ow}; C, cos θ *vs.* $1/\gamma_{ow}$ (○ = PTFE, △ = polyethylene).

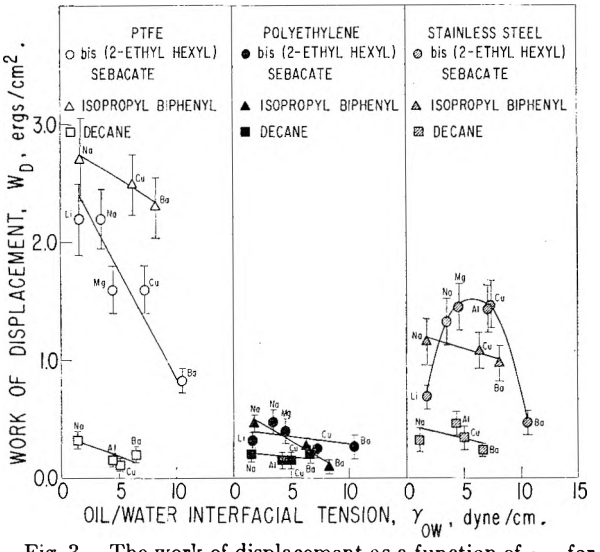

Fig. 3.—The work of displacement as a function of γ_{ow} for water drops on solid surfaces submerged in oil solutions of the dinonylnaphthalene sulfonate soaps.

oil solution on metal oxide surfaces to form close packed monolayers that have surface properties comparable with those of the surface of polyethylene.[5] It should be noted that the contact angles obtained for a given oil solution on the sulfonate films fall between those obtained on polytetrafluoroethylene and those obtained on polyethylene for the same solutions. That is, the soap monolayer adsorbed at the oil–oxide interface has a water wettability intermediate between that of the two polymers in these oil solutions.

In the absence of polar–non-polar solutes in the liquid phases the contact angles obtained on the polymer surfaces in the three oils all were greater than 175°. On a clean stainless steel surface submerged in the oils, the water drops all gave contact angles less than 10°; by making extraordinary efforts to eliminate polar impurities it was possible to obtain contact angles very near zero degrees.

The relationship between cos θ and γ_{ow} at higher values of the oil–water interfacial tension than can be obtained with the dinonylnaphthalene sulfonates was determined by measuring the contact angles formed by water drops containing different concentrations of sodium dodecyl sulfate (NaLS). Observations were made on polytetrafluoroethylene and polyethylene submerged in isopropylbiphenyl; the data are indicated in Fig. 2A.

The experimental data also provide an index of the relative adhesional tendency of water and oil to these non-polar surfaces, the reversible work of displacing unit area of water, W_D.[15] This quantity is defined as the work involved in the disappearance of one cm.^{2} of water–solid interface with simultaneous formation of one cm.^{2} of oil–water interface and one cm.^{2} of oil–solid interface. A summation of the energy changes gives an expression for the work of displacement

$$W_D = \gamma_{os} + \gamma_{ow} - \gamma_{ws} \qquad (2)$$

The value of W_D for any system can be calculated from the experimental data by substituting equation 1 into the expression for W_D to obtain

$$W_D = \gamma_{ow}(\cos\theta + 1) \qquad (3)$$

In Fig. 2B and 3 the work of displacement calculated from the experimental data is plotted as a function of γ_{ow}. The vertical lines extending from each point represent the probable error in W_D and were calculated taking a probable error of ± 0.2 dyne/cm. in γ_{ow} and ± 2° in θ. Generally, the work required to displace water from polytetrafluoroethylene is larger than that required to displace water from polyethylene.

Discussion

The Oil–Water–Polymer Systems.—In order to interpret the observed relationship between cos θ and γ_{ow}, consideration must be given to the relative orders of magnitude of the interfacial energies acting at the oil–water–solid line of intersection and to the effect that polar–non-polar solutes have on these energies. It is assumed that, in the absence of surface active solutes, the interfacial energy existing between water and the organic polymer surface is comparable in magnitude to that existing at the interface between water and the organic oil. It also is assumed that both these energies are large in comparison with the interfacial energy at the organic liquid–organic solid boundary. These assumptions are reasonable because interaction between the relatively polar water molecules and a non-polar organic liquid such as decane should not be greatly different from that between water and an organic solid such as polyethylene. The interfacial energy between decane and polyethylene is much smaller

(15) H. Freundlich, "Colloid and Capillary Chemistry," Methuen and Co., London, 1926, p. 159.

than the other two because methylene groups preponderate in both.

It is expected that the solutes employed will be strongly adsorbed at both the oil–water and water–solid boundaries but that little adsorption of solute will occur at the interface between the oil and the organic solid. Adsorption at the oil–water interface involves ionic interactions of the polar head of the solute molecule with the aqueous phase. Similar interactions are possible when the molecule is at the water–organic polymer interface. Fowkes and Harkins[16] have measured the film pressure of solutes adsorbed at the water–paraffin interface and Bernett and Zisman[9] have demonstrated the adsorption of polar–non-polar solutes at the water–polyethylene and water–polytetrafluoroethylene interfaces. The interfacial energy at the boundary between a non-polar organic liquid and a non-polar organic polymer, however, is not likely to be of sufficient magnitude to favor the specific adsorption of surface active solute.

The contact angles of near 180° obtained on the submerged polymer surfaces in the absence of surface active solutes, and the parabolic relationship observed between $\cos\theta$ and γ_{ow}, are consistent with the preceding assumptions concerning the relative magnitudes of the interfacial energies. In order to obtain contact angles near 180°, *i.e.*, $\cos\theta = -1$, the numerator of the Young-Dupre equation (equation 1) must be negative and nearly equal to the denominator. In other words, the water–polymer interfacial tension, γ_{ws}, must exceed the oil–polymer interfacial tension, γ_{os}, by an amount nearly equal to the oil–water interfacial tension, γ_{ow}. A decrease in the contact angle as a result of decreasing γ_{ow} requires that in eq. 1 the numerator must take less negative values, *i.e.*, γ_{ws} must decrease. Thus the progressive decrease in the contact angle with increased adsorption at the oil–water interface must be the result of simultaneous adsorption of solute at the water–polymer interface.

It is possible to examine the data more critically by rewriting the Young–Dupre equation in the form

$$\cos\theta = \gamma_{os}\left(\frac{1}{\gamma_{ow}}\right) - \frac{\gamma_{ws}}{\gamma_{ow}} \qquad (4)$$

This equation will be linear (in $1/\gamma_{ow}$) if γ_{os} and γ_{ws}/γ_{ow} are constant. Because the surface energies of the oil and polymer are small and comparable, it is unlikely that the solutes are adsorbed at the oil–polymer interface, so that γ_{os} may reasonably be expected to be constant for a given oil–polymer combination regardless of the solute present. The term γ_{ws}/γ_{ow}, on the other hand, can be constant only if adsorption at the respective interfaces changes the interfacial energies by proportional amounts. In Fig. 2C and 4 the data are plotted as $\cos\theta$ against $1/\gamma_{ow}$. Of the eleven solvent–solid systems investigated, only one shows unquestionable departures from linearity. For the systems that do give a linear relation between $\cos\theta$ and $1/\gamma_{ow}$, the slope of the line represents an estimate of the value of γ_{os}, the oil–solid interfacial tension. Therefore, to the extent the assumptions can be justified, this analytic treatment provides a novel means of obtaining numerical values of the interfacial tension between non-polar solids and liquids. In the oil–polymer systems, the data obtained on polymer surfaces in the oil solutions of the dinonylnaphthalene sulfonates (Fig. 4) either are clearly linear when plotted as $\cos\theta$ against $1/\gamma_{ow}$ or are consistent with a linear plot but lack enough points to confirm linearity. The slopes of these lines are taken as estimates of γ_{os} and are listed in Table I. The interfacial tensions between polytetrafluoroethylene and bis-(2-ethylhexyl)-sebacate or isopropylbiphenyl are an order of magnitude greater than the interfacial tensions between polyethylene and these same liquids. There is only a small difference in the value of γ_{os} for the two polymers in decane. The data for the polymers in isopropylbiphenyl using the aqueous solutions of sodium dodecyl sulfate also give slopes that indicate a much larger value of γ_{os} for polytetrafluoroethylene than for polyethylene against this aromatic liquid (Fig. 2C).

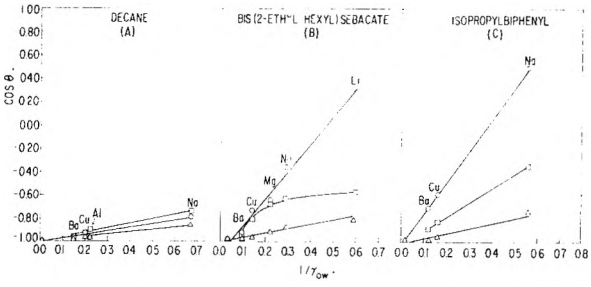

Fig. 4.—Cos θ *vs.* $1/\gamma_{ow}$ for water drops on solid surfaces submerged in oil solutions of the dinonylnaphthalene sulfonated soaps: ○, polytetrafluoroethylene; △, polyethylene; □, stainless steel.

TABLE I

ESTIMATED OIL–SOLID INTERFACIAL TENSIONS, γ_{os} (FROM EQ. 4 AND FIG. 4)

Solid surface	γ_{os}, dyne/cm. For isopropylbiphenyl	For bis-(2-ethylhexyl)-sebacate	For decane
PTFE	2 7	2.2	0.3
Polyethylene	0 4	0.4	.2
Sulfonate monolayer on stainless steel	1 2		.4

TABLE II

COMPARISON OF $\gamma_{LV} - \gamma_c$ WITH TWO ESTIMATES OF γ_{os} FOR VARIOUS OIL–POLYMER PAIRS

Oil–polymer interface	$\gamma_{LV} - \gamma_c$, dynes/cm.	Estimated value of γ_{os}, dynes/cm. From Fig. 4	From eq. 5
Isopropylbiphenyl–polytetrafluoroethylene	17	2.7	2.8
Isopropylbiphenyl–polyethylene	3	0.4	0.2
Bis-(2-ethylhexy)-sebacate–polytetrafluoroethylene	13	2.2	1.8
Bis-(2-ethylhexyl)-sebacate–polyethylene	1	0.4	0.1
Decane–polytetrafluoroethylene	6	.3	.4
Decane–polyethylene	−8	.2	.6

(16) F. M. Fowkes and W. D. Harkins, *J. Am. Chem. Soc.*, **62**, 3377 (1940).

The interfacial energy between a non-polar liquid and a non-polar solid may be considered the result of a difference in their chemical constitution. More specifically, it is the result of differences in the magnitude of the unsatisfied molecular dispersion forces at the surfaces of the two phases. The best indices of the magnitude of these unsatisfied forces are the surface tension of the liquid (γ_{LV}) and the critical surface tension[17] of the solid (γ_c), and it may be expected that the solid–liquid interfacial tension will be greater as the difference between these two quantities is greater. Critical surface tensions of the solid surfaces of interest here are: polytetrafluoroethylene, 18 dynes/cm.,[18] dinonylnaphthalene sulfonate monolayer on stainless steel, 29 dynes/cm.,[5] and polyethylene, 32 dynes/cm.[18] The surface tensions of the model oils employed are: decane, 24 dynes/cm., bis-(2-ethylhexyl)-sebacate, 31 dynes/cm., and isopropylbiphenyl, 35 dynes/cm. The differences in the surface tension of the liquid and the critical surface tension of the solid, γ_c, for various oil–polymer pairs are listed in column 2 of Table II. Reference to column 3 of this table shows that the interfacial tensions estimated from Fig. 4 do fall into the general order to be expected from column 2, although there is no simple proportionality when the value of γ_{os} is less than 0.5 dyne/cm.

The estimated values of γ_{os} listed in Table I for polyethylene against the various oils are small quantities, a result of the similarity in chemical constitution of these organic liquids and the surface of the hydrocarbon polymer. There do not appear to be any experimental data available for the interfacial tension between liquid polyethylene and other hydrocarbon liquids with which to make comparisons since such pairs of liquids usually are miscible in one another. This miscibility is evidence in itself that they would have only a small interfacial energy. The values of γ_{os} for polytetrafluoroethylene against the hydrocarbon liquids (Table I) are smaller by a factor of three or four than the experimental values reported in the literature for the interfacial tension between pairs of liquids having comparable differences in chemical composition. For example, a value of 12.5 dynes/cm. has been measured for the interfacial tension between α-methylnaphthalene and a high molecular weight fluorocarbon[19] as compared to 2.7 dynes/cm. for isopropylbiphenyl against polytetrafluoroethylene. Jarvis and Zisman[20] have estimated the interfacial tension for a perfluoroalkane against a polyethylene glycol fluid as 5.7 dynes/cm. and against hexadecane as 8.8 dynes/cm. These values are considerably greater than the 2.2 dynes/cm. obtained for polytetrafluoroethylene against the diester oil and the 0.3 dynes/cm. obtained against decane.

The smaller values for the interfacial tensions at the oil–polymer boundaries compared to the values for the interfacial tension between liquids having similar differences in chemical constitution suggests that the overlying oil alters the apparent surface energy of the polymer. This would be the case if the molecules of the oil at the polymer surface are less mobile than the oil molecules further removed from the surface. For oil–polymer pairs that are similar in chemical constitution, such as polyethylene and decane, it is possible that there is a penetration or solution of the oil into the amorphous polymer surface. It also is conceivable, since the solid surfaces are not smooth on an atomic scale, that there is an entanglement of the molecules of the organic liquid with the polymer. A weak adsorption of oil or solute molecules, particularly at the surface of polytetrafluoroethylene, cannot be excluded. Studies of the heat of immersion of this polymer[21] indicate the presence of a small number of relatively active adsorption sites. In any event, oil displacement will be from a surface that is comprised of polymer molecules and a few relatively immobile molecules of the oil itself. Because of the immobilized oil molecules, the solid surface will have properties less unlike the overlying organic liquid, and the apparent oil–polymer interfacial energy will be less than if all the oil molecules could be displaced.

Girifalco and Good have proposed an equation[22]

$$\gamma_{ab} = \gamma_a + \gamma_b - 2\phi(\gamma_a\gamma_b)^{1/2} \qquad (5)$$

which expresses the interfacial tension between two liquids, γ_{ab}, in terms of their individual surface tensions, γ_a and γ_b. This expression was arrived at by analogy from the Berthelot relation for the interaction between like and unlike molecules. The term ϕ is an empirical factor which corrects for systems that deviate from the simple Berthelot relation. Computed values of γ_{ab} are particularly sensitive to small alterations in ϕ, and this correction term approaches one (*i.e.*, systems conform to the Berthelot relation) only when the liquids are mutually soluble. Listed in column 4 of Table II are values of γ_{os} for the oil–polymer pairs investigated here, calculated using equation 5 and employing γ_c as the surface tension of the solid phase and assuming $\phi = 1$. Considering the uncertainties introduced by using the critical surface tension, values of γ_{os} calculated in this way are in surprisingly good agreement with the values estimated from Fig. 4 provided ϕ is taken as unity. If instead, a value of 0.95 is used for ϕ, as suggested by Girifalco and Good[22] for non-polar but mutually insoluble liquid pairs, the computed values of γ_{os} are considerably greater than the values estimated from Fig. 4. The results of these calculations are a further indication that the value of γ_{os} estimated here from relative wettability data expresses the interfacial tension between oil and a polymer surface more or less modified by immobilized oil molecules.

(17) The critical surface tension, γ_c, is the surface tension of a liquid that will just spread on a non-polar solid surface (H. W. Fox and W. A. Zisman, *J. Colloid Sci.*, **5**, 514 (1950); E. G. Shafrin and W. A. Zisman, *J. Phys. Chem.*, **64**, 519 (1960)). The value of γ_c is less than the actual surface energy of the solid by the quantity of γ_{sl}, the interfacial energy between the solid and the liquid that just spreads. With suitably chosen spreading liquids, γ_{sl} may be assumed to be very small so that the critical surface tension may be taken as a reasonable approximation of the surface energy of the solid. W. D. Bascom and C. R. Singleterry, *ibid.*, **65**, 1683 (1961).

(18) E. G. Shafrin and W. A. Zisman, *ibid.*, **64**, 519 (1960).

(19) F. M. Fowkes and W. M. Sawyer, *J. Chem. Phys.*, **20**, 1650 (1952).

(20) N. L. Jarvis and W. A. Zisman, *J. Phys. Chem.*, **63**, 727 (1959).

(21) A. C. Zettlemoyer, *Chem. Revs.*, **59**, 937 (1959).

(22) L. A. Girifalco and R. J. Good, *J. Phys. Chem.*, **61**, 904 (1957).

For the polymer surfaces studied here, some inferences concerning the relative values of γ_{ws} and γ_{ow} may be derived from a consideration of eq. 1, 2 and 4. If the data give a linear plot of cos θ *vs.* $1/\gamma_{ow}$, *i.e.*, if γ_{os} and γ_{ws}/γ_{ow} are constant in eq. 4, it follows from eq. 2 that a plot of W_D *vs.* γ_{ow} also must be linear. When the assumption of a constant γ_{os} for solutions of different soaps in the same oil is justifiable, the departures of the W_D plot from linearity may be unambiguously associated with departures from constancy of γ_{ws}/γ_{ow}. Unfortunately, the value of W_D is extremely sensitive to errors in the measurement of either cos θ or γ_{ow} from which it is calculated. These uncertainties for the present work are indicated for each datum point in Figs. 2B and 3. More precise data obviously are necessary for a decisive test of the assumption that the ratio γ_{ws}/γ_{ow} is constant. Nevertheless, for all of the present data involving polymer surfaces, a linear plot is possible within the limits of error indicated. For stainless steel the points for isopropylbiphenyl are easily compatible with a linear plot and those for decane are approximately so, but those for bis-(2-ethylhexyl)-sebacate deviate well beyond the experimental uncertainty. Since the solid surfaces in this case are adsorbed monolayers of polar organic compounds, the assumption of a constant γ_{os} is questionable. The diester is subject to hydrolysis in the presence of water and a catalyst; it is possible that varying amounts of hydrolytic products adsorb to modify the surface energy of the soap monolayer, and so γ_{os}.

The measurements with sodium dodecyl sulfate were taken for the specific purpose of extending the wettability study into the range of higher oil–water interfacial tensions. The plot of W_D *vs.* γ_{ow} (Fig. 2B) can be associated reasonably with a straight line for all values of γ_{ow} below 25 dynes/cm., but the points for the more dilute solutions and for pure water do not fall on this line. Since γ_{os} may be expected to be constant, the deviation is attributed to a relatively slower increase in γ_{ws} than in γ_{ow} as the soap concentration is decreased in this range. Beyond γ_{ow} values of 25 dynes/cm., W_D is close to zero and γ_{ow} and γ_{ws} change in such a way that their difference rather than their ratio is nearly constant and this difference approaches the value of γ_{os}.

The Oil–Water–Metal Systems.—The conclusions arrived at in considering the relative wettability of submerged polymer surfaces may be applied directly to the data obtained on stainless steel surfaces submerged in oil solutions of the dinonylnaphthalene sulfonates. The sulfonate molecules are adsorbed on stainless steel as monolayers with their polar heads on the metal oxide surface and their hydrocarbon portion oriented away from this surface.[b] Films adsorbed from isopropylbiphenyl solutions that previously have been saturated with water have surface properties that are independent of the sulfonate cation. The critical surface tension for these monolayers is 29 dynes/cm.; this is lower than that of polyethylene and is presumed to indicate that a substantial fraction of the surface of the sulfonate film is occupied by methyl groups which give a lower polarizability of the surface than is found for polyethylene. Thus, these films have surface properties between those of polytetrafluoroethylene and polyethylene.

In the absence of solute, the low contact angles observed on steel surfaces submerged in the oils are consistent with the oil–metal interface being a boundary between the highly polar metal oxide and the non-polar oil; the value of γ_{os} in the Young–Dupre equation must be high. When the surface of the metal specimen is coated with an adsorbed soap film, the relationship between cos θ and γ_{ow} is comparable with that obtained for the polymer surfaces in these same oil solutions.

An analysis of the data according to eq. 4 provides some indication of the interfacial energy at the boundary between the sulfonate monolayers and the oils (Fig. 4, Table I). For the monolayers against decane the estimated value of γ_{os} is 0.4 dyne/cm. A low value of γ_{os} for the decane–sulfonate monolayer interface is consistent with the similarity between the atomic groups in the monolayer surface and the characteristic atomic groups of the oil molecule. On the other hand, the end groups of the soap monolayers differ sufficiently from the molecular configuration of isopropylbiphenyl to give a larger oil–solid interfacial energy. The value of γ_{os} for the sulfonate monolayers in isopropylbiphenyl is between the values of γ_{os} for the polymer surfaces in this liquid, as would be expected from a comparison of the values of $\gamma_{LV}-\gamma_c$ for the three oil–solid pairs.

The results obtained on stainless steel surfaces in the diester oil solutions of the sulfonate soaps raise a question as to whether the monolayers formed by the individual soaps are in this case identical in surface energy. The relation between cos θ and γ_{ow} is not parabolic, the work of displacement goes through a pronounced maximum when plotted as a function of γ_{ow}, and there is considerable curvature in the plot of cos θ against $1/\gamma_{ow}$. As suggested in the foregoing discussion, the diester oil may be hydrolyzed at the metal surface and the resulting hydrolysis products mixed with the adsorbed monolayer. The hydrolysis and the adsorption of hydrolyzed fragments of diester oils on clean metal surfaces has been demonstrated previously.[23] Unfortunately, it has not been possible to isolate films adsorbed from the solutions of the sulfonates in this oil to study their surface properties in air because diester–sulfonate solutions do not retract cleanly from the films they deposit on stainless steel.

Conclusions

(1) The work required to displace water from a non-polar solid surface by a non-polar organic liquid will be least when the surface tension of the liquid and the critical surface tension of the solid surface are as nearly the same as possible.

(2) Dinonylnaphthalene sulfonates present in these systems are adsorbed onto polar solid surfaces to form close packed films that are comparable with the surfaces of non-polar solids. They also

(23) E. F. Hare and W. A. Zisman, *J. Phys. Chem.*, **59**, 335 (1955).

are adsorbed over the entire surface of the water drop, although solute adsorption at the water–oil interface may not exactly parallel that at the water–solid interface.

(3) While the analytic treatment of the data does not lead to an assumption-free determination of γ_{os}, there is good reason for believing that it furnishes a useful relative index of the interfacial energy of a non-polar liquid against a non-polar solid surface.

THEORY OF RADIATION CHEMISTRY. V. GENERALIZED SPUR DIFFUSION MODEL

BY ARYEH H. SAMUEL

Stanford Research Institute, Menlo Park, California

Received July 10, 1961

The sharp-boundary model of Magee[1] for diffusion and recombination of radicals and ions produced by ionizing radiation is extended to the case of a spherically symmetrical spur. The paper includes sample calculations and asymptotic solutions for the high- and low-background regimes; the importance of the transition region between these is emphasized.

In the first paper of this series, Magee[1] constructed a simple, but general, model of geometrical effects in radiation chemistry. Features of this model were a definite volume of the expanding track and a discontinuity in the value of the concentration at the track boundary. A closed-form solution of the diffusion–recombination equations was obtained, and a number of valuable relationships were deduced. Chief among these was the definition of "low-background" and "high-background" regimes.

Since the appearance of that paper, the study of track effects in radiation chemistry has been devoted largely to specific systems, notably water.[2] (A recent paper by Ivanov[3] is based partially on the Magee model.)

In this paper we re-examine the original model for two reasons: (1) It applies to all states of aggregation and to radicals as well as ions (provided termination is second order). (2) It identifies the irradiation conditions having background ratios near unity as those most useful for determination of diffusion and recombination parameters. In the low-background regime, yields do not depend on dose rate; in the high-background regime, they do not depend on track parameters; but in the region of transition between the two regimes they depend on dose rates and track parameters.

To develop the Magee model into one which can be applied to physical systems, four steps appear to be necessary.

1. The Magee model, which applies to cylindrical tracks, must be extended to include tracks made up of spherically symmetrical spurs, independent of each other, and corresponding to individual primary ionizations or excitations. Such tracks are typical of ionizing radiations of low linear energy transfer.

2. The model must be extended to include reactions of active species with a homogeneously distributed substrate. These correspond to many actual cases of radical and ion reactions.

3. The dependence of yields on dose rate must be obtained as a function of the background ratio (which we shall call β/κ as in ref. 1). We may write $G \propto I^n$, where G is the yield of products per unit dose (molecules/100 e.v.), I is the dose rate, and n is 0 in the low-background region and $-1/2$ in the high-background region. To obtain track parameters from studies of the transition region, we must be able to find β/κ from an experimental determination of the change of n with I.

4. Since many of the experiments at high dose rates are performed using pulsed radiation, the model must be suitably adapted. This involves making the background concentration, y_0, a variable which is zero at the beginning of a pulse and increases toward its steady-state value. (y_0 is taken as a constant in ref. 1 and in this paper.)

This paper deals with the first of these four steps. Diffusion and bimolecular recombination in spherically symmetrical spurs are considered. The model applies primarily to systems in which the only reactions involve active species, *e.g.*, H atoms in pure hydrogen or ion pairs in rare gases, in any state of aggregation. It also applies to other systems in which radical–substrate reactions are slow compared to diffusion and recombination.

Spur Diffusion Model.—The notation of ref. 1 is followed as much as possible (k = recombination rate constant, D = diffusion constant.) The spur volume v is taken as

$$v = (v_0^{2/3} + Dt)^{3/2} \qquad (1)$$

The background concentration of active species is y. The number of particles initially formed in the spur is w_0. The initial number present is

$$N_0 = w_0 + v_0 y_0 \qquad (2)$$

The time dependence of the number N of active particles is

$$\frac{dN}{dt} = -kN(N-1)/v + y\,dv/dt \qquad (3)$$

As in ref. 4, $N(N-1)$ is substituted for N^2 be-

(1) J. L. Magee, *J. Am. Chem. Soc.*, **73**, 3270 (1951); Appendix: ADI-3217 (see footnote 10 in Magee's paper; photocopy price now $1.25 from Photoduplication Service, Library of Congress, Washington 25, D. C.).

(2) A very complete review is given by A. Kuppermann, in "Actions Chimiques et Biologiques des Radiations," M. Haïssinsky, ed., Vol. 5, Masson et Cie., Paris, 1961, pp. 85–166.

(3) V. I. Ivanov, *Atomnaya Energ.*, **7**, 73 (1959); *Reactor Sci.*, **12**, 128 (1960).

(4) A. H. Samuel and J. L. Magee, *J. Chem. Phys.*, **21**, 1080 (1953).

cause w_0 is a small number and because a radical or ion cannot recombine with itself.

The following approximate solution to this equation was found to be more useful than the exact analytical solution which is given in the Appendix. To render the equations tractable, we take $N' = N - 1/2$ and approximate $N(N-1) = N'^2$. This introduces an error of 1/4. An average value of w_0 is about 5 (Samuel and Magee[4]), so that the over-all error will be between 1 and 2%.

Dividing equation 3 by dv/dt gives

$$\frac{dN}{dv} = \frac{dN'}{dv} = -\frac{2kN'^2}{3Dv^{4/3}} + y \tag{4}$$

Outside the spur, the change in y is given by

$$\frac{dy}{dt} = -ky^2 \tag{5}$$

which can be solved to give

$$y = \frac{y_0}{1 + \frac{ky_0}{D}(v^{2/3} - v_0^{2/3})} \tag{6}$$

Introducing this result in equation 4, and substituting

$$u = \frac{1}{N' - vy} \tag{7}$$

the linear differential equation obtained is

$$\frac{du}{dv} = u\frac{4ky_0}{3Dv^{1/3}\left[1 + \frac{ky_0}{D}(v^{2/3} - v_0^{2/3})\right]} + \frac{2}{3}\frac{k}{Dv^{4/3}} \tag{8}$$

with the boundary condition $v = v_0$, $u = 1/(w_0 - 1/2)$.

The solution is

$$N = \frac{[1 + ky_0(v^{2/3} - v_0^{2/3})/D]^2}{(w_0 - 1/2)^{-1} + 2k^3y_0^2(v - v_0)/3D^3 + (4k^2y_0/D^2 - 4k^3y_0^2v_0^{2/3}/D^3)(v^{1/3} - v_0^{1/3}) + (-2k/D - 4k^2y_0v_0^{2/3}/D^2 - 2k^3y_0v_0^{4/3}/D^3)(v^{-1/3} - v_0^{-1/3}) + \frac{vy_0}{1 + ky_0(v^{2/3} - v_0^{2/3})/D} + \frac{1}{2}} \tag{9}$$

Substituting $x = v/v_0$, $\kappa = kw_0/Dv_0^{1/3}$, $\beta = ky_0v_0^{2/3}/D$, $w = N - vy$, this reduces to

$$\kappa = \frac{(w - 1/2)^{-1}[1 + \beta(x^{2/3} - 1)]^2 - (w_0 - 1/2)^{-1}}{\frac{2}{3}\beta^2(x - 1) + 4\beta(1 - \beta)(x^{1/3} - 1) + 2(1 - \beta)^2(1 - x^{-1/3})} \tag{10}$$

In order to eliminate w, a termination condition is required. Let us assume initially that w_0 is the same for all spurs. Then the terminating condition is the same as in ref. 1. Let the subscript m refer to the situation at the end of the spur's lifetime. At the termination time t_m, when another spur is formed in the volume $v = v_m$, the concentration in the spur is

$$N_m/v_m = y_0 \tag{11}$$

and

$$w_m = v_m(y_0 - y_m) = \frac{\beta w_0 x_m}{\kappa} \times \frac{\beta(x_m^{2/3} - 1)}{1 + \beta(x_m^{2/3} - 1)} \tag{12}$$

Introducing this into equation 10, w can be eliminated, giving

$$\kappa = \frac{[1 + \beta(x_m^{2/3} - 1)]^3}{\frac{2}{3}\beta^2(x_m - 1) + 4\beta(1 - \beta)(x_m^{1/3} - 1) + 2(1 - \beta)^2(1 - x_m^{-1/3})} - \frac{\beta^2 x_m(x_m^{2/3} - 1) - \kappa[1 + \beta(x_m^{2/3} - 1)]/2w_0}{w_0/\kappa(w_0 - 1/2)} \tag{13}$$

This is a relation involving only β, κ, x_m and w_0. It is easiest to assume values of β, x_m and w_0 and to calculate κ.

In Figs. 1 and 2, solutions of equation 13 are shown for $w_0 = 5$, $x_m = 10^6$, 10^3 and 8, and β ranging from 10^6 to 10^{-6} inclusive. Figure 1 is a logarithmic plot of β *vs.* κ, and Fig. 2 is a logarithmic plot of β *vs.* β/κ, the background ratio. As expected, lower values of x_m and lower values of β are associated with higher values of β/κ, as in the cylindrical model. An unsteadiness of trend in the $x_m = 10^3$ and $x_m = 8$ curves is believed to be a mathematical artifact. The high- and low-background regimes show up clearly.

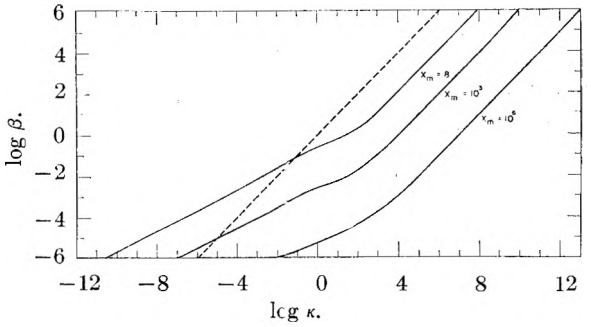

Fig. 1.—Plot of log κ *vs.* log β. The broken line represents $\beta = \kappa$.

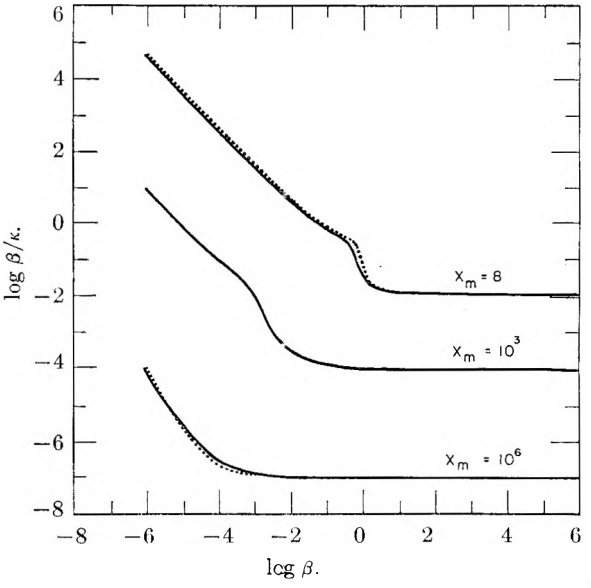

Fig. 2.—Plots of log β/κ *vs* log β: solid lines, $w_0 = 5$; broken lines, distribution of spur sizes.

A second approach permits consideration of the spur size distribution. Assume v_m = const, $v_0' = v_0/w_0$ = const. Then $x_m' = \text{const} = x_m w_0$. For a given set of physical constants, N_m and w_m will vary with w_0, and average values would be obtained by averaging over the distribution of values of w_0. Since this is not feasible, we shall instead pretend that w_m is constant, thus obtaining fictitious κ values for each spur size. The values of β/κ thus obtained will be averaged and weighted in accordance with the distribution of spur sizes. The values of β and κ are proportional to $w_0^{2/3}$.

For comparison with the values previously obtained, the spur size distribution used was

$w_0 = 2$	Frequency = 0.43
4	.22
6	.12
8	.10
14	.13
	1.00

This distribution is based on cloud chamber observations by Wilson.[5] It has been shown previously[6] that this approximation to the actual spur size distribution yields acceptable results. The mean value of w_0 in this distribution is 5.08.

Values of κ and β/κ were calculated for these values of w_0 and for values of x_m and β corresponding to those used in the previous calculation, except that no calculations paralleling the previous ones for $x_m = 10^3$ were made. For each calculation, the new x_m was the previous x_m multiplied by $5/w_0$, and the new β was the previous β multiplied by $(w_0/5)^{2/3}$. The values of β/κ were averaged and are shown as broken lines in Fig. 2. It will be seen that they are not very different from the solid lines except in the transition region. It is apparent that qualitative conclusions can be drawn from calculations using a single value of w_0.

Asymptotic expressions also were obtained for κ in the high-background and low-background regions.

In the low-background region

$$\kappa = 2\beta x_m w_0 = 2\beta x_m' \qquad (14)$$

In the high-background region

$$\kappa = \beta^2 x_m(x_m^{2/3} - 1) \qquad (15)$$

From the low-background asymptotic value, one can obtain a rather remarkable conclusion. Substituting

$$\beta/\kappa = y_0 v_0/w_0 \qquad (16)$$

we obtain

$$2y_0 v_0 x_m = 2y_0 v_m = 1 \qquad (17)$$

and from (11)

$$N_m = 1/2$$

Thus, in the low-background limit, and in the absence of scavengers, the average population of a spur at the end of its expansion would be 1/2 radical. However, the obvious relation of this result to the substitution $N' = N - 1/2$ casts doubt on its physical significance. A similar asymptotic development of equation A15 (see Appendix) yields

$$N_m = 1 \qquad (19)$$

It is interesting that the value for N_m in the low-background regime is found to be independent of track parameters and dose rate by two independent methods.

The physical significance of the model has been been treated before[7] and will be summarized briefly.

Under low-background conditions, the yield is the sum of chemical changes in the individual spurs, and is proportional to the dose. Under high-background conditions, the kinetics are similar to those of photochemistry, since the spurs have radical (or ion) concentrations similar to those of the bulk medium. The transition between these regimes is observed only under special conditions, which it is our aim to identify. Figure 2 seems to show that the transition region is not that at which $\beta/\kappa = 1$, but is rather that given by a line running through the bends of the curves.

High-background conditions are favored by low values of w_0 and k, and by high values of D and the dose rate I; low-background conditions conversely. All of these quantities except I appear explicitly in the equations. To point up the physical meaning of the model, let us show how I is present implicitly.

Let us suppose that the average value for the energy lost by the primary particle in producing a spur is 100 e.v. Then a dose rate of I rad/sec. is equivalent to the formation of $6.25 \times 10^{11} I$ spurs/g./sec., or $6.25 \times 10^{11} I\rho$ spurs/cc./sec., where ρ is the density of the medium.

In our model, the volume of the spur at t_m is the same as the volume in which one new spur is created in time t_m

$$(v_0^{2/3} + Dt_m)^{3/2} = (6.25 \times 10^{11} I\rho t_m)^{-1} \qquad (20)$$

This equation relates I to the track parameters. The equation can be simplified further for $x_m >> 1$, *i.e.*, $Dt_m >> v_0^{2/3}$. Then

$$t_m = 1.9 \times 10^{-5} (I\rho)^{-0.4} D^{-0.6} \qquad (21)$$

$$x_m = (Dt_m)^{3/2}/v_0 = 8.4 \times 10^{-3} (D/I\rho)^{0.6}/v_0 \qquad (22)$$

Thus the parameter x_m is substituted for I.

An application of these equations to an actual case is possible for electron irradiation of water. Rotblat and Sutton[8] have shown that the transition from the low-background to the high-background regime in water occurs at about 10^{10} rad/sec. Assuming $D = 2 \times 10^{-5}$cm.^{2}/sec., $v_0 = 10^{-21}$ cm.^{3}, we obtain from (22) $x_m = 1.3 \times 10^5$. This high value justifies the use of (22). Taking this dose rate as corresponding to the center of the bend in the plot of log β/κ *vs.* log β, we find by interpolation in Fig. 2 that log $\beta \approx -3.5$, log $\beta/\kappa \approx -5.7$, therefore log $\kappa \approx 2.2$. From the definition of κ we then obtain for the radical recombination rate constant $k = 8 \times 10^{-11}$ cm.^{3}/particle-sec., which may be considered plausible in view of the roughness of the calculation. Similar calculations can be carried out for other systems.

(5) C. T. R. Wilson, *Proc. Roy. Soc.* (London), **A104**, 192 (1923); D. E. Lea, "Actions of Radiations on Living Cells," Cambridge University Press, Cambridge, England, 2nd ed., 1955, p. 27.

(6) A. H. Samuel, Ph.D. Thesis, University of Notre Dame, 1952, pp. 46–48.

(7) A. H. Samuel, *Trans. Am. Nuclear Soc.*, **2**, 390 (1960).

(8) J. Rotblat and H. C. Sutton, *Proc. Roy. Soc.* (London), **A255**, 490 (1960).

Further development of the Magee model is planned, along the lines which have been mentioned. The next step is to introduce a reaction with substrate molecules. It is believed that analytical solutions may not be attainable in this case; if so, computer programs in ALGOL language will be substituted.

Acknowledgments.—It is a pleasure to thank Dr. Edwin M. Kinderman and Dr. Samuel I. Taimuty for their encouragement, and Dr. Joel L. Brenner for many helpful discussions and particularly for finding the solution given in the Appendix.

Appendix

Substituting equation 6 in equation 3 gives

$$\frac{dN}{dv} = -\frac{2}{3}\frac{kN(N-1)}{Dv^{4/3}} + \frac{y_0}{1 + ky_0(v^{2/3} - v_0^{2/3})} \quad (A1)$$

To solve this equation, we substitute

$$N' = N - 1/2 \quad (A2)$$

$$M = \frac{2k}{D} v^{-1/3} \quad (A3)$$

$$a = k^3 y_0 / D^3 \quad (A4)$$

and

$$b = 1 - k y_0 v_0^{2/3}/D \quad (A5)$$

The equation then becomes

$$\frac{dN'}{dM} = N'^2 - \frac{24a + aM^2 + bM^4}{4aM^2 + 4bM^4} \quad (A6)$$

If a function $f(M)$ can be found which satisfies

$$\frac{1}{f}\frac{d^2f}{dM^2} = \frac{24a + aM^2 + bM^4}{4aM^2 + 4bM^4} \quad (A7)$$

then the solution[9] of the Riccati equation A6 is

$$N' = \frac{1}{f}\frac{df}{dM} + \frac{1}{f^2(C - \int dM/f^2)} \quad (A8)$$

where C is a constant of integration.

The function f is obtained as an infinite series. There are two solutions

$$\text{(I)} \quad f(M) = M^{-2} + z_1 + z_2 M^2 + \ldots\ldots + z_n M^{2n-2} + \ldots\ldots \quad (A9)$$

with the recurrence formula

$$z_n = \frac{-bz_{n-2} + z_{n-1}[4b(2n-4)(2n-5) - a]}{24a - 4a(2n-2)(2n-3)}, \quad z_0 = 1, z_1 = \frac{b}{a} - \frac{1}{24} \quad (A10)$$

and

$$\text{(II)} \quad f(M) = M^3 + q_1 M^5 + q_2 M^7 + \ldots\ldots + q_n M^{2n+3} + \ldots\ldots \quad (A11)$$

with the recurrence formula

$$q_n = \frac{-bq_{n-2} + q_{n-1}[8bn(2n-1) - a]}{24a - 4a(2n+3)(2n+2)}, \quad q_0 = 1, q_1 = -\frac{3}{7}\frac{b}{a} + \frac{1}{56} \quad (A12)$$

This solution has not been found useful for further development. However, a low-background limit can be obtained. If y_0 is very small, and $bM^4 >> 24a$, (A6) reduces to

$$\frac{dN'}{dM} = N'^2 - \frac{1}{4} \quad (A13)$$

which has the solution

$$M - M_0 = \frac{2\kappa}{w_0}(x^{-1/3} - 1) = \ln \frac{1 - \frac{1}{N}}{1 - \frac{1}{N_0}} \quad (A14)$$

where again

$$x = v/v_0$$

Substituting equations 2 and 16, the number of active particles at time t_m is

$$N_m = \frac{1}{1 - \left[1 - \frac{1}{w_0(\beta/\kappa + 1)}\right] \exp\left[\frac{2\kappa}{w_0}(x_m^{-1/3} - 1)\right]} \quad (A15)$$

Since, from equations 11 and 16

$$N_m = \frac{\beta w_0 x_m}{\kappa}$$

this is another equation in the four parameters β, κ, w_0, x_m and is comparable to equation 13 for the low-background region. For large κ, the right-hand side of equation A15 reduces to 1—just twice the asymptotic value obtained in equation 18.

(9) E. Kamke, "Differentialgleichungen: Lösungsmethoden und Lösungen," Chelsea Publishing Co., New York, N. Y., 3rd ed., 1948, equation 1.33, p. 298.

METAL–POLYELECTROLYTE COMPLEXES. IX. THE POLY-N-ETHYLENEGLYCINE–COPPER(II) COMPLEX

BY DANIEL H. GOLD[1] AND HARRY P. GREGOR

Department of Chemistry of the Polytechnic Institute of Brooklyn, Brooklyn, N. Y.

Received July 21, 1961

The synthetic polyampholyte poly-N-ethyleneglycine demonstrated a weak binding for sodium and potassium ions. Spectrophotometric studies in the presence of Cu(II) showed that complexes were formed with an absorption maxima in the 680–780 mμ region. Continuous variations analysis showed that three glycine ligands were bound to a copper ion indicating 6-fold coördination. Potentiometric titrations of the polyampholyte in the presence of Cu(II) showed the simultaneous binding of two glycine units with a formation constant log k_1k_2 = 12.04, with a third glycine unit being weakly bound with a formation constant log k_3 = 2.88.

Introduction

The preparation and general properties of a new synthetic polyampholyte poly-N-ethyleneglycine (PEG) were described recently.[2] In contrast to other synthetic polyampholytes reported by Alfrey, *et al.*,[3–5] Wagner and Long,[6] Schloegl and Fabitschowitz,[7] Katchalsky and Miller[8] and Morris, *et al.*,[9] this polymer was of a relatively low base molecular weight (101) and was soluble in the region of the isoelectric point. Previous papers in this series have reported the binding of alkali, alkaline earth and transition metals with polyacids,[10,11] and of copper and silver with the polybase poly-N-vinylimidazole.[12] This communication deals with a study of the binding of sodium, potassium and copper(II) ions by poly-N-ethyleneglycine.

Experimental

The synthesis of PEG *via* the polymerization of the methyl ester of N-ethyleneglycine yielded a product free of salts and other low molecular weight contaminants.[2] As indicated by diffusivity through membranes and moving boundary experiments, its estimated molecular weight was in the range 5,000–15,000. The polymer was soluble over the *p*H range 1–12 at polymer concentrations as high as 1 *M* (base moles); more dilute (0.1 *M*) polymer solutions were not salted out by ordinary 1–1 electrolytes at concentrations as high as 1 *M*. The isoelectric point determined viscometrically was 2.75 while from electrophoretic mobility measurements it was 2.9. The isoionic point or the *p*H of the pure ampholyte (0.01 *M*) in water was 3.45.

The neutral salts used were of reagent grade with in no case a heavy metals content greater than 0.001%. Titrations of PEG in the absence of copper were carried out as follows: Identical polymer solutions were titrated by adding acid to one solution, base to the other and the two titration curves joined. Titrations in the presence of an excess of neutral salt were performed by adding acid to the polymer solution and back-titrating with base. Titrations were performed at 25.0 ± 0.1° under nitrogen; carbon dioxide-free water was used throughout. A Beckman Model G *p*H meter was employed. Because of possible gel formation during titrations in the presence of Cu(II), a stepwise procedure similar to that previously reported[12] was employed where measurements were made after equilibration at 25 ± 0.1°.

Absorption spectra were measured at room temperature (25 ± 3°) with 1-cm. silica cells against water blanks; a Beckman Model DU spectrophotometer was used.

Results and Discussion

Titrations of 0.01 *M* PEG in the presence of no salt, 1 *M* sodium nitrate and 1 *M* potassium nitrate in the *p*H 2.5 range are shown in Fig. 1. The isoelectric point of PEG can be calculated from its titration behavior, using the method of Edsall, *et al.*[13] Letting B represent amino functional groups and A the carboxyl groups, hydrolysis produces equal concentrations of BH^+ and OH^- with the former and A^- and H^+ with the latter and

$$[BH^+] + [H^+] = [A^-] + [OH^-]$$

where the brackets represent concentrations. Since the isoionic point is at *p*H 3.45, $[H^+] > [OH^-]$ and $[A^-] > [BH^+]$ or the solution is above the isoelectric *p*H where $[A^-] = [BH^+]$. If a strong acid is added then $[A^-]$ is lowered as $[BH^+]$ is raised, and the *p*H when they are equal is the isoelectric point. Analysis of the titration data of Fig. 1 taken in the absence of salt and assuming an activity coefficient of unity led to a calculated isoelectric point of 2.84 in excellent agreement with the point established by electrophoretic mobility and viscosity.

The titration of polyelectrolytes generally can be expressed in terms of a modified Henderson–Hasselbach relationship[10,14]

$$pH = pK_a - n \log (1 - \alpha)/\alpha \qquad (1)$$

where α is the degree of neutralization by acid or base and n and pK_a are constants. With titration data taken in the absence of added salt this plot yielded a curved line at low *p*H levels (titration of the $RCOO^-$ groups) with a pK_a value of 2.2 and a slope n of unity; the titration of the amino group gave a somewhat better line with pK_a = 8.15 with a slope of 7.45. This latter, extremely high slope may result because protons are being extracted from a positively charged backbone which is shielded by negatively charged carboxyl groups, the latter acting to repel the hydroxide ions added.

(1) Taken in part from the Dissertation of Daniel H. Gold, submitted in partial fulfillment of the requirements for the degree of Doctor of Philosophy in Chemistry, Polytechnic Institute of Brooklyn, June, 1957.

(2) H. P. Gregor, D. H. Gold and G. K. Hoeschele, *J. Am. Chem. Soc.*, **77**, 4743 (1955).

(3) T. Alfrey, Jr., H. M. Morawetz, E. B. Fitzgerald and R. M. Fuoss, *ibid.*, **72**, 1864 (1950).

(4) T. Alfrey, Jr., and H. M. Morawetz, *ibid.*, **74**, 436 (1952).

(5) T. Alfrey, Jr., R. M. Fuoss, H. Morawetz and H. Pinner, *ibid.*, **74**, 438 (1952).

(6) H. L. Wagner and F. A. Long, *J. Phys. Colloid Chem.*, **55**, 1512 (1951).

(7) K. Schloegl and H. Fabitschowitz, *Monatsh. Chem.*, **85**, 1223 (1954).

(8) A. Katchalsky and I. R. Miller, *J. Polymer Sci.*, **13**, 57 (1954).

(9) L. R. Morris, R. A. Mock, C. A. Marshall and J. H. Howe, *J. Am. Chem. Soc.*, **81**, 377 (1959).

(10) H. P. Gregor and M. Frederick, *J. Polymer Sci.*, **23**, 451 (1957).

(11) H. P. Gregor, L. B. Luttinger and E. M. Loebl, *J. Phys. Chem.*, **59**, 34, 366, 559, 990 (1955).

(12) D. H. Gold and H. P. Gregor, *ibid.*, **64**, 1461, 1464 (1960).

(13) J. T. Edsall, H. Edelhoch, R. Lontie and P. R. Morrison, *J. Am. Chem. Soc.*, **72**, 4641 (1950).

(14) A. Katchalsky and P. Spitnik, *J. Polymer Sci.*, **2**, 432 (1947).

As α increases the shielding effect similarly increases, tending to make for particularly high slopes.

Inspection of Fig. 1 discloses certain unusual aspects. Considering the polyzwitterionic structure given below it is apparent that the addition of

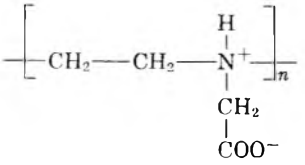

neutral salt will cause the polyampholyte to act like a stronger base when titrated with acid and a stronger acid when titrated with base with the *p*H of the isoelectric point remaining unchanged if both acidic and basic dissociation constants are affected in a like manner. As a consequence, polyampholyte titration curves usually rotate about their isoelectric points when neutral salt is added, an effect observed by Sorenson[15] with natural polyampholytes and applied by Alfrey and co-workers[5] for the detection of the isoelectric point of a synthetic polyampholyte.

When PEG was titrated in the presence of 1 *M* sodium and potassium nitrates a rotation of the titration curves about the isoelectric point was not observed; rather, a downward shift of the titration curves resulted. This behavior is consistent with a binding of the sodium and potassium ions by the polymer, with the release of hydrogen ions. This view is supported by observations of Schwarzenbach and co-workers[16,17] on the binding of sodium and potassium by ethylenediaminetetraacetic acid, which is structurally similar to PEG.

In order to separate this binding effect from a pure salt effect, PEG was titrated in the presence of tetramethylammonium bromide; the quaternary ammonium cations are not bound by EDTA. Here the normal salt effect with rotation is observed corroborating the view that sodium and (to a lesser extent) potassium ions are bound by this protein-like structure.

The absorbancy (log I^0/I) of copper nitrate, PEG and a mixture of PEG with copper in solutions adjusted to *p*H 3.6 was measured in the 400–900 mμ region, where PEG absorbs weakly. When the two reactants were mixed a new species was formed as shown by the formation of an extremely strong absorption band at low wave lengths (< 400 mμ) and a new absorption peak in the 700 mμ region. An evaluation of the predominant moiety present under these experimental conditions was made using the method of continuous variations described by Job.[18] Mixtures of the reactants at different ratios keeping the total concentration constant at 0.02 *M* were prepared. Assuming Beer's law, the solution absorbancy was corrected for reactant absorbancy assuming no reaction had taken place and was plotted against the mole fraction of the copper present. As the PEG–Cu ratio was increased from 1:3 to 3:1 the absorbancy increased and the peak shifted to shorter wave lengths. Still further increases in the PEG–Cu ratio resulted in a decreased absorbancy and a shift of the peaks back to longer wave lengths.

A continuous variation analysis of the PEG–Cu system at 610 and 700 mμ is shown in Fig. 2. At both wave lengths sharp peaks were found at a copper mole fraction of 0.25, corresponding to a complex of 3 glycine-type ligands with one copper ion. Since each glycine ligand has two coördinating positions, 6-fold copper-(II) coördination is indicated.

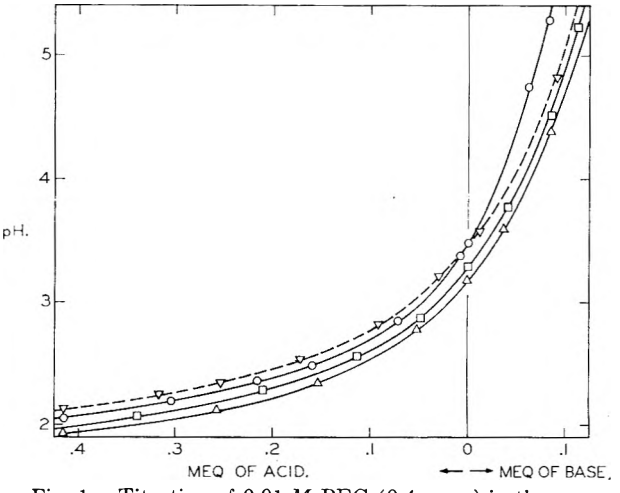

Fig. 1.—Titration of 0.01 *M* PEG (0.4 meq.) in the presence of no salt ○, 1 *M* sodium nitrate △, 1 *M* potassium nitrate □ and 1 *M* tetramethylammonium bromide ▽.

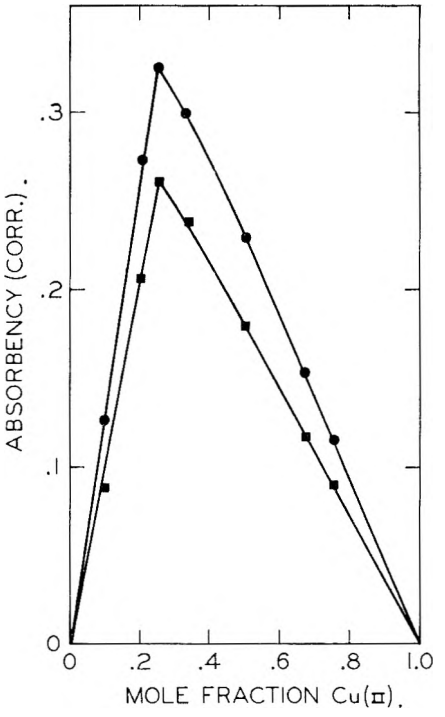

Fig. 2.—Continuous variations analysis of the poly-N-ethyleneglycine–Cu(II) complex, adjusted to *p*H 3.60 and measured at 700 mμ (●) and 610 mμ (■) using a 0.02 *M* total solution concentration.

(15) S. P. L. Sorenson, *Compt. rend. trav. lab. Carlsberg*, **12**, 68 (1919).

(16) G. Schwarzenbach and H. Ackerman, *Helv. Chim. Acta*, **30**, 1798 (1947).

(17) G. Schwarzenbach, E. Kampitsch and R. Steiner, *ibid.*, **28**, 828 (1945).

(18) P. Job, *Ann. Chim.* (Paris), [10], **9**, 113 (1928); [11], **6**, 97 (1936).

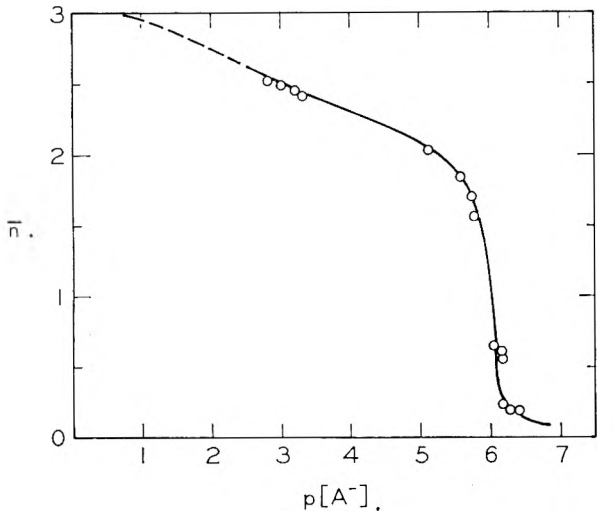

Fig. 3.—Formation curve for the poly-N-ethyleneglycine–copper(II) nitrate complex at 25°.

It is of interest to compare this with the results of Quintin[19] who investigated glycine–copper complexes spectrophotometrically and found a 1:1 complex at low *p*H and a 2:1 complex at *p*H 7 and above. From an analysis of his results, Quintin also concluded that a 3:1 complex also might exist but could not directly identify it. Bjerrum, Ballhausen and Jorgenson[20] found that the Cu(II)–ammine complexes also show a coördination number of 6, with 4 of the ligands in the planar positions and two perpendicular to the plane and somewhat farther from the central atom. The placement of the last two ligands required a higher solution concentration than for the others.

Assuming complete reaction, the molar absorptivity ($1/bc \log I^0/I$) of the PEG–Cu complex is 74 ±2 at 690 mμ. Dean and Soonpaa[21] found the 2:1 glycine–copper complex had an absorptivity of 46.

The titration of PEG in the presence of several concentrations of Cu(II) was carried out. A pronounced shift to lower *p*H values was observed as the copper ion concentration was increased, typical of complex-forming systems. The method of Bjerrum[22] for the calculation of individual formation constants was employed. Here the average number of ligands bound per metal ion present is

$$\bar{n} = \frac{[A_T] - [A^-] - [HA] - [H_2A^+]}{[Cu_T^{++}]} \qquad (2)$$

where $[A_T]$ is the total base molar concentration of PEG, $[A^-]$ the concentration of negatively charged glycine units ($RNCH_2COO^-$), [HA] the concentration of zwitterionic glycine ($RNH^+CH_2COO^-$), $[H_2A^+]$ the concentration of diacidic glycine (RNH^+CH_2COOH) and $[Cu_T^{++}]$ the total molar concentration of cupric ion. From the results of the continuous variations analysis

$$[A_T] = [A^-] + [HA] + [H_2A^+] + 3[CuA_3^-] \qquad (3)$$

$$[Cu_T^{++}] = [Cu^{++}] + [CuA_3^-] \qquad (4)$$

From equations 3 and 4 and the solution electroneutrality requirement it readily may be shown that

$$[HA] = [A_T](1 - \alpha) - [H^+] + [OH^-] - 2[H_2A^+] \qquad (5)$$

Since only titration data below *p*H 5 were used in the analysis, $[OH^-]$ was negligible in comparison to the other terms in equation 5 and was neglected. Also, it easily may be demonstrated that $[HA] >> [H_2A^+]$ over the *p*H range treated if the second polyampholyte acid dissociation constant is less than 2.5×10^{-5}; this will be demonstrated subsequently.

In some of the studies previously reported in this series[10,11] the values of $\bar{n}$ and $[A^-]$ could be calculated using the functional relationship between the concentration of charged and uncharged ligand groups as expressed by a suitably modified Henderson–Hasselbach equation. However, since the titration of PEG in the absence of a coördinating metal did not give a linear plot of *p*H against log $(1-\alpha)/\alpha$, a different relationship was used.[23] Here the polyacid dissociation constant is taken as a function of the degree of chain charging or α

$$K_a' = \frac{[H^+][A^-]}{[HA]} = f(Z) \qquad (6)$$

where (Z) is $[A^-]/[A_T]$ and in the absence of a coordinating metal is equal to α. Since when $(Z) > 0.1$, K_a' is smaller than 2.5×10^{-5}, and the previous simplifying assumption is justified.

In the presence of copper

$$(Z) = \alpha + \frac{[CuA_3^-]}{[A_T]} = \frac{1}{3[A_T]}\{\alpha[A_T] + [H^+] + 2[A^-]\} \qquad (7)$$

On the basis that coördination does not alter the dissociation relation 6 but changes only the degree of charge on the polymeric chain, equations 6 and 7 will produce a consistent value for $[A^-]$ by an iterative procedure.

TABLE I

FORMATION CONSTANTS FOR POLY-N-ETHYLENEGLYCINE, GLYCINE AND N-SUBSTITUTED GLYCINES WITH COPPER(II) AT 25°

Ligand	Log k_1	Log K_2
PEG		12.04
Glycine[a]		15.10
Glycine[b]	8.28	16.0
Glycine[c]	8.38	15.17
N-Methylglycine[c]	7.94	14.59
N-Ethylglycine[c]	7.34	13.55
N-Propylglycine[c]	7.25	13.31
N-Butylglycine[c]	7.32	13.50
N,N-Dimethylglycine[c]	7.30	13.65
N,N-Diethylglycine[c]	6.88	12.86

[a] N. C. Li and E. Doody, *J. Am. Chem. Soc.*, 76, 221 (1954). [b] R. M. Keefer, *ibid.*, 70, 476 (1948). [c] Ref. 24.

The calculated formation function is shown in Fig. 3. It is observed that the PEG–Cu system forms a strong 2:1 complex and a considerably weaker 3:1 complex. The 2:1 complex is appar-

(19) M. Quintin, *Compt. rend.*, **231**, 1226 (1950); **232**, 228 (1951).

(20) J. Bjerrum, C. J. Ballhausen and C. K. Jorgenson, *Acta Chem. Scand.*, **8**, 1275 (1954).

(21) R. B. Dean and H. Soonpaa, *J. Am. Chem. Soc.*, **74**, 6108 (1952).

(22) J. Bjerrum, "Metal Ammine Formation in Aqueous Solution," P. Haase and Son, Copenhagen, 1941.

(23) J. B. Andelman, G. K. Hoeschele and H. P. Gregor, *J. Phys. Chem.*, **63**, 206 (1959).

ently formed in a one-step process since the slope of the formation curve is quite steep up to $\bar{n} = 2$. The third step is displaced considerably from the first two and is weaker. Formation constants for PEG–Cu are listed in Table I together with values for glycine and substituted glycines. The 2:1 PEG–Cu complex is weaker than the glycine–Cu complex and comparable with the N,N-diethylglycine–Cu complex. Basolo and Chen[24] concluded that the progressive decline in stability between the substituted glycines and copper as the alkyl substituents became larger was indicative of steric hindrance. Agreement between the log K_2 values for the PEG–Cu and N,N-diethylglycine–Cu systems is consistent with the planarity requirement for the first four Cu(II) coördination positions where steric hindrance makes for a lowered stability constant.

The observation of a 3-step reaction indicating 6-fold Cu(II) coördination is in agreement with the spectroscopic data presented earlier.

Acknowledgment.—This investigation was supported in part by the Public Health Service Research Grant RG-2934 from the Division of General Medical Sciences, Public Health Service.

(24) F. Basolo and Y. T. Chen, *J. Am. Chem. Soc.*, **76**, 953 (1954).

THE POLAROGRAPHIC DETERMINATION OF THE FORMATION CONSTANTS OF THE OXALATE COMPLEXES OF COPPER(II) AND CADMIUM(II) IN LIGHT AND HEAVY WATER

BY DONALD L. MCMASTERS, JOSEPH C. DIRAIMONDO, LOWELL H. JONES, R. PHILIP LINDLEY AND EUGENE W. ZELTMANN

Department of Chemistry of Beloit College, Beloit, Wisconsin

Received July 31, 1961

The formation constants of the dioxalato cuprate(II) complex and the cadmium(II)–oxalate complexes have been determined polarographically in light water (H_2O) and heavy water (D_2O). The over-all formation constant of the dioxalato cuprate(II) complex in light water is 1.87×10^9 ($\log K_2 = 9.27$) and in heavy water is 3.27×10^9 ($\log K_2 = 9.51$). The over-all formation constants for the cadmium(II)–oxalate complexes in light water are 4.10×10^2 for K_1 ($\log K_1 = 2.61$), 1.29×10^4 for K_2 ($\log K_2 = 4.11$) and 1.15×10^5 for K_3 ($\log K_3 = 5.06$). In heavy water the over-all formation constants are 4.60×10^2 for K_1 ($\log K_1 = 2.66$), 1.60×10^4 for K_2 ($\log K_2 = 4.20$) and 1.49×10^5 for K_3 ($\log K_3 = 5.17$). All these constants were determined at $25.0 \pm 0.05°$ and at an ionic strength of 1.00 with sodium nitrate. These results indicate that light water is more strongly solvating than heavy water.

Introduction

Very few studies have been reported on the polarography of solutions in heavy water, D_2O. Studies have been made on the discharge of hydrogen and deuterium at the dropping mercury electrode from mixtures of light and heavy water.[1,2] The hydrogen overvoltages in light and heavy water and in their mixture are discussed in a paper by Heyrovsky.[3]

As far as these authors know, there have been no published reports on the determination of the half-wave potentials of either simple or complexed metal ions in heavy water. Nor have any type of measurements been reported on the deuterium solvent isotope effect on the formation of metal coördination complexes.[3a] However, a considerable amount has been done on acid dissociation effects. Reference is made to three recent papers.[4–6]

This paper reports the results of the polarographic determination of the over-all formation constant of the dioxalato cuprate(II) complex and the formation constants of the cadmium(II)–oxalate complexes in light and heavy water. The formation constant of the copper(II) oxalate ion-pair was not determined because of the difficulty in obtaining the necessary low concentration of oxalate. In the concentration range studied, no evidence was obtained to indicate that the trioxalato cuprate(II) complex would form.

The formation constant of the dioxalato cuprate(II) complex, K_2, in light water has been reported by several investigators. Their results are summarized in Table I.

TABLE I

LITERATURE VALUES OF LOG K_2 FOR THE DIOXALATO CUPRATE(II) COMPLEX

Log K_2	Ionic strength	Method	Ref.
8.3	0.06	E.m.f.(Cu)	7
8.5	.1	E.m.f.(Cu)	8
10.3	.3	Polarography	9
9.24	1.0	Polarography	10
9.36	1.1	*p*H titration	11
9.70	1.0	Polarography	12

The formation constants of the cadmium(II)–oxalate complexes have been investigated pre-

(1) J. Heyrovsky and O. H. Muller, *Collection Czechoslov. Chem. Communs.*, **7**, 281 (1935).

(2) J. Novak, *ibid.*, **9**, 207 (1937).

(3) J. Heyrovsky, *ibid.*, **9**, 273 (1937).

(3a) See also N. C. Li, P. Tang and R. Mathur, *J. Phys. Chem.*, **65**, 1074 (1961), on deuterium isotope effects on dissociation constants and formation constants.

(4) C. A. Bunton and V. J. Shiner, Jr., *J. Am. Chem. Soc.*, **83**, 42 (1961).

(5) E. A. Halevi, F. A. Long and M. A. Paul, *ibid.*, **83**, 305 (1961).

(6) V. J. Shiner, Jr., and M. L. Smith, *ibid.*, **83**, 593 (1961).

(7) H. T. S. Britton and M. E. D. Jarrett, *J. Chem. Soc.*, 1489 (1936).

(8) H. S. Riley, *ibid.*, 1307 (1929).

(9) L. Meites, *J. Am. Chem. Soc.*, **72**, 184 (1950).

(10) D. L. McMasters, Ph.D. Thesis, Indiana University, 1959.

(11) J. I. Watters, *J. Am. Chem. Soc.*, **81**, 1560 (1951).

(12) R. DeWitt and J. I. Watters, *ibid.*, **76**, 3810 (1959).

viously by the methods of solubility and conductivity. The experimental results are summarized in Table II. None of these papers lists a value for the formation of the trioxalato-cadmiate(II) complex. Cadmium has a coördination number of six and should be capable of coördinating three oxalate ions. Polarographic evidence is reported in this paper that indicates the presence of this third complex.

TABLE II

LITERATURE VALUES OF LOG K_1 AND LOG K_2 FOR THE CADMIUM(II)–OXALATE COMPLEXES

Log K_1	Log K_2	Ionic strength	Method	Ref.
3.52	..	$\rightarrow 0$	Solubility	13
4.00	5.77	$\rightarrow 0$	Conductivity	14
3.89	..	$\rightarrow 0$	Solubility	15
..	5.66	$\rightarrow 0$	Solubility	16

Experimental

Reagents and Chemicals.—Distilled water and 99.5+% pure heavy water, D_2O, were used as solvents. All other chemicals were reagent grade and were used without further purification. Anhydrous cadmium nitrate[17] was used in the preparation of the heavy water stock solution. All the copper nitrate and cadmium nitrate solutions were standardized by electrodeposition. A 0.25 M stock solution of sodium oxalate was made in light water and a 0.20 M stock solution in heavy water; both were prepared from primary standard sodium oxalate. A 5.00 M solution of sodium nitrate in light water and a 2.50 M solution in heavy water were used in the preparation of the supporting electrolyte. (The concentrations of the stock solutions are given because the solubility of the salts varies considerably between the two solvents.) No maximum suppressor was required.

All solutions used in the polarographic measurements had, in addition to a varying sodium oxalate concentration, a copper ion concentration of 5.78×10^{-4} M in light water and 5.56×10^{-4} M in heavy water; a cadmium ion concentration of 5.50×10^{-4} M in light water and 5.59×10^{-4} M in heavy water. The ionic strength of the working solutions was adjusted to 1.00 by using the appropriate amounts of sodium nitrate electrolyte. Just prior to usage, the working solutions were freed of oxygen by bubbling a stream of prepurified nitrogen through them.

Apparatus.—The polarograms were recorded at 25.0 ± 0.05° with a Sargent Model XXI polarograph. An H-type cell, very similar to that described by Kolthoff and Lingane,[18] was used in light water. The agar bridge was made from 3% agar in 1.0 M potassium nitrate and a water-jacketed, bulb-type saturated calomel reference electrode was inserted into a 1.0 M potassium chloride solution in the reference side of the cell.

In heavy water, a modified H-type cell was used for the copper(II) solution. One section was a demountable saturated calomel reference electrode constructed with heavy water. The horizontal part of the reference electrode was filled with 3% agar containing saturated potassium chloride in heavy water. The other two sections were filled with the deaerated working solution and were separated by a medium porosity sintered Pyrex disk to minimize the diffusion of chloride ions from the S.C.E. to the working side of the cell. For the cadmium(II) solutions a two-compartment, demountable H-cell was used in heavy water instead of the more elaborate three-compartment cell.

The same dropping mercury electrode was used in all this work. In light water the D.M.E. had a drop time of 4.07 sec. and a rate of flow of mercury of 1.57 mg./sec. at a height of 62.50 cm. (open circuit). Similar figures in heavy water are: drop time, 4.29 sec., a rate of flow of mercury of 1.56 mg./sec.

The span of the polarograph was set at 0.5 volt and the initial and final potentials were measured to ±0.01 mv. with a Rubicon Model B potentiometer. The resistance of the cell system was measured at 1000 cycles per sec. with a Model RCM 15Bl Serfass conductivity bridge.

Calculations.—Current measurements were made using the maximum currents as suggested by Hume, *et al.*,[19] for the Sargent Model XXI polarograph. Corrections were made for the residual current and for the iR drop due to the recorder sensitivity setting (446.5 ohms at 0.020 μamp./mm.) and the cell system resistance (approximately 100 ohms). The half-wave potential calculations were made on an IBM 650 electronic computer.[20]

Seven values of the half-wave potential were averaged for the uncomplexed copper in light water, and eight values of the half-wave potential were averaged for the uncomplexed copper in heavy water. Four independent values of the half-wave potential were averaged for each oxalate concentration in both light and heavy water. The range of the half-wave potentials used was well within 1.0 mv. in the majority of cases but occasionally the difference between the highest and lowest values for a given concentration slightly exceeded 2 mv. For all polarograms the slope of the plot log $(i_d-i)/i$ *vs.* voltage indicated reversibility. The value for the slope was +0.030 ± 0.001 or less better than 80% of the time and the maximum deviation did not exceed ±0.006.

For the cadmium(II)–oxalate system from four to six independent values of the half-wave potentials were averaged for each solution. The range of the half-wave potentials used was well within 1.0 mv. in the majority of instances. The slope of the plot of log (i_d-i) *vs.* potential indicated reversibility. The value of the slope was 0.030 ± 0.001 or less better than 70% of the time and only two times outside the limits of 0.030 ± 0.002.

The half-wave potentials were not corrected for liquid junction potentials, but it is assumed that no serious errors would result from neglecting the probably-small junction potentials.

The $F_j(X)$ terms are defined by DeFord and Hume[21] for

TABLE III

EXPERIMENTAL RESULTS. DIOXALATO CUPRATE(II) COMPLEX IN LIGHT WATER

$[C_2O_4^=]$, m	$E_{1/2}$, *vs.* S.C.E., v.	i_d, mm.	$F_0(X)$	$F_1(X)$	$F_2(X)$
0.0000	$+0.025_{16}$	202.6			
.1017	$-.191_0$	194.4	2.11×10^7	2.075×10^8	2.04×10^9
.08643	$-.186_4$	191.6	1.50×10^7	1.74×10^8	2.01×10^9
.07118	$-.181_1$	194.7	9.78×10^6	1.37×10^8	1.93×10^9
.05592	$-.173_9$	197.6	5.50×10^6	9.84×10^7	1.76×10^9
.04067	$-.165_9$	190.5	3.06×10^6	7.53×10^7	1.85×10^9
.02542	$-.153_6$	195.0	1.15×10^6	4.52×10^7	1.78×10^9
.01017	$-.129_9$	196.3	1.80×10^5	1.77×10^7	1.74×10^9

Av. $F_2(X) = 1.87 \times 10^9 = K_2$

TABLE IV

EXPERIMENTAL RESULTS. DIOXALATO CUPRATE(II) COMPLEX IN HEAVY WATER

$[C_2O_4^=]$, m	$E_{1/2}$ *vs.* S.C.E., v.	i_d, mm.	$F_0(X)$	$F_1(X)$	$F_2(X)$
0.000	$+0.031_9$	177.4			
.08037	$-.184_2$	172.7	2.79×10^7	2.59×10^8	3.22×10^9
.06831	$-.180_4$	173.4	1.54×10^7	2.26×10^8	3.30×10^9
.05626	$-.175_8$	170.1	1.10×10^7	1.95×10^8	3.47×10^9
.04420	$-.168_8$	174.2	6.22×10^6	1.41×10^8	3.18×10^9
.03215	$-.160_5$	173.6	3.27×10^6	1.02×10^8	3.16×10^9

Av. $F_2(X) = 3.27 \times 10^9$

(13) W. J. Clayton and W. C. Vosburgh, *J. Am. Chem. Soc.*, **59**, 2414 (1937).

(14) W. C. Vosburgh and J. F. Beckman, *ibid.*, **62**, 1028 (1940).

(15) R. W. Money and C. W. Davies, *Trans. Faraday Soc.*, **28**, 609 (1923).

(16) J. E. Barney, W. J. Argersinger, Jr., and C. A. Reynolds, *J. Am. Chem. Soc.*, **73**, 3785 (1951).

(17) G. Malguori, *Gazz. chim. ital.*, **58**, 209 (1928).

(18) I. M. Kolthoff and J. J. Lingane, "Polarography," Interscience Publishers, New York, N. Y., 1952, p. 354.

(19) D. N. Hume, D. D. DeFord and G. C. B. Cave, *J. Am. Chem. Soc.*, **73**, 5323 (1951).

(20) D. L. McMasters and W. B. Schaap, *Proc. Indiana Acad. Sci.*, **67**, 111 (1958).

(21) D. D. DeFord and D. N. Hume, *J. Am. Chem. Soc.*, **73**, 5321 (1951).

TABLE V

EXPERIMENTAL RESULTS. CADMIUM(II)–OXALATE COMPLEXES IN LIGHT WATER

$[C_2O_4^=]$, m	$E_{1/2}$ vs. S.C.E., v.	i_d, mm.	$F_0(X)$	$F_1(X)$	$F_2(X)$	$F_3(X)$
0.0000	−0.5754	180.0				
.2010	− .6685	164.5	1542	7667	3.61×10^4	1.154×10^5
.1610	− .6609	165.1	850.5	5277	3.023×10^4	1.076×10^5
.1416	− .6569	156.7	656.5	4628	2.979×10^4	1.193×10^5
.1217	− .6532	162.2	475.4	3898	2.866×10^4	1.295×10^5
.1014	− .6468	166.2	282.0	2771	2.329×10^4	1.025×10^5
.06080	− .6331	166.7	96.76	1575		
.04020	− .6221	174.7	39.22	950.7		
.02062	− .6089	166.8	14.70	664.4		
.01444	− .6022	161.4	9.018	555.3		
.01238	− .6002	162.4	7.668	538.6		
.00618	− .5920	178.9	3.915	476.4		

TABLE VI

EXPERIMENTAL RESULTS. CADMIUM(II)–OXALATE COMPLEXES IN HEAVY WATER

$[C_2O_4^=]$, m	$E_{1/2}$ vs. S.C.E., v.	i_d, mm.	$F_0(X)$	$F_1(X)$	$F_2(X)$	$F_3(X)$
0.0000	−0.5963	165.5				
.1807	− .6622	152.8	1507	8333	4.356×10^4	1.525×10^5
.1622	− .6586	148.6	1171	7215	4.165×10^4	1.581×10^5
.1406	− .6537	156.1	760.7	5404	3.517×10^4	1.363×10^5
.1205	− .6495	154.8	552.8	4580	3.420×10^4	1.510×10^5
.1004	− .6440	156.1	357.3	3549	3.077×10^4	1.471×10^5
.08033	− .6380	162.0	215.7	2673	2.755×10^4	1.438×10^5
.06024	− .6300	156.4	119.8	1972	2.510×10^4	1.511×10^5
.04054	− .6208	139.9	65.40			
.02001	− .6050	160.6	16.64			
.01801	− .6030	149.0	15.34	796.1	1.866×10^4	1.477×10^5
.01635	− .6009	144.3	13.45	761.6	1.844×10^4	1.492×10^5
.01401	− .5990	157.6	10.64	687.8		
.01201	− .5962	147.9	9.102	674.7	1.788×10^4	1.565×10^5
.008005	− .5899	141.8	5.811	600.9	1.760×10^4	

the system as

$$F_0(X) = \text{antilog } \langle (n/0.05916)([E_{1/2}]_s - [E_{1/2}]_c) + \log [(i_d)_s/(i_d)_c] \rangle$$

$$F_0(X) = K_0 + K_1[\text{ox}] + K_2[\text{ox}]^2 + K_3[\text{ox}]^3$$

$$F_1(X) = [F_0(X) - K_0]/[\text{ox}] = K_1 + K_2[\text{ox}] + K_3[\text{ox}]^2$$

$$F_2(X) = [F_1(X) - K_1]/[\text{ox}] = K_2 + K_3[\text{ox}]$$

$$F_3(X) = [F_2(X) - K_2]/[\text{ox}] = K_3$$

Since the values of the several activity coefficients which appear in the fundamental equations are unknown at present, the formation constants will be in terms of molarities instead of activities, with reference to the ionic strength used. Additional details may be secured from other papers by Hume, *et al.*[19,21,22]

Results and Discussion

Copper(II)–Oxalate Complex System.—The experimental results and calculations are summarized in Table III for light water and in Table IV for heavy water. A graph of log $F_0(X)$ *vs.* log [ox] indicates that the dioxalato cuprate(II) complex is the predominating species in the concentration range studied. The slope of the lines is 2.05 instead of the theoretical 2.00 for the number of ligands attached.

The results of an experiment of this type usually are presented in graphical form. Because of the large range of values, this is impossible for the $F_0(X)$ and $F_1(X)$ data. A graph of $F_2(X)$ *vs.* [ox] will produce a straight line, horizontal to the [ox] axis. The intercept at zero concentration of oxalate is theoretically the value of the formation constant, K_2. However, a graph is not usually drawn for this last step and an average of the $F_2(X)$ values is taken to be the best value of the formation constant.

The over-all formation constant of the dioxalato cuprate(II) complex in light water is $1.87 \pm 0.12 \times 10^9$, where the range is the observed standard deviation of the mean ($\log K_2 = 9.27$). The over-all formation constant of the dioxalato cuprate(II) complex in heavy water is $3.27 \pm 0.13 \times 10^9$ ($\log K_2 = 9.51$).

These results indicate that light water is more strongly solvating than heavy water.

Cadmium(II)–Oxalate Complex System. Light Water.—The experimental results and calculations are summarized in Table V for light water. A graph of log $F_0(X)$ *vs.* log [ox] indicates that, in the concentration range covered, all three complexes were present.

The graph of $F_0(X)$ *vs.* [ox] has an extrapolated intercept equal to the theoretical value of 1. The graph of $F_1(X)$ *vs.* [ox] has an extrapolated intercept equal to $4.10 \pm 0.15 \times 10^2$ for K_1 ($\log K_1 = 2.61$). The plot of $F_2(X)$ *vs.* [ox] has an extrapolated intercept equal to $1.29 \pm 0.15 \times 10^4$ for K_2 ($\log K_2 = 4.11$). The average of the $F_3(X)$ values is $1.15 \pm 0.15 \times 10^5$ for K_3 ($\log K_3 = 5.06$).

Heavy Water.—The experimental and calculated results for heavy water are summarized in Table VI. All three complexes again were present.

The graph of $F_0(X)$ *vs.* [ox] has an extrapolated intercept equal to the theoretical value of 1. The graph of $F_1(X)$ *vs.* [ox] has an extrapolated inter-

(22) R. E. Frank and D. N. Hume, *J. Am. Chem. Soc.*, **75**, 1736 (1953).

cept equal to $4.60 \pm 0.15 \times 10^2$ for K_1 ($\log K_1 = 2.66$). The plot of $F_2(X)$ *vs.* [ox] has an extrapolated intercept equal to $1.60 \pm 0.15 \times 10^4$ for K_2 ($\log K_2 = 4.20$). The average of the $F_3(X)$ values is $1.49 \pm 0.15 \times 10^6$ for K_3 ($\log K_3 = 5.17$).

These results also indicate that light water is more strongly solvating than heavy water.

Acknowledgments.—The authors wish to express appreciation to the National Science Foundation (Grant NSF-G12235) for their financial assistance *via* an Undergraduate Research Training Program Grant. Appreciation also is extended to the Research Corporation for a grant that made possible the purchase of the equipment used in this research problem. We thank Fairbanks Morse and Co., Beloit Division, Beloit, Wisconsin, for donating time on their IBM 650.

EFFECT OF SEVERAL PHOSPHATES ON THE CRYSTALLIZATION AND CRYSTAL HABIT OF STRONTIUM SULFATE

BY MASAJI MIURA, SADAICHI OTANI, MINEKAZU KODAMA AND KOZO SHINAGAWA

Department of Chemistry, Faculty of Science, Hiroshima University, Hiroshima, Japan

Received July 21, 1961

The crystallization of strontium sulfate was remarkably retarded when an extremely small amount of sodium pyro- or triphosphate was added to the solution, the habit of the resultant crystals being modified to the spherulitic. The effect of either sodium trimetaphosphate or the orthophosphate was insignificant. The effect of the phosphate on the crystallization rate, estimated by conductometric measurements, was attributed to adsorption of the phosphate on the strontium sulfate crystals. In the case of the pyro- and triphosphates, there was a rapid increase in the amount adsorbed with increasing phosphate concentration. The large differences in adsorption were correlated with the solubilities of the strontium phosphate salts and with the ability of the phosphates to form complexes with strontium. The low values for the amount of trimetaphosphate adsorbed were partially ascribed to the rigidity of its ionic structure, which might prevent its adaptation to the crystal lattice of strontium sulfate.

Introduction

It was reported previously that the crystallization of strontium sulfate is retarded by the presence of an extremely small amount of sodium triphosphate, and that the habit of the crystals is modified with the formation of spherulites.[1] On the basis of measurements of the crystallization rate, the adsorption of phosphate on the strontium sulfate crystals, coprecipitation and observations on the growth process of the crystals, the author ascribed the retarding action of the triphosphate to its adsorption on the crystal nuclei or the growing crystals. The mechanism of the habit modification as well as of the spherulite formation was explained in terms of the adsorption.[2]

To find out whether other phosphates exert an effect similar to that of the triphosphate, we investigated the crystallization rate of strontium sulfate in the presence of the ortho-, pyro-, tri- and trimetaphosphates; measurements also were made on the adsorption of these phosphates on strontium sulfate crystals. A correlation was found between the effect on crystallization and adsorption. The dependence of the adsorption upon the ionic structure of the phosphate is discussed.

Experimental

Materials.—Strontium chloride and potassium sulfate were purified by recrystallization as previously described.[1] Analytical grade sulfuric acid was purified by distillation. Strontium hydroxide was crystallized from a mixture containing equivalent amounts of strontium chloride and sodium hydroxide solutions which had been freed from carbonate by treatment with calcium hydroxide; the product was recrystallized twice from carbon dioxide-free water. To obtain sodium pyrophosphate, $Na_4P_2O_7$, analytical grade disodium orthophosphate was heated for 5 hr. at 550°, and then cooled slowly; after three recrystallizations from water, it was heated again for 5 hr. at 550°.[3] Sodium triphosphate, $Na_5P_3O_{10}$, was prepared by the procedure previously reported.[1,2] Sodium trimetaphosphate, $(NaPO_3)_3$, prepared from monosodium orthophosphate,[4] was recrystallized three times from aqueous solution by adding ethanol. To obtain the radioactive salts of the pyro-, tri- and trimetaphosphates ^{32}P-labeled orthophosphate was added to the starting materials. Paper chromatographic tests showed that the individual phosphates were not contaminated by each other.

The strontium sulfate crystals used as the adsorbent were precipitated by the addition of 0.025 *M* strontium hydroxide solution to an equal volume of sulfuric acid of the equivalent concentration. The precipitate was allowed to stand for 5 days with occasional stirring at room temperature, washed thoroughly with carbon dioxide-free water by decantation, and then dried at 150°.

Procedures.—The crystallization experiments were carried out with solutions prepared by mixing equal volumes of equivalent solutions of strontium chloride and potassium sulfate. The phosphate always was added to the sulfate solution prior to mixing. Procedures for the qualitative tests are given in the previous paper.[1]

The amount of crystals precipitated within a given period was determined by weighing. The effect of each phosphate on the crystallization rate was estimated quantitatively by conductometry.[2]

Phosphate adsorption was measured with the aid of labeled phosphate as described in the previous paper.[2] The amount of adsorbent used in each run ranged from 0.05 to 2 g. according to the adsorbability of the phosphate.

Results

Effect on the Crystal Habit.—The influence of each phosphate on the crystal habit of the strontium sulfate precipitated was observed over a wide range of phosphate concentration; Fig. 1 shows the relation between the phosphate concentration

(1) S. Otani *Bull. Chem. Soc. Japan*, **33**, 1543 (1960).

(2) S. Otani, *ibid.*, **33**, 1549 (1960).

(3) "Inorganic Syntheses," Vol. 3, McGraw-Hill Book Co., Inc., New York, N. Y., 1950, p. 100; "Jikken Kagaku Koza [Handbook of Experimental Chemistry]," ed. by the Chemical Society of Japan, Maruzen Co., Tokyo, Vol. 9, 1958, p. 74.

(4) L. T. Jones, *Ind. Eng. Chem., Anal. Ed.*, **14**, 537 (1942).

and the habit of the crystals formed for solutions which initially were 0.02 M with respect to strontium sulfate. The effect of sodium ortho- or trimetaphosphate was insignificant. Sodium pyrophosphate exhibited a marked effect similar to that of sodium triphosphate, which has been described in a previous paper.[1]

Effect on the Rate of Crystallization.—The effect of the individual phosphates on the amount of deposit is illustrated in Fig. 2. The influence of the individual phosphates on the crystallization rate is illustrated more quantitatively by the conductometric data in Figs. 3–6 which give the decrease in specific conductivity during the crystallization in the presence of various amounts of the phosphates.

Adsorption.—The adsorption of six kinds of phosphates on the strontium sulfate was measured with ^{32}P, as shown in the adsorption isotherms in Fig. 7. In the case of sodium pyrophosphate, measurements were impossible if the phosphate concentration exceeded 1×10^{-5} M, at which strontium pyrophosphate precipitated.

To determine the specific surface area of the adsorbent used, the adsorption of stearic acid from benzene solution was measured[5] and recorded in Fig. 8. The specific area evaluated from this isotherm by the BET equation is 0.29 m.^{2}/g.; the area occupied per molecule of stearic acid was assumed to be 20 Å.^{2}. The value estimated from microscopic inspection of the crystals was of the same order of magnitude.

Discussion

It is obvious from Figs. 1 and 2 that the four phosphates studied differ markedly in their effect on the precipitation and crystal habit of strontium sulfate. The conductometric data in Figs. 3–6 furnish quantitative information about the crystallization rate. For convenience, we have expressed the rate as the time required for the deposition of one-half of the total precipitate (half-time). The horizontal broken lines in Figs. 3–6 represent one-half of the total decrease in conductivity, and the points of intersection of these lines with the curves give the half-times, since the decrease in conductivity practically was proportional to the decrease in the concentration of strontium sulfate in all cases. In Fig. 9 the half-times thus obtained are plotted against the concentration of each phosphate; this figure shows the striking difference between the effect of the pyro- and triphosphates and that of the ortho- and trimetaphosphates. In fact, the presence of only 5×10^{-6} M triphosphate or 7×10^{-6} M pyrophosphate is sufficient to practically inhibit precipitation from 0.01 M strontium sulfate solution, while approximately a hundred times as much ortho- or trimetaphosphate is necessary merely to retard precipitation. As is seen in Fig. 9, the effect of the orthophosphate decreased after its concentration exceeded 5×10^{-4} M, at which strontium phosphate precipitated. The retarding action of the phosphate in this case may be offset by the precipitation of strontium phosphate, which might accelerate the nucleation of the strontium sulfate.

(5) E. Suito, M. Arakawa and T. Arakawa, *J. Chem. Soc. Japan, Pure Chem. Sec.* (*Nippon Kagaku Zasshi*), **75**, 596 (1954).

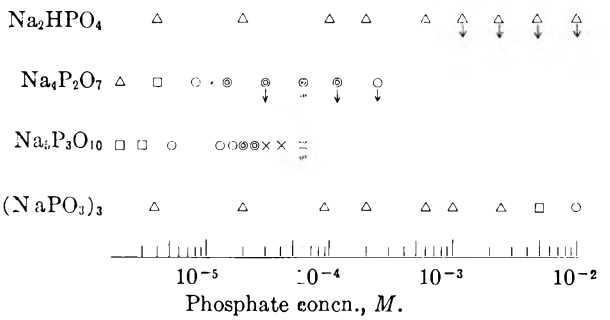

Fig. 1.—Effect of four phosphates on the habit of crystals grown from 0.02 M $SrSO_4$ solution: Δ, slightly modified single crystals; □, irregular crystalline aggregates; O, spherulitic aggregates having irregular shapes; ⊙, spherulites having spherical shapes; ×, no strontium sulfate deposits; ↓, deposition of the phosphate is accompanied.

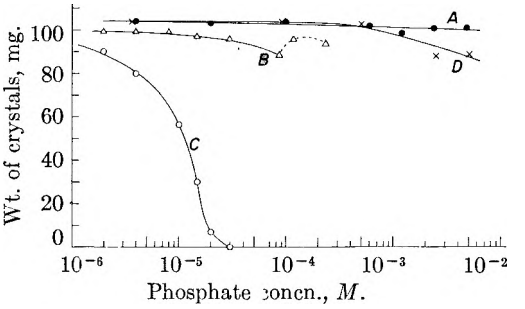

Fig. 2.—Relation between the phosphate concentration and the amount of crystals deposited from 30 ml. solution within 24 hr.: A, Na_2HPO_4; B, $Na_4P_2O_7$; C, $Na_5P_3O_{10}$; D, $(NaPO_3)_3$.

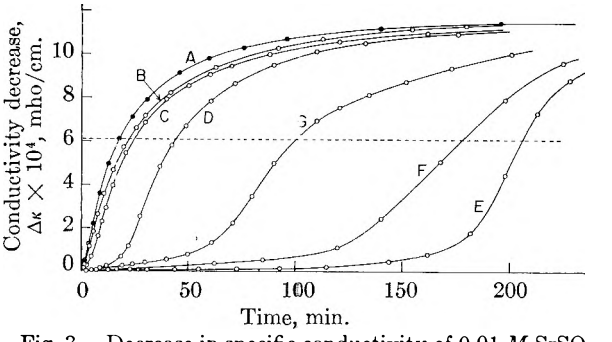

Fig. 3.—Decrease in specific conductivity of 0.01 M $SrSO_4$ solutions containing (A) no additive, (B) 1×10^{-5} M, (C) 2×10^{-4} M, (D) 3×10^{-4} M, (E) 5×10^{-4} M, (F) 1×10^{-3} M, and (G) 2×10^{-3} M Na_2HPO_4, respectively.

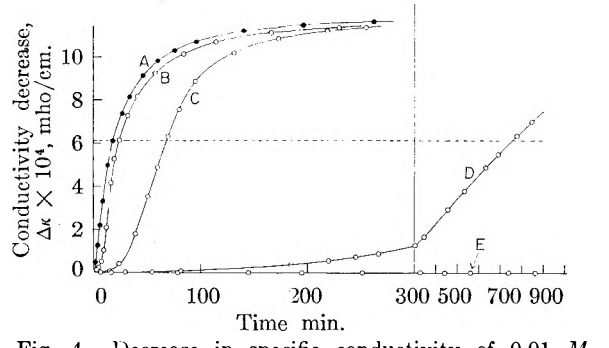

Fig. 4.—Decrease in specific conductivity of 0.01 M $SrSO_4$ solutions containing (A) no additive, (B) 2.5×10^{-6} M, (C) 4.0×10^{-6} M, (D) 5.0×10^{-6} M, and (E) 1.0×10^{-5} M $Na_4P_2O_7$, respectively.

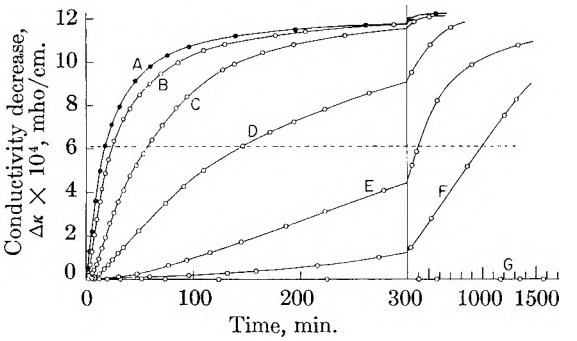

Fig. 5.—Decrease in specific conductivity of 0.01 M $SrSO_4$ solution containing (A) no additive, (B) 7×10^{-7} M, (C) 1.25×10^{-6} M, (D) 2×10^{-6} M, (E) 3×10^{-6} M, (F) 4×10^{-6} M, and (G) 5×10^{-6} M $Na_5P_3O_{10}$, respectively.

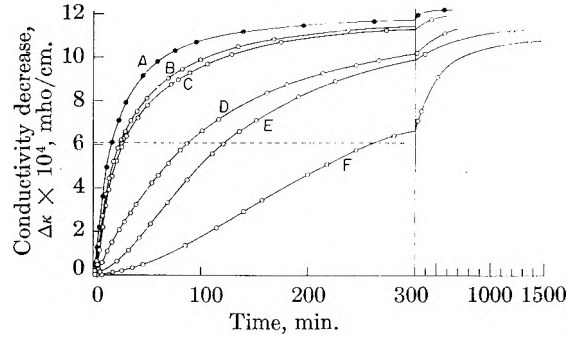

Fig. 6.—Decrease in specific conductivity of 0.01 M $SrSO_4$ solutions containing (A) no additive, (B) 2.5×10^{-5} M, (C) 5×10^{-5} M, (D) 1×10^{-4} M, (E) 2×10^{-4} M, and (F) 3×10^{-4} M $(NaPO_3)_3$, respectively.

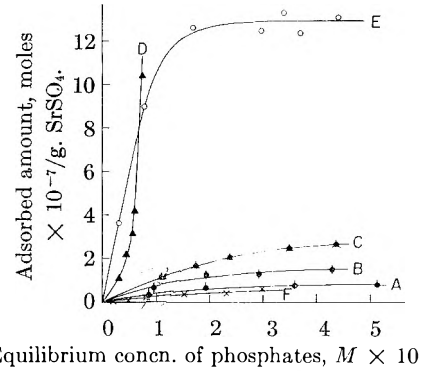

Fig. 7.—Adsorption isotherms of phosphates at 25.0°: A, NaH_2PO_4; B, Na_2HPO_4; C, Na_3PO_4; D, $Na_4P_2O_7$; E, $Na_5P_3O_{10}$; F, $(NaPO_3)_3$.

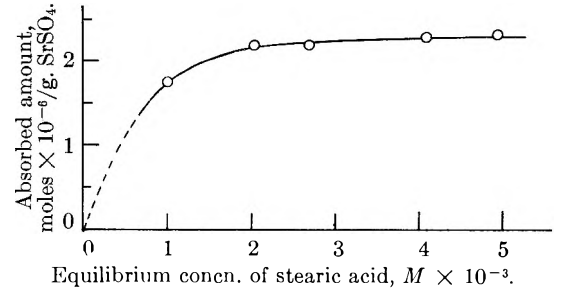

Fig. 8.—Adsorption isotherm of stearic acid at 25.0°.

For the same reason, sodium pyrophosphate cannot prevent the precipitation of strontium sulfate if the concentration of the latter is 0.02 M or higher, and there is a break in the curve, pyrophosphate concentration *vs.* weight of precipitate (B, Fig.

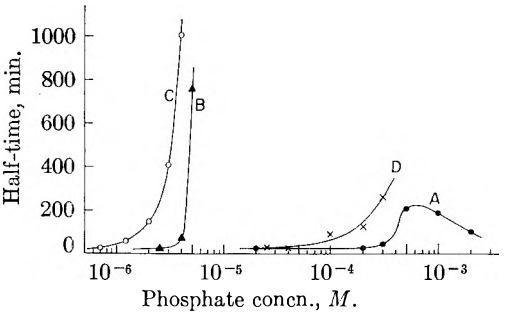

Fig. 9.—Half-time of crystallization *vs.* phosphate concentration at 25°: A, Na_2HPO_4; B, $Na_4P_2O_7$; C, $Na_5P_3O_{10}$; D, $(NaPO_3)_3$.

2), at a pyrophosphate concentration of 1×10^{-4} M. On the other hand, the triphosphate, whose strontium salt does not precipitate in the concentration investigated, inhibited crystallization almost perfectly when its concentration exceeded 3×10^{-5} M; see curve C in Fig. 2.

A comparison of Fig. 7 with Figs. 1 and 2 shows that there is a close correlation between the adsorption of the phosphates and their effects on the precipitation rate and crystal habit. In the case of the pyro- and triphosphate which exert a marked effect on the crystallization rate and crystal habit, the amount adsorbed increases rapidly with the concentration, whereas in the case of the ortho- and trimetaphosphate, the gradual increase in the amount adsorbed corresponds to their small effect.

The pyrophosphate adsorption isotherm differs in shape from those of the other phosphates (Fig. 7). Its form, which belongs to the Type III isotherm named by Brunauer and his co-workers,[6] suggests that pyrophosphate ions have a stronger affinity for the ions already adsorbed than for the clean surface of the adsorbent. This view seems reasonable in view of the low solubility of strontium pyrophosphate.

In the case of sodium triphosphate, the amount adsorbed tended to reach a saturation value at about 1.3×10^{-6} mole per gram adsorbent, within the concentration range examined. From this value we obtain 37 A.^{2} as the area occupied per molecule of triphosphate, using 0.29 m.^{2}/g. as the specific surface area of the adsorbent. This value is in close agreement with the maximum cross-sectional area of triphosphate ion, 33 A.^{2}, which is estimated from the data of Davies and Corbridge[7] on the crystal structure of sodium triphosphate, Phase II; the radius of oxygen atom was assumed to be 0.66 Å.[8] Thus, in the presence of a large amount of the triphosphate, above 3×10^{-5} M, the surface of the crystals or nuclei of strontium sulfate may be regarded as being covered with a monomolecular adsorbed layer, and the deposition of strontium sulfate onto such a surface may be strongly inhibited.

In the case of the orthophosphate, which has a far smaller ionic dimension than triphosphate, and

(6) S. Brunauer, L. S. Deming, W. E. Deming and E. Teller, *J. Am. Chem. Soc.*, **62**, 1723 (1940).

(7) D. R. Davies and D. E. C. Corbridge, *Acta Cryst.*, **11**, 315 (1958).

(8) L. Pauling, "The Nature of the Chemical Bond," 3rd Ed., Cornell Univ. Press, Ithaca, N. Y., 1960, p. 246.

of the trimetaphosphate, which shows very little adsorption, the adsorbed phosphates must cover merely a small fraction of the adsorbent surface even at the highest concentration used.

These pronounced differences in adsorption may be attributed primarily to the differences in the affinity of strontium ion for the various phosphate ions. This affinity may be related to the solubility of the individual strontium phosphates and also to the ability of the phosphates to form complexes with strontium. As there are few data in the literature on the solubilities of these salts, we studied the precipitation of strontium with each of the phosphates by means of the Tyndall effect. The minimum phosphate concentrations at which a 0.02 M strontium chloride solution became turbid were 2×10^{-4} M, 1×10^{-5} M, 4×10^{-5} M, and above 1×10^{-1} M, for the ortho-,[9] pyro-, tri-, and trimetaphosphates, respectively. These data suggest the familiar relation that the smaller the solubility, the greater is the adsorption.

The stability of the strontium complexes with these phosphates are given in van Wazer and Callis' comprehensive review[10]; the pK_D-values (negative logarithms of the dissociation constants) are 1.52 for the ortho- and 3.35 for the trimetaphosphate. Values for the chain phosphates are lacking, but we were able to estimate them from the relationship between the relative pK_D-values for alkaline earth complexes and the number of phosphorus atoms per chain; the values obtained are 4.8 and 6.1 for the pyro- and triphosphates, respectively. These data confirm qualitatively the expected relation between the complexing ability and adsorption.

The very small adsorption of the trimetaphosphate may be attributed, in part, to the rigidity of its ionic structure. As has been pointed out by Raistrick,[11] the rigid cyclic structure may prevent adaptation of the ions to the crystal lattice of strontium sulfate.

The mechanism, which first was suggested to explain the inhibition of the crystallization of strontium sulfate by triphosphate,[2] has been confirmed, and it also serves to explain the effect of the other condensed phosphates. This work also may afford some insight into the relation between the behavior of the condensed phosphates and their ionic structure. We now are working with tetra- and pentaphosphates to find out the relationship between the length of the ion and its effect on crystallization rate.

Acknowledgment.—The authors wish to thank Mrs. A. Weissberger for her help in preparing the manuscript.

(9) Disodium salt was used and the pH of the system was 7.1 at the concentration just referred to.

(10) J. R. Van Wazer and C. F. Callis, *Chem. Revs.*, **58**, 1011 (1958).

(11) B. Raistrick, *Discussions Faraday Soc.*, **5**, 234 (1949).

A DETERMINATION OF SOME RATE CONSTANTS FOR THE RADICAL PROCESSES IN THE RADIATION CHEMISTRY OF WATER[1]

BY HAROLD A. SCHWARZ

Chemistry Department, Brookhaven National Laboratory, Upton, Long Island, New York

Received July 24, 1961

The steady-state concentrations of H_2O_2 and O_2 produced by a 1.5 Mev. electron beam in pure water have been investigated. Both steady states increase with the square root of the intensity, I. The ratio $(O_2)/(H_2O_2)$ is 0.86; $(H_2O_2)^2/I = 2.4 \times 10^{-16}$ M^2 sec./rad. It is shown that a general mechanism including any number of radical combination reactions and radical-product reactions predicts a square root intensity dependence for all products. The results are interpreted in terms of a mechanism including the following reactions: $OH + H_2O_2 \rightarrow H_2O + HO_2$ (2), $H + H_2O_2 \rightarrow H_2O + OH$ (3), $OH + HO_2 \rightarrow H_2O + O_2$ (7), $OH + OH \rightarrow H_2O_2$ (8), and $H + HO_2 \rightarrow H_2O_2$ (9). k_8/k_2^2 is found to be 1.9×10^{-6} M sec., and k_7k_3/k_2k_9 is found to be 74. The electron beam then was pulsed and the H_2O_2 steady state followed as a function of the pulse rate. The resulting curve is interpreted in terms of the lifetime of the OH radical, giving $k_2 = 4.5 \times 10^7$ M^{-1} sec.$^{-1}$ and $k_8 = 4 \times 10^9$ M^{-1} sec.$^{-1}$.

A considerable body of data on the radiation chemistry of aqueous solutions has accumulated in the literature. These data have been interpreted in terms of a free radical model in which it is assumed that "spurs" of radicals are formed by the radiation containing about three pairs of H and OH in a volume of a few thousand cubic Ångströms. The subsequent reactions of these radicals with each other and the solutes yield the products that are observed.

This model has been very successful in explaining the observations. The high local concentration of the radical favors radical recombination which accounts for the production of the hydrogen and hydrogen peroxide that are observed as well as the dependence of their yields on solute concentration and their independence of intensity. The oxidation or reduction yields of the solutes generally can be expressed in terms of the yields of the radicals and the yield of hydrogen peroxide. Many systems have been studied in which two solutes compete for one radical species and the relative rate constants for the reactions have been obtained.

There are several gaps in our knowledge which reduce the utility of this wealth of data. There is no firm demonstration that the active intermediates produced by the radiation really are radical in nature, and there is scant information on the absolute rate constants of their reactions. Information on both of these points can be obtained by studying solutions with high intensity radiation. If it could be shown that the active

(1) Research performed under the auspices of the U. S. Atomic Energy Commission.

species undergo exclusively second-order disappearance it would be strong evidence for their radical character rather than excited-state character. The application of pulsed-beam techniques to an intensity dependent system will yield information on absolute rate constants.

In 1956, Ghormley[2] published his results on the irradiation of pure water with an electron beam. He observed a steady-state concentration of hydrogen peroxide which varied with the intensity. Upon placing a rotating sector in front of the beam, he determined that the lifetime of the rate-controlling species was of the order of a millisecond under his conditions.

At that time, there was a plethora of data on the low-intensity radiation chemistry of dilute solutions of H_2, H_2O_2 and O_2, which was not adequately understood. Consequently the high intensity experiments could not be interpreted. Quantitative agreement between much of the low intensity data and a simple six-step mechanism was reached by Allen and Schwarz[3] in 1958 and it appeared that it was time to reconsider and extend the high intensity work.

Experimental

Triply-distilled water was used in this work with and without further purification by pre-irradiation with Co^{60} γ-rays and subsequent photolysis by 2537 Å. light to destroy the hydrogen peroxide.[4] Slightly different results were obtained with the two different preparations, as will be explained in the section on results.

The radiation cells were flat cylinders of Pyrex glass, 14 mm. i.d. and an average of 2.7 mm. inside length in the direction of the beam. This is about half the range of the electrons. The front face of the cell was about 0.2 mm. thick. There was a single entrance to the cell from the edge made of 0.5 mm. i.d. capillary, 1 cm. long, which was left open and filled with water during the irradiation.

The water for irradiation was deaerated by bubbling helium through it for about 1 hr. The helium first was passed through a trap of activated charcoal at liquid nitrogen temperature, through a fritted disk into a tube containing pure water and then through a capillary bubbler into the water used for the irradiation. The deaerated solution was forced into the cells through a fine capillary with a slight helium pressure. There were no visible bubbles in the cells before or after irradiation.

A deaerated solution standing in a cell for an hour exposed to the atmosphere contained less than 0.3 μM O_2. This time is long compared to the time between filling and irradiating the cells. Each day the cells were filled with deaerated water and preirradiated with the electron beam for about 100 watt-seconds in order to clean the surface. They were not exposed to the air until after they had been used.

During the irradiation, the cell was placed behind a grounded $1/4''$ aluminum plate, 3" in diameter with a 15 mm. hole directly in front of the cell. Behind the cell, a $1/4''$ aluminum plate collected the current that went through. A 0.05 mm. platinum wire attached to the back plate was inserted a few millimeters into the neck of the cell.

The cell was mounted with its window 9 cm. from the window of the machine. At this distance the beam has diverged considerably and only 14% of it passes through the hole in the guard plate. The intensity distribution across the cell was checked by irradiating blue cellophane in a similar holder and was found to vary by about 4% from the center of the cell to the outside edge. The maximum intensity variation from front to back of the cell should not exceed ± 13% of the average.[5]

Hydrogen peroxide was determined by the iodide method of Ghormley.[6] The sample was removed from the irradiation cell with an eyedropper and a 0.200-cc. aliquot mixed with 0.144 cc. of the reagent directly in a dry Beckman microcell. The O.D. of known samples were reproducible to 0.002 unit out of 0.15 O.D. unit.

The sum of peroxide concentration plus twice the oxygen concentration was found by a modified Winkler analysis.[7] The reagents are: A, 27 g. $MnSO_4 \cdot H_2O$/100 ml.; B, 18 g. NaOH + 30 g. KI/100 ml.; C, 4.2 M HCl. These reagents are deaerated by bubbling N_2 through them. First 3.6 μl. of A is added to the sample in the irradiation cell from a capillary pipet and mixed by rotating the cell. Then 3.6 μl. of B is added, mixed and the precipitate allowed to settle. Next 4.6 μl. of C is added and after the precipitate is completely dissolved the solution is removed with an eyedropper and the O.D. of the triiodide complex is read in the Beckman microcell at 350 mμ. Calibration of the method with a peroxide solution gave the relation

$$(H_2O_2),\ \mu M = 41.3 \times \text{O.D.}$$

This factor may be calculated from the extinction coefficient of the iodide method for H_2O_2 at this I^- concentration[8] and the expected factor is also 41.3. A dilute oxygen sample prepared by adding nitrogen-saturated water to air-saturated water in a syringe indicated that the oxygen response was twice the peroxide response within 5%, which was the limit of precision in preparing the sample. In general, it was found that the precision of the determination of $(H_2O_2)+2(O_2)$ was about ± 0.5 μM, not as precise as the peroxide method.

The electron beam was produced by a Van de Graaff accelerator operating at 1.5 Mev. The pulsing circuit for the Van de Graaff was developed by S. Wagner and W. Higginbotham of Brookhaven National Laboratory. This circuit switches the beam on for a variable period of time and then off for a longer period. The ratio of the off to on time is kept constant and was 7.5 for most of the work. The period for the whole cycle can be varied from 5×10^{-5} to 5 sec. The rise time when the beam is turned on is about 1 μsec., so that the pulses are square shaped. There is a 480 cycle wobble in the beam current due to the alternator driving the filament, but this did not exceed ± 5%.

Results

Pure helium-saturated water was irradiated with no intentional impurities added. Hydrogen peroxide came to a steady-state concentration with a total dose of less than 10^{18} e.v./cc., which was the smallest used. The radiation doses given in the experiments reported ranged between 10^{19} and 10^{20} e.v./cc.

Some of the data obtained are given in Fig. 1. The lower curve indicates that the steady-state concentration of H_2O_2 increases with the square root of the intensity (represented as the beam current). The upper curve is the sum of (H_2O_2) + $2(O_2)$ steady-states. This is the quantity given by the Winkler analysis, and by material balance should be equal to the hydrogen concentration which was not determined. This sum also increases with the square root of the intensity. The ratio of the slopes of the two curves, which is believed to be the significant quantity, is 2.72 with a probable error of the mean of ± 0.14.

In two other sets of experiments, larger intercepts were observed for the (H_2O_2) + $2(O_2)$ and the peroxide curves (~7 and 2 μM). The ratio of the slopes was 2.85, which agrees with Fig. 1 within error. These runs and those of Fig. 1 were made on

(2) J. A. Ghormley, *Radiation Research*, **5**, 247 (1956).

(3) A. O. Allen and H. A. Schwarz, Paper P/1403, "Proc. Intern. Conf. Peaceful Uses Atomic Energy, 2nd Conf.," Geneva (1958).

(4) A. O. Allen and R. A. Holroyd, *J. Am. Chem. Soc.*, **77**, 5852 (1955).

(5) J. G. Trump, R. J. Van de Graaff and R. W. Cloud, *Am. J. Roentgenol. Radium Therapy*, **43**, 728 (1940).

(6) C. J. Hochanadel, *J. Phys. Chem.*, **56**, 587, ref. 6 (1952).

(7) "Scott's Standard Methods of Chemical Analysis," fifth edition, N. H. Furman, Editor, D. Van Nostrand Co., Inc., New York, N. Y., 1939, p. 2079.

(8) H. A. Schwarz and A. J. Salzman, *Radiation Research*, **9**, 502 (1958).

water that had been pre-irradiated and photolyzed. In some earlier experiments using triply distilled water without further purification, the oxygen steady-state concentration increased with $I^{1/2}$ but appeared to be zero below a beam current of 5×10^{-7} amp. while (H_2O_2) varied strictly with $I^{1/2}$ with no intercept. The ratio of the slopes between 5×10^{-7} and 3×10^{-6} amp. was 2.4. The error on this ratio was larger, and it is likely that it is a lower limit, as the current range is near the threshold for oxygen production. The ratio of the slopes of the curves in Fig. 1, 2.72, will be used in the discussion.

The intercepts observed in various sets of curves were not reproducible and probably are due to impurities. On the basis of the mechanism presented later, it would appear that the positive intercepts could be produced by either O_2 of the order of 10^{-6} M or active impurities such as Br^- at concentrations of the order of 10^{-7} M. The negative intercept observed for O_2 in water not purified by pre-irradiation likely is due to traces of organic matter being converted to H_2, CO_2 and H_2O, which would leave the solution in a net reducing atmosphere.

The radiation intensity was calibrated by the Fricke ferrous sulfate dosimeter.[9] The ratio of the Fe(III) concentration produced to the charge collected was 3.04×10^3 M/coulomb. The dosimeter was irradiated in all cells used and the average deviation of the determinations was $\pm 2\%$. The average of the slopes of the (H_2O_2) *vs.* intensity curves was 6.7×10^{-3} M amp.$^{-1/2}$ with a probable error of the slopes of $\pm$ 0.3×10^{-3}. Combining this with intensity calibration gives the equation

$$\frac{(H_2O_2)^2}{I} = 1.40 \times 10^{15} \frac{(\text{molecules})^2 \text{ sec.}}{\text{l. e.v.}}$$

$$= 2.40 \times 10^{-16} \frac{M^2 \text{ sec.}}{\text{rad.}}$$

A different set of units will be used in the discussion due to a personal preference for molar units and a habit of expressing yields in units of G. Since G = molecules/100 e.v., it also is equal to moles/100 volt-faraday. Expressing the intensity in terms of 100 volt-faradays l.$^{-1}$ sec.$^{-1}$

$$\frac{(H_2O_2)^2}{I} = 2.31 \times 10^{-7}$$

In these units, $G_H I$ becomes the rate of production of H in units of M sec.$^{-1}$. A 10^{-6} ampere beam corresponds to 1.92×10^{-4} (100 volt-faradays) l.$^{-1}$ sec.$^{-1}$.

Figure 2 shows the effect of pulsing the beam in a manner analogous to the effect of a rotating sector. In these experiments the beam was on for the first 11.8% of the cycle and off the rest. Thus the effective intensity varies from full intensity with slow pulses at the upper right of the figure to 0.118 with very fast pulses at the lower left. In this figure, the ratio of the observed steady-state peroxide concentration to the steady state that would be observed if the beam were continuous is plotted *vs.* the product of the length of time the beam is on and the continuous-beam steady-state peroxide concentration. This plot is used to normalize data obtained at various intensities. The currents used in obtaining the data of Fig. 2 ranged from 2 to 17 μamp.

(9) J. Weiss, A. O. Allen and H. A. Schwarz, *Proc. Intern. Conf. Peaceful Uses Atomic Energy*, **14**, 179 (1955).

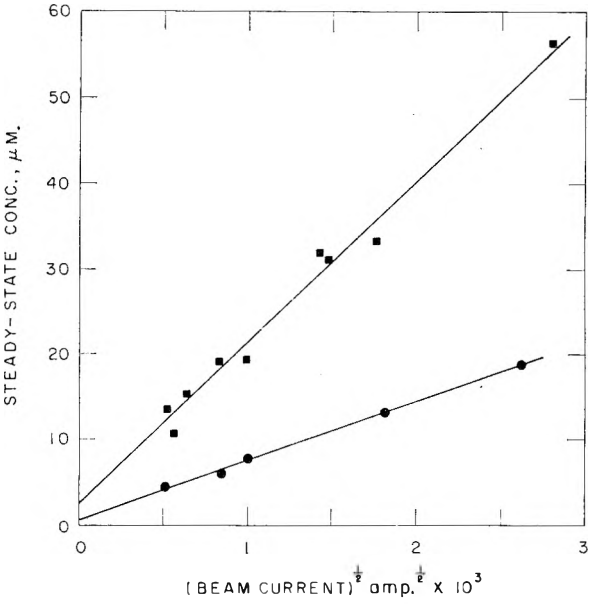

Fig. 1.—Variation of steady-state concentrations with the square root of the intensity: top curve, $(H_2O_2) + 2(O_2)$, bottom curve, (H_2O_2).

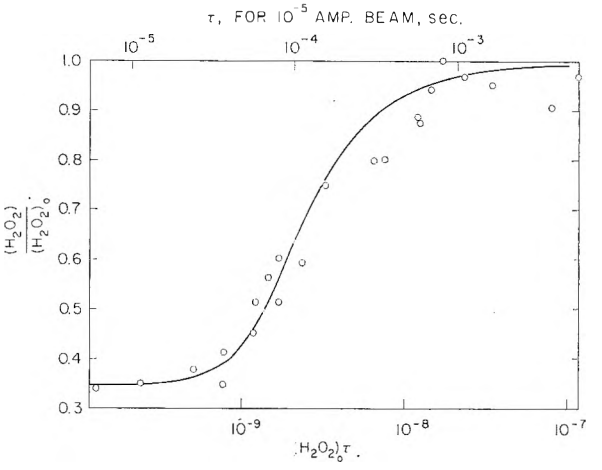

Fig. 2.—Variation of H_2O_2 steady state with pulse period. The beam is on for a time τ and off for a time 7.5 τ and the cycle is repeated until steady state is obtained. Ordinate is the ratio of the observed steady state, (H_2O_2), to the steady state for a steady beam of the same intensity, $(H_2O_2)_0$. The abscissa normalizes results obtained at various intensities. τ for a 10^{-6} amp. beam is given at the top of the figure.

Steady-beam irradiations were made at the same time as the pulsed-beam experiments in order to check for intercepts at low intensity, such as were observed in Fig. 1. Such intercepts existed in about half the runs, and in order to use the pulsed beam data corrections had to be applied. The intercept was subtracted from the observed peroxide concentration and only runs in which the intercept was less than 15% of the observed peroxide concentration are reported in order to minimize any possible effect of this correction.

Insofar as these data are comparable to Ghormley's, the agreement is good.[2] His curve of per-

oxide steady-state concentration as a function of $I^{1/2}$ curves slightly, the slope being smaller below 10^{-7} amperes. He irradiated water in a flow system at 0.1 ml./sec. in order to obtain larger samples for analysis. It is likely that this small initial slope is due to a penumbra effect, H_2O_2 being destroyed as the solution entered a small region of low intensity while leaving the beam. He measured the hydrogen from several samples and found that the hydrogen steady-state concentration was "about twice" the peroxide steady state. This is comparable to the ratio of the slopes of the two curves in Fig. 1, which is 2.72. Ghormley used a rotating sector to produce an intermittent beam and the mid-point of his sector curve and the pulsed-beam curve of Fig. 2 agree within 50%. His peroxide steady-state concentration approached about one half the steady-beam value at long pulse times, however, whereas the peroxide steady-state concentration for the experiments reported herein averaged about 0.95 of the full beam value with pulse lengths of the order of 2×10^{-3} sec. [$(H_2O_2)\ \tau \sim 4 \times 10^{-8}$]. A rotating sector produces trapezoidal pulses, and this discrepancy probably results from the products tending to follow the slow decrease in intensity as the sector edge passes in front of the beam.

Discussion

A homogeneous distribution of the radicals is assumed in the discussion and is justified by the lifetime observed. In Fig. 2, the peroxide concentration is at the mid-point of its fast and slow pulse extremes when $(H_2O_2)_0\ \tau = 2.5 \times 10^{-9}\ M$ sec. For a 10^{-5} amp. beam, this corresponds to a lifetime of about 1.3×10^{-4} sec. for the radicals involved in the rate-controlling step. Even though the radicals presumably are formed in "spurs," the concentration of radicals in these spurs will drop down to the background concentration (10^{-6} to $10^{-7}\ M$) in the order of 10^{-6} sec.[10]

Treatment of the Mechanism.—The reactions that take place between the radicals produced in water and the reaction products, H_2, H_2O_2 and O_2, are well understood kinetically.[3] They constitute the first five reactions of the mechanism proposed, the numbering system corresponding to that of Allen and Schwarz. Three radical combination reactions are added to complete the mechanism. R_1, R_2, etc., are the rates at which the corresponding reactions are occurring, I is the intensity and G_{H_2}, $G_{H_2O_2}$, G_H and G_{OH} are the "molecular" yields and radical yields produced by the radiation in units of molecules per 100 e.v. absorbed.

$H_2O \longrightarrow H_2, H_2O_2, H, OH$	$R_{H_2} = G_{H_2}I,\ R_H = G_HI$, etc.
$OH + H_2 \longrightarrow H_2O + H'$[11]	$R_1 = k_1(OH)(H_2)$
$OH + H_2O_2 \longrightarrow H_2O + HO_2$	$R_2 = k_2(OH)(H_2O_2)$
$H + H_2O_2 \longrightarrow H_2O + OH$	$R_3 = k_3(H)(H_2O_2)$
$H + O_2 \longrightarrow HO_2$	$R_4 = k_4(H)(O_2)$
$H' + O_2 \longrightarrow HO_2$	$R_5 = k_5(H')(O_2)$
$OH + HO_2 \longrightarrow H_2O + O_2$	$R_7 = k_7(OH)(HO_2)$
$OH + OH \longrightarrow H_2O_2$	$R_8 = k_8(OH)^2$
$H + HO_2 \longrightarrow H_2O_2$	$R_9 = k_9(H)(HO_2)$

(10) A. Kupperman, "Actions Chimique et Biologiques des Radiations, 5° serie," (Edited by M. Haissinsky), Academic Press, Ltd., London, 1961, p. 122.

Since all products are at a steady state, the rates of formation and destruction are equal for each species.

$$\begin{aligned} \text{For}\quad [H]&: G_HI = R_3 + R_4 + R_9 \\ [OH]&: G_{OH}I + R_3 = R_1 + R_2 + R_7 + 2R_8 \\ [HO_2]&: R_2 + R_4 + R_5 = R_7 + R_9 \\ [H']&: R_1 = R_5 \\ [H_2]&: G_{H_2}I = R_1 \\ [H_2O_2]&: G_{H_2O_2}I + R_8 + R_9 = R_2 + R_3 \\ [O_2]&: R_7 = R_4 + R_5 \end{aligned} \qquad (1)$$

The equation of material balance in the system (ignoring the contribution of the radicals) is

$$(H_2) = (H_2O_2) + 2(O_2) \qquad (2)$$

Equations 1 and equation 2 predict that the steady-state concentrations of all the species will vary with the square root of the intensity. This may be shown by making the seven substitutions $(H_2) = A_{H_2}I^{1/2}$, $(H) = A_HI^{1/2}$, $(H_2O_2) = A_{H_2O_2}I^{1/2}$, etc. The problem then reduces to demonstrating that the A factors are independent of intensity. With these substitutions, equations 1 become

$$[H]: G_H = k_3A_HA_{H_2O_2} + k_4A_HA_{O_2} + k_9A_HA_{HO_2}$$

$$[OH]: G_{OH} + k_3A_HA_{H_2O_2} = k_1A_{OH}A_{H_2} + k_2A_{OH}A_{H_2O_2} + k_7A_{OH}A_{HO_2} + 2k_8A_{OH}^2 \text{ etc.}$$

while equation 2 becomes $A_{H_2} = A_{H_2O_2} + 2A_{O_2}$. Thus there are eight equations from which the seven unknown A's may be determined as a function of the rate constants and G_H, G_{OH}, G_{H_2} and $G_{H_2O_2}$. (The extra equation is due to the set of equations 1 not being independent of material balance in the form $2G_{H_2} + G_H = 2G_{H_2O_2} + G_{OH}$. Any six of the seven equations 1 are independent, however.) The A's are independent of the intensity, as I has cancelled out in the new set of equations. From the defining equations for the A's, the concentration of each species is seen to be proportional to the square root of the intensity.

It is clear from the method of deriving the square-root intensity dependence that the conclusion is not peculiar to this mechanism. Any number of radical combination reactions, such as H + OH, H + H, etc., could be added, and square-root intensity dependence still would be predicted. It also is clear that the observation of a square-root intensity dependence places a requirement on the mechanism that all reactions be second order in the reactants. Thus the production of a species such as an excited water molecule that may react with itself or another reactant or undergo first-order decay is ruled out

$$H_2O \longrightarrow X$$
$$X + H_2O_2, H, \text{etc.} \longrightarrow \text{products}$$
$$X \longrightarrow H_2O$$

Pseudo-first-order reactions such as $H + H_2O \rightarrow H'$ also are ruled out. If this reaction were included, an A_{H_2O} parameter would be defined by $(H_2O) = A_{H_2O}I^{1/2}$ and the assumption that

(11) There are two reducing agents present in the system which have different kinetic behaviors called H and H', described by N. Barr and A. O. Allen, *J. Phys. Chem.*, **63**, 928 (1959). H reacts readily with H_2O_2 and H' does not. Recent work in our Laboratory has demonstrated that H is negatively charged, suggesting that it is the basic form of the hydrogen atom, H', in water. However, this description is unnecessary for the present work.

A_{H_2O} is independent of intensity would clearly violate the corresponding material balance equation. The requirement that all reactions must be second order is strong evidence in favor of the intermediates being free radical in nature, as it is characteristic of free radicals to undergo second-order recombination.

The set of equations 1 may be reduced to the following form, where $v = 2(O_2)/(H_2O_2)$, $(H_2) = (H_2O_2)(1+v)$ and[6] $k_1/k_2 = 1.0$

$$\begin{aligned} R_6 &= R_1 = G_{H_2} I \\ R_9 &= R_2 = \frac{k_2(H_2O_2)}{k_1(H_2)} R_1 = \frac{G_{H_2} I}{1+v} \\ R_3 &= G_{H_2O_2} I + R_8 \\ R_4 &= \left(G_H - G_{H_2O_2} - \frac{G_{H_2}}{1+v}\right) I - R_8 \\ R_7 &= \left(G_{OH} + G_{H_2O_2} - G_{H_2} - \frac{G_{H_2}}{1+v}\right) I - R_8 \end{aligned} \tag{3}$$

From these

$$\frac{R_4}{R_3} = \frac{k_4}{2k_3} v = \frac{\left(G_H - G_{H_2O_2} - \frac{G_{H_2}}{1+v}\right) I - R_8}{G_{H_2O_2} I + R_8} \tag{4}$$

The yields of molecular products and radicals are taken as $G_{H_2} = 0.44$, $G_{H_2O_2} = 0.70$, $G_H = 2.76$ and $G_{OH} = 2.24$.[3] Equation 4 and the experimental observation that $v = 1.72$ may be used to evaluate R_8, as k_4/k_3 has been determined[12] to be 2.1. The rest of the yields follows from equations 3

$$\begin{aligned} R_8 &= 0.22I \quad R_4 = 1.67I \\ R_1 = R_5 &= 0.44I \quad R_7 = 2.12I \\ R_2 = R_9 &= 0.16I \\ R_3 &= 0.92I \end{aligned} \tag{5}$$

The intensity coefficients in the above equations correspond to the yields of the reactions in units of G.

Two rate-constant ratios may be derived from the data. From the definitions of the rates

$$\frac{k_7 k_3}{k_2 k_9} = \frac{R_7 R_3}{R_2 R_9} = 74 \pm 10$$

and

$$\frac{k_8}{k_2^2} = \frac{R_8}{R_2^2}(H_2O_2)^2 = \frac{G_8}{G_2^2}\frac{(H_2O_2)^2}{I} =$$

$$(1.9 \pm 0.3) \times 10^{-6}\ M \text{ sec.}$$

Choice of Mechanism.—In view of the general nature of the $I^{1/2}$ relationship the decision about which radical combination reactions to include must rest largely on external grounds. The rate constants k_3 and k_4 are in the diffusion-controlled region.[13] k_1 and k_2 must be smaller than k_3 and k_4, as k_1 and k_2 are several orders of magnitude smaller than the rate constants for the reactions of OH with NO_2^-[14] and Br^-.[15] HO_2 does not react with the products at all. This suggests that $(HO_2) > (OH) > (H)$, and that reactions 7, 8 and 9 should be important reactions decreasing in that order. The major question is the elimination of reaction 6 from the mechanism.

$$HO_2 + HO_2 \longrightarrow H_2O_2 + O_2 \quad R_6 = k_6(HO_2)^2$$

This reaction is considered to be of overwhelming importance in the irradiation of H_2, H_2O_2, O_2 systems at lower intensities.[3]

If reaction 6 is included, the rate equations for HO_2 and O_2 would be

$$\frac{d(HO_2)}{dt} = 0 = R_2 + R_4 + R_5 - 2R_6 - R_7 - R_9$$

$$\frac{d(O_2)}{dt} = 0 = R_6 + R_7 - R_4 - R_5$$

Addition of these two equations gives

$$R_2 = R_5 + R_9$$

showing that (6) and (9) are in competition with each other for the small proportion of HO_2 radicals produced in reaction 2.

R_6 may be found by the equations

$$\frac{R_7^2 I}{R_2^2 R_6} = \frac{k_7^2}{k_2^2 k_6}\frac{I}{(H_2O_2)^2}$$

or

$$\frac{R_6}{I} = \frac{k_2^2 k_6}{k_7^2}\frac{R_7^2}{R_2^2}\frac{(H_2O_2)^2}{I}$$

A value for the rate constant ratio $k_2^2 k_6/k_7^2$ may be obtained from an analysis of the intensity dependence observed by Schwarz, Caffrey and Scholes[16] in the hydrogen, oxygen system when irradiated with a cyclotron deuteron beam. They found that the yield of H_2O_2 produced in a solution containing 5×10^{-4} M H_2 and 4×10^{-4} M O_2 decreased with increasing beam current. The curve observed agrees with a mechanism consisting of reactions 1 and 4 through 7. Allen[17] has analyzed these data and finds that $k_2^2 k_6/k_7^2 = 500$ M^{-1} sec.$^{-1}$, approximately.

The rates, R_7 and R_2, for a mechanism consisting of reactions 1 through 9 are given by the same expression as in the set of equations 3. R_8 depends somewhat on the ratio of R_9 to R_6, but this affects R_7 to at most 5%. Taking $R_2 = 0.16I$ and $R_7 = 2.12I$, the above equations give $R_6 \approx 0.015I$ and $R_9 = 0.15I$, so reaction 6 may be neglected.

This conclusion is peculiar to the present system of pure water irradiated with an electron beam. The concentration of HO_2 is not negligible compared to H_2O_2 and O_2 since the steady-state concentrations of these products are so low. With deuteron beams, the ratio of molecular yields to radical yields is larger, so that a much higher steady state of products is expected. Under these conditions reaction 6 should predominate. Some preliminary results with a cyclotron deuteron beam indicate this to be the case.

Pulsed Beam Experiments.—In rotating sector studies, it is usual to follow a rate of production or disappearance which is proportional to the average concentration of the rate controlling intermediate.[18]

(12) G. Czapski, private communication. This value is higher than the value 1.85 reported in reference 3. It was determined by the same method but with increased precision.

(13) A. R. Anderson and E. J. Hart, *J Phys. Chem.*, **65**, 804 (1961).

(14) H. A. Schwarz and A. O. Allen, *J. Am. Chem. Soc.*, **77**, 1324 (1955).

(15) E. R. Johnson and A. O. Allen, *ibid.*, **74**, 4147 (1952).

(16) H. A. Schwarz, J. M. Caffrey and G. Scholes, *ibid.*, **81**, 1801 (1959).

(17) A. O. Allen, "The Radiation Chemistry of Water and Aqueous Solutions," D. Van Nostrand Co., New York, N. Y., 1961, p. 97.

(18) G. M. Burnett and H. W. Melville, "Techniques of Organic Chemistry," Vol. 8, "Investigation of Rates and Mechanisms of Reactions," Interscience Publishers, Inc., New York, N. Y., 1953.

In this work, the concentration of the measurable species are at steady state and a different analysis is needed.

At steady state, the concentration of any species at the beginning of one cycle must be the same as it is at the beginning of the next. Hence the integral of the rate of production of any species over a complete cycle must be zero.

$$\oint \frac{d(H_2)}{dt}\,dt = 0 = G_{H_2} I\tau - \oint R_1 dt$$

$$\oint \frac{d(OH)}{dt}\,dt = 0 = G_{OH} I\tau + \oint R_3 dt - \oint R_1 dt - \oint R_2 dt - \oint R_7 dt - 2\oint R_8 dt, \text{ etc.}$$

τ is the time the beam is on. There are seven equations of this type, one for each species, analogous to the set of equations 1. The average rate of a reaction, during the cycle $\bar{R}$, is given by

$$\oint R dt = \bar{R}(r+1)\tau$$

where r is the ratio of the time the beam is off to the time it is on, 7.5 in the present case.

These integral rate equations combine into a set analogous to equations (3)

$$\bar{R}_1(r+1) = \bar{R}_6(r+1) = G_{H_2} I$$

$$\bar{R}_9(r+1) = \bar{R}_2(r+1) = \frac{G_{H_2} I}{1+v}$$

$$\bar{R}_3(r+1) = G_{H_2O_2} I + \bar{R}_8(r+1) \qquad (6)$$

$$\bar{R}_4(r+1) = \left(G_H - G_{H_2O_2} - \frac{G_{H_2}}{1+v}\right) I - \bar{R}_8(r+1)$$

$$\bar{R}_7(r+1) + \bar{R}_8(r+1) = \left(G_H + G_{H_2O_2} - G_{H_2} - \frac{G_{H_2}}{1+v}\right) I$$

At this point, some assumptions about the relative lifetimes ($\bar{l}$) of the three radicals, HO_2, OH and H must be made in order to obtain rate constants from the pulsed-beam H_2O_2 curve (Fig. 2). The most reasonable assumptions are that $\bar{l}_{HO_2} >> \bar{l}_{OH} >> \bar{l}_H$. This is analogous to the earlier statement that $(HO_2) > (OH) > (H)$ made on the grounds that $k_3 >> k_2$ while the rate constants for reactions between HO_2 and the stable products are negligibly slow. The experimental data presented here are consistent with these assumptions, as it was found that $R_7 > R_8 > R_9$. Since k_7, k_8 and k_9 are probably of similar magnitude, this again gives $(HO_2) > (OH) > (H)$. If it is assumed that the concentration of HO_2 is large enough so that it does not change appreciably during the cycle, then

$$\bar{R}_7 = k_7(HO_2)(\overline{OH}) \text{ and } \bar{R}_9 = k_9(HO_2)(\overline{H})$$

where $(\overline{OH})$ and $(\overline{H})$ are the average concentrations of OH and H over the cycle. Also, $\bar{R}_2 = k_2 \times (H_2O_2)(\overline{OH})$, $\bar{R}_4 = k_4(O_2)(\overline{H})$ and $\bar{R}_3 = k_3(H_2O_2)(\overline{H})$, giving

$$\frac{\bar{R}_7\bar{R}_3}{\bar{R}_2\bar{R}_9} = \frac{k_7k_3}{k_2k_9} \text{ and } \frac{\bar{R}_4}{\bar{R}_3} = \frac{k_4}{2k_3} v \qquad (7)$$

These are the same equations that applied in the steady-beam analysis, and lead to the conclusion that v and $\bar{R}_8$ are independent of τ. This may be seen by inserting the corresponding equations from the set of equations 6 into 7, giving two equations in v and $\bar{R}_8$ independent of τ.

$$\frac{k_7k_3}{k_2k_9} = \frac{\left\{\left(G_H + G_{H_2O_2} - G_{H_2} - \frac{G_{H_2}}{1+v}\right) I - \bar{R}_8(r+1)\right\}\{G_{H_2O_2} I + \bar{R}_8(r+1)\}(1+v)^2}{G_{H_2}{}^2 I^2}$$

$$\frac{k_4}{2k_3} v = \frac{\left(G_H - G_{H_2O_2} - \frac{G_{H_2}}{1+v}\right) I - \bar{R}_8(r+1)}{G_{H_2O_2} I + \bar{R}_8(r+1)}$$

Since v and $\bar{R}_8$ are fixed all the average rates are fixed by equations 6. The yields assigned to the various rates in equations 5 apply here to $\bar{R}(r+1)$; *i.e.*, $\bar{R}_2(r+1) = 0.16$, $\bar{R}_8(r+1) = 0.22$, etc. While it would seem to be instructive to follow (O_2) as a function of τ, the lower precision of the analysis compared to H_2O_2 coupled with the other sources of error in the pulsed beam work were not encouraging enough to make the attempt attractive.

The relationship between the observed peroxide steady state and the average radical concentration during the pulse may be found from the relationship $\bar{R}_2(r+1) = R_2{}^0$. (Superscript or subscript zero refers to steady-beam conditions at the same intensity.)

$$\frac{(H_2O_2)}{(H_2O_2)_0} = \frac{(OH)_0}{(\overline{OH})(r+1)}$$

The ratio $(\overline{OH})/(OH)_0$ may be found by integrating the OH concentration over the cycle. The rate equation for (OH) when the beam is on is

$$d(OH)/dt = G_{OH} I + R_3 - R_1 - R_2 - R_7 - 2R_8$$

The assumption that $\bar{l}_H << \bar{l}_{OH}$ is equivalent to assuming that R_3 is independent of time while the beam is on and zero when it is off, giving $R_3 = \bar{R}_3(r+1)$. Since the HO_2 concentration is assumed to be constant throughout the cycle, we may write $R_1 + R_2 + R_7 = (\bar{R}_1 + \bar{R}_2 + \bar{R}_7)(OH)/(\overline{OH})$ and finally, $(\overline{OH})$ is obtained from the expression $k_2(H_2O_2)(\overline{OH})(r+1) = G_{H_2} I/(1+v)$. The rate equation for (OH) while the beam is on now becomes

$$\frac{d(OH)}{dt} = G_{OH} I + \bar{R}_3(r+1) - k_2(H_2O_2)(1+v) \times \frac{(\bar{R}_1 + \bar{R}_2 + \bar{R}_7)(r+1)}{G_{H_2} I}(OH) - 2k_8(OH)^2 \qquad (8)$$

When the beam is off

$$\frac{d(OH)}{dt} = -k_2(H_2O_2)(1+v) \times \frac{(\bar{R}_1 + \bar{R}_2 + \bar{R}_7)(r+1)}{G_{H_2} I}(OH) - 2k_8(OH)^2 \qquad (9)$$

This type of equation, involving first-order and second-order terms, has been solved by Burnett and Melville[18] in connection with rotating sector treatments for the case where the coefficient of the first-order term is a constant. The fact that it is proportional to (H_2O_2) introduces a minor modification to the solution, leading to the squaring of $(H_2O_2)_0/(H_2O_2)$ in the equation below. The solution is[19]

(19) Some of the signs in the expression for P_1 as a function of a, b and c are printed wrong in the chapter by Burnett and Melville.

$$\left\{\frac{(H_2O_2)_0}{(H_2O_2)}\right\}^2 = (\gamma_0^{-1} - 1)^{-1}\left\{-1 + (\gamma m)^{-1} \times \ln\left[\frac{P_2 + 2\gamma}{P_1 + 2\gamma}\{1 + (P_1 + \gamma)\tanh m\}\cosh m\right]\right\}$$

where

$$\gamma = \left[1 + \frac{8\bar{R}_8\{G_{OH}I + \bar{R}_3(r+1)\}}{(\bar{R}_1 + \bar{R}_2 + \bar{R}_7)^2(r+1)}\left\{\frac{(H_2O_2)_0}{(H_2O_2)}\right\}^2\right]^{-1/2}$$

γ_0 is γ at steady-beam, *i.e.*, when $(H_2O_2) = (H_2O_2)_0$

$$m = k_2(H_2O_2)_0\tau \times \left[\gamma^{-1}(1+v)\frac{(\bar{R}_1 + \bar{R}_2 + \bar{R}_7)(r+1)}{2G_{H_2}I}\frac{(H_2O_2)}{(H_2O_2)_0}\right]$$

$$P_1 = \frac{(a^2 + 4bc)^{1/2} - a}{2b} \qquad P_2 = \frac{2\gamma\exp(2\gamma rm)P_1}{\{1 - \exp(2\gamma rm)\}P_1 + 2\gamma}$$

and $a = -\tanh m(1 - 3\gamma^2) - 2\gamma + \exp\{2\gamma rm\}[(1+\gamma^2)\tanh m + 2\gamma]$

$b = -1 + \gamma\tanh m + \exp\{2\gamma rm\}(1 + \gamma\tanh m)$

$c = 2\gamma(1 - \gamma^2)\tanh m$

In spite of its messy appearance, there is only one variable parameter (m) in the equation, all other quantities being fixed by the determination of the ratio of (O_2) to (H_2O_2) under steady-beam conditions. That is, formally the equation may be represented as $(H_2O_2)_0/(H_2O_2) = f(m, v)$. γ is an intermediate function introduced as a convenience in the solution and unfortunately depends on the answer. Consequently, the solution was found by trial and error, recalculating $(H_2O_2)_0/(H_2O_2)$ for various values of γ until the input and output γ agreed. Since the quantity in brackets in the definition of m is known, the solution is readily expressed as a curve relating $(H_2O_2)/(H_2O_2)_0$ and $k_2(H_2O_2)_0\ \tau$. This is the curve given in Fig. 2. From this curve it is found that

$$k_2 = 4.5 \times 10^7\ M^{-1}\ \text{sec.}^{-1}$$

The probable error of the mean, including the error in determination of v, k_4/k_3, and the fit to the curve, is $\pm\ 0.4 \times 10^7\ M^{-1}\ \text{sec.}^{-1}$. Combining this with the value of k_8/k_2^2 found from the absolute slopes of Fig. 1 gives

$$k_8 = 4.0 \times 10^9\ M^{-1}\ \text{sec.}^{-1}$$

with a probable error of $\pm\ 25\%$.

Since $k_7k_3/k_2k_9 = 74$, $k_7k_3/k_9 = 3.3 \times 10^9\ M^{-1}\ \text{sec.}^{-1}$. If it is assumed that $k_9 \approx k_3$, $k_7 \approx 3 \times 10^9\ M^{-1}\ \text{sec.}^{-1}$. By extension to $k_6k_2^2/k_7^2 = 500$, $k_6 \approx 2 \times 10^6\ M^{-1}\ \text{sec.}^{-1}$. Due to the presence of a squared assumption here, this estimate may be wrong by an order of magnitude in either direction. It agrees well with the measurement reported by Dainton and Rowbottom,[20] however.

The calculated pulsed beam curve of Fig. 2 lies consistently above the experimental points at the upper end. There is probably a second step in the curve representing the last 5%, due to the occurrence of reaction 6. In this region, τ is long compared to the lifetimes of H and OH, but short compared to the lifetime of HO_2. Reaction 6 will be exaggerated in importance since it occurs during the complete time cycle, while the other reactions are complete shortly after the beam is off. For this reason, only those points below $(H_2O_2)_0\ \tau = 3 \times 10^{-9}$ were used in calculating k_2.

Alternative Mechanisms. (a) Independent Yield of H′.—It has been suggested that both H and H′ are produced when water is irradiated.[21] Estimates of the relative contributions of these species vary, but the yield of H′ is probably small. The value for G_H used in this discussion, 2.76, was determined in the hydrogen, oxygen system[6,11] and represents both forms. If it is assumed that 10% of the species are H′, which is believed to be a maximum, the various rate constants become

$$\frac{k_4}{k_3} = 1.9;\quad k_1 = 4.5 \times 10^7\ M^{-1}\ \text{sec.}^{-1};\quad k_8 = 3.4 \times 10^9\ M^{-1}\ \text{sec.}^{-1}$$

$$\frac{k_7k_3}{k_2k_9} = 73$$

(b) $H + HO_2 \rightarrow 2OH$ (9′).—It is possible that reaction 9 does not occur, but that instead the products are OH radicals. Under these conditions the same parameters may be evaluated.

$$k_1 = 4.2 \times 10^7\ M^{-1}\ \text{sec.}^{-1};\quad k_8 = 6.0 \times 10^9\ M^{-1}\ \text{sec.}^{-1}$$

$$\frac{k_7k_3}{k_2k_9'} = 74$$

Another possible set of products for this reaction is $H_2 + O_2$. If this were the case, the mechanism is incomplete without reaction 6, and we would have $R_6 = R_2$. Using the value of $k_2^2k_6/k_7^2 = 500$, the mechanism predicts the peroxide steady state to be about 10 times that observed. One of the distinctions between H and H′ seems to be that H does not readily abstract hydrogens.[21]

Effect of H Lifetime.—The only way in which the lifetime of H can affect the sector curve is through the rate R_3. Even though the general solution is difficult, an extreme case can be treated in which it is assumed that the lifetimes of H and OH are equal, that is $(H) = k(OH)$. With this assumption R_3 is no longer a constant in equation 8 but enters the coefficient of (OH). The calculated values of k_2 and k_3 are then 6.4×10^7 and $8.2 \times 10^9\ M^{-1}\ \text{sec.}^{-1}$. Since the average lifetime of H is probably only a tenth of OH, it is doubtful that the assumption that it is zero will introduce more than a few per cent. error.

TABLE I

SOME RATE CONSTANTS FOR REACTIONS OF OH BASED ON $k_2 = 4.5 \times 10^7\ M^{-1}\ \text{sec.}^{-1}$

Reactant	(H^+)	k, M^{-1} sec.$^{-1}$	Reference
NO_2^-	Neutral	2.5×10^9	14
H_2	Neutral	4.5×10^7	6
FeII	10^{-2}	2.6×10^8	[a]
HCOOH	0.4	4.2×10^7	[b]
CeIII	0.4	7.2×10^7	[c]
H_2SO_4	0.4	1×10^5	[c]
Tl^+	0.4	2.7×10^9	[d]

[a] W. G. Rothschild and A. O. Allen, *Radiation Research*, **8**, 101 (1958). [b] E. J. Hart, *J. Am. Chem. Soc.*, **74**, 4174 (1952). [c] T. J. Sworski, *Radiation Research*, **6**, 645 (1957). [d] T. J. Sworski, *ibid.*, **4**, 483 (1956).

Derived Rate Constants.—The absolute measurement of the rate constant for reaction 2 allows absolute values to be assigned to the rate constants for many other reactions, as relative rate constants have been accumulating for years. Some of these are given in Table I. No attempt has been made

(20) F. S. Dainton and J. Rowbottom, *Trans. Faraday Soc.*, **49**, 1160 (1953).

(21) J. T. Allan and G. Scholes, *Nature*, **187**, 218 (1960).

for an exhaustive search of the literature in the table, and only relative rate constants determined from the irradiation of aqueous solutions are included. Many other ratios have been observed for OH radicals produced by Fenton's reagent. Even this short table includes one inconsistency. Hart[22] has found that $k_{OH+HCOOH}/k_{OH+H_2O_2} = 10$ in 10^{-3} M H_2SO_4, which would give a value of 4.5×10^8 M^{-1} sec.$^{-1}$ for $k_{OH+HCOOH}$. It would appear that this rate constant is a function of acid concentration.

(22) E. J. Hart, *J. Am. Chem. Soc.*, **73**, 68(1951).

Acknowledgment.—The author would like to express appreciation to S. Wagner and W. Higinbotham for designing and constructing the beam-pulsing circuits. Also, this work has benefited greatly from discussions with A. O. Allen.

THE REDUCING RADICALS PRODUCED IN WATER RADIOLYSIS: SOLUTIONS OF OXYGEN–HYDROGEN PEROXIDE–HYDROGEN ION[1]

BY GIDEON CZAPSKI AND A. O. ALLEN

Department of Chemistry, Brookhaven National Laboratory, Upton, Long Island, New York

Received July 24, 1961

The reducing radical "H" or "H_2O^-" arising from the γ-radiolysis of water is shown to react competitively with dissolved O_2 and H_2O_2; the ratio of the respective rate constants is 2.0. It also reacts in a simple competitive bimolecular fashion with hydrogen ion, H^+, to give an acid form of the radical which reacts several thousand times as fast with O_2 as with H_2O_2. The rate constants for reaction of "H" with O_2 and with H^+ are equal. The yield of "H" deduced from the O_2–H_2O_2 competition in neutral solution is 2.85, which is equal to the standard value of the total yield of reducing radicals. Thus essentially none of the reducing radicals appear to be generated initially in the acid form, a conclusion which disagrees with recently proposed interpretations of some other radiolytic reactions.

Introduction

It has been clear for some time that the reducing free radicals, usually called H, formed in radiolysis of water, can exist in two different forms. Barr and Allen[2] showed that the H atom formed by free radical oxidation of H_2 reacts preferentially with oxygen rather than with hydrogen peroxide, whereas radicals produced in water radiolysis react with these solutes at comparable rates. It was suggested that the product of H_2 oxidation was an acidic form of this radical, and that the radical produced in water radiolysis might in fact be a solvated electron. Hayon and Weiss[3] showed that the acid form of H attacks chloroacetic acid to form mainly H_2, whereas the basic form originally produced from water gives mainly chloride ion in this solution. Later Hayon and Allen[4] showed that the reaction of the basic form with chloroacetic acid appeared to stand in simple competition with its reaction with hydrogen ion to yield the acid form. It seemed of interest to demonstrate the direct competition between hydrogen peroxide and hydrogen ion for the radical, which could be shown by studying the variation of the yield of peroxide formation or destruction in systems containing various concentrations of oxygen, peroxide and acid. This system also affords a means of determining the amount of the two different forms which may be produced in water radiolysis. Allan and Scholes[5] have evidence from radiolysis of solutions of organic compounds that a yield $G = 0.6$ of the acid form is produced in water radiolysis, the balance $G = 2.2$ of the total production of reducing species being in a basic form, and Kelly and Smith[6] have quoted similar results.

Experimental

Materials and Methods.—The purification of water was as described by Allen and Holroyd,[7] except that after the distillation apparatus had been cleaned thoroughly it was not found necessary to purify the water further by radiolysis and photolysis. Most of the solutions were air-saturated; oxygen concentration was varied in some cases by bubbling purified tank oxygen through the water in the irradiation tubes, or by using nitrogen–oxygen mixtures obtained from the Matheson Co., Inc. and stated to contain 50.6 and 5.16% oxygen. Acidities were determined with a Beckman *p*H meter. Peroxide was determined by the Ghormley method.

Treatment of the Data.—In solutions initially not containing any hydrogen peroxide, the peroxide concentration increased linearly with dose and G-values were obtained without difficulty. In some runs in which hydrogen peroxide was added initially, however, the yield of peroxide changed so rapidly with increasing dose that an accurate determination of the initial yield was difficult. An example of high curvature is shown in Fig. 1. To extrapolate to the initial yield in such cases an algebraic method of correction was used. The rate of change of peroxide concentration in these systems is fixed by the ratio of oxygen concentration to peroxide concentration present at any time in the solution. By material balance, the change in oxygen concentration must be related to the changes in hydrogen and hydrogen peroxide concentrations by the relation $2\Delta O_2 = \Delta H_2 - \Delta H_2O_2$. In solutions containing bromide, hydrogen will be produced with a yield $G = 0.45$, so that for ΔH_2 we may write simply $0.45D$, where D is the dose given the solution (in units of e.v. l.$^{-1}$ $(6.02 \times 10^{25})^{-1}$ if the concentrations are in moles per liter). For each experimental point the concentration of oxygen was calculated and it always was found that the ratio of oxygen to peroxide could be represented within experimental error as a linear function of the dose

$$(O_2)/(H_2O_2) = (O_2)_0/(H_2O_2)_0 + bD = \rho_0 + bD$$

According to the results of Allen and Schwarz[8] (confirmed by the present work) the yield of peroxide then will be given by

(1) Research performed under the auspices of the U. S. Atomic Energy Commission.

(2) N. F. Barr and A. O. Allen, *J. Phys. Chem.*, **63**, 928 (1959).

(3) E. Hayon and J. Weiss, *Proc. Second Intern. Conf. Peaceful Uses Atomic Energy*, **29**, 80 (1958).

(4) E. Hayon and A. O. Allen, *J. Phys. Chem.*, **65**, 2181 (1961).

(5) J. T. Allan and G. Scholes, *Nature*, **187**, 218 (1960).

(6) P. Kelly and M. Smith, *J. Chem. Soc.*, 1479 (1961).

(7) A. O. Allen and R. A. Holroyd, *J. Am. Chem. Soc.*, **77**, 5852 (1955).

(8) A. O. Allen and H. A. Schwarz, *Proc. Second Intern. Conf. Peaceful Uses Atomic Energy*, **29**, 30 (1958).

$$G = d(H_2O_2)/dD = G_0 - 2G_H/(1 + k(\rho_0 + bD))$$

This equation integrates into a logarithmic form which after expansion and neglect of higher-order terms becomes

$$(H_2O_2) - (H_2O_2)_0 = \left(G_0 - \frac{2G_H}{1 + K\rho_0}\right) D + \frac{KG_H bD^2}{(1 + K\rho_0)^2}$$

The coefficient of D in the first term is the value of the initial yield being sought. The final term shows the deviation of the peroxide concentration from what it would be if the initial yield were maintained throughout the irradiation. The value of the final term was determined for each point, using reasonable values of K and G_H, and the resulting numbers were subtracted from the observed concentrations. The corrected values for the run of Fig. 1 are shown on the figure and were found to fall on a straight line. The difficulty with this method was that the values of K and G_H were precisely the quantities to be found. It was necessary, after this preliminary correction of all the runs had been made and better values of these constants determined as described below, to repeat the entire procedure on all the runs using the improved values of K and G_H in order to obtain the final best values of these constants. Since the corrected initial yield values are not very sensitive to the assumed values of these constants, a third approximation was not necessary.

Results

All solutions used contained 10^{-4} M KBr to protect the hydrogen from radical attack. After some difficulty with water purification, reproducible yields of peroxide were obtained in the irradiation of neutral air-saturated water. The results agree closely with those of Allen and Holroyd.[7] The line representing peroxide concentration as a function of dose has an intercept of about 0.25 μM, which is of about the same magnitude as that found by Allen and Holroyd, and presumably arises from impurities. The yield of peroxide $G(H_2O_2)$ obtained from the slope of the line is 0.87, in good agreement with their value, 0.85. In acid solutions the reproducibility seemed a little better than in neutral solutions. Values of the peroxide yield in air-saturated water are shown in Fig. 2 as a function of $(H^+)^{1/3}$ where (H^+) is defined as 10^{-pH}. These values for each pH are hereinafter called G_0.

Solutions in which peroxide as well as oxygen was added initially gave peroxide yields which could be either positive or negative, depending on the amount of peroxide present. The results obtained in neutral solution are shown graphically in Fig. 3, in which the quantity $1/(G_0 - G(H_2O_2))$ is plotted against the ratio of the oxygen to peroxide concentration. Similar results have been presented by Allen and Schwarz.[8] The present data are much more extensive and precise. The initial yields obtained for acid solutions with peroxide and oxygen initially present are shown in Table I.

Discussion

Neutral Solutions.—The mechanism of the reaction in neutral solutions has been discussed by Sworski[9] and by Allen and Schwarz.[8] If we denote the reducing radical produced in water radiolysis as H and the oxidizing radical as OH, the equations representing the mechanism appear as

$$H_2O \longrightarrow H, OH, H_2, H_2O_2$$

$$OH + Br^- = Br + OH^- \quad (1)$$

$$Br + H_2O_2 = HO_2 + H^+ + Br^- \quad (2)$$

$$H + H_2O_2 = OH + H_2O \quad (3)$$

$$H + O_2 = HO_2 \quad (4)$$

$$2HO_2 = H_2O_2 + O_2 \quad (6)$$

(9) T. J. Sworski, *J. Am. Chem. Soc.*, **76**, 4687 (1954).

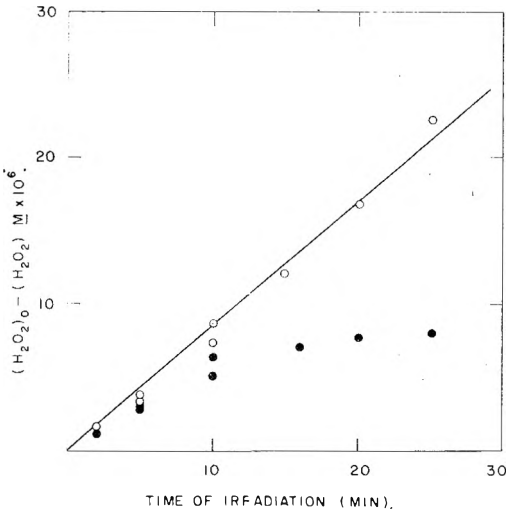

Fig. 1.—Peroxide destruction in a solution containing initially 120 μM (H_2O_2) and 270 μM (O_2). Dose rate (Fricke dosimetry) 99 μM Fe^{III}/min.: ●, observed values; ○, corrected values.

TABLE I

PEROXIDE YIELDS IN 10^{-4} M KBr SOLUTIONS CONTAINING PEROXIDE, OXYGEN AND ACID

$(H_2O_2)_0$, $M \times 10^4$	$(O_2)_0$, $M \times 10^4$	pH	$G(H_2O_2)$	$\frac{1}{G_0 - G(H_2O_2)}$	Acid
1.19	2.7	3.8	0.168	1.40	H_2SO_4
1.58	2.7	3.8	− .019	1.11	H_2SO_4
2.38	2.7	3.8	− .30	0.84	H_2SO_4
3.96	2.7	3.8	− .84	.58	H_2SO_4
6.44	2.7	3.43	− .93	.54	H_2SO_4
4.30	2.7	3.43	− .405	.76	H_2SO_4
2.15	2.7	3.43	.093	1.23	H_2SO_4
1.29	2.7	3.43	.38	1.93	H_2SO_4
3.43	2.7	3.43	− .226	0.88	H_2SO_4
3.90	2.7	3.12	.045	1.14	H_2SO_4
10.33	2.7	3.12	−1.13	0.49	H_2SO_4
6.62	2.7	3.12	−0.44	.73	H_2SO_4
7.78	2.7	3.12	− .760	.59	H_2SO_4
5.24	2.7	3.12	− .235	.87	H_2SO_4
7.77	2.7	2.85	− .17	.90	H_2SO_4
5.02	2.7	2.85	.16	1.28	H_2SO_4
10.33	2.7	2.85	− .37	0.76	H_2SO_4
6.20	2.7	2.85	.079	1.16	H_2SO_4
4.14	2.7	2.85	.335	1.64	H_2SO_4
4.54	2.7	3.05	0	1.09	HCl
7.76	2.7	3.05	−0.40	0.76	HCl
3.88	2.7	3.05	.117	1.25	HCl
11.6	2.7	3.05	− .83	0.57	HCl
15.5	2.7	3.05	−1.24	.46	HCl
18.7	13.0	3.12	−0.84	.56	H_2SO_4
14.9	13.0	3.12	− .55	.67	H_2SO_4
11.2	13.0	3.12	− .39	.76	H_2SO_4
7.46	13.0	3.12	− .13	.95	H_2SO_4
3.74	13.0	3.12	.38	1.84	H_2SO_4
4.95	6.56	3.12	.097	1.21	H_2SO_4
7.47	6.56	3.12	− .29	0.82	H_2SO_4
3.70	6.56	3.12	.29	1.58	H_2SO_4
12.37	6.56	3.12	− .77	0.59	H_2SO_4
9.91	6.56	3.12	− .67	0.62	H_2SO_4
5.26	2.7	3.03	− .143	0.95	$HClO_4$
4.20	2.7	3.03	.025	1.13	$HClO_4$
6.29	2.7	3.03	− .34	0.80	$HClO_4$
7.34	2.7	3.03	− .46	0.73	$HClO_4$

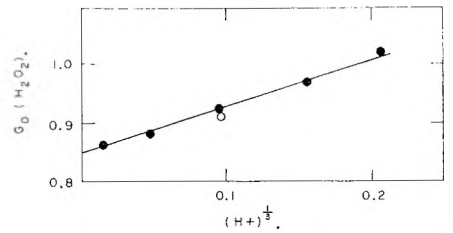

Fig. 2.—Peroxide yields in air-saturated solutions of 10^{-4} M KBr at different acidities: ●, H_2SO_4; ○, $HClO_4$.

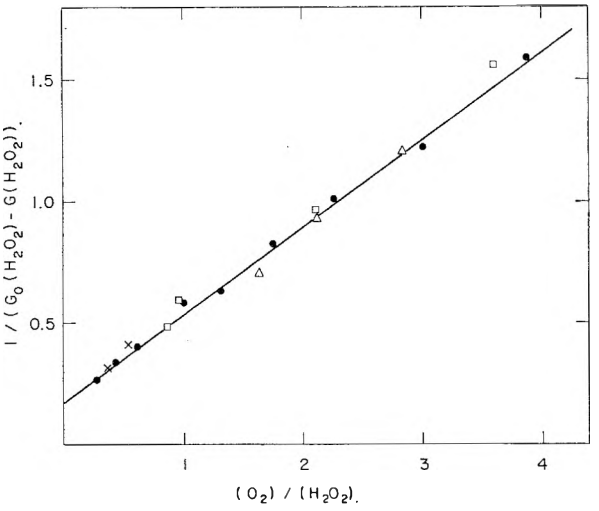

Fig. 3.—Initial peroxide yields in neutral 10^{-4} M KBr solutions containing O_2 and added H_2O_2: ●, saturated with air; △, with 100% O_2; □, with 50.6% O_2; X, with 5.15% O_2. The solubility of oxygen at 1 atm. total pressure and room temperature (22.5°) was taken as 1.29 mM.

This mechanism predicts that the initial peroxide yield in dilute bromide solution containing oxygen but no peroxide is given by [10]

$$G_0 = G_{H_2O_2} + \frac{1}{2}(G_H - G_{OH}) \qquad (A)$$

and that the yield in the presence of added hydrogen peroxide is

$$G(H_2O_2) = G_0 - \frac{2G_H}{1 + [k_4(O_2)/k_3(H_2O_2)]} \qquad (B)$$

The data of Fig. 3 show that equation B is accurately borne out by experiment. The slope and intercept of the line of Fig. 3 were determined by a number of separate least mean square calculations, using different methods of weighting the individual points. The statistical probable error in the intercept is only about ±6%, and in the slope much less; but the different weighting schemes gave "best" intercepts corresponding to values of G_H ranging from 2.73 to 3.01. We believe, therefore, the data indicate that G_H probably lies between 2.7 and 3.0, and write $G_H = 2.85 \pm 0.15$, where the limits represent "probable error." From the ratio of slope to intercept, $k_4/k_3 = 2.0 \pm 0.1$.

If some of the reducing radicals are produced in an acid form which reacts preferentially with oxygen then the peroxide yield, with no peroxide added initially, will be governed by the total yield of both species. When peroxide is added initially, however, the difference $G_0 - G(H_2O_2)$ produced by the presence of the peroxide will depend only on the yield of radicals produced in the basic form, which does react with hydrogen peroxide. Thus the intercept in Fig. 3 is a measure of the quantity of radicals produced in the more reactive basic form. This may be shown formally if we introduce another radical, H′, into the scheme which is assumed always to react with oxygen in the solutions. To the above scheme we formally write as the initial equation

$$H_2O \longrightarrow H_2, H_2O_2, OH, H, H'$$

and add the equation

$$H' + O_2 = HO_2 \qquad (5)$$

Including (5) in the scheme we find for G and G_0

$$G_0 = G_{H_2O_2} + \frac{1}{2}(G_H + G_{H'} - G_{OH})$$

$$G = G_0 - \frac{2G_H}{1 + [k_4(O_2)/k_3(H_2O_2)]}$$

Thus the intercept of Fig. 3 refers only to G_H, not to G_H'.

A word may be said here about the notation to be used in equations such as the above, which tends to become very confusing. There is a growing belief that the basic form called H in the above equations really is to be thought of as a solvated electron, which for purposes of balancing chemical equations is most conveniently represented as H_2O^-. Oxidation–reduction equations such as the above can be written in equivalent forms for either formulation of the reducing radical without changing the significance of the reactions in any way, since the postulated forms differ only by the presence or absence of a proton in the formulas of the reactants and products. Thus equations 3 and 4 above could be written

$$H_2O^- + H_2O_2 = OH + OH^- + H_2O \qquad (3)$$

$$H_2O^- + O_2 = HO_2 + OH^- \text{ or } O_2^- + H_2O \qquad (4)$$

without affecting any conclusions to be drawn from the reaction mechanism.

The value of the total yield of reducing radicals has been determined at neutral pH from the yield of peroxide in solutions containing hydrogen and oxygen,[2,11] formate ion and oxygen,[12] and ethanol and oxygen.[13] The best value, 2.8, is obtained from the hydrogen–oxygen solutions. A slightly higher value appears from the ethanol solutions, but here the concentration of ethanol as well as oxygen was somewhat higher and the value of G_H may have been somewhat elevated due to scavenging of radicals from the spurs. If we accept the value 2.8 for the total yield of the reducing radical, the results of Fig. 3 show that essentially all of these radicals are produced in the basic form, which is reactive with hydrogen peroxide, and little or none in the acid form. This conclusion is in direct conflict with the proposal by the Durham workers[5,6] of an independent yield of the acid form, arising from their interpretation of the hydrogen yields

(10) The initial yields of the water radiolysis products are denoted by $G_{H_2O_2}$, G_H, etc. The net observed yield of hydrogen peroxide is denoted by $G(H_2O_2)$.

(11) C. J. Hochanadel, *J. Phys. Chem.*, **56**, 587 (1952).

(12) E. J. Hart, *J. Am. Chem. Soc.*, **76**, 4198 (1954).

(13) G. G. Jayson, G. Scholes and J. Weiss, *J. Chem. Soc.*, 1358 (1957).

found in neutral solutions of organic compounds. Since the chemistry of the peroxide–oxygen system seems clean and simple compared to that of most organic systems, we believe that the present conclusion should be given more weight, and that some other interpretation of the hydrogen yields obtained in solutions of organic compounds should be looked for.

Acid Solutions.—The discussions of Barr and Allen[2] and of Allen and Schwarz[8] show that the form of hydrogen atom produced by free radical oxidation of H_2 reacts preferentially with oxygen and much more slowly with hydrogen peroxide. The work of Hayon[3,4] appears to show that the form produced in water radiolysis is converted to an acid form by simple bimolecular reaction with hydrogen ion. If the form resulting from oxidation of H_2 is the same as that produced on reaction of the water radiolysis product with acid, then the kinetics of peroxide formation in acid solution should give evidence of simple competition for the radical between H_2O_2, O_2 and H^+. The expected mechanism then would consist of reactions 1, 2, 3, 4, 5, 6 and

$$H + H^+ = H' \qquad (7)$$

if we denote the form produced in the radiolysis of water as H and that produced by reaction with acid as H′. A more reasonable-looking form of (7) is

$$H_2O^- + H^+ = H_2O + H$$

In the above mechanism with its double competition the following expression is obtained for the peroxide yield as a function of the initial concentration of H_2O_2, O_2 and H^+

$$G(H_2O_2) = G_0 - \frac{2G_H}{1 + [k_4(O_2)/k_3(H_2O_2)] + [k_7(H^+)/k_3(H_2O_2)]}$$

The results of Table I consist of a number of experimental series, the initial oxygen and acid concentration in each series being held constant while the peroxide concentration was varied. For each of these series a plot was made of the same quantity shown in Fig. 3, but with only five points to each plot. Because of the scatter of the points and their small number, the least-squares value of the intercept in these plots was quite uncertain and the best lines were drawn by assuming an appropriate value of G_H to fix the intercept. Since the total G_H is known to increase with increasing acidity, and since it is not known whether the additional H formed in acid solutions is produced in the acid or the basic form, two calculations were made for each plot: one assuming G_H in all cases equal to 2.85, the other taking G_H at each acidity from the graph of G_H *vs.* *p*H given by Rothschild and Allen.[14] If the assumed mechanism is correct the slopes of these lines, divided by their intercepts, should be given by the expression $(k_7(H^+) + k_4(O_2))/k_3$. This quantity for all the runs in acidified air-saturated water is plotted against the concentration of H^+ in Fig. 4. The points fall on a good straight line with a slope giving $k_7/k_3 = 2.2$, while the intercept gives $k_4/k_3 = 1.9$, in good agreement with the value obtained from the data of Fig. 3. This plot is obtained from points calculated using for G_H the total H atom yield of Rothschild. If constant G_H of 2.85 is assumed the points are displaced slightly and the constants of the line are $k_7/k_3 = 2.0$ and $k_4/k_3 = 2.05$. It is seen that the results depend only on the *p*H of the solution used and not on the nature of the acid used to obtain the *p*H.

(14) W. G. Rothschild and A. O. Allen, *Radiation Research*, **8**, 101 (1958).

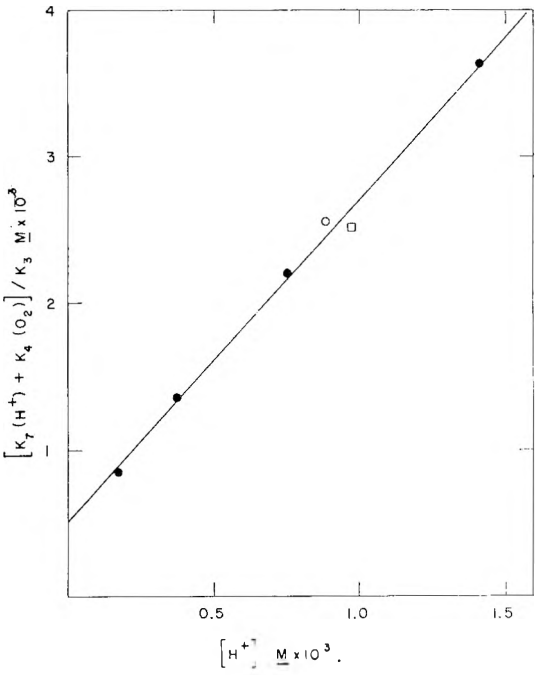

Fig. 4.—Results of the peroxide yield determinations in acid solutions, plotted as described in the text: ●, H_2SO_4; ○, HCl; □, $HClO_4$.

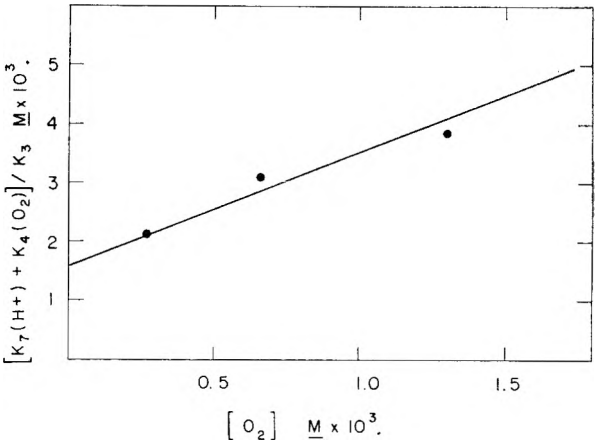

Fig. 5.—Results of the peroxide yield determinations at *p*H 3.1 for different oxygen concentrations.

Figure 5 shows results obtained at *p*H 3.12 for different concentrations of oxygen plotted against the oxygen concentration. If the mechanism is correct the points should lie on a line having an intercept of 2.0 times the H^+ concentration and a slope of 2.0 ($= k_4/k_3$). The expected line is shown on the figure and the points agree within experimental error.

The system thus behaves in every way as expected from a simple competition for the initial water radiolysis product between the three react-

ants H_2O_2, O_2 and H^+. The rates of reaction with O_2 and H^+ are seen to be equal within a few per cent.

To obtain some idea of the preference of the acid form for reaction with oxygen over hydrogen peroxide, we determined the yield of oxygen produced in the irradiation of deaerated solutions of 10^{-4} M KBr at pH 2.85. According to Hochanadel,[11] considerable oxygen is produced in the irradiation of neutral bromide solutions, but in acid solutions practically none is formed and the peroxide yield equals that of the hydrogen. In three experiments we found $G(H_2)$ = 0.46, 0.45 and 0.43, and the ratios of oxygen to hydrogen were, respectively, 0.004, 0.004 and 0.0012. In this solution the H is all converted to the acid form. From the very low yield of O_2 found here we calculate that the ratio of specific rates for the acid form to react, respectively, with O_2 and H_2O_2 is greater than 3000. Hochanadel[15] has obtained a value for this ratio of the order of 1000.

(15) C. J. Hochanadel, in "Comparative Effects of Radiation," ed. by M. Burton, J. S. Kirby-Smith and J. L. Magee, John Wiley and Sons, Inc., New York, N. Y., 1960, p. 167.

THE THERMAL EXPANSION OF LEAD[1]

BY THOR RUBIN, H. L. JOHNSTON AND HOWARD W. ALTMAN

Cryogenic Laboratory of The Ohio State University, Columbus 10, Ohio

Received July 26, 1961

Measurements of the expansion coefficients of lead from 20 to 300°K. have been made by use of a Fizeau Interferometer. A correlating function of heat capacity and expansion coefficients has been derived by means of which it has been shown that lead obeys Grüneisen's law between 25 and 300°K. A method for calculating the compressibility of lead as a function of temperature between 25 and 300°K. has been suggested. A correlation of the expansion coefficient data for lead with those for copper and rock salt has been given.

Introduction

The apparatus and experimental technique for determination of the expansion coefficient of lead were the same as those described for synthetic rock salt[3] and single crystal copper.[2]

The lead, obtained from the National Bureau of Standards, was melting point purity material containing 99.99% lead. It was used without further purification. The sample was cut to three pillars filed to the same length within $^1/_5$ wave length of sodium-D radiation. These pillars served to separate the interference plates.

Results

The absolute values for the expansion coefficients are given in Table I. v_1^2 and v_2^2 are the squares of the apparent fringe diameter measured at temperature equilibrium by means of a filar micrometer eye piece. The optical constant, O, is a measure of the change in the square of the fringe diameter on increasing the fringes by one order. The values for O are those which result from smoothing according to the method already outlined.[3] F is the number of fringes passing a fiduciary mark when the temperature changed by ΔT degree, l_0 = 0.49670 cm. is the length of the sample measured at 25°, T(°K.) is the mean of the initial and final temperature of a determination and α is the expansion coefficient. Runs 24 to 28 inclusive are determined by use of the standard thermocouple alone. The rest of the measurements were obtained by using a resistance thermometer wound on the cell in conjunction with the thermocouple. The data from this resistance thermometer were smoothed and tabulated at equal temperature intervals between 30 and 300°K. This resistance data table was used to calculate the temperatures of the cell above 30°K. All temperatures were based on The Ohio State University Cryogenic Laboratory temperature scale.[4] All fringe measurements were referred to length measurements in terms of the mean wave length of sodium-D radiation.

Seven sets of length (arbitrary) temperature measurements are exhibited in Table I. They begin at runs 1, 9, 13, 24, 33, 36 and 40 where T average in most cases is given three significant figures to the right of the decimal. In each of these series the α-values were computed by the method of divided differences.[5,6] Only third divided differences and first divided differences were used to calculate the derivative of length with respect to temperature.

Errors.—The absolute temperature values are known to about 0.03°K. Temperature intervals measured by the thermocouple are precise to about 0.02°K. Intervals measured by means of the resistance thermometer are precise to a few thousandths of a degree. The error in the length measurement is about 0.008 fringe order. However, because of the rather large heat capacity of the sample, thermal equilibrium was much more difficult to obtain for these measurements than in the case of the rock salt. A smooth curve was drawn within 0.2% of all data above 40°K., except for runs 36 and 37 which could not be reconciled with the rest of the data.

Nix and MacNair[7] have determined integral expansions for lead at a number of temperatures

(1) This work was supported in part by the Air Material Command, Wright Field.

(2) T. Rubin, H. W. Altman and H. L. Johnston, *J. Am. Chem. Soc.*, **76**, 5289 (1954).

(3) T. Rubin, H. L. Johnston and H. W. Altman, *J. Phys. Chem.*, **65**, 65 (1961).

(4) T. Rubin, H. L. Johnston and H. Altman, *J. Am. Chem. Soc.*, **73**, 3401 (1951).

(5) F. A. Willers, "Practical Analysis," Dover Publications, 1947, p. 77.

(6) J. B. Scarborough, "Numerical Mathematical Analysis," Johns Hopkins Press, Baltimore, Maryland, 1930, p. 115.

(7) F. C. Nix and D. MacNair, *Phys. Rev.*, **61**, 74 (1942).

TABLE I

Lead l_0 = 0.49670 cm.

Run	ΔT	T avg., °K.	O smoothed	v_1^2	v_2^2	F	$\alpha \times 10^6$
1	7.492	82.817	14.80	20.521	22.801	3.1541	2.497
2	8.121	90.62	14.80	22.801	29.485	3.4516	2.521
3	10.369	99.87	14.80	29.485	21.064	4.4312	2.536
4	9.868	109.99	14.81	21.064	25.000	4.2658	2.564
5	11.917	120.88	14.82	25.000	27.931	5.1978	2.594
6	13.564	133.62	14.84	27.931	28.729	6.0538	2.646
7	14.430	147.03	14.83	28.729	20.931	6.4735	2.682
8	15.537	162.62	14.80	20.931	22.515	7.1071	2.717
9	19.603	213.157	14.88	37.39	38.50	9.0874	2.750
10	22.224	234.07	14.83	38.50	45.02	10.439_9	2.787
11	21.012	255.73	14.79	45.02	45.56	10.036_4	2.822
12	24.063	278.32	14.80	45.56	39.00	11.556_6	2.849
13	5.973	61.091	14.84	13.141	18.275	2.3457	2.327
14	8.133	68.14	14.82	18.275	22.231	3.2710	2.385
15	7.684	76.05	14.82	22.231	25.100	3.1939	2.466
16	7.553	83.67	14.80	25.100	27.615	3.1699	2.489
17	10.039	92.47	14.80	27.615	16.605	4.256_1	2.515
18	10.592	102.78	14.81	16.605	29.750	4.549_6	2.547
19	13.875	115.02	14.83	24.750	25.050	6.020_2	2.575
20	11.991	127.95	14.83	25.050	29.214	5.281_0	2.613
21	13.660	140.77	14.83	29.214	15.563	6.078_9	2.640
22	14.148	154.68	14.81	15.563	21.114	6.375_1	2.673
23	4.072	16.873	14.96	16.646	25.250	0.575_1	0.840
24	4.097	20.96	14.95	25.250	22.091	0.788_6	1.144
25	3.808	24.91	14.94	22.091	20.521	0.8949	1.396
26	3.539	28.59	14.92	20.521	19.669	0.9429	1.580
27	3.350	32.04	14.92	19.669	19.428	0.9839	1.725
28	3.169	35.30	14.92	19.428	19.009	0.9719	1.841
29	4.225	38.98	14.91	19.009	25.250	1.4187	1.991
30	4.807	43.50	14.90	25.250	20.295	1.6675	2.058
31	5.978	48.89	14.88	20.295	22.848	2.1716	1.155
32	6.872	55.32	14.86	22.848	17.015	2.6075	2.252
33	23.739	173.413	14.76	31.81	29.00	10.8096	2.702
34	24.471	197.52	14.72	29.00	33.29	11.291_8	2.737
35	24.691	222.10	14.71	33.29	41.35	11.547_6	2.774
36	12.172	125.442	15.18	37.64	42.38	5.314_7	...
37	13.998	138.53	15.11	42.38	30.31	6.198_7	...
38	12.622	151.84	15.08	30.31	40.45	5.672_3	2.666
39	12.185	164.24	15.05	40.45	33.12	5.512_8	2.684
40	29.538	184.895	14.52	30.14	38.32	13.563_1	2.724
41	30.918	215.12	14.46	38.32	44.36	14.417_6	2.766
42	29.394	247.90	14.52	44.36	43.30	13.927_1	2.811
43	19.757	269.86	14.66	43.30	35.58	9.473_7	2.845
44	24.769	292.12	14.78	35.58	35.17	11.971_9	2.868

above that for liquid air and have compared their results with the data of numerous authors. These were determined at various restricted temperatures. The comparison of Nix and MacNair's results at a few temperatures with those of the present research are shown in Table II. The deviations of their values from those of the present work are never more than about 0.3%. Dorsey[8] has determined α between 113 and 273°K. His results are about 2% higher at room temperature than those of the present work. The deviations decrease steadily at lower temperatures, become negative, then finally reach values within 2% of the values of the present research at 113°K.

TABLE II

t, °C.	$\frac{\Delta l}{l_0} \times 10^4$, Nix and MacNair	$\frac{\Delta l}{l_0} \times 10^4$, present work
−188	−50.398	−50.719
−143.5	−39.423	−39.323
−103.0	−28.775	−28.567
− 79.5	−22.155	−22.234
− 48.1	−13.520	−13.524
− 17.4	− 4.916	− 4.928
0	0	0

(8) M. G. Dorsey, *Phys. Rev.* **27**, 1 (1908).

Theory.—Since the compressibility of lead is not known reliably as a function of temperature, a discussion of these results directly in terms of Gruneisen's theory is not possible.

Instead of the quotient $C_P/\alpha T$ was computed for not only lead but also for copper and rock salt where reliable heat capacity and thermal expansion are known. This function has the dimensions of PV/T which suggests that $C_P/\alpha T$ can be considered as a type of corresponding state function, so that the data of the three solids can be plotted as a function of a reduced temperature and compared.

Two types of deviations from the corresponding state curve will be discussed, the effect of anharmonicity, if any, and the effect of variations of the Gruneisen parameter at lower temperatures which has been presented at length by Barron.[9,10] By thermodynamics

$$\frac{C_p}{3\alpha T} = V\left(\frac{\partial P}{\partial T}\right)_s \qquad (1)$$

for a crystal containing one kind of particle the pressure[11] is

$$P = -\frac{\partial E_0}{\partial V} - \frac{1}{V}\sum_{i=1}^{3N}\frac{h\nu_i\,\gamma_i}{e^{h\nu i/RT}-1} - \frac{1}{2V}\sum_{i=1}^{3N} h\nu_i\gamma_i + kV\frac{\partial ln\,\sigma_0}{\partial V} \qquad (2)$$

where E_0 is the zero point energy, ν_i is the frequency, V the volume, T the temperature, $\gamma_i = \partial \ln \nu_i/\partial \ln V)_T$, σ_0 is the number of states of lowest energy, the other symbols have their usual meaning. Since $(\partial V/\partial T)_s = -V/\gamma T$ and $\partial(\nu_i/V/\partial T)_s = 0$ where $\gamma = \alpha V/CvK$, the Gruneisen[12] function, where α is the expansion coefficient and K is the isothermal compressibility.

$$\frac{C_p}{3\alpha T} = \frac{\partial^2 E_0}{\partial V^2}\frac{V^2}{\gamma T} - k\left(\sum_{i=1}^{3N}\frac{k\nu_i}{kT}\gamma_i\Big/e^{h\nu i/kT}-1 + \sum_{i=1}^{3N}\frac{h\nu_i\gamma_i}{2kT}\right) + kV\frac{\partial \ln \sigma_0}{\partial V} \qquad (3)$$

$$= \frac{\partial^2 E_0}{\partial V^2}\frac{V^2}{\gamma T} - \frac{\gamma_E\,(E-E_0)}{T} + k\frac{\partial \ln \sigma_0}{\partial \ln V} \qquad (4)$$

where

$$\gamma_E = \frac{k\left(\sum_{i=1}^{3N}\frac{h\nu_i\,\gamma_i}{kT}\Big/(e^{h\nu i/kT}-1) + \sum_{i=1}^{3N}\frac{h\nu_i\,\gamma_i}{2\,kT}\right)}{k\left(\sum_{i=1}^{3N}\frac{h\nu_i}{kT}\Big/(e^{h\nu i/kT}-1) + \sum_{i=1}^{3N}\frac{h\nu_i}{2\,kT}\right)} \qquad (5)$$

$$\frac{\partial^2 E_0}{\partial V^2} = 1/K_0 v_0 \qquad (6)$$

and $E - E_0$ is the denominator of (5). In relation 2 (6) $\partial^2 E_0/\partial \nu^2 = 1/K_0 V_0$ at the absolute zero, assuming central forces.

K_0 is the isothermal compressibility, V_0 is the molar volume, both at the absolute zero.

Inserting 6 in 4 yields after approximating V_0 for V

(9) T. H. K. Barron, *Phil. Mag.*, [7] **46**, 720 (1955).

(10) T. H. K. Barron, *Ann. Phys.*, **1**, 77 (1957).

(11) R. C. Tolman, "Statistical Mechanics," Oxford Press, 1938, p. 589.

(12) E. Grüneisen, "Handbuch der Physik," Vol. 10, Julius Springer, Berlin, 1926, p. 1.

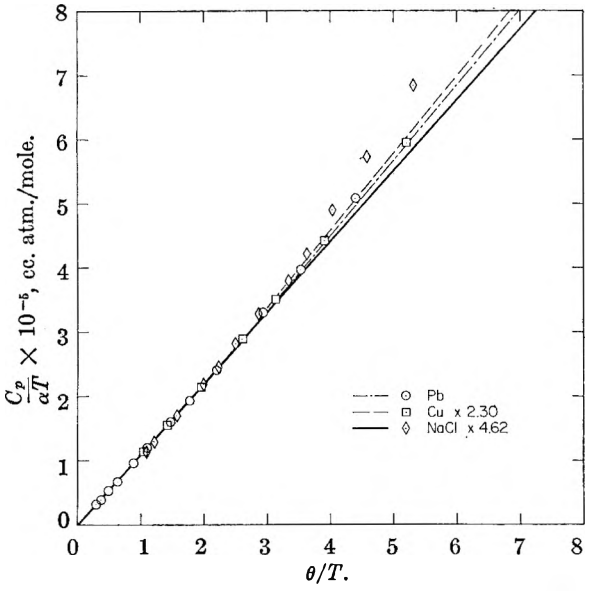

Fig. 1.

$$\frac{C_p}{3\,\alpha T} = \frac{V_0}{K_0 \gamma T} - \frac{\gamma_E(E - E_0)}{T} \qquad (7)$$

Except for the last term on the right-hand side, this relation resembles Gruneisen's relation for γ. However, (7) involves the compressibility as a constant and the more easily measured C_p rather than C_v. Still, with this relation deviations from Gruneisen's law can be discussed. We will retain the temperature terms in relation 7 only so that the entire relation is a function of θ/T.

The best way of using relation 7 as a corresponding state function seems to be by comparing the results of this research for lead with previous work for copper and rock salt. The heat capacity of copper taken from the work of Giauque and Meads,[13] the values for lead from that of Meads, Forsythe and Giauque,[14] and the values for rock salt of Clusius, Goldman and Perlick,[15] together with the expansion coefficients of lead, copper[2] and rock salt[3] were used to give numerical values of $C_p/\alpha T$. θ was taken as 88[16] for lead, 312.8[13] for copper and 280[15] for rock salt. The graph of $C_P/\alpha T$ *vs.* θ/T is shown in Fig. 1, where all of the results for copper and rock salt have been superimposed on the results for lead. This has been done by multiplying the copper values by 2.30 and the rock salt values by 4.62. The straight line portion of the curve of Fig. 1 extrapolates to a negative value of about 3000 cc. atm./deg. mole. Thus, the value corresponds roughly to the second term of (7). Anharmonic effects are absent.

The large deviations from the straight line occur at low temperatures where θ/T is greater than 5. This is expected, as at low temperatures, γ should decrease.[10] Using Barron's relation[9] for γ corresponding to the nearest neighbor model for both lead and copper, the deviations from the straight line function are shown for these two substances as the dotted curves. The agreement is satisfactory.

The deviations of the rock salt points do not agree with Barron's relation[3] for that substance. The experimental points deviate by over a factor of three from a curve demanded by the theory.

From the results shown in Fig. 1, the heat capacity and thermal expansion data for lead, copper and rock salt are quite self consistent. Lead obeys Gruneisen's law between 25 and 300°K. Satisfactory values (within a few per cent.) for the compressibility of lead as a function of temperature to about 25°K. can be computed, assuming that γ is independent of temperature. Using Barron's deviation function for γ, the compressibility of both lead and copper can be computed for temperatures from 300 to about 11°K. for lead and to about 39°K. for copper.

(13) W. F. Giauque and P. F. Meads, *J. Am. Chem. Soc.*, **63**, 1897 (1941).

(14) P. F. Meads, W. R. Forsythe, and W. F. Giauque, *ibid.*, **63**, 1902 (1941).

(15) K. Clusius, J. Goldman and A. Perlick, *Z. Naturforschung*, **4**, 424 (1949).

(16) R. H. Fowler, "Statistical Mechanics," Cambridge University Press, 2nd Edition, 1936, p. 126.

N.M.R. STUDY OF THE IONIZATION OF ARYL SULFONIC ACIDS

BY ROBERT H. DINIUS AND GREGORY R. CHOPPIN

Department of Chemistry, Florida State University, Tallahassee, Florida

Received July 31, 1961

Nuclear magnetic resonance spectra of *p*-toluenesulfonic acid, 2-naphthalenesulfonie acid and 2,7-naphthalenedisulfonic acid were measured as a function of concentration. The acid ionization constant for *p*-toluenesulfonic acid calculated from the chemical shifts is 22 ± 3. A comparison of the chemical shifts for these sulfonic acids and Dowex-50 cation exchange resin of 4 and 16% divinylbenzene content indicates that the cation exchanger resin is the stronger acid.

Aryl sulfonic acids such as *p*-toluenesulfonic acid have been used in a number of investigations[1,2] as model compounds for the elucidation of the complex physical chemistry of polystyrene–divinylbenzene sulfonic acid ion exchange resins such as Dowex-50. In conjunction with an investigation of hydrated Dowex-50 resin by nuclear magnetic resonance techniques,[3] it has seemed feasible to study these model compounds by the same techniques. Several previous reports[4,5] have demonstrated the

(1) G. E. Meyers and G. E. Boyd, *J. Phys. Chem.*, **60**, 521 (1956).

(2) O. D. Bonner, V. F. Holland and L. L. Smith, *ibid.*, **60**, 1102 (1956).

(3) R. H. Dinius, G. R. Choppin and M. T. Emerson, to be submitted for publication.

(4) H. S. Gutowsky and H. Saika, *J. Chem. Phys.*, **21**, 1688 (1953).

(5) G. C. Hood, O. Redlich and C. A. Reilly, *ibid.*, **22**, 2067 (1954); also G. C. Hood, A. C. Jones and C. A. Reilly, *J. Phys. Chem.*, **63**, 101 (1959).

value of the study of strong acids by nuclear magnetic resonance and recently the results of such an investigation of polystyrene sulfonic acid have been reported.[6]

Experimental

Reagents.—C.P. *p*-toluenesulfonic acid was used as obtained from Eastman Chemical Co. with no further purification. 2-Naphthalenesulfonic acid and 2,7-naphthalenedisulfonic acid were purified from technical grade material by recrystallization from concentrated hydrochloric acid solutions. Saturated aqueous solutions were prepared from the purified crystals and the desired concentrations obtained by dilution with distilled water. The molarities of all solutions were determined by titration with standard sodium hydroxide solution.

N.M.R. Spectra.—The proton magnetic resonance spectra of these three acids were measured as a function of the acid solution concentration using a Varian Associates high resolution N.M.R. spectrometer operating at 60 megacycles per sec. The side band technique utilizing external standards was used to obtain reference signals. The room and magnet gap were thermostated to 25°.

Cyclohexane was used as the external reference and from a knowledge of the difference in resonance frequencies of cyclohexane and water, the chemical shifts of the acid solutions were calculated with respect to the frequency of pure water. All the shifts, expressed in cycles per second, were toward lower field strengths. The observed chemical shifts were corrected for changes in the bulk magnetic susceptibility of the solutions. The magnetic susceptibilities were obtained by observing the splitting of the resonance lines induced by shaping the sample container from a cylinder to a sphere and placing the transition zone in the magnetic field.[7] The susceptibilities obtained in this way have been compared with the values obtained from Pascal's constants and found to agree within 3–5%. The results of the n.m.r. measurements are presented in Table I.

TABLE I

CHEMICAL SHIFTS

Molarity	Density	Frequency, c.p.s.	Resonance shift (*S*), p.p.m. Obsd.	Cor.	*P*
		p-Toluenesulfonic acid			
0.064	1.002	214.0	0.020	0.024	0.0017
.300	1.017	219.1	.105	.115	.0084
.590	1.034	224.6	.197	.221	.017
1.181	1.063	236.8	.401	.439	.036
2.373	1.115	267.2	.908	.964	.087
2.885	1.135	286.0	1.221	1.282	.117
3.787	1.170	326.8	1.901	1.989	.186
4.733	1.208	383.6	2.847	2.929	.291
5.075	1.229	415.4	3.377	3.469	.342
		2-Naphthalenesulfonic acid			
0.232	1.014	217.6	0.081	0.087	0.0065
.462	1.040	221.2	.141	.174	.0132
.940	1.053	231.4	.311	.346	.0294
1.880	1.119	257.2	.741	.808	.069
		2,7-Naphthalenedisulfonic acid			
0.1631	1.009	220.3	0.126	0.120	0.0096
.4570	1.042	230.9	.302	.312	.0310
.9125	1.115	251.5	.646	.704	.0517
1.368	1.175	276.3	1.059	1.163	.0918
1.825	1.251	300.8	1.467	1.632	.1302

The n.m.r. spectra of the undissociated acids were measured in non-ionizing solvents ($CHCl_3$ and C_7H_{16}) and the shifts with respect to water within experimental error were found to be 6.51 p.p.m. This compares with the reported value of 6.7 ± 0.3 p.p.m. for the alkyl and benzene sulfonic acids.[8]

(6) L. Kotin and M. Nagasawa, *J. Am. Chem. Soc.*, **83**, 1026 (1961).

(7) W. Stewart and R. Glick, private communication.

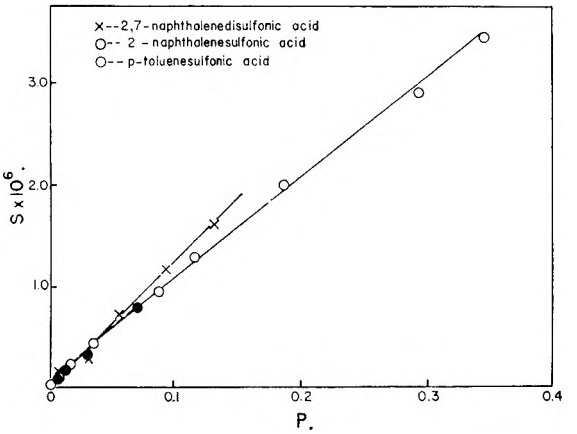

Fig. 1.—The chemical shift plotted as a function of the mole fraction of protons on hydronium ions.

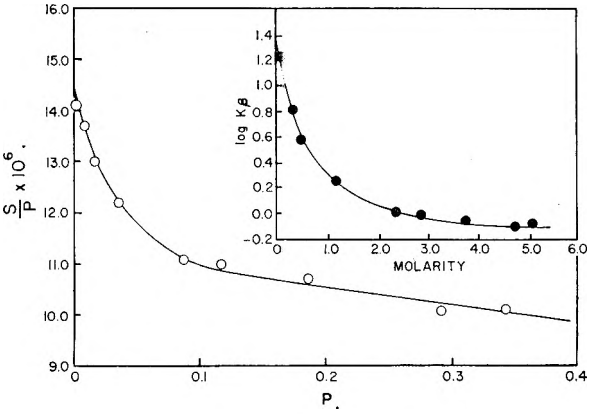

Fig. 2.—The ratio of chemical shift to mole fraction of protons on hydronium ions as a function of the mole fraction of protons on hydronium ions for *p*-toluenesulfonic acid.

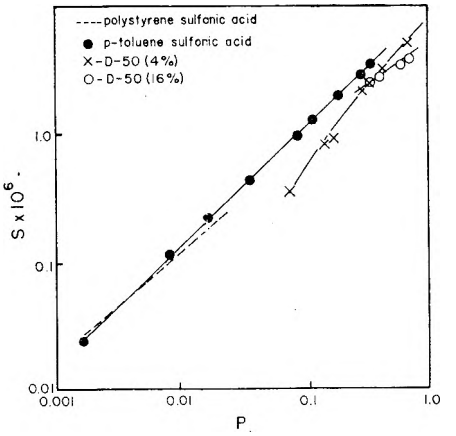

Fig. 3.—Log of the chemical shift plotted as a function of the log of the mole fraction of protons on hydronium ions.

During the course of this investigation, it was observed that solutions of *p*-toluenesulfonic acid underwent photochemical decomposition in the presence of ultraviolet radiation, resulting in the development of a yellow color with evolution of SO_2. Prolonged heating on a steam-bath in the dark failed to provide any visible evidence of this decomposition.

(8) L. H. Meyer, A. Saika and H. S. Gutowsky, *J. Am. Chem. Soc.*, **75**, 4567 (1953).

Discussion

Figure 1 indicates that *p*-toluenesulfonic acid and 2-naphthalenesulfonic acid have a very similar curve for the chemical shift plotted as a function of P, the mole fraction of protons on hydronium ions. In calculating P, only the acid group and water protons are considered and not the aromatic hydrogens. Assuming complete dissociation, if x is the stoichiometric mole fraction of the acid, P equals $3x/(2\text{-}x)$ for the monobasic acids and $3x$ for the dibasic acid. The greater slope for 2,7-naphthalenedisulfonic acid possibly could be interpreted as meaning that it is a stronger acid than the *p*-toluenesulfonic or 2-naphthalenesulfonic acid (see equation). However, the two sulfonic acid groups of this dibasic acid are not completely independent and the effect of the ionization of one group upon the ionization of the second group is uncertain. Consequently, the suggested interpretation of relative acid strength must be regarded as only tentative.

Only for *p*-toluenesulfonic acid is the solubility sufficiently large to allow high enough values of P to be investigated so that analysis of the data to calculate the acid constant is possible. The degrees of dissociation were calculated from the shifts by the equation

$$S/P = \alpha S_1 + (1 - \alpha)S_2 \qquad (1)$$

where S is the total chemical shift in p.p.m., S_1 is the shift of the hydronium ion and S_2 is the shift of the undissociated acid. For S_2 the value of 6.51 p.p.m. was used. Although the value of S_1 would be expected to be the same in all acids, it has been found that in fact the anion influences the observed hydronium ion shift. The value of S_1 is obtained by plotting the values of the slope S/P as a function of P as in Fig. 2 and extrapolating to $P = 0$. A value of 14.5 p.p.m. is obtained for the *p*-toluenesulfonic acid as compared to previously reported valves of 11.8, 9.2 and 13.1 p.p.m. for HNO_3, $HClO_4$ and H_2SO_4.[5,9] The calculation of α, the degree of dissociation, is more sensitive to the value of S_1 than of S_2 as can be seen from the revision of the S/P equation to the form

$$\alpha = \frac{S/P - S_2}{S_1 - S_2} \qquad (2)$$

The equation for the acid dissociation constant is

$$K\beta = \frac{a}{C(1 - \alpha)} \qquad (3)$$

(9) G. C. Hood and C. A. Reilly, *J. Chem. Phys.*, **27**, 1126 (1957).

where β is the acitivity coefficient of the undissociated molecule, C is the concentration of the acid in moles per liter and a is the activity of *p*-toluenesulfonic acid. In the insert in Fig. 2, log $K\beta$ is plotted *vs.* molarity. The values of a were calculated using data of Bonner, *et al.*[10] The value of K calculated in this fashion is 22 ± 3, which is comparable to that of nitric acid. Bonner and Rogers[11] report that mesitylenesulfonic acid has an ionization constant of the same order of magnitude but lower than nitric acid.

In Fig. 3, the chemical shifts are shown on a log–log plot as a function of P for *p*-toluenesulfonic acid, polystyrenesulfonic acid[6] and Dowex-50 cation exchange resin of 4 and of 16% divinylbenzene content.[3] Both this curve and an analysis of the polystyrenesulfonic acid for the acid dissociation constant indicate that the latter is quite similar to *p*-toluenesulfonic acid in its acid strength. Although the resin is too concentrated even in the most hydrated state to allow reliable calculation of an acid constant, the indications are that the 4% DVB resin is stronger than the *p*-toluenesulfonic acid. Also the indication that the 4% DVB resin is stronger than the 16% DVB is reasonable, since the more extensive organic crosslinking would result in a lower effective dielectric constant in the vicinity of the sulfonate group, lowering the acid constant. It must be understood that this analysis of the relative acid strengths of the resins and *p*-toluenesulfonic acid is based on equation 2, assuming S_2 is the same for all these sulfonic acids and that S_1 for the resin is equal to or greater than 14.5 p.p.m., which does not seem unreasonable.

The observed line widths for dilute solutions of the *p*-toluenesulfonic, the 2-naphthalenesulfonic and the 2,7-naphthalenedisulfonic acids were approximately 0.9 cycle. As the concentrations of the solutions approached saturation and increased in viscosity, the absorption line width increased to 1.5-2 cycles. This broadening is consistent with reported viscosity effects.[12]

The authors wish to thank Drs. E. Grunwald and M. Emerson for their assistance in this research. The Atomic Energy Commission has supported this research under Contract AT-(40-1)-1797.

(10) O. D. Bonner, G. D. Easterling, D. L. West and V. F. Holland, *J. Am. Chem. Soc.*, **77**, 242 (1955).

(11) O. D. Bonner and O. C. Rogers, *J. Phys. Chem.*, **64**, 1499 (1960).

(12) J. N. Shoolery and B. Alder, *J. Chem. Phys.*, **23**, 805 (1955).

RADIOLYTIC AND PHOTOCHEMICAL DECOMPOSITION AND EXCHANGE IN LIQUID AND GASEOUS CCl_3Br[1]

BY AUSTIN H. YOUNG AND JOHN E. WILLARD

Department of Chemistry of the University of Wisconsin, Madison, Wisc.

Received August 3, 1961

This paper reports studies of the radiolysis of liquid and gaseous CCl_3Br, of the photolysis of gaseous CCl_3Br and of the radiation induced exchange of bromine between Br_2 and CCl_3Br in the liquid and the gaseous phases. Co^{60} γ-rays and 2537 Å. light were the activating radiations. Typical product yields in units of molecules/100 e.v. absorbed are

	Dose, e.v./g.	CCl_4	CCl_2Br_2	$CClBr_3$	C_2Cl_6	Br_2	C_2Cl_5Br
Radiolysis (liq., 20°)	1×10^{21}	3.5	2.9	0.1	0.5	1	0.15
Rad. (gas, 108°)	1×10^{21}	7.5	6.1	.82	1.2	1.2	0
Rad. (gas, 108°, 1 mole % Br_2)	1×10^{21}	5.1	5.7	.3	0	0	0
Photolysis (gas, 108°)	1×10^{22}	0.5	0.5	.01	0.9	0.7	0

The apparent activation energies for the formation of the products are about 3 kcal./mole, which is lower than required for thermal radical and atom abstraction reactions in this system. This may result from a small contribution from thermal processes superimposed on a major contribution from temperature insensitive reactions of vibrationally excited species or ions. The reaction cross sections for these hot processes must be significantly lower than the collision cross sections since the yields are reduced by 1 mole % added Br_2. The G-values for the exchange caused by γ-rays in the gas and in the liquid at 108° are both of the order of 600 atoms/100 e.v. absorbed while that in the liquid at 20° is about 150. These values indicate chain reactions with an over-all activation energy which appears to be too low to be explained on the basis of the known thermal chemistry of the system, and so may include a contribution from ion molecule reactions. G(exchange) is sensitive to some unknown variable but is not affected significantly by 2 mole % O_2 in the presence of 1 mole % Br_2.

Introduction

This work was initiated to compare the radiolysis of CCl_3Br in the gas phase with that in condensed phases.[2] It was designed to determine to what extent the yields, the temperature effects and the scavenger effects in the condensed phases are dependent upon diffusion controlled and caging processes. Characteristics of the gas phase radiolysis, in which ions are formed, have been compared with the photolysis, in which no ions are formed. Previous work on the radiolysis of the liquid has been extended by gas chromatographic analysis of the organic products. The exchange of gaseous CCl_3Br with Br_2 induced by γ-rays has been investigated and found to occur by a chain reaction.

Experimental[1b]

The purification and sample preparation procedures used were, with some variations, similar to those described earlier.[2] Irradiation of samples to be analyzed spectrophotometrically was carried out in an annular vessel[3] into the center of which a 400 curie Co^{60} source about 1.6 cm. diam. and 2 cm. long could be inserted to give a dosage rate of about 1×10^{20} e.v. hr.$^{-1}$ (g. of CCl_3Br)$^{-1}$. A Beckman-type cell of square Pyrex tubing attached to the annular vessel by several inches of glass tubing was used for spectrophotometric analysis of the liquid or gas after each of successive periods of irradiation. For analysis of gaseous samples steam heated "thermospacers" were used on the Beckman DU spectrophotometer cell compartment, which was provided with an electrically heated cover box to accommodate the protruding annular vessel. Care was taken to mix thoroughly the irradiated and unirradiated portions of the sample before analysis. The absorbancy index of Br_2 in gaseous CCl_3Br at 4160 Å. was determined to be 166 l. mole^{-1} cm.$^{-1}$. Gas phase γ-irradiations were carried out in a thermostated mineral oil-bath in which was mounted a lead shield to reduce the exposure of the spectrophotometer cell to irradiation while the gas in the annular vessel was being exposed. Br^{82} for exchange studies was prepared by irradiation of small ampoules of liquid Br_2 at a flux of 10^{12} neutrons sec.$^{-1}$ cm.$^{-2}$ in the CP-5 reactor of the Argonne National Laboratory. Mixtures of CCl_3Br and radiobromine which had undergone exchange were partitioned between CCl_4 and aqueous sulfite solution to determine by counting methods the extent of exchange.

The 0.3-ml. liquid samples to be analyzed by gas chromatography were sealed in 6 cm. long 4 mm. i.d. Pyrex tubes following degassing, and during irradiation were positioned so that they received the same dose rate as samples irradiated in the annular vessel. Detection of the components in the effluent from the silicone-oil-on-firebrick chromatographic columns was done with a Gow Mac thermal conductivity detector. When radiobromine had been used in the sample a scintillation counter also was used.[4]

The photochemical experiments were carried out in a 10 cm. long, 2.5 cm. diam. quartz cell with flat end windows, mounted in an aluminum block furnace. The radiation source was a Hanovia SC 2537 low pressure mercury arc, filtered by a Vycor plate to exclude wave lengths below 2100 Å. All of the incident 2537 Å. radiation was adsorbed by the CCl_3Br at the pressures used. The intensity was assumed to be the same as that previously found[5] for the same type of lamp at the same current and used at the same geometry with respect to the reaction cell.

Results

$G(Br_2)$ of Liquid Phase Radiolysis.—It has been reported[2] that $G(Br_2)$ for the radiolysis of liquid CCl_3Br at 20° decreases with increasing bromine concentration up to about 0.02 M and then remains constant, the value at 10^{-3} M Br_2 being 1.5 and the "terminal" value being 0.94. These observations were made at a dose rate of 1×10^{19} e.v. g.$^{-1}$ hr.$^{-1}$ and total doses up to 2×10^{20} e.v. g.$^{-1}$. The present work has shown that the same trend occurs with a 10-fold higher intensity (1×10^{20} e.v. g.$^{-1}$ hr.$^{-1}$) and for 10-fold higher doses (2×10^{21} e.v. g.$^{-1}$). The absolute G-values at the lower bromine concentrations show evidence of being slightly higher at the higher intensity but the terminal G-values appear to be indistinguish-

(1) (a) Presented at the International Congress of Radiation Research, Burlington, Vt., Aug. 1958; (b) Additional details of work are given in the Ph.D. thesis of A. H. Young filed with the University of Wisconsin Library in 1958 and available from University Microfilms, Ann Arbor, Mich.

(2) R. F. Firestone and J. E. Willard, *J. Am. Chem. Soc.*, **83**, 3551 (1961).

(3) R. F. Firestone and J. E. Willard, *Rev. Sci. Instr.*, **24**, 904 (1953).

(4) J. B. Evans, J. E. Quinlan and J. E. Willard, *Ind. Eng. Chem.*, **50**, 192 (1958).

(5) G. M. Harris and J. E. Willard, *J. Am. Chem. Soc.*, **76**, 4678 (1954).

able at the two intensities and different total doses.

Organic Products of Liquid Phase Radiolysis.—CCl_4 and CCl_2Br_2 are the predominant products of the radiolysis of liquid CCl_3Br at 20°. They are formed with constant G-values of 3.5 and 2.9, respectively, up to doses of at least 2×10^{21} e.v. g.$^{-1}$. Other organic products, produced with much lower G-values, are C_2Cl_6 (0.5), C_2Cl_5Br (0.15) and $CClBr_3$ (0.1). The accuracy of the low G-value measurements is not adequate to indicate whether the rate of formation of these is independent of bromine concentration.

Br_2–CCl_3Br Exchange during Liquid Phase Radiolysis.—Some thirty determinations of the exchange reaction $CCl_3Br + Br_2^* \rightarrow CCl_3Br^* + Br_2$ were made using Br_2 labeled with Br^{82}. G-(exch.) is about 650 at 108° and 150 at 28°, apparently independent of radiation intensity over a 50-fold range from 0.03×10^{18} to 1.5×10^{18} e.v. g.$^{-1}$ min.$^{-1}$, and independent of Br_2 concentration over the twenty-fold range from 5×10^{-3} to 1×10^{-1} M. Rather large unexplained fluctuations in individual G-values were observed between certain supposedly duplicate runs, the extreme values at 28° being 30 and 350. Control runs in which the samples were prepared, heated and analyzed in the standard manner but not subjected to radiation showed negligible exchange.

Gas Phase Radiolysis.—Typical G-values for the products of radiolysis of CCl_3Br in the gas phase at 108° both with and without added Br_2 are tabulated in the Abstract. The values without added Br_2 are slightly higher than those in the liquid at 20°, except for C_2Cl_5Br which is not observed in the gaseous products. The presence of 1 mole % added Br_2 reduces all of the yields slightly and seems to completely eliminate C_2Cl_6 and Br_2 production.

A comparison of the solid lines of Fig. 1 illustrates the increase in $G(Br_2)$ with temperature in the radiolysis of gaseous CCl_3Br. The G-values calculated from the slopes at 0.2 mole % Br_2 concentration on the 108 and 177° radiolysis curves are 1.2 and 2.2. A value of 1.5 was obtained for a similar determination at 141°. Other experiments in which the bromine concentration was followed as a function of dose at various temperatures up to 177° and at doses up to 18×10^{21} e.v. g.$^{-1}$ showed that $G(Br_2)$ approaches zero for prolonged irradiations at 108 and 141°. At 177° the data also show this trend, but at a dose as high as 17×10^{21} e.v. g.$^{-1}$ $G(Br_2)$ is still 0.9 for an average bromine concentration of 3.2 mole %. The Br_2 concentrations at which $G(Br_2)$ becomes zero increase with increasing temperature, being about 1.5 mole % at 108°, 2.5 mole % at 141° and higher than 3.5 mole % at 177°. When a sample of CCl_3Br vapor in which 1.5 mole % Br_2 had been produced by irradiation was allowed to stand for 18 hr. at 177° without irradiation no increase in the Br_2 concentration occurred, showing thermal decomposition to be negligible. Likewise an unirradiated sample showed negligible bromine production when held for 37 hours at 180°.

When the radiolysis was carried out at 182° with an absorbed dose of 1.5×10^{21} e.v. g.$^{-1}$ the G-values of the organic products shown for 108° all increased by a factor of 1.4 to 1.5 except for $CClBr_3$ which increased from $G = 0.82$ to $G = 1.8$.

Br_2–CCl_3Br Exchange during Gas Phase Radiolysis.—When gaseous CCl_3Br at 108° was radiolyzed in the presence of 1–11 mole % Br_2 labeled with Br^{82} well over 90% of the Br^{82} in organic combination appeared as CCl_3Br (Table I). In 15 experiments in which G(exchange) was determined the average value for atoms exchanged per 100 e.v. was 497 ± 225 in the absence of oxygen and 266 ± 95 in the presence of 0.04 to 2 mole % oxygen (Table II). From the data it may be said that the exchange must be a chain reaction, and that it is not highly sensitive to Br_2 concentration, radiation dose or oxygen concentration within the ranges tested but is sensitive to some unknown variable, as in the case of the liquid phase exchange reported above.

TABLE I

DISTRIBUTION OF Br^{82} AMONG ORGANIC PRODUCTS OF THE RADIOLYSIS OF GASEOUS CCl_3Br–Br_2 MIXTURES CONTAINING Br_2(Br-82)

(108°, 1.64×10^{21} e.v. absorbed per g.)

$[Br_2]$, mole %	$[O_2]$, mole %	Fraction of organic Br^{82} in CCl_3Br	CCl_2Br_2	$CClBr_3$
1	0	0.97	0.032	Trace
5.3	1.2	.92	.077	Trace
10	0	.94	.048	0.01
10	1.2	.97	.027	None

TABLE II

G(EXCHANGE) DURING RADIOLYSIS OF GASEOUS CCl_3Br–Br_2 MIXTURES CONTAINING Br_2(Br-82)

(108°, 7.7×10^{19} e.v. g.$^{-1}$ hr.$^{-1}$)

$[Br_2]$, mole %	$[O_2]$, mole %	Energy absorbed, (e.v. g.$^{-1}$ $\times 10^{19}$)	F/F_∞ [a]	G(exchange), atoms/100 e.v.
1	..	1.96	0.90	680
1	..	0.78	.54	590
1	..	.13	.26	1400
1.4	..	.78	.43	620
1.3	..	.78	.42	540
1.2	..	.78	.13	140
0.5	..	.78	.74	500
0.5	..	.78	.58	330
0.2	..	.39	.42	170
1	..	.76	.27	250
1	..	.76	.43	460
1	..	.76	.31	280
1	2	.76	.21	190
1	0.4	.76	.23	200
1	0.04	.76	.41	410

[a] F/F_∞ is the fraction of equilibrium exchange achieved.

Gas Phase Photolysis.—Gaseous CCl_3Br illuminated with 2537 Å. radiation produces Br_2 at a rate which decreases with increasing bromine concentration and increases with increasing temperature, as shown by the broken lines of Fig. 1. The initial yield of Br_2 per unit of energy absorbed is somewhat higher for the photolysis than the radiolysis. The initial G of photolysis decreases more rapidly with increasing Br_2 concentration than that of radiolysis but, in contrast to the radiolysis, is not reduced to zero at 108° at the bromine concentrations achieved in Fig. 1. Following the

determination of bromine production as a function of time of photolysis shown in Fig. 1 the two samples used to define the curve at 108° each were analyzed by gas chromatography. The yields of organic products for these samples which had each been exposed to 10^{22} e.v. g.$^{-1}$ of 2537 Å. radiation are given in Table III both as G-values and as quantum yields.

TABLE III

YIELDS OF PRODUCTS PRODUCED BY THE PHOTOLYSIS OF GASEOUS CCl_3Br AT 108° WITH 10^{22} e.v. g.$^{-1}$ OF 2537 Å. RADIATION

	Sample 1		Sample 2	
Compound	G-value	Quantum yield	G-value	Quantum yield
CCl_4	0.33	0.016	0.47	0.023
CCl_3Br	−2.48	− .121	−2.77	− .136
CCl_2Br_2	0.56	.027	0.52	.026
$CClBr_3$	..	...	.01	.0005
C_2Cl_6	.80	.039	.90	.044
Br_2 (spectrophotometrically)	.69	.034	.70	.034

From the curves of Fig. 1 it is apparent that the *average* quantum yields of Br_2 for the complete experiment are much smaller than the initial yields. This presumably is true also for C_2Cl_6, one molecule of which is produced for each molecule of Br_2 formed.

Discussion

Mechanism of Br_2 Production in Radiolysis.—$G(Br_2)$ as estimated from the slope of the 108° curve of Fig. 1 at 0.2 mole % Br_2 is 1.2, which is similar to the value of 1.7 obtained[2] at this bromine concentration in the liquid at 98°. The absence of a sharp discontinuity in yield at the liquid n vapor transition probably is fortuitous. Caging effects in the liquid undoubtedly cause some primary recombination with no net product yield, while reactions of adjacent radicals in the spurs must lead to Br_2 production which could not occur in the gas phase, where the radicals must react with Br_2 in the bulk of the gas because the high localized radical concentration of the spurs does not exist. It has been noted earlier[2] that there is no discontinuity in $G(Br_2)$ at the solid phase transitions at −33.5 and −13.5° or at the melting point at −5.6°. These transitions are not, however, accompanied by a density change of the magnitude involved in the change from liquid to vapor.

An immediately apparent difference between the liquid and gas phase radiolysis is that in the latter $G(Br_2)$ decreases with increasing Br_2 concentration, approaching zero at a concentration which is dependent on temperature. This was observed in the range of 0.1 to 3 mole % Br_2, while in the overlapping range of 0.01 to 0.3 mole % in the liquid constant G-values were observed above 0.1 mole % at all temperatures.

Three types of available evidence are helpful in considering the mechanism of bromine production in the gas phase radiolysis, *i.e.*, the temperature dependence, the dependence on bromine concentration, and comparison with the photolysis. A comparison of the rates of the gas phase radiolysis at 0.2 mole % Br_2 at 108, 140 and 177° shows an

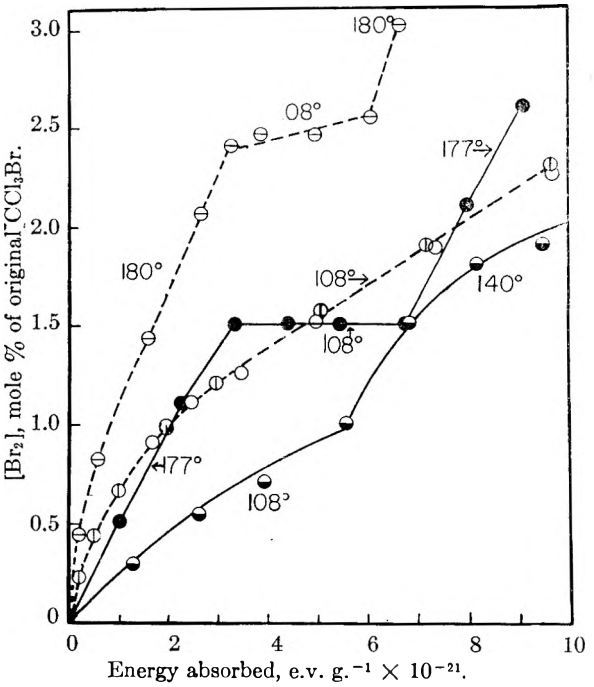

Fig. 1.—Production of bromine by the radiolysis (solid lines) and photolysis (dashed lines) of gaseous CCl_3Br.

apparent activation energy of only 3 kcal./mole. The similar apparent activation energy in the liquid phase radiolysis seemed to be ascribed best to the increasing probability of CCl_3 and Br atoms escaping primary or secondary recombination.[2] Such recombination does not occur in the gas so the temperature coefficient in this phase must be associated with a chemical process. Three kcal./mole is, however, much lower than the activation energy (8–10 kcal./mole)[6] of reaction 6 listed below, or the activation energy of reaction 7, which appears to be about 24 kcal./mole.[7] Reactions 5 and 7, utilizing CCl_3 radicals formed by (1) and (4) or (6) appear to be the only plausible thermal reactions of neutral species which can lead to net bromine production in the system. Ion–molecule reactions cannot be excluded, but the photochemical production of Br_2 with similar low activation energy (Fig. 1) indicates that neutral species can give yields of the magnitude observed. The fact that Br_2 and C_2Cl_6 production can be eliminated by the presence of a few mole % of Br_2 and that the Br_2 concentration required to accomplish this increases with increasing temperature indicates that the reactive species must undergo on the average many

$$CCl_3Br \rightsquigarrow CCl_3 + Br \quad (1)$$
$$CCl_3Br \rightsquigarrow CCl_3Br^+ + e^- \quad (2)$$
$$CCl_3Br \rightsquigarrow CCl_3^+ + Br + e^- \quad (3)$$
$$CCl_3 + M \longrightarrow CCl_3 + M \quad (4)$$
$$CCl_3 + CCl_3 \longrightarrow C_2Cl_6 \quad (5)$$
$$CCl_3Br + Br \longrightarrow CCl_3 + Br_2 \quad (6)$$
$$CCl_3 + CCl_3Br \longrightarrow C_2Cl_6 + Br \quad (7)$$
$$CCl_3 + CCl_3Br \longrightarrow C_2Cl_6 + Br \quad (7')$$
$$CCl_3 + Br_2 \longrightarrow CCl_3Br + Br \quad (8)$$

(6) (a) A. A. Miller and J. E. Willard, *J. Chem. Phys.*, **17**, 168 (1949); (b) N. Davidson and J. H. Sullivan, *ibid.*, **17**, 176 (1949).

(7) E. N. Becker, Ph.D. thesis, University of Wisconsin, 1953.

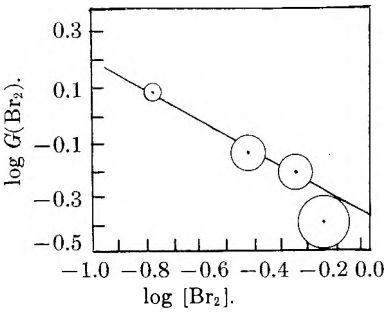

Fig. 2.—Evaluation of dependence of $G(Br_2)$ on bromine concentration. $G(Br_2)$ is in units of molecules produced/100 e.v. absorbed during the particular interval of irradiation; bromine concentration is in units of mole % of original CCl_3Br and is the average concentration during the interval for which G is calculated.

collisions with CCl_3Br before consummating the bromine producing reaction, and that the probability of reaction on collision is increased by increasing the temperature. The most plausible explanation of the observed results seems to be that the major portion of bromine production is the result of the temperature independent reaction of vibrationally excited CCl_3 radicals by (7′), combined with a small yield of the temperature dependent reaction 7. Vibrationally excited CCl_3 radicals which undergo many collisions before reacting and which can be scavenged by Br_2 before reacting likewise have seemed to offer the best explanation of the bromine dependence of $G(Br_2)$ in the liquid phase radiolysis. Clear evidence for the role of vibrationally excited CH_3 radicals in the gas phase radiolysis of CH_3I has been observed.[8] The hot CCl_3 radicals from the gas phase radiolysis of CCl_3Br must be vibrationally rather than kinetically hot because kinetic energy would be lost in a very few collisions with CCl_3Br molecules and so the reaction of the radicals would not be subject to the scavenger action of bromine at the concentrations used.

The question of whether C_2Cl_6 production (and hence Br_2 production) occurs predominantly by reaction 5 or reactions 7 and 7′ also can be examined by estimating the relative probability of these reactions from estimated steady-state concentrations and rate constants. Such estimates are highly uncertain, with the greatest uncertainties arising from lack of information on the relative frequency factors of the radical reactions. Assuming equal frequency factors, a Br_2 concentration of 0.1 mole %, and activation energies for reactions 7 and 8 which are 24 and 4 kcal./mole, respectively, higher than that of (5) the calculated rates of (7) and (5) are 6×10^{-9} and 3×10^{-6} of that of (8). Since the rate of (5) is second order with respect to $[CCl_3]$, it increases rapidly with decreasing concentration of Br_2. Fragmentary evidence that such increase is observable experimentally at concentrations in the range below 0.2 mole % Br_2 was given by the fact that $G(C_2Cl_6)$ for an exposure of gaseous CCl_3Br to 1.5×10^{21} e.v. g.$^{-1}$ (maximum $[Br_2] = 0.2$ mole %) was 1.2 while it was 5.2 for an exposure of 0.13×10^{21} e.v. g.$^{-1}$ (max. $[Br_2] = 0.02$ mole %).

(8) (a) G. M. Harris and J. E. Willard, *J. Am. Chem. Soc.*, **76**, 4678 (1954); (b) F. P. Hudson, R. R. Williams, Jr., and W. H. Hamill, *J. Chem. Phys.*, **21**, 1894 (1953).

(Studies at doses below about 2×10^{21} e.v. g.$^{-1}$ required the combination of separately irradiated samples in order to obtain enough product for analysis.)

If the steady-state concentration of CCl_3 radicals is controlled by reaction 8, as appears to be the case at most of the Br_2 concentrations used in this work, their concentration will be inversely proportional to the Br_2 concentration. In this case the rate of production of Br_2 would be proportional to $1/[Br_2]$ if reaction 7 is responsible and to $1/[Br_2]^2$ if reaction 5 is responsible. Reaction 7′ also would give a $1/[Br_2]$ dependence if it involves long lived vibrationally excited radicals which may be deactivated, and so prevented from reacting, by collision with Br_2. The bromine dependence for a run at 108° with a total dose of 4.9×10^{21} e.v. g.$^{-1}$ and a final Br_2 concentration of 0.8 mole % has been determined by evaluating b in the relation $G(Br_2) = a\,[Br_2]^b$ from the slope of the plot of log $G(Br_2)$ *vs.* log $[Br_2]$ shown in Fig. 2. The slope of the line which has been drawn is −0.75. Within the experimental accuracy (diameters of circles indicate error of ± 0.001 absorbance unit) the slope of the correct line could be −1 but not −2.

Mechanism of Br_2 Production in the Photolysis.—Absorption of a photon of 2537 Å. radiation gives a CCl_3Br molecule sufficient energy to break the C–Br bond (49 kcal./mole)

$$CCl_3Br \longrightarrow CCl_3 + Br \qquad (9)$$

plus 64 kcal. which must appear as vibrational energy of the CCl_3 radical or kinetic energy of the CCl_3 and of the Br atom. If the energy in excess of the bond energy all appears as kinetic energy conservation of momentum requires that it be divided, 26 kcal. to the CCl_3 and 38 kcal. to the Br. Comparison of the curves for bromine production as a function of dose for the radiolysis and photolysis (Fig. 1) indicates that $G(Br_2)$ decreases with increasing $[Br_2]$ concentration at low $[Br_2]$ concentrations for both methods of activation. Above about 1 mole % Br_2 the G of bromine production by the photolysis at 108° is constant at 0.5 to at least 2.3 mole % (lower dashed line); whereas $G(Br_2)$ for the radiolysis is zero at 1.5 mole %, as seen from the horizontal portion of the upper solid line plot of Fig. 1. The linear portion of the 108° photolysis curve indicates that Br_2 is being formed by a hot process which is not susceptible to scavenging by Br_2 molecules in this concentration range. The vibrationally or kinetically excited CCl_3 radicals involved in this process must have a high probability of reacting with CCl_3Br or being deactivated by it before reacting with or being deactivated by Br_2 present at 2 mole %. If CCl_3 radicals are formed with 26 kcal./mole of kinetic energy they might meet this criterion, some of them producing 1/2 Br_2 by reaction 7′ and others being reduced to energies below the necessary activation energy on the first few collisions. The slope of the straight line portion of the 108° curve (lower dashed line) indicates a quantum yield of about 0.025.

If the rate of the hot photolysis reaction shown by the straight portion of the 108° curve is subtracted from the rates of the reaction below 1 mole

% Br_2 at both 108 and 180° the rates of the bromine sensitive reaction are given. Comparison of these yields gives an apparent activation energy of about 5 kcal./mole. This is lower than the activation energy of either reaction 6 or 7 and suggests that, as in the radiolysis discussed above, there may be both a thermal and a hot reaction contributing to the bromine sensitive yield, processes 7 and 7′ being possible reactions.

Organic Products of the Radiolysis and Photolysis.—The presence of CCl_4, CCl_2Br_2 and $CClBr_3$ as products of both the radiolysis and photolysis of gaseous CCl_3Br and of C_2Cl_5Br as a product of the radiolysis in the liquid phase indicates that some or all of the following reactions must be occurring

$$CCl_3 + CCl_3Br \longrightarrow CCl_4 + CCl_2Br \quad (10)$$

$$CCl_3 + CCl_3Br \longrightarrow CCl_4 + CCl_2Br \quad (10')$$

$$CCl_3 + CCl_2Br_2 \longrightarrow CCl_4 + CClBr_2 \quad (11)$$

$$CCl_3 + CCl_2Br_2 \longrightarrow CCl_4 + CClBr_2 \quad (11')$$

$$CCl_3Br \rightsquigarrow CCl_2Br + Cl \quad (12)$$

$$CCl_xBr_{3-x} + Br_2 \longrightarrow CCl_xBr_{4-x} + Br \quad (13)$$

$$CCl_3 + CCl_2Br \longrightarrow C_2Cl_5Br \quad (14)$$

(omitting consideration of possible ion–molecule reactions). One mole % of initially added Br_2 reduces the yields of CCl_4, CCl_2Br_2 and $CClBr_3$ in the gas phase radiolysis slightly (see table in Abstract for comparison of typical runs), but does not eliminate them. That portion of the products not eliminated by the added Br_2 must be produced as a result of the hot processes 10′ and 11′ or 12. If reaction 12 does not occur stoichiometry requires that $G(CCl_4) = G(CCl_2Br_2) + 2G(CClBr_3)$. Within the precision of the data the results are in agreement with this requirement indicating that C–Cl bond rupture in the radiolysis occurs as a very minor process if at all. The material balance observed in the photolysis suggests that 1% or so of the photons absorbed may cause primary rupture of a C–Cl bond rather than a C–Br bond.

The yields of CCl_4 and CCl_2Br_2 from the radiolysis exceed the yields of C_2Cl_6 and Br_2, but the reverse is true for the photolysis under the conditions of the table given in the Abstract. In view of the great differences in both kinetic energy and vibrational energy which may exist between the CCl_3 radicals formed by the absorption of 2537 Å. radiation and those formed by excitation by electrons or by neutralization of ions in the radiolysis system it is plausible that the relative probability of reactions 7′ and 10′ would be distinctly different for the photolysis and radiolysis.

The yields of organic products from the radiolysis at 180° are somewhat higher than at 108°, indicating some contribution from the thermal reactions 10 and 11. This might be expected from the finding of Becker[7] (using CCl_3 radicals labeled with Cl^{36}) that the analogous chlorine abstraction reaction

$$CCl_3^* + CCl_4 \longrightarrow CCl_4^* + CCl_3$$

has an activation energy of about 10 kcal./mole.

The presence of C_2Cl_5Br among the products of the liquid phase radiolysis but not those of the gas phase presumably is the result of reaction 14 occurring in the spurs. Similar reactions of CCl_3 and CCl_2Br radicals to form C_2Cl_5Br are indicated by earlier studies of solutions of Br_2 in CCl_4 activated by the $Br^{81}(n,\gamma)Br^{82}$ process.[9]

Br_2–CCl_3Br Exchange during Radiolysis.—Significant characteristics of the exchange reaction induced by Co^{60} radiation include: (1) the G-values in the range of several hundred indicate that it is a chain reaction; (2) comparison of the G-values at 108 and 28° in the liquid phase indicates that the activation energy probably lies between 4 and 6 kcal./mole; (3) the G-values in the gas and liquid phases at the same temperature are indistinguishable; (4) the yield is not markedly affected by the presence of O_2 at a concentration equal to that of the Br_2 present.

The only possible mechanism for a chain reaction for the exchange seems to be a repeating sequence of reactions 6 and 8 or an ion–molecule sequence.[10]

If the observed temperature dependence, suggesting an apparent activation energy of 4–6, is correct the sequence 6 and 8 cannot be responsible for the total exchange since the activation energy of (6) is 8 kcal./mole or more.[6] The evidence at present available suggests that the chain is the result of the (6)-(8) sequence occurring simultaneously with an ion–molecule reaction of lower activation energy.

Schulte[11] has found $G(C_2Cl_6) = 0.86$ for the Co^{60} irradiation of liquid CCl_4 at 21°, a value similar to those we have observed in both liquid CCl_3Br at 20° and in gaseous CCl_3Br at 108°. He finds a value of G for the exchange of Cl_2 with CCl_4 of 3.5, much lower than our observation for the Br_2–CCl_3Br exchange. The comparisons suggest that the C_2Cl_6 may be formed in the two systems by analogous hot processes of the type of (7′). The fact that the activation energy for $Cl + CCl_4 \rightarrow CCl_3 + Cl_2$ is at least 14 kcal./mole[12] may account in part for the lower yield of the exchange reaction.

Acknowledgment.—This work was supported in part by the United States Atomic Energy Commission (Contract AT(11-1)-32) and in part by the University Research Committee with funds made available by the Wisconsin Alumni Research Foundation. During part of the work one of the authors (A.H.Y.) held a fellowship given by the Standard Oil (Indiana) Foundation.

(9) J. F. Hornig and J. E. Willard, *J. Am. Chem. Soc.*, **75**, 461 (1953).

(10) By analogy with the mechanism postulated by Thompson and Shaeffer (*ibid.*, **80**, 553 (1958)) for the H_2–D_2 exchange the ion molecule sequence might be

$$CCl_3Br^+ + Br_2^* \longrightarrow CCl_3Br_2^{*+} + Br$$

$$CCl_3Br_2^{*+} + CCl_3Br \longrightarrow CCl_3Br^* + CCl_3Br_2^+$$

$$CCl_3Br_2^+ + Br_2^* \longrightarrow CCl_3Br_2^{*+} + Br_2$$

(11) J. W. Schulte, *J. Am. Chem. Soc.*, **79**, 4643 (1957).

(12) F. J. Johnston and J. E. Willard, *J. Phys. Chem.*, **65**, 317 (1961).

ELECTRON PARAMAGNETIC RESONANCE ABSORPTION OF CHROMIA–ALUMINA CATALYSTS[1]

BY D. E. O'REILLY AND D. S. MACIVER

Gulf Research & Development Company, Pittsburgh 30, Pa.

Received August 10, 1961

The electron paramagnetic resonance absorption of chromia supported on alumina has been investigated at X-band (9.5 kMcps.) and K-band (23.9 kMcps.). Spectra of chromia–alumina reduced in hydrogen at 500° show two distinct phases: a dispersed (δ) phase which predominates at low concentrations of chromium and a bulk (β) phase which is prevalent at the higher concentrations. The temperature dependence of the intensity of these phases indicates the δ-phase consists of rather isolated Cr^{+3} ions not coupled electronically and the β-phase consists of clusters of Cr^{+3} ions with strong exchange coupling of 3d electrons. Intensity calibrations of e.p.r. spectra have been made and these indicate all the chromium present in the reduced catalysts to be in the trivalent state. Absolute amounts of δ- and β-phase chromium also are given. A relatively sharp resonance absorption appears upon oxidation of reduced chromia–alumina with oxygen. A spin-Hamiltonian for each of the observed types of resonances is proposed and discussed.

Introduction

Chromia supported on alumina is an active catalyst in many diverse chemical reactions and has been studied by measurements of magnetic susceptibility,[2,3] oxygen chemisorption,[4] electrical conductivity[5] and thermoelectric power.[6,7] Pure chromia has been studied by paramagnetic resonance absorption[8a,8b] and by antiferromagnetic resonance absorption.[8c] More recently, the technique of electron paramagnetic resonance (e.p.r.) absorption has been applied to the chromia–alumina system.[1,9,10] In the present work, e.p.r. data at various temperatures from 77 to 425°K. of chromia supported on alumina reduced and oxidized at 500° are reported. An interpretation of this data is given in terms of the crystal field theory[11] of Cr^{+3} and spin-Hamiltonians[12] for Cr^{+3} and Cr^{+5}. The data so obtained provide detailed information on the nature of the chromia–alumina system not readily obtained by other techniques. A model for this system is proposed and compared with other models[10] and activity data.

Experimental

In this investigation microwave bridges operating in the X-band (9.39, 4.47 kMcps.) and K-band (23.9 kMcps.) were used. The e.p.r. spectrometer consisted of Varian Associates' automatic frequency control unit, klystron power supply, klystrons (VA6312, VA98), output control unit, sweep generator, amplifier, 12-inch electromagnet, electromagnet power supply, field scanning unit, X-band microwave bridge, and rectangular cavity. The K-band microwave system consisted of a cylindrical TE_{011} mode cavity and K-band bridge components. Microwave power measurements were made with a Hewlett-Packard Model 430C power meter; frequencies were measured with Hewlett-Packard X530A and Douglas 450K frequency meters. The klystrons were operated at constant frequencies stabilized to one part in 10^6 by the above-mentioned AFC unit. Magnetic fields were measured with a Numar Model M-2 gaussmeter. Peak to peak modulation amplitudes from 5 to 20 gauss were used in recording paramagnetic resonance spectra. A cylindrical microwave cavity and cavity arm, described elsewhere,[9] was used in X-band e.p.r. measurements at temperatures ranging from −196 to 100°. Measurements at temperatures above 100° were performed using a microwave cavity and oven described in the literature.[13]

1,1-Diphenyl-2-picrylhydrazyl obtained from the Aldrich Chemical Company was employed as a standard in g-factor measurements. Pure, synthetic vanadyl etioporphyrin I[14a] obtained from Dr. J. Gordon Erdman of Mellon Institute was used in intensity calibrations.

All samples were sealed in 5 mm. o.d. quartz tubes since Pyrex glass was unsatisfactory due to e.p.r. absorption by ferric ion in the glass. Very pure γ-alumina was impregnated with chromic nitrate, calcined and reduced at 500°, as described elsewhere.[15] Oxidized samples were prepared by calcination of reduced chromia–alumina in air at 500° for five hr. Samples were analyzed both gravimetrically and photometrically for Cr; the results of both methods agreed well. The BET surface areas of all samples were within 10% of 160 m.²/g. Sample I of chromia was prepared by precipitation of the gel from a solution of $Cr(NO_3)_3 \cdot 9H_2O$; this gel then was dried at 250° and reduced at 500° with hydrogen. Sample II (Fig. 5) was obtained from Baker Chemical Company and the ruby sample from Linde Air Products Company.

Blank e.p.r. runs of the empty cavity and alumina support were made periodically; a weak, broad resonance generally appeared from the empty cavity and this signal was subtracted from the chromia–alumina spectra when necessary.

Results

Reduced Chromia–Alumina.—Samples of chromia–alumina containing 0.078, 0.55, 1.2, 2.0, 3.6 and 10.1 wt. % chromium were examined in both the reduced and oxidized states. The reduced samples at the lower concentrations were blue in color, the more concentrated samples were green. X-Band e.p.r. spectra of the reduced 1.2, 3.6 and 5.8 wt. % samples at −196° are shown in Fig. 1.

(1) Presented at the Symposium on Instrumental Techniques in Study of Catalysis Mechanism, Division of Petroleum Chemistry, American Chemical Society Meeting, April 5–10, 1959, Boston, Mass.

(2) R. P. Eischens and P. W. Selwood, *J. Am. Chem. Soc.*, **69**, 1590, 2698 (1947).

(3) Y. Matsunaga, *Bull. Chem. Soc. Japan.* **30**, 868 (1957).

(4) S. W. Weller and S. E. Voltz, *J. Am. Chem. Soc.*, **76**, 4695 (1954).

(5) S. E. Voltz and S. W. Weller, *ibid.*, **75**, 5227 (1953).

(6) P. R. Chapman, R. H. Griffith and J. D. F. Marsh, *Proc. Roy. Soc.* (London), **A224**, 419 (1954).

(7) P. B. Weisz, C. D. Prater and K. D. Rittenhouse, *J. Chem. Phys.*, **21**, 2236 (1953).

(8) (a) E. P. Trounson, D. F. Bleil, R. K. Wangsness and L. R. Maxwell, *Phys. Rev.*, **79**, 542 (1950); (b) L. R. Maxwell and T. R. McGuire, *Rev. Mod. Phys.*, **25**, 279 (1953); (c) E. S. Dayhoff, *Phys. Rev.*, **107**, 84 (1957).

(9) D. E. O'Reilly, *Advances in Catalysis*, **12**, 31 (1960).

(10) (a) P. Cossee and L. L. Van Reijen, Preprints, Second International Congress on Catalysis, Paris, France, 1960, Paper No. 82; (b) Y. I. Pecherskaya, V. B. Kozansky and V. V. Voevodsky, *ibid.*, Paper No. 108.

(11) C. F. Davis and M. W. P. Strandberg, *Phys. Rev.*, **105**, 447 (1957).

(12) A. Abragam and M. H. L. Pryce, *Proc. Roy. Soc.* (London), **A205**, 135 (1951).

(13) C. P. Poole, Jr., and D. E. O'Reilly, *Rev. Sci. Instr.*, **32**, 460 (1961).

(14) (a) D. E. O'Reilly, *J. Chem. Phys.*, **29**, 1188 (1958); (b) R. H. Sands, *Phys. Rev.*, **99**, 1222 (1955).

(15) J. M. Bridges, D. S. MacIver and H. H. Tobin, Second International Congress on Catalysis, Paris, France, 1960, Paper No. 110.

These spectra are the first derivatives of the resonance absorptions. The spectra consist of two principal resonances as shown by the changes in the spectra with increasing concentration of chromium and by examination of the samples at 23.9 kMcps. The first of these is characterized by a maximum in the first derivative in the vicinity of 1500 gauss at X-band; this resonance has been referred to as the δ-phase resonance. The second resonance yields a symmetrical derivative centered near 3400 gauss; this resonance has been referred to as the β-phase resonance.

The δ-phase resonance dominates in intensity in the low concentration chromium samples, while the β-phase resonance dominates in intensity at the higher concentrations. This effect is illustrated by the spectra of Fig. 1. A third type of resonance was observed at $-196°$ but not at higher temperatures in the reduced samples. This resonance, referred to as the γ-phase resonance, is described in detail below.

At 23.9 kMcps. only symmetrical β-phase type resonances were observed, unchanged in shape and width from the corresponding β-phase resonances at 9.5 kMcps. The shape of the β-phase resonance was represented quite well by a Lorentzian shape function for all samples examined. Sample 1–128–1 (5.8 wt. % Cr) was calibrated at 25° with a standard solution of vanadyl etioporphyrin I in benzene by means of the equation

$$N_{Cr} = \left(\frac{A_{Cr}}{A_{Vs}}\right) \frac{3N_{Vs}}{g_{Cr}^2 S_{Cr}(S_{Cr}+1)} \qquad (1)$$

where A_{Cr} and A_{Vs} are the areas under the resonance absorption curves of the chromia–alumina sample and the vanadyl standard, respectively; N_{Cr} and N_{Vs} are the number of Cr atoms and vanadyl units in the chromia–alumina sample and vanadyl standard, respectively; S_{Cr} is the spin of the Cr which may be 0, 1/2, 1, 3/2 or 2 depending on the valence state of the chromium and g_{Cr} is the g-factor of the Cr. Placing $g = 2.0$, $S_{Cr} = 3/2$, one obtains $N_{Cr} = 5.2 \times 10^{20}$ cm.$^{-3}$ for sample 1–128–1 (reduced in hydrogen at 500°), in good agreement with the chemical value of 5.0×10^{20} cm.$^{-3}$. Thus the valence state of chromium in this reduced sample is three. Integration of spectra of samples of reduced chromia–alumina at 9.5 and 23.9 kMcps. permits evaluation of the relative amounts of chromium in the δ- and β-phases. The results of these calculations are given in Table I

TABLE I

CONCENTRATIONS OF CHROMIA IN δ- AND β-PHASE RESONANCE ABSORPTIONS

Sample no.	Concn. wt. % Cr (chemical analysis)	C_{δ},[a] g.$^{-1}$ $\times 10^{-20}$	C_{β},[b] g.$^{-1}$ $\times 10^{-20}$	C_t,[c] g.$^{-1}$ $\times 10^{-20}$
1–30–3	0.07	0.060	0.015	0.075
1–30–2	0.55	.40	.13	.53
1–30–1	1.2	.73	.21	.94
1–138–1	2.0	.81	.62	1.43
1–90–1	3.6	.64	2.67	3.31
1–128–1	5.8	.34	6.38	6.72
1–105–1	10.1	.20	11.75	11.95

[a] C_{δ} is the chromium concentration of the δ-phase. [b] C_{β} is the chromium concentration of the β-phase. [c] C_t is the total chromium concentration.

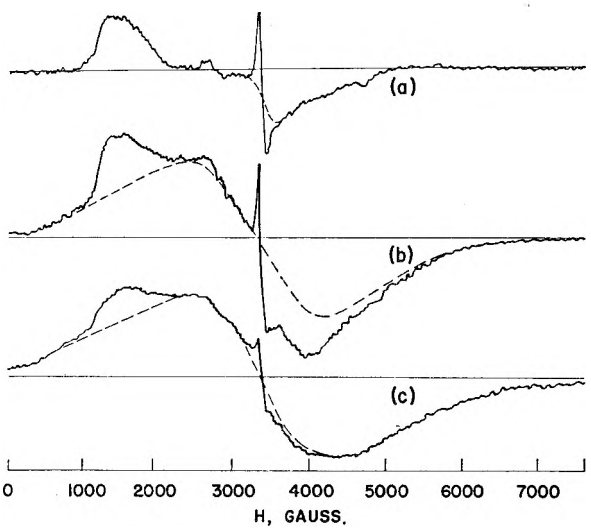

Fig. 1.—Paramagnetic resonance absorption derivatives of (a) 1.2 wt. %, (b) 3.6 wt. % and (c) 5.8 wt. % reduced chromia–alumina samples at 77°K. Dashed lines separate β-, δ- and γ-phase resonances. A very weak γ-phase type resonance appears in each sample.

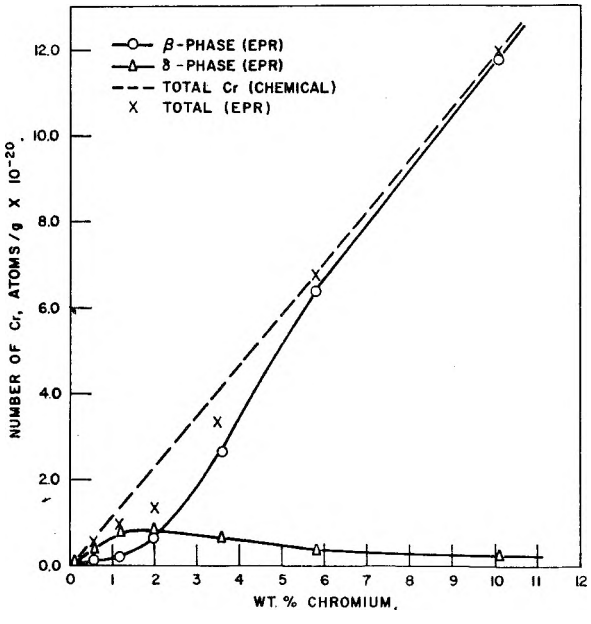

Fig. 2.—Calibrated intensity of δ- and β-phase chromia *versus* total Cr concentration.

and Fig. 2. The sum of the amounts of chromium in the δ- and β-phases is in good agreement with the total amount of Cr determined by chemical analyses, except in the range from 1 to 4% Cr wherein the Cr content determined by e.p.r. is somewhat less than the Cr content by chemical analysis.

The Cr^{+3} content of the β-phase resonance was measured for the 3.6, 5.8 and 10.1 wt. % Cr samples at various temperatures and the results of these measurements are given in Fig. 3. The amount of Cr contributing to the δ-phase resonance was found to be independent of temperature for the 1.2, 3.6 and 5.8 wt. % Cr samples from -195 to 162°. The width between points of maximum slope, ΔH_{ms}, of the β-phase resonance was found to vary with temperature, as given in Fig. 4. At all temperatures, the shape of the β-phase resonance was

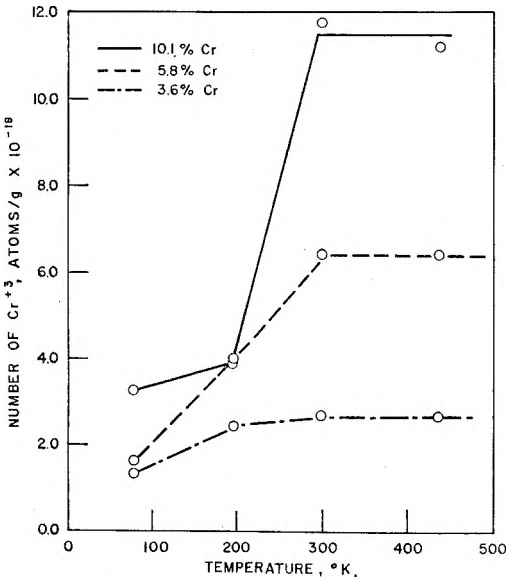

Fig. 3.—Temperature dependence of the number of Cr contributing to β-phase resonance.

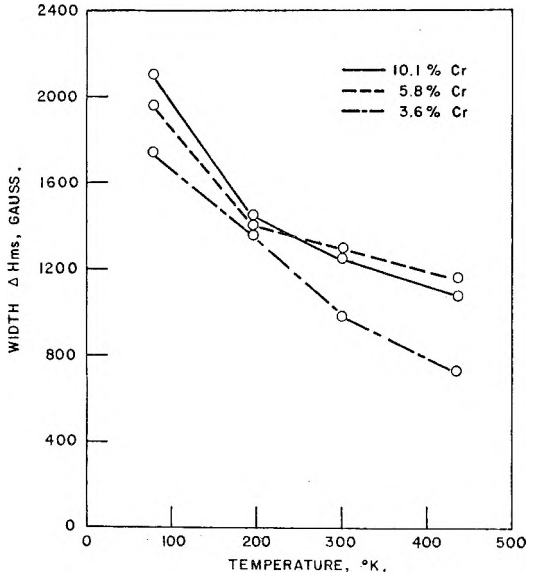

Fig. 4.—Temperature dependence of the line width of the β-phase resonance.

Lorentzian. The width between points of maximum slope of the symmetrical β-phase resonance ranges from about 700 gauss at the lower (0.55 and 1.2 wt. %) concentrations to about 1300 gauss at the higher concentrations (5.8 and 10.1%) at 25°.

Oxidized Chromia–Alumina.—Upon oxidation of chromia–alumina samples an additional, sharp resonance was obtained. The intensity width and spectroscopic splitting factor of this resonance as well as its temperature dependence has been given previously[1,9] and will not be repeated here.

Chromia.—Several samples of bulk chromia were examined at X- and K-bands. α-Cr_2O_3 is known to be antiferromagnetic with a Curie point near 30° by magnetic susceptibility and electron resonance measurements.[8] Spectra of two samples of chromia were obtained. The first shows no absorption 15° below the Curie point. However, in sample II an unsymmetrical resonance persists to temperatures well below the Curie point, as shown in Fig. 5. ΔH_{ms} is equal to 600 gauss for sample I and 700 gauss for sample II above the Curie point.

Discussion

Spin-Hamiltonian.—Paramagnetic resonance spectra are most conveniently discussed in terms of a spin-Hamiltonian operator. The spin-Hamiltonian appropriate to Cr^{+3} ($3d^3$) in tetragonal or trigonal symmetry is[11]

$$\mathcal{H} = g\beta\vec{H}\cdot\vec{S} + D(S_{z'^2} - 5/4) \qquad S = 3/2 \qquad (2)$$

Equation 2 is the magnetic energy operator for the Cr^{+3} ion and is written relative to a coördinate system having the z'-axis along the symmetry axis of the crystal field; this axis is a fourfold rotation axis in tetragonal symmetry and a threefold axis in trigonal symmetry. It is assumed that the octahedral crystal field splitting is large compared to the trigonal or tetragonal splitting so that the g-factor (g) may be taken as isotropic. The first term in eq. 2 represents the energy of interaction of the electronic magnetic moment $g\beta\vec{S}$ with the externally applied magnetic field $\vec{H}$, where β is the Bohr magneton and $\vec{S}$ is the total spin operator. The second term is the energy of the splitting in zero magnetic field due to the crystal field and to spin–orbit coupling. Here D is the crystal field splitting energy, while $S_{z'}$ is the component of S along the z'-axis and $\vec{S}$ is the total electronic spin of the ion.

The eigenvalues E of eq. 2 satisfy the equation

$$\mathcal{H}\psi = E\psi \qquad (3)$$

where the ψ are spin wave functions for Cr^{+3}. Since $2S + 1 = 4$, eq. 2 gives rise to a 4×4 matrix. This matrix has been solved by perturbation theory for the following situations: $|D| >> g\beta H$ and $g\beta H >> |D|$; as described in the Appendix. For values of D intermediate to these, the eigenvalues of eq. 3 have been obtained by diagonalization of the 4×4 matrix on an IBM 704 computer. All possible values of θ, the angle between z' and the applied magnetic field, occur in a sample of chromia on γ-alumina and in order to obtain a powder pattern spectrum from the results of the solution of eq. 3, an appropriate average must be made over all angles. In the case of axial symmetry, the intensity of resonance absorption is readily shown[14b] to be proportional to the product of d cos θ/dH and the transition probability at the angle θ. From plots of the field H necessary for resonance *vs.* cos θ and the transition probability[11] for the transition considered *vs.* H, the powder pattern line shape may be obtained.

Another term involving an exchange integral must be added to eq. 2 in order to account for the effects of the exchange interactions between chromium ions which become important at higher chromium concentrations. The effect of this interaction when the exchange integral is fairly large and there are a large number of ion neighbors is an exchange narrowing of the resonance absorption line. This effect has been described quantita-

tively by Anderson and Weiss.[16] For α-Cr_2O_3 the line width[17] resulting from the local fields produced by the electron magnetic moments is approximately 6,000 gauss; the exchange interaction reduces this width to about 600 gauss.

With this background in mind, each of the observed types of resonance absorption will be discussed below.

δ-Phase.—Through the use of plots of $g\beta H/D$ *vs.* $\cos\theta$, a range of zero field splittings which possibly may account for the main features of the δ-phase spectrum can be obtained. The approximate line shape is obtained by subtraction of the symmetrical β-phase resonance; the width and shape of the β-phase resonance are known from the K-band spectra. The intense peaks near 1000 and 1500 gauss in the derivative curves of the X-band δ-phase resonance spectra are expected from the G/D *vs.* $\cos\theta$ plots for $D > 0.2$ cm.$^{-1}$; the positions of these two peaks are rather insensitive to D for larger values of D, as shown in the Appendix. Dipole–dipole broadening or a range of D values can account for the broadness of the resonance; the breadth in regions where sharp maxima are expected appears to be about 200 gauss. In order to account for the broad maximum in the δ-phase absorption curve corresponding to the derivative of Fig. 1a, it appears to be necessary to invoke lower symmetry, that is, to introduce an additional $E(S_{x'}^2 - S_{y'}^2)$ term[12] in eq. 2 where E is an additional crystal field splitting energy and $S_{x'}$ and $S_{y'}$ are the components of $\vec{S}$ along the axis perpendicular to the z'-axis (see above). An upper limit for D or E appears to be about 1 cm.$^{-1}$ from consideration of the optical spectra[18] of chromia–alumina at low concentrations of chromia. With D sufficiently large the peak intensity at K-band of the first derivative of the δ-phase resonance will diminish by about a factor of six over the peak intensity at X-band, due to the greater range of field strength spanned by the resonance. This effect is sufficient to explain the apparent absence of the δ-phase from the K-band derivative spectrum.

The range of D values (0.2 cm.$^{-1} < D < 1$ cm.$^{-1}$) which can account for the δ-phase resonance represents rather strong axial distortions. For ruby[19] (Cr^{3+}–doped α-Al_2O_3) $D = 0.193$ cm.$^{-1}$; the powder pattern of ruby containing about 1 wt. % chromia is shown in Fig. 6. The positions of the crossover points of this spectrum are in excellent agreement with those expected from the plot of G/D *vs.* $\cos\theta$ corresponding to $D = 0.193$ cm.$^{-1}$. As can be seen from the spectrum, many of the peaks in the derivative curve are relatively sharp since the dipole–dipole broadening is small and a unique D value accounts for the spectrum.

In summary, the δ-phase resonance can be interpreted as due to Cr^{+3} ions in relatively strong axial crystal fields with distortions of lower symmetry.

β-Phase.—The β-phase resonance is similar to that observed from α-chromia, except that it is broader and does not exhibit a distinct antiferromagnetic Curie point near room temperature. This resonance is interpreted as due to Cr^{+3} ions clustered in such a way that there is sufficient exchange coupling of spins to cause exchange narrowing of the resonance and partially "wash out" line broadening effects due to the dipolar interaction and the D term of the crystal field. The β-phase, however, is different from large crystallites of α-chromia and corresponds more closely to the chromia gels which are paramagnetic at room temperature.

Anderson and Weiss[16] have shown that the width

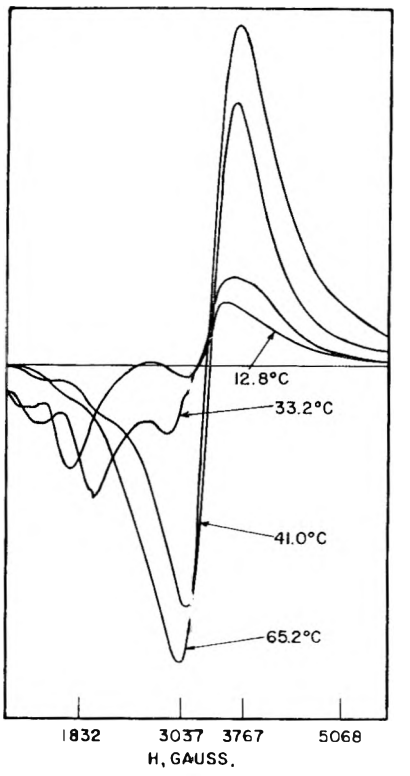

Fig. 5.—Paramagnetic resonance of sample II of chromia at various temperatures.

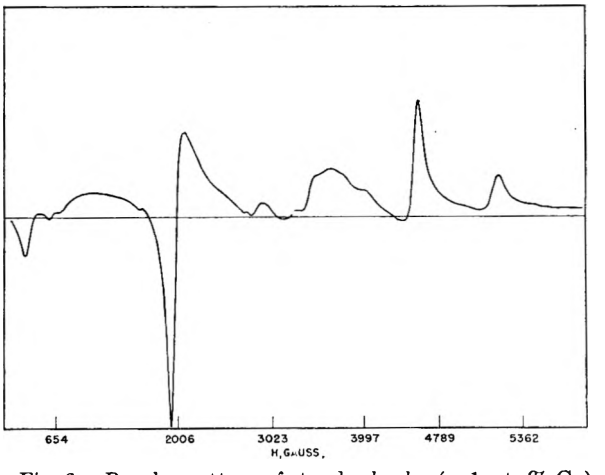

Fig. 6.—Powder pattern of standard ruby (~1 wt. % Cr) at 9.47 kMc./s. A very weak hump not shown in this scan occurs at about 7800 gauss.

(16) P. W. Anderson and P. R. Weiss, *Rev. Mod. Phys.*, **25**, 269 (1953).

(17) J. H. Van Vleck, *Phys. Rev.*, **74**, 1168 (1948).

(18) J. R. Tomlinson and D. E. O'Reilly, Preprints, Division of Petroleum Chemistry, American Chemical Society Meeting, Boston, Mass., **4**, No. 2, C-51 (1959).

(19) J. E. Geusic, *Phys. Rev.*, **102**, 1252 (1956).

δH (at half the maximum absorption) to be given by

$$\delta H = \frac{H_p^2}{H_e} \qquad (4)$$

where H_p^2 is the mean square magnetic field produced by the dipolar interaction between electron spins and H_e is the average exchange field produced by the exchange interaction. As is pointed out by Anderson and Weiss, a given spin (chromium ion) should have several neighbors to which it is coupled by the exchange interaction so that the narrowing effect may occur. The line shape under such circumstances is Lorentzian.[16] To first approximation H_p^2 may be considered to be proportional to Z, the number of Cr^{+3} nearest neighbors of a Cr^{+3} ion and H_e to be proportional to J, the exchange integral between Cr^{+3} ions.

$$J = \frac{3k\theta'}{2ZS(S+1)} \qquad (5)$$

where θ' is the Weiss constant of the material. Hence

$$\delta H \propto \frac{Z}{J} \qquad (6)$$

The data of Fig. 3 indicate that with a decrease in temperature below 300°K., only a portion of the β-phase chromia is observed by electron resonance, presumably due to the onset of anti-ferromagnetism in the β-phase. Clusters of chromia which are antiferromagnetic will not, of course, be observed by paramagnetic resonance. The Curie point of a given type of β-phase cluster will vary with both J and Z. Since the line widths given in Fig. 4 increase with decrease in temperature, the chromia which comprises the β-phase resonance at the lower temperatures has lower average values of J than the values of J at room temperature. An increase of δH with concentration may be interpreted as due to an increase in the average value of Z with concentration. The data of Fig. 3 indicate that the average Curie point of the β-phase increases with concentration and that there is no α-Cr_2O_3 present in the samples.

γ-Phase.—This relatively sharp resonance which results upon the oxidation of chromia–alumina may conceivably be due to Cr^{+3}, Cr^{+4}, Cr^{+5} or color centers in the oxidized chromia. Since the resonance line shape and width are independent of concentration of the chromia–alumina, this resonance appears to be characteristic of a distinct phase. Magnetic susceptibility[3] and optical spectra[18] data show that a considerable amount of Cr^{+6} is formed upon oxidation at 500°. Several of the characteristics of the γ-phase resonance indicate that this resonance is due to single electrons trapped on Cr^{+6} ions, that is, Cr^{+5} ions. Since the δ-phase resonance is changed only slightly in intensity by oxidation, while the β-phase changes considerably, the γ-phase resonance is at least partially associated with the β-phase (*i.e.*, clusters of Cr^{+3} ions.) This conclusion is corroborated by the fact that the specific number of electrons in the γ-phase (*i.e.*, electrons per chromium atom) is a maximum near 1 wt. % chromium and decreases with decrease in concentration below 1 wt. % chromium.

In non-cubic symmetry isolated Cr^{+3} and Cr^{+4} will not give rise to a sharp, symmetrical powder pattern resonance due to the D terms in the spin-Hamiltonian. Also at K-band a small D term will not produce broadening and slight asymmetry as observed. On the other hand, the spin-Hamiltonian corresponding to a single 3d electron does not contain a D term. Anisotropy of the g-factor, however, often is present,[14] as is illustrated by the following spin-Hamiltonian for a single 3d electron in axial symmetry

$$\mathcal{H} = g_{\parallel}\beta H_z'S_z' + g_{\perp}\beta\,(H_x'S_x' + H_y'S_y') \qquad (7)$$

The powder pattern resonance corresponding to eq. 7 will be asymmetric[14]; however, sufficient width of the individual resonance lines may make it appear symmetrical. At K-band the anisotropy will be enhanced by a factor of approximately 2.5 so that asymmetry and broadening of the resonance may appear.

The spin-Hamiltonian of eq. 7 could describe the resonance of an F-center with no nuclear hyperfine interaction terms from Cr^{53}. However, g-factors for F-centers usually are close to 2.0023 as for alkali halides[20] and MgO,[21] so that the hypothesis of F-centers as the source of the γ-phase resonance appears unlikely since the observed g-factor is 1.967.

Chromia.—As had been reported previously,[8] the e.p.r. of α-Cr_2O_3 disappears rather abruptly near the antiferromagnetic Curie point, as shown in Fig. 5. A change in the resonance condition is caused by the intense local magnetic fields resulting from the antiferromagnetic alignment. In sample II a strong resonance signal persists well below the Curie temperature which is associated with a paramagnetic portion of the sample.

Relation of E.P.R. Results to Other Data.—In summary, the e.p.r. spectrum reveals three distinct chemical species in the chromia–alumina system: Cr^{+3} ions which are electronically decoupled (δ-phase), Cr^{+3} ions which are coupled electronically (β-phase), and electrons trapped in the oxidized chromia (γ-phase).

Cossee and Van Reijen[10a] have proposed a very similar model for this system on the basis of e.p.r. and magnetic susceptibility data obtained on samples of chromia–alumina with varying degrees of reduction. In addition, these authors suggested that at intermediate degrees of reduction, and also for the silica–chromia system, chromium is present in the +4 oxidation state. No appreciable amount of Cr^{+4} was detected in samples reduced in hydrogen at 500° in the present work as illustrated by the intensity calibration of the resonance given under Results. Thus the fully reduced samples consist exclusively of Cr^{+3} although it is possible that Cr^{+4} in tetrahedral interstices will contribute to the resonance of partially oxidized samples as proposed by Cossee and Van Reijen.

Pecherskaya, Kozansky and Voevodsky,[10b] on the other hand, propose that the γ-phase consists of isolated Cr^{+3} ions. This assignment is unlikely

(20) A. F. Kip, C. Kittel, R. A. Levy and A. M. Portis, *Phys. Rev.*, **91**, 1066 (1953).

(21) J. E. Wertz, P. Auzins, R. A. Weeks and R. H. Silsbee, *ibid.*, **107**, 1535 (1957).

since the symmetry of the environment of such isolated Cr^{+3} ions must be nearly perfectly octahedral cubic to produce such a sharp resonance line as is observed, and the mechanism of formation of such ions upon oxidation is difficult to envision. A more serious objection to this assignment is afforded by the increase in asymmetry in the γ-phase resonance line observed at K-band which cannot be accounted for by a small D term in the spin-Hamiltonian of Cr^{+3} since the asymmetry due to this term will *decrease* with increase in resonance frequency rather than increase with increase in frequency. A similar statement is true for any small E term present in the spin-Hamiltonian of Cr^{+3}. However, as discussed above, this effect is readily explained by the spin-Hamiltonian for Cr^{+5}. Pecherskaya, *et al.*, also find that the width of the γ-phase resonance at X-band is dependent on the partial pressure of oxygen over the sample, which indicates the paramagnetic species are in the surface phase of the solid and hence not likely to be situated in an environment of cubic symmetry.

The e.p.r. data are of course intimately related to magnetic susceptibility data. The Weiss constant of the δ-phase chromia is proportional to D, which will amount to only a few degrees Kelvin at most, while the Weiss constant of the β-phase chromia is due largely to the large exchange effects in this phase. The Weiss constant obtained from a magnetic susceptibility measurement thus is due predominantly to the β-phase.

The relation of e.p.r. data to other susceptibility, conductivity and catalytic data for the chromia–alumina system already has been discussed.[9] It is of interest to note that the δ- and β-phase behavior appears to occur in other transition metal oxide–alumina systems.[22] From the point of view of e.p.r. the division between the two classes of chromium is rather sharp but not completely inclusive of all the chromium present, as indicated by the intensity data of Fig. 2. Intermediate types of Cr may involve small clusters of Cr^{+3} ions which, due to dipolar and, in particular, exchange interactions, do not contribute to either the δ- or β-phase type resonance.

Appendix

For certain situations the Hamiltonian of eq. 2 can readily be solved by the application of perturbation theory. First we consider the case $D \gg g\beta H = G$. It then is convenient to write eq. 2 in a coördinate system whose z-axis is along the static laboratory magnetic field. In this reference frame eq. 2 becomes

$$\mathcal{H} = GS_z + \frac{3}{2} D\{S_z^2 - 5/4\}(\cos^2\theta - 1/3) + \frac{1}{2} D \sin\theta\cos\theta\,[(S_zS_+ + S_+S_z)e^{-i\phi} + (S_zS_- + S_-S_z)e^{i\phi}] + \frac{1}{4} D \sin^2\theta\,(S_+^2 e^{-2i\phi} + S_-^2 e^{2i\phi})$$

$$S_+ = S_x + iS_y \quad (8)$$

θ and ϕ are the polar and azimuthal coördinates of the symmetry axis of the Cr^{+3} ion relative to the laboratory coördinate system. To first order one finds, taking diagonal matrix elements of eq. 8

$$E_{\pm 3/2} = \pm\frac{3}{2} G + \frac{3}{2} D(\cos^2\theta - 1/3)$$

$$E_{\pm 1/2} = +\frac{1}{2} G - \frac{3}{2} D(\cos^2\theta - 1/3) \quad (9)$$

E_{ms} denotes the energy of the state with the quantum number m_s. The positions of main peaks of the powder pattern spectra of potassium ammonium sulfate at X-band and K-band and of ruby at K-band are represented fairly well by the differences between the levels of eq. 10 with $\theta = \pi/2$ ($dH/d\cos\theta = 0$).

When $D >> G$, eq. 2 may be used to obtain the levels; to first order of perturbation theory the levels are

$$E_{\pm 1/2} = -D \pm \frac{1}{2} G(4 - 3\cos^2\theta)^{1/2}$$

$$E_{\pm 3/2} = D \pm \frac{3}{2} G\cos\theta \quad (10)$$

Powder pattern maxima occur at

$$\frac{h\nu}{3g\beta}(3/2 \longleftrightarrow -3/2, \text{ weak}); \quad \frac{h\nu}{2g\beta}, \frac{h\nu}{g\beta}(1/2 \longleftrightarrow -1/2)$$

in this case; these correspond to fields of 1137, 1705 and 3410 gauss for $\nu = 9.47$ kMcps. and $g = 1.98$. Powder patterns from the δ-phase of the chromia–alumina system correspond approximately to this case, although a term $E(S_x^2 - S_y^2)$ must be added to eq. 2 to fully account for the shape of the δ-phase resonance. The absorption curve corresponding to the $(1/2 \longleftrightarrow -1/2)$ transition is drawn in Fig. 7.

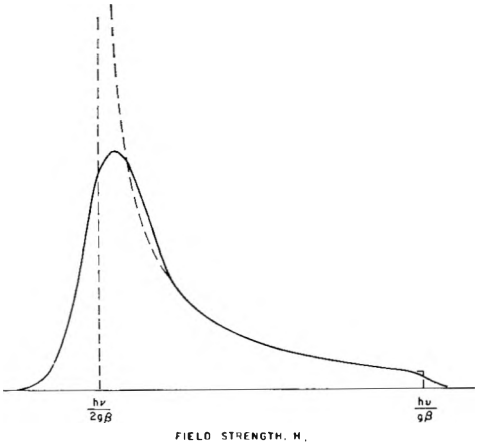

Fig. 7.—Line shape corresponding to the $(1/2 \longleftrightarrow -1/2)$ transition in the event that $D >> g\beta H$. Dashed curve represents powder pattern for zero width of the individual resonance lines.

(22) J. R. Tomlinson, R. O. Keeling, G. T. Rymer and J. M. Bridges, Preprints, Second International Congress on Catalysis, Paris, France, 1960, Paper No. 90.

KINETICS OF THE PRODUCTION OF C_2 DURING THE PYROLYSIS OF ETHYLENE

BY W. TSANG, S. H. BAUER AND F. WAELBROECK

Department of Chemistry, Cornell University, Ithaca, New York

Received August 14, 1961

The rate of production of C_2 in the lowest vibrational level of the $X,^3\Pi_u$ state has been measured *via* absorption spectrometry at λ5165 (0,0 Swan band) in back reflected shocks propagated in 8% C_2H_4–92% Ar. The temperature range covered was 2600–3600°K., with shock densities one-third to two atm., NTP. The initial rate was found to be of the first order in the ethylene concentration; the rate constant has an activation energy of 50 kcal. These data can be explained by assuming that the ethylene was decomposed to acetylene and hydrogen by the incident shock, either in whole or in part, depending on the shock strength. The acetylene thus generated then was converted to a large variety of C/H fragments by decomposition, abstractions, polymerization, etc. One of the products of this complex chain was C_2. A steady-state concentration of C_2 was reached, which was essentially at equilibrium with various C/H species (excluding solid carbon), prior to the appearance of a continuum absorption. The latter presumably was due to high molecular weight conjugated ring or chain polymers.

Introduction

The thermal decomposition of simple hydrocarbons (CH_4, C_2H_6, C_2H_4, C_2H_2, etc.) has been studied extensively. As yet, there is no general agreement on specific mechanisms for the progressive degradation of any of these to the elements. The key to unraveling these complex kinetics is the identification of intermediates. Unfortunately, these are short lived and, hence, present in low concentrations. Nevertheless, there have been attempts to identify them directly. Greene and co-workers[1] analyzed residues from acetylene shocked to about 2000°K. and found that diacetylene (C_4H_2) was a prominent product. Glick,[2] in his studies with a single-pulse shock tube, isolated small amounts of allene, benzene and methylacetylene, in addition to diacetylene, following the pyrolysis of various hydrocarbons at about 2000°K. Bradley and Kistiakowsky[3] coupled a rapid-scan mass spectrometer into the reflecting wall of a shock tube. They found that, in the reflected shock region, acetylene was converted to a variety of polymers (C_8, C_6, C_4) of which C_4H_4 was quite prominent. Many other studies have been reported[4–8] covering material which is related to our problem.

The characteristic spectrum of C_2 radicals, the transition being $A,^3\Pi_g \rightarrow X,^3\Pi_u$, consisting of a regular series of bands centered in the green and degraded to the violet, has been found in emission from many types of high temperature carbon-bearing flames, in heavy current electrical discharges through carbon-bearing vapors, in carbon furnaces at high temperatures, in flash photolysis of hydrocarbons, and in the wake of strong shock waves through carbon compounds. In the last three types of experiments, C_2 also has been recorded in absorption. Its ubiquitous presence naturally has led to speculations on the mechanism of its formation[9] and on the reactions it undergoes. Gaydon and Wolfhard[10] have computed the absolute concentration of C_2 radicals in an acetylene–air flame and found this to be in excess of the amount which would be present were the system in equilibrium with carbon, but not enough to satisfy any theory which assumes C_2 polymerization as the main source of carbon formation. The latter is confirmatory of other observations regarding the relative positions of C_2 emission and the carbon zone in flat diffusion flames and in some premixed flames (ethylene and benzene). With regard to the source of C_2, Gaydon favors its formation from large unsaturated hydrocarbon species. This appears to be at variance with results of Ferguson,[11] who used C^{13} as a tracer in acetylene–air flames. From the relative intensity of C^{12}–C^{12}, C^{12}–C^{13} and C^{13}–C^{13} (1,0) Swan peaks, he concluded that there is almost complete randomization of isotopic species. Hence, he favors a mechanism which involves first the splitting of the hydrocarbon into single atom units and then reactions of the type

$$2CH \longrightarrow C_2 + H_2$$

Some investigators[12] favor oxygen as an intermediate in the generation of C_2, according to the reaction

$$C_4H_2 + O_2 \longrightarrow C_4H_2O_2 \longrightarrow C_2 + H_2 + 2CO$$

However, Gaydon and Fairbairn[13] observed C_2 emission in acetylene–argon mixtures when subjected to shock heating; this indicates that oxygen is not essential.

Scope of the Present Study.—Our objective has been to find conditions under which the pyrolysis of ethylene might follow a relatively simple mechanism. It was presumed that the higher the temperature, the fewer and simpler are the species which would be involved. In the investigation described below, the pyrolysis of ethylene was

(1) E. Greene, R. Taylor and W. Patterson, *J. Phys. Chem.*, **62**, 238 (1958).

(2) H. S. Glick, "Seventh Symposium (International) on Combustion," Butterworths, London, 1959, p. 98.

(3) J. Bradley and G. B. Kistiakowsky, Symposium on Experimental and Theoretical Advances in Elementary Gas Reactions, 139th National Meeting, A.C.S., Div. Phys. Chem., St. Louis (March, 1961); *J. Chem. Phys.*, **35**, 264 (1961).

(4) N. Milberg, *J. Phys. Chem.*, **63**, 578 (1959).

(5) R. Norrish, G. Porter and B. Thrush, *Proc. Roy. Soc.* (London), **A227**, 432 (1955).

(6) G. Herzberg and J. Shoosmith, *Can. J. Phys.*, **34**, 523 (1956).

(7) J. Harshbarger, Ph.D. Thesis, California Institute of Technology, 1956.

(8) "Seventh Symposium (International) on Combustion," Butterworths, London, 1959, pp. 150, 247, 264.

(9) E. Smith, *Proc. Roy. Soc.* (London), **A174**, 110 (1940).

(10) A. G. Gaydon and H. G. Wolfhard, *ibid.*, **A201**, 570 (1950).

(11) R. E. Ferguson, *J. Chem. Phys.*, **23**, 2085 (1955).

(12) K. Laidler, "The Chemical Kinetics of Excited States," Clarendon Press, Oxford, 1955, p. 168.

(13) A. R. Fairbairn and A. G. Gaydon, *Proc. Roy. Soc.* (London), **A239**, 464 (1957).

studied in back-reflected shocks by estimating spectrophotometrically the concentration of C_2 as it changed with time, for a variety of initial conditions. Specifically, the characteristic absorption of C_2 at the (0,0) band head of the $X,^3\Pi_u \rightarrow A,^3\Pi_g$ transition was measured. Two postulates were made in this experiment: (a) With regard to translation, rotation and vibration of all the molecular species involved, equilibrium is rapidly attained in the shock front, in a time small compared to the changes in concentration of C_2, and (b) equilibrium is not attained with regard to the precipitation of carbon even at the end of an observation time which is of the order of 1 millisecond.

In all of our experiments, an 8% mixture of ethylene in argon was used. The range of temperatures covered was 2600–3600°K., and the density range was one-third to two atmospheres (NTP) under shock conditions. These experimental conditions were required to generate a sufficient concentration of absorbing molecules at a measurable rate. However, an undesirable change in temperatures thus is imposed on the shocked samples. The initial reactions, preceding the reactions in which we are interested, modify the sample temperature due to their endothermicity. The effect is present in both the incident and reflected shock regions. With respect to the former, an examination of the possible equilibria and relevant rates shows that at these temperatures (1500–2000°K.) the predominant reaction is the dehydrogenation of ethylene, which is endothermic to the extent of about 40 kcal. per mole. Thus, a drop in temperature is introduced. Fortunately, the rate has been measured recently by Skinner,[14] who found the unimolecular rate constant to be

$$\log k = 8.87 - 10{,}130/T$$

over the temperature range 1300–1800°K. From the known and/or calculated time between the passage of the incident shock and the arrival of the reflected shock at a given sample location, it was possible to estimate the extent of the dehydrogenation reaction by an iterative procedure. We found that for the strongest shocks (u incident = 1.57 mm./μsec.) about 60% of the ethylene was converted, while for the weaker shocks there was almost no conversion.

It thus appears that the reflected shock wave entered a mixture of C_2H_4, C_2H_2, H_2 and Ar. The rise in temperature due to shock reflection increased the dehydrogenation rate. We estimated that under these conditions the dehydrogenation process was completed in a few microseconds. The actual gas temperatures consequently were lower than those we would have computed on the assumption of "no reaction." If this final value is taken as the temperature of the test sample, it is equivalent to making the assumption that all the other reactions either have no thermal effect or have not had sufficient time to occur. It is likely that, for the region immediately after the passage of the reflected shock (within 30–40 μsec.), this is valid. Some of the initial polymerization reactions are indeed thermally neutral; for example

$$2C_2H_2 \longrightarrow C_4H_2 + H_2, \qquad \Delta H^0 \approx 2.7 \text{ kcal.}$$

has been considered by Greene to be one of the key steps in the decomposition of acetylene. For the remaining test time (200–500 μsec.) the temperature probably was lowered again due to endothermic dissociations which lead to the production of species the relavent portions of such as C_2H, C_4H.

For this study, shock parameters were calculated[15] on the assumption that equilibrium was established behind both the incident and reflected shocks, with twelve species (C_2H_4, C_2H_2, H_2, H, Ar, C_2H_3, C_2H, C_2, C_3, C_4H_2, C_4H, C_4H_3) present. Of course, equilibrium was not fully attained behind the incident shock. Unfortunately, no programs were available which allowed the calculation of shock parameters for kinetic systems. As a result the computed temperatures were somewhat higher than the actual ones for weaker shocks. In any case, the temperatures and densities computed probably are correct for the last half of the testing time.

Experimental Details

The ethylene was dried by passing it over P_2O_5 and further purified by pumping on it while it was frozen by liquid nitrogen. Mass spectrometric analyses showed after a period of several months a slight trace of acetylene and less than 0.1% of O_2 or other impurities. The argon was supplied by Matheson, with a stated purity of 99.998%, and used without further treatment.

To record the changes in the absorption spectrum of the sample which had been subjected to a shock, two types of experimental arrangements were used. In the first, a continuum of wave lengths was generated by discharging a condenser (1.0 μf., 10 kv.) through a small quartz tube through which argon was flowing at a pressure of approximately 50 mm.[16] This produced an intense emission which initially rose sharply and fell to half of the peak intensity in about 10 μsec. The light which passed through the shocked gas was picked up by a mirror and sent to a grating spectrograph. By delaying the source trigger pulse, the argon continuum was generated at predetermined times after passage of the reflected shock past the observation ports. The transmission spectra then were photographed (at 16 A. per mm. dispersion) over the range λ3900 to λ6000, thus providing a record of the absorption intensity as a function of wave length at specified intervals after initiation of the reaction. The photographs show a general absorption which is fairly uniform over the longer wave lengths but increases rapidly below some critical wave length which depends on the time interval. Upon this background there was clearly superposed a well developed Swan band system, the intensity of which increased with temperature. Below 2500°K., it was barely discernible. As far as we can tell, no measurable absorption due to C_3 was evident at λ4050, although there are indications from preliminary experiments that a small amount of absorption by this species did appear during the higher temperature runs. No CH absorption was observed.

To permit reduction of these data to semi-quantitative absorptions, the lamp was flashed a number of times prior to running the shock, with various gray filters of different densities placed in front of the spectrograph slit. In this manner, a series of calibration exposures were recorded on the plate. For selected wave lengths, a sensitometric curve was drawn and the per cent. transmitted at the "background" read from this curve. The ratio

$$[\log (I_\lambda{}^0/I_\lambda)]_t = \frac{\epsilon c l}{2.3}$$

at 100, 200 and 300 μsec. intervals after passage of the reflected shock was plotted against the wave length, Fig. 1. Note the sudden increase in absorption which appears below

(14) G. B. Skinner and E. Sokolski, *J. Phys. Chem.*, **64**, 1028 (1960).

(15) Code set up for IBM-704 Computer by Russell E. Duff, Los Alamos Scientific Laboratory.

(16) D. A. Ramsay, *Ann. N. Y. Acad. Sci.*, **67**, 485 (1957); J. H. Collomon and D. A. Ramsay, *Can. J. Phys.*, **35**, 129 (1957).

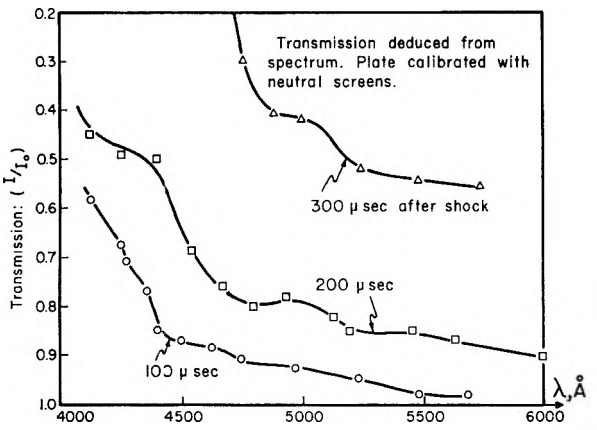

Fig. 1.—Background continuous absorption $T_{reflected} \sim 3700°K.$; $\rho_{reflected} \sim 800$ mm. (NTP).

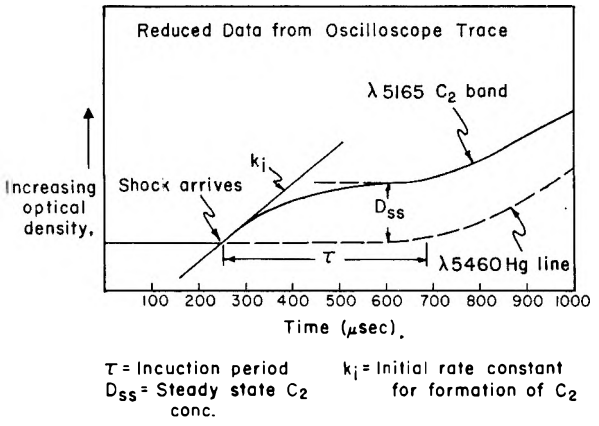

Fig. 2.—Typical features of reduced oscilloscope trace.

λ4300 and the change with the passage of time, both in the level of absorption and in the shift toward the red of the wave length at which the increase occurs. In the visible, this absorption shows an induction period which increases with decreasing density of the shocked gas, as will be demonstrated below. However, we infer from qualitative observations that the length of this induction period decreases with decreasing wave length, and in the ultraviolet the background absorption can be detected even in the incident shock.

The Kinetics of Production of C_2 from $[I(t)/I_0(t)]_{\lambda 5165}$.—To study the rate of appearance of C_2, a characteristic source was positioned in place of the continuum source. The light was split with a half-silvered mirror, so that a JAco monochromator phototube monitored the intensity over a small wave length interval near λ5165, while the small grating spectrograph with a phototube attachment monitored the intensity of the mercury line at λ5460. The characteristic source was generated by discharge of a 2 μf. condenser at about 12 kv. through a tube filled with butane, helium and mercury. The outputs of the two 1P28 photocells were led to a 100 kc. electronic switch, so that the relative absorption by the shock sample of the two characteristic emission regions was displayed on one oscilloscope record. The optical window was 0.5 Å. wide and set at the band head of the (0,0) band of the $^3\Pi_g \rightarrow {}^3\Pi_u$ transition for a C_2 ($J = 11$ to $J = 18$ in the P branch). The per cent. absorption recorded in this manner is thus a measure of the population of the C_2 species present in the zero vibration level of the $^3\Pi_u$ state. Because a continuum absorption is superposed on the characteristic absorption, a correction for the former should be made. It was convenient to monitor the background absorption at the λ5460 mercury line. The error introduced by the 300 Å. displacement is of secondary significance, since the essential kinetic data were derived during the induction period, when the background absorption was negligible. Since the populations of the lower states for these lines change with the temperature, a correction was made in reducing the per cent. absorption to relative concentration.

An idealized reduced oscilloscope record of the measured quantities (C_2 absorption and continuum absorption) is shown in Fig. 2. The solid line is the intensity recorded at the C_2 band head, and the dashed line is that recorded at λ5460 Hg line. It is characteristic that the C_2 absorption reached a plateau and that there was an induction time for the absorption at λ5460, as indicated in the preliminary discussion. The measurements of slope and steady-state concentration are subject to some uncertainties. An examination of our data indicates this to be about ±30% for the rate determination and ±50% for the equilibrium measurements. Since the relevant quantities here are ln I_0/I, these errors should not be too important. The temperature uncertainties due to the endothermicity of the reactions are probably more important, especially in the steady-state studies; here the uncertainties may well be of the order of 50°K.

Consider first the steady-state concentration of C_2 radicals. Following the nomenclature and treatment of Penner,[17] one may write (concentrations of C_2 are expressed in partial pressures)

$$\frac{1}{pl}\int_{\Delta w} \ln\left(\frac{I_0}{I}\right) dw = P_{\Delta w}\, dw$$

w is in wave numbers; Δw is the band width
p is the partial pressure of C_2
P_w is the spectral absorption coefficient
l is the path length

$$\int_{\Delta w} P_w dw = \frac{\pi e^2}{mc^2}\frac{A}{RT} f_{1\rightarrow u}\, Q_T$$

A is Avogadro's number
Q_T is a term expressing the fact that only the molecules in a few levels are being obsd.

Since at the band head there is such a profusion of overlapping lines that the entire wave number interval passed by the monochromator (ΔW_s) is fully covered, one may use an average effective absorption coefficient. Then

$$p_{(atm)} = \frac{T}{Q_T}\frac{\ln (I_0/I)_{av}\Delta w_s}{6.5 \times 10^9 l f_{1\rightarrow u}} = \frac{T}{Q_T}\frac{1.2 \times 10^{-10}}{f_{1\rightarrow u}} \ln(I_0/I)_{av}$$

for $l = 3.81$ cm. and Δw_s corresponds to 3 cm.$^{-1}$. For the temperature, we used the values estimated under conditions of total equilibrium for the twelve species listed above. This is not critical since the temperature dependence is rather weak. With regard to the f-number, the value available is of dubious accuracy since numbers ranging from

(17) S. S. Penner, "Quantitative Molecular Spectroscopy and Gas Emissivities," Addison-Wesley, London, 1959, p. 17.

0.02 to 0.5[18] have been reported. However, an error in the f-value selected will affect the absolute concentration but not the relative concentrations.

For a system in which there is such a plethora of products generated in the forward zone of the shock, the final density ratio, temperature ratio, and mole fractions of the different species depend not only on the shock velocity but also on the initial pressure of the test gas. To reduce the data obtained in these experiments, for which a wide variety of initial pressures was used, it is necessary to determine the relationship between initial pressure and C_2 steady state concentrations at a given shock velocity. Figure 3 is a plot of ln (p_{initial}) *vs.* ln $(C_2)_{ss}$ at a velocity of approximately 1.485 mm./μsec. The scatter is rather large, but the best fit is close to a line with unit slope. With this relation, the partial pressures of C_2 radicals were reduced to a common initial pressure (0.1 atm.). Figure 4 is a plot of the ln p_{C_2} *vs.* the shock velocity, normalized to 0.1 atm. initial pressure. For the purposes of this calculation, an f-number of 0.034 (the value reported by Hicks)[19] was selected. (The f-value pertinent to our calculations is $\backsim$ 0.01, since account must be taken of transitions to the Q and R branches and in the 1,0 sequence. For the latter, we arbitrarily assigned a relative probability of 16% with respect to the 0,0 sequence, as in the case of CN.) The partial pressure of C_2 so estimated can be corrected when a new f-value is established. If f = 0.02 were used, the calculated partial pressures would be about twice those given. The point of interest here is that, if one plots the C_2 partial pressure at equilibrium with the twelve species mentioned above against the temperature (using shock speed as the actual variable), the curve is nearly the same as that obtained experimentally. (See Fig. 4, dotted line.)

The rate of formation of C_2 is measured by the initial slope (Fig. 2). In reducing these data, one is faced with the uncertainty in sample temperature. The use of either of the two possibilities outlined above implies certain assumptions with regard to the mechanism. If one uses the temperature velocity relationships obtained from the steady-state measurements, he assumes that substantially all the other species, especially the C_4H, C_2H and H radicals, were in equilibrium concentration previous to C_2 formation. This is a questionable postulate; since C_2 formation was observed almost immediately upon the passage of the shock, the rates of formation of C_4H, C_2H, etc., would have to be extremely fast. For this reason, the temperature–velocity relations derived for partial dehydrogenation in the incident shock and complete dehydrogenation in the reflected shock were used.

The gross rate law for the initial formation of C_2 was established as follows. The quantity measured is $(I_0/I)_i$. For experiments performed at the same

$$\left[\frac{d(C_2)}{dt}\right]_i = \frac{1}{\langle\mu\rangle l}\left[\frac{d(\ln I_0/I)_c}{dt}\right]_i = k\rho^n$$

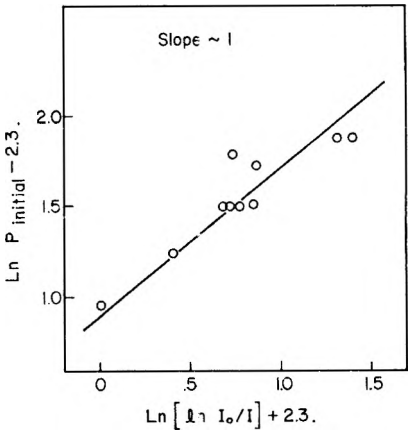

Fig. 3.—Dependence of absorption intensity on initial pressure of test gas, at constant shock velocity, 1.485 mm./μsec.; pressure in mm.

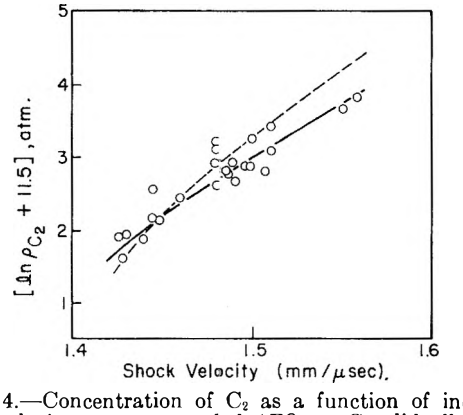

Fig. 4.—Concentration of C_2 as a function of incident shock velocity: ———, calcd. (*EQ*, no C solid allowed); ———, exptl. (f = 0.034).

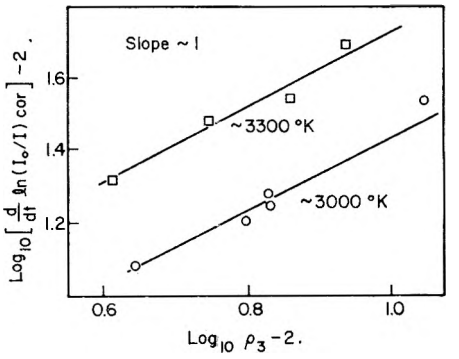

Fig. 5.—Initial rate of production of C_2 *vs.* shock density; density in mm.; t in sec.

k is the rate constant
ρ is the density (total)
n is the order of reaction
$\langle\mu\rangle$ absorption coefficient (av.)
l path length
$(I_0/I)_c$ is the cor. ratio for energy level population dependence on T

temperature, a plot of log $[d(\ln I_0/I)_c/dt]_i$ *vs.* log ρ yields n as the slope. This is shown in Fig. 5; n = 1 is a good fit.

For the determination of the activation energy, write

$$k = Ae^{-E/RT} = \frac{1}{\rho\langle\mu\rangle l}\left[\frac{d(\ln I_0/I)_c}{dt}\right]_i$$

Thus, a plot of log $1/\rho[d(\ln I_0/I_c)/dt]_i$ *versus* $1/T$

(18) W. Benedict and E. K. Plyler, Natl. Bur. Standards Circular 523, 1954, p. 57.

(19) W. Hicks, Ph.D. Thesis, Univ. of California, 1957.

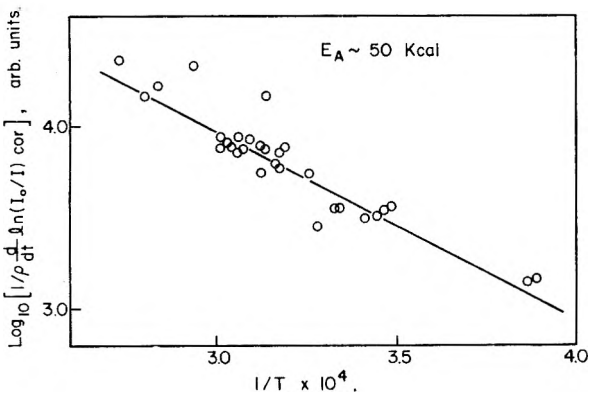

Fig. 6.—Determination of the activation energy for C_2 production.

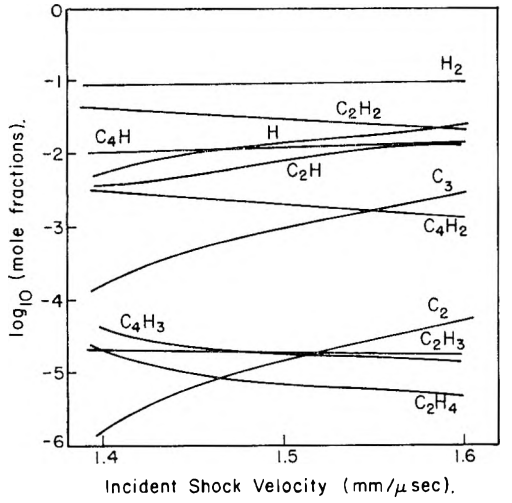

Fig. 7.—Calculated equilibrium composition in reflected shock; C_2H_4 (8%) + Ar (92%); *EQ*; no C solid.

gives the gross activation energy for the initial production of C_2. This is shown in Fig. 6; a value of approximately 50 ± 10 kcal. was obtained.

Discussion of Data

The results reported above agree in general with previous work. The continuum absorption recorded has almost the same characteristics as that obtained from samples subjected to flash photolysis, in diffusion flames, and from hydrocarbon systems flowing through hot tubes. The shift toward the red of the wave length, at which the sudden rise in absorption coefficient appears, is explainable in terms of the growth of ringed carbon compounds. A comparison of the well-known polynuclear substances and our data suggests that several hundred microseconds after passage of the shock, four-membered ring compounds appeared in appreciable concentrations. The substances used as models need not have been present, but similar substances (with some of the hydrogen atoms ripped off) probably were. This supports the surmise of Norrish and co-workers[5] and the work of those investigators who found multi-ringed compounds in soot.

The detection of appreciable concentrations of C_2 radicals in absorption was not unexpected. The absence of oxygen in these shock tube experiments is definite proof that an oxidation step need not play a role in the mechanism of C_2 formation. The measured steady-state concentration of C_2 is also of interest. Figure 4 strongly suggests that, at a given temperature, the steady-state partial pressure is dependent on the total pressure. Note that under the assumption of equilibrium among twelve selected species the final temperature also is dependent on density. The spread in temperature, due to changes in the latter, is nevertheless small (≈ 100°K.), and the distribution of the points is random about the line drawn. Were the steady-state set by an equilibrium between solid carbon and C_2, at any temperature, one would have found

$$K_p = p_{C_2} = \text{const.}$$

The estimated partial pressure of C_2 in these experiments was somewhat higher than that computed for equilibrium with the solid. For example, at 3000°K., $p_{est}(C_2) \approx 2 \times 10^{-4}$ atm., while p_{cal}(eq. with C solid) $\approx 2 \times 10^{-5}$ atm. However, were a higher f-value assumed, a lower p_{est} would have been deduced. Finally, if the continuum is regarded as a manifestation of the carbon forming process, the fact that C_2 reaches a steady state very rapidly, in some cases within ~ 60 μsec., means that carbon solid has not yet had time to be formed. These arguments are in line with the results of Gaydon and Wolfhard.[10] They assumed an f-value of 0.5 and that a Boltzmann distribution was attained among electronic levels and estimated from spectroscopic data the partial pressure of C_2 in a 5.5 mm. (pressure) flame consisting of a stoichiometric mixture of C_2H_2–O_2. At 2700°K., $p(C_2) \approx 11 \times 10^{-7}$ atm., which is appreciably higher than that expected assuming equilibrium with solid carbon. They assumed $\Delta H_f^0(C_2) =$ 233 kcal. instead of 198 kcal., the currently accepted value. The latter figure raises the calculated equilibrium partial pressure at 2700°K. to approximately 2×10^{-7} from the 9×10^{-10} atm. given by Gaydon and Wolfhard. Their conclusions still hold.

In spite of the uncertainties in the f-value, the close correlation between the measured C_2 partial pressure and that calculated assuming equilibria involving eleven low molecular weight hydrocarbon fragments is intriguing. During the course of the pyrolytic reaction, especially at the beginning, one would expect a large number of relatively low molecular weight fragments, and these may attain "local" equilibria. Figure 7 is a plot of the equilibrium concentrations of the different species *vs.* the shock velocity, for an initial pressure of 0.1 atm. and where no solid carbon is formed. The species present in relatively large concentrations are C_2H_2, C_4H, C_2H, H_2 and H; C_4H_2 and C_3 are intermediate, with C_2H_3, C_4H_3 and C_2 several orders of magnitude less. A particular point of interest is the large amounts of C_3. It is rather disappointing not to have observed its well known spectrum at approximately 4050 Å. This may have been due to its low absorption coefficient or the obscuring effect of the continuum absorption. There is also the possibility that C_3 and other species with odd numbers of C atoms are present in substantially less than their equilibrium amounts.

For C_4H_2–C_2H_4–C_2H_2–C_2, etc., the basic building blocks are two carbon atoms joined by a multiple bond; the formation of C_3 at any early stage thus would require the scission of a strong bond. The absence of C_3 would not disturb the general equilibrium situation very much since its total contribution is no more than $\sim 10^{-3}$ in mole fraction.

The kinetic data, which follow a first-order density dependence for the rate of C_2 formation and an activation energy of approximately 50 kcal., effectively rule out two possible sources for C_2 formation: *e.g.*, the direct formation from acetylene

$$C_2H_2 + X \longrightarrow C_2H_2^* + X$$
$$\hookrightarrow C_2 + H_2$$

and evaporation from solid carbon. In both cases the activation energies would have to be much higher, 140 and 200 kcal., respectively. The conclusion is that the C_2 radicals are formed during the course of a complex chain reaction. If one accepts the postulate that C_2 is formed in an early part of the polymerization process and that its concentration is near that at equilibrium, a glance at Fig. 7 suggests possible reaction paths. Consider only those which have low ΔH^0's, since these place lower limits on the activation energy. Estimates show that those reactions which involve the direct scission of either a C–C or a C–H bond involve enthalpy changes of $\approx$ 100 kcal. or over. To net a relatively low activation energy, a combination of abstraction reactions must be used, as indicated in Table I. The ΔH_0's used are those estimated by Cowperthwaite, Duff and Bauer.[20] Clearly these kinetic data are insufficient to permit development of a detailed mechanism. It also is worth noting that a large variety of other species may be formed depending upon the reaction conditions. At the higher temperatures, where polymerization is less likely, the low molecular weight species dominate, but the longer chains (C_6H_2, C_6H_4, etc.) may be important intermediates in the carbon forming process. Indeed, the formation of C_2 and C_3 may be competitive with polymerization.

In the reactions listed above the line (Table I), di-carbon units remain intact. For these, the transition states are readily visualized. Reactions which produce fragments with odd numbers of carbons necessitate more involved rearrangements and may have low P factors. Ferguson[11] using C^{13}-labeled acetylene in a flame found almost complete isotopic mixing in the products. However, the fact that in the shock tube experiments less C_2 was found than in flames, as reported by Gaydon,[10] leads to the suspicion that C_2 formation in flames may be influenced by factors not present in shocks. Specifically, reaction with O_2 and OH may reduce the formation of long chained or ringed molecules which are precursors of carbon formation. Fairbairn[21] reported that in C^{13}-labeled acetylene approximately two-thirds of the carbon atoms in the spectroscopically recorded C_2 were scrambled. It thus appears that the odd number species participate in the C/H shuffling reactions soon after shock initiation.

TABLE I

	ΔH^0_0, kcal. mole^{-1}
$C_2H_4 + X \longrightarrow C_2H_4^* + X \longrightarrow C_2H_2 + H_2$	39.8
$C_2H_2 + C_2H_2 \longrightarrow C_4H_2 + H_2$	2.7
$C_2H_2 + C_2H_2 \longrightarrow C_2H_3 + C_2H$	74
$C_4H_2 + C_2H_2 \longrightarrow C_4H_3 + C_2H$	54
$C_4H_2 + C_2H_2 \longrightarrow C_2H_3 + C_4H$	58
$C_4H_3 + C_2H_2 \longrightarrow C_4H_2 + C_2H_3$	21
$C_2H_3 + C_2H_2 \longrightarrow C_2H_4 + C_2H$	10
$C_4H_2 + C_2H \longrightarrow C_4H_3 + C_2$	72.5
$C_2H + C_2H \longrightarrow C_2H_2 + C_2$	19
$C_4H + C_2H \longrightarrow C_4H_2 + C_2$	35
$C_4H + C_2H \longrightarrow C_2H_2 + C_4$	22
$C_4H + C_4H \longrightarrow C_4H_2 + C_4$	42
$C_4H + C_2H \longrightarrow C_6H_2$	−102
$C_2H + C_2H_2 \longrightarrow C_3H_3 + C$	76
$C_2H + C_2H_2 \longrightarrow C_3H + CH_2$	23
$C_4H + C_2H_2 \longrightarrow C_3H + C_3H_2$	35.5
$C_4H + C_2H_2 \longrightarrow C_3H_3 + C_3$	58

Conclusions

In the pyrolysis of ethylene, C_2 is produced by a pseudo-first order process, with an activation energy of 50 kcal. A steady-state C_2 ($^3\Pi$) concentration soon is reached and its magnitude is compatible with the assumption that C_2 is in equilibrium with a number of low molecular weight C/H fragments. C_2 formation appears to be a consequence of abstraction reactions. The principal problem encountered in these studies was the uncertainty in the estimation of the temperature. In future work, it will prove advisable to use lower ethylene concentrations and to make measurements in the incident shock region. Of course, a direct measurement of the temperature behind the shock wave would be desirable.

Further pyrolytic studies must be carried out before sufficient data will be available to permit specification of a mechanism. The use of isotopically labeled molecules has been mentioned. Of special interest is the possible role of the singlet levels in attaining the equilibrium condition for C_2. To determine whether the singlet levels are populated *via* collisions, we propose to record the simultaneity of absorption by the Swan and the Deslandres systems.

Acknowledgments.—This work was supported by the Department of the Air Force, Wright Air Development Center, under Contract No. AF 33(616)-6694, for which grateful acknowledgment is made. We also thank Dr. Russell E. Duff (Los Alamos Scientific Laboratory) for providing us with an IBM-704 program for the computation of equilibrium shock conditions in a reacting gas mixture and Mr. Paul Marrone for supervising our computations at the Cornell Aeronautical Laboratory facility.

(20) M. Cowperthwaite, R. E. Duff and S. H. Bauer, "Estimation of Molecular Parameters of C/H Fragments" and "The Equilibrium Composition of the C/H System at Elevated Temperatures," submitted for publication in *J. Chem. Phys.*

(21) A. R. Fairbairn, "Eighth Symposium (International) on Combustion," Butterworths, to appear.

HEATS OF FORMATION OF BROMINE FLUORIDES[1]

BY LAWRENCE STEIN

Argonne National Laboratory, Argonne, Illinois

Received August 31, 1961

Heats of reaction of F_2 with Br_2 were measured with an adiabatic calorimeter in the vicinity of 25 and 105°. When excess F_2 was used, BrF_3 and BrF_5 were formed in the 25° region, and BrF_5 alone was formed in the 105° region. The standard heats of formation [ΔH^0_f] of BrF_5, BrF_3 and BrF calculated from the measurements and data in the literature are −106.2, −64.8 and −17.7 kcal./mole, respectively (reactants and products in the gaseous state at 25°). The standard free energies of formation [ΔF^0_f] are −84.1, −55.2 and −18.0 kcal./mole, respectively.

The heats of formation of BrF, BrF_3 and BrF_5 previously have been derived from spectroscopic and equilibrium data, and from estimates of bond energies, rather than from thermochemical measurements. The dissociation limit of BrF was found to be 21,370 cm.$^{-1}$ by Broderson and Schumacher[2] from absorption spectra and 21,190 cm.$^{-1}$ by Durie[3] from emission spectra. Cole and Elverum[4] published tables of thermodynamic properties which listed two possible values for $\Delta H^0_{f,BrF}$ at 25°, −9.44 or −19.59 kcal./mole, since it was not known whether the dissociation of BrF left the bromine or the fluorine atom in an excited state. Evans, Munson and Wagman[5] considered excited fluorine to be more probable and obtained −18.36 kcal./mole for $\Delta H^0_{f,BrF}$. Both calculations depended upon the authors' selected values for the dissociation energies of Br_2 and F_2. A new dissociation limit of 22,915 cm.$^{-1}$ for BrF was reported recently by Broderson and Sicre,[6] and bromine was assumed to be the excited atom. This would lead to still a different value of −13.9 kcal./mole for $\Delta H^0_{f,BrF}$.

Steunenberg, Vogel and Fischer[7] studied the equilibrium between Br_2, BrF_3 and BrF, and obtained −75 kcal./mole for $\Delta H^0_{f,BrF_3}$, using liquid Br_2 and BrF_3 and gaseous F_2 for the standard states. Since then, infrared studies[8] have shown that low concentrations of BrF_5 also are present in the mixtures, but the effect on the equilibrium constants is small. The heat of formation of BrF_5 has not been measured previously but has been estimated[5] as −124 kcal./mole from bond energies of Slutsky and Bauer.[9] Thermodynamic functions derived from molecular constants have been published for BrF_3[10] and BrF_5.[5,11,12] Although BrF_3 formerly was thought to have a pyramidal structure, it is known now to have a planar "T" structure, and the functions have been computed on this basis in reference 10.

In considering the reactions which might be used to obtain heats of formation of BrF_3 and BrF_5, it was found that very few could be selected with certain knowledge of the products and the final states. Heat-of-solution methods appeared to be out of the question, since both compounds react explosively with water, yielding complex mixtures of HF, HBr, HBrO, $HBrO_3$, Br_2 and O_2. When the compounds are reduced by substances which are fluorinated readily, such as silicon or sulfur, mixtures of Br_2 and BrF generally are produced. Although Schmitz and Schumacher[13] were able to use the reaction of ClF_3 with NaCl, the analogous reaction of BrF_3 with NaBr was considered unfavorable due to the formation of $NaBrF_4$ and intermediate products.[14] The direct combination of Br_2 and F_2 appeared to be the simplest choice for a reaction, particularly since the products were well-known from earlier studies.[8,15]

Apparatus.—The calorimeter consisted of a nickel reaction vessel surrounded by an adiabatic shield, both of which were supported inside a brass submarine by a thin-walled gas inlet tube. The reaction vessel, which will be referred to hereafter as the calorimeter, was a welded cylinder 10.0 cm. tall, 5.2 cm. in outer diameter, with a wall thickness of 0.060 cm. A layer of copper approximately 0.013 cm. thick was electroplated on the outside to improve the thermal conductivity. The Monel inlet tube, with an inner diameter of 0.157 cm. and a wall thickness of 0.022 cm., extended into the middle of the calorimeter; it was hard-soldered to the lid and to a Hoke 411 diaphragm valve on the top plate of the submarine. Before assembly, the volume of the calorimeter and inlet tube was found to be 212.88 ml. at 25° by calibration with degassed distilled water. The leg of the valve below the needle point was filled with a nickel insert, so that the tube and valve comprised less than 0.15% of the total volume.

For electrical calibration, the top, bottom and sides of the calorimeter were covered with a bifilarly-wound heater of B & S gage No. 28 glass-covered Nichrome wire, with a total series resistance of approximately 300 ohms. Leads were of No. 36 glass-covered copper wire. One potential lead to the heater terminated at the calorimeter and the other at the shield to compensate for heat losses in the current leads. A 28-ohm resistance thermometer of No. 36 glass-covered copper wire was bifilarly wound on the sides of the calorimeter (superimposed on the heater). One junction of a Chromel-P Alumel thermocouple was placed in the center of the thermometer windings and the other was formed in an ice-bath, where copper leads were attached. The thermocouple was not calibrated directly, but e.m.f. corrections of the same Chromel-P Alumel wire were determined elsewhere with a platinum resistance thermometer. Copper-constantan difference thermocouples were attached to adjacent positions of the calorimeter and shield, at the top and at the side. When in place, all wires were varnished with Formvar, which was air dried and baked in an oven at 170°. A layer of shiny aluminum foil was attached to the

(1) Based on work performed under the auspices of the U. S. Atomic Energy Commission.

(2) P. H. Broderson and H. J. Schumacher, *Z. Naturforsch.*, **2a**, 358 (1947).

(3) R. A. Durie, *Proc. Roy. Soc.* (London), **A207**, 388 (1951).

(4) L. G. Cole and G. W. Elverum, Jr., *J. Chem. Phys.*, **20**, 1543 (1952).

(5) W. H. Evans, T. R. Munson and D. D. Wagman, *J. Research Natl. Bur. Standards*, **55**, 147 (1955).

(6) P. H. Broderson and J. E. Sicre, *Z. Physik*, **141**, 515 (1955).

(7) R. K. Steunenberg, R. C. Vogel and J. Fischer, *J. Am. Chem. Soc.*, **79**, 1320 (1957).

(8) L. Stein, *ibid.*, **81**, 1273 (1959).

(9) L. Slutsky and S. H. Bauer, *ibid.*, **76**, 270 (1954).

(10) H. H. Claassen, B. Weinstock and J. G. Malm, *J. Chem. Phys.*, **28**, 285 (1958).

(11) C. V. Stephenson and E. A. Jones, *ibid.*, **20**, 1830 (1952).

(12) T. G. Burke and E. A. Jones, *ibid.*, **19**, 1611 (1951).

(13) H. Schmitz and H. J. Schumacher, *Z. Naturforsch.*, **2a**, 362 (1947).

(14) A. G. Sharpe and H. J. Emeleus, *J. Chem. Soc.*, 2135 (1948).

(15) L. Stein, *J. Am. Chem. Soc.*, **81**, 1269 (1959).

surface of the calorimeter with Formvar to reduce radiation losses.

The shield consisted of a gold-plated copper cylinder of 15.2 cm. height, 8.9 cm. outer diameter, and 0.080 cm. wall thickness, which was assembled around the calorimeter with 0–80 machine screws. No. 28 glass-covered Nichrome wire was bifilarly wound on the sides in upper and lower sections and on the top and bottom in flat coils. The windings were connected to form separate heaters for the upper and lower halves of the shield, each with 400 ohms resistance. All lead wires from the calorimeter and shield were combined into a spiral cable, brought into good thermal contact with with the shield and submarine lids, and sealed through a vacuum pumping leg with Apiezon-W wax. An oil diffusion pump was used to evacuate the submarine, which was sealed with a Neoprene "O" ring at the top and was immersed in a well-stirred water-bath, regulated to ± 0.05°.

The valve on the top plate of the submarine was connected through a manifold of nickel tubing to a fluorine storage pot and pressure transducer (both immersed in the bath) and lines for evacuating the calorimeter or introducing Br_2 or F_2. Hoke 411 valves in the legs of the manifold were partly immersed in the bath, with their handles above the surface. The transducer, consisting of a bellows and differential transformer, has been described previously.[15] Pressure measurements were made by balancing fluorine or bromine pressure on one side of the bellows with an equal helium pressure on the other side, then reading the helium pressure to ± 0.05 mm. with a mercury manometer and cathetometer. Pressures were corrected to 0° and standard gravity. The total volume of the manifold, fluorine pot and transducer was obtained by measuring pressure changes on expansion of helium into the evacuated calorimeter, assuming the helium to be an ideal gas.

Current and potential measurements were made with a White double potentiometer and the circuits generally used in this Laboratory for heat capacity measurements.[16] The galvanometer used with the potentiometer had a working sensitivity of 0.04 μv./mm. Time intervals for electrical calibration were measured with a synchronous clock and controlled-frequency generator. The shield was manually controlled by observing the deflections of two galvanometers connected to the difference thermocouples and adjusting the currents in the upper and lower shield heaters.

Reagents.—Baker and Adamson reagent grade bromine, with a stated chlorine content of 0.3% or less, was dried over phosphorus pentoxide and vacuum distilled. A middle fraction was collected and stored in a Pyrex bulb attached to a small Monel valve. Before each loading of the calorimeter, the bromine was frozen and thawed under vacuum several times to remove any dissolved air.

Fluorine was obtained from the General Chemical Company and purified by distillation at liquid nitrogen temperature in a metal still.[17] The fraction used in the present experiments was of 99.84% purity, as determined by titration with mercury. Mass spectrographic analyses indicated that the impurities consisted chiefly of nitrogen, oxygen and argon.

Experimental

The heat capacity of the calorimeter (with 10 mm. of helium added for exchange purposes) was determined in calories per ohm resistance change of the thermometer by electrical calibration. In the interval 25.0–43.1°, the heat capacity increased from 158.34 to 161.01 cal./ohm; the experimental points, plotted against resistance, were represented by a linear equation (least squares) with a standard deviation of 0.15 cal./ohm. In each Br_2–F_2 reaction, the appropriate value of the heat capacity then was obtained from the equation, using the resistance at the midpoint of the reaction interval. The heat capacity of the contents of the calorimeter was computed separately from the molar heat capacities.

Temperatures on the Centigrade scale were determined initially with the Chromel–Alumel thermocouple. From the measured resistance of the thermometer at each temperature, a table of resistance ratios at fixed intervals was prepared, similar to that of Dauphinee and Preston-Thomas.[18]

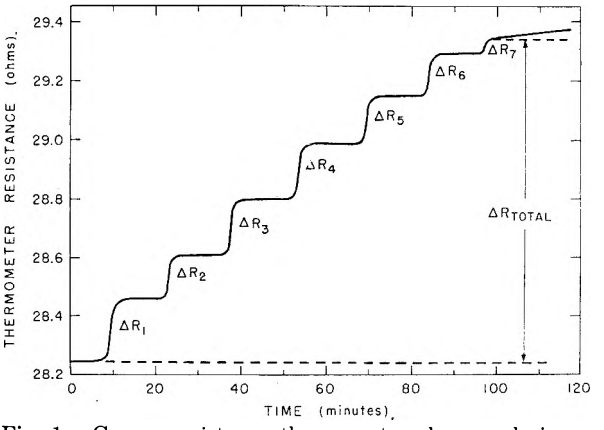

Fig. 1.—Copper resistance thermometer changes during a typical Br_2–F_2 reaction; initial temperature was 25.0°.

Temperatures thereafter were obtained from the table by interpolation.

Before each reaction, the calorimeter was prefluorinated with F_2, then highly evacuated. In the first experiments, designated as Series A, Br_2 vapor was added to a measured pressure with the calorimeter initially at the bath temperature of 25.0°. Due to the compressive work done by the incoming Br_2, the temperature rose slightly and was remeasured after several minutes, when it was again constant. The number of moles of Br_2 in the calorimeter was calculated from a virial equation of state.[15] The F_2, at higher pressure than the Br_2, was added gradually in fractional amounts, at about 15-minute intervals. The number of moles of F_2 admitted each time was calculated from the pressure change in the manifold and storage pot, assuming the F_2 to be an ideal gas, since the second virial coefficient is small at 25°.[19] After each addition, the resistance increase (temperature rise) was measured. The F_2 reacted rapidly and quantitatively with Br_2 and with the intermediate product, BrF. After the last addition, when the Br_2 and BrF had been consumed, the excess F_2 reacted very slowly with BrF_3. The successive steps were

$$Br_2 + F_2 \longrightarrow 2BrF \quad \text{(rapid)} \qquad (1)$$

$$BrF + F_2 \longrightarrow BrF_3 \quad \text{(rapid)} \qquad (2)$$

$$BrF_3 + F_2 \longrightarrow BrF_5 \quad \text{(slow)} \qquad (3)$$

Reaction 3 was detected as an apparent "drift," which was extrapolated back to the time of the last F_2 addition to obtain the final resistance or "end-point." A typical curve of "Resistance" *vs.* "Time" is shown in Fig. 1.

At the end-point, the calorimeter contained BrF_3, excess F_2 and BrF_5, which had been formed by reaction 3 to a slight extent during each F_2 addition. In the last addition, the amount of F_2 consumed was determined from the end of the rapid heat evolution by making use of the ratio $\Delta R/\Delta n_a$, the increase in resistance per mole of F_2 reacting. The ratio was known for each of the preceding steps, in which the F_2 reacted quantitatively. When plotted as a function of the total F_2 added, $\Delta R/\Delta n_a$ increased very slowly, and the value at the end-point was obtained by a short extrapolation from the preceding points. The F_2 consumed in the last step then was given by

$$\frac{(\Delta R)_{\text{Final}}}{\left(\frac{\Delta R}{\Delta n_{F_2}}\right)_{\text{Final}}}$$

where the numerator is the last resistance increase (ΔR_7 in Fig. 1) and the denominator is the ratio obtained in the extrapolation. The amounts of BrF_3 and BrF_5 then were calculated from the amount of Br_2 present at the start and the total amount of F_2 consumed. As a check on the present method, the end-point also was determined by the pressure minimum of the reaction, which has been described elsewhere.[15] Although the pressure in the calorimeter was

(16) E. F. Westrum, Jr., J. B. Hatcher and D. W. Osborne, *J. Chem. Phys.*, **21**, 419 (1953).

(17) L. Stein, E. Rudzitis and J. L. Settle, Report ANL-6364, Argonne National Laboratory, June 1961.

(18) T. M. Dauphinee and H. Preston-Thomas, *Rev. Sci. Instr.*, **25**, 884 (1954).

(19) D. White, J. H. Hu and H. L. Johnston, *J. Chem. Phys.*, **21**, 1149 (1953).

TABLE I

HEATS OF REACTION OF F_2 WITH Br_2

n_{Br_2}	n_{F_2}	n_{BrF_3}	n_{BrF_5}	ΔR	ΔH_1	ΔH_3	ΔH	$\Delta H^0_{f,BrF_3}$ at 25°	$\Delta H^0_{f,BrF_5}$ at 25°
(millimoles)				(ohms)	(cal.)			(kcal./mole)	(kcal./mole)
Series A, 25 to 44°									
1.1752	3.759	2.237	0.113	1.13065	−0.43	23.42	−180.25	−64.94	.....
1.9822	6.335	3.794	.170	1.88454	− .70	39.82	−301.85	−64.49	.....
0.6344	2.093	1.150	.119	0.62193	− .18	11.66	− 98.85	−64.99	.....
0.5490	1.970	1.037	.061	0.52640	− .29	10.42	− 83.80	−64.79	.....
2.1622	7.362	4.128	.196	2.06167	− .46	43.28	−330.64	−64.68	.....
							Mean =	−64.78	
							Std. dev. =	0.20	
Series B, 105 to 128°									
0.9611	6.845	0	1.9222	1.18837	2.44	0	−205.95	.....	−106.01
.5244	5.620	0	1.0488	0.65131	2.85	0	−113.90	.....	−106.01
.9827	6.869	0	1.9654	1.22255	2.38	0	−211.20	.....	−106.39
.4987	4.046	0	0.9974	0.61604	1.64	0	−107.16	.....	−105.91
1.5290	9.386	0	3.0580	1.89324	2.78	0	−328.03	.....	−106.48
								Mean =	−106.16
								Std. dev. =	0.26

known only approximately after each F_2 addition, the pressure end-point agreed with the resistance end-point within ± 0.5% in each experiment.

Most of the BrF_3 and a small fraction of the BrF_5 condensed into a liquid phase. The composition of the liquid was calculated from the vapor pressures of BrF_3[20] and BrF_5[21] at the final calorimeter temperature and the approximate activity coefficients of 1.0 and 1.5, respectively.[21] The vapors were assumed to be ideal gases, and the excess F_2 was assumed to be insoluble in the liquid phase.

In the second group of experiments, designated as Series B, the bath was kept at 65.0°, and the shield and calorimeter were heated initially to the vicinity of 105°. The shield current was increased to compensate for the larger heat leak of the shield, but the drift of the calorimeter remained very small as before. In the electrical calibration, the heat capacity of the calorimeter increased approximately linearly from 171.23 to 174.38 cal./ohm in the interval 106.8 to 125.1°, with a standard deviation of 0.11 cal./ohm. The Br_2 and F_2 added to the calorimeter both were assumed to be ideal gases at these elevated temperatures. The experiments were far less complicated than the preceding ones, since no liquid phase appeared, and BrF_5 alone was obtained as the final product. After the initial rapid reaction, which again produced a mixture of BrF_3 and BrF_5, the excess F_2 reacted at a moderately fast rate with the BrF_3. By adding a large excess of F_2, the reaction was made to go to completion in 30 to 50 minutes. It therefore was necessary to measure only the initial and final thermometer resistance, rather than the small resistance increments which were required in Series A.

Results and Discussion

The results obtained in Series A, between 25.0 and 43.8°, and Series B, between 104.9 and 128.2°, are given in Table I. The first four columns show the amounts of Br_2 and F_2 added to the calorimeter (F_2 corrected for impurities) and the total amounts of BrF_3 and BrF_5 produced. In the next column, ΔR is the total resistance change of the thermometer. Since the F_2 was added from an external source, work was done on the contents of the calorimeter, which contributed to the temperature rise. The compressive work has been described for a non-ideal gas by Gillespie and Coe.[22]

In the present experiments, correction was made for an ideal gas as $1/2\ n_{F_2}R_G(T_1 + T_2)$, where T_1 and T_2 are the initial and final calorimeter temperatures, respectively, and R_G is the gas constant. (The subscript G is added to avoid confusion with resistance.) The gas constant was taken as 1.9872 cal./degree-mole and the ice point as 273.15°K. Since the total number of moles of gas decreased in each reaction, due to the stoichiometry and due to the condensation of liquid in Series A, a PV correction to the enthalpy also was required. This was computed from the initial amounts of Br_2 and F_2 and final amounts of gaseous products, assuming all components to be ideal. The sum of the corrections for compressive work and $\Delta(PV)$ is given by ΔH_1 in column 6.

The next term, ΔH_2, is the heat of vaporization of the liquid phase at the final temperature, which must be added in Series A to convert all products to the gas phase. It was computed from the heats of vaporization of BrF_3[20] and BrF_5[21] and the amounts of these components in the liquid. No correction was made for the heat of mixing, which is believed to be small. The enthalpy change for cooling the calorimeter and gaseous products (through resistance interval ΔR) is given by ΔH_3. In Series B, $\Delta H^0_{f,BrF_5}$ was computed from the sum of ΔH_1 and ΔH_3 and the amount of BrF_5 formed. The results, corrected to 25°, are given in column 10. In Series A, $\Delta H^0_{f,BrF_3}$ then was obtained by subtracting the contribution of the BrF_5 in the mixture from the total enthalpy change

$$\Delta H^0_{f,BrF_3} = \frac{\Delta H_1 + \Delta H_2 + \Delta H_3 - n_{BrF_5}\Delta H^0_{f,BrF_5}}{n_{BrF_3}} \quad (4)$$

The results are given in column. 9. The tabulated values are the heats of formation of gaseous BrF_3 and BrF_5 from the gaseous elements at 25°. The energy unit is the defined thermochemical calorie, equal to 4.1840 absolute joules. Although the standard deviations for $\Delta H^0_{f,BrF_3}$ and $\Delta H^0_{f,BrF_5}$ are 0.20 and 0.26 kcal./mole, respectively, the uncertainties are estimated as ± 0.7 and ± 0.5 kcal./mole, respectively, using the simplifying assumptions which have been made concerning heats of

(20) G. D. Oliver and J. W. Grisard, *J. Am. Chem. Soc.*, **74**, 2705 (1952).

(21) R. D. Long, Report ANL-5405, Argonne National Laboratory, March, 1955.

(22) L. J. Gillespie and J. R. Coe, *J. Chem. Phys.*, **1**, 103 (1933).

mixing of the liquids and ideality of the vapors. At present, no correction is made for partial dimerization of BrF_3, since the proportion of dimer in the vapor at 25° is not accurately known. The equilibrium constant for dimerization has been estimated[10] from approximate vapor densities at 75 and 100°, but the extrapolation to lower temperatures probably is subject to very large error.

Steunenberg, Vogel and Fisher[7] found $\Delta F^0 = 1.2$ kcal. and $\Delta H^0 = 11.9$ kcal. for the gas phase reaction

$$Br_2 + BrF_3 \rightleftarrows 3BrF \qquad (5)$$

at 25°. If ΔS^0 is obtained from tables of entropy[5,10]

$$\Delta F^0 + T\Delta S^0 = 11.8 \text{ kcal.} \qquad (6)$$

which is in very good agreement with their value of ΔH^0 derived from the temperature coefficient of the equilibrium constant. It then is possible to obtain $\Delta H^0_{f,BrF}$ from $\Delta H^0_{f,BrF_3}$ by the reverse of the calculation which they made

$$\Delta H^0_{f,BrF} = {}^1/_3(\Delta H^0 + \Delta H^0_{f,BrF_3}) \qquad (7)$$
$$= {}^1/_3(11.8 - 64.8)$$
$$= -17.7 \text{ kcal./mole at } 25°$$

Since this agrees within 0.7 kcal./mole with $\Delta H^0_{f,BrF}$ computed by Evans, Munson and Wagman[5] from the dissociation limit of BrF, the assumption of these authors that the dissociation leaves fluorine in an excited state apparently is correct.

The free energies of formation, ΔF^0_f, of BrF, BrF_3 and BrF_5 at 25° are calculated as −18.0, −55.2 and −84.1 kcal./mole, respectively, from the present heats of formation and tables of entropy.[5,10] The entropy of BrF_3 is taken as 69.905 cal./degree mole, even though this is derived with certain assumptions about the degree of dimerization of BrF_3[10] and subsequently may be revised. The free energies at elevated temperatures indicate that BrF_5 dissociates into BrF_3 and F_2 above 550° and that BrF_3 dissociates into BrF and F_2 above 800° (F_2 also dissociates into atoms in the latter region). The dissociation of BrF_5 has been verified by approximate PVT measurements. Above 1000°, BrF is expected to be the stable species over a wide range of composition, in equilibrium with atomic bromine or fluorine.

Acknowledgment.—The author wishes to thank Dr. D. W. Osborne for advice regarding the calorimetric techniques and both Mr. J. L. Tague and Mr. B. T. Cope, Jr., for operating the shield at various times during the experiments.

THE REACTIVITY OF HYDROGEN ATOMS IN THE LIQUID PHASE. III. THE REACTIONS WITH OLEFINS

BY T. J. HARDWICK

Gulf Research & Development Company, Pittsburgh 30, Pennsylvania

Received September 7, 1961

The rates of reaction of hydrogen atoms with a series of olefins in *n*-hexane solution have been measured at 23°. Both addition and abstraction of hydrogen occur. For olefins within a given structural type, *e.g.*, RCH=CHR, the rates of reaction are the same, although these rates vary from one structural type to another. Hydrogen abstraction appears to take place only from the olefinic hydrogens, although the individual factors affecting the rate have not been determined. The reactivity of hydrogen atoms is similar to that of alkyl radicals, but different from that of oxygen atoms.

Introduction

The reactivity of hydrogen atoms with olefins in the gas phase has been studied extensively. Until ten years ago, however, experiments were confined to a study of ethylene, propylene and the butenes; such work has been critically reviewed by Steacie.[1] Addition of hydrogen was the main observed reaction; evidence for hydrogen abstraction was found in some cases.

The most comprehensive work has been carried out by Melville, Robb and their co-workers.[2-8] The rate constants for hydrogen atom reaction with ten olefins were determined at 18°. Their measurements represent the sum of the addition and abstraction reactions, but in a later paper[8] they found addition to be the most probable reaction in the case of ethylene and propylene. Absolute constants were measured, varying in value from 1.8–8.0 × 10^{11} cc. $mole^{-1}$ $sec.^{-1}$. Toby and Schiff[9] found the rates of H and D addition to ethylene to be the same, confirming earlier work by Melville.[10]

Some very interesting studies have been made of the reaction of hydrogen atoms with propylene in the solid state.[11-14] Propylene molecules form part of a solid matrix (maintained near liquid nitrogen temperatures). Hydrogen or deuterium atoms, formed by dissociation of the corresponding molecules on a hot wire, diffuse into the matrix and form radicals by addition. An activation energy of 1.5 kcal. was found for the formation of isopropyl radicals. In contrast to propylene, both addition and

(1) See "Atomic and Free Radical Reactions," E. W. R. Steacie, Reinhold Publ. Corp., New York, N. Y., 1954, Chap. V.
(2) H. W. Melville and J. C. Robb, *Proc. Roy. Soc.* (London), **A196**, 445 (1949).
(3) H. W. Melville and J. C. Robb, *ibid.*, **A196**, 466 (1949).
(4) H. W. Melville and J. C. Robb, *ibid.*, **A196**, 479 (1949).
(5) H. W. Melville and J. C. Robb, *ibid.*, **A196**, 494 (1949).
(6) H. W. Melville and J. C. Robb, *ibid.*, **A202**, 181 (1950).
(7) P. E. M. Allen, H. W. Melville and J. C. Robb, *ibid.*, **A218**, 311 (1953).
(8) J. N. Bradley, H. W. Melville and J. C. Robb, *ibid.*, **A236**, 454 (1956).
(9) S. Toby and H. I. Schiff, *Can. J. Chem.*, **34**, 1061 (1956).
(10) H. W. Melville, *J. Chem. Soc.*, 1243 (1934).
(11) R. Klein and M. D. Scheer, *J. Phys. Chem.*, **62**, 1011 (1958).
(12) R. Klein, M. D. Scheer and J. G. Waller, *ibid.*, **64**, 1247 (1960).
(13) R. Klein and M. D. Scheer, *ibid.*, **65**, 324 (1961).
(14) M. D. Scheer and R. Klein, *ibid.*, **65**, 375 (1961).

hydrogen abstraction were found for butene-1 and isopentene on reaction in the solid state.[14]

The present work concerns the reactivity of hydrogen atoms with olefins in the liquid phase. In the technique used, as described previously,[15-17] it is required that the olefins be liquid at room temperature. As this precludes the use of olefins of fewer than five carbon atoms, the only work with which direct comparison may be made is that of Allen, *et al.*[7]

In measuring the reactivity of hydrogen atoms in the liquid phase, the hydrogen atoms are formed by the radiolysis of an alkane solvent (RH), and react competitively with solvent and added solute (S). The kinetic expression derived from the steady state kinetics is[15,16]

$$\frac{1}{G_{H_2(O)} - G_{H_2(S)}} = \frac{1}{\Delta G_{H_2}} = \frac{1}{G_2} \times \frac{[RH]}{[S]} \times \frac{k_3}{k_4} + \frac{1}{G_2}\left(\frac{k_5}{k_4} + 1\right) \quad (I)$$

where $G_{H_2(O)}$ and $G_{H_2(S)}$ are the radiolytic hydrogen gas yields without and with added solute. G_2 is the thermal hydrogen atom yield (= 3.16 for *n*-hexane); k_3, k_4 and k_5 are the rate constants for the reactions

$$H + RH \xrightarrow{k_3} H_2 + R$$

$$H + S \xrightarrow{k_4} HS$$

$$H + S \xrightarrow{k_5} H_2 + R'$$

If the kinetics are followed, a plot of $1/\Delta G_{H_2}$ *vs.* [RH]/[S] gives a straight line, the slope of which is $(k_3/k_4)(1/G_2)$, and the intercept $(k_5/k_4 + 1)(1/G_2)$. It is the purpose of this paper to study the reactivity of hydrogen atoms on olefins in *n*-hexane solution, with particular attention to the effect of olefin structure on the rates of reaction.

Experimental

Materials.—The following olefins were Phillips Pure Grade: 2-methylbutene-1, pentene-1, pentene-2, hexene-1, hexene-2, heptene-1, heptene-2, octene-1, cyclohexene. Cyclopentene was Phillips Reagent Grade. Decene-1, 2,4,4-trimethylpentene-1, 2-methylpentene-1, 2-methylheptene-1, 2-methylpentene-2, trimethylethylene, tetramethylethylene, 2-ethylbutene-1, 3-ethylpentene-2, and vinylcyclohexane were obtained from K and K laboratories. All olefins tested to 99–101% unsaturation. *n*-Hexane was Phillips Pure Grade, and was further purified by sulfuric acid to lower the unsaturation below a measured value of 0.15 m*M*/l.

Normal hexane was used as the solvent and source of hydrogen atoms. The techniques of sample preparation, irradiation and analysis have been described previously.[15,16] Corrections were made to the measured hydrogen gas yields to allow for direct absorption of the radiation by the solute.[17] In general the solute concentration ranged between 0.3 and 1.5% by volume. All irradiations were made at 23 ± 1°.

Results

As required by equation I, a plot of $1/\Delta G_{H_2}$ *vs.* [hexane]/[olefin] gave a straight line for all olefins studied. Such plots for hexenes of five different structural types are shown in Figs. 1 and 2. The relative rate constants obtained from such plots were converted into absolute values by taking $k_3 = 4.9 \times 10^9$ cc. mole^{-1} sec.$^{-1}$.[16] The results are shown in Table I, where the olefins are listed by structural type.

Addition of H Atoms to Olefins.—For all olefins of a similar structure, *e.g.*, RCH = CHR, the rates of addition of hydrogen atoms are the same. A minor variation is found with R_2C = CHR. This rate of addition varies, however, from one structural group to another, R_2C = CH_2 having the fastest rate, R_2C = CR_2 the slowest.

TABLE I

REACTIVITY OF HYDROGEN ATOMS WITH OLEFINS IN *n*-HEXANE (T = 23 ± 1°)

Olefin	k_4 (addition) cc. mole^{-1} sec.$^{-1}$ × 10^{11}	k_5 (H abstraction)	k_5/k_4
	RCH=CHR		
Cyclopentene	5.3	1.33	0.25
Cyclohexene	4.9	1.12	.23
Pentene-2	5.5	1.23	.22
Hexene-2	5.2	1.27	.25
Heptene-2	5.1	1.35	.27
	5.2	1.26	0.24
	$RCH=CH_2$		
Pentene-1	7.8	2.3	0.30
Hexene-1	7.9	2.4	.31
Heptene-1	8.2	2.9	.35
Octene-1	7.6	2.0	.27
Decene-1	7.9	2.5	.32
	7.9	2.4	0.30
	$R_2C=CH_2$		
2,4,4-Trimethylpentene-1	10.8	3.4	0.32
2-Methylbutene-1	10.8	3.4	.32
2-Methylpentene-1	11.7	3.7	.32
2-Methylheptene-1	11.0	3.1	.28
2-Ethylbutene-1	11.5	3.7	.33
	11.2	3.4	0.31
Vinylcyclohexane	7.6	2.1	0.28
	$R_2C=CHR$		
Trimethylethylene	7.5	0.6	0.085
2-Methylpentene-2	6.6	1.2	.17
3-Ethylpentene-2	7.1	1.8	.26
	$R_2C=CR_2$		
Tetramethylethylene	5.5	<0.1	<0.03

Abstraction of H Atoms from Olefins.—In a manner parallel to the results for H atom addition, the rate of hydrogen abstraction is the same for all olefins of one structure, but varies between the different structure types. It follows that the ratio of abstraction to addition (k_5/k_4) is constant for a particular structure.

It is a feature of the kinetic development that the collision diameter of the solute is taken as that of the reactive portion of the molecule. Thus for a given type of olefin, the relative frequency of collision of hydrogen atoms with the olefinic group and with *n*-hexane, although not accurately known, will remain constant at a given concentration and temperature, regardless of the length and structure of the alkyl chains on the olefin.

Within all but one of the olefin groups it was found experimentally that the rates of reaction are

(15) T. J. Hardwick, *J. Phys. Chem.*, **64**, 1623 (1960).
(16) T. J. Hardwick, *ibid.*, **65**, 101 (1961).
(17) T. J. Hardwick, *ibid.*, **66**, 117 (1962).

the same. It would appear therefore that within each group the probability of reaction on collision is the same, the steric factors are equal and the activation energies are identical. For the same reasons it may be presumed that the activated complex has the same general structure, and that the entropy of activation is the same for all similar olefins.

Although this consistency is found within groups, the rates of both addition and abstraction reactions vary from one structural type to another. Such a variation may be due to a change in effective collision diameter, a different reaction probability, or a difference in activation energy, or a combination of these effects. A distinction is not possible from the present data.

Within the group $R_2C{=}CHR$ there is a distinct difference in the rates, particularly for hydrogen abstraction. It would appear that the lone olefinic hydrogen is more reactive when ethyl rather than methyl groups are attached to the olefinic carbon atoms.

Structurally, vinylcyclohexane belongs to the group $R_2C{=}CH_2$. In view of the blocked rotation of the adjacent methylene groups, and possibly greater shielding effects from the cyclohexane ring, it is understandable that a lower rate of reaction should exist. As the ratio k_5/k_4 is that expected for type $R_2C{=}CH_2$, it would appear likely that a decrease in the frequency of encounters between hydrogen atoms and the olefin bond is the reason for the lower rate. Perhaps coincidentally, the rates for vinylcyclohexane are typical of those for $RCH{=}CH_2$ type olefins.

From the data in Table I it has been concluded that hydrogen abstraction takes place from olefinic carbon atoms only. Within a given structural type of hydrogen abstraction is the same regardless of length and structure of the alkyl substituents. In the case of tetramethylethylene, with no olefinic hydrogens, hydrogen abstraction is not observed. If the alkyl chains react in a fashion similar to alkanes, a rate of hydrogen abstraction $<10^{10}$ cc. mole^{-1} sec.$^{-1}$[16] would be expected. Such a rate is below the limit of detection in the systems used. This inert behavior of alkyl chains has been found in other aliphatic compounds, *e.g.*, esters, acids, aldehydes and alcohols.[17]

Abstraction of olefinic hydrogens by hydrogen atoms has been demonstrated in studies of *n*-hexane radiolysis.[15] In this case about 25% of the monoolefins formed in the C_8-C_{12} fraction were of the type $R_2C{=}CHR$. These unsaturated products were formed by the abstraction of hydrogen from an olefin (hexene-1, -2 or -3) by a hydrogen atom to give a hexenyl radical, followed by a combination of this alkenyl radical with an alkyl radical to give the product olefin. If olefinic hydrogens were not abstracted, the formation of $R_2C{=}CHR$ could not occur.

Two mechanisms of hydrogen abstraction are possible. In the first, it is assumed that the activated complex may break up in two ways—to form an alkyl radical, or to eliminate a molecule of hydrogen and form an alkenyl radical. The relative probabilities of these two events will be the same for the same type of activated complex, *i.e.*, from reaction with the same type of olefin. Each type of olefin, however, with its individual structure of the activated complex, should give differing results.

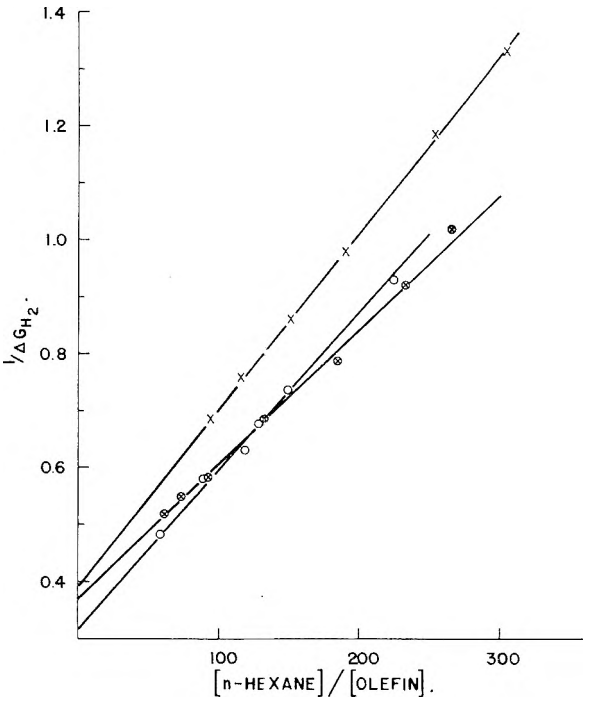

Fig. 1.—Kinetic plot for the reaction of hydrogen atoms on C_6 olefins in *n*-hexane solution at 23°: ○, tetramethylethylene; ×, hexene-2; ⊗, 2-methylpentene-2.

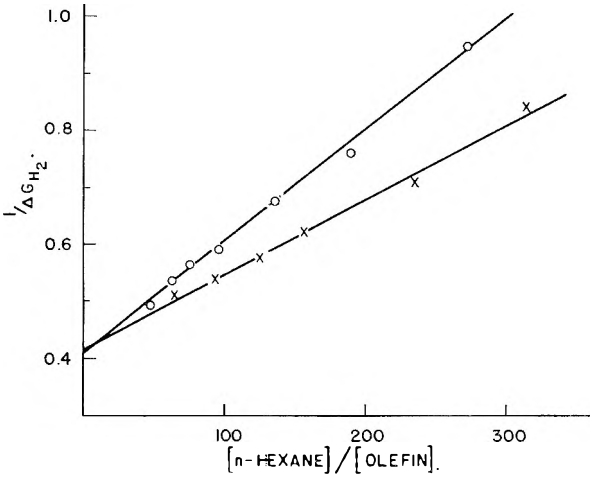

Fig. 2.—Kinetic plot for the reaction of hydrogen atoms on C_6 olefins in *n*-hexane at 23°: ○, hexene-1; ×, 2-methylpentene-1.

The second mechanism assumes that abstraction and addition are independent and competing processes, the extent of each depending on the geometry of the effective reaction center. It might be expected that terminal olefins with their more readily accessible hydrogen would have a higher probability of abstraction than internal olefins with their more highly shielded hydrogens. This is so in general, but further explanation is needed to understand why the rate of abstraction from $R_2C{=}CH_2$ is higher than from $RCH{=}CH_2$.

It is not possible to choose between these two mechanisms on the basis of the data available in Table I.

Comparison with Previous Results.—The reaction of hydrogen atoms with four of the olefins in Table I has been studied in the gas phase.[7] Two of them, cis-pentene-2 and cyclohexene, together with benzene, were used previously to establish the absolute value of the rate constant k_3 in the liquid phase. In Table II a comparison is made between the measured rate of hydrogen atom attack in the gas phase and the ratio of rate constants $k_3/(k_4 + k_5)$ derived from Table I. The product of these two values gives the rate of hydrogen atom reactivity with *n*-hexane. Results from the two last-studied compounds (tri- and tetramethylethylene) are in good agreement with those previously obtained and further increase confidence in our absolute values.

TABLE II

DATA FOR ESTABLISHING ABSOLUTE RATE CONSTANTS IN *n*-HEXANE

$T = 23°$

Solute	Measured rate H + S ($k_4 + k_5$) in gas phase,[a] cc. mole^{-1} sec.$^{-1}$	Measured ratio $\frac{k_3}{k_4 + k_5}$ in liquid phase	Rate H + *n*-hexane in liquid phase, cc. mole^{-1} sec.$^{-1}$
cis-Pentene-2	6.7×10^{11}	7.3×10^{-3}	4.9×10^{9}
Cyclohexene[b]	9.2	8.1	7.4
Benzene	1.25	39	4.9
Trimethylethylene	8.5	6.0	5.1
Tetramethyleth-ylene	5.6	8.9	5.0

Standard value k_H + *n*-hexane 4.9×10^9 cc. mole^{-1} sec.$^{-1}$.

[a] Data of Allen, Melville and Robb, *Proc. Roy. Soc.* (London), **A218**, 311 (1953). [b] Values for cyclohexene have been redetermined for this paper.

Comparison of Hydrogen Atom Reactivity with that of Other Radicals. Methyl Radical.—Buckley and Szwarc[18] studied the reactivity of methyl radicals on a series of α-olefins in isooctane solution. Within experimental error, they concluded that the rates for addition to butene-1, pentene-1, heptene-1, decene-1, hexadecene-1 and 3-methylbutene-1 were equal.

Ethyl Radical.—James and Steacie[19] found the identical rates of addition of ethyl radicals to hexene-1, heptene-1 and octene-1 in the gas phase. In other experiments[20] these authors found the abstraction of hydrogen by ethyl radicals proceeded at the same rate for heptene-1 and octene-1. Abstraction from cyclohexene and octene-4 took place at the same rate, which, however, was different from that of the α-olefins. More detailed comparison is not justified, mostly because of the differing temperatures at which the experiments were carried out.

In any case, differences in steric factors are expected as steric hindrance obviously will be more severe with alkyl radicals than with hydrogen atoms. The important result is that, regardless of the radical (methyl, alkyl, hydrogen atom) and regardless of the phase (gaseous or liquid), the rate of reaction for that radical with all members of a given olefin type is the same.

(18) R. P. Buckley and M. Szwarc, *Proc. Roy. Soc.* (London), **A240**, 396 (1957).

(19) D. G. L. James and E. W. R. Steacie, *ibid.*, **A244**, 297 (1958).

(20) D. G. L. James and E. W. R. Steacie, *ibid.*, **A244**, 289 (1958).

Oxygen Atoms.—Cvetanovic, in a series of papers,[21-24] has studied the rate of oxygen atom attack on olefins. His results apparently are not related to structure in the same manner as we have found, and this difference may be due, as he suggests, to the electrophilic character of the oxygen atoms. Clearly a different set of forces exist when using oxygen atoms, compared to free radicals. Hydrogen atoms clearly behave as alkyl radicals, rather than as oxygen atoms.

Trichloromethyl Radicals.—Kharasch and Sage[25] studied the addition of CCl_3 to a series of olefins in the liquid phase. A comparison has been made in Table III of the relative rates of reaction of various types of olefins with hydrogen atoms and with trichloromethyl radicals. With the exception of RCH=CHR, the agreement is striking. It would appear that trichloromethyl radicals react as a true free radical and not through any particular electrophilic property of the group.

The rate of addition of hydrogen atoms to the various olefins decreases in the order $R_2C{=}CH_2$, $RCH{=}CH_2$, $R_2C{=}CHR$, $RCH{=}CHR$, $R_2C{=}CR_2$. It does not appear worthwhile to compare such a result with other work, first because the complete rate expression should be used in any comparison, and secondly because the steric factors, which affect the extent of collision of methyl and ethyl radicals with the olefin bond, may be much less significant when considering hydrogen atom collisions.

The activation energy for the reactivity of hydrogen atoms with propylene has been determined in the solid phase $E = 1.5$ kcal. It would be interesting to apply such a value in the liquid phase data, but for several reasons this is undesirable. In the gas phase the reactivity of hydrogen atoms with propylene is anomalously low by a factor of 4 when compared to other olefins.[7] Secondly, whereas in the solid phase propylene reacts by hydrogen addition only, butene-1 and 3-methylbutene-1 react by both addition and abstraction.[14] In view of the somewhat unique behavior of propylene, quantitative comparisons of the data will not be attempted.

TABLE III

COMPARISON OF RATES OF REACTION OF H AND CCl_3 ON OLEFINS IN SOLUTION

Olefin type	Relative value: H atoms—over-all rate	Relative value: CCl_3 radical addition
$RCH{=}CHR$	0.7	0.2
$R_2C{=}CHR$	0.8	0.9
$RCH{=}CH_2$	1.0	1.0
$R_2C{=}CH_2$	1.4	1.4

Results such as are reported in this paper should furnish a basis for calculating the configurations of the various transition state complexes. For example, the transition state complex formed on the addition of a hydrogen atom to cyclopentene should vary from that of cyclopentyl radical only in bond angles and interatomic distances. All reac-

(21) R. J. Cvetanovic, *J. Chem. Phys.*, **30**, 19 (1959).

(22) R. J. Cvetanovic, *ibid.*, **33**, 1063 (1960).

(23) R. J. Cvetanovic, *Can. J. Chem.*, **38**, 1678 (1960).

(24) R. J. Cvetanovic and L. C. Doyle, *ibid.*, **38**, 2187 (1960).

(25) M. S. Kharasch and M. Sage, *J. Org. Chem.*, **14**, 537 (1949).

tants are electronically in their ground state, and reaction takes place at a conveniently low temperature.

Although this study does not indicate a specific reaction, there is evidence that hydrogen atoms add almost exclusively to the terminal carbon of α-olefins[26,27]

$$R(H,R)C{=}CH_2 + H \longrightarrow R(H,R)C{-}CH_3$$

giving a secondary or tertiary radical. On the basis of such information the properties of the transition state likewise can be calculated.

(26) P. J. Boddy and J. C. Robb *Proc. Roy. Soc.* (London), **A249**, 518 (1959).

(27) P. J. Boddy and J. C. Robb *ibid.*, **A249**, 532 (1959).

NON-IONIC–CATIONIC MICELLAR PROPERTIES OF DIMETHYLDODECYLAMINE OXIDE[1]

By K. W. Herrmann

Miami Valley Laboratories, The Procter & Gamble Company, Cincinnati, Ohio

Received September 13, 1961

The micellar properties of a surfactant showing both non-ionic and cationic character in aqueous solution, depending on *p*H, were determined using light scattering methods. Differences in the critical micelle concentrations, micelle molecular weights and interaction coefficients shown by the neutral and positively charged surfactant species in water and in 0.2 *M* NaCl are noted and discussed. Although the micellar results are consistent for each individual species, a direct comparison of the properties of the cationic and non-ionic modifications shows some inconsistencies when current concepts of micelle formation are considered. In addition, changes in micellar properties have been determined as a function of non-ionic surfactant (dimethylalkylamine oxide) chain length and as a function of temperature for the C_{12} homolog. These results were used to calculate thermodynamic quantities for micelle formation.

Much of the controversy over the interpretation of light scattering data obtained on solutions of ionic surface active agents is due to the electrical charge carried by the micelles. Since Debye first showed that micellar information can be obtained by applying light scattering methods to detergent solutions,[2] most of the work reported in the literature has dealt with the micellar properties of anionic and cationic detergent systems.[3] Attempts have been made to avoid electrical interactions by using non-ionic surfactant molecules; however, these substances have been polymeric condensates with large polar heads which, although fractionated, may consist of a distribution of chain lengths.[4–6] It is desirable that well characterized, non-ionic surfactants be investigated if the theory of micellar solutions is to be developed further.

The present work deals with the micellar molecular weights and critical micelle concentrations of a pure species which can exist in both non-ionic and cationic form depending upon the *p*H of the solution. These two forms are: dimethyldodecylamine oxide (DDAO), $C_{12}H_{25}N(CH_3)_2 \rightarrow O$ and dimethyldodecyl-N-hydroxyammonium chloride (DDHAC), $[C_{12}H_{25}N(CH_3)_2OH]$ Cl. They are related by the equilibrium

$$C_{12}H_{25}N(CH_3)_2OH^+ \rightleftharpoons C_{12}H_{25}N(CH_3)_2 \rightarrow O + H^+$$

The micellar properties of each species have been determined in the presence and absence of added electrolyte.

Since the steric properties of DDAO and DDHAC are similar, the effect of charge on micellar character can be evaluated. Variations in the critical micelle concentrations, micelle molecular weights, and interaction coefficients are discussed in light of current concepts of micelle formation and possible experimental limitations.

In addition, the effect of hydrocarbon chain length (C_8–C_{14}) and temperature (DDAO, 1–50°) on the micellar properties of the amine oxides in H_2O are presented and compared with those of ionic surfactants. The thermodynamic quantities pertinent to micelle formation have been calculated for DDAO using these results.

Experimental

Turbidity Measurements.—Turbidities were determined with a commercial apparatus (Phoenix Precision Instrument Company, Philadelphia, Pa.) similar to that described by Brice, *et al.*[7] The narrow slits provided with this instrument were employed along with a cylindrical cell (Cat. No. C-101) which was painted black except for the window.[8] The apparatus was calibrated with a 0.5% solution of Debye's Dow Styron in reagent grade toluene which has a reported excess turbidity at 90° of 3.51×10^{-3} cm.$^{-1}$. After calibration, the Rayleigh ratios (R_{90}) for freshly distilled benzene and toluene were found to be 48.9×10^{-6} and 56.1×10^{-6}, respectively, using light of wave length 4358 Å. These values agree well with those previously reported.[9] In addition, the fluorescence from an ethanol solution of fluorescein was found to be symmetrical within 1% over the angular range 25 to 135°.

When the turbidity measurements were carried out at room temperature, the temperature within the light scattering instrument was approximately 27°. For the determination of the temperature dependence of the micellar

(1) Paper presented to the Division of Colloid and Surface Chemistry, at the 140th National Meeting of the American Chemical Society, Chicago, Ill., September 3, 1961.

(2) (a) P. Debye, *J. Appl. Phys.*, **15**, 338 (1944); (b) *J. Colloid Sci.*, **3**, 407 (1948).

(3) M. M. Fishman, "Light Scattering by Colloidal Systems, An Annotated Bibliography," Tech. Service Labs., River Edge, N. J., 1958.

(4) L. M. Kushner and W. D. Hubbard, *J. Phys. Chem.*, **58**, 1163 (1954).

(5) A. M. Mankowieh, *ibid.*, **58**, 1027 (1954).

(6) L. M. Kushner and W. D. Hubbard, *ibid.*, **61**, 371 (1957).

(7) B. A. Brice, M. Halwer and R. Speiser, *J. Opt. Soc. Am.*, **40**, 768 (1950).

(8) P. F. Onyon, *J. Polymer Sci.* **24**, 493 (1957).

(9) K. A. Stacey, "Light Scattering in Physical Chemistry," Academic Press, Inc., New York, N. Y., 1956, p. 103.

properties the heating unit described by Trementozzi[10] and purchased from the Phoenix Precision Instrument Company Cat. No. (CCJ-2) was employed. The cell temperature was determined by prior calibration with a constant temperature bath (± 0.2°) whose fluid was continuously pumped through the cored cell heating jacket. The blue line of mercury (λ = 4358 Å.) was used throughout. Dissymmetry values were calculated from the scattered intensities observed at 45 and 135° (Z_{45}).

Refractive Index Increments.—The dn/dc values were determined with a Brice–Phoenix differential refractometer at 27° using light of λ = 4358 Å. The instrument was calibrated with sucrose solutions.

Materials.—Dimethyldodecylamine oxide (DDAO) was prepared by H_2O_2 oxidation of the dimethyldodecylamine. Excess H_2O_2 was catalytically decomposed by the addition of platinum black. Unreacted amine was removed by repeated extraction with petroleum ether; the residue from freeze drying was repeatedly recrystallized from acetone previously dried over $CaSO_4$.

The starting dimethyldodecylamine was obtained by repeated fractional distillation of Armour's Armeen DMC-D (dimethylcoconutamine-distilled). The fraction used in the preparation of the amine oxide was shown to be 99.8% pure dimethyldodecylamine by vapor phase chromatography methods. Conductivity measurements showed the DDAO to be free of ionic impurities and the presence of free amine in the amine oxide could not be detected by a non-aqueous titration of a petroleum ether extract using brom cresol purple as the titrant for free amine.

The preparations of the other amine oxides were similar except that the starting dimethylalkylamines were prepared by reacting the alkyl bromides with dimethylamine. Vapor phase chromatography methods showed the selected portions of the fractionally distilled dimethylalkylamines to have greater than 99.5% purity.

Preparation of Solutions.—Stock DDAO solutions were prepared on a weight/volume basis and diluted volumetrically. Double distilled water was used in preparing all solutions. The non-ionic form (DDAO) was investigated at the natural *p*H of the solutions (*p*H 7.2–8.5 depending on concentration). The cationic form (DDHAC) was examined at *p*H 2 and 3, the *p*H being adjusted with HCl just before the final volumes were reached in each dilution. The solutions of other chain length amine oxides were prepared similarly and examined at their natural *p*H's.

All solutions were clarified by nitrogen pressure filtration through a 0.45 μ pore size Millipore filter at flow rates of 2–3 ml./min. Freedom from extraneous particles was determined by observing the fluctuation in scattered intensity at a scattering angle of 25°. Solutions were repeatedly filtered until their scattered intensity at 25° remained essentially constant.

The cell and the bottles in which the solutions were kept were made dust-free using the technique described by Thurmond.[11]

Results

Cationic–Non-ionic Equilibrium.—Nylen has reported *pK* values for the dissociation

$$R_3NOH^+ \rightleftarrows R_3NO + H^+$$

of 4.65 and 5.13 when R is CH_3 and C_2H_5, respectively.[12] Replacement of one CH_3 group with $C_{12}H_{25}$ should result in a *pK* between these values. An approximate measurement of the *pK* of DDHAC supported an estimated value of 5.0. This was considered adequate since a precise knowledge of the dissociation constant is unnecessary for interpreting the light scattering results which follow. Above *p*H 7 the surfactant will virtually all be in the non-ionic form (DDAO) and below *p*H 3 it will essentially all be in the cationic form (DDHAC).

At *p*H 3 the electrolyte (HCl) in excess of DDHAC will be no greater than 10^{-3} *M*. Earlier work reported in the literature indicates that such a small amount of electrolyte will have very little effect on cationic micelle properties,[13] particularly when the critical micelle concentration (c.m.c.) is greater than the added electrolyte concentration. Also, it has been previously that shown it is chiefly the salt anions which affect the micelle properties of cationic detergents.[14]

Micelle Properties.—Values for the critical micelle concentration (c.m.c.) were determined by plotting turbidity against detergent concentration and noting the concentration where a sharp increase in turbidity occurs.

Micelle molecular weights (m.m.w.) were calculated using Debye's equation

$$\frac{H(c - c_0)}{\tau - \tau_0} = \frac{1}{M} + 2B(c - c_0)$$

where

- H = a constant that includes the refractive index increment (dn/dc)
- τ = turbidity of the solution
- τ_0 = turbidity at the c.m.c. (equal to the solvent turbidity in almost all cases)
- c = detergent concn. in g./100 ml.
- c_0 = detergent concn. at the c.m.c.
- M = micelle molecular weight
- B = interaction coefficient which is a measure of non-ideality (interaction between micelles)

Although Debye's equation is strictly valid only for uncharged colloidal particles, Prins and Hermans have reported that the m.m.w.'s of ionic detergents determined using this relationship will be only about 10% too low if examined in the absence of added electrolyte.[15] Since there is still some controversy over the quantitative interpretation of the interaction coefficient (B)[16–18] and since the m.m.w. correction factor depends on this interpretation, Debye's equation has been used in calculating all m.m.w.'s. The m.m.w.'s were calculated from the intercepts and the slopes were taken as an indication of the non-ideality of the system.

Dissymmetry values for the surfactant solutions in the absence of added electrolyte could not be determined accurately; however, in the presence of 0.2 *M* NaCl all solutions showed dissymmetries of 0.98 to 1.02 over the entire concentration range studied. These values indicate that the micelles are small compared to the wave length of light employed.

DDHAC–DDAO.—The experimental data from which the micellar properties of DDHAC and DDAO were determined are shown in Figs. 1 and 2. The results are summarized in Table I.

In order to more easily compare the micelle properties of the cationic and non-ionic forms shown by DDAO, the detergent concentrations, c.m.c.'s,

(10) Q. A. Trementozzi, *J. Polymer Sci.*, **23**, 887 (1957).
(11) C. D. Thurmond, *ibid.*, **8**, 607 (1952).
(12) P. Nylen, *Z. anorg. u. allgem. Chem.*, **246**, 227 (1941).
(13) L. M. Kushner, W. D. Hubbard and R. A. Parker, *J. Research Natl. Bur. Standards*, **59**, 113 (1957).
(14) M. L. Corrin and W. D. Harkins, *J. Am. Chem. Soc.*, **69**, 683 (1947).
(15) W. Prins and J. J. Hermans, *Proc. Koninkl. Ned. Akad. Wetenschap.*, **B59**, 298 (1956).
(16) K. J. Mysels, *J. Colloid Sci.*, **10**, 507 (1955).
(17) W. Prins and J. J. Hermans, *Proc. Koninkl. Ned. Akad. Wetenschap.*, **B59**, 162 (1956).
(18) D. Stigter, *J. Phys. Chem.*, **64**, 842 (1960).

TABLE I

SUMMARY OF MICELLAR PROPERTIES (DDHAC-DDAO)

Form of detergent	Added Cl^- concn. (M)	C.m.c.[a] (g./100 ml.)	M.m.w.[a]	Monomers/micelle
DDAO	0	0.048	17,300	76
DDAO	0.2	0.034	17,800	78
DDHAC	1×10^{-3}	0.19	20,400	89
DDHAC	1×10^{-2}	.18	20,700	90
DDHAC	0.1	.048	26,000	114
DDHAC	0.2	.034	31,100	136

[a] Determined from Figs. 1 and 2 wherein the cationic properties have been expressed in terms of the non-ionic formula weight (see text).

and micelle molecular weights (m.m.w.) of the cationic form have been expressed in terms of the non-ionic formula weight in Figs. 1 and 2 and Table I, *i.e.*, all of the above values of the cationic species have been reduced by the factor $M.W._{DDAO}/M.W._{DDHAC}$.

Chain Length Effects.—The experimental data for the C_8 and C_{10} dimethylalkylamine oxides were similar to those of DDAO in that a sharp increase in turbidity occurred at their respective c.m.c. values and the slopes of their $H(c-c_0)/(\tau-\tau_0)$ *vs.* $(c-c_0)$ plots were zero. In addition, the c.m.c. of C_{14} dimethylalkylamine oxide was determined by noting the concentration at which a slope change occurred in the surface tension *vs.* log concentration plot. Surface tensions were determined by the pendant drop method. The micellar properties at 27° for this homologous series of amine oxides are summarized in Figs. 3 and 4.

Figure 3 compares the c.m.c. variation with chain length of non-ionic dimethylalkylamine oxides with those of cationic alkyltrimethylammonium bromide[19] and anionic sodium alkyl sulfonate.[20]

Figure 4 compares the aggregation number variation with chain length for the various surfactant types.

Temperature Effects.—Light scattering data again were used to determine the c.m.c. and m.m.w. values of DDAO at temperatures ranging from 1 to 50°. Zero slopes were obtained in the $H(c-c_0)/(\tau-\tau_0)$ *vs.* $(c-c_0)$ plots at all temperatures. The micellar results are given in Table II.

TABLE II

VARIATION OF DDAO MICELLAR PROPERTIES WITH TEMPERATURE

Temp., °C.	C.m.c. (moles/l.)	M.m.w.
1.0	0.00284	17,700
27.0	.00210	17,300
40.0	.00183	17,900
50.0	.00175	16,600

Discussion

DDHAC-DDAO.—If one considers the micelle properties shown by the cationic and non-ionic forms individually, one finds that the c.m.c., m.m.w., and interaction coefficient change as expected when electrolyte is added.

The non-ionic form (DDAO) behaves ideally (no

(19) H. J. L. Trap and J. J. Hermans, *Proc. Koninkl. Ned. Akad. Wetenschap.*, **B58**, 97 (1955).

(20) H. V. Tartar and A. L. M. LeLong, *J. Phys. Chem.*, **59**, 1185 (1955).

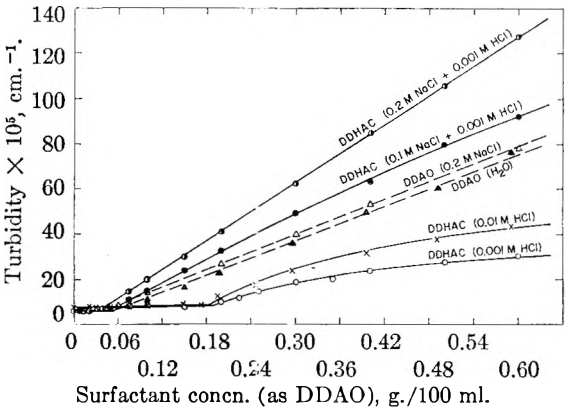

Fig. 1.—Turbidity measurements in the presence and absence of added electrolyte.

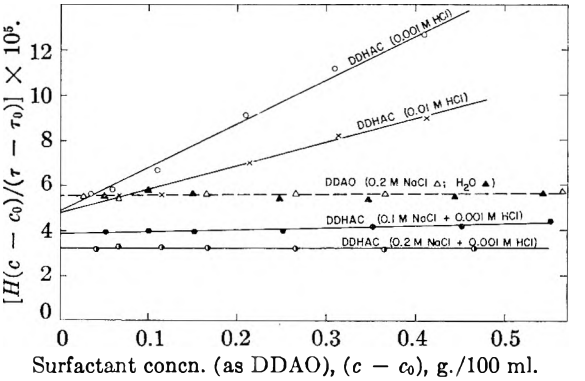

Fig. 2.—Light scattering results in the presence and absence of added electrolyte.

interaction between micelles as indicated by the zero slope in the Hc/τ *vs.* c plots) in both water and 0.2 M NaCl and the m.m.w. is not significantly influenced by the presence of electrolyte. The c.m.c. is, however, appreciably lowered when electrolyte is added. These data support the use of the estimated pK value for DDHAC since a zero slope in the absence of electrolyte indicates that there is no appreciable concentration of the cationic form present.

Results obtained with the cationic form (DDHAC) show, as expected, that both the c.m.c. and interaction coefficient decrease while the m.m.w. increases with increasing salt concentration. The very slight variation in micelle properties on going from pH 3 to pH 2 again suggests that a pK value of 5.0 is a reasonable one.

Although the results are as expected for the individual surfactant species, some anomalies are observed when the micellar properties of the cationic and non-ionic are compared. These comparisons are based on the fact that the only difference between the two solution species is that the cationic form contains a proton which gives it a positive charge.

It can be seen from the results given in Table I that the c.m.c. ratio of cationic to non-ionic is about 4 in the absence of appreciable added electrolyte, and essentially 1 in 0.2 M NaCl solution. Current concepts of micelle formation which include a consideration of short range van der Waals forces, long range electrostatic forces, and the effect of increased ionic strength on the latter forces, would indicate that these comparative c.m.c. values are of reason-

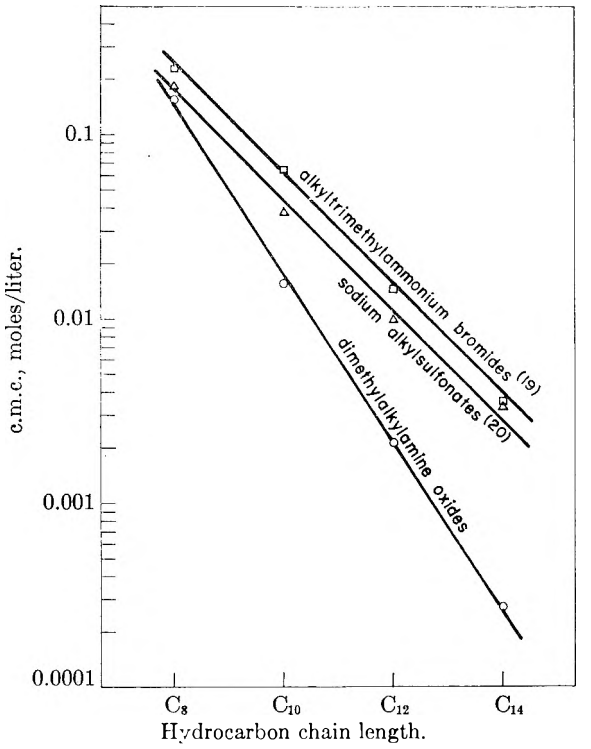

Fig. 3.—Critical micelle concentration variation with hydrocarbon chain length.

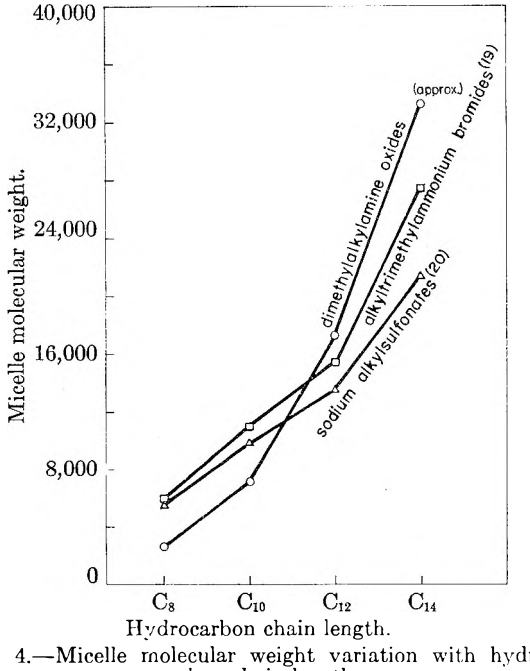

Fig. 4.—Micelle molecular weight variation with hydrocarbon chain length.

able magnitudes and change in the direction expected when electrolyte is added.[21-24] More specifically, earlier arguments state that the micelle structure of an ionic detergent can be represented as an equilibrium between the attractive forces (*e.g.*, van der Waals forces) and the electrical repulsive forces. The net result will be reflected in the heat term ($\Delta\bar{H}_m$) for micelle formation. It also has been reported that the work done in forming micelles is directly related to the c.m.c. The c.m.c. of a non-ionic detergent should, therefore, be less than that of an ionic since there is no zeta potential electrical work to be overcome in the non-ionic case. Furthermore, in the presence of a swamping excess of added electrolyte, where the charge effects are minimized, it might be expected that the cationic form should have a c.m.c. similar to that of the non-ionic. Certainly the absence of electrical interaction between micelles in 0.2 *M* NaCl is shown by the zero slope obtained in the Hc/τ plot for the cationic species under these conditions (Fig. 2). Thus, existing theory would predict changes in the c.m.c. similar to those observed experimentally.

Further comparison shows that the m.m.w. ratio of cationic to non-ionic is about 1 in the absence of appreciable electrolyte and almost 2 in 0.2 *M* NaCl. If arguments similar to those used to explain the c.m.c. results are valid and sufficient, then these m.m.w. ratios are unexpected. Since the electrical repulsive forces developed within the micelles should be greater for the micelles of the cationic species (ion–ion repulsion) than for the non-ionic (dipole–dipole repulsion), a larger m.m.w. would be expected for the non-ionic than for the cationic form. This is not observed. Also, even in the presence of a swamping excess of electrolyte (0.2 *M* NaCl) there is no satisfactory explanation for the m.m.w. of the cationic form being greater than that of the non-ionic form. It is apparent from these relative results that other factors are operating in the process of micellization. Different models for the micelles of the two detergent forms might be used to explain these results, however, no valid reason for expecting a model difference has been presented to date. Marked variations in the solvation of monomers and/or micelles, which would alter the entropy of the system, also might aid in explaining the experimental observations. That solvation is a factor in micelle formation has been recognized by several authors[25-27] but no quantitative treatment of its influence has been presented as yet.

The unexpected cationic/non-ionic m.m.w. ratios might in part be explained experimentally. Eisenberg and Casassa[28] have shown that added electrolyte preferentially concentrates around polyelectrolytes in aqueous solution. If the added electrolyte in micellar solutions of ionic detergents behaves similarly, one might conclude that the experimental refractive index increments (dn/dc) for the cationic form are too low, thereby causing the m.m.w. values to be too high. However, errors in the molecular weight of only about 10% were found if the apparent dn/dc values were employed with polyelectrolytes. A similar error in the m.m.w.'s of the cationic form would not greatly change the cationic/non-ionic m.m.w. ratio. Un-

(21) P. Debye, *Ann. N. Y. Acad. Sci.*, **51**, 575 (1949).
(22) K. Shinoda, *Bull. Chem. Soc. Japan*, **26**, 101 (1953).
(23) D. Stigter, *Rec. trav. chim.*, **73**, 593 (1954).
(24) H. V. Tartar, *J. Phys. Chem.*, **59**, 1195 (1954).
(25) E. D. Goddard, C. A. J. Hoeve and G. C. Benson, *ibid.*, **61**, 593 (1957).
(26) E. Matijević and B. A. Pethica, *Trans. Faraday Soc.*, **54**, 587 (1958).
(27) R. H. Aranow and L. Witten, *J. Phys. Chem.*, **64**, 1643 (1960).
(28) H. Eisenberg and E. F. Casassa, presented at the 137th National Meeting of the American Chemical Society, Cleveland, Ohio, April 8, 1960.

fortunately, the dialysis technique used to obtain the more correct dn/dc values of polyelectrolytes cannot be used with micellar solutions because of their monomer–micelle equilibrium.

Chain Length Effects.—It can be seen from Figs. 3 and 4 that the c.m.c. decrease with increased chain length and the aggregation number increase with increased chain length are greater for the non-ionic dimethylalkylamine oxides than for either the cationic or anionic surfactants.

The treatments of Phillips[29] and Overbeek[30] for the thermodynamics of micelle formation result in the following expression for non-ionic surfactants of relatively high aggregation number (>50 monomers/micelle),

$$\Delta\bar{F}_m^0 = \Delta\bar{H}_m^0 - T\Delta\bar{S}_m^0 \cong RT \ln \text{c.m.c.}$$

where $\Delta\bar{F}_m^0$, $\Delta\bar{H}_m^0$ and $\Delta\bar{S}_m^0$ are the standard state thermodynamic changes per mole of monomer on micelle formation. The above expression is valid as long as the c.m.c. is sufficiently small so that the monomer activity coefficient approximates unity. From Fig. 3 we also can determine empirically that $\log \text{c.m.c.} = -0.477N + A$ where N = the number of CH_2 groups, A = constant.

Therefore,

$$\Delta\bar{F}_m^0 = 2.3RT(-0.477N + A)$$

$$\Delta\bar{F}_m^0 = -1.10RTN + 2.3RTA$$

or

$$\frac{\Delta(\Delta\bar{F}_m^0)}{\Delta N} = -1.10RT$$

This value for the standard free energy change per CH_2 group for non-ionic amine oxides agrees well with Overbeek's[30] calculated value for anionic sodium dodecyl sulfate ($\Delta(\Delta\bar{F}_m^0)/\Delta N = -1.0RT$) and with that found by Shinoda[22] from the solubilities of aliphatic homologous series ($\Delta(\Delta\bar{F}_m^0)/\Delta N = -1.08RT$).

Temperature Effects.—No significant change in DDAO micelle aggregation number occurs over the temperature range 1–50°. The c.m.c., however, decreases with increasing temperature. A straight line with slope equal to 410 degrees is obtained when log c.m.c. is plotted against $1/T$.

From this slope and the relationship for non-ionic surfactants

$$\frac{\mathrm{d} \ln \text{c.m.c.}}{\mathrm{d}T} = \frac{-\Delta\bar{H}_m}{RT^2}$$

where $\Delta\bar{H}_m$ is the partial molal heat of micelle formation, a $\Delta\bar{H}_m$ of +1.9 kcal./mole is obtained. In published derivations of the above expression[26,31,32] the micellar phase is treated as a separate phase much as is a precipitate in equilibrium with its saturated solution. If this analogy is strictly adhered to, the composition of the micellar phase must remain constant over the temperature range examined. Although composition data are not available for DDAO micelles, the calculated $\Delta\bar{H}_m$ is likely to be valid since the aggregation number is constant.

Because of the equilibrium conditions, $\Delta\bar{F}_m = \Delta\bar{H}_m - T\Delta\bar{S}_m = 0$,

$$\overline{\Delta S_m} = \frac{\Delta\bar{H}_m}{T} = 6.3 \text{ cal./mole deg.}$$

These $\Delta\bar{H}_m$ and $\overline{\Delta S_m}$ values are the partial molal quantities usually obtained from calorimetric heat measurements.

Thermodynamics of Micelle Formation.—It already has been shown that micelle formation of non-ionic sufactants can be described by

$$\Delta\bar{F}_m^0 = \Delta\bar{H}_m^0 - T\overline{\Delta S_m}^0 \cong RT \ln \text{c.m.c.}$$

The solvated monomer standard state may be taken as the hypothetical state obtained by extrapolation of Henry's law to mole fraction unity; the micelle standard state conveniently can be taken as the solvated micelle at mole fraction unity.

It also can be shown that $\Delta\bar{H}_m = \Delta\bar{H}_m^0$ if the system under consideration behaves ideally. Calorimetric measurements on the higher chain length amine oxide–water systems do indeed indicate that ideality is approached.[33] Therefore, for DDAO at 27°, using the above equation and the c.m.c. of 3.77×10^{-5} mole fraction, $\Delta\bar{F}_m^0 = -10.2RT$ or −6.1 kcal./mole. Since $\Delta\bar{H}_m^0 \cong \Delta\bar{H}_m = +1.9$ kcal./mole

$$\overline{\Delta S_m}^0 = \frac{\Delta\bar{H}_m^0 - \Delta\bar{F}_m^0}{T} = +26.6 \text{ cal./mole deg.}$$

In addition, the thermodynamic changes which occur on dilution of the monomer from the hypothetical standard state to the c.m.c. under isothermal and isobaric conditions can be calculated from

$$\Delta\bar{F}_d = RT \ln \frac{\gamma_1' X_1'}{\gamma_1 X_1}$$

where γ_1 and γ_1' are the activity coefficients of the monomer in the hypothetical standard state and at the c.m.c., respectively, and X_1 and X_1' are the mole fractions of the monomer in the above states. Since the monomer hypothetical standard state is obtained by extrapolation of Henry's law to $X_1 = 1$, $\gamma_1 = 1$ by definition. Also, since the c.m.c. for DDAO in water is small $\gamma_1' \cong 1$ at the c.m.c. (X'). Since this system does indeed approach ideality, than $\Delta\bar{H}_d \cong 0$. Therefore

$$\Delta\bar{F}_d = RT \ln \text{c.m.c.} = -6.1 \text{ kcal./mole}$$

$$\Delta\bar{H}_d = 0$$

$$\Delta\bar{S}_d = -R \ln \text{c.m.c.} = 20.3 \text{ cal./mole deg.}$$

The above calculations allow completion of the cycle

(29) J. N. Phillips, *Trans. Faraday Soc.*, **51**, 561 (1955).

(30) J. Th. G. Overbeek, *Chem. Weekblad.*, **54**, 687 (1958).

(31) G. Stainsby and A. E. Alexander, *Trans. Faraday Soc.*, **46**, 587 (1950).

(32) E. Hutchinson, A. Inaba and L. G. Baley, *Z. physik. Chem.* (Frankfurt), **5**, 344 (1955).

(33) L. Benjamin, private communication.

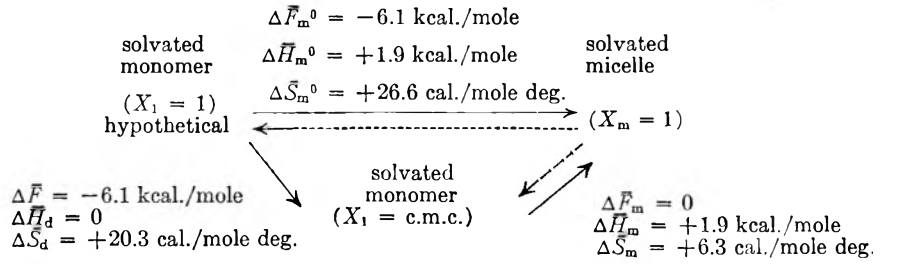

This diagram clearly shows the relationships between the thermodynamic quantities frequently cited for micelle formation. Note that the heat and entropy terms for micelle formation are positive and remain positive over the temperature range 1–50°. One must conclude, since the standard free energy is negative and the heat term is positive, that it is the entropy change that is responsible for the formation of amine oxide micelles. A positive entropy change indicates increased randomness. It does not appear likely that increased disorder would result from the aggregation of surfactant monomers into micelles, therefore one looks to solvation changes to explain the positive $\Delta\bar{S}_m$.

Goddard and Benson[34] studied the variation of sodium alkyl sulfate c.m.c.'s with temperature over the range 10–55° and found that $\Delta\bar{H}_m$ changes sign between 25–30°. An explanation of the positive $\Delta\bar{H}_m$ and $\Delta\bar{S}_m$ values was given by Goddard, Hoeve and Benson[25] based on modification of the postulated water structure surrounding the monomer hydrocarbon chains. The ordering of water ("iceberg" formation) by relatively large organic ions has been discussed previously by Frank and coworkers.[35,36]

Although solvent modification does seem likely to occur when micelles are formed, an exact description of the solvent's role in micelle formation still is lacking. Information on the degree of association of water with monomers and micelles and on the heat of monomer solvation would be helpful in understanding solvent participation in micellization.

Acknowledgments.—The author is indebted to Mr. P. Baumgardner who assisted in making the light scattering measurements.

(34) E. D. Goddard and G. C. Benson, *Can. J. Chem.*, **35**, 986 (1957).

(35) H. S. Frank and W. W. Evans, *J. Chem. Phys.*, **13**, 507 (1945).

(36) H. S. Frank and W. Y. Wen, *Discussions Faraday Soc.*, **24**, 133 (1958).

RECOIL REACTIONS WITH HIGH INTENSITY SLOW NEUTRON SOURCES. IV. THE RADIOLYSIS OF CRYSTALLINE ALKALI METAL BROMATES WITH γ-RAYS

BY G. E. BOYD, E. W. GRAHAM AND Q. V. LARSON

Oak Ridge National Laboratory, Oak Ridge, Tennessee

Received September 15, 1961

The radiolysis of the alkali metal bromates by Co^{60} γ-rays was effected to decompositions greater than three mole per cent. The amounts of bromate ion decomposed increased linearly with dose at first, but subsequently the dependence became non-linear for all salts except $LiBrO_3$. The initial 100 e.v. radiolytic yields or "G_0" values for bromate decomposition were: 0.31, 1.46, 1.71, 2.33, 3.4 and 5.1 for $LiBrO_3$, $NaBrO_3$, $KBrO_3$, $RbBrO_3$, $CsBrO_3$ and $TlBrO_3$, respectively. The yields increased only slightly with temperature between −195 and 85°, and for $CsBrO_3$ were almost independent of the dose rate from 8.8×10^{14} to 7.6×10^{16} e.v. g.$^{-1}$ sec.$^{-1}$. The radiolysis of bromate ion gave bromite, hypobromite, bromide and oxygen gas in amounts which varied with the alkali metal cation in the salt and with the total dose absorbed. Virtually all the oxidizing fragments produced in the crystalline salts by irradiation could be removed by thermal annealing. The radiolytic yields for bromate decomposition could not be correlated either with the thermodynamic stability of the salts or with their isothermal decomposition rates observed in the absence of radiation. However, an exponential dependence of "G_0" on the crystal "free space" was found, and a mechanism for the decomposition of the molecular bromate ion could be proposed.

This study deals with the radiation chemistry of molecular ions in crystals, and it is an extension of our earlier researches[1a,b,2] on the decomposition of the bromate ion in crystalline potassium bromate when this compound was exposed to various types of energetic nuclear radiation. The chief concern has been in determining the importance of crystal structure and binding to the radiolysis of the alkali metal bromates by γ-rays, and in determining the details about the radiolytic decomposition of the bromate group. It was of interest, also, to discover if any of the other bromates were more radiation stable than the potassium salt, if susceptibility to radiolysis were dependent on the manner in which the crystals were prepared or on the impurities they contained, and if conditions during the irradiations such as temperature could be chosen to minimize decomposition.

The decompositions produced by Co^{60} γ-rays were measured because it was expected that the

(1) (a) G. E. Boyd, J. W. Cobble and S. Wexler, *J. Am. Chem. Soc.*, **74**, 237 (1952); (b) J. W. Cobble and G. E. Boyd, *ibid.*, **74**, 1282 (1952).

(2) G. E. Boyd and J. W. Cobble, *J. Phys. Chem.*, **63**, 919 (1959).

dependence of these on the absorbed dose, etc., would afford a basis for comparison with the more complex radiolytic effects produced by neutron reactor radiations to be reported in a subsequent paper. In addition, Co^{60} γ-radiations are preferred for fundamental studies, because the methods for radiation dose measurement on them are well established in contrast to the situation with respect to the dosimetry of pile radiations where appreciable uncertainty persists.

There are no publications which report other than the formation of bromide in the radiolysis of the alkali metal bromates, or which attempt to give a mechanism for their radiation decomposition. The production of chloride, hypochlorite and chlorite has been observed in preliminary investigations of the decomposition of $KClO_3$ by X-rays,[3] and recently Co^{60} γ-rays have been reported to give chlorite, chloride and oxygen gas.[4] A radiolytic chlorite yield of 1.2 molecules per 100 e.v. was observed, which could be reduced to 0.8 on heating the irradiated salt at 200°. The conversion of chlorite to chloride and oxygen was reported to be responsible for the yield reduction. The radiolysis of the molecular chlorate ion was interpreted as proceeding through intermediate ClO_3 free radicals which decomposed either to chlorite or to chloride.

Experimental

Preparation of Anhydrous Compounds.—The lithium, sodium and potassium bromates employed were either spectrochemically pure commercial products or reagent grade chemicals. Rubidium and cesium bromate were synthesized starting with the pure carbonates or with CsCl. Procedures described elsewhere[5] were followed. Thallium bromate was prepared by a double decomposition reaction between $TlNO_3$ and $KBrO_3$. The $TlNO_3$ was made by dissolving thallium metal (American Platinum Works) in concentrated nitric acid and recrystallizing once from water containing HNO_3 to minimize hydrolysis. The slightly soluble $TlBrO_3$ formed was separated by filtration and washed twice with cold water.

The bromide contents of the alkali metal salts were reduced to acceptably low levels (Table I) by recrystallizations from water. All compounds were dried in air at 110° and stored away from light in closed vessels. The formation of $LiBrO_3 \cdot H_2O$ was prevented by storing the anhydrous salt over a desiccant; further, the loading of samples into paraffin-sealed glass-stoppered vials for irradiation was conducted in a dry box. The crystals appeared to be stable over many months, excepting $TlBrO_3$ which decomposed slowly on standing in air. Both $RbBrO_3$ and the $CsBrO_3$-1 preparations were found to be quite free from the other alkali metals by flame spectrophotometric analysis. The $CsBrO_3$-2 preparation, however, was contaminated with 4.6% potassium and 0.73% rubidium by weight.

Characterization of the Alkali Metal Bromate Preparations.—Results from several measurements to characterize the alkali metal bromate preparations described above are summarized in Table I. The melting points listed in column 3 were determined by differential thermal analysis (DTA) techniques using a heating rate of 9.5 degrees per minute. Good agreement with literature values for $RbBrO_3$ and $CsBrO_3$ was obtained, but not with $NaBrO_3$ (381°) and $KBrO_3$ (434°). No melting point temperature for $LiBrO_3$ has been reported hitherto. The DTA studies showed that no phase transitions occurred in any of the alkali metal bromates below their melting points. Above 200° the decomposition of the compounds was accompanied by the evolution of heat, and above their melting points the reaction became strongly exothermic. This behavior is consistent with the standard heats, ΔH^0_{dec}, for decomposition to alkali bromide and oxygen gas.

The standard free energies of decomposition, ΔF^0_{dec}, (Table I, col. 5) were derived from estimations of the free energies of formation, ΔF^0_f, based on calorimetric measurements of the heats of solution of the crystalline bromates.[5] The ΔF^0_{dec}. values reveal that all of the salts are thermodynamically unstable at 298.1°K. Despite this instability the crystals did not decompose at an appreciable rate until they were heated well above their melting points. This behavior suggests that the thermal decomposition of bromate must occur with an appreciable activation energy.

Columns 6 and 7, Table I, summarize published information to be employed later in this paper on the crystal symmetry and X-ray density of the alkali metal bromates. Anhydrous $LiBrO_3$, whose structure previously was unknown, was demonstrated as orthorhombic in a special study. X-Ray diffraction powder patterns were taken on all of the preparations, and an excellent agreement with the N.B.S. Circular 539 crystal constants was obtained. The structures of $KBrO_3$, $RbBrO_3$, $CsBrO_3$ and $TlBrO_3$ were hexagonal-(trigonal) and hence these compounds are isomorphous.

Irradiation of Samples.—The irradiations were conducted in the 10.5″ × 10.5″ × 12″ cavity of the ORNL Cobalt Storage Facility where dose rates of 3.4 to 5.1 × 10^{16} e.v. $g.^{-1}$ $sec.^{-1}$ in water were observed during the period of our investigations. The temperature of the chamber was uniform and varied between 80 and 105°. The thermal decomposition of the crystalline bromates was negligibly small at 105°. Approximately 5-g. amounts of salt contained in glass-stoppered, 1.15-cm. diameter by 4.0 cm. high glass vials were irradiated at the center of the floor of the chamber in a fixed geometry arrangement. Dose rate measurements were made for almost every irradiation. Irradiations at −195° were performed in 500-ml. stoppered wide-mouth Dewars filled with liquid nitrogen. The samples were suspended in the center of the bath.

Three other Co^{60} irradiation facilities were employed in studies of the dose rate dependence of the radiolysis: nominal 300,[6] 1100 and 10,000[7] curie sources giving dose rates in water of 1.22 × 10^{15}, 7.45 × 10^{15} and 1.08 × 10^{17} e.v. $g.^{-1}$ $sec.^{-1}$, respectively.

Dosimetry.—Gamma-ray dose rate measurements were made with approximately 0.025 *M* ceric sulfate solutions 0.4 *M* in H_2SO_4.[8] This solution was prepared from carefully purified reagents and water and was "aged" by heating overnight at 90°. It was stored away from light and was stable over many months.[9] In the measurements 15 ml. was placed in glass tubes (2.5 cm. diameter by 4.5 cm. deep) which were closed-off with Bakelite screw-top caps. Dose rates were computed from the equivalents of Ce(IV) reduced, as determined by potentiometric titration with standardized $FeSO_4$ solutions, and the yield values (eq. per 100 e.v.) given by the equation:[10] $G(CeIII) = 2.35 + 0.37(Ce(IV))^{1/3}$, which holds for concentrations from 10^{-4} to 10^{-1} *M*. The reduction of the initial Ce(IV) concentration by radiation varied from 20 to 60%.

The precision of the dose rate measurements (including the reproducibility of the exposure geometry) appeared to lie between one and three per cent. as indicated by results obtained at frequent intervals.

The precision of the analytical determinations of the amounts of Ce(IV) reduced was about 0.2%. The reliability of the Ce(IV) dosimetry measurements was established by periodic comparisons with the dose rate obtained with the ferrous sulfate (Fricke) dosimeter.

Analysis for Radiolytic Products.—Weighed amounts usually (*ca.* 1.0 g.) of irradiated crystals were analyzed for bromide ion after dissolving them in distilled water containing excess 0.1 *N* sodium arsenite and allowing the solution to stand for at least 30 min. After making up to 25.00-

(3) H. G. Heal, *Can. J. Chem.*, **31**, 91 (1953).

(4) A. S. Bakerkin, "The Action of Ionizing Radiation on Inorganic and Organic Systems," Moscow, Acad. Sci. U.S.S.R. Press, 1958, p. 187.

(5) G. E. Boyd and F. Vaslow, *J. Chem. Eng. Data*, in press.

(6) J. A. Ghormley and C. J. Hochanadel, *Rev. Sci. Instr.*, **22**, 473 (1951).

(7) W. Davis, Jr., "The Chemical Technology Division Co^{60} Source," ORNL-CF-60-3-82, March, 1960.

(8) S. I. Taimuty, L. H. Towle and D. L. Peterson, *Nucleonics*, **17**, 103 (1959).

(9) J. T. Harlen and E. J. Hart, *ibid.*, **17**, 102 (1959).

(10) C. J. Hochanadel, private communication, June, 1959.

TABLE I

CHARACTERIZATION OF ALKALI METAL BROMATE PREPARATIONS

Salt	Residual bromide content (p.p.m.)	M.p., °C.	$\Delta H°$dec. kcal. mole^{-1}	$\Delta F°$dec.	Crystal structure: Symmetry	Crystal structure: X-Ray density
$LiBrO_3$-1; -2	19; <5	254	+1.5	−19.2	Orthorhombic[a]	3.766
$NaBrO_3$	40	355	−4.1	−22.7	Cubic[b]	3.325
$KBrO_3$-1; -2	40; 9	396	−5.7	−23.7	Hexagonal[c]	3.256
$RbBrO_3$-1; -2	25; <6	426	−4.0	−22.3	Hexagonal[d]	3.919
$CsBrO_3$-1; -2	14; <5	420	−4.7	−23.6	Hexagonal[e]	4.306
$TlBrO_3$	26	..	...	....	Hexagonal[f]	6.188
$Ba(BrO_3)_2$	55	288	...	....	.....	...

[a] J. H. Burns, private communication, October, 1960; *Acta Cryst.*, in press (1961). [b] N. B. S. Circular 539, **5**, 65 (1955). [c] *Ibid.*, **7**, 38 (1957). [d] *Ibid.*, **8**, 60 (1958). [e] *Ibid.*, **8**, 18 (1958). [f] *Ibid.*, **8**, 45 (1958).

ml. volume three (or more) aliquots were titrated micropotentiometrically with 0.01 *N* (or 0.1 *N*) $AgNO_3$ which had been compared with a standardized NaBr solution. The amounts of bromide ion found were expressed in p.p.m. (*i.e.*, μg. Br/g. $MBrO_3$). A small, usually negligible, correction was made for bromide in the crystals before irradiation (Table I). The foregoing procedure measures the total non-bromate bromine produced by radiolysis. Bromite, hypobromite and bromine which may have been formed either in the crystal or on dissolution were reduced by arsenite to bromide before titration. The bromide analyses therefore give the number of bromate ions decomposed, and total yields were calculated on this basis. The precision of the analyses usually was better than ±0.2% as shown by numerous determinations in triplicate. The method was checked by standard addition techniques.

Titrations were conducted in a number of cases without added arsenite to permit estimations of the yield for the direct formation of bromide ion. The precision of these determinations was less than when excess AsO_2^- was present.

Total oxidizing fragments produced by radiolysis (bromite, hypobromite, etc.) were determined by adding weighed quantities of irradiated salt to an excess of 0.1000 *N* sodium arsenite solution containing bicarbonate buffer and back-titrating with standardized 0.1009 *N* iodine solution.

The amount of bromite formed was measured following a procedure based on the work of Chapin.[11] Here, *ca.* 0.5 g. of irradiated bromate was dissolved in a solution containing 1 ml. of 5% phenol and sufficient NaOH to give an excess of at least 0.1 *N*. Within 10 sec. standardized arsenious oxide was added in an amount sufficient to give an excess of at least 0.2 meq. After 5 min. 0.2 g. of $NaHCO_3$ was added, and then a 10% solution of acetic acid was added slowly with constant agitation to the point of free effervescence. Excess arsenite was titrated immediately with standardized iodine solution. The phenol in this procedure acted preferentially to consume all hypobromite so that the arsenite oxidized was equivalent, presumably, to the amount of bromite present. The amount of hypobromite plus bromine was estimated from the difference between the total oxidizing power shown by the irradiated crystals and the amount of bromite found.

Aqueous dissolution methods for the analysis of the radiolysis products are limited in that the primary radiolytic products may differ greatly from the species formed and detected on dissolving irradiated crystals in water. Accordingly, infrared absorption and X-ray diffraction examinations were carried out, but, unfortunately, the sensitivity of these techniques was too low; as much as 5% decomposition of bromate was required to distinguish an irradiated from an unirradiated crystal. Thus, $CsBrO_3$-1 radiolyzed to 7.3 mole % decomposition showed characteristic powder diffraction lines of CsBr; however, $LiBrO_3$ and $KBrO_3$ in which 0.3 and 2.1 mole % bromide had been produced showed no diffraction lines attributable to LiBr or KBr, respectively. In the infrared studies pellets containing *ca.* 1% by weight radiolyzed $KBrO_3$ mixed into "infrared" quality KBr were examined with a Beckman IR-7 spectrometer. The strong absorption band for BrO_3^- ion at 795 cm.$^{-1}$ was found to decrease with increased radiation dose. Unidentified weaker bands at 875, 1025 (broad) and 1085 cm.$^{-1}$ caused by irradiation were observed in addition.

(11) R. M. Chapin, *J. Am. Chem. Soc.*, **56**, 2211 (1934); L. Farkas and M. Lewin, *Anal. Chem.*, **19**, 662, (1947).

Isothermal Decomposition of the Alkali Metal Bromates.—A number of auxiliary experimental studies were conducted to give a basis for an interpretation of the observed radiolytic decompositions. One of these involved the measurement of the isothermal decomposition rates in air of $LiBrO_3$, $KBrO_3$-2 and $CsBrO_3$-2 in experiments where *ca.* 5 g. of crystals in a porcelain boat were heated at various temperatures between 150 and 350° in a tube furnace controlled to ±2°. The decomposition to form bromide at a given temperature increased linearly with time and the rates, *k* (p.p.m. hr.$^{-1}$), when plotted as log *k* *vs.* $1/T$ gave parallel straight lines whose slopes corresponded to an apparent activation energy, E_a, of 40 ± 2 kcal. mole^{-1}.[12] This value is approximately the same as the dissociation energy for the Br–O bond. The thermal decomposition rates at constant temperature were: $LiBrO_3 > KBrO_3 > CsBrO_3$. An aliquot of $KBrO_3$ heated for 24 hr. at 325° was titrated for oxidizing power and none was found; the thermal decomposition appeared to go entirely to bromide and oxygen gas.

Role of Surface Area in Thermal and Radiolytic Decomposition.—A possible dependence of radiolysis on surface was investigated using the $RbBrO_3$-1 preparation which was obtained in large crystals. An aliquot was pulverized and irradiated together with some of the original preparation to a dose of 0.478 × 10^{23} e.v. mole^{-1}: 668 ± 4 and 671 ± 1 p.p.m. Br^- ion were produced, respectively, indicating that the extent of surface was unimportant. In another experiment $KBrO_3$-2 was irradiated to a dose of 5.51 × 10^{23} e.v. mole^{-1} to give a decomposition of 1.15 mole %. A measurement of its specific surface by krypton gas adsorption at −195° gave 0.022 m.^{2} g.$^{-1}$; the same $KBrO_3$ before irradiation showed an area of 0.0225 ± 0.0005 m.^{2} g.$^{-1}$. A surface area determination on an aliquot of $KBrO_3$-2 heated at 322° for 16 hr. to give a 1.19 mole % decomposition gave 0.0364 ± 0.0020 m.^{2} g.$^{-1}$ suggesting, in contrast to radiolysis, that pyrolysis occurred on external surfaces.

Determination of Oxygen Gas in Irradiated Salts.—The irradiated salts were found to evolve gas in perceptible quantities when they were dissolved in water. Accordingly, several quantitative measurements (Table II) were made of the amounts of oxygen released using a gas chromatographic method. Extensively irradiated crystals were placed in a closed vessel connected with a vacuum line and were dissolved in de-gassed water after the system had been evacuated. The gases liberated were transferred under low pressure (<5 mm.) to a Perkin–Elmer Model 154C chromatograph with which a separation and determination of oxygen was performed using an 8-ft. column of Linde Type 5A Molecular Sieves at 100°. Blank determinations with unirradiated samples gave 13 to 19 μl./g. (STP) of gas which appeared to be occluded air because a nitrogen "peak" was noted also. The gas yields reported in Table II may be low; the salts measured were irradiated in air and some oxygen may have escaped from the crystals.

Optical and Electron Microscope Examinations of Irradiated $CsBrO_3$-1.—A series of eight samples of variously irradiated $CsBrO_3$-1 showing decompositions from 0.3 to 7.34 mole % were examined under an optical microscope at 1000× magnification using dark-field illumination. Significant changes in appearance with increasing dose were observed: (a) initially the crystals were translucent and of

(12) Recent observations on the rate of decomposition of bromate in molten salts have given 42 kcal. mole^{-1} for E_a: F. R. Duke and W. W. Lawrence, *J. Am. Chem. Soc.*, **83**, 1269 (1961).

TABLE II

GAS YIELDS FROM RADIOLYZED ALKALI METAL BROMATES

Salt	E.v. absorbed/mole × 10^{-23}	μl. O_2/g.	Mmoles O_2 / Mole BrO_3^-	$G(O_2)$, molecules / 100 e.v.	$G(BrO_3^-)$, molecules / 100 e.v.
$LiBrO_3$-1	9.84	453 ± 10	2.725	0.17	0.32
$KBrO_3$-2	11.99	3571 ± 58	26.60	1.29	1.07
$CsBrO_3$-1	16.22	6757 ± 13	78.61	2.92	2.73

regular geometric shape, but, at 1.14% decomposition, they became "milky" and the surfaces appeared "soft." For larger doses the crystals became opaque and appeared to be filled with a large number of minute bubbles. The bubbles (or light-scattering centers) were less than 0.1 μ in diameter; (b) no shattering of the crystals to give smaller particles was observed as reported for irradiated $KClO_4$[3] except with the most highly irradiated sample where an internal fragmentation seemed to occur. These observations appear to be consistent with the lack of change in surface area with irradiation noted above. Gas bubble formation has been reported to occur in the radiolysis of alkali metal nitrates,[13] and pressures of several hundreds of atmospheres in them have been estimated.

Formation of Oxidizing Species in Radiolysis.—The intermediate oxidation states of bromine appeared to be formed in significant yields (Table III). The value, "G(Ox.)," for the yield[14] of the oxidizing fragments may be compared with the yield for bromate decomposition, $G(BrO_3^-)$, and with the yield for the direct formation of bromide, $G(Br^-)$. It may be noted that "G(Ox.)" and the average oxidation number decreased with the absorbed dose and for approximately equal doses were dependent on the alkali metal cation in the salt. The average oxidation number for $LiBrO_3$ appeared to correspond closely with that expected for an equimolar mixture of hypobromite and bromite, but with the other salts the formation of bromite seemed to be favored relatively.

TABLE III

FORMATION OF OXIDIZING SPECIES IN ALKALI METAL BROMATE RADIOLYSIS

Salt	Dose (e.v. mole^{-1} × 10^{-23})	"Oxidizing power" (meq. mole^{-1})	"Av. oxidation no."	Radiolytic yields (molec./100 e.v.) "G(Ox.)"	$G(Br^-)$	$G(BrO_3^-)$
$LiBrO_3$-2	6.44	6.70	2.0	0.21	0.13	0.33
$NaBrO_3$	0.491	2.69	2.8	.87	.65	1.52
$NaBrO_3$	5.30	16.4	2.4	.55	.98	1.52
$NaBrO_3$	6.06	20.8	2.3	.64	.88	1.48
$KBrO_3$-2	0.547	3.01	2.8	.87	.83	1.61
$KBrO_3$-2	5.90	15.0	2.4	.46	1.07	1.53
$KBrO_3$-2	6.56	15.5	2.5	.41	.97	1.35
$RbBrO_3$-2	9.99	49.1	2.6	.82	1.02	1.85
$CsBrO_3$-1	16.22	45.3	2.4	.49	2.23	2.73

The amount of bromite formed in the $CsBrO_3$-1 preparation (Table III) was determined as 8.2 mmole mole^{-1} following the Chapin procedure. The amount of hypobromite, estimated from the difference between the total "oxidizing power" (45.3 meq. mole^{-1}) and that by the bromite (32.6 meq. mole^{-1}) assuming no other oxidizing species were present, was 6.4 mmole mole^{-1}. The yield values, $G(BrO_2^-)$ and $G(BrO^-)$, were 0.30 and 0.24, respectively.

The color of the irradiated salts varied from light yellow to gold with increasing dose absorbed. A gentle heating virtually bleached the color and this change was accompanied by a nearly complete reduction in the oxidizing power of the crystals (Table IV). Interestingly, the bromate decomposition, measured as total bromide after the addition of excess arsenite in the standard procedure, decreased slightly suggesting that while most of the oxidizing fragments decomposed to give bromide (and oxygen gas) a small fraction must have re-formed bromate. The "direct" bromide contents of the irradiated crystals (no arsenite) increased after heating. A measurement of the infrared absorption by the annealed crystals also showed that the weak, γ-ray induced bands at 875 and *ca.* 1025 cm.$^{-1}$ noted earlier had been removed.

The *p*H of 0.14 *M* aqueous solutions formed by dissolving unirradiated, irradiated and annealed $CsBrO_3$-2 in 25 ml. of freshly boiled triple-distilled water were 7.2, 9.4 and 6.8, respectively. Dissolution of equal weights of irradiated and unirradiated $LiBrO_3$-2 in water gave solutions (0.74 *M*) with *p*H's of 5.3 and 9.3, respectively. The alkalinity increase, however, may not be ascribed solely to the reaction of trapped electrons with water to give hydrogen gas and OH^- ion as in experiments with irradiated $Ba(NO_3)_2$.[15] Hypobromite ion was formed in amounts easily sufficient to produce the observed alkalinity.

Experimental Results

Treatment of Data.—The measured decompositions determined as p.p.m. Br^- were converted to a mmole Br^- per mole alkali metal bromate to place the various salts on a comparable basis. The absorbed doses were estimated as follows: (a) The total dose (e.v. g.$^{-1}$) in ceric sulfate was computed from the measured dose rate and the time of irradiation, which was determined with good accuracy; (b) the dose absorbed by a given salt (e.v. g.$^{-1}$) was found by multiplying the "ceric sulfate dose" by the ratio of the electrons per gram for the salt to that for the dosimeter solution (3.346 × 10^{23}), and this result was multiplied by the molecular weight of the salt to give the dose as e.v. mole^{-1}. The employment of an "electron per gram ratio" for the conversion factor may be less accurate than the use of the ratio of the respective energy absorption mass attenuation coefficients at 1.25 Mev. for the ceric sulfate dosimeter and the salt. The ratios of the latter conversion factor to the former for $CsBrO_3$ and for $LiBrO_3$, for example, are 1.084 and 0.988, respectively. A more serious error in absorbed dose estimates with Co^{60} γ-rays may arise if low energy scattered radiation is present inside the source.[16] Because of the strong energy dependence of the absorption of low energy γ-rays by high Z elements, much more dose may be absorbed by them than will be estimated from the average energy. The absence of significant amounts of soft radiation in the source used in this work was demonstrated by experiments wherein duplicate samples of dosimeter solution, $LiBrO_3$-2 and $RbBrO_3$-2, were irradiated with and without a 6-mm. lead sheath surrounding the samples. This thickness was sufficient to remove most of the low energy component. Photoelectrons from the lead were absorbed in 3.2 mm. of aluminum between the sample and the lead. The observed ratios of decomposition yield in the shielded to the unshielded sample irradiated simultaneously were 0.596, 0.589 and 0.593 for the Ce(IV) dosimeter, $LiBrO_3$ and $RbBrO_3$, respectively.

The yields for the radiolytic decomposition of bromate ion (G_0 values in molecules per 100 e.v. absorbed) in the various alkali metal salts were derived from the *initial* slopes of the curves in

(13) G. Hennig, R. Lees and M. S. Matheson, *J. Chem. Phys.*, **21**, 664 (1953).

(14) The difference in the titers of the radiolyzed salts for bromide ion with and without added arsenite gave the number of mmoles bromine per gram associated with the oxidizing fragments. The ratio of the "oxidizing power" (meq./g.) to the mmoles Br/g. so determined will give the change in the bromine oxidation number relative to bromide, and hence the "average oxidation number" of the oxidizing fragments in the crystal lattice.

(15) A. O. Allen and J. A. Ghormley, *J. Chem. Phys.*, **15**, 208 (1947).

(16) W. Bernstein and R. H. Schuler, *Nucleonics*, **13**, [11], 110 (1955).

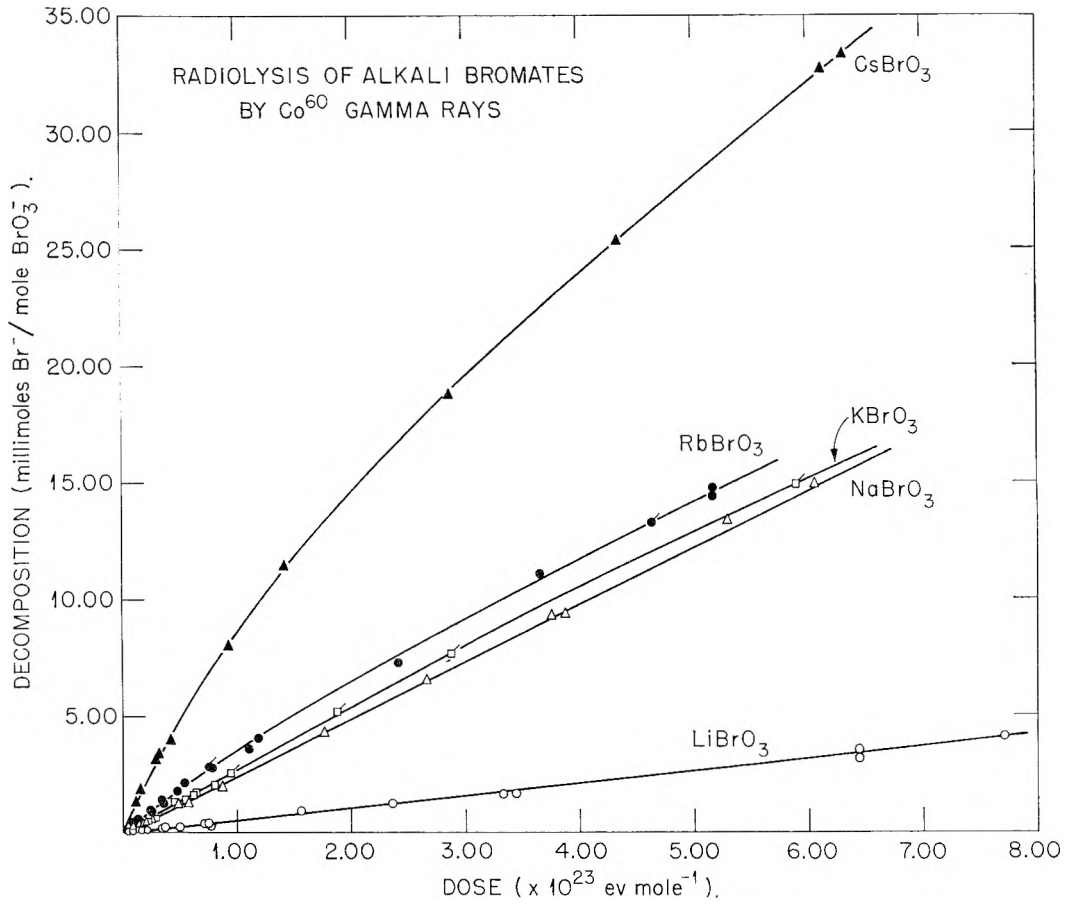

Fig. 1.—Radiolysis of the alkali metal bromates by Co^{60} γ-rays (symbols with "flags" for second preparations of salt).

Table IV

Thermal Annealing of Oxidizing Species in Radiolyzed Alkali Metal Bromates

Salt	Dose (e.v. mole^{-1} × 10^{-23})	"Oxidizing power" (meq. mole^{-1}) Initial	"Oxidizing power" (meq. mole^{-1}) After heating	Total bromide content (mmole Br$^-$ mole^{-1}) Initial	Total bromide content (mmole Br$^-$ mole^{-1}) After heating	Direct bromide content (mmole Br$^-$ mole^{-1}) Initial	Direct bromide content (mmole Br$^-$ mole^{-1}) After heating
$NaBrO_3$	5.30	16.4	0.34[a]	13.4	11.8[a]	8.64	11.6[a]
$KBrO_3$-2	5.90	15.0	1.2[a]	15.0	14.7[a]	10.5	14.8[a]
$CsBrO_3$-2	13.8	65.6	3.6[b]	60.5	54.6[b]	...	...

[a] Heated 20 min. at 300°. [b] Heated 1 hr. at 250°.

Fig. 1 and are plotted in Fig. 3. Numerical values for these slopes were taken from least squares fits which were made to a linear equation for the data on $LiBrO_3$ and $NaBrO_3$, and on $KBrO_3$ except at large doses. The dose dependences of the decomposition of the other alkali metal salts were sufficiently non-linear that the data were better fitted by an equation of the form: $y = k_1x/(1 + k_2\sqrt{x})$, where y is the decomposition and x is the absorbed dose.

Qualitative Features of the Radiolytic Decompositions.—As may be observed in Fig. 1 and 2, the radiation decompositions uniformly increased with dose, and there were no discontinuities in this dependence in contrast to the reported behavior with the alkali metal nitrates.[17,18] The decomposition increase with dose was linear initially; however, above about 1 mole % radiolysis the increase was less rapid with $RbBrO_3$ and $CsBrO_3$ and possibly with $KBrO_3$. A strong dependence on the nature of the cation may be noted, there being at least a ten-fold difference in yield between the cesium and lithium salts. In some cases electron structure may have been important: $TlBrO_3$, for example, appeared to be much more decomposed than $RbBrO_3$ with which it is isomorphic. No difference between $^7LiBrO_3$ and $LiBrO_3$ was found, but the actual difference in isotopic composition was not large, so that if a small isotope effect in radiolysis existed it probably would not have been detected. No apparent dependence on the crystal preparation was observed with the lithium or rubidium bromates where two independent syntheses were performed. The $CsBrO_3$-1 preparation differed significantly from $CsBrO_3$-2 (Tables IV and VI); much of this can be attributed to the inadvertent contamination of the latter with potassium, however.

Temperature Dependence of Radiolysis.—Measurements of radiolytic yields at liquid nitrogen tem-

(17) J. Cunningham and H. G. Heal, *Trans. Faraday Soc.*, **54**, 1355 (1958).

(18) E. R. Johnson and J. Forten, *J. Phys. and Chem. Solids*, **15**, 218 (1960).

perature and at *ca.* 85° for the same absorbed dose are compared in Table V. The decomposition was greater at the higher temperature and the increase appeared the largest for $LiBrO_3$. Considering the appreciable temperature interval (*ca.* 280°), however, the augmentation was quite small. Small temperature coefficients also have been observed over the same temperature range for the radiolysis of the alkali metal nitrates.[17] It was of particular interest, furthermore, to observe that the formation of oxidizing products in the radiolysis of $NaBrO_3$ and $KBrO_3$-2 was greater at −195° than at 85°. The ratios of the yield at the higher to that for the lower temperature were 0.87 and 0.73, respectively.

TABLE V

TEMPERATURE DEPENDENCE OF RADIOLYSIS OF ALKALI METAL BROMATES

Salt	Temp. (°C.)	Dose, e.v. mole^{-1} × 10^{-23}	Decomposition Mmoles Br^-/ Mole BrO_3^-	Molec./ 100 e.v.	$G(85°)/G(-195°)$
$LiBrO_3$-1	85	0.363	0.256	(0.42)	
	−195	.363	.172	.29	1.37 ± 0.14
$LiBrO_3$-1	85	.753	.408	.33	
	−195	.753	.327	.26	
$NaBrO_3$	85	.150	.361	1.45	
	−195	.150	.251	1.01	1.35 ± 0.09
$NaBrO_3$	85	.491	1.235	1.52	
	−195	.491	0.980	1.20	
$KBrO_3$-2	85	.167	.476	1.72	
	−195	.167	.368	1.33	
$KBrO_3$-2	85	.457	1.360	1.79	
	−195	.457	1.064	1.40	
$KBrO_3$-2	85	.547	1.465	1.61	1.23 ± 0.13
	−195	.547	1.313	1.45	
$KBrO_3$-2	85	.615	1.628	1.59	
	−195	.615	1.490	1.45	
$KBrO_3$-2	85	.947	2.560	1.63	
	−195	.947	1.883	1.20	
$RbBrO_3$-2	85	.762	2.700	2.14	1.47
	−195	.762	1.837	1.45	
$CsBrO_3$-1X	75	.903	5.424	3.62	1.16
	−195	.903	4.678	3.12	
$Ba(BrO_3)_2$	95	.373	1.188	1.92	1.12 ± 0.01
	−195	.373	1.063	1.72	

Dose Rate Dependence of Radiolysis.—Measurements were conducted to determine if, for a constant total dose, the radiolysis was dependent on the dose rate. The results with $CsBrO_3$-2 (Table IV) indicate only a small dependence as the dose rate was increased by 85-fold.

TABLE VI

DOSE RATE DEPENDENCE OF THE RADIOLYSIS OF $CsBrO_3$-2

(Dose = 0.831 × 10^{23} e.v./mole $CsBrO_3$)

Dose rate (e.v. g.$^{-1}$ sec.$^{-1}$)	Decomposition (mmoles Br^-/mole BrO_3^-)	$G(BrO_3^-)$ molecules/100 e.v.
8.86 × 10^{14}	4.637	3.36
5.46 × 10^{15}	4.436	3.21
3.21 × 10^{16}	4.672	3.38
7.51 × 10^{16}	4.903	3.55

Discussion

Correlations of Susceptibility to Radiolysis.—From the data presented in Table I and in Fig. 1

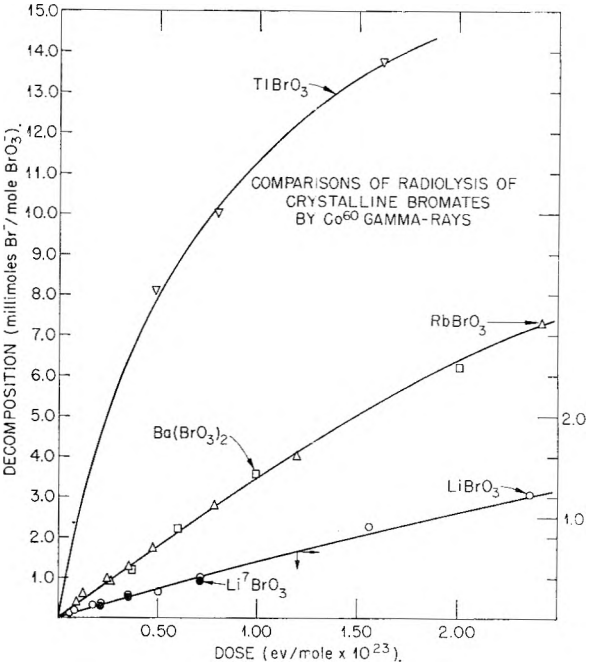

Fig. 2.—Comparisons of radiolysis of crystalline bromates for small doses.

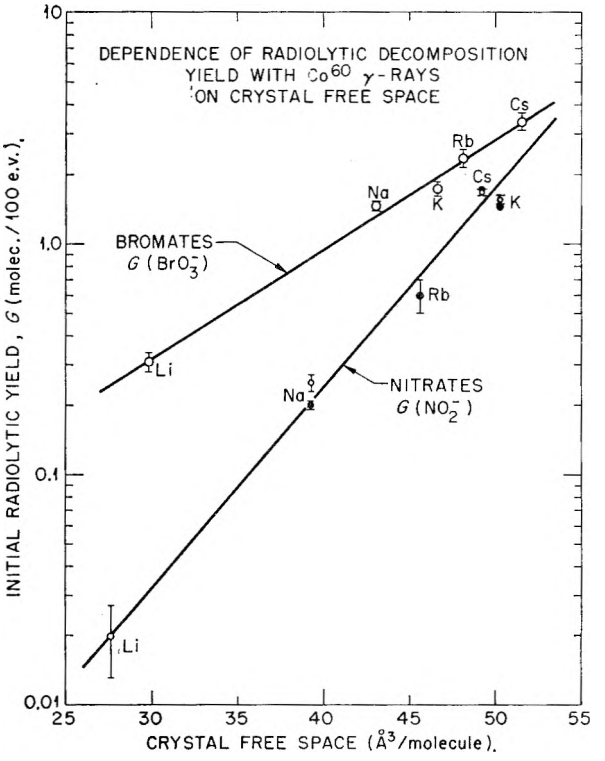

Fig. 3.—Dependence of initial radiolytic yields on "crystal free space." (Data for nitrates from ref. 21, open circles; and from ref. 22, filled circles.)

it may be concluded that no correlation exists between the radiolytic yield and either the standard free energy of formation of the alkali metal bromates or the standard free energy for their decomposition to bromide and oxygen gas. The ΔF^0_{dec} values for the salts differ slightly, whereas their G_0 values for decomposition vary by an order of magnitude. This lack of parallelism is, of course, not surprising

when it is remembered that radiolysis is a rate and not an equilibrium process.

The lack of a similarity in the mechanisms governing the rates of thermal and radiation decomposition perhaps is more interesting. The evidence for a difference may be summarized: (a) Thermal decomposition occurs with an appreciable activation energy (*ca.* 40 kcal. mole^{-1}) while radiolysis, at least up to *ca.* 100°, is almost temperature independent. (b) The order for increasing the thermal decomposition rate at a given temperature was $LiBrO_3 > KBrO_3 > CsBrO_3$, whereas the reverse order held for radiation decomposition. (c) Thermolysis produced an increase in the surface, but no detectable change in area occurred in the radiolyzed crystals. Further, radiolytic yield did not appear to depend on particle size. (d) The alkali metal bromates are colored by exposure to γ-rays, and oxidizing fragments are produced in them. No coloration nor oxidizing fragments were observed in the thermally decomposed compounds. The foregoing observations have led to the view that thermal decomposition takes place largely at the crystal surface, possibly through the formation of nuclei of alkali metal bromide followed by an interface reaction between this product and bromate. Radiolysis, in contrast, must occur mainly at random in the crystal lattice or possibly in the vicinity of defects.

Support for the hypothesis that the mode of radiolytic decomposition of the alkali metal bromates must be dependent on crystal lattice properties has been found in the apparent correlation of their initial yields (G_0 values) with the "crystal free space." The latter quantity[18] may be defined as the difference between the volume per mole of crystal derived from the X-ray density and the volume per mole of constituent ions. The "free space" volumes per molecule of alkali metal bromate plotted in Fig. 3 were estimated using the densities in Table I. The volume per bromate ion was computed as 28.7 Å.^{3} from the Br–O bond distance[19] and the radius[20] of Br^{+5}. The volumes of the alkali metal cations were derived from the accepted crystal radii. The "free space" in the alkali metal nitrate crystals was estimated in a similar manner using a volume of 19.6 Å.^{3} for the nitrate ion. Initial radiolytic yield values at 25° for the decomposition of the nitrates by Co^{60} γ-rays were taken from two independent sources.[21,22] The exponential dependence (Fig. 3) of G_0 on the "free space" over a ten-fold range for the alkali metal bromates and over nearly 100-fold for the nitrate is of interest because it emphasizes the importance of crystal environment to radiolytic processes. Furthermore, the existence of such an empirical relationship might be expected from an elementary model for the dependence. However, the correlation noted in Fig. 3 may be subject to limitations: For example, the G_0 value for $TlBrO_3$, which possesses nearly the same "free space" as $RbBrO_3$, was much higher than expected from Fig. 3. Additionally, the G_0 for $AgNO_3$ has been found[17] to fall below the smooth curve relating the alkali metal nitrates, whereas the curve for the alkaline earth nitrates lies above the latter. On the other hand, the high G_0 value observed with $TlBrO_3$ may have been caused in part by the thermal decomposition of this highly unstable compound, and it has been suggested[17] that the low value for $AgNO_3$ results from the efficient trapping and degradation of energy by silver ions.

The apparent exponential dependence of G_0 on crystal free space is reminescent of the well-known exponential dependence of reaction rates in solution on pressure.[23] The analogy between these processes and the case in hand is re-enforced by the observation that the disruption of a bromate ion to yield bromide plus three oxygen atoms gives a 37.3 Å.^{3} volume increase. Alternatively, decomposition to give oxygen molecules would be accompanied by a volume increase of 58.6 Å.^{3} per ion. The amount of activation energy required for the diffusion of radiolytic oxygen from the site of decomposition should be proportional to the strain it causes in the crystal; this strain, for a given volume increase, will be the greater the smaller the interstitial space in the lattice and the greater the crystal binding.

State of Dissociation and Fate of Absorbed Energy.—The first step in the radiolytic process, of course, is the absorption of energy which subsequently can be utilized in a chemical process. For small decompositions it seems reasonable to assume that the break-up of excited or ionized bromate ions occurs at widely separated lattice sites in the crystal; otherwise, it is difficult to understand the apparent importance of the crystal "free-space" noted above. Exciton migration to lattice defects or special trapping centers where a preferred decomposition of bromate might occur would afford an alternative mechanism. This alternative is regarded as an unlikely one, however, because an exceptionally large defect concentration would be required to sustain the initial radiolytic rate, which is estimated as 4.7×10^{15} bromate ions per cm.^{3} per sec. in $CsBrO_3$-1 exposed to a dose rate of 3.2×10^{16} e.v. g.$^{-1}$ sec.$^{-1}$. If, for example, the energy required to produce a lattice vacancy at room temperature is taken as one e.v., the concentration of Schottky defects will be only 4×10^5 per cm.^{3}.

An appreciable fraction of the electronically excited bromate ions formed in the lattice must decompose. Thus, for $CsBrO_3$-1 it can be estimated that roughly 30 e.v. of energy is absorbed per BrO_3^- ion. If the first excited electronic state of the ion lies at 4.6 e.v. above the ground state, as is indicated by the strong optical absorption band at 2700 Å. found with aqueous solutions, then at least 15% of the excited bromates decompose.

Mechanism of Decomposition of the Molecular Bromate Ion.—Assuming that the γ-ray energy

(19) "Interatomic Distances," The Chemical Society, London, 1958.

(20) L. H. Ahrens, *Geochim. Cosmochim. Acta*, **2**, 155 (1952).

(21) C. J. Hochanadel and T. W. Davis, *J. Chem. Phys.*, **27**, 333 (1957).

(22) J. Cunningham, *J. Phys. Chem.*, **65**, 628 (1961).

(23) S. Glasstone, K. Laidler and H. Eyring, "The Theory of Rate Processes," McGraw-Hill Book Co., Inc., New York, N. Y., 1941, pp. 470–474.

absorbed divides approximately equally into exciting and ionizing bromate ions, the primary radiolytic act may be depicted as

$$BrO_3^- \xrightarrow{h\nu} BrO_3^{-*} \quad (1A)$$

$$BrO_3^- \xrightarrow{h\nu} BrO_3 + e^- \quad (1B)$$

The decomposition reactions following excitation are, then, formally

$$BrO_3^{-*} \longrightarrow BrO_2^- + O, \text{ or, } BrO_2 + O^- \quad (2A)$$

$$BrO_3^{-*} \longrightarrow BrO^- + O_2 \quad (2B)$$

$$BrO_3^{-*} \longrightarrow Br^- + O + O_2 \quad (2C)$$

Abstraction reactions

$$BrO_3^- + O \longrightarrow BrO_2^- + O_2(g), \quad (3)$$

recombination reactions

$$O + O \longrightarrow O_2(g) \quad (4A)$$

$$BrO_2^- + O_2 \longrightarrow BrO_3^- + O \quad (4B)$$

and thermal decomposition reactions

$$BrO_2^- \longrightarrow Br^- + O_2 \quad (5)$$

must be considered in addition because of their possible role in determining the net yields of gas and oxidizing fragments.

The experimental evidence bearing on the occurrence of these reactions may be examined

(1) The analytical determinations of oxidizing fragments, of bromite and hypobromite in radiolyzed $CsBrO_3$-1 and of bromide by argentiometric titration and by X-ray diffraction suggest that reactions 2A-C, inclusive, may occur. Bromite and hypobromite, which were observed only in aqueous solutions, may have been formed by the reaction of trapped bromate (or other) free radicals with water on dissolving the radiolyzed crystals. The formation of a relatively large number of free radicals would have been required, however, and it seems more likely that BrO_2^- and BrO^- were present in the crystal instead. For example, the average oxidation number of the oxidizing bromine species in the crystals was much lower (*e.g.*, 2.0 to 3.0 meq./mmole) than that expected (*e.g.*, 6.0 meq./mmole) if bromate free radicals or if BrO_2 were present (Table III). It was assumed in (2A-C) that negatively charged bromine species and neutral oxygen atoms were formed. The electron affinities[24] for atomic bromine (3.54 e.v.) and oxygen (2.34 e.v.) are such as to favor the formation of Br^- and O rather than Br + O^-. Values for the other bromine oxidation states are unknown, but, if their electron affinities are nearly the same as for ClO_2 and ClO, respectively, then BrO_2^- and BrO^- will be favored over BrO_2 and BrO.

(2) The abstraction reaction 3 would be expected to be temperature and dose rate dependent. The over-all bromate decomposition, however, appeared to be almost independent of these variables (Tables V and VI), so that it must be concluded that the formation of BrO_2^- *via* (3) was relatively minor.

(3) The occurrence of reaction 4A is supported by the fact that oxygen gas is released either on dissolving or heating the radiolyzed crystals, and by the observation of microscopic bubbles of gas formed in the body of the crystals. Oxygen atoms are sufficiently small (*ca.* 12 Å.[3] per atom) that they should diffuse through the crystal easily. The concentration of uncombined atoms should be extremely small; reaction (4A) is highly exothermic.

(4) Reactions 4B and 5 have been postulated to explain the fact that radiolytically produced oxidizing fragments in the crystal can be removed by thermal annealing. Reaction 4B must have occurred to a relatively minor extent as only a small fraction of the fragments recombined to give bromate on heating. Reaction 5 may only represent the net of reaction 2A to give BrO_2 + O^- followed by

$$BrO_2 \longrightarrow Br + O_2 \quad (5A)$$

$$Br + O^- \longrightarrow Br^- + O \quad (5B)$$

Bromine dioxide is known to be quite unstable and to exist only below −40°.

(5) It will be assumed that reaction 4B can proceed by radiation excitation of the trapped O_2 molecules (exciton transfer) held under high pressures within the crystals. This reaction would account, at least in part, for the non-linear dependence of bromate ion radiolysis on dose (Fig. 1) for large absorbed doses. Evidence for this kind of a radiation annealing reaction has been published recently[25]: a KBr pellet was irradiated in an atmosphere of dry oxygen with 1.5 Mev. electrons to a dose of about 10^{21} e.v. g.$^{-1}$ and examined for its infrared absorption. In addition to an absorption band at 1440 cm.$^{-1}$ (which could have been from KBrO) the principal band for $KBrO_3$ at 795 cm.$^{-1}$ was observed. The potential importance of exciton trapping by radiolytic products in determining the kinetics of the radiation decomposition of solids has been pointed out already.[17] The presence of these processes in the alkali metal bromates must be recognized.

Acknowledgments.—It is a pleasure to acknowledge the assistance given by several members of the ORNL Analytical Chemistry Division in various phases of our researches: D. E. LaValle for the synthesis of the $^7LiBrO_3$, $RbBrO_3$ and $CsBrO_3$ preparations and C. A. Pritchard for the flame photometric analysis of the latter two compounds; C. M. Boyd for the DTA and TGA examinations and R. Sherman for the X-ray powder pattern identifications of all the salts; A. S. Myers and I. Rubin for the micro-oxygen analyses on the irradiated crystals; T. E. Willmarth for the optical and electron microscope studies and C. A. Horton for the preliminary infrared measurements.

(24) H. O. Pritchard, *Chem. Revs.*, **52**, 529 (1953).

(25) A. R. Jones, *Science*, **127**, 234 (1958).

DISSOCIATION CONSTANT OF 2-AMMONIUM-2-METHYL-1,3-PROPANEDIOL IN WATER FROM 0 TO 50° AND RELATED THERMODYNAMIC QUANTITIES

BY HANNAH B. HETZER AND ROGER G. BATES

National Bureau of Standards, Washington 25, D. C.

Received September 16, 1961

The base 2-amino-2-methyl-1,3-propanediol, like the closely related compound tris-(hydroxymethyl)-aminomethane, is a solid substance of considerable use as a biological buffer material. The acidic dissociation constant, K_{bh}, of the substituted ammonium ion conjugate to the free base now has been determined at 11 temperatures from 0 to 50° by measurement of the electromotive force of hydrogen–silver chloride cells without liquid junction. The results are given as a function of the temperature (T) in °K. by the equation $-\log K_{bh} = 2952.00/T - 2.2652 + 0.0039092T$. The standard changes of free energy, enthalpy, entropy and heat capacity for the dissociation process have been calculated from the temperature coefficient of the dissociation constant. For the acidic dissociation of 2-ammonium-2-methyl-1,3-propanediol at 25°, the following results were obtained: $\Delta G^0 = 50{,}238$ j. mole^{-1}, $\Delta H^0 = 49{,}860$ j. mole^{-1}, $\Delta S^0 = -1.3$ j. deg.$^{-1}$ mole^{-1}, and $\Delta C_p^0 = -45$ j. deg.$^{-1}$ mole^{-1}. For the basic dissociation of 2-amino-2-methyl-1,3-propanediol at 25°, the corresponding quantities are $\Delta G^0 = 29{,}656$ j. mole^{-1}, $\Delta H^0 = 6720$ j. mole^{-1}, $\Delta S^0 = -76.9$ j. deg.$^{-1}$ mole^{-1}, and $\Delta C_p^0 = -150$ j. deg.$^{-1}$ mole^{-1}.

Introduction

The dissociation constant of the protonated acid form of 2-amino-2-(hydroxymethyl)-1-,3-propanediol, known also as tris-(hydroxymethyl)-aminomethane, from 0 to 50° was determined recently in this Laboratory.[1] This base is obtainable in highly pure form and has been employed extensively as an acidimetric standard and in the preparation of buffer solutions of particular use in biological studies in the *p*H range 7 to 9. The related compound, 2-amino-2-methyl-1,3-propanediol, also a solid at room temperature, is a water-soluble aminoglycol which has found some use as a biological buffer. As might be expected, it is a stronger base than tris-(hydroxymethyl)-aminomethane. The negative logarithm of the basic dissociation constant of this compound has been found from *p*H measurements with the glass electrode to be 5.24 at 25°.[2]

The acidic dissociation constant of 2-ammonium-2-methyl-1,3-propanediol ion in water now has been determined by the electromotive force method over the temperature range 0 to 50°. The changes of free energy, enthalpy, entropy and heat capacity for the dissociation of the free base and its conjugate acid have been derived from the change of the dissociation constant with temperature.

Method

The electromotive force method used[3,4] is essentially that devised by Harned and Ehlers[5] for the study of acetic acid. It has been modified as necessary to apply it to bases in whose solutions the silver–silver chloride electrode has an appreciable solubility. A cell without liquid junction was employed

Pt; H_2(g, 1 atm.)$(HOCH_2)_2C(CH_3)NH_3Cl(m_1)$, $(HOCH_2)_2C(CH_3)NH_2(m_2)$, AgCl; Ag

where m_1 and m_2 represent the molalities of 2-ammonium-2-methyl-1,3-propanediol chloride and that of the corresponding free base, respectively.

The base reacts with the silver–silver chloride electrode (to form the silver–amine complex) to such an extent that cell vessels with large-bore stopcocks separating the electrode compartments were required.[3] Since the stopcock was opened only at the time of measurement, diffusion of silver ion to the hydrogen electrodes was largely prevented, as evidenced by the absence of a gray deposit of silver on the hydrogen electrodes at the conclusion of the experiments.

The dissociation of 2-ammonium-2-methyl-1,3-propanediol ion may be formulated as

$$BH^+ + H_2O \rightleftarrows B + H_3O^+ \qquad (1)$$

The general equation for calculating the acidic dissociation constant, K_{bh}, is obtained by combining the mass-law expression for equation 1 with the Nernst equation for the cell and with the Debye–Hückel expression for the activity coefficients (γ_i) of the ions concerned. The resulting equations are

$$-\log K_{bh}' \equiv -\log K_{bh} - \beta I = p(a_H \gamma_{Cl}) + \log \frac{m_{BH^+}}{m_B} - \frac{2A\sqrt{I}}{1 + Ba^*\sqrt{I}} \qquad (2)$$

where

$$p(a_H \gamma_{Cl}) \equiv -\log (\gamma_H \gamma_{Cl} m_H) = \frac{E - E^0}{2.30259RT/F} + \log m_{Cl} \qquad (3)$$

In these equations, E and E^0 are the e.m.f. and standard potential of the cell, A and B are Debye–Hückel constants, I is the ionic strength, and a^* and β are adjustable parameters of which the former is termed the "ion size parameter." It is evident in equation 2 that K_{bh}' is an "apparent" dissociation constant which becomes equal to the true K_{bh} at an ionic strength of zero.

In the application of these equations to the data obtained for approximately equimolal buffer solutions of 2-amino-2-methyl-1,3-propanediol and its hydrochloride, two corrections were considered. First, the computation of $p(a_H \gamma_{Cl})$ by equation 3 may have to take into account the increase in m_{Cl} in the vicinity of the silver–silver chloride electrode resulting from the formation of the amine–silver complex ion, and second, allowance for the effect of hydrolysis on the equilibrium concentrations of B and BH^+ in the second term on the right of equation 2 may have to be made.

To derive m_{BH^+}/m_B from m_1/m_2, corrections for hydrolysis were made with the aid of hydroxyl ion concentrations estimated directly from the e.m.f. and the dissociation constant of water in the manner suggested in an earlier paper.[6] In the extreme case, however, the correction amounted to only 0.0005 in $\log K_{bh}'$.

The increase of m_{Cl} in the immediate vicinity of the silver–silver chloride electrode is equal to the molality of diammine–silver complex formed in the reaction

$$AgCl + 2B \rightleftarrows AgB_2^+ + Cl^- \qquad (4)$$

The true molality of chloride was calculated at 0, 25 and 50°

(1) R. G. Bates and H. B. Hetzer, *J. Phys. Chem.*, **65**, 667 (1961).

(2) S. Glasstone and A. E. Schram, *J. Am. Chem. Soc.*, **69**, 1213 (1947).

(3) R. G. Bates and G. D. Pinching, *J. Research Natl. Bur. Standards*, **42**, 419 (1949).

(4) R. G. Bates and G. D. Pinching, *ibid.*, **46**, 349 (1951).

(5) H. S. Harned and R. W. Ehlers, *J. Am. Chem. Soc.*, **54**, 1350 (1932).

(6) R. G. Bates, G. L. Siegel and S. F. Acree, *J. Research Natl. Bur. Standards*, **31**, 205 (1943).

from m_1, the solubility product constants of silver chloride,[7] and values of K_f (the stability constant of the diammine–silver complex ion) derived from measurements of the solubility of silver chloride in 0.1 M solutions of the base. The calculation has been described by Bates and Pinching.[3] For $m_1 = m_2 = 0.1$, the correction increases $p(a_H \gamma_{Cl})$ by only 0.0006 at 0°, 0.0010 at 25°, and 0.0014 at 50° above the values calculated on the assumption that $m_{Cl} = m_1$. For $m_1 = m_2 = 0.15$, the correction is 0.0011 at 50°. The effect of solubility is therefore almost, but not quite, negligible.

The following values of log K_f were found by solubility measurements

0°	log K_f = 7.79
25°	6.90
50°	6.18

Datta and Grzybowski[8] assumed that the ammine complex forms in two steps and, by a titration procedure, obtained log $K_1 = 3.20$ and log $K_2 = 3.67$ for the successive stability constants at 25°. The sum of these two figures (6.87) is in good agreement with the value 6.90 found by us.

Experimental

Electromotive force measurements were made of 19 buffer solutions in four series. Each series of solutions was prepared by diluting a stock solution made by combining standard hydrochloric acid, the solid base and carbon dioxide-free water. Before the cells were filled, the solutions in each series were deaerated with purified hydrogen saturated with water vapor. The preparation of the acid and the electrodes, the sequence of the e.m.f. measurements, and other details have been described previously.[1,3,9]

The free base, 2-amino-2-methyl-1,3-propanediol,[10] was recrystallized three times from reagent-grade methanol, dried first in a stream of dry nitrogen at room temperature and then in a vacuum oven at 55°, and stored over calcium chloride. The melting point was 111° with a rate of heating of approximately 1.5° min.$^{-1}$. The material assayed 100.0 ± 0.1% when titrated with the standard solution of hydrochloric acid, precautions being taken to minimize access of carbon dioxide. The end-point, calculated from the approximately known strength of the base, was taken as pH 5.0 for a solution 0.05 M at the equivalence point. Adjustment to the end-point was made with the aid of a pH meter with a glass electrode.

Results

The e.m.f. values listed in Table I are the averages of the readings of two hydrogen–silver chloride electrode combinations in the same cell, corrected as usual to a partial pressure of 1 atm. of dry hydrogen. The average difference between the duplicate readings at 25° was 0.02 mv.

Values of $-\log K_{bh}'$ were calculated by equation 2 for several values of a^*. The value $a^* = 0$ gave a straight line plot at all temperatures and therefore was used for the evaluation of $-\log K_{bh}$. The extrapolation lines for 0, 25 and 50° are shown in Fig. 1. The best rectilinear fit of the calculated values of $-\log K_{bh}'$ was obtained with the aid of the IBM 704 computer.

The values of $-\log K_{bh}$ (the intercepts at $I = 0$), together with the standard deviations of the intercepts (σ_i) and values of K_b, are summarized in Table II. The basic dissociation constant, K_b, was obtained from K_{bh} by the relation

$$K_b = K_w/K_{bh} \qquad (5)$$

where K_w is the ion product constant for water.[11]

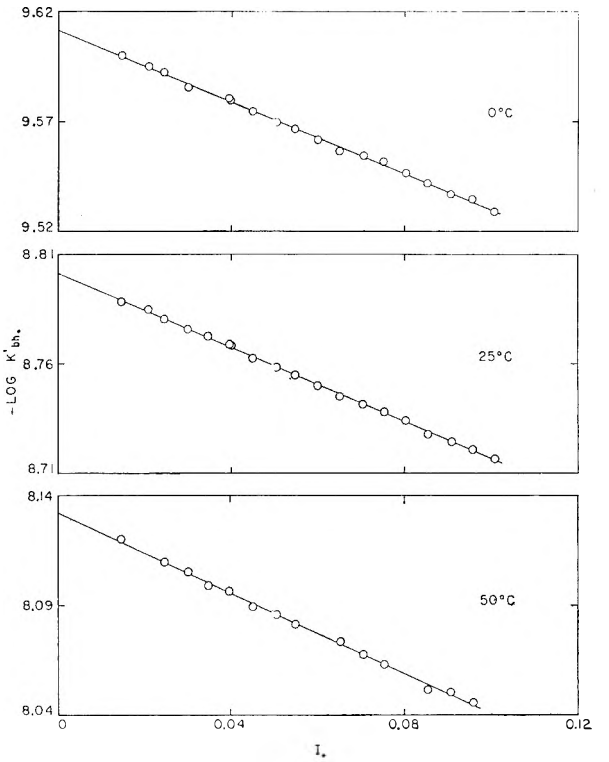

Fig. 1.—Plots of $-\log K'_{bh}$ at 0, 25 and 50° as a function of ionic strength. The value $a^* = 0$ was used in equation 2.

The value of $-\log K_{bh}$ at 25° (8.801) may be compared with 8.76 computed from $pK_b = 5.24$ obtained by Glasstone and Schram,[2] and with 8.799 listed by Datta and Grzybowski.[8] While this work was under way, the authors learned that Everett and Timimi[12] have recently completed the measurement of $-\log K_{bh}$ for this base. Their value at 25°, obtained by an e.m.f. method that differs somewhat from that used in this work, is 8.790.

The optimum buffer range of 2-amino-2-methyl-1,3-propanediol is approximately pH 7.8 to 9.8. Gomori[13] pointed out that buffers formed by partially neutralizing aqueous solutions of this base with hydrochloric acid are of considerable use in many biological studies, as they do not precipitate calcium and do not inhibit the action of enzymes. This buffer system has been used successfully by London and Hudson[14] in studies of the activity of uricase.

Thermodynamic Constants.—The values of $-\log K_{bh}$ given in Table II were fitted to the Harned–Robinson equation,[15] the constants being determined by the IBM 704 digital computer. The following result, valid from 0 to 50°, was obtained

$$-\log K_{bh} = \frac{2952.00}{T} - 2.2652 + 0.0039092T \qquad (6)$$

(7) B. B. Owen and S. R. Brinkley, Jr., *J. Am. Chem. Soc.*, **60**, 2233 (1938).

(8) S. P. Datta and A. K. Grzybowski, *J. Chem. Soc.*, 1091 (1959).

(9) R. G. Bates, "Electrometric pH Determinations," John Wiley and Sons, Inc., New York, N. Y., 1954, pp. 166, 167, 205, 206.

(10) Supplied through the courtesy of Dr. John A. Riddick of Commercial Solvents Corp.

(11) H. S. Harned and B. B. Owen, "The Physical Chemistry of Electrolytic Solutions," 3rd Ed., Reinhold Publ. Corp., New York, N. Y., 1958, Chap. 15.

(12) B. A. Timimi, Thesis, Bristol, 1960; D. H. Everett, private communication.

(13) G. Gomori, *Proc. Soc. Exptl. Biol. Med.*, **62**, 33 (1946).

(14) M. London and P. B. Hudson, *Biochim. et Biophys. Acta*, **21**, 290 (1956).

(15) H. S. Harned and R. A. Robinson, *Trans. Faraday Soc.*, **36**, 973 (1940).

TABLE I

ELECTROMOTIVE FORCE OF THE CELL: Pt;H_2(g, 1 atm.), $(HOCH_2)_2C(CH_3)NH_3Cl(m_1)$, $(HOCH_2)_2C(CH_3)NH_2(m_2)$, AgCl; Ag, FROM 0 TO 50° (IN V.)

m_1	m_2	0°	5°	10°	15°	20°	25°	30°	35°	40°	45°	50°
0.10060	0.10149	0.82400	0.82256	0.82113	0.81958	0.81785	0.81623	.....	.....	.....	.....	.....
.09558	.09561	.82490	.82350	.82207	.82055	.81888	.81711	0.81523	0.81324	0.81116	0.80903	0.80674
.09051	.08951	.82560	.82433	.82290	.82136	.81971	.81793	.81611	.81415	.81210	.80994	.80769
.08503	.08760	.82779	.82644	.82505	.82352	.82190	.82023	.81829	.81639	.81432	.81219	.81000
.07998	.08069	.82854	.82717	.82583	.82432	.82273	.82110	.81907	.....	.....	.....	.....
.07502	.07505	.82965	.82833	.82695	.82551	.82393	.82223	.82042	.81850	81655	.....	.81220
.07031	.06954	.83059	.82935	.82796	.82653	.82495	.82329	.82155	.81964	.81767	.81560	.81340
.06490	.06686	.83298	.83189	.83059	.82914	.82763	.82597	.82430	.82247	.82044	.81848	.81642
.05982	.06035	.83416	.83288	.....	.....	.....	.82719	.....	.....	.....	.....	.....
.05477	.05479	.83576	.83458	.83333	.83198	.83053	.82891	.82728	.82548	.82356	.82159	.81945
.05033	.04978	.83712	.83599	.83476	.83342	.83197	.83041	.82875	.82696	.82512	.82316	.82105
.04491	.04627	.84036	.83922	.83805	.83672	.83538	.83388	.83224	.83050	.82864	.82677	.82477
.03987	.04022	.84233	.84120	.84000	.83869	.....	.83599	.83429	.....	.....	.....	.....
.03958	.04077	.82499	.84195	.84085	.83954	.83820	.83669	.83515	.83347	.83168	.82978	.82787
.03460	.03461	.....	.84380	.84275	.84155	.84024	.83885	.83729	.83562	.83388	.83203	.83005
.02999	.02966	.84746	.84653	.84550	.84437	.84309	.84164	.84020	.83862	.83695	.83517	.83324
.02458	.02532	.85259	.....	.....	.....	.....	.84709	.84574	.84421	.84255	.84085	.83905
.02093	.02112	.85540	.85435	.85349	.....	.....	.85023	.....	.....	.....	.....	.....
.014602	.014607	.86267	.86193	.86115	.86028	.85929	.85800	.85696	.85561	.85418	.85268	.85096

TABLE II

SUMMARY OF VALUES FOR K_{bh} AND K_b FROM 0 TO 50°

t, °C.	$-\log K$	σ_i	$-\log K_b$
0	9.6116	0.0011	5.331
5	9.4328	.0013	5.301
10	9.2658	.0010	5.269
15	9.1049	.0011	5.241
20	8.9508	.0010	5.216
25	8.8013	.0007	5.195
30	8.6588	.0014	5.174
35	8.5193	.0011	5.161
40	8.3854	.0014	5.150
45	8.2569	.0016	5.139
50	8.1322	.0012	5.130

where T is the absolute temperature. The average difference between "observed" $-\log K_{bh}$ values and those calculated by equation 6 was 0.0008 unit.

By applying the usual thermodynamic formulas to equation 6 the changes of free energy, ΔG^0; of enthalpy, ΔH^0; of entropy, ΔS^0; and of heat capacity, ΔC_p^0 which accompany the dissociation of 1 mole of the substituted ammonium ion (BH^+) in the standard state were calculated. The results are summarized in Table III.

TABLE III

THERMODYNAMIC QUANTITIES FOR THE ACIDIC DISSOCIATION OF 2-AMMONIUM-2-METHYL-1,3-PROPANEDIOL (BH^+) FROM 0 TO 50°

t, °C.	ΔG^0, j. mole^{-1}	ΔH^0, j. mole^{-1}	ΔS^0, j. deg.$^{-1}$ mole^{-1}	ΔC_p^0, j. deg.$^{-1}$ mole^{-1}
0	50,253	50,930	2.5	−41
5	50,243	50,720	1.7	−42
10	50,236	50,510	1.0	−42
15	50,233	50,300	0.2	−43
20	50,234	50,080	−0.5	−44
25	50,238	49,860	−1.3	−45
30	50,246	49,640	−2.0	−45
35	50,258	49,410	−2.8	−46
40	50,274	49,180	−3.5	−47
45	50,293	48,940	−4.3	−48
50	50,317	48,700	−5.0	−48

The corresponding thermodynamic quantities for the basic dissociation of the amine B can be derived by combining these results with comparable data for the dissociation of water,[16] as suggested by equation 5. In this way, one finds

$$-\log K_b = \frac{1519.33}{T} - 3.8194 + 0.013144T \quad (7)$$

from which these quantities are obtained at 25°

Process: $B + H_2O = BH^+ + OH^-$

$\Delta G^0 = 29{,}656$ j. mole^{-1}
$\Delta H^0 = 6{,}720$ j. mole^{-1}
$\Delta S^0 = -76.9$ j. deg.$^{-1}$ mole^{-1}
$\Delta C_p^0 = -150$ j. deg.$^{-1}$ mole^{-1}

The thermodynamic quantities at 25° given in Table III are in excellent agreement with the values found by Everett and Timimi,[12] as the following comparison demonstrates

	ΔG^0, j. mole^{-1}	ΔH^0, j. mole^{-1}	ΔS^0, j. deg.$^{-1}$ mole^{-1}	ΔC_p^0, j. deg.$^{-1}$ mole^{-1}
Everett and Timimi[12]	50,176	49,724	−1.5	−46
This investigation	50,238	49,860	−1.3	−45

Although the error in determining ΔG^0 should not exceed 10 j. mole^{-1} in either investigation, the difficulties in establishing accurate values of the first and second derivatives of $\log K_{bh}$ with respect to temperature endow the other thermodynamic quantities with larger uncertainties, estimated to be as follows: ΔH^0, ± 150 j. mole^{-1}; ΔS^0, ±1.0 j. deg.$^{-1}$ mole^{-1}; and ΔC_p^0, ±5 j. deg.$^{-1}$ mole^{-1}.

Discussion

The sixfold increase in basic strength resulting from the replacement of one hydroxymethyl group of "tris" by methyl is easily understood in terms of the known electron-attracting properties of the hydroxyl group.[2] This diminution of basic strength with progressive substitution of OH groups perhaps is best observed in the series of ethanolamines.[4,17,18]

Certain qualitative conclusions also can be drawn

(16) R. A. Robinson and R. H. Stokes, "Electrolyte Solutions," 2nd Ed., Academic Press, Inc., New York, N. Y., 1959, p. 363.

(17) V. E. Bower, R. A. Robinson and R. G. Bates, *J. Research Natl. Bur. Standards*, to be published.

(18) R. G. Bates and G. F. Allen, *ibid.*, **64A**, 343 (1960).

by comparing the changes of entropy and heat capacity for the dissociation process with the alteration in gross structural features of the amine molecule.[1] Everett and his co-workers[19,20] and Evans and Hamann[21] have considered these matters in some detail and have been able to identify several factors that appear to be of primary importance in determining the sign and magnitude of the thermodynamic quantities associated with the ionization process.

The most illuminating comparisons, however, utilize the *changes* of these quantities upon passing from one member to the next in a series of compounds of similar structure. An interpretation of the differences between tris-(hydroxymethyl)-aminomethane and 2-amino-2-methyl-1,3-propanediol therefore should be postponed until similar data for all four members of this series are available. The base with one hydroxyl group, namely, 2-amino-2-methyl-1-propanol, has been studied recently by Everett and Timimi,[12] and a similar study of the last member of the series (*t*-butylamine) already has been undertaken in this Laboratory.

(19) D. H. Everett and B. R. W. Pinsent, *Proc. Roy. Soc.* (London), **215A**, 416 (1952).

(20) D. H. Everett, D. A. Landsman and B. R. W. Pinsent, *ibid.*, **215A**, 403 (1952).

(21) A. G. Evans and S. D. Hamann, *Trans. Faraday Soc.*, **47**, 34 (1951).

RARE EARTH CHELATE STABILITY CONSTANTS OF SOME AMINOPOLYCARBOXYLIC ACIDS[1]

BY J. L. MACKEY, M. A. HILLER AND J. E. POWELL

Institute for Atomic Research and Department of Chemistry, Iowa State University, Ames, Iowa

Received September 23, 1961

Stability constants of the complexes formed between the rare earths and 1,2-bis-[2-di-(carboxymethyl)-aminoethoxy]-ethane (EGTA) and 2,2′-bis-[di-(carboxymethyl)-amino]-diethyl ether (EEDTA) have been determined by the polarographic and mercury electrode methods at a temperature of 20° and an ionic strength of $\mu = 0.1$. Some of the trends in the stabilities of rare earth aminopolycarboxylate chelates have been discussed.

Introduction

The interaction of lanthanide ions with aminopolycarboxylic acids is of practical interest because the use of chelating agents in conjunction with ion-exchange resins has proved to be an effective method for separating rare earths. Stability constants of individual rare earth chelates indicate the applicability of the respective chelating agents to this separation process. On a theoretical level studies of chelation have been made for the purpose of relating metal–chelate stability to the structure of the chelating agent and to the nature of the metal ion.[2] The tervalent rare earth ions, having the same electronic configuration in the outer orbitals, provide a unique opportunity for study of the effects of ionic size and inner electronic structure on chelate formation.

Studies of stability constants of rare earth aminopolycarboxylate chelates have been limited to ethylenediaminetetraacetic acid (EDTA),[3,4] 1,2-diamino-cyclohexane-N,N,N′,N′-tetraacetic acid (DCTA),[4] N-hydroxyethylethylenediaminetetraacetic acid (HEDTA),[5] nitrilotriacetic acid (NTA),[6,7] and diethylenetriaminepentaacetic acid (DTPA).[8] The present authors have extended the measurement of rare earth chelate stability constants to two additional chelating agents, 1,2-bis-[2-di-(carboxymethyl)-aminoethoxy]-ethane (EGTA) and 2,2′-bis-[di-(carboxymethyl)-amino]-diethyl ether (EEDTA), and have considered some of the trends in rare earth chelate stability sequences. The structures of EEDTA and EGTA are given below. A discussion of these chelating agents as eluents for rare earths has been presented elsewhere.[9]

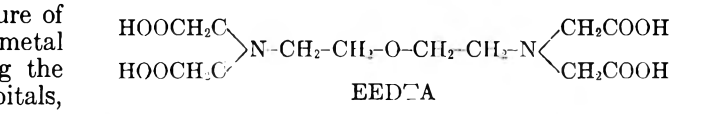

EEDTA

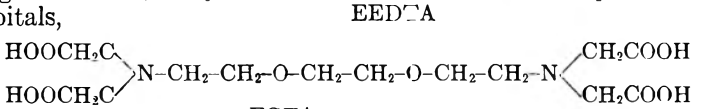

EGTA

Methods of Measurement.—The rare earth aminopolycarboxylate stability constants have been determined generally either by the modified *p*H method[3,5,8] or by a polarographic method.[3-5] Recently the mercury electrode has been used to determine stable chelate constants.[10,11] In the

(1) Contribution No. 955. Work was performed in the Ames Laboratory of the U. S. Atomic Energy Commission.

(2) (a) S. Chaberek and A. E. Martell, "Organic Sequestering Agents," John Wiley and Sons, New York, N. Y., 1959, pp. 124–170; (b) A. E. Martell and M. Calvin, "Chemistry of the Metal Chelate Compounds," Prentice–Hall, Inc., New York, N. Y., 1952.

(3) E. H. Wheelwright, F. H. Spedding and G. Schwarzenbach, *J. Am. Chem. Soc.*, **75**, 4196 (1953).

(4) G. Schwarzenbach, R. Gut and G. Anderegg, *Helv. Chim. Acta*, **37**, 937 (1954).

(5) F. H. Spedding, J. E. Powell and E. J. Wheelwright, *J. Am. Chem. Soc.*, **78**, 34 (1956).

(6) G. Schwarzenbach and R. Gut, *Helv. Chim. Acta*, **39**, 1589 (1956).

(7) G. Anderegg, *ibid.*, **43**, 825 (1960).

(8) R. Harder and S. Chaberek *J. Inorg. & Nuclear Chem.*, **11**, 197 (1959).

(9) J. E. Powell, "Separation of Rare Earths by Ion Exchange" in F. H. Spedding and A. H. Daane, "The Rare Earths," Chap. 5, John Wiley & Sons, New York, N. Y., 1961.

present work the mercury electrode (pHg) was used to determine rare earth chelate stability constants for EEDTA and EGTA. These constants also have been measured independently by the polarographic method.

The pHg Method.—In the pHg method equimolar amounts of rare earth and mercury(II) ions are mixed with an amount of chelating agent equal to about half the sum of the concentrations of the two metal ions. The basic reaction which takes place is shown by eq. I

$$R^{+3} + HgY^{-} \rightleftharpoons RY^{-} + Hg^{2+} \qquad (I)$$

R^{3+} in this equation represents rare earth ion and Y^{4-} is the anion of the aminopolycarboxylic acid H_4Y, which can be either EEDTA or EGTA. The equilibrium constant for reaction I can be written as

$$K_I = \frac{[RY^-][Hg^{+2}]}{[R^{+3}][HgY^-]} = \frac{K_{RY}}{K_{HgY}} \qquad (1)$$

K_I is calculated from the equilibrium concentrations of the four ionic species in 1. The mercury(II) concentration and pH are measured directly and the other concentration terms are evaluated from material balance equations which describe the concentrations of all species in a solution of the two metals and a chelating agent. These equations are

$$[R]_t = [R^{3+}] + 2[R_2Y^{2+}] + [RHgY^+] + \sum_{h=0}^{h} [H_hRY^{h-1}] \qquad (2)$$

$$[Hg]_t = [Hg^{2+}] + 2[Hg_2^{2+}] + [RHgY^+] + \sum_{p=0}^{p} [H_pHgY^{p-2}] \qquad (3)$$

$$[Y]_t = \sum_{h=0}^{h} [H_hRY^{h-1}] + \sum_{p=0}^{p} [H_pHgY^{p-2}] + \sum_{n=0}^{n} [H_nY] + [R_2Y^{2+}] + [RHgY^+] \qquad (4)$$

$$[H]_t = [H^+] - [OH^-] + \sum_{h=0}^{h} h[H_hRY^{h-1}] + \sum_{p=0}^{p} p[H_pHgY^{p-2}] + \sum_{n=0}^{n} n[H_nY] \qquad (5)$$

In their general form these equations are difficult to solve; however, for the chelating agents and circumstances studied here, some of the terms are negligible and may be omitted. The metal chelates considered here are very stable ($K_{RY} > 10^{15}$) and in all cases $K_{HgY} > 10^3 K_{RY}$. Due to these conditions the concentrations of free mercury ions are so small that they do not affect the material balance equations to an appreciable extent. The term $\sum_{n=0}^{n} [H_nY]$ is insignificant due to the high stability of the chelates and the presence of excess metal ions.

For chelating agents of the type studied, it is necessary to consider only singly-protonated metal chelates[12]; however, values for $K_{HMY} = [HMY]/[H][MY]$ were not available for the rare earth chelates studied here. Since protonated chelates are generally fairly strong acids,[12,13] the pH range for the measurement of constants was maintained sufficiently high that these protonated species could be neglected. Species of the form R_2Y and RHgY also were neglected in our calculations. With these simplifications the equations easily were solved for the concentration terms required in (1).

It should be noted that the validity of the above assumptions can be checked easily. If the assumptions are correct, the experimentally determined values of K_{RY} calculated from the simplified material balance equations should be constant in spite of appreciable changes in pH or the composition of the solutions on which the measurements were made.

K_{RY} can be found by applying eq. I, provided K_{HgY} has been determined independently. The mercury–chelate constants (K_{HgY} for EGTA and EEDTA) also were measured with the mercury electrode. The details of the method have been given by Schwarzenbach, *et al.*[11] The values obtained in the present study are reported in Table I along with previously reported values.

Experimental Procedure

Two separate series of solutions were prepared in the case of each chelating agent by mixing proper proportions of standardized solutions of rare earth nitrate, chelating agent, mercuric nitrate and enough potassium nitrate to adjust the ionic strength of each preparation to $\mu = 0.1$. A drop of mercury was added to each solution and all were placed in a constant temperature-bath at 20° for 24 hr. Each solution then was placed in a titration cell and the pH and potential of the mercury electrode were recorded periodically as the pH was varied from 3.5 to 4.5 by addition of KOH. The pH was measured by means of a Beckman G.S. meter using the regular scale. The potential of the mercury electrode was measured with a Rubicon potentiometer and can be represented by the equation

$$E = E_0' + S/2 \log [Hg^{2+}] \qquad (6)$$

where

$$E_0' = E^0 + E_j + E_j' + S/2 \log \gamma_{Hg}{}^{2+} \qquad (7)$$

In the above equation E^0 is a term that consists of the reduction potential of Hg^{2+} to Hg^0 and the potential of a 0.1 M calomel cell, E_j and E_j' are liquid–liquid junction potentials, and $S = 2.3026RT/F$. E_0' was evaluated by measuring the potential of a solution of known mercury(II) ion concentration at an ionic strength of $\mu = 0.1$ (KNO_3). The equilibrium $Hg + Hg^{2+} \rightarrow Hg_2^{+2}$ must be accounted for. For a detailed description of how E^0 is found, the paper by Schwarzenbach and Anderegg should be consulted.[11]

Polarographic Method.—In this method equimolar amounts of cadmium chelate and rare earth nitrate are combined. The rare earth ion and cadmium then compete for the complexing agent as shown in eq. II. The polarograph is used to measure the concentration of

$$CdY^{2-} + R^{3+} \rightleftharpoons Cd^{2+} + RY^- \qquad (II)$$

uncomplexed cadmium ions in the equilibrated mixture. When the rate of formation and dissociation of the metal chelate is slow, both Cd^{2+} and CdY^- are reduced at the dropping mercury electrode, and a distinct reduction wave is observed for each species. The diffusion current, i_d, of the first wave is proportional to the concentration of free cadmium ion in solution.

The equilibrium constant for eq. II can be written as

$$K_{II} = \frac{[CdY^{2+}][R^{3-}]}{[Cd^{2-}][RY^+]} = \frac{K_{RY}}{K_{CdY}} \qquad (8)$$

(10) C. N. Reilley and R. W. Schmid, *J. Am. Chem. Soc.*, **78**, 5513 (1956).

(11) G. Schwarzenbach and G. Anderegg, *Helv. Chim. Acta*, **40**, 1773 (1957).

(12) G. Schwarzenbach, H. Senn and G. Anderegg, *ibid.*, **40**, 1886 (1957).

(13) J. E. Powell, J. S. Fritz and D. B. James, *Anal. Chem.*, **32**, 954 (1960).

Since the reactants are combined in equimolar quantities, the following expressions hold at equilibrium

$$[RY^-] = [Cd^{2+}] \quad (9)$$

and

$$[CdY^{2-}] = [R^{3+}] = C - [Cd^{2+}] \quad (10)$$

where C is the initial concentration of each reactant. Substituting these quantities into (8) gives

$$K_{II} = \frac{[Cd^{2+}]^2}{(C - [Cd^{2+}])^2} \quad (11)$$

The rare earth-chelate stability constant can be calculated from eq. 12

$$K_{RY} = K_{CdY}\frac{(\%Cd^{2+})^2}{(100 - \%Cd^{2+})^2} \quad (12)$$

Experimental Procedure.—The polarograms were obtained from solutions prepared by mixing 10 ml. of 0.0100 M $R(NO_3)_3$, 10 ml. of 0.0100 M $Cd(NO_3)_2$, 10 ml. of 0.0100 M tetrapotassium salt of the chelating agent, 10 ml. of 0.1 M sodium acetate, 10 ml. of 0.1 M acetic acid and enough potassium nitrate to adjust the ionic strength to $\mu = 0.1$. The mixtures then were diluted to a total volume of 100 ml. The acetic acid–sodium acetate mixture buffered the solutions at a pH of 4.65. After mixing, the solutions were allowed to equilibrate for 24 hr. in a constant temperature bath at 20°.

The measurements were made with a Sargent Model XXI polarograph. The cell was fashioned from a 100-ml. beaker, and a saturated calomel electrode was connected to the cell by a potassium nitrate–agar bridge. Helium or argon was bubbled through the cell prior to making measurements. Reference i_d values were obtained from solutions with 100% uncomplexed cadmium and 100% complexed cadmium. The stability constants were calculated from i_d values by use of eq. 12. The cadmium–EGTA and EEDTA stability constants were determined by the pHg method. The values are based on the mercury–chelate stability constants, and are listed in Table I.

TABLE I

STABILITY CONSTANTS OF THE CADMIUM AND MERCURY CHELATES AT 20° AND IONIC STRENGTH OF $\mu = 0.1$ (KNO_3)

Metal chelate	K_{MY} This work	K_{MY} Lit.[12]
Hg–EEDTA	22.88 ± 0.10	23.09
Hg–EGTA	23.12 ± .12	23.20
Cd–EEDTA	16.64 ± .06	16.27
Cd–EGTA	16.70 ± .10	16.73

Preparation of Solutions.—The EGTA and EEDTA used were obtained from Geigy Industrial Chemicals, Ardsley, New York and were further purified by double recrystallization from ethanol. The solutions of chelating agents were standardized by the following two methods: potentiometric titration with standard potassium hydroxide; and complexometric titration against standard mercuric nitrate solution using the mercury indicator electrode.[14,15]

The rare earths were supplied by the rare earth separation group at the Ames Laboratory of the Atomic Energy Commission and were 99.9% pure or better. Stock solutions of nitrates were prepared by dissolving the respective oxides in nitric acid. Aliquots of each solution were titrated potentiometrically to determine the pH of the neutral equivalence point, and the solutions then were adjusted to that pH. Standardization was done gravimetrically by precipitation with oxalic acid followed by ignition to oxides. Carbonate-free potassium hydroxide was prepared by the method of Powell and Hiller[16] and was standardized against potassium acid phthalate.

Results

The results of the determination of the rare earth–chelate stability constants are listed in Table II. The errors shown for the constants determined by the pHg method are the maximum deviations from the mean of some ten determinations on two series of solutions in the pH range 3.5–4.5. For the polarographic measurements the errors made in the determination of the per cent. uncomplexed metal ion amount to ±2%. This would introduce uncertainties of ±0.08 to ±0.17 in the log K_{RY} values in Table II. The two methods give results of comparable accuracy

TABLE II

STABILITY CONSTANTS OF THE RARE EARTH EGTA AND EEDTA CHELATES AT 20° AND IONIC STRENGTH $\mu = 0.1$ (KNO_3)

Rare earth	EGTA pHg log K_{RY}	EGTA Polar. log K_{RY}	EEDTA pHg log K_{RY}	EEDTA Polar. log K_{RY}
La	15.55 ± 0.20	15.84	16.00 ± 0.20	16.29
Ce	15.70 ± .10	16.06	16.69 ± .10	17.13
Pr	16.05 ± .08	16.17	17.36 ± .06	17.61
Nd	16.28 ± .10	16.59	17.67 ± .10	17.81
Sm	16.88 ± .16	17.25	18.19 ± .08	18.25
Eu	17.10 ± .10	17.77[a]	18.31 ± .10	18.38[a]
Gd	16.94 ± .10	17.50	18.13 ± .08	18.21
Tb	17.27 ± .10	17.80	18.31 ± .10	18.31
Dy	17.42 ± .04	17.84	18.21 ± .20	18.29
Ho	17.38 ± .05	17.90	18.13 ± .10	18.17
Er	17.40 ± .05	18.00	17.99 ± .15	18.18
Tm	17.48 ± .05	17.96	17.83 ± .11	18.01
Yb	17.78 ± .05	18.22	17.85 ± .20	18.06
Lu	17.81 ± .10	18.48	17.75 ± .23	17.92
Y	16.82 ± .05	17.16	17.54 ± .10	17.79

[a] Europium could not be measured *vs.* cadmium because the half-wave potentials of the metals were too close. The value given here was obtained by comparing europium to neodymium, gadolinium and dysprosium.

Discussion

A comparison of the values obtained by the two methods shows that in both cases the polarographic values are higher than those of the pHg method. In the case of EEDTA the two sets of values are within the limits of error, if the uncertainty of the cadmium–chelate stability constant is considered. For EGTA the difference between the two sets of constants is definitely greater than the experimental error. The exact reasons for this difference in the two sets of constants is not clear. A consideration of possible metal acetate complexes of cadmium and the rare earths in the case of the polarographic measurements would tend to increase rather than decrease the difference. It might be noted that Schwarzenbach and Anderegg[11] also have reported a difference between the calcium–EDTA stability constant measured with the mercury electrode and the equally accurate pH method. In any case the relative values of the constants determined by the two methods are in good agreement. Both sets of constants for both ligands show a "gadolinium break" and, in the case of EEDTA, an inflection is apparent in both sets at thulium. The use of the rare earth stability constants in obtaining separation factors in ion-exchange separations depends upon relative values so that either set of constants would suffice.

It is interesting to compare the stability constants of the rare earths with EEDTA and EGTA with the stability constants of other rare earth

(14) C. N. Reilley and R. W. Schmid, *Anal. Chem.*, **25**, 1640 (1953).

(15) J. S. Fritz, M. J. Richard and S. K. Karraker, *ibid.*, **30**, 1347 (1958).

(16) J. E. Powell and M. A. Hiller, *J. Chem. Educ.*, **34**, 330 (1957).

aminopolycarboxylate chelates. The stability sequences for DCTA and EDTA chelates of the rare earths show similar behavior. These constants increase rather regularly with increasing atomic number and decreasing ionic radius. The two sets of constants are nearly parallel with the DCTA constants somewhat higher than those for EDTA. The trend with EGTA resembles that with HEDTA. Both sets of constants reveal an increase in chelate stability from lanthanum to europium; whereupon the values remain nearly constant up to erbium and then increase again from thulium to lutetium. Both the DTPA and EEDTA sequences show an unusual reversal in chelate stability. The heavier rare earth stability constants decline in magnitude and a few become lower than some of the light rare earth stability constants. For DTPA the reversal in chelate stability occurs at dysprosium, while for EEDTA it occurs in the vicinity of europium.

For almost all chelating agents there is a noticeable irregularity in the case of the gadolinium chelate. Spedding, *et al.*,[3] noted this phenomenon in the EDTA constants, and Schwarzenbach and Gut[17] called attention to the "gadolinium break" in the stability sequences of both DCTA and nitrilotriacetate (NTA) chelates. Many other properties of the rare earths also show a discontinuity at gadolinium. The irregularity is marked in both the EGTA and EEDTA rare earth–chelate stability sequences.

It is interesting to note the position of yttrium in stability constant series. In every case it falls below the position it should occupy from a consideration of its ionic radius. Furthermore, its position relative to individual rare earths changes with the chelating agent.

In all stability sequences the constants increase rather regularly up to europium, but beyond europium they increase in some cases and decrease in others. Comparing the regular portions of the rare earth series, the increasing order of stability for the chelating agents is NTA < HEDTA < EDTA $\leq$ EGTA < EEDTA $\leq$ DCTA < DTPA.

Ionic radii are believed to play an important role in determining differences in the chemical behavior of individual rare earths, and a correlation of increasing chelate stability with decreasing ionic radius has been made for the rare earth series.[1,3] A recent discussion by Duncan[18] has shown the theoretical significance of such a correlation. He has treated the formation of complexes in terms of simple electrostatic forces and has shown that the enthalpy change in complex formation is linear with respect to the reciprocal of the metal ion radii within the restricted range of ionic radii found in nature. If the entropy change is negligible compared to ΔH or is a linear function of ΔH, the free energy also will be a linear function of the reciprocal radii of the metal ions. It was not possible to check the requirements on ΔS for linear behavior of the free energy, since precise data regarding entropies of chelation were not available. However, plots of log K *vs.* $1/r$, using the radii values of Templeton and Dauben,[19] show that only DCTA and EDTA approach linear behavior. One of the possible reasons for non-linearity and even reversal of the trend in chelate free energy with ionic radius may be a change in the coördination requirements of the ions within the rare earth series.[3,8] Such a change in coördination requirement would allow a different number of donor sites of the chelating agent to be used. The different types of behavior observed for the rare earths beyond europium thus might be dependent on the structure of the chelating agent, for it would be possible to utilize the changed coördination requirements in some cases and not in others. Another factor that may be significant in the behavior of rare earth chelates is ligand-field stabilization. It has been suggested that a correlation of the stability constants of rare earth chelates should take into account the effect of a ligand field on the inner 4f electrons.[20] Such ligand field stabilization might explain the gadolinium irregularity and the low position of yttrium in the stability sequences. Yttrium with no inner 4f electrons and gadolinium with a half-filled shell would not be stabilized by a ligand field. More studies will be required if these various trends in rare earth chelate stability are to be fully understood.

(17) G. Schwarzenbach and R. Gut, *Helv. Chim. Acta*, **39**, 1589 (1956).

(18) J. F. Duncan, *Australian J. Chem.*, **12**, 356 (1959).

(19) D. H. Templeton and C. H. Dauben, *J. Am. Chem. Soc.*, **76**, 5237 (1954).

(20) L. A. K. Stancley and T. Randall, *Discussions Faraday Soc.*, **26**, 157 (1958).

SYSTEM $CaO-P_2O_5-HF-H_2O$: THERMODYNAMIC PROPERTIES[1]

BY THAD D. FARR AND KELLY L. ELMORE

Division of Chemical Development, Tennessee Valley Authority, Wilson Dam, Alabama

Received September 21, 1961

Thermodynamic data for solutions of the system $CaO-P_2O_5-HF-H_2O$, saturated at 25° with both fluorapatite and calcium fluoride, were used in estimating the activities of water and undissociated phosphoric acid, the activities of the dihydrogen phosphate and calcium ions, and the activity solubility product of fluorapatite.

For that portion of the system $CaO-P_2O_5-HF-H_2O$ where fluorapatite (FA) and calcium fluoride are the solid-phase pair in equilibrium with the solutions,[2] the activity relationships may be written

$$\frac{K_{FA}}{K_{CaF_2}} = \frac{a_{Ca}^{10}\, a_{PO_4}^{6}\, a_F^{2}}{a_{Ca}\, a_F^{2}} \qquad (1)$$

The activity of the phosphate ion is represented by

$$a_{PO_4} = \frac{K_1K_2K_3a_u}{a_H^{3}} \qquad (2)$$

where $K_1K_2K_3$ is the product of the three dissociation constants of orthophosphoric acid and a_u is the activity of undissociated orthophosphoric acid. Substitution yields

$$K_{FA} = \frac{a_{Ca}^{9}\, a_u^{6}\, (K_1K_2K_3)^{6}\, K_{CaF_2}}{a_H^{19}} \qquad (3)$$

Values for the activities of the undissociated phosphoric acid, the calcium ion and the hydrogen ion were estimated from the experimental data[2] relative to composition, vapor pressure and *p*H of the pertinent saturated solutions of the quaternary system at 25°. Values for the three dissociation constants of phosphoric acid have been published.[3] The solubility product of calcium fluoride, 1.612×10^{-10}, was calculated from free energy values.[4]

Experimental values of the basic thermodynamic variables and derived values for parameters of the several functional relationships are given in Tables I and II and Figs. 1 through 4.

TABLE I

LIQUID PHASES IN EQUILIBRIUM WITH THE SOLID-PHASE PAIR FLUORAPATITE AND CALCIUM FLUORIDE AT 25°

P_2O_5, %	m_P	CaO, %	m_{Ca}	F, %	*p*H	Vapor pressure, mm.	Activity[a] of water, a_1
5.73	0.8862	1.330	0.2604	0.002	1.76	23.60	0.9933
9.70	1.6080	2.159	.4530	.004	1.55	23.28	.9798
12.97	2.2856	2.860	.6379	.005	1.41	22.97	.9667
16.00	2.9961	3.562	.8442	.035	1.28	22.61	.9516
17.91	3.4883	3.917	.9656	.019	1.20	22.31	.9390
20.01	4.0804	4.377	1.1297	.027	1.11	22.03	.9272
23.01	5.0255	4.965	1.3725	.008	0.96	21.45	.9028
24.38	5.4973	5.144	1.4681	.012	.89	21.20	.8923
25.78	6.0226	5.466	1.6162	.024	.81	20.78	.8746

[a] $a_1 = p/p_0$, where p_0 is 23.76 mm., the vapor pressure of pure water at 25° determined with the same null-point mercury isoteniscope used for the saturated solutions (ref. 2).

(1) Presented before the Division of Physical and Inorganic Chemistry, 132nd National Meeting of the American Chemical Society, New York, N. Y., September 1957.

(2) T. D. Farr, G. Tarbutton and H. T. Lewis, Jr., *J. Phys. Chem.*, **66**, 318 (1962).

(3) $K_{H_3PO_4} = 7.145 \times 10^{-3}$; R. G. Bates, *J. Research Natl. Bur. Standards*, **47**, 127 (1951). $K_{H_2PO_4} = 6.339 \times 10^{-8}$; R. G. Bates and S. F. Acree, *ibid.*, **30**, 129 (1943). $K_{HPO_4} = 4.73 \times 10^{-13}$; N. Bjerrum and A. Unmack, *Kgl. Danske Videnskab. Selskabs, Mat.-fys. Medd.*, **9**, 5 (1929).

(4) National Bureau of Standards Circular 500, U. S. Govt. Printing Office, Washington, D. C., 1952.

TABLE II

THERMODYNAMIC PROPERTIES OF SOLUTIONS SATURATED WITH FLUORAPATITE AND CALCIUM FLUORIDE AT 25°

a_{H_2O}	$a_{H_2PO_4}$	$a_{H_3PO_4}$	c_{Ca}	*p*H	pK_{FA}	$K_{FA} \times 10^{121}$
0.9933	0.209	0.506	0.061	1.76	120.859	1.4
.9798	.276	1.050	.097	1.55	120.908	1.2
.9667	.321	1.755	.134	1.41	120.815	1.5
.9516	.357	2.653	.185	1.28	120.831	1.5
.9390	.374	3.391	.222	1.20	120.905	1.2
.9272	.394	4.369	.288	1.11	120.845	1.4
.9028	.419	6.339	.447	0.96	120.865	1.3
.8923	.428	7.668	.545	.89	120.855	1.4
.8746	.440	9.428	.764	.81	120.434	3.7

Activities of Undissociated Phosphoric Acid and Dihydrogen Phosphate Ion.—According to the Gibbs–Duhem equation as developed by Van Rysselberghe,[5] solutions of the system $CaO-P_2O_5-HF-H_2O$ may be represented by the relationship

$$-55.5062\ d\ln a_{H_2O} = m_u\, d\ln a_u + m_{H_2PO_4}\, d\ln a_{H_2PO_4} + m_{HPO_4}\, d\ln a_{HPO_4} + m_{PO_4}\, d\ln a_{PO_4} + m_{HF}\, d\ln a_{HF} + m_F\, d\ln a_F + m_H\, d\ln a_H + m_{Ca}\, d\ln a_{Ca} \qquad (4)$$

The three dissociation products of orthophosphoric acid and that for hydrofluoric acid yield

$$d\ln a_{H_2PO_4} = d\ln a_u - d\ln a_H$$
$$d\ln a_{HPO_4} = d\ln a_u - 2d\ln a_H$$
$$d\ln a_{PO_4} = d\ln a_u - 3d\ln a_H$$
$$d\ln a_F = d\ln a_{HF} - d\ln a_H$$

Substitution in equation 4 and rearrangement gives

$$-55.5062\ d\ln a_{H_2O} = [m_u + m_{H_2PO_4} + m_{HPO_4} + m_{PO_4}]\, d\ln a_u + [m_{HF} + m_F]\, d\ln a_{HF} + [m_H - m_{H_2PO_4} - 2m_{HPO_4} - 3m_{PO_4} - m_F]\, d\ln a_H + m_{Ca}\, d\ln a_{Ca}$$

By setting $[m_u + m_{H_2PO_4} + m_{HPO_4} + m_{PO_4}]$, the total phosphorus concentration, equal to m_P, and $[m_{HF} + m_F]$, the total fluorine concentration, equal to m_F, and by using the electroneutrality equation in the form

$$m_H - m_{H_2PO_4} - 2m_{HPO_4} - 3m_{PO_4} - m_F = -2m_{Ca}$$

general equation 4 is reduced to

$$-55.5062\ d\ln a_{H_2O} = m_P\, d\ln a_u + m_F\, d\ln a_{HF} - 2m_{Ca}\, d\ln a_H + m_{Ca}\, d\ln a_{Ca} \qquad (5)$$

From equation 3, or its equivalent

$$K_{FA} = \frac{a_{Ca}^{10}\, a_u^{6}\, a_{HF}^{2}}{a_H^{20}}\, (K_1K_2K_3)^{6}\, K_{HF}^{2}$$

is obtained

$$d\ln a_{Ca} + 3/5\ d\ln a_u + 1/5\ d\ln a_{HF} = 2\ d\ln a_H$$

which, when multiplied by calcium and substituted in equation 5, gives

$$-55.5062\ d\ln a_{H_2O} = [m_P - 3/5\ m_{Ca}]\, d\ln a_u + [m_F - 1/5\ m_{Ca}]\, d\ln a_{HF}$$

(5) P. Van Rysselberghe, *J. Phys. Chem.*, **39**, 403 (1935).

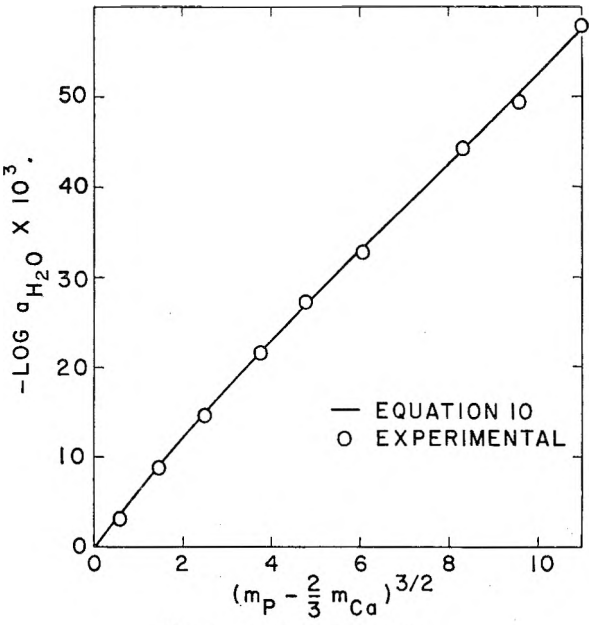

Fig. 1.—Activity of water.

or the equivalent

$$\left[\frac{-55.5062}{m_F - 1/5\, m_{Ca}}\right] d \ln a_{H_2O} - \left[\frac{m_P - 3/5\, m_{Ca}}{m_F - 1/5\, m_{Ca}}\right] d \ln a_u = d \ln a_{HF} \quad (6)$$

From the relationship

$$K_{CaF_2} = a_{Ca}\, a_F^2$$

or its equivalent

$$\frac{K_{CaF_2}}{K_{HF}^2} = \frac{a_{Ca}\, a_{HF}^2}{a_H^2}$$

is obtained

$$d \ln a_{Ca} + 2\, d \ln a_{HF} = 2\, d \ln a_H$$

which, when multiplied by calcium and substituted in equation 5, gives

$$-55.5062\, d \ln a_{H_2O} = m_P\, d \ln a_u + [m_F - 2m_{Ca}]\, d \ln a_{HF}$$

or the equivalent

$$\left[\frac{-55.5062}{m_F - 2m_{Ca}}\right] d \ln a_{H_2O} - \left[\frac{m_P}{m_F - 2m_{Ca}}\right] d \ln a_u = d \ln a_{HF} \quad (7)$$

Equating expressions 6 and 7, and simplifying, one obtains

$$55.5062\,[-9/5\, m_{Ca}]\, d \ln a_{H_2O} = [9/5\, m_{Ca} m_P - 6/5\, m_{Ca}^2 + 3/5\, m_{Ca} m_F]\, d \ln a_u$$

or

$$-55.5062\, d \ln a_{H_2O} = (m_P - 2/3\, m_{Ca} + 1/3\, m_F)\, d \ln a_u \quad (8)$$

which represents the Gibbs–Duhem–Van Ryssel-berghe relationship for solutions of the system CaO–P_2O_5–HF–H_2O saturated with both fluorapatite and calcium fluoride. As the concentration of fluorine (< 0.04%) in the saturated solution is negligible, the function reduces to

$$d \ln a_u = -\frac{55.5062}{(m_P - 2/3\, m_{Ca})}\, d \ln a_{H_2O} \quad (9)$$

The vapor pressures and compositions of the saturated solutions are related by the expression

$$\log a_1 \times 10^3 = 5.541x^{3/2} - 21.803x^2 + 13.369x^{5/2} - 2.5857x^3 \quad (10)$$

where a_1 is the activity of water and the concentration variable $x = m_P - 2/3\, m_{Ca}$. The parameters of equation 10 were determined by the method of least squares; its probable error is ± 0.00036, and it reproduces the experimental values in Table I with a maximal deviation of 0.18% and an average deviation of 0.08%. The activity of water is plotted in Fig. 1.

Substitution of equation 10 into equation 9, and integration, yields

$$\log a_u = -0.9227x^{1/2} + 2.4204x - 1.2368x^{3/2} + 0.2153x^2 + I \quad (11)$$

The activity of the undissociated phosphoric acid is expressed also by

$$\log a_u = \log a_H + \log a_{H_2PO_4} - \log K_1 \quad (12)$$

where K_1 is the first dissociation constant for phosphoric acid. Equating expressions 11 and 12, and rearranging, one obtains

$$\log a_{H_2PO_4} = -\log a_H + \phi + I + \log K_1$$

or its equivalent

$$\log \gamma_{H_2PO_4} = -\log m_{H_2PO_4} + pH + \phi + I + \log K_1 \quad (13)$$

where

$$\phi = -0.9227x^{1/2} + 2.4204x - 1.2368x^{3/2} + 0.2153x^2$$

By use of the Debye–Hückel relationship in the form

$$\log \gamma_{H_2PO_4} = -0.5091\mu^{1/2} \pm A\mu \pm \ldots$$

equation 13 may be written

$$\log m_{H_2PO_4} - pH - 0.5091\, \mu^{1/2} - \phi + pK_1 = I \pm A\mu \pm \ldots \quad (14)$$

Since the saturated solutions have negligibly small concentrations of fluorine and have pH's of less than 1.8, the concentration of the dihydrogen phosphate ion is

$$m_{H_2PO_4} = 2m_{Ca} + m_H$$

and the ionic strength is

$$\mu = 3m_{Ca} + m_H$$

Values for the terms on the left-hand side of equation 14, as calculated for each of the nine saturated solutions described in Table I, were used in the least-squares computation of the linear relationship

$$y = -0.6069 - 0.0503\, \mu$$

In the solutions saturated with fluorapatite and calcium fluoride, therefore, the activity of the undissociated phosphoric acid is represented by

$$\log a_u = -0.9227\,(m_P - 2/3\, m_{Ca})^{1/2} + 2.4204\,(m_P - 2/3\, m_{Ca}) - 1.2368\,(m_P - 2/3\, m_{Ca})^{3/2} + 0.2153\,(m_P - 2/3\, m_{Ca})^2 - 0.6069 \quad (15)$$

which is plotted in Fig. 2, and the activity coefficient of the dihydrogen phosphate ion is represented by

$$\log \gamma_{CH_2PO_4} = -0.5091\, \mu^{1/2} + 0.0503\, \mu \quad (16)$$

which is plotted in Fig. 3.

Activity of Calcium Ion.—Equating the two expressions for the activity of the undissociated phosphoric acid (eq. 15 and the logarithmic form of eq. 3), dividing by 1.5, and rearranging, one obtains

$$-\log a_{Ca} = 2\, pH + 2/3\, \phi - 1/9 \log K_{FA} = 15.9387$$

or its equivalent

$$-\log \gamma_{Ca} = \log m_{Ca} + 2\,p\mathrm{H} + 2/3\,\phi - 1/9 \log K_{FA} - 15.9387 \quad (17)$$

where γ_{Ca} is the activity coefficient of the calcium ion. Since the modified Debye–Hückel relationship

$$\log \gamma_{Ca} = \frac{-2.0364\,\mu^{1/2}}{1 + 1.9512\,\mu^{1/2}} \pm B\mu \pm C\mu^2 \pm \ldots$$

where ionic strength $\mu = 3m_{Ca} + m_H$, has been found to apply for many calcium phosphate systems, equation 17 may be written

$$\alpha = A \pm B\mu \pm C\mu^2 \pm \ldots$$

where

$$\alpha = \frac{2.0364\,\mu^{1/2}}{1 + 1.9512\,\mu^{1/2}} - \log m_{Ca} - 2\,p\mathrm{H} - 2/3\,\phi + 15.9387$$

A plot of α as a function of the ionic strength (Fig. 4) shows a parabolic curve, which was defined by the method of least squares from eight of the nine saturated solutions described in Table I. The point representing the solution with the greatest ionic strength was discarded statistically. The resultant equation

$$\alpha = 13.429 + 0.0436\,\mu - 0.00729\,\mu^2 + 0.00388\,\mu^3 \quad (18)$$

has a probable error of ± 0.00026; it reproduces the experimental data with a maximal deviation in α of 0.04% and a mean deviation of 0.02%.

The activity coefficient of the calcium ion therefore is represented by the function

$$\log \gamma_{Ca} = \frac{-2.0364\,\mu^{1/2}}{1 + 1.9512\,\mu^{1/2}} + 0.0436\,\mu - 0.00729\,\mu^2 + 0.00388\,\mu^3 \quad (19)$$

which is plotted in Fig. 3.

Evaluation of K_{FA}.—By combining the experimental data in Table I with equations 15 and 19, nine values of the activity solubility product of fluorapatite were calculated through the relationship

$$\log K_{FA} = 9 \log a_{Ca} + 6 \log a_u - 18 \log a_H + 6 \log (K_1K_2K_3) + \log K_{CaF_2} \quad (20)$$

which must exist among the activities of calcium and hydrogen ions and of the free phosphoric acid in solutions that are in equilibrium with mixtures of fluorapatite and calcium fluoride. The constancy of eight of the nine values given in Table II, $1.4 \pm 0.2 \times 10^{-121}$, shows a high degree of consistency of the experimental results and suggests that physicochemical laws generally applied to dilute electrolytic solutions can be applied in this system to solutions of high concentrations.

It may be of interest to compare the solubility product of fluorapatite, $pK_{FA} = 120.86 \pm 0.05$, derived from the equilibrium data for the quaternary system with some of the values that may be calculated from thermochemical data. For example, values of pK_{FA} ranging from 114.25 to 120.08 were calculated from (a) the average heat of formation of fluorapatite, −3267.2 ± 0.4 kcal./mole, as determined for the process

$$6H_3PO_4 + 9Ca(OH)_2 + CaF_2 = Ca_{10}(PO_4)_6F_2 + 18H_2O$$

from published data[4] for the heats of formation of $Ca(OH)_2$, CaF_2 and H_2O, together with unpublished

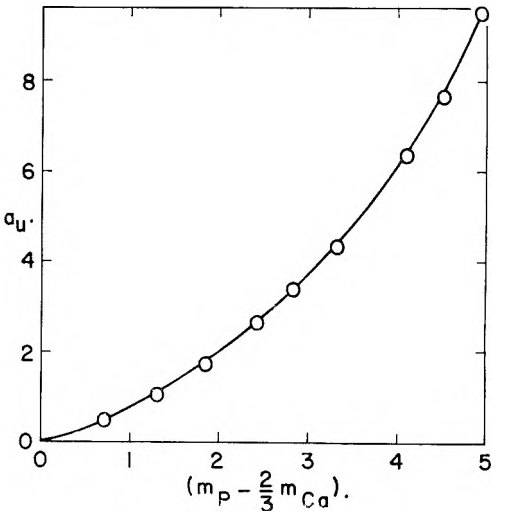

Fig. 2.—Activity of undissociated phosphoric acid.

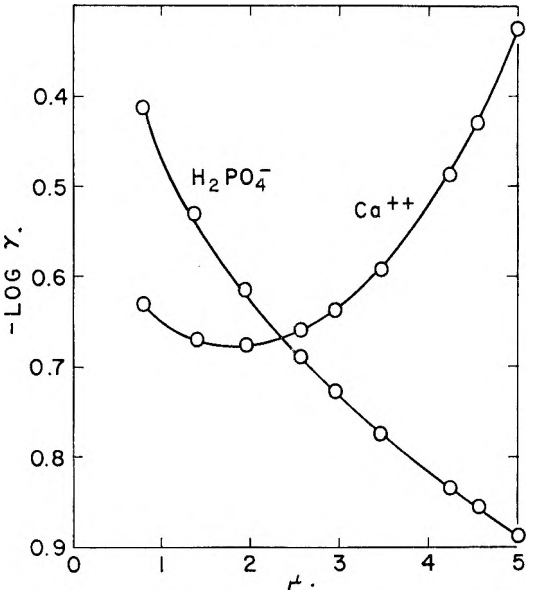

Fig. 3.—Activity coefficients of calcium and dihydrogen phosphate ions.

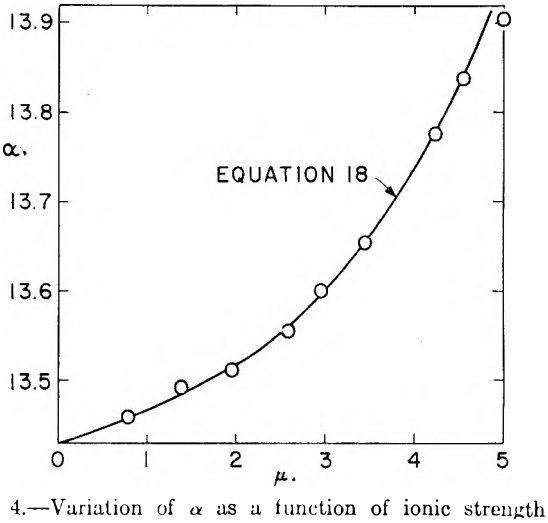

Fig 4.—Variation of α as a function of ionic strength.

TVA data for the heats of solution of the respective calcium compounds and for the heats of formation and dilution of phosphoric acid; (b) published data for the heats of formation[4] of Ca^{++}, PO_4^{3-} and F^-, for the entropies[4] of Ca^{++}, F^-, Ca(s), F_2(g) and O_2(g), for the entropy[6] of PO_4^{3-} (-52 ± 2 e.u.), and for the entropy[7] of fluorapatite.

(6) C. C. Stephenson, *J. Am. Chem. Soc.*, **66**, 1436 (1944).
(7) E. P. Egan, Jr., Z. T. Wakefield and K. L. Elmore, *ibid.*, **73**, 5581 (1951).

SYSTEM CaO–P_2O_5–HF–H_2O: EQUILIBRIUM AT 25 AND 50°[1]

BY THAD D. FARR, GRADY TARBUTTON AND HARRY T. LEWIS, JR.

Division of Chemical Development, Tennessee Valley Authority, Wilson Dam, Alabama

Received September 21, 1961

Phase equilibria in the system CaO–P_2O_5–HF–H_2O at 25 and 50° were determined for the region represented by liquid phases containing 4 to 35% P_2O_5, 0.7 to 5.5% CaO and less than 0.07% F. The stable solid phases in equilibrium with the saturated solutions were calcium fluoride and fluorapatite or calcium fluoride and monocalcium phosphate monohydrate. The invariant points representing solutions saturated with all three compounds were located at both temperatures. Measurements on the saturated solutions included *p*H, density and vapor pressure.

The presence of fluorapatite, $Ca_{10}(PO_4)_6F_2$, as a major component in rock phosphate focuses interest on the system CaO–P_2O_5–HF–H_2O in its relation to the manufacture and use of phosphatic fertilizers. Phase equilibrium in a portion of the system was studied with three major objectives: To determine whether dicalcium phosphate fertilizer can be made directly from rock phosphate and the stoichiometric proportion of phosphoric acid at temperatures in the range 25 to 50°, to determine the relative rates of equilibration from the directions of supersaturation and of undersaturation, and to determine some of the thermodynamic properties of the saturated solutions.

Materials and Methods

Monocalcium phosphate monohydrate, dicalcium phosphate and phosphoric acid were crystallized twice from the reagent materials. Hydrofluoric acid was redistilled in platinum and the middle fraction was retained. Calcium fluoride was prepared from twice-recrystallized calcium nitrate and the purified hydrofluoric acid. Tricalcium phosphate and fluorapatite were prepared by methods described previously.[2]

About half the equilibration mixtures were prepared from phosphoric acid and fluorapatite to approach equilibrium from the direction of undersaturation. The other mixtures were prepared from phosphoric acid and various combinations of monocalcium phosphate monohydrate, dicalcium phosphate, tricalcium phosphate, fluorapatite, calcium fluoride and hydrofluoric acid.

The mixtures were equilibrated in 500-ml. hard rubber or polyethylene screw-cap bottles that were rotated end over end in water-baths at 25 ± 0.08° or 50 ± 0.04°. The wet solids were identified petrographically, with some confirmations by X-ray diffraction.

Slow settling of solids complicated sampling of the liquid phases, which were analyzed in duplicate. The phosphorus content generally was determined by double precipitation as magnesium ammonium phosphate, with ignition to magnesium pyrophosphate. A few phosphorus determinations were made by a differential spectrophotometric method.[3] Calcium was determined by double precipitation as the oxalate, generally with ignition to calcium oxide. Some of the precipitates were ignited at 475 to 500° and weighed as calcium carbonate. Fluorine was determined by a method that has been described.[4]

Densities of the solutions were measured in 25-ml. pycnometers calibrated at 25 ± 0.005° or 50 ± 0.005°.

The *p*H's of the solutions were measured by means of a Beckman Model H-2 meter, with glass and saturated calomel electrodes calibrated at 25 and 50°. A few check determinations of *p*H were made with a hydrogen half-cell in a different system.

In measuring the vapor pressure of a saturated solution, a technique of alternate stirring and freezing was used for removal of dissolved extraneous gases without changing the composition of the solution. The solution was stirred in a 25-ml. bulb by means of a perforated platinum disk, lifted magnetically 8 times per min. After 5 to 10 min. of stirring, the liquid was frozen quickly at −78° and evacuated. The solid was melted at room temperature with the bulb isolated from the vacuum system and the cycle was repeated until the pressure over the solid was 10^{-4} mm. on a McLeod gage (usually 8 to 10 cycles).

The bulb with degassed test solution and stirring mechanism, a mercury isoteniscope, and the critical connecting lines were immersed in a water-bath at 25 ± 0.005° or 50 ± 0.005°. The nitrogen pressure needed to balance the isoteniscope, as indicated by an electronic relay system, was measured with a manometer containing Monsanto Arochlor No. 1242, which gave a magnification factor of 9.78. The manometer was read with a cathetometer.

The apparatus was tested by measuring the vapor pressure of conductivity water. The results of replicate determinations, 23.76 ± 0.01 mm. at 25° and 92.58 ± 0.01 mm. at 50°, are compared with the value 0.032287 kg./cm.² (23.75 mm.) for 25° recommended by Osborne, Stimson and Ginnings[5] from their compilation of published vapor pressures and the value 92.56 mm. for 50° given by Keyes.[6]

Equilibration at 25°.—Most of the complexes at 25° were sampled at 12, 16, 21 and 24 months. Some of the more viscous liquids were sampled only twice because of slow settling and the difficulty of getting clear samples. Neither the compositions of the liquid phases nor the forms of the solid phases changed significantly after 16 months.

Properties of the system at equilibrium are summarized in Table I. The low fluorine content of the liquid phases (<0.07%) permits a plot of the compositions on a ternary diagram, as in Fig. 1, without significant projection error. For comparison, a portion of the 25° isotherm of the ternary system CaO–P_2O_5–H_2O[7,8] is included in Fig. 1.

(1) Presented before the Division of Physical and Inorganic Chemistry, 132nd National Meeting of the American Chemical Society, New York, N. Y., September 1957.
(2) E. P. Egan, Jr., Z. T. Wakefield and K. L. Elmore, *J. Am. Chem. Soc.*, **73**, 5581 (1951).
(3) A. Gee and V. R. Deitz, *Anal. Chem.*, **25**, 1320 (1953).
(4) D. S. Reynolds and W. L. Hill, *Ind. Eng. Chem., Anal. Ed.*, **11**, 21 (1939).
(5) N. S. Osborne, H. F. Stimson and D. C. Ginnings, *J. Research Natl. Bur. Standards*, **23**, 261 (1939).
(6) F. G. Keyes, *J. Chem. Phys.*, **15**, 602 (1947).

TABLE I

SYSTEM $CaO-P_2O_5-HF-H_2O$ AT 25°

Liquid phase					Vapor pressure, mm.	Solid phase[a]
P_2O_5, %	CaO, %	F, %	Density, g./ml.	pH		
Approach from undersaturation						
3.81	0.922	0.002	1.0388	1.90	23.75	FA + CF
5.73	1.330	.002	1.0600	1.73	23.60	FA + CF
8.79	1.978	.004	1.0925	1.60	...	FA + CF
9.70	2.159	.004	1.1058	1.55	23.28	FA + CF
11.96	2.643	.004	1.1332	1.46	...	FA + CF
12.97	2.860	.005	1.1430	1.41	22.97	FA + CF
16.00	3.562	.035	1.1838	1.23	22.61	FA + CF
17.91	3.917	.019	1.2040	1.20	22.31	FA + CF
18.40	3.999	.011	1.2092	1.19	22.34	FA + CF
20.01	4.377	.027	1.2322	1.11	22.03	FA + CF
20.73	4.489	.019	1.2400	..	...	FA + CF
23.01	4.965	.008	1.2710	0.96	21.45	FA + CF
24.38	5.144	.012	1.2816	.89	21.20	FA + CF
25.78	5.466	.024	1.3042	.81	20.78	MC + CF + FA
31.90	4.217	.017	1.3571	.26	18.76	MC + CF
33.85	3.729	.064	1.3710	.00	17.93	MC + CF
Approach from supersaturation						
8.61	1.938	0.004	1.0930	1.61	...	FA + CF
8.68	1.962	.004	1.0945	1.61	...	FA + CF
20.40	4.433	.037	1.2370	1.10	...	FA + CF
20.71	4.510	.029	1.2405	1.07	...	FA + CF

[a] Identified petrographically in wet solids; first symbol represents major phase: FA = fluorapatite, CF = calcium fluoride, MC = monocalcium phosphate monohydrate.

Petrographic examination of the wet solids consistently showed the presence of three solid phases—fluorapatite, monocalcium phosphate monohydrate and calcium fluoride—in one mixture whose liquid phase at equilibrium contained 25.78% P_2O_5, 5.47% CaO and 0.02% F; the solid phases were fluorapatite and calcium fluoride in the mixtures whose liquid phases contained less P_2O_5—monocalcium phosphate monohydrate and calcium fluoride in the mixtures whose liquid phases contained more P_2O_5. The dicalcium phosphate used in several of the charges disappeared before the first examination at 12 months and did not reappear.

The thermodynamic properties of the saturated solutions (Table I) can be represented by smooth curves. Some of these data are evaluated further in a companion article[9] concerning calculation of the activity solubility product of fluorapatite.

Equilibration at 50°.—Most of the complexes at 50° were sampled at 9.5, 12, 15, 17, 19 and 22 months. Some of the more viscous liquids were sampled only at 12 and 22 months because of slow settling.

Properties of the system at 22 months are summarized in Table II. Compositions of the liquid phases in complexes prepared from fluorapatite and phosphoric acid (top of Table II) remained essentially constant after 12 months.

Petrographic examination of the wet solids consistently showed the presence of three solid phases—fluorapatite, monocalcium phosphate monohydrate and calcium fluoride—in one mixture whose liquid phase at 22 months contained 29.87% P_2O_5, 5.51% CaO and 0.02% F; the solid phases were fluorapatite and calcium fluoride in the mixtures whose liquid phases contained less P_2O_5—monocalcium

(7) H. Bassett, *Z. anorg. u. allgem. Chem.*, **59**, 1 (1908).
(8) K. L. Elmore and T. D. Farr, *Ind. Eng. Chem.*, **32**, 580 (1940).
(9) T. D. Farr and K. L. Elmore, *J. Phys. Chem.*, **66**, 315 (1962).

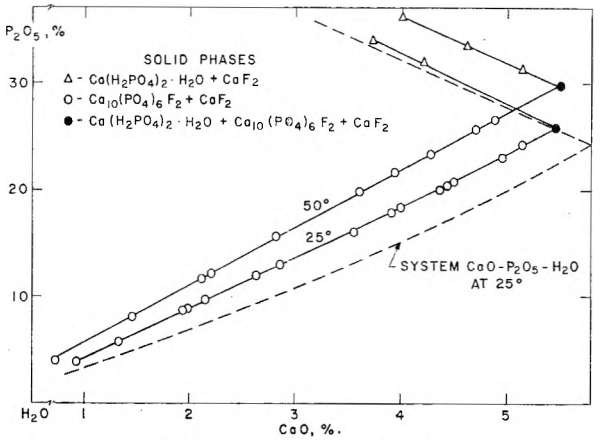

Fig. 1.—The system $CaO-P_2O_5-HF-H_2O$.

TABLE II

SYSTEM $CaO-P_2O_5-HF-H_2O$ AFTER 22 MONTHS AT 50°

Liquid phase					Vapor pressure, mm.	Solid phase[a]
P_2O_5, %	CaO, %	F, %	Density, g./ml.	pH		
Approach from undersaturation						
3.98	0.736	0.005	1.0276	1.80	92.08	FA + CF
8.00	1.451	.007	1.0686	1.58	91.40	FA + CF
11.72	2.107	.007	1.1083	1.38	90.51	FA + CF
12.21	2.207	...	....	..	...	FA + CF
15.71	2.825	.007	1.1537	1.20	89.04	FA + CF
19.85	3.612	.007	1.2043	1.00	86.65	FA + CF
21.70	3.941	.007	1.2291	0.92	85.39	FA + CF
23.41	4.284	.009	1.2523	.83	83.87	FA + CF
25.64	4.704	.008	1.2822	.73	81.96	FA + CF
26.57	4.831	.013	1.2921	.69	80.90	FA + CF
29.87	5.505	.021	1.3401	.51	77.03	MC + CF + FA
31.25	5.145	.022	1.3512	.38	75.60	MC + CF
33.41	4.636	.013	1.3671	.19	71.72	MC + CF
36.32	4.053	.040	1.3909	− .04	67.34	MC + CF
Approach from supersaturation						
9.75	1.941	0.006	1.0899	1.56	90.67	FA + CF
9.93	1.951	.003	1.0913	1.55	90.39	FA + CF
17.49	3.378	.010	1.1786	1.22	87.54	FA + CF
16.75	3.177	.007	1.1687	1.25	...	FA + CF
12.27	2.475	.003	1.1185	1.42	89.65	CF + FA
12.29	2.283	.007	1.1102	1.49	...	FA + CF
26.30	5.071	.014	1.2935	0.79	80.87	FA + CF

[a] Identified petrographically in wet solids; first symbol represents major phase: FA = fluorapatite, CF = calcium fluoride, MC = monocalcium phosphate monohydrate.

phosphate monohydrate and calcium fluoride in the mixtures whose liquid phases contained more P_2O_5. The dicalcium phosphate used in four of the charges disappeared before the first examination at 9.5 months and did not reappear.

The compositions of the three liquid phases associated with the solid phases monocalcium phosphate monohydrate and calcium fluoride fall on a smooth solubility curve (Fig. 1) that joins the invariant point representing the composition of the liquid phase associated with three solid phases.

The compositions of the liquid phases associated with the solid phases fluorapatite and calcium fluoride fall on two curves (Fig. 2) that were practically constant after the first sampling at 9.5 months. Complexes prepared from fluorapatite and phosphoric acid yielded liquid phases whose compositions fall uniformly along curve I, whereas the compositions of the liquid phases from the complexes prepared from monocalcium phosphate

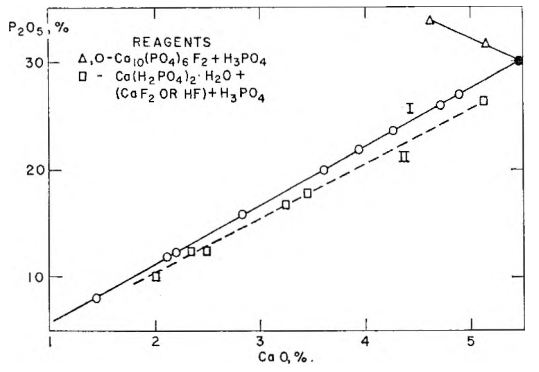

Fig. 2.—Solutions of the system $CaO-P_2O_5-HF-H_2O$ after 12 months at 50°.

monohydrate, calcium fluoride or hydrofluoric acid, and phosphoric acid (together with small amounts of dicalcium phosphate and fluorapatite) fall, less uniformly, along curve II. The $CaO:P_2O_5$ weight ratios (0.19 to 0.20) for points along curve II are higher than the ratio 0.18 for curve I. There was some evidence of a slight shift of three of the points along curve II in the direction of lower $CaO:P_2O_5$ ratios in the interval 9.5 to 22 months. The liquid phases contained little fluorine; apparent irregularities among the fluorine contents probably were within the limits of precision of the analytical method and cannot account for the two curves. The density, *p*H and vapor pressure of the two groups of liquid phases were consistent with their composition.

Despite the essential constancy of composition of the liquid phases after 9.5 months, all the mixtures could not have been at equilibrium. To determine whether formation of an impervious film on the solid phases might be inhibiting the approach to equilibrium[10,11] wet solids from the two groups after 19 months were ground for 5 min. in a mullite mortar, recharged to the liquid phases and rotated in the 50° bath for 2 months. The compositions of the liquid phases remained constant.

When fluorapatite and calcium fluoride are the saturating solids, a decrease in the $CaO:P_2O_5$ ratio in solution is associated with dissolution of calcium fluoride and concomitant precipitation of fluorapatite (the amount of calcium immobilized by a given weight of fluorine being ten times as great in fluorapatite as in calcium fluoride). The very slow approach to equilibrium from the direction of high $CaO:P_2O_5$ ratios is attributed to the very low rate of solution of calcium fluoride. The low rate of solution of calcium fluoride was observed in other tests in which the concentrations of calcium fluoride and phosphoric acid were comparable to those in this study.

Because of its importance in relation to the manufacture and use of phosphatic fertilizers, the rate of approach to equilibrium was explored further. Fourteen mixtures were prepared to simulate those in the earlier work at 50°. Four were prepared without fluorapatite to determine definitely whether this compound is a stable solid phase in the quaternary system. Tricalcium phosphate was used in the preparation of three of the mixtures.

The approach of the new complexes to equilibrium was checked at 3.5, 7 and 11 months. The compositions of the liquid phases at 3.5 and 11 months are given in Table III. Complexes 1 through 4, prepared from fluorapatite and phosphoric acid, yielded liquid phases whose compositions at 3.5 months fell on a smooth curve representing $CaO:P_2O_5$ ratios of 0.17 to 0.18 and lying quite near curve I of Fig. 2 ($CaO:P_2O_5$ ratio, 0.18); at 11 months, the compositions fell on curve I.

The other complexes listed in Table III yielded liquid phases whose compositions scattered and whose $CaO:P_2O_5$ ratios (0.19 to 0.27) corresponded to widely differing degrees of supersaturation with respect to calcium. Complexes 11 through 14, for example, in which no fluorapatite was added, yielded liquid phases whose compositions fell on or quite near the solubility isotherm for the ternary system $CaO-P_2O_5-H_2O$ at 50.7° as reported by Bassett.[7]

The two sets of results establish curve I of Fig. 2 as the solubility isotherm for 50°. The results show also that the phosphoric acid solutions of fluorapatite were more than 97% saturated in a 3.5-month period and were saturated in an 11-month period.

Petrographic examinations of the wet solids (Table III) showed several significant features. Calcium fluoride was found in the solids from all the complexes.

At 3.5 months, the nature of the wet solids from solutions supersaturated with respect to calcium suggested a marked influence of seed crystals on the rate of precipitation of fluorapatite. No fluorapatite was found in the solids from three (12, 13 and 14) of the four complexes in which fluorapatite was not part of the charge, whereas fluorapatite was found in complex 11 as radial clusters of acicular crystals on seeds of the original dicalcium phosphate. The wet solids from complexes in which fluorapatite was part of the charge contained two types of fluorapatite—solution-rounded polycrystalline masses (the type charged) and precipitated fluorapatite in various degrees of crystal growth on nuclei of monocrystalline apatite.

Dicalcium phosphate was part of the charge for complexes 8 through 12. None was found in the solids from complexes 8, 9, 10 and 12 at 3.5 and 7 months. In complex 11, whose liquid phase had the highest $CaO:P_2O_5$ ratio, dicalcium phosphate was found at 3.5 months as slightly eroded crystal fragments (essentially the form charged) and as nuclei for precipitated fluorapatite; at 7 months, the dicalcium phosphate was a minor phase, present only as nuclei for fluorapatite; at 11 months, no dicalcium phosphate was found.

Tricalcium phosphate was part of the charge for complexes 13 and 14. At 3.5 months, all the tricalcium phosphate in complex 14 and about half that in complex 13 had disappeared, and dicalcium phosphate had precipitated in complex 13. At 7 months, neither of the complexes contained tricalcium phosphate; in complex 13, dicalcium phosphate had increased to the proportions of a

(10) K. S. Krasnov, *Zhur. Priklad. Khim.*, **26**, 1114 (1953).

(11) E. B. Brutskus and M. L. Chepelevetskii, *Izvest. Sektora Fiz.-Khim. Anal., Akad. Nauk S.S.S.R.*, **20**, 383 (1950).

TABLE III

APPROACH TO EQUILIBRIUM IN THE SYSTEM $CaO-P_2O_5-HF-H_2O$ AT 50°

Complex	Reagents charged[a]	Compn. of liquid phase: P_2O_5, % 3.5 mo.	P_2O_5, % 11 mo.	CaO, % 3.5 mo.	CaO, % 11 mo.	Solid phase[b]: 3.5 mo.	7 mo.	11 mo.
1	FA	8.05	7.99	1.42	1.44	FA + CF	FA + CF	.....
2	FA	15.88	15.82	2.77	2.84	FA + CF	FA + CF	.....
3	FA	24.08	23.84	4.28	4.34	FA + CF	FA + CF	.....
4	FA	30.34	29.89	5.47	5.48	FA + CF	FA + CF	FA + CF + MC
5	MC + CF + FA	9.99	9.96	1.96	1.92	FA + CF	FA + CF	.....
6	MC + HF + FA	17.67	17.74	3.32	3.22	FA + CF	FA + CF	.....
7	MC + CF + FA	16.79	16.89	3.19	3.15	FA + CF	FA + CF	.....
8	MC + CF + FA + DC	12.59	12.64	2.68	2.64	FA + CF	FA + CF	.....
9	MC + CF + FA + DC	12.63	12.67	2.37	2.35	FA + CF	FA + CF	.....
10	MC + CF + FA + DC	26.59	26.65	5.14	5.15	CF + FA	CF + FA	FA + CF
11	MC + CF + DC	4.71	4.95	1.24	1.06	DC + FA + CF	FA + DC + CF	FA + CF
12	MC + CF + DC + HF	26.91	26.93	5.36	5.30	CF	CF	CF + FA
13	MC + CF + TC	4.11	4.21	1.11	1.13	TC + CF + DC	FA + DC + CF	FA + CF + DC
14	MC + CF + TC + HF	26.56	26.55	5.61	5.56	CF	CF	CF

[a] Aqueous H_3PO_4 was part of each charge; FA = fluorapatite, MC = monocalcium phosphate monohydrate, CF = calcium fluoride, DC = dicalcium phosphate, TC = α-tricalcium phosphate, HF = hydrofluoric acid. [b] Identified petrographically in wet solids; first symbol represents major phase.

major phase, and fluorapatite was observed as a precipitated phase in various degrees of crystal growth (acicular to well-formed hexagonal prisms) on nuclei of dicalcium phosphate. At 11 months, dicalcium phosphate had decreased to a minor phase comprising skeletal prisms that had grown on tricalcium phosphate cores no longer present; fluorapatite, the major phase, was present as rod crystals in radial clusters around dicalcium phosphate seeds. The change in complex 14 was extremely slow; calcium fluoride was the only solid phase that could be identified petrographically at 11 months. Most of the fluorine in complex 14 was added as hydrofluoric acid.

Conclusions

Fluorapatite and calcium fluoride are the stable solid phases in equilibrium with saturated liquid phases whose compositions cover the respective ranges

	P_2O_5, %	CaO, %
At 25°	4 to 25.8	0.9 to 5.47
At 50°	4 to 29.9	0.7 to 5.51

In this region, tri- and dicalcium phosphates are metastable phases; tricalcium phosphate, when added to the system, was converted to dicalcium phosphate and, in turn, to fluorapatite.

Monocalcium phosphate monohydrate and calcium fluoride are the stable solid phases in equilibrium with saturated liquid phase whose compositions cover the respective ranges

	P_2O_5, %	CaO, %
At 25°	25.8 to 33.9	5.47 to 3.73
At 50°	29.9 to 36.3	5.51 to 4.1

The saturated solutions contain less than 0.07% F. The results fix neither the lower limit of stability of the solid-phase pair fluorapatite–calcium fluoride nor the upper limit of stability of the pair monocalcium phosphate monohydrate–calcium fluoride at either temperature.

The invariant point representing a solution saturated with fluorapatite, calcium fluoride and monocalcium phosphate monohydrate contains, at 25°, 25.8% P_2O_5, 5.47% CaO, 0.024% F—at 50°, 29.9% P_2O_5, 5.51% CaO, 0.021% F.

Fluorapatite dissolves incongruently and relatively fast in phosphoric acid. When similar mixtures are prepared from mono- and dicalcium phosphates and calcium fluoride or hydrofluoric acid, the solution phases become saturated with calcium, and the approach to equilibrium is impeded by the low rate of dissolution of calcium fluoride.

The relatively fast ionic reaction of fluoride and calcium to form difficultly soluble calcium fluoride helps explain why acid phosphates revert only slowly to less available apatitic forms on ammoniation or when added to soils.

THE RADIOLYSIS OF ETHYLENE: DETAILS OF THE FORMATION OF DECOMPOSITION PRODUCTS[1]

BY MYRON C. SAUER, JR., AND LEON M. DORFMAN

Chemistry Division, Argonne National Laboratory, Argonne, Illinois

Received September 25, 1961

The radiolysis of ethylene has been studied with emphasis on the decomposition products. The G-values of hydrogen and acetylene are independent of ethylene pressure from 150 to 1000 mm., being 1.2 and 2.4, respectively, but increase significantly below this pressure. Isotopic and scavenger data for the system C_2H_4–C_2D_4 are presented. The bearing of the experimental data on the relative importance of ionic and excited states in the formation of hydrogen and acetylene is discussed.

Introduction

The radiolysis of ethylene has been studied by Mund and Koch,[2] Lind, *et al.*,[3] and more recently by Lampe[4] and Yang and Manno,[5] among others. The mercury-photosensitized decomposition has been the subject of extensive investigations,[6] and isotopic methods have been used[7] to establish the primary process in that reaction. A recent study,[8] in our Laboratory, of the vacuum-ultraviolet decomposition, has established the primary processes in the direct photolysis, and has provided results which show an interesting comparison with the radiolysis.

The principal decomposition products in the radiolysis of ethylene are hydrogen and acetylene. The acetylene accounts for only about 10% of the ethylene which is used up, the remainder undergoing condensation reactions to form products of higher molecular weight. In attempting to understand the primary processes in this radiolysis, we have examined the details of the formation of the decomposition products. Isotopic experiments have been carried out to provide information about the molecular detachment processes, the occurrence of which already has been indicated by scavenger experiments.[5] The pressure-dependence of the yields has been examined over a broad range, particularly in the low pressure region over which collisional de-excitation effects may manifest themselves. The pressure-dependence is also of importance in connection with any possible competition between unimolecular dissociation of ions and ion–molecule reactions. And finally, it was desirable to resolve some existing discrepancies between reported yields[4,5] of decomposition products.

Experimental

The materials were purified as follows. Matheson C.P. ethylene was degassed at −196° and distilled from a trap at −150° to a trap at −196°, a middle fraction of about 2/3 being collected. Gas chromatographic analysis showed no impurities which would interfere with the products to be analyzed. The C_2D_4 was obtained from Merck and Co. and was purified by degassing at −196° and by a bulb-to-bulb distillation at −150°.

The isotopic purity of the C_2D_4 was determined mass spectrometrically to be one atom of H per 100 atoms of D. Matheson Co. C_2H_2 was purified by degassing at −196° and distilling from −120 to −196°. Matheson Co. NO was degassed at −196° and distilled from a trap at liquid O_2 temperature to a trap at −196°.

Irradiations were carried out with both a Co^{60}-γ source[9] and a beam of 1 Mev. electrons from a Van de Graaff accelerator. The vessels used for Co^{60} irradiations were Pyrex cylinders, about 14 cm. long and 37 mm. in diameter, with a breakseal for removal of the sample after irradiation. Each vessel was used only once, and the samples were irradiated to about 5% consumption of the ethylene.

Several similar vessels were used for the Van de Graaff irradiations. They were about 17 cm. long and 35 to 40 mm. in diameter. The beam entered through a 2 mil thick, 30 mm. diameter stainless steel window which was either welded or silver soldered to Kovar metal. The Kovar was sealed to 7052 Pyrex which was used for the body of the vessel. The cell was reproducibly positioned for each run. The current striking the window was between 30 and 60 μamp. and a jet of air was directed on the window to prevent heating. Samples were irradiated 3 to 4 min., giving about 5% consumption of the ethylene. It was found experimentally that an accurate relative measure of the beam current passing through the window could be obtained by electronically integrating, over the length of the irradiation, the current from a lead attached to the edge of the window.

The polymerization of acetylene was used as a chemical dosimeter, the value $G(-C_2H_2) = 72$ being used.[3,10] The absorbed intensity was determined for the γ-irradiations to be 1.27×10^{20} e.v. hr.$^{-1}$g.$^{-1}{}_{C_2H_2}$ over the measured range of 80 to 500 mm. A few γ-irradiations were carried out at an intensity of 2.8×10^{19} e.v. hr.$^{-1}$g.$^{-1}{}_{C_2H_2}$. The absorbed intensity in the Van de Graaff runs was approximately 2700 times the latter figure, and was shown by 15 experiments, where the acetylene pressure varied from 50 to 450 mm., to be independent of acetylene pressure. To calculate the absorbed intensity for ethylene samples, the experimental figure for C_2H_2 was multiplied by the electron density ratio of ethylene to acetylene.

Because of uncertainty involved in extrapolating $G(-C_2H_2)$ for the acetylene dosimeter to the high radiation intensity of the Van de Graaff irradiations, the product yields obtained in Van de Graaff radiolyses are reported in a relative manner to be described in the discussion.

The analytical methods used were as follows. The gases non-condensable at −196° were removed and the PV product measured in a McLeod gage. Mass spectral analysis gave the percentages of hydrogen and methane, and in the case of isotopic experiments, the relative amounts of H_2, HD and D_2. Acetylene was analyzed by gas chromatography using a 25-foot, 0.19-in. i.d. column of 25% by weight hexadecane on 30–60 mesh Chromosorb Regular (from Wilkens Instrument and Research, Inc.). At room temperature and a flow rate of about 20 ml./min., this was found to cleanly separate, in order of retention times, C_2H_2, C_2H_4 and C_2H_6 when an aliquot of the irradiated C_2H_4 of size smaller than about 100 cc.-cm. was used. When the isotopic distribution of the acetylenes was to be determined, the acetylene "peak" was collected as it emerged from the chromatograph, and analyzed mass spectrometrically. The pressure of ethylene was measured initially in a known

(1) Based on work performed under the auspices of the U. S. Atomic Energy Commission. Presented in part at the 137th National Meeting of the American Chemical Society, Cleveland, Ohio, March, 1960.

(2) W. Mund and W. Koch, *Bull. soc. chim. Belges*, **34**, 119 (1925).

(3) S. C. Lind, D. C. Bardwell and J. H. Perry, *J. Am. Chem. Soc.*, **48**, 1556 (1926).

(4) F. W. Lampe, *Radiation Research*, **10**, 691 (1959).

(5) K. Yang and P. J. Manno, *J. Phys. Chem.*, **63**, 752 (1959).

(6) A. B. Callear and R. J. Cvetanović, *J. Chem. Phys.*, **24**, 873 (1956).

(7) R. J. Cvetanović and A. B. Callear, *ibid.*, **23**, 1182 (1955).

(8) M. C. Sauer, Jr., and L. M. Dorfman, *ibid.*, **35**, 497 (1961).

(9) R. A. Blomgren, "Proc. Sixth Hot Laboratories and Equipment Conference," p. 229, March, 1958.

(10) L. M. Dorfman and F. J. Shipko, *J. Am. Chem. Soc.*, **77**, 4723 (1955).

TABLE I

RESULTS OF ISOTOPIC EXPERIMENTS[a]

Irradiated system	Source of radiation	Total pressure (mm.)	Composition of products, % H_2	HD	D_2	C_2H_2	C_2HD	C_2D_2
C_2D_4	1 Mev. e^-	104	0	2.6	97	..	..	..
C_2H_4, C_2D_4[b]	1 Mev. e^-	200 to 400 (av. of 4 runs)	47.4 ± 0.6	5.5 ± 1.0	47.1 ± 0.7	..	..	..
C_2D_4, 10% NO	Co^{60} γ's		0	1.4	99	0	4.3	96
C_2H_4, C_2D_4[c]	Co^{60} γ's	260 (av. of 2 aliquots)	...	...	...	32 ± 1	45 ± 1	23 ± 1
C_2H_4, C_2D_4, 10% NO[c]	Co^{60} γ's	180	...	...	...	48	4	49
C_2H_4, C_2D_4[b]	Co^{60} γ's	20 to 25 (av. of 2 runs)	49.9 ± 0.1	5.2 ± 0.3	44.9 ± 0.1	..	..	..

[a] For mixtures containing C_2H_4 and C_2D_4, the results have been corrected to a 50–50 mixture. [b] Results corrected for HD which results when the C_2D_4 is irradiated. [c] Results corrected for C_2HD which results when the C_2D_4 is irradiated.

volume at a known temperature. After radiolysis and removal of hydrogen and methane, the residual pressure was measured in the same volume. From this and additional information on the *G*-values of the volatile products, $G(-C_2H_4)$ was calculated.

Results and Discussion

The results of isotopic experiments, in which equimolar mixtures of ethylene and ethylene-d_4 were irradiated with both Co^{60} γ-rays and 1 Mev. electrons, are shown in Table I. It may be seen, after correction for the HD originating from the isotopic impurity in the C_2D_4, that only 4% of the total hydrogen consists of HD. Thus it is clear that almost all of the hydrogen product is formed by molecular detachment. A significant atomic contribution to the hydrogen would not be expected, on the basis of self-scavenging of the hydrogen atoms by ethylene. Molecular detachment has been observed also in the mercury-photosensitized decomposition[7] and in the direct photolysis[8] of ethylene.

The situation with respect to the isotopic composition of the acetylene product is not as simple. The acetylene shows extensive isotopic mixing, consisting of 45% C_2HD. However, if 10% nitric oxide is added prior to irradiation, the isotopic mixing of the acetylene is eliminated almost completely, the C_2HD amounting to only 4%. The presence of nitric oxide does not lower the *G*-value for acetylene formation. Only an approximate value of $G(\text{acetylene}) \approx 2.8$ has been obtained in the presence of NO, but it is clear that the acetylene yield is not decreased by added NO. It appears from this, along with the following observations, that the isotopic mixing of the acetylenes in the absence of nitric oxide is due largely to an efficient secondary exchange between the acetylene molecules which also must involve the ethylene. The acetylene is formed initially isotopically unmixed, and the exchange apparently is inhibited by nitric oxide. No such isotopic mixing of the acetylene is observed in either the mercury photosensitized decomposition[7] or the direct photolysis[8] of ethylene.

Table II shows the results of four experiments performed to investigate the nature of the reactions leading to C_2HD formation. These runs all were carried out in the all-glass cells using the γ-source because the cells used for the electron irradiations exhibited exchange of the acetylene even in the absence of radiation, presumably because of catalysis by the metal surfaces. Experiment 1 shows the amount of C_2H_2 formed when pure C_2H_4 is irradiated. Experiments 2 and 3 contain C_2D_2 initially added. Examination of the data shows that C_2D_2 is consumed, that there is a deficiency of C_2H_2 formed and an excess of C_2HD compared with expt. 1. These results indicate that exchange must involve the C_2D_2 and the C_2H_2, the latter being continuously produced during the radiolysis. However, some C_2HD also must be formed from an exchange between C_2D_2 and some species other than C_2H_2. This may be seen by comparison, as in expt. 2, of the amount of C_2HD formed with the deficiency in C_2H_2. This conclusion also is indicated by the fact that, in the absence of NO, there is an isotope effect in acetylene formation (see Table I). An over-all isotope effect could not, of course, result from exchange among the acetylene molecules themselves. In expt. 4, both C_2D_2 and C_2H_2 were added initially in amounts considerably in excess of the acetylene formed in such a run. Under this condition, the exchange involving C_2H_2 and C_2D_2 is far more important than exchange between acetylene and some other species. Although the material balance in these runs is far from perfect, the conclusions drawn seem fully warranted.

TABLE II

FORMATION OF C_2HD IN THE RADIOLYSIS OF C_2H_4, C_2D_2, C_2H_2 MIXTURES[a]

			1	2	3	4
Initial	μmoles	C_2H_4	1880	1880	1860	1870
	μmoles	C_2D_2	0	20.2	103	99
	μmoles	C_2HD	0	0.31	1.6	1.5
	μmoles	C_2H_2	0	0	0	104
Final	μmoles	C_2D_2	0	10.1	84	48
	μmoles	C_2HD	0	13.0	21.4	110
	μmoles	C_2H_2	9.3	4.4	1.5	64

[a] All samples irradiated the same length of time at the same intensity.

The lack of isotopic mixing in the acetylenes rules out the formation of acetylene by combination of CH_2 radicals. The possibility that C_2H_3 radicals are precursors of the acetylene is ruled out on the basis of information on higher molecular weight products[11] which indicates that C_2H_3 is not an important radical. It appears then, that acetylene is formed by molecular detachment from

(11) M. C. Sauer, Jr., unpublished results.

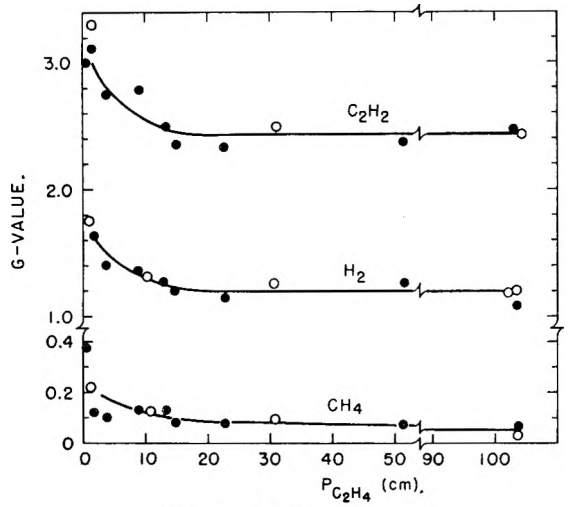

Fig. 1.—Co^{60} irradiations.

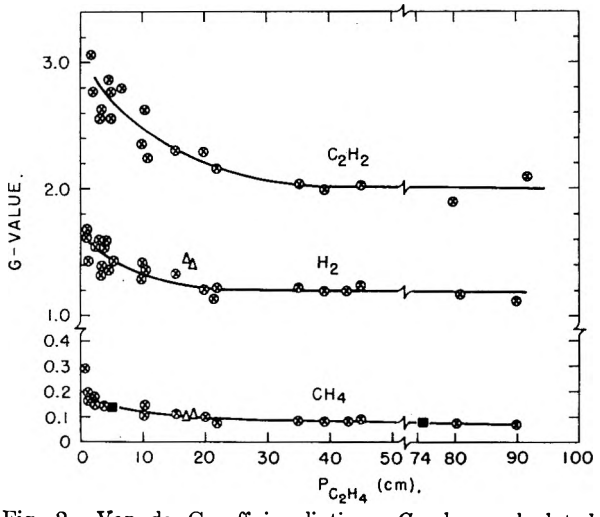

Fig. 2.—Van de Graaff irradiations, G-values calculated relative to $G(H_2) = 1.2$ as stated in text.

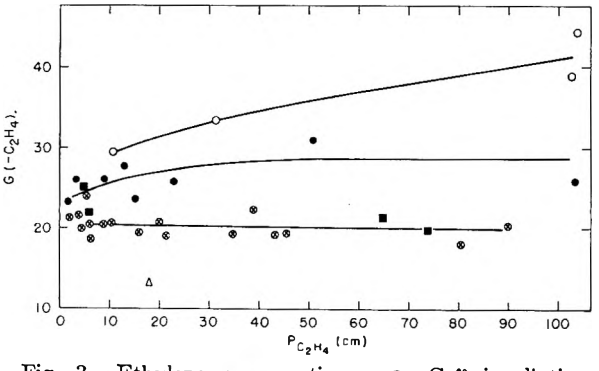

Fig. 3.—Ethylene consumption: O, Co^{60} irradiation, 2.8×10^{19} e.v. hr.$^{-1}$ g.$_{C_2H_2}^{-1}$; ●, Co^{60} irradiation, 12.7×10^{19} e.v. hr.$^{-1}$ g.$_{C_2H_2}^{-1}$; ⊗, Van de Graaff irradiation, $\sim 8 \times 10^{22}$ e.v. hr.$^{-1}$ g.$_{C_2H_2}^{-1}$; G-values calculated relative to $G(H_2) = 1.2$ as stated in text; ■, same as ⊗ but −78°; △, same as ⊗ but 10% NO present. Note: these symbols apply to all three figures.

an excited state of ethylene and/or by the ion-molecule reaction of $C_2H_3^+$ with C_2H_4.

The dependence of the product yields upon pressure has been examined over the pressure range 15 to 1000 mm. The yields for H_2, C_2H_2, CH_4 and for ethylene disappearance are shown in Fig. 1–3. The yields for H_2 and C_2H_2 clearly are independent of pressure in the region 150 to 1000 mm. As the pressure is decreased below 150 mm. these yields show a gradual increase amounting to over 40% at the lowest pressures studied.

The increase in the yield of H_2 and C_2H_2 probably is due to a contribution from additional processes at lower pressures. Two such processes immediately suggest themselves. Callear and Cvetanović[6] have shown, in the mercury photosensitized decomposition of ethylene, that below 150 mm. dissociation of a long-lived excited state of ethylene occurs to give H_2 and C_2H_2. At higher pressures this dissociation is eliminated by collisional deactivation. Our data are qualitatively in accord with the postulate that decomposition of such a long-lived excited state is occurring in the radiolysis, and that the hydrogen and acetylene produced simply add to the amounts of these products formed in the pressure-independent processes. Alternatively, or in addition, the increase in the product yields at the lower pressures could result from dissociation of an ethylene molecule–ion, which at the higher pressures undergoes reaction with ethylene rather than dissociating. That is, at the lower pressures, dissociation occurs

$$C_2H_4^+ = C_2H_2^+ + H_2 \qquad (1)$$

and

$$C_2H_4^+ = C_2H_3^+ + H \qquad (2)$$

followed by

$$C_2H_3^+ + C_2H_4 = C_2H_5^+ + C_2H_2 \qquad (3)$$

to yield acetylene, as Lampe has suggested.[4] Whereas, as the pressure is increased, the ion–molecule reaction

$$C_2H_4^+ + C_2H_4 = C_3H_5^+ + CH_3 \qquad (4)$$

becomes more probable. Stevenson[12] has discussed this competition on the basis of the statistical theory of ion dissociation, and has concluded that, in the case of ethylene at one atmosphere pressure, reaction 4 is strongly favored. The questionable quantitative validity of the quasi-equilibrium theory, judging from recent publications[13,14] on the subject, would argue against placing complete reliance on such a calculation, at least where absolute rate constants are involved. Our observation of pressure independent yields from 150 to 1000 mm. is, however, rather strong evidence that a competition between reactions 1 and 4 is not occurring over that range.

The over-all isotope effects observed are compatible with the first of the two interpretations discussed above. Table I shows that in the region where G-values are independent of pressure there is no over-all isotope effect in hydrogen formation, the ratio being $H_2/D_2 = 1.00 \pm 0.02$. There is furthermore no isotope effect in acetylene formation in the presence of nitric oxide, the ratio being $C_2H_2/C_2D_2 = 0.98 \pm 0.05$. In the mercury

(12) D. P. Stevenson, *Radiation Research*, **10**, 610 (1959).

(13) E. M. Eyring and A. L. Wahrhaftig, *J. Chem. Phys.*, **34**, 23 (1961).

(14) B. Steiner, C. F. Giese and M. G. Inghram, *ibid.*, **34**, 189 (1961).

photosensitized decomposition at 20 to 25 mm., an isotope effect of about 1.5 is observed.[7] At 20–25 mm. pressure (see Table I), the radiolysis of an equimolar mixture of C_2H_4–C_2D_4 shows an isotope effect of $H_2/D_2 = 1.11 \pm 0.02$. This is, within experimental error, the predicted value obtained by applying the isotope effect of Callear and Cvetanović to the additional hydrogen formed at the lower pressure and combining this with the isotope effect of unity in the pressure-independent region to obtain the over-all isotope effect at the lower pressures.

The following data, which appear in Fig. 2, should be mentioned briefly. The *G*-value of methane formation is not affected by the presence of 10% NO or by lowering the irradiation temperature to −78°. These facts suggest that methane is not formed *via* a thermal methyl radical precursor.

The results of our studies of the photolysis of ethylene at 1470 Å., taken together with the conclusions reached by Lassettre[15] in his investigations of excitation processes by electron impact spectroscopy, lead to the conclusion that there is *some contribution* to molecular hydrogen and acetylene by dissociation of an excited state of ethylene, formed by electron impact. Lassettre has shown that, under certain conditions of electron energy and scattering angle, the selection rules for molecular excitation by electron impact are the same as the selection rules for absorption of light quanta. Since molecular detachment of hydrogen and acetylene occurs in the photolysis,[8] a contribution by molecular detachment from excited states is to be expected in the radiolysis. The quantitative extent of such a contribution cannot reliably be estimated on the basis of existing information. It is a consequence of this conclusion that a precise correlation between molecular detachment yields in ethylene and the mass spectrum[16] is fortuitous to the extent that the contribution from neutral excited states has been omitted, as stated, and must be included. A similar conclusion has been reached from isotopic experiments.[17]

The *G*-values for hydrogen and acetylene formation have been determined for the Co^{60} irradiations in the pressure region 150–1000 mm. and are 1.2 and 2.4, respectively. These values are based on chemical dosimetry using the value $G(-C_2H_2) = 72$ in the acetylene polymerization.[3,10] The hydrogen yield is in agreement with the value of Lampe[4] and somewhat lower than reported by Yang and Manno,[5] who used a liquid dosimeter. The observed C_2H_2/H_2 ratio, however, is in very close agreement with the data of Yang and Manno,[5] and the indication, therefore, is that the acetylene *G*-value of Lampe is low.

We do not feel justified in reporting *G*-values for the electron irradiations at very high intensity. The use of the acetylene dosimeter at these intensities would involve a very long extrapolation (as a function of intensity) which might be in error. All *G*-values for Van de Graaff irradiations therefore have been calculated relative to $G(H_2) = 1.2$ at $P_{C_2H_4} = 40$ cm.

Conclusions

The conclusions we have reached may be stated as follows: 1. Hydrogen is formed by molecular detachment. The data do not allow us to specify the relative importance of ionic and excited states in the formation of hydrogen. 2. Acetylene is formed by molecular detachment from an excited ethylene molecule and/or an ion–molecule reaction involving $C_2H_3^+$. 3. The yields in the pressure independent region above 150 mm. are $G(H_2) = 1.2$, $G(C_2H_2) = 2.4$ molecules/100 e.v. 4. These yields increase with decreasing pressure below 150 mm., but the role of ion dissociation or of excited state dissociation in this effect cannot be resolved by the present data. 5. The pressure-independence of the yields above 150 mm. indicates that, in this region, a competition between unimolecular dissociation and ion–molecule reactions of the parent ion is highly unlikely. 6. The results of photolysis at 1470 Å. indicate that some contribution to H_2 and C_2H_2 formation by dissociation of neutral excited states must occur in the radiolysis, a conclusion which also has been reached on the basis of isotopic studies.[17] 7. The precise correlation between H_2 yield and ionic processes alone, based on the mass spectral pattern, must be regarded as fortuitous, to the extent that a contribution from neutral excited states must be added to the calculated values.

(15) E. N. Lassettre, *Radiation Research*, Supplement **1**, 530 (1959).

(16) L. M. Dorfman and M. C. Sauer, *J. Chem. Phys.*, **32**, 1886 (1960).

(17) P. Ausloos and R. Gorden, Jr., *ibid.*, in press.

ADSORPTION AND DIELECTRIC STUDIES OF THE ALUMINA–ETHYL CHLORIDE SYSTEM AT 35°[1]

BY R. A. YOUNT

Department of Chemistry, University of North Carolina, Chapel Hill, N. C.

Received October 2, 1961

The adsorption isotherm of ethyl chloride on alumina was determined at 35.0°. The shape of this isotherm resembled that classified by S. Brunauer as Type IV. In conjunction with the isotherm determination, dielectric studies were made on the system. The dielectric constant and loss were measured at frequencies between 100 c. and 100 kc. for various amounts of adsorbed ethyl chloride. The dielectric loss exhibited an increase until monolayer completion; then it became relatively constant upon further amounts adsorbed. The dielectric constant increased with increasing amount adsorbed. For any given amount adsorbed, both the dielectric constant and loss decreased with increasing frequency.

Introduction

This work constitutes a determination of the adsorption isotherm of ethyl chloride on powdered alumina. At various points along the isotherm, dielectric studies were made to see if there is a possible correlation between dielectric properties and the amount of ethyl chloride adsorbed.

The alumina-ethyl chloride system was chosen for several reasons. First of all, the alumina used has a very large surface area. Because of this and the ionic nature of the alumina, one would expect the dipolar ethyl chloride to be adsorbed readily. Secondly, ethyl chloride was chosen as an adsorbate with a relatively large dielectric constant, so that the heterogeneous system would exhibit measurable changes in dielectric properties upon increasing amounts adsorbed. Finally, study of this system affords an opportunity to contrast results with those obtained for the system alumina–water,[2] and with ethyl chloride on adsorbents other than alumina.[3–6]

Experimental

Materials.—The alumina used was Merck and Co. reagent grade aluminum oxide for use in chromatographic adsorption. Before use, the alumina was vacuum degassed at 300° for six hr. and cooled under vacuum. After heating at 300° for 16 hr. more in the adsorption cell, constant values of the capacitance of the cell were obtained.

The ethyl chloride used was Matheson Co. U. S. P. grade dried over calcium chloride before use.

Apparatus.—The dielectric cell consisted of concentric nickel cylinders held rigidly in two concentric sections of large diameter Pyrex tubing. The capacitance of the empty cell *in vacuo* at 35.0° was 57.1 ± 0.1 μμf. between 50 c. and 100 kc. At the same temperature and frequencies the capacitance was 131.75 ± 0.25 μμf. when the cell was filled with alumina.

The gas buret was kept at 31.0° and the cell at 35.00 ± 0.03°.

Dielectric measurements were made with a General Radio Type 1610–A Capacitance Measuring Assembly. Using the Substitution Method[7] measurements could be made to an accuracy of ± 0.1% or ∓ 0.8 μμf., whichever is larger, in the dielectric constant. The dissipation factor could be measured within ± 2%.

Procedure.—Using both adsorption and desorption procedures, the 35° isotherm was established for values of P/P_0 between 0 and 0.825, where P = equilibrium pressure, and P_0 = vapor pressure of liquid ethyl chloride at 35.0°.

For various amounts of ethyl chloride adsorbed, the dielectric constant, ϵ', and dielectric loss, ϵ'', were determined at frequencies between 100 c. and 100 kc.

Results and Discussion

Adsorption Studies.—For the P/P_0 ranges 0.825–0.600 and 0.200–0.000, adsorption and desorption curves (Fig. 1) were coincident. Values of W/g, the number of milligrams of ethyl chloride per gram of alumina, obtained on desorption are greater than those obtained on adsorption in the P/P_0 range 0.600–0.200, the maximum discrepancy being about 5% at $P/P_0 = 0.350$. For values of P/P_0 less than 0.05, the desorption points fell on a smooth curve, whereas the adsorption points had been distributed very erratically. Additional adsorption points, determined after completion of the desorption isotherm, fell on the desorption branch of the isotherm, thus defining the hysteresis as irreversible. This probably is due to impurities, mostly permanent gases, originally adsorbed on the adsorbent.[8]

The isotherm has the same general shape as that classified by Brunauer[9] as Type IV. This isotherm represents multimolecular adsorption with capillary condensation at high pressure. Brunauer, Deming, Deming and Teller,[10] discussing a model system with the above features, obtained the isotherm

$$V = V_m \left\{ \frac{X}{1-X} + \frac{2(C-1)X + 2(C-1)^2X^2 + (\bar{n}C^2 + \bar{n}h - 2\bar{n}C - \bar{n}^2C^2)X^{\bar{n}}}{2[1 + 2(C-1)X + (C-1)^2X^2 + (C^2 + h - 2C - \bar{n}C^2)X + (2C + \bar{n}^2C^2 + 2\bar{n}C - 2C^2 - \bar{n}C^2 - 2h - 2\bar{n}h)X^{\bar{n}+1} + (\bar{n}C^2 + 2C - 2C^2 - 2h)X^{\bar{n}+1} + (\bar{n}h + 2h)X^{\bar{n}+2} + hX^{\bar{n}+2}]} \right\} \quad (1)$$

where $\bar{n}$ = maximum number of layers that can fit into the capillary; $h = (\bar{n}C^2 - 2C^2 + 2C)g$, if the $\bar{n}$ layers do not exactly fill the capillary; or $h = C^2g$, if the $\bar{n}$ layers exactly fill the capillary; C = constant; g = constant; $X = P/P_0$; V =

(1) Based on a thesis by the author submitted to the Graduate School, University of North Carolina, in partial fulfillment of the requirements for the degree of Master of Arts, 1960.

(2) M. G. Baldwin, Doctoral Thesis, Dept. of Chemistry, University of North Carolina, 1958.

(3) E. Channen and R. McIntosh, *Can. J. Chem.*, **33**, 172, 341 (1955).

(4) R. McIntosh, E. Rideal and J. A. Snelgrove, *Proc. Roy. Soc.* (London), **A208**, 292 (1957).

(5) J. A. Snelgrove, H. Greenspan and R. McIntosh, *Can. J. Chem.*, **31**, 72 (1953).

(6) J. A. Snelgrove and R. McIntosh, *ibid.*, **31**, 84 (1955).

(7) This method is described fully in the instruction booklets accompanying the Measuring Assembly. Forms 681-G, 844-B, 785-B and 661-F.

(8) R. Zsigmondy, *Z. anorg. u. allgem. Chem.*, **71**, 356 (1911).

(9) S. Brunauer, "The Adsorption of Gases and Vapors," Vol. 1, Princeton University Press, Princeton, N. J., 1943.

(10) S. Brunauer, L. S. Deming, W. E. Deming and E. Teller, *J. Am. Chem. Soc.*, **62**, 1723 (1940).

volume adsorbed; and V_m = volume that must be adsorbed to cover the surface with one complete unimolecular layer.

Equation 1 gives a fair representation of the experimental isotherm for ethyl chloride on alumina. From the linear portion of a BET[11] plot, there was obtained V_m = 48.51 mg./g. and C = 27.74. Using these values, $\bar{n}$ and h were obtained from equation 1, the best fit being produced with $\bar{n}$ = 6, and h = 30,000 cal. Typical points are: V = 62.4 at X = 0.25, V = 82.6 at X = 0.36, V = 104.3 at X = 0.50, and V = 130.9 at X = 0.75 (Fig. 1). The discrepancy above X = 0.50 may arise from the use of a model capillary consisting of open-ended parallel walls. If the capillary walls are not parallel, a fifth constant will appear in the adsorption isotherm. If the capillaries are completely enclosed, and if V_m is taken as the amount of adsorbate to cover the walls of all the capillaries with one unimolecular layer, V_m will be a function of $\bar{n}$ and will decrease with amount adsorbed. The calculated values of X suggest that enclosed capillaries may exist in the alumina used in this work.

It is instructive to compare the above BET area for ethyl chloride with that for nitrogen on the same adsorbent. The BET area using nitrogen at 77°K. has been determined to be 270 sq. m./g.[2] Comparing this with the value of V_m for ethyl chloride, we see that an area of 63 Å.[2] is available for each molecule of ethyl chloride, assuming one molecule adsorbed on each site.

Using a relation given by Emmett and Brunauer,[12] the area actually needed by each molecule can be obtained. The average cross section of the adsorbed molecule is assumed to be the same as that corresponding to the plane of closest packing in the solidified gas.

$$A = 4(0.866)(M/4\sqrt{2}\,ND_L)^{2/3} \qquad (2)$$

where D_L is the density of the liquefied gas, which is 0.903 g./cm.[3] at 10°,[13] M is the molecular weight of the gas, and N is Avogadro's number. Substituting these values into equation 2 gives a value of 28 Å.[2] for the area needed by each molecule. Thus each molecule occupies only about half of the area that is available to it. This would seem to indicate that the molecules are oriented with their long axes parallel to the surface since they are not close enough together for mutual repulsion to have set in.

Dielectric Studies.—Plots were prepared of the dielectric constant, ϵ', and of the dielectric loss, ϵ'', *vs.* the natural logarithm of the frequency, f, for various amounts of ethyl chloride adsorbed (Fig. 2). Clearly the curves for ϵ'' *vs.* ln f exhibit no maxima such as those characteristic of a Debye-like system for which

$$\epsilon'' = (\epsilon_0 - \epsilon_\infty)\omega\tau/(1 + \omega^2\tau^2 -) \qquad (3)[14]$$

where ϵ_0 = static dielectric constant, ϵ_∞ = optical dielectric constant, ω = angular frequency, and

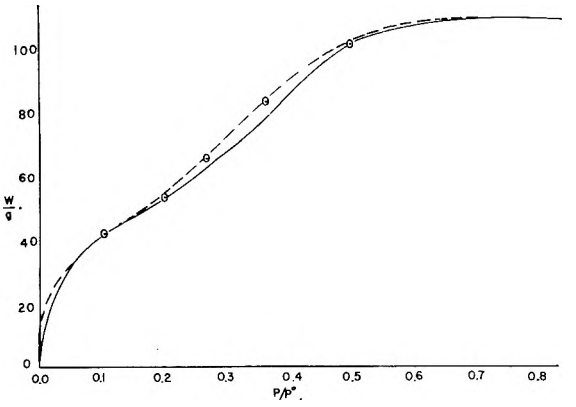

Fig. 1.—The adsorption isotherm of ethyl chloride on alumina at 35.0°: solid line, adsorption; broken line, desorption; circles, points calculated from Brunauer, Deming, Deming and Teller equation.

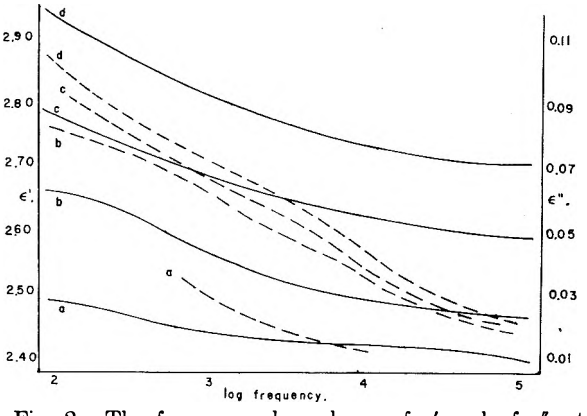

Fig. 2.—The frequency dependence of ϵ' and of ϵ'' at various amounts of ethyl chloride adsorbed: a, 27.48 mg./g.; b, 46.17 mg./g.; c, 73.52 mg./g.; d, 90.15 mg./g.; solid lines, ϵ'; broken lines, ϵ''.

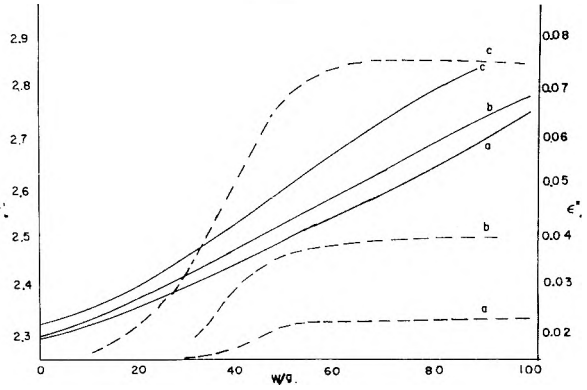

Fig. 3.—The dependence of ϵ' and of ϵ'' on the amount of ethyl chloride adsorbed at various frequencies: a, 1 kc.; b, 10 kc.; c, 50 kc.; solid lines, ϵ'; broken lines, ϵ''.

τ = dipole relaxation time, although such maxima may occur at frequencies less than 100 c.

Plots of ϵ' and ϵ'' *vs.* W/g (Fig. 3) are consistent with Debye-type behavior. As the amount of ethyl chloride adsorbed increases, sites of lower binding energy are progressively occupied, giving a system characterized by shorter and shorter relaxation times. The less strongly the molecules are held to the surface, the easier it will be for them to return to their original random orientation once the field is removed and ϵ'' increases.

(11) S. Brunauer, P. H. Emmett and E. Teller, *J. Am. Chem. Soc.*, **60**, 309 (1938).

(12) P. H. Emmett and S. Brunauer, *ibid.*, **59**, 2682 (1937).

(13) J. Timmermans, "Physico-Chemical Constants," Elsevier Publishing Co., New York, N. Y., 1950.

(14) P. Debye, "Polar Molecules," Chemical Catalog, New York, N. Y., 1929.

For the low values of W/g, the molecules of ethyl chloride occupy the sites of highest binding energy, and the dipole relaxation time is much larger than the phase interval between reversals of the field. Thus $\omega\tau$ is very much greater than 1, and ϵ'' is immeasurably small. Almost until the completion of the monolayer, ϵ'' remains small. Near the completion of the monolayer, sites of lower binding energy begin to be occupied, and τ becomes smaller so that $\omega\tau$ approaches unity. Thus a measurable absorption region arises, ϵ'' increasing as amount adsorbed increases because τ decreases. This continues until the monolayer is completed.

Because of the difference in heat of adsorption for the first and subsequent layers, a rather sharp decrease in relaxation time is to be expected at monolayer completion. (Perhaps even the mechanism of orientation changes.) For such a sudden decrease, $\omega\tau$ becomes much less than 1. Thus amounts adsorbed past the monolayer will not contribute appreciably to ϵ'', but those molecules already adsorbed before completion of the monolayer retain their characteristic relaxation times, producing a plateau in the curve for amounts adsorbed past the monolayer. This is in contrast to the alumina–water system in which Baldwin[2] found that ϵ'' did not begin to increase until after the monolayer had been completed. The studies of McIntosh and co-workers[3-6] of ethyl chloride on silica gel and on rutile were made in the megacycle region and thus cannot be compared with the alumina–ethyl chloride system. The values of V_m as found by identifying the point of monolayer completion from the plateau characteristics are in good agreement with those found from the adsorption isotherm. At a frequency of 1 kc., V_m = 51 mg./g.; at 10 kc., V_m = 50 mg./g.; and at 50 kc., V_m = 49 mg./g. Thus it seems reasonable to identify the beginning of the plateau in the ϵ'' *vs.* amount adsorbed curve with the completion of the monolayer.

The author wishes to thank Professor J. C. Morrow for his valuable suggestions and criticisms. The help of Mr. D. E. Sampson and Dr. M. G. Baldwin in the construction of the vacuum system and dielectric cell is gratefully acknowledged.

SURFACE ACTIVITY OF FLUORINATED ORGANIC COMPOUNDS AT ORGANIC LIQUID–AIR INTERFACES. PART IV. EFFECT OF STRUCTURE AND HOMOLOGY[1]

BY MARIANNE K. BERNETT, N. LYNN JARVIS AND W. A. ZISMAN

U. S. Naval Research Laboratory, Washington 25, D. C.

Received October 2, 1961

Previous investigations have shown that partially fluorinated carboxylic esters adsorb at organic liquid–air interfaces as monomolecular films, thus depressing the surface tension of the organic liquid. In this investigation the surface activities of specially designed fluorinated solutes were studied in seven organic solvents of different compositions and surface tensions. By varying the structure and composition of the organophobic, the organophilic and the connecting polar groups, their contribution to solubility, adsorptivity, and orientation and packing of the solute molecules at the organic liquid–air interface could be investigated. The degree of solubility, as well as the packing of the molecules at the surface, was shown to be dependent upon fluorination, length and number of the organophobic chain, and the structure of the organophilic portion. From the force–area isotherms the lowest area per molecule attainable in each solvent was calculated. The relation of these lowest areas to the corresponding lowest values of surface tension obtained was discussed in terms of solute structure and orientation at the interface. As indicated by surface tension values and the steep initial slopes of the surface tension *vs.* concentration curves, several of the new fluorinated solutes have much higher surface activity than those previously reported.

Introduction

In Part I[2] of this investigation it was shown that the initial spreading coefficient can be used to rapidly screen a large number of amphipathic compounds for possible surface activity in organic liquids. By using this technique several classes of partially fluorinated organic compounds were shown qualitatively to be promising surface active agents for organic liquids. In Part II[3] it was demonstrated that the partially fluorinated carboxylic esters were surface active in various organic liquids, the surface tension depression in any one organic liquid being a function of the balance between the organophobic and organophilic constituents of the molecule. These fluoroester solutes adsorbed at the organic liquid–air interfaces as unimolecular films whose orientation and packing depended upon the molecular structure, solubility and extent of association of the solute and solvent molecules. From the F *vs.* A isotherms, equations of state were calculated in Part III[4] for each adsorbed monomolecular film. It was concluded that the adsorbed molecules fail to form close-packed condensed monolayers even at the highest film pressures; at low film pressures all films are gaseous monolayers.

In the present study emphasis is given to the search for fluorinated solutes having the highest possible surface activities in organic liquids. For this purpose selected types of partially fluorinated compounds were designed, synthesized and studied, some in homologous series. The previous studies suggested some primary qualifications for optimum surface activity, such as low volatility, organophobic fluorocarbon chains so situated as to present

(1) Presented before the Division of Colloid and Surface Chemistry, American Chemical Society, at the 140th National Meeting in Chicago, Illinois, September 4–8, 1961.

(2) N. L. Jarvis and W. A. Zisman, *J. Phys. Chem.*, **63**, 727 (1959).

(3) N. L. Jarvis and W. A. Zisman, *ibid.*, **64**, 150 (1960).

(4) N. L. Jarvis and W. A. Zisman, *ibid.*, **64**, 157 (1960).

close packing on adsorption at the solvent surface, and organophilic constituents sufficiently soluble to impart desirable orientation of the molecule at the interface. With these requirements in mind, as well as obvious requirements of reasonable oxidative and hydrolytic stability, compounds were designed in which straight chain or highly branched hydrocarbon groups, benzene rings or chlorine-substituted benzene rings were used as the organophilic constituents of the molecules. To study the effects of homology, the number or length of the organophobic fluorocarbon chains in the molecule was varied. The effect of the replacement of the terminal fluorine atom of a fluorocarbon chain by hydrogen also was investigated. Since the organophobic and organophilic portions of the molecule may be connected by polar groups, which may be either organophilic or organophobic depending upon their structure and the nature of the substrate, a variety of these were included in this study.

Materials and Experimental Procedures

All of the compounds used as surface active agents, with the exception of the ϕ'-octyl alcohol, were synthesized for this investigation by J. G. O'Rear and P. J. Sniegoski of the Surface Chemistry Branch of this Laboratory. Each compound was a small scale preparation of high purity; the methods of preparation will be described in a subsequent publication by O'Rear and Sniegoski. Table I lists the compounds investigated along with selected physical constants. Using previously established nomenclature,[5] the perfluoro alcohol derivatives are denoted as ϕ'-derivatives and ω-monohydroperfluoro alcohol derivatives as ψ'-derivatives.

Seven organic liquids with graded surface tensions and different chemical compositions were used as solvents. The source, method of purification, and essential physical constants of propylene carbonate (γ = 41.1 dynes/cm.), tricresyl phosphate (γ = 40.2 dynes/cm.), Alkazene 42 (γ = 38.2 dynes/cm.), nitromethane (γ = 36.4 dynes/cm.) and hexadecane (γ = 27.6 dynes/cm.) are given in Part I.[2] The additional organic liquids used in this study were dioxane (γ = 32.9 dynes/cm.) and ethylbenzene (γ = 28.6 dynes/cm.), both of which were obtained from Eastman Organic Chemical Company. The dioxane was dried just before use with Linde Molecular Sieves.

Solutions of the surface active agents were prepared and their surface tensions measured using the procedures described in Part II.[3] The same method of preparation was used for the solid fluorocompounds as for the liquids, except that in the former case they were weighed on a semimicro balance. All surface tension measurements were made at 20 ± 0.4° and 50% R.H.

Results and Discussion

Surface Tension Lowering and Solubility.— Figures 1a–1h summarize the results of the surface tension measurements made for each fluorinated solute in the various organic solvents. Due to limiting solubility all the solutes were not studied in every solvent, the choice of solvent being predicated upon the structure of the respective fluorochemical.

The derivatives of the ψ'-alcohols, compounds 5–8 and 10–11 of Table I, all had higher surface tensions than the derivatives of the ϕ'-alcohols, but they were also more soluble in the polar organic solvents studied. It was suggested in Part II that the terminal hydrogen of a ψ'-compound weakly associates with the polar oxygen group in

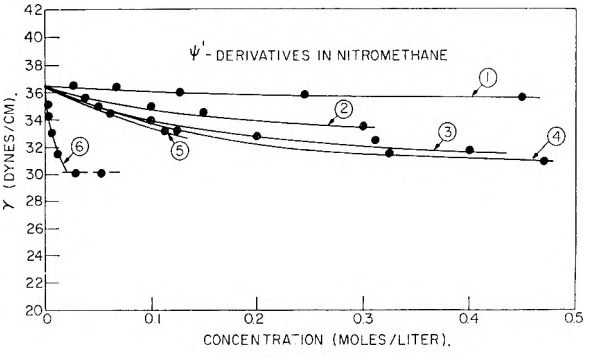

Fig. 1a

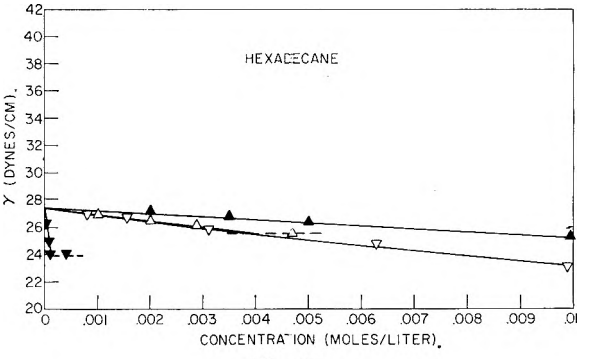

Fig 1b

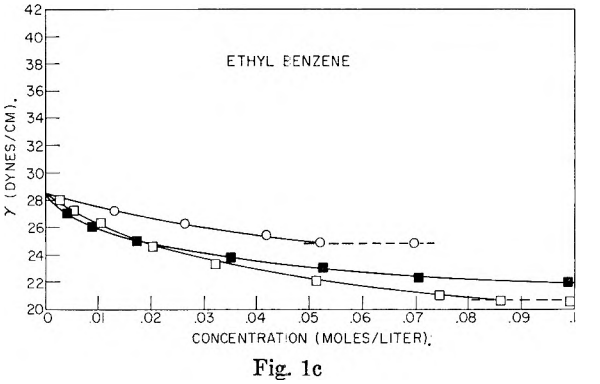

Fig. 1c

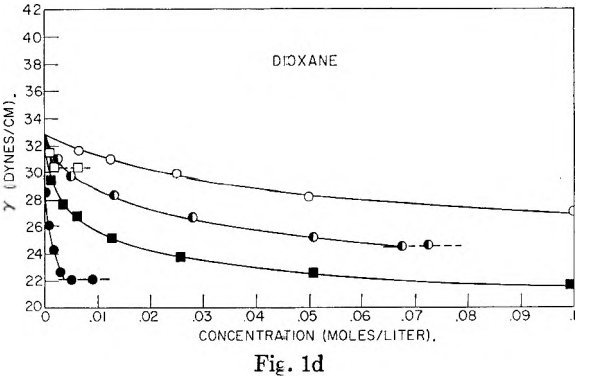

Fig. 1d

the more highly associating organic solvents, thus imparting high solubility to the ψ'-compound. As can be seen in Fig. 1e this combination of high surface tension and high solubility resulted in very low surface activity for the ψ'-alcohol derivatives, with the exception of tris-(ψ'-nonyl)-tricarballylate. This low surface activity is reflected

(5) P. D. Faurote, C. M. Henderson, C. M. Murphy, J. G. O'Rear and H. Ravner, *Ind. Eng. Chem.*, **48**, 445 (1956).

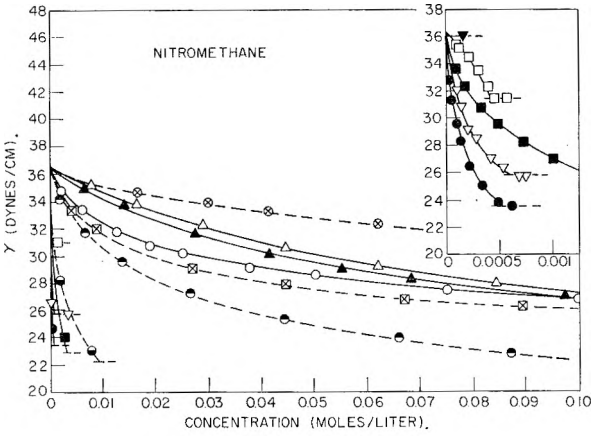

Fig. 1e

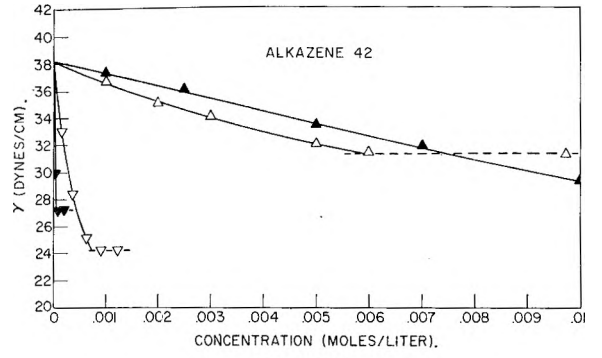

Fig. 1f

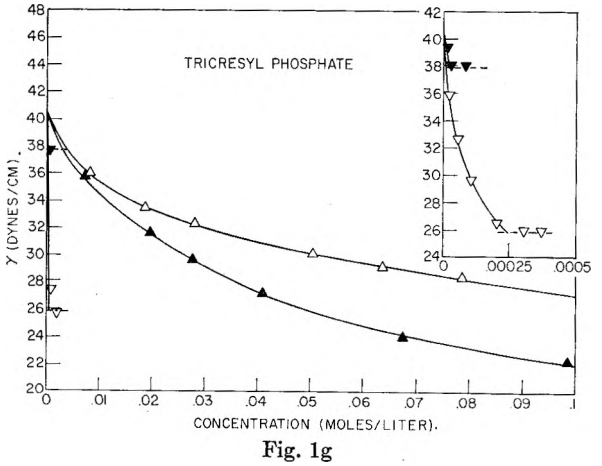

Fig. 1g

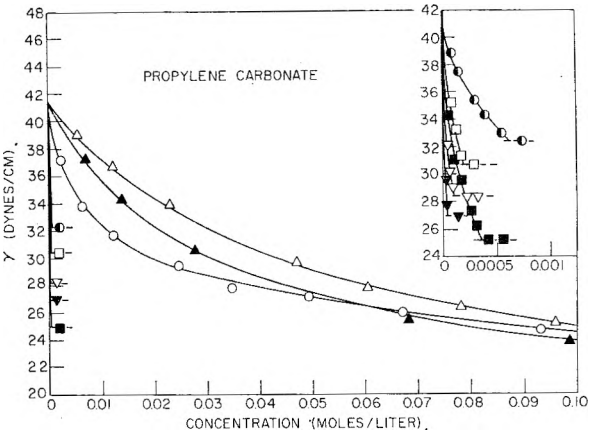

Fig. 1h

Fig. 1.—Surface tensions of partially fluorinated compounds in organic liquids: 1, tris-(ψ'-propyl)-tricarballylate; 2, tetrakis-(ψ'-amyl)-butane tetracarboxylate; 3, bis-(ψ'-heptyl)-phenyl succinate; 4, bis-(ψ'-heptyl)-tetrachlorophthalate; 5, bis-(ψ'-heptyl)-phenyl glutarate; 6, tris-(ψ'-nonyl)-tricarballylate. △, ϕ'-octyl alcohol; ▲, ϕ'-octyl ethanesulfonate; ▽, bis-(ϕ'-octoxy)-bis-(t-butoxy)-silane; ▼, tris-(ϕ'-octoxy)-t-butoxysilane; □, bis-(ϕ'-octyl)-tetrachlorophthalate; ○, tris-(ϕ'-butyl)-tricarballylate; ●, tris-(ϕ'-octyl)-tricarballylate; ■, bis-(ϕ'-octyl)-dodecenyl succinate; ◐, bis-(ϕ'-octyl)-toluene dicarbamate; ⊗, hexyl ϕ'-butyrate[3]; ⊠, 1,2,3-trimethylolpropane tris-(ϕ'-butyrate)[3]; ◓, bis-(ϕ'-hexyl)-3-methylglutarate[3]; ◒, bis-(ϕ'-octyl)-3-methylglutarate.[3]

TABLE I

PHYSICAL CONSTANTS OF PARTIALLY FLUORINATED SURFACE ACTIVE COMPOUNDS (AT 20°)

Number	Surface active solute	Density, g./ml.	Surface tension, dynes/cm.
1	ϕ'-Octyl alcohol	Solid	..
2	ϕ'-Octyl ethanesulfonate	1.709	19.1
3	Bis-(ϕ'-octoxy)-bis-(t-butoxy)-silane	1.525	18.4
4	Tris-(ϕ'-octoxy)-t-butoxysilane	1.702	18.5
5	Bis-(ψ'-heptyl)-α-phenyl glutarate	1.6164	26.2
6	Bis-(ψ'-heptyl)-phenyl succinate	1.6400	25.9
7	Tetrakis-(ψ'-amyl)-1,2,3,4-butane tetracarboxylate	Solid	..
8	Bis-(ψ'-heptyl)-tetrachlorophthalate	Solid	..
9	Bis-(ϕ'-octyl)-tetrachlorophthalate	Solid	..
10	Tris-(ψ'-propyl)-tricarballylate	1.4012	31.0
11	Tris-(ψ'-nonyl)-tricarballylate	Solid	..
12	Tris-(ϕ'-butyl)-tricarballylate	1.613	18.5
13	Tris-(ϕ'-octyl)-tricarballylate	Solid	..
14	Bis-(ϕ'-octyl)-α-n-dodecenyl succinate	1.484	19.4
15	Bis-(ϕ'-octyl)-2,4-toluene dicarbamate	Solid	..

in the small values given in the sixth column of Table II for the initial slopes of the surface tension *vs.* concentration curves in Fig. 1a. Due to the low surface activity of the derivatives of the ψ'-alcohols, no study was made of their behavior in solvents other than nitromethane.

The solubility of the ϕ'-compounds generally followed the pattern outlined in Part II, where the solubility was shown to be a function of the balance between the organophobic and organophilic constituents in the molecule. The polar groups used to join the fluorocarbon and hydrocarbon groups in the molecule were organophilic to the extent that they associated with the solvent molecules. Table III lists the estimated solubility values for the fluorocarbons obtained by extrapolating the surface tension *vs.* concentration curve for each solution until it intersected a horizontal line representing the surface tension of the saturated solution. The contributions of the polar connecting groups to the solubility in both polar and non-polar solvents is made evident by the higher solubility of the tricarballylates in the associating solvents than in non-polar ethylbenzene. In the ethylbenzene solu-

TABLE II

INITIAL SLOPE OF SURFACE TENSION *vs.* CONCENTRATION CURVES (AT 20°)

Surface active solute	Surface tension, γ, dynes/cm.	Initial slope × 10^2						
		Propylene carbonate (γ = 41.1)	Tricresyl phosphate (γ = 40.2)	Alkazene (γ = 38.2)	Nitro-methane (γ = 36.4)	Dioxane (γ = 32.9)	Ethyl-benzene (γ = 28.6)	Hexa-decane (γ = 27.6)
ϕ'-Octyl alcohol	..	0.36	0.56	1.4	0.25	...	..	0.56
ϕ'-Octyl ethanesulfonate	19.1	0.90	0.6	0.9	0.2	...	..	.24
Bis-(ϕ'-octoxy)-bis-(*t*-butoxy)-silane	18.4	410	280	64	60	...	..	.80
Tris-(ϕ'-octoxy)-*t*-butoxysilane	18.5	455	120	380	40	...	..	10.0
Bis-(ψ'-heptyl)-α-phenyl glutarate	26.2	....	....	...	0.035	...	..	...
Bis-(ψ'-heptyl)-phenyl succinate	25.9	....	....	...	.028	...	..	...
Tetrakis-(ψ'-amyl)-1,2,3,4-butane tetracarboxylate	..	....	....	...	.018	...	..	...
Bis-(ψ'-heptyl)-tetrachlorophthalate	..	....	....	...	.036	...	..	...
Bis-(ϕ'-octyl)-tetrachlorophthalate	..	72	....	...	11	1.6	0.20	...
Tris-(ψ'-propyl)-tricarballylate	31.0	....	....	...	0.004	...	..	...
Tris-(ψ'-nonyl)-tricarballylate	..	....	....	...	.8	...	..	...
Tris-(ϕ'-butyl)-tricarballylate	18.5	2.6	....	...	.56	0.2	.12	...
Tris-(ϕ'-octyl)-tricarballylate	..	....	....	...	110	14	..	...
Bis-(ϕ'-octyl)-α-*n*-dodecenyl succinate	19.4	310	....	...	30	4.8	.60	...
Bis-(ϕ'-octyl)-2,4-toluene dicarbamate	..	32	....	...	.....	0.56	..	...

TABLE III

SOLUBILITY OF PARTIALLY FLUORINATED SURFACE ACTIVE COMPOUNDS IN ORGANIC LIQUIDS (AT 20°)

Surface active solute	Surface tension, γ, dynes/cm.	Solubility (moles/l.) of solute						
		Propylene carbonate (γ = 41.1)	Tricresyl phosphate (γ = 40.2)	Alkazene 42 (γ = 38.2)	Nitro-methane (γ = 36.4)	Dioxane (γ = 32.9)	Ethyl-benzene (γ = 28.6)	Hexa-decane (γ = 27.6)
ϕ'-Octyl alcohol	Solid	>0.1	>0.1	5.9×10^{-2}	>0.1			9.5×10^{-3}
ϕ'-Octyl ethanesulfonate	19.1	>0.1	>0.1	1.85×10^{-2}	>0.1			1.54×10^{-2}
Bis-(ϕ'-octoxy)-bis-(*t*-butoxy)-silane	18.4	8.8×10^{-5}	2.3×10^{-4}	7.9×10^{-4}	5.5×10^{-4}			1.78×10^{-2}
Tris-(ϕ'-octoxy)-*t*-butoxysilane	18.5	2×10^{-5}	2×10^{-5}	4.9×10^{-5}	1×10^{-5}			9.5×10^{-4}
Bis-(ϕ'-octyl)-tetrachlorophthalate	Solid	1.7×10^{-4}			4.3×10^{-4}	1.9×10^{-3}	8.5×10^{-2}	
Bis-(ϕ'-octyl)-α-*n*-dodecenyl succinate	19.4	3.5×10^{-4}			2.93×10^{-3}	>0.1	>0.1	
Bis-(ϕ'-octyl)-2,4-toluene dicarbamate	Solid	6.2×10^{-4}			$<5 \times 10^{-5}$	6.6×10^{-2}	$<5 \times 10^{-5}$	
Tris-(ϕ'-butyl)-tricarballylate	18.5	1.02×10^{-1}			>0.1	>0.1	5.25×10^{-2}	
Tris-(ϕ'-octyl)-tricarballylate	Solid	$<5 \times 10^{-5}$			5.2×10^{-4}	3.25×10^{-3}	$<5 \times 10^{-5}$	
Tris-(ψ'-nonyl)-tricarballylate	Solid	.....			2.2×10^{-2}	.....	.....	

tion of bis-(ϕ'-octyl)-tetrachlorophthalate the solubility of the carboxyl group is obscured by the structural similarity between the hydrophilic portion of the solute molecule and the solvent molecules.

From Fig. 1a–1h it is possible to reach the following conclusions regarding the contribution of the various component groups in the surface active fluoroesters to the solubility of these compounds: (1) the ψ'-derivatives are much more soluble than the ϕ'-derivatives of approximately the same chain length; (2) compounds with an organophobic group consisting of only one perfluoroöctyl chain (ϕ'-octyl ethanesulfonate and ϕ'-octyl alcohol) are very soluble in polar solvents; (3) within an homologous series, such as the tricarballylates, tetrachlorophthalates, succinates, or silanes, the solubility decreases with increasing number and length of the ϕ'-chain; (4) a chlorine-substituted benzene ring is more organophilic than an unsubstituted one; (5) the polar connecting groups are decidedly organophilic in polar solvents; however, their actual contribution to the solubility of the surface active agent varies from one solvent to another.

Effect of Structure on Surface Tension Lowering. —Some of these new compounds are more surface active in organic solvents than any compounds reported previously, which is evident from the large initial slopes of the surface tension *vs.* concentration curves. Table II points out that these slopes are an order of magnitude steeper than even the highest ones previously observed.[3] Figure 1e, which is representative of the other solvents as well, clearly shows the increase in slope for most of the new solutes over the previously reported compounds in solutions of nitromethane.

Inspection of Fig. 1a–1h and Table II shows that with any one solvent the slope increases with the organophobic–organophilic ratio of the fluorocarbon derivatives, and that with a given solute the initial slope of the surface tension *vs.* concentration curve increases with increasing solvent surface tension. Ellison and Zisman[6] and Jarvis and Zisman[3] found that their data fitted the equation

$$-\frac{\partial\gamma}{\partial c_{\text{initial}}} = \alpha e^{\beta(\Delta\gamma_{\max})}$$

where α and β are constants depending upon the solute used and the degree of association in the organic solvents, and $\Delta\gamma_{\max} = \gamma_{\text{solvent}} - \gamma_{\text{solute}}$. Hence, a plot of log $(-\partial\gamma/\partial c)_{\text{initial}}$ *vs.* $\Delta\gamma_{\max}$ is a

(6) A. H. Ellison and W. A. Zisman, *J. Phys. Chem.*, **63**, 1121 (1959).

TABLE IV

SURFACE TENSIONS OF SATURATED SOLUTIONS IN VARIOUS ORGANIC LIQUIDS (AT 20°)

Surface active solute	Surface tension, γ, dynes/cm.	Surface tension of saturated solution (dynes/cm.) Propylene carbonate (γ = 41.1)	Tricresyl phosphate (γ = 40.2)	Alkazene 42 (γ = 38.2)	Nitromethane (γ = 36.4)	Dioxane (γ = 32.9)	Ethylbenzene (γ = 28.6)	Hexadecane (γ = 27.6)
φ′-Octyl alcohol	Solid	24.9[a]	27.6[a]	31.2	26.8[a]			25.4
φ′-Octyl ethanesulfonate	19.1	23.8[a] (22.3 at 0.16)	22.1[a] (20.9 at 0.14)	23.4	26.7[a]			23.8
Bis-(φ′-octoxy)-bis-(t-butoxy)-silane	18.4	28.3	25.9	24.2	25.7			21.2
Tris-(φ′-octoxy)-t-butoxysilane	18.5	28.3	38.0	27.4	36.0			24.0
Bis-(φ′-octyl)-tetrachlorophthalate	Solid	30.7			31.2	30.4	20.7	
Bis-(φ′-octyl)-α-n-dodecenyl-succinate	19.4	25.3			23.1	21.9[a]	21.9[a]	
Bis-(φ′-octyl)-2,4-toluene dicarbamate	Solid	32.5			Too insol.	24.7	Too insol.	
Tris-(φ′-butyl)-tricarballylate	18.5	24.5[a]			27.1[a] (22.2 at 0.688 *M*)	27.2[a] (23.6 at 0.559 *M*)	24.9	
Tris-(φ′-octyl)-tricarballylate	Solid	28.2			23.6	22.1	Too insol.	

[a] At 0.1 mole/l.

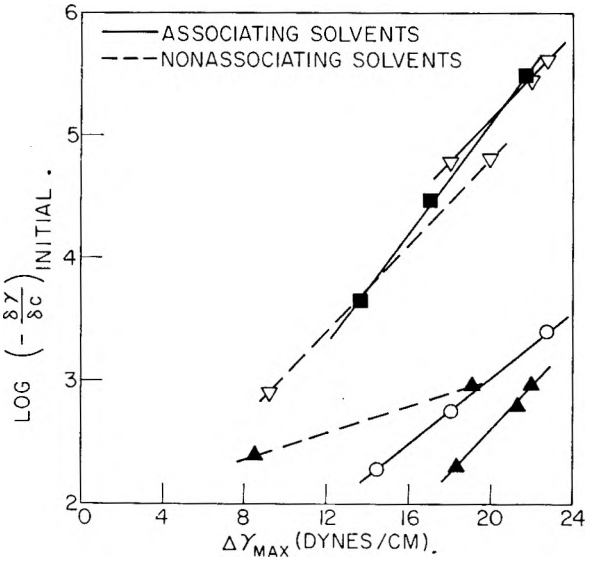

Fig. 2.—Relation of log $(-\partial\gamma/\partial c)_{initial}$ to maximum possible surface tension lowering of partially fluorinated compounds in organic liquids: ▲, φ′-octyl ethanesulfonate; ▽, bis-(φ′-octoxy)-bis-(t-butoxy)-silane; ○, tris-(φ′-butyl)-tricarballylate; ■, bis-(φ′-octyl)-dodecenyl succinate.

straight line. In verifying this relationship, we necessarily are limited to solutions containing solutes which are liquid at 20°. In agreement with the results reported in Part II,[3] two families of straight line graphs (see Fig. 2) were obtained for solutes dissolved in associating and non-associating solvents, respectively. Of course, only one curve was obtained where the solvents were limited to the associating type.

A large initial slope, however, does not necessarily imply a large surface tension depression. In order to greatly depress the surface tension of each solvent, the solute used should be soluble enough to permit the adsorption of a high concentration of perfluoro groups at the organic liquid–air interface. Figures 1a–1h show that the highly fluorinated solutes, especially those containing several φ′-octyl chains, are so slightly soluble that they are unable to depress significantly the surface tension of many of the solvents. The surface tensions of each of the saturated solutions at 20° are given in Table IV. It can be seen that in some systems the surface tension was depressed below 22–24 dynes/cm., that surface tension value corresponding to the closest packing of hydrocarbon groups at a liquid–air interface.[7] Since surface tension values as low as 20.7 dynes/cm. were obtained, it can be concluded that an excess of perfluoro groups over hydrocarbon groups is exposed at the liquid–air interface. Surface tensions below 22–24 dynes/cm. have been reported previously for aqueous solutions of highly fluorinated surface active compounds added as pure compounds[6,8–11] or as additives used in combination with conventional hydrocarbon-type wetting agents.[12]

The surface active efficiency of the solute has been defined in Part II as 100 $(\Delta\gamma/\Delta\gamma_{max})$, where $\Delta\gamma$ stands for the observed surface tension lowering, and $\Delta\gamma_{max} = \gamma_{solvent} - \gamma_{solute}$, which represents the maximum possible surface tension lowering, *i.e.*, the lowering of the solvent surface tension until it corresponds to the surface tension of the pure liquid solute. The efficiency of each solute in saturated solutions of the various solvents is reported in Table V; where data on saturated solutions were not available, the efficiencies were calculated on the basis of a 0.1 *M* solution (footnote *a*). The results should be quite comparable because, if the solute is to be useful as a surface active agent, only a small concentration should be required to give the maximum possible surface tension lowering. The necessity of a proper solubility balance is evident in Table V. If the solubility is too high, as with tris-(φ′-butyl)-tricarballylate in nitromethane or dioxane, or too low as with tris-(φ′-octoxy)-t-butoxysilane in nitromethane, the surface active efficiency is decreased. Solutes exhibiting the highest efficiencies in all solvents, φ′-octyl ethanesulfonate and bis-(φ′-octyl)-α-n-

(7) N. L. Jarvis and W. A. Zisman, "The Stability and Surface Tension of Teflon Dispersions in Water," presented before Div. of Colloid Chemistry A.C.S. Meeting, Atlantic City, Sept., 1959. NRL Report 5306, May, 1959 (to be published).

(8) H. B. Klevens and M. Raison, *J. chim. phys.*, **51**, 1 (1954).

(9) H. M. Scholberg, R. A. Guenthner and R. I. Coon, *J. Phys. Chem.*, **57**, 923 (1953).

(10) C. H. Arrington and G. D. Patterson, *ibid.*, **57**, 247 (1953).

(11) M. K. Bernett and W. A. Zisman, *ibid.*, **63**, 1911 (1959).

(12) M. K. Bernett and W. A. Zisman, *ibid.*, **65**, 448 (1961).

TABLE V

SURFACE ACTIVE EFFICIENCY OF PARTIALLY FLUORINATED COMPOUNDS IN ORGANIC LIQUIDS AT SATURATION (AT 20°)

Surface active solute	Surface tension, γ, dynes/cm.	Surface active efficiency of solute, %: Propylene carbonate (γ = 41.1)	Tricresyl phosphate (γ = 40.2)	Alkazene 42 (γ = 38.2)	Nitromethane (γ = 36.4)	Dioxane (γ = 32.9)	Ethylbenzene (γ = 28.6)	Hexadecane (γ = 27.6)
ϕ'-Octyl ethanesulfonate	19.1	78.7[a] (85.4 at 0.16 M)	85.9[a] (91.5 at 0.14 M)	76.9[a]	55.6[a]			44.7
Bis-(ϕ'-octoxy)-bis-(t-butoxy)-silane	18.4	56.8	65.9	70.7	59.4			46.7
Tris-(ϕ'-octoxy)-t-butoxysilane	18.5	56.4	11.0	54.7	2.2			39.5
Bis-(ϕ'-octyl)-α-n-dodecenyl succinate	19.4	70.5			78.4	81.4[a]	72.8[a]	
Tris-(ϕ'-butyl)-tricarballylate	18.5	73.4			52.2[a] (78.9 at 0.688 M)	39.6[a] (64.6 at 0.559 M)	36.6	

[a] At 0.1 mole/l.

dodecenyl succinate, have as an organophilic constituent a straight hydrocarbon chain containing a terminal $-CH_3$ group. This structure apparently has some solubility advantage in the systems studied, for even with bis-(ϕ'-octyl)-α-n-dodecenyl succinate in propylene carbonate, which has a low saturation concentration (3.5×10^{-4} M), the surface active efficiency is still 70.5%.

Adsorption Isotherms.—The surface excess of solute molecules adsorbed at each interface was calculated from the surface tension *vs.* concentration curves in Fig. 1, using the Gibbs equation in the form

$$\Gamma = -\frac{c}{RT}\left(\frac{\partial\gamma}{\partial c}\right)$$

where Γ is the "surface excess" of solute, c the concentration and γ the solution surface tension. Rigorously, the equation should be expressed in terms of activities rather than concentrations; however, for the dilute solutions used, concentration was assumed to be a good approximation of the activity in calculating the surface excess. In the case of the ψ'-derivatives, where concentrations went above 0.1 M, this approximation may be invalid, and the simple Gibbs equation may no longer be useful.

The calculated adsorption isotherms shown in Fig. 3a and 3b for several partially fluorinated agents in nitromethane and propylene carbonate are typical of those obtained in the other solvents. Variations in solubility and orientation of the adsorbed molecules at the interface are responsible for the differences in the initial slopes and the maximum values of the Γ *vs.* concentration curves. No further increase in Γ above the first plateau in the adsorption curves was observed in any system studied. It was observed, as in Part II, that compounds such as tris-(ϕ'-butyl)-tricarballylate or bis-(ϕ'-octyl)-α-n-dodecenyl succinate, whose organophilic groups give them appreciable solubility in the polar solvents, often caused a greater total surface tension lowering than compounds with an initially steeper adsorption isotherm but a lower solubility. It also was found that at very low concentrations only these Γ *vs.* concentration curves obey the Langmuir adsorption isotherms.

Force *vs.* Area Isotherms.—A graph of F *vs.* A at 20° for the adsorbed film at the organic liquid–air interface was computed for every fluorinated solute in each liquid substrate. The total surface

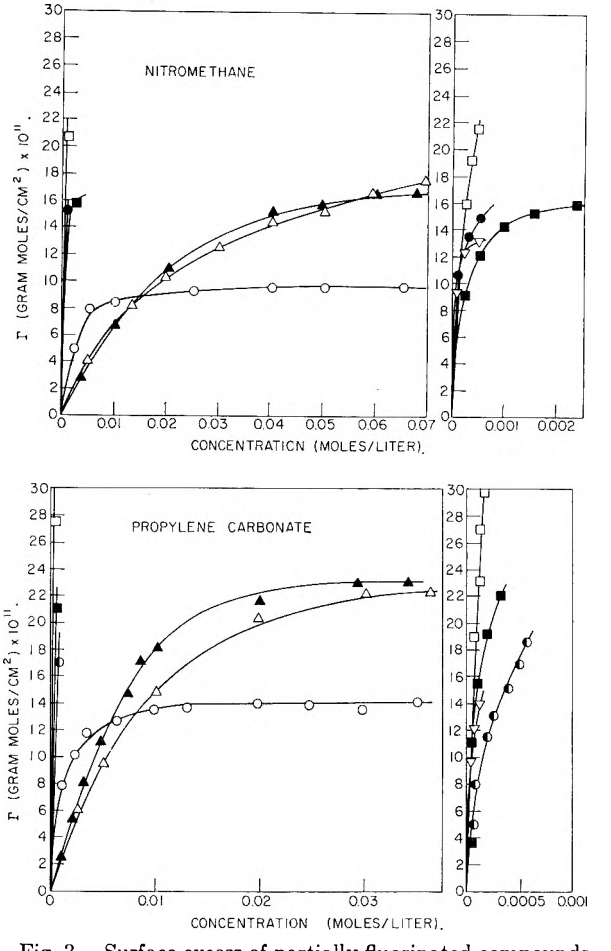

Fig. 3.—Surface excess of partially fluorinated compounds in organic liquids: △, ϕ'-octyl alcohol; ▲, ϕ'-octyl ethanesulfonate; ▽, bis-(ϕ'-octoxy)-bis-(t-butoxy)-silane; □, bis-(ϕ'-octyl)-tetrachlorophthalate; ○, tris-(ϕ'-butyl)-tricarballylate; ●, tris-(ϕ'-octyl)-tricarballylate; ■, bis-(ϕ'-octyl)-dodecenyl succinate; ◐, bis-(ϕ'-octyl)-toluene dicarbamate.

tension lowering caused by the solute was replaced by the film pressure (F); the area (A) per adsorbed molecule for each solute concentration was determined from the surface excess Γ, assuming always that the solute adsorbed as a unimolecular layer. The resulting F *vs.* A graphs for the partially fluorinated surface active agents dissolved in nitromethane or in propylene carbonate are shown in Fig. 4a and 4b. No extrapolation to a limiting area per molecule (A_0) could be made since the isotherms usually did not exhibit rectilinear be-

TABLE VI

LOWEST VALUES OF A OF SURFACE ACTIVE SOLUTES OBTAINED IN ORGANIC LIQUIDS (AT 20°)

Surface active solute	Lowest value of A (Å.²/molecule) Propylene carbonate (γ = 41.1)	Tricresyl phosphate (γ = 40.2)	Alkazene 42 (γ = 38.2)	Nitromethane (γ = 36.4)	Dioxane (γ = 32.9)	Ethylbenzene (γ = 28.6)	Hexadecane (γ = 27.6)
ϕ'-Octyl alcohol	69	105		78[a]			
ϕ'-Octyl ethanesulfonate	69	67	42	84[a]			110
Bis-(ϕ'-octoxy)-bis-(t-butoxy)-silane	119	97	107	124			96
Tris-(ϕ'-octoxy)-t-butoxysilane	Too insol.	Too insol.	104	Too insol.			162
Bis-(ϕ'-octyl)-tetrachlorophthalate	56			75	219[b]	117	
Bis-(ϕ'-octyl)-α-n-dodecenyl succinate	66			101	165	143[a]	
Bis(ϕ'-octyl)-2,4-toluene dicarbamate	86[b]			Too insol.	145[b]	Too insol.	
Tris-(ϕ'-butyl)-tricarballylate	104			134 (88 at 0.3 M)	138[a]	127[b]	
Tris-(ϕ'-octyl)-tricarballylate	Too insol.			109	141	Too insol.	

[a] Too soluble to approach limiting area at concentration reported. [b] Too insoluble to form close-packed monolayer.

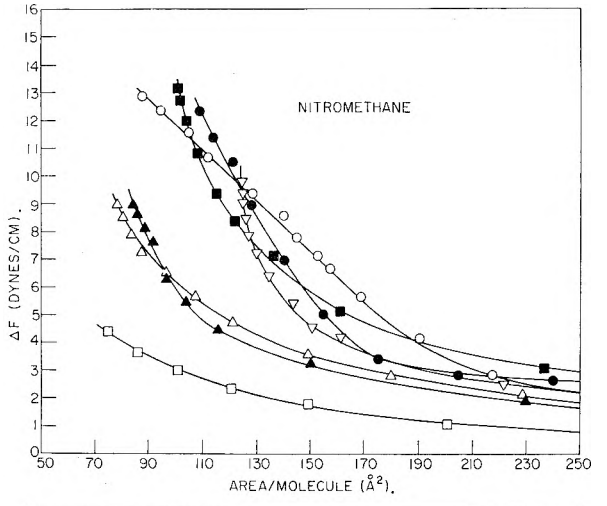

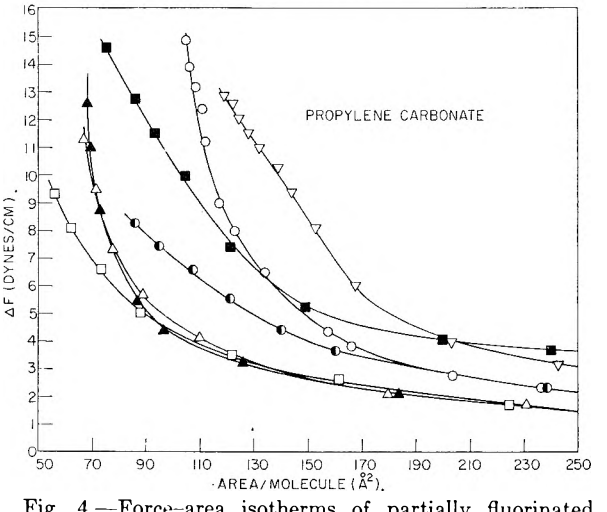

Fig. 4.—Force–area isotherms of partially fluorinated compounds in organic liquids: △, ϕ'-octyl alcohol; ▲, ϕ'-octyl ethanesulfonate; ▽, bis-(ϕ'-octoxy)-bis-(t-butoxy)-silane; □, bis-(ϕ'-octyl)-tetrachlorophthalate; ○, tris-(ϕ'-butyl)-tricarballylate; ●, tris-(ϕ'-octyl)-tricarballylate; ■, bis-(ϕ'-octyl)-dodecenyl succinate; ◐, bis-(ϕ'-octyl)-toluene dicarbamate.

havior in any region; at best a liquid condensed film was formed, as with bis-(ϕ'-octoxy)-bis-(t-butoxy)-silane or bis-(ϕ'-octyl)-α-n-dodecenyl succinate in propylene carbonate.

The lowest value of A calculated for each solute (Table VI) varied with the structure of the compound and its solubility in the organic solvent. When the solubility was very low, close packing of the monolayer was not attained; when the solubility was high, low values of A were not reached in the concentration range studied. An exception was the system tris-(ϕ'-butyl)-tricarballylate in nitromethane where the curves were extended to a fairly high concentration (0.3 M); at or above this concentration the Gibbs equation as used here became invalid, as the solution concentration no longer approximated the activity of the solute molecules.

Relation of Minimum Surface Tension to Surface Constitution.—In aqueous solutions of conventional wetting agents, the lowest surface tensions are attained when the surface of the liquid is covered with a close-packed monolayer of vertically oriented hydrocarbon chains in which a continuous layer of $-CH_3$ groups is exposed to the surface.[7] By analogy the surface tension of a solution of a fluorinated solute in an organic liquid would be at a minimum when there is a closely packed film of perfluoro groups adsorbed at the interface with the $-CF_3$ groups exposed at the surface. Surface tensions of pure fluorocarbons are quite low[9,13,14]; for example, the surface tension of pure perfluorooctane is 13.6 dynes/cm. at 20°.[9] Aqueous solutions of pure perfluorocarboxylic acids have been reported with surface tensions of 15–18 dynes/cm.[8,9] and aqueous systems containing mixtures of perfluoroöctyl alcohol and conventional wetting agents reached surface tensions as low as 15.2 dynes/cm.[12] These low surface tensions correspond to rather close-packed films of $-CF_2-$ and $-CF_3$ groups at the water–air interface. As an indication of the surface free energy of a $-CF_2-$ saturated surface, Zisman and co-workers found the critical surface tension of polytetrafluoroethylene (primarily $-CF_2-$) to be 18.4 dynes/cm.,[15] while for a closely packed $-CF_3$ surface it is about 6 dynes/cm.[16] The importance of orientation of the fluorocarbon

(13) G. H. Rohrback and G. H. Cady, *J. Am. Chem. Soc.*, **71**, 1938 (1949).

(14) J. H. Simon, "Fluorine Chemistry," Academic Press Inc., New York, N. Y., 1950, p. 438.

(15) H. W. Fox and W. A. Zisman, *J. Colloid Sci.*, **5**, 514 (1950).

chain on surface tension depression thus is quite evident. Using this information on the effect of structure and orientation of fluorocarbon groups on surface tension, in conjunction with the calculated areas per molecule, certain conclusions can be reached regarding solute orientation at an organic liquid–air interface.

Inspection of Table VI shows that the lowest values of A calculated for compounds containing only one fluorinated chain (ϕ'-octyl ethanesulfonate and ϕ'-octyl alcohol) are considerably larger than the cross-sectional area of 24.5 Å.^{2} determined from the Stuart–Briegleb ball models. These solutes are too soluble in the polar solvents propylene carbonate, tricresyl phosphate and nitromethane to give saturated solutions in the concentration range studied. The lowest values of A observed, which vary from about 70 to 80 Å.^{2} at 0.1 M in these solvents, are presumed to correspond to the adsorption of the molecules lying in the surface rather than orienting vertically in close packing. Where the solubility is not so great, as with ϕ'-octyl ethanesulfonate in Alkazene, the lowest value of A obtained from a saturated solution is 42 Å.^{2}; this suggests adsorption of the solute with the organophobic fluorocarbon chains oriented away from the liquid in a tilted position. The minimum surface tension recorded for this solution was 23.4 dynes/cm., which is much higher than the surface tension of pure fluorocarbons or of a closely packed adsorbed film of perfluorochains exposing $-CF_3$ groups at the surface. If such an orientation and packing were obtained, surface tensions of 15 dynes/cm. or less would be possible. The much higher value recorded for ϕ'-octyl ethanesulfonate in Alkazene makes it apparent that even though the fluorocarbon group is oriented away from the liquid, the surface of the substrate is by no means covered with a continuous fluorocarbon film. The very large values for the most concentrated solutions of ϕ'-octyl ethanesulfonate and ϕ'-octyl alcohol in hexadecane may be due to the absence of an adequate organophilic group able to anchor the solute molecule sufficiently firmly in the liquid phase to give it an orientation favorable for close packing at the interface.

The compounds containing two fluorinated chains so placed as to allow vertical orientation and close packing have lowest values of A in some solvents which correspond to such orientations and packing of their chains. The smallest value of A obtainable for the four solutes of this type, as determined from ball models, is about 50 Å.^{2} when the fluorocarbon chains are vertically oriented and at their closest packing. Bis-(ϕ'-octyl)-tetrachlorophthalate, with a lowest value of A of 56 Å.^{2} in propylene carbonate, closely approaches this limiting area. This same solute has lowest values of A of 75 and 219 Å.^{2}/molecule in nitromethane and dioxane, respectively, even though the minimum surface tensions found with each of the three solutions are about the same, 30.7, 31.2 and 30.4 dynes/cm., much higher than would be expected for a fluorine-rich surface. On the basis of ball model studies the correlation of the small area per molecule in propylene carbonate with the high surface tension value is rather difficult unless one supposes that portions of the chlorinated benzene ring are entering the interface. Quite another situation occurs with the tetrachlorophthalate in ethylbenzene, where the minimum surface tension attained is only 20.7 dynes/cm., but A still has the high value of 117 Å.^{2}, or 58 Å.^{2} per fluorocarbon chain. The solubility of this compound in ethylbenzene is so much greater than in the other solvents that the chlorinated benzene ring apparently remains in the solvent and does not enter the interface. The large value of A may indicate the fluorocarbon chains are more or less tilted or oriented horizontally, perhaps interspersed with solvent molecules. If the fluorocarbon groups orient horizontally in close-packed arrangement, one would expect the low surface tension of a surface containing a larger percentage of $-CF_2-$ groups than $-CF_3$ groups.

Bis-(ϕ'-octyl)-α-n-dodecenyl succinate reaches lowest values of A in propylene carbonate and nitromethane of 66 and 101 Å.^{2}, respectively, indicating the two fluorocarbon constituents are oriented away from the surface, although tilted or staggered in varying degrees. In dioxane it is possible that one or both of the fluorocarbon chains are lying parallel to the surface. The lowest values of A of bis-(ϕ'-octoxy)-bis-(t-butoxy)-silane in each of the solvents ranged from 96 to 124 Å.^{2}/molecule, which suggests that one fluorocarbon chain is oriented vertically and the other horizontally, or more likely both of them are adsorbed in a somewhat canted position.

On the basis of the bis-(ϕ'-octyl) derivatives studied, the carboxyl group exhibited greater interaction with the associating solvents than the other polar connecting groups; its immersion in the bulk liquid caused the fluorocarbon chains to be oriented away from the interface, thus allowing for closer packing of the solute molecules. In the non-associating liquids, the carboxyl groups appear to have as little contact as possible with the substrate, giving the organophobic chains more freedom of rotation; the tilt away from the vertical then may be increased until one or both chains lie horizontally in the interface, increasing the area per molecule. The silicate group acts much like the carboxyl group, but other parameters, such as solubility, do not allow a direct comparison. This also is true for the carbamate group, which was quite insoluble.

Four homologous tricarballylates also were investigated. Of the two ψ'-derivatives studied, tris-(ψ'-propyl)-tricarballylate was found to be too soluble in nitromethane to approach a limiting area per molecule in the concentration range studied, and tris-(ψ'-nonyl)-tricarballylate was too insoluble even in nitromethane to form a close-packed monolayer. Although quite soluble in propylene carbonate, nitromethane and dioxane, tris-(ϕ'-butyl)-tricarballylate formed adsorbed films, the lowest values of A being 104, 134 and 138 Å.^{2}, respectively. These values are not too different from those of 109 Å.^{2} in nitromethane and 141 Å.^{2} in dioxane of the much less soluble derivative tris-(ϕ'-octyl)-

(16) E. F. Hare, E. G. Shafrin and W. A. Zisman, *J. Phys. Chem.*, **58**, 236 (1954).

tricarballylate. Several possible orientations at the organic liquid–air interface can be postulated for these solutes, the most plausible suggesting random orientation away from the interface for all three fluorocarbon chains. However, it also is possible that only two of the fluorocarbon groups are oriented out of the interface and the third group remains behind in the solvent. In all instances the lowest value of A obtained for each system is consistent with the areas measured by the Stuart–Briegleb ball models arranged in the proposed configurations.

General Discussion.—Although it was thought that a closer packing of the fluorocarbon groups could be achieved by increasing the number or length of the organophobic fluorinated alkane substituents, the results show that other factors also play an important role. Since the lowest value of A obtained is a measure of the closeness of packing obtained, it is concluded that the dicarboxylic esters in polar solvents adsorbed as the most condensed monolayers in the systems studied. Factors that contribute to this close packing are: (1) structure and solubility of the organophilic constituent; either a long straight-chain hydrocarbon group, or a hydrocarbon constituent made more soluble by chlorine substitution seemed to be the most effective; (2) type and position of the polar connecting group; (3) fluorination, length and number of organophobic chains; a terminal hydrogen in an otherwise fluorinated alkyl chain increases solubility in polar solvents and decreases adsorptivity; longer chains decrease solubility and often lead to a closer packed monolayer, but too many chains attached in close proximity to the same organophilic portion of the molecule will interfere sterically with each other.

Possibly the molecules cannot adsorb from solution at the interface in a close-packed orientation because the average adsorption lifetime is too short. Equally large areas per molecule at about the same film pressures were reported long ago[17] for butyl alcohol in aqueous solutions; in order for A to be small enough to indicate close packing, the film pressure F had to be about three times higher than the highest values we were able to attain. Close packing may be prevented in these organic solutions due to a more marked competitive adsorption than occurs in aqueous solutions.

The most surface active compounds studied did orient to cause large surface tension decreases, but in no case was the depression as great as one might expect from a liquid completely covered with perfluorinated alkyl groups. Nevertheless, some of the new solutes reported were more surface active in organic solvents than any previously reported compounds, as evident by the much steeper initial slopes of the graphs of surface tension *vs.* concentration and adsorption *vs.* concentration. These and similar surface active agents should prove interesting in their ability to adsorb and modify the surface composition and other surface properties of organic liquids.

Where the solubility is too low to permit the use of these compounds as surface active agents for solutions, they may be spread upon organic substrates as insoluble films or monolayers, or as "piston monolayers" for measuring high equilibrium spreading pressures of organic liquids by extending the method of Washburn and Keim[18] to non-aqueous substrates.

(17) W. D. Harkins, "The Physical Chemistry of Surface Films," Reinhold Publ. Corp., New York, N. Y., 1952, p. 210.

(18) E. R. Washburn and C. P. Keim, *J. Am. Chem. Soc.*, **62**, 1747 (1940).

GROSS AND NET QUANTUM YIELDS AT 2537 Å. FOR FERROUS TO FERRIC IN AQUEOUS SULFURIC ACID AND THE ACCOMPANYING REDUCTION OF WATER TO GASEOUS HYDROGEN[1]

BY LAWRENCE J. HEIDT, MARY G. MULLIN, WILLIAM B. MARTIN, JR., AND ANN MARIE JOHNSON BEATTY

Chemistry Department, Massachusetts Institute of Technology, Cambridge, Mass.

Received October 2, 1961

Gross, ϕ_g, and net, ϕ_n, quantum yield measurements have been made for the photochemical conversion by light of 2537 Å. of up to 1.4% of the ferrous to ferric sulfate and of the accompanying production of gaseous hydrogen in aqueous sulfuric acid at 25°. In each solution ϕ_g decreased as the reaction progressed but ϕ_n remained constant. In the different solutions ϕ_n remained at 0.4 between 0.1 and 0.8 M ferrous sulfate in 2 M H_2SO_4 but increased from 0.16 to 0.74 between 0.15 and 6.0 M sulfuric acid. The data support the hypothesis that in 2 M and more dilute sulfuric acid ferrous sulfate exists mostly as ion pairs which in 6.0 M sulfuric acid are partly replaced by contact ferrous sulfate complexes.

Introduction

The photochemical production of gaseous hydrogen from water by light absorbed by cerous and ferrous species in aqueous acid has been under investigation for some time in this Laboratory as a part of our physicochemical research program on solar energy conversion.[2] Energy of the light absorbed by these systems is converted into chemical

(1) We wish to acknowledge financial support for this research from the G. L. Cabot Fund of M.I.T. on a continuing basis, the C. F. Kettering Foundation for the exploratory part of this research and the Air Research and Development Command, United States Air Force. W. B. Martin, Jr., worked on this problem as a National Institutes of Health Special Research Fellow, United States Public Health Service, and a Fellow of the M.I.T. School for Advanced Study for the period October 1, 1959 to September 30, 1961. He is Professor of Organic Chemistry at Union College, Schenectady, New York. This is publication No. 73 of the M.I.T. Solar Energy Conversion Project.

(2) (a) L. J. Heidt and A. F. McMillan, *Science*, **117**, 75 (1953); (b) *J. Am. Chem. Soc.*, **76**, 2135 (1954).

TABLE I

NOMINAL (N) AND ACTUAL (A) WAVE LENGTHS IN Å. APPLICABLE TO CARY MODEL 11, No. 69

N:	4000	3940	3900	3840	3800	3740	3700	3640	3600	3540	3500	3440	3400
A:	4040	3974	3930	3864	3820	3757	3715	3651	3609	3547	3505	3443	3401
N:	3340	3300	3240	3200	3140	3100	3040	3000	2940	2900	2840	2800	2537
A:	3340	3299	3238	3198	3138	3098	3037	2997	2938	2898	2838	2798	2537

energy available as fuel in the form of gaseous hydrogen which is especially suitable for use in fuel cells.

The trends of our results, our conclusions and our working hypotheses have become known to many by means of our unpublished reports and lectures as well as through visits to our Laboratory. Among those favoring us with such visits have been Dainton,[3] Weiss[4] and Stein,[5] who since have published related results although not on a quantum yield basis. Similar results also not on a quantum yield basis have been published by Lefort and Douzou.[6]

We present here our gross and net quantum yields and the related essential measurements on the conversion of ferrous to ferric and the accompanying production of gaseous hydrogen in aqueous sulfuric acid at 25° by light of 2537 Å.

$$\phi_n = \phi_g(\epsilon_2 c_2 + \epsilon_3 c_3)/\epsilon_2 c_2 \qquad (1)$$

where ϵ and c represent molar absorptivities and concentrations, respectively, in terms of gram atoms of iron per liter per cm. Negligible amounts of 2537 Å. were absorbed by the other solute species.

Materials.—The solutions were prepared by employing conductivity water and the purest Baker, du Pont, Fisher or Merck analyzed reagent grade chemicals. The ferric solutions intentionally added to the ferrous solutions were made up from Fisher certified $Fe_2(SO_4)_3$ powder.

Reaction vessels were of cylindrical fused quartz and were like those previously described.[2] Each vessel was of uniform diameter but the different vessels had diameters ranging from 2.56 to 2.76 cm.

Photolyses were carried out at 25° with monochromatic light of 2537 Å. in the manner previously employed here.[7] In every case 30 ± 0.01 ml. of solution was photolyzed for 1 to 16 min. but in most cases for 1 or 2 min.

Measurements of the light flux incident upon the solution in each reaction vessel were made in the manner previously described.[2]

Actinometry was carried out with a solution about 0.001 *M* in $UO_2C_2O_4$ and 0.004 *M* in $H_2C_2O_4$. Decomposition of the oxalate by the light was kept below 20% by adjustment of the time of photolysis. The change in oxalate concentration brought about by the absorbed light was determined by addition of excess ceric sulfate solution followed by titration of the excess ceric sulfate with ferrous sulfate solution using as an indicator 1 ml. of 0.0013 *M* "Ferroin." A correction was made for the ceric consumed by the indicator. The quantum yield at 25° for the actinometer was taken as 0.63 mole oxalate decomposed to material non-oxidizable by ceric per mole of quanta of 2537 Å. absorbed by the solution.

Optical densities were measured over the wave length range 4000 Å. to about 1900 Å. by means of Cary recording spectrophotometers Models 11 and 14. Nominal scale readings of wave lengths and the corresponding actual values are given in Table I. In the other tables only the nominal values are given.

Absorbance values, *A*, of the ferrous and ferric species were determined from the optical density values in the manner previously described for cerous species in cerous perchlorate solutions in order to allow for light absorbed by other components of the solution.[8]

Solutions employed for the photochemical and light absorbance measurements were freed and kept free of air, sulfur dioxide and other obnoxious gases. This was done by sweeping out these gases with Airco prepurified nitrogen, carbon dioxide or U.S.N. approx. 100% pure oil-free Grade A helium.

The quantum yield measurements were made mostly on the solutions while under an atmosphere of helium. Carbon dioxide was used only for the solutions employed to determine also the ratio of gaseous hydrogen produced to ferrous converted to ferric.

Ferrous solutions were made up from iron wire and sulfuric acid. Care was taken to minimize the reduction of sulfate and the oxidation of ferrous to ferric by employing sulfuric acid of less than 0.2 *M* to dissolve the iron wire and by carrying out in an inert atmosphere all operations involving the solutions. The carbon and any other suspended materials produced on dissolving the iron wire were removed by filtration through a sintered glass plug of medium porosity.

Initial compositions of the solutions photolyzed are given in Table II under the headings (H_2SO_4) and ($FeSO_4$). The column headed "Range of Fe(III) added as $Fe(SO_4)_{3/2}$" applies only to the solutions used for the determination of ϵ_3.

TABLE II

SOLUTION COMPOSITIONS

Concentrations are expressed in gram formula weights per liter of solution at 25°

Soln.	(H_2SO_4)	($FeSO_4$)	Range of Fe(III) added as $Fe(SO_4)_{3/2}$
A	1.99	0.10	0.00024 to 0.0038
B	1.98	.50	.001 to 0.008
C	1.87	.70	.0005 to 0.008
D	1.97	.80	None
E	6.0	.10	0.0002 to 0.003
F	0.15	.10	0.0004 to 0.007

Concentrations of ferrous sulfate were determined from the weighed amount of iron employed to prepare a solution and by titration with ceric sulfate solution as described under "Actinometry."

Sulfuric acid concentrations were determined by titration with sodium hydroxide solution using phenolphthalein or a *p*H meter to determine the end-point.

Ferric sulfate concentrations were determined in two ways. When sufficiently large, ferric was determined by reduction to ferrous with a Jones reductor and titration of the ferrous to ferric. Titrations were made in an atmosphere of nitrogen, and care was taken to sweep all molecular hydrogen and other reducing gases out of the solution before addition of excess ceric sulfate.

The small ferric concentrations produced by photolyses were determined from optical density measurements of the solution while kept sealed in the reaction vessel. This was done mainly at 3000, 3040 and 3100 Å. where there is a peak in the absorption spectrum of ferric sulfate species and where ϵ_3/ϵ_2 is greater than 100,000. The optical densities were obtained by placing the reaction vessel in the cell compartment of the Cary Model 11 recording spectrophotometer and appropriately adjusting the vessel's position and

(3) (a) F. S. Dainton, *Discussions Faraday Soc.*, **29**, 257 (1960); (b) F. S. Dainton and D. B. Peterson, *Nature*, **186**, 878 (1960); (c) F. S. Dainton and S. A. Sills, *ibid.*, **186**, 879 (1960); (d) G. Czapski and J. Jortner, *ibid.*, **188**, 50 (1960).

(4) E. Hayon and J. Weiss, *J. Chem. Soc.*, 3866 (1960).

(5) (a) G. Stein, Fifth International Symposium on Free Radicals, Inst. Phys. Chem., Univ. of Uppsala, Uppsala, Sweden, July 6–7, 1961, Paper 67. The symposium papers were published in 1961 by Almqvist and Wiksell, Stockholm, Sweden; (b) G. Czapski, J. Jortner and G. Stein, *J. Phys. Chem.*, **65**, 956 (1961); (c) J. Jortner, R. Levine, M. Ottolenghi and G. Stein, *ibid.*, **65**, 1232 (1961).

(6) M. Lefort and P. Douzou, *J. chim. phys.*, **53**, 536 (1956).

(7) L. J. Heidt, *Science*, **90**, 473 (1939).

(8) L. J. Heidt and J. Berestecki, *J. Am. Chem. Soc.*, **77**, 2049 (1955).

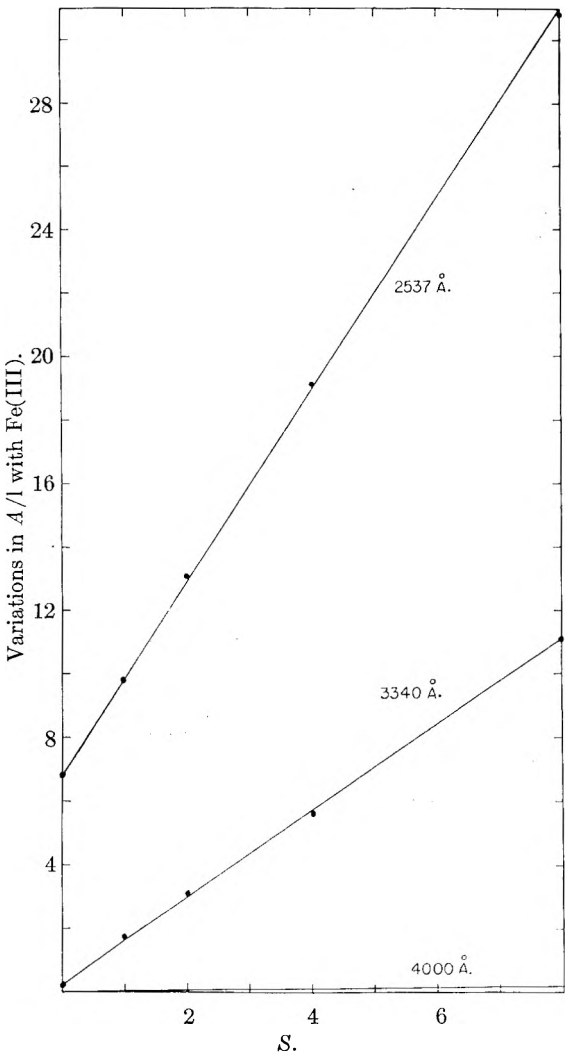

Fig. 1.—Plot illustrating the method of determining the molar absorptivities, ϵ_3, of the ferric iron in our sulfate solutions. The values of A/l are for solution B containing different added concentrations of ferric iron while all other variables were held constant. The points are seen to fall on straight lines at each wave length. This was true for all our solutions at all wave lengths. The best straight lines were obtained by the method of least squares. The slopes of these lines equal ϵ_3 multiplied by the value of the added ferric concentration in changing from $s = 1$ to $s = 2$ as explained in the text. The points at 4000 Å. are not shown because they do not fall significantly off the corresponding straight line in the plot.

the shape and size of the beam of light passing through the reaction vessel. The chart paper recordings of the optical density were kept within suitable limits by attenuation of the light beam passing through the reference compartment by placing therein appropriate screens of square-woven single strands of brass wire.[9]

The evaluation of ϵ_3 was carried out by noting that for only the ferrous and ferric species

$$A/l = \epsilon_2 c_2 + \epsilon_3 c_3 = \epsilon_2 c_2 + \epsilon_3 c_3^0 + \epsilon_3 c_3^a = A_0 + \epsilon_3 c_3' s \quad (2)$$

where c_3^0 and $c_3^a = c_3' s$ represent the ferric inadvertently present and added to the solution, respectively. We used s in this way because the values of c_3^a were obtained by dilution of a solution containing the maximum value of c_3^a and the other solutes at the concentrations prevailing in the ferrous solutions where $c_3 = c_3^0$. Equation 2 is limited to solutions containing negligible amounts of iron species having more than one atom of iron.

Figure 1 presents typical plots of A/l *vs.* $s = c_3^a/c_3'$ when c_2 and c_3^0 were kept constant while only c_3^a was varied. It follows that under these conditions the slopes of the lines equal $\epsilon_3 c_3'$.

The numerical values of ϵ_3 determined by the method of least squares applied to the values of A/l *vs.* s are given in Table III.

TABLE III

MOLAR ABSORPTIVITIES, ϵ_3, OF THE FERRIC IRON IN THE DIFFERENT SULFATE SOLUTIONS AT 25°

	Solution				
mμ	F	A	B	C	E
400	21.0	17.2	19.4	18.4	22.0
390	47.7	37.9	42.4	41.9	48.9
380	103	83.2	90.0	93.1	106
370	205	172	181	186	221
360	391	327	350	362	431
350	693	582	609	634	754
340	1140	944	1010	1050	1240
330	1640	1420	1520	1550	1860
320	2110	1840	1980	2040	2480
314	2320	2080	2240	2290	2810
310	2400	2200	2370	2400	3000
304	2450	2290	2490	2510	3140
300	2430	2320	2510	2530	3180
294	2330	2290	2490	2480	3130
290	2230	2230	2420	2410	3070
280	1960	2040	2240	2210	2910
254	2600	2840	2990	2710	2960

It should be recognized that $\epsilon c = \Sigma \epsilon_i c_i$ so that ϵ_3 and ϵ_2 are weighted average values. In the case of the ferric species the c_i represent mostly different ferric sulfate complexes, namely, $[Fe(SO_4)_n]^{3-2n}$ where $n = 1$, 2 or 3. The variations in ϵ_3 brought about by the changes in c_2 and in the concentration of sulfuric acid probably are produced mostly by changes in the bulk concentration of sulfate and not by any interaction between the ferrous and ferric.

The evaluation of ϵ_2 followed a circuitous procedure which is presented in Table IV.

Luckily, one of the concentrated ferrous sulfate solutions prepared for photolysis displayed an absorption spectrum having no maximum in the region of the absorption peak of ferric iron at about 3000 Å. This is shown in Fig. 2, so as a first approximation this solution was assumed to contain no ferric iron. Even in this solution, however, the values of ϵ_2 were the same within 1% in three different reaction vessels only at 2840 and 2860 Å. The pertinent data are presented in Table IV, Part A.

At wave lengths outside the range 2840 to 2860 Å. the values of ϵ_2 were less reproducible. At longer wave lengths the optical densities of the solution in the reaction vessels were too small and at shorter wave lengths they either changed too rapidly with wave length or exceeded the range of the chart paper.

In order to obtain better values for ϵ_2 in this solution at wave lengths outside the range 2840 to 2860 Å., we prepared for use with the absorbance cells another solution of ferrous sulfate of about the

(9) L. J. Heidt and D. E. Bosley, *J. Opt. Soc. Am.*, **43**, 760 (1953).

TABLE IV

Data pertaining to the evaluation of the molar absorptivities, ϵ_2, of the ferrous sulfate in the different sulfate solutions at 25°. The explanation of the table is given in the text. *Part A:* Data pertaining to the ferric free solution C which was 0.70 *M* in $FeSO_4$ and 2 *M* in H_2SO_4.

mμ	Reaction vessel	A	Sol'n. depth l, in cm.	A/l or ϵ_2c_2	ϵ_2	$\bar{\epsilon}_2$
284	B	0.334	2.76	0.121	0.173	
284	D	.331	2.70	.122	.175	0.174
284	E	.328	2.67	.123	.175	
286	B	.223	2.76	.0809	.116	
286	D	.221	2.70	.0817	.117	0.117
286	E	.219	2.67	.0821	.117	

Part B: Data pertaining to the evaluation of the trace amount of ferric, c_3^0, inadvertently in the solution 0.688 *M* in $FeSO_4$ and 2 *M* in H_2SO_4. The solution was about the same composition as solution C so the values of $\bar{\epsilon}_2$ at 284 and 286 mμ obtained for solution C were assigned to this solution.

mμ	$\bar{\epsilon}_2$	ϵ_2c_2	A	l	$\epsilon_3c_3^0$	ϵ_3	$10^5 \times c_3^0$	$10^5 \times \bar{c}_3^0$
284	0.174	0.120	0.291	1.00	0.171	2200	7.78	7.80
286	.117	.080	.255	1.00	.175	2240	7.82	

Part C: Data pertaining to the evaluation of ϵ_2 at 300, 304 and 310 mμ in the above solution 0.688 *M* in $FeSO_4$ and 2 *M* in H_2SO_4 which contained no added ferric iron but in which $c_3 = c_3^0 = 7.80 \times 10^{-5}$ *M* as determined above.

mμ	ϵ_3	ϵ_3c_3	A		ϵ_2c_2	ϵ_2	$\bar{\epsilon}_2$	"Best" values chosen for ϵ_2
300	2530	0.197	1.045	5.00	0.012	0.017	0.013	0.015
300	2530	.197	0.203	1.00	.006	.009		
304	2508	.196	1.023	5.00	.009	.013	.009	.011
304	2508	.196	0.199	1.00	.003	.004		
310	2404	.188	.983	5.00	.009	.013	.008	.011
310	2404	.188	.190	1.00	.002	.003		

same composition. This solution, however, inadvertently contained a significant amount, c_3^0, of ferric, which was determined as outlined in Table IV, Part B.

The values of ϵ_2c_2 and subsequently of ϵ_2 outside the range 2840 to 2860 Å. next were determined in the manner outlined in Table IV, Part C.

Eventually the values of ϵ_2 given in the last column of Table IV, Part C were selected as the "best" values because their use combined with the values of c_2 and ϵ_3 gave, within the limits of error, reasonable values for c_3^0 in all of our solutions.

Our best estimates of the values of ϵ_2 are given: between 300 and 400 mμ there is in every case a peak at about 384 mμ. In the case of solutions A, B, C and F, ϵ_2 is about 0.03 at this peak and no greater than its value at 300 mμ outside the range 380 to 390 mμ; in the case of solution E the corresponding values of ϵ_2 are about three times larger. At 2537 Å., however, ϵ_2 is about 12.5 and 7.2, respectively, in the corresponding solutions.

It seems worthwhile to point out that our charts also revealed an absorption peak for ferrous sulfate at about 2360 Å. which remained unchanged in our solutions up to 2 *M* in sulfuric acid but became sharper when the acidity was increased to 6 *M*. This effect produced the decrease in ϵ_2 of about two-fold at 2537 Å.

Gross quantum yields are in terms of gram atoms of ferrous converted to ferric per mole of quanta of all the light of 2537 Å. absorbed by the solution. The decrease in these yields as the reaction progressed is illustrated in Fig. 3.

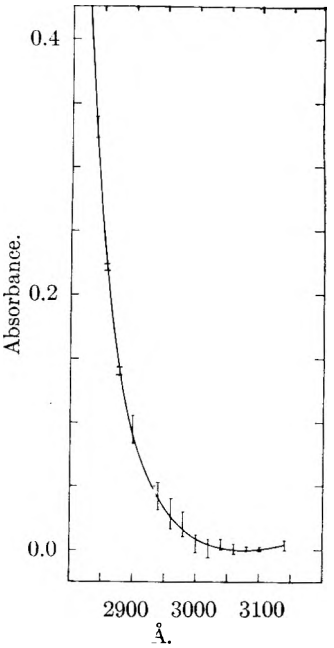

Fig. 2.—Absorbance values, A, for our ferrous solution containing the least amount of ferric iron which happened to be less than the amount measurable. The values are for a water solution 0.70 *M* $FeSO_4$ and 1.9 *M* H_2SO_4 in the three different reaction vessels having solution light paths of 2.76, 2.70 and 2.67 cm. The A values adjusted for these small differences in depths would reduce the spread of the data at every wave length and this was taken into account in the calculations of the molar absorptivities, ϵ_2, of the ferrous iron as indicated in Table IV. Evidence for the lack of ferric iron in the solution is indicated by the absence of an absorbance maximum in the region of 3000 Å. where ferric iron in sulfate solution has an absorption peak. The values of ϵ_2 calculated from the data at 2340 and 2860 Å. are considered to be accurate within one per cent. and equal 0.174 and 0.117, respectively.

Net quantum yields based on the light of 2537 Å. absorbed only by the ferrous sulfate remained constant in any given solution as also is illustrated in Fig. 3.

Table V presents the values of ϕ_g and ϕ_n together with pertinent information. It should be noted in this table that the light intensity incident on the photolyzed solutions did not vary greatly. The intensity available to the ferrous sulfate, however, decreased several-fold during the course of photolysis of a given solution because of increases in the fraction of light absorbed by the ferric sulfate.

Figure 4 displays the independence of ϕ_n upon the concentration of ferrous sulfate in our solutions. The apparent slight increase in ϕ_n is partly the result of our assumption that the actinometer and ferrous sulfate solutions under investigation absorbed the same fraction of light of 2537 Å. incident upon them. This is strictly true, however, only when both solutions have the same optical density. Actually our most dilute ferrous sulfate solution had initially a slightly lower optical density at 2537 Å. than the actinometer solution and the fraction of light absorbed by the ferric iron was small. Thus, initially, slightly less light than we have calculated actually was absorbed by the more dilute solutions photolyzed so both ϕ_g and ϕ_n actually are larger than calculated. The optical den-

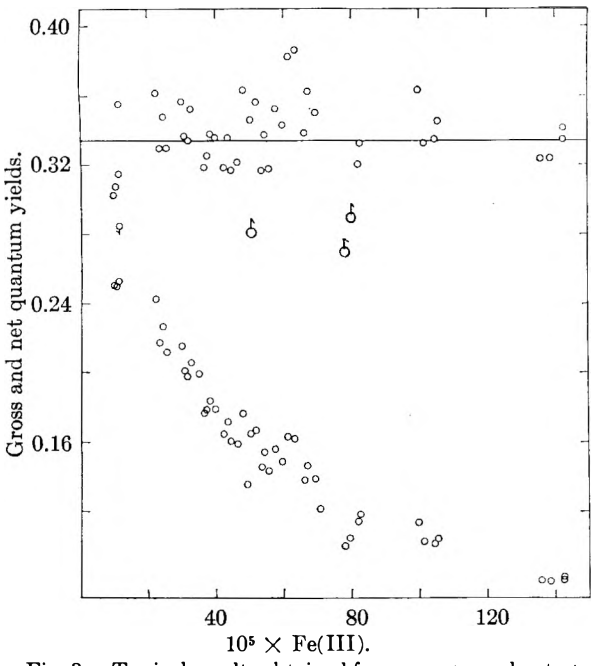

Fig. 3.—Typical results obtained for gross, ϕ_g, and net, ϕ_n, quantum yields during the course of the photolysis of the ferrous sulfate solutions at 25°. The results are for solution A which was 0.10 *M* in $FeSO_4$ and 2.0 *M* in H_2SO_4. The upper points represent ϕ_n and fall on the horizontal line within the limits of error. The lower points falling away from the horizontal line represent the values obtained for ϕ_g. The constancy of ϕ_n, which is based only on the light absorbed by the ferrous iron, is strong evidence that in these solutions the ferric iron acts mainly as an inner filter.

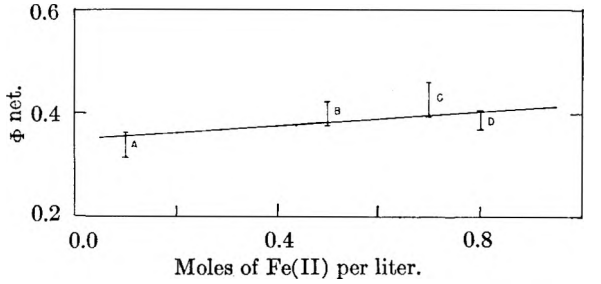

Fig. 4.—Plots showing that the net quantum yields in our sulfate solutions A, B, C and D, which were 2.0 *M* in sulfuric acid, are nearly independent of the concentration of the ferrous sulfate over the range 0.10 to 0.80 *M*. The apparent slight increase in ϕ_n probably is the result of a small error in evaluating the light of 2537 Å. absorbed by the system, as explained in the text.

sities at 2537 Å. of all the photolyzed solutions, however, eventually became greater than the optical density of the actinometer solution as the ferrous was converted to ferric iron because of the greater values for ϵ_3 than for ϵ_2 at 2537 Å. This effect at first decreased the error in both the gross and net quantum yields and eventually changed the sign of the error as the reaction progressed.

Figure 5 shows that an increase in the sulfuric acid brings about a significant increase in ϕ_n. The linear relationship between ϕ_n and the concentration of sulfuric acid is quite surprising since it does not lead to a linear relationship between $1/\phi_n$ and $1/(H^+)$ as in the case of cerous perchlorate solutions.[2b] We plan to carry out experiments designed to reveal the reason for this difference. It should be noted, however, that cerous sulfate solutions in contrast to cerous perchlorate solutions are not measurably sensitive to light of 2537 Å.[2b]

TABLE V

Gross and net quantum yields for the oxidation of ferrous to ferric and the accompanying reduction of water to gaseous hydrogen under an inert atmosphere by light of 2537 Å. absorbed by solutions of the compositions given in Table II. The solutions were at 25° when photolyzed. The values of I_g are expressed in moles of quanta of 2537 Å. incident per second upon a square cm. of the photolyzed solution. The amount of ferrous converted to ferric was at the most 1.4%.

Soln.	ϕ_g	ϕ_n	$10^8 I_g$	% 2537 Å. abs. by Fe(II)	No. of expts.
A	0.080 to 0.285	0.334 ± 0.024	3.5	24 to 80	47
B	.278 to .410	.398 ± .023	2.1	78 to 96	38
C	.304 to .455	.426 ± .034	1.6	79 to 99	21
D	.306 to .400	.386 ± .018	1.7	82 to 97	35
E	.183 to .504	.737 ± .036	2.7	26 to 77	27
F	.091 to .132	.155 ± .005	4.5	56 to 81	8

The ratio of hydrogen produced to ferrous converted to ferric was determined in solution C which was 0.70 *M* in ferrous sulfate and 2 *M* in sulfuric acid and under an atmosphere of carbon dioxide instead of helium. The amount of hydrogen produced was varied over a range of about threefold by varying the extent (time) of photolysis.

The procedure for determining the amount of hydrogen was a tracer technique employing a mass spectrograph. Briefly, a measured amount of helium was added to the system containing all the solution photolyzed and the products of photolysis. The hydrogen and added helium, as well as the carbon dioxide and water vapor, were allowed to equilibrate for about an hour. Then a measured fraction of the system containing a finger and closed off evacuated sampling flask was isolated from the rest of the system and the carbon dioxide and water vapor in this part were frozen out by immersing the finger in liquid nitrogen. Finally, the sample flask was opened and the gases entered it by passing through the cold finger. After allowing sufficient time for equilibration, the sample flask was closed off, and the ratio of H_2 to He in the flask was determined.

A calibration curve for the analyses was constructed from the results of ratios of known mixtures of hydrogen and helium in the range of those found in the analyses. Allowance was made for the contribution He^{++} by measuring the ratios of the 2 and 4 mass to charge peaks in pure He blanks. Drs. Klaus Biemann and Gottfried Deffner of this Laboratory kindly helped with these analyses.

About 10^{-5} mole of hydrogen should have been produced by these photolyses. The amounts obtained by the analyses were about 40% lower. The difference is believed due to failure of the hydrogen formed in the solution to come into equilibrium with its gas phase and to preferential adsorption of the gaseous hydrogen compared to the dilutent carrier gas helium on the surfaces of the system especially on the carbon dioxide and water snow in the cold finger through which the mixture of hydrogen and helium passed on its way to the sampling flask for subsequent analysis with the mass spectrograph.

The over-all reaction in our acidic solutions can be represented within the limits of error by the equation

$$Fe(II) + H^+ + light = Fe(III) + 1/2\ H_2(g)$$

Our measured net quantum yield of about 74% for light of 2537 Å. absorbed by ferrous in 6 *M* H_2SO_4 is to be compared to yields of about 0.1% and of less than 0.001% for the conversion of cerous to ceric in perchloric and sulfuric acids, respectively.[2b]

Discussion

We had anticipated a maximum value of about 0.4 for ϕ_n based on extrapolation to infinite acidity and sulfate concentration of the linear plots obtained for $1/\phi_n$ *vs.* $1/(H^+)$ at 2 *M* and less sulfuric acid. The unexpectedly large value of 74% for ϕ_n in 6 *M* sulfuric acid we believe is due to the existence of significant amounts of a new kind of ferrous sulfate complex at the larger concentrations of sulfuric acid.

In 2 *M* and less sulfuric acid the ferrous sulfate complex appears to exist mainly as an ion pair of the type $Fe(H_2O)_nSO_4$ in which there are more than two ($n > 2$) layers of water molecules between the ferrous and sulfate ions. More than two layers of water appear to be necessary to keep the electrostatic forces between the oppositely charged ferrous and sulfate ions from squeezing out the intervening water.

This concept is based on conductivity,[10a,b] solubility,[11a,b] isopiestic[12] and freezing point[13] measurements of aqueous solutions of 2–2 sulfates compared to 2–1 chlorides[14a,b] in particular of $CaSO_4$ and $MgSO_4$ compared to $CaCl_2$, $MgCl_2$ and $FeCl_2$ which have been found to be weak and strong electrolytes, respectively. Absorption spectra measurements of $CuSO_4$ in water[15] also support the hypothesis that the 2–2 sulfate is a weak electrolyte. That the associated ferrous sulfate in dilute acid exists as ion pairs of the kind first proposed by Bjerrum[16] is supported by the lack of any measurable difference in the absorption spectra of ferrous perchlorate and ferrous sulfate in dilute aqueous acid as obtained in this Laboratory at 2000 to 8000 Å.

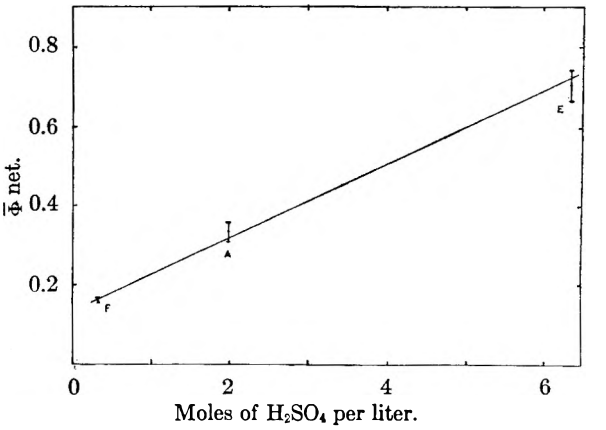

Fig. 5.—Plot showing the linear dependence of the net quantum yields upon the concentrations of sulfuric acid in solutions F, A and E, which contained 0.10 *M* $FeSO_4$ in 0.15, 2.0 and 6.0 *M* H_2SO_4, respectively.

In 6 *M* sulfuric acid the amount of water available for the ion pair type of complex is reduced because of the large affinity of sulfuric acid for the water. This brings the ferrous and sulfate ions closer together which increases the electrostatic pull between the oppositely charged ions. When this pull becomes dominant, the intervening water molecules are squeezed out and the ferrous and sulfate ions come into intimate contact. Thus both our absorption spectra and net quantum yield measurements support the hypothesis that as the sulfuric acid concentration is increased the ion pair type of complex gives way to the contact type of complex between ferrous and sulfate ions in water.

The unexpectedly large net quantum yield of 74% also suggests that the atomic hydrogen produced by the primary reaction escapes from the reaction cage more often the shorter the time required to form the resulting comparatively very stable contact ferr*ic* sulfate complex. The photon excited contact ferr*ous* sulfate complex would require less time than the ion pair to form the contact ferric sulfate complex since the iron and sulfate are already in intimate contact thereby eliminating the time required to squeeze out intervening water.

Our sulfuric acid concentrations do not extend down into the lower range of values employed by Lefort and Douzou[6] nor do the latter give enough information regarding the optical densities and the total ferric in their solutions to make possible any kind of a valid comparison with our results. The lack of similar information given by the other workers on this system cited in the introduction of the manuscript also renders such a comparison highly speculative.

(10) (a) H. S. Dunsmore and J. C. James, *J. Chem. Soc.*, 2925 (1951); (b) H. S. Harned and B. B. Owen, "The Physical Chemistry of Electrolyte Solutions," Reinhold Publishing Co., New York, N. Y., ed. 2, 1950, pp. 423–426.

(11) (a) R. P. Bell and J. H. B. George, *Trans. Faraday Soc.*, **49**, 619 (1953); (b) H. W. Jones and C. B. Monk, *ibid.*, **48**, 929 (1952).

(12) R. A. Robinson and R. H. Stokes, "Electrolyte Solutions," Butterworths Scientific Publications, London, England, 1955, pp. 390–485.

(13) P. G. M. Brown and J. E. Prue, *Proc. Roy. Soc.* (London), **A232**, 320 (1955).

(14) (a) D. L. Leussing and I. M. Kolthoff, *J. Am. Chem. Soc.*, **75**, 2476 (1953); (b) S. R. Carter and N. J. L. Megson, *J. Chem. Soc.*, 2023 (1927).

(15) R. Näsänen, *Acta Chem. Scand.*, **3**, 179 and 959 (1949).

(16) N. Bjerrum, "Selected Papers," No. 9, Einar Munksgaard, Copenhagen, 1949, p. 108. Later information on this subject is given by Y. H. Inami, H. K. Bodenseh and J. B. Ramsey, *J. Am. Chem. Soc.*, **83**, 4745 (1961).

INTERMOLECULAR ENERGY TRANSFER IN GAS REACTIONS[1]

BY NARL CHOW AND DAVID J. WILSON

Department of Chemistry, University of Rochester, Rochester 20, New York

Received October 2, 1961

Photochemical and unimolecular reactions in which a reactive molecule may react by two different paths to yield distinguishable products are analyzed theoretically. In contrast to reactions which take place by only one path, reactions of this type may be expected to yield considerable qualitative information about the nature of collisional energy transfer processes involving highly energetic molecules.

I. Introduction

A large number of papers have appeared in the last few years on the subject of internal energy transfer by molecular collisions in gases.[2] A difficulty noticed previously by several authors is that of distinguishing, by conventional photochemical[3a] or unimolecular thermal[3b] reaction rate studies, between the various types of plausible collisional energy transfer mechanisms. For unimolecular thermal reactions the situation appears hopeless; theoretical curves of rate constant *vs.* pressure are essentially indistinguishable for strong and stepwise collision mechanisms. (A strong collision mechanism is one in which the average amount of energy transferred per effective collision is large compared to kT; a stepwise collision mechanism is one in which this quantity is comparable to kT.) Porter and Connelly showed that the situation was almost as bad for photochemical reactions; that very precise measurements of quantum yield as a function of pressure at relatively low pressures would be necessary to distinguish between strong and stepwise collision mechanisms. Carrington[2] has indicated the difficulties of extracting precise quantitative information even from transient or steady-state spectroscopic measurements. (If one is interested in only a qualitative discrimination between strong and stepwise collision mechanisms, however, we find that the situation is not so black for spectroscopic studies.[2,4])

Recently, however, some results on a particular type of unimolecular reaction were published by Chesick,[5] Rabinovitch,[6] Walters,[7] Frey,[8] and their co-workers. In these reactions a reactant molecule can react unimolecularly by two (or more) different modes to yield chemically distinguishable products. We felt that the dependence of the ratio of the rate constants of the different modes on pressure might yield information about the nature of collisional energy transfer in gas reactions not obtainable from conventional rate studies in which there is only one mode of reaction. It also was suggested to us by Dr. R. Srinivasan (then at the University of Rochester) that photochemical reactions in which a reactant molecule in one excited electronic state can decompose by two or more different modes to yield chemically distinct products might be of interest. We are indebted to Dr. Srinivasan for this suggestion and for discussing with us his results on what appears to be one such reaction, the photolysis of cyclopentanone.

The remainder of this paper describes briefly and reports the results of calculations on these unimolecular and photochemical "bireactions."

II. Unimolecular Bireactions

The commonly accepted mechanism for a unimolecular reaction is[9]

$$\begin{aligned} A_i + M &\longrightarrow A_j + M \quad a_{ji} \\ A_i &\longrightarrow (\text{Products})_1 \quad c_i^1 \end{aligned} \tag{1}$$

A_i represents a reactant molecule in its ith internal energy state, M represents an inert "heat-bath" molecule (the inert gas is presumed present in large excess in comparison with reactant, and is assumed to be in thermal equilibrium), and a_{ji} and c_i are the microscopic rate constants for the processes with which they are associated. We generalize this mechanism to include a second mode of decomposition by including the process

$$A_i \longrightarrow (\text{Products})_2 \quad c_i^2 \tag{2}$$

where $(\text{Products})_2$ are chemically distinguishable from $(\text{Products})_1$.

Kassel's model of a reacting molecule[10] as a system of s coupled degenerate harmonic oscillators was used to calculate the microscopic decomposition rate functions c_i^1 and c_i^2.

$$c_i^1 = \nu_1 g_s(i - n^{*1})/g_s(i) \tag{3}$$

where $g_s(j)$ is the degeneracy of the jth energy state of the system (containing j quanta of vibrational energy), ν_1 is a frequency factor, and n^{*1} is the minimum number of quanta required to yield $(\text{Products})_1$ from a molecule of reactant. A similar expression was used to compute c_i^2. The quantities a_{ji} were computed according to two models: (1) the strong collision model used by Kassel,[10] Slater,[11a] and others,[11b] in which activated molecules are deactivated into an equilibrium distribution (essentially) by single collisions, and (2) the stepwise collision mechanism we treated earlier,[3b] in which $a_{n,n+1} = a(n+s)e^{-\theta}$, where a is

(1) This work was supported by grants from the Research Corporation and the National Science Foundation.

(2) See, for example, T. Carrington, *J. Chem. Phys.*, **35**, 807 (1961); D. J. Wilson, *ibid.*, to be published (this paper contains several recent references); K. E. Shuler, *ibid.*, **32**, 1692 (1960); E. W. Montroll and K. E. Shuler, "Advances in Physics," Interscience Publishers, Inc., New York, 1958, Vol. I (this article lists many of the earlier papers).

(3) (a) G. B. Porter and B. T. Connelly, *J. Chem. Phys.*, **33** 81 (1960); (b) F. P. Buff and D. J. Wilson, *ibid.*, **32**, 677 (1960).

(4) D. J. Wilson, B. Noble and B. Lee, *ibid.*, **34**, 1392 (1961).

(5) J. P. Chesick, *J. Am. Chem. Soc.*, **82**, 3277 (1960).

(6) B. S. Rabinovitch, E. W. Schlag and K. B. Wiberg, *J. Chem. Phys.*, **28**, 504 (1958).

(7) H. R. Gerberich, Ph.D. Thesis, University of Rochester, 1959.

(8) M. C. Flowers and H. M. Frey, *J. Chem. Soc.*, 3953 (1959).

(9) See H. S. Johnston and J. R. White, *J. Chem. Phys.*, **22**, 1969 (1954), for example.

(10) L. S. Kassel, "Kinetics of Homogeneous Gas Reactions," Chemical Catalog Co., Inc., New York, N. Y., 1932.

(11) (a) N. B. Slater, "Theory of Unimolecular Reactions," Cornell University Press, Ithaca, New York, 1959; (b) C. Steel, *J. Chem. Phys.*, **31**, 899 (1959), for example.

a constant, θ is $h\nu_{vib}/kT$, and ν_{vib} is the frequency of the oscillators representing the molecule. (Microscopic reversibility then yields $a_{n+1,n} = a(n+1)$.)

Plots of $k_1/k_{1\infty}$ and $k_2/k_{2\infty}$ as functions of $k_{10}M/k_{1\infty}$ then were computed on the Cornell Aeronautics Laboratories' IBM 704 computer. The computation based on the strong collision model employed the quantum mechanical analog of the formula mentioned by Chesick.[5] The computation based on the stepwise collisional model was performed by means of slight modifications of the procedure used by Buff and Wilson[3b] to handle the case in which only one reaction occurs.[12]

We found that plots of log $k_1/k_{1\infty}$ *vs.* the log of the dimensionless pressure $k_{10}M/k_{1\infty}$ were essentially indistinguishable for the strong and stepwise mechanisms, as we had suspected from our earlier work.[3b] (It is assumed here and following that n_1^* is less than n_2^*— that is, that the reaction producing $(Products)_2$ has the higher critical energy.) This is demonstrated in Fig. 1 and 2; the curves for the two collision mechanisms are essentially indistinguishable over the entire pressure range.

Log–log plots of k_1/k_2 *vs.* dimensionless pressure were markedly different for the two mechanisms at low pressures, and the differences were more marked the greater the difference $E_2 - E_1$. We therefore investigated Chesick's data on the pressure dependence of the ratio of the rate constants for the production from methylcyclopropane of the two normal butenes and of isobutene. We took Chesick's value of 2.3 ± 0.7 kcal. for $E_2 - E_1$, increased this difference to 3.7 kcal., and adjusted the ratio of the pre-exponential factors so as to retain agreement with Chesick's value of k_2/k_1 at high pressures. In this way we hoped to detect, by leaning over backwards, any discrepancy between the stepwise collision theory and Chesick's data. (Chesick had shown previously that his results were consistent with the appropriate modification of Kassel theory.[5]) As is shown in Fig. 3, our attempt to use these data to eliminate the stepwise mechanism from consideration was a failure. However, there remains a definite possibility of discriminating between the strong and stepwise collision mechanisms by means of the study of unimolecular reactions of this type at sufficiently low pressures.

Figures 4 and 5 demonstrate the feasibility of discriminating between the two mechanisms by a study of the rate constant of the reaction having the higher activation energy. We had remarked above that the larger the difference $E_2 - E_1$, the better the discrimination between the two mechanisms; in these figures we see that the simpler the molecule, the better the discrimination, also.

Figure 6 shows the ratio k_1/k_2 as a function of the dimensionless pressure for the two collision mechanisms. The marked difference in the ratio at low pressures, especially for fairly simple molecules, indicates that one could run such a reaction nearly

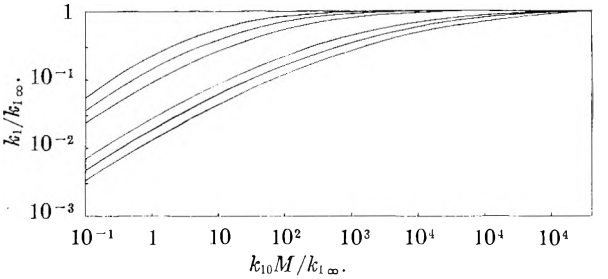

Fig. 1.—Rate constant of the reaction having the lower activation energy *versus* reduced pressure. The symbols are described in the text. Strong collision mechanism. From top to bottom s = 5, 7, 9, 15, 17, 19, $n_2^* - n_1^* = 5$; $e^{-\theta} = 0.6$; $\nu_2/\nu_1 = 1.13$.

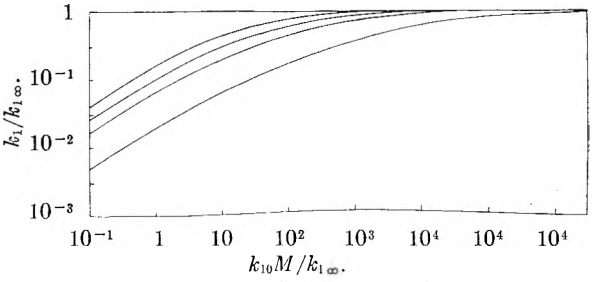

Fig. 2.—Rate constant of the reaction having the lower activation energy *versus* reduced pressure. Stepwise collision mechanism. From top to bottom s = 5, 7, 9, 15; $n_2^* - n_1^* = 5$; $e^{-\theta} = 0.6$; $\nu_2/\nu_1 = 1.13$.

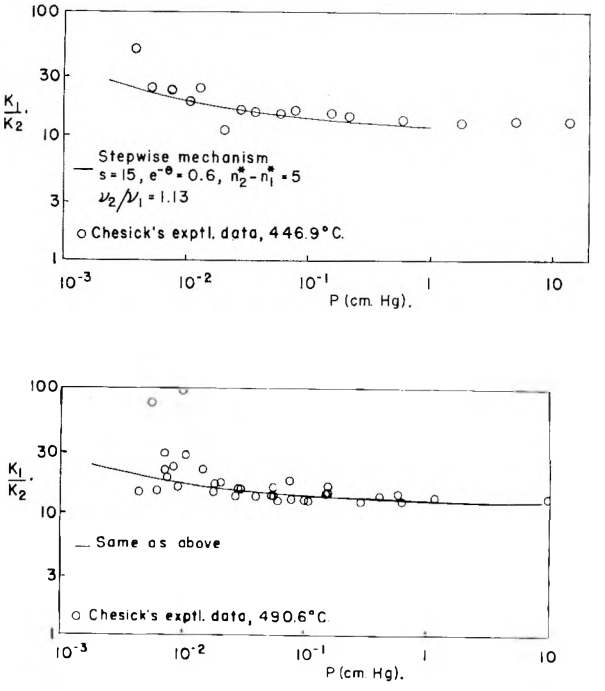

Fig. 3.—Comparison of the stepwise theory with Chesick's results.

(12) The only modifications made were (1) the inclusion of an extra term in Buff and Wilson's equations 40 and 41, corresponding to the disappearance of reactant *via* the second mode of reaction, and (2) the partitioning of λ (their notation) into k_1 and k_2. This last is readily accomplished by accumulating the expressions

$$\sum_i c_i^1 A_i \quad \text{and} \quad \sum_i c_i^2 A_i$$

during the numerical solution of the difference equations above i_1^* (reaction 1 is presumed to have the lower activation energy) and then noting that

$$\left(\sum_i c_i^1 A_i \lambda\right) \Big/ \left(\sum_i c_i^1 A_i + \sum_i c_i^2 A_i\right)$$

is just k_1; the expression for k_2 is obtained by permuting the subscripts 1 and 2.

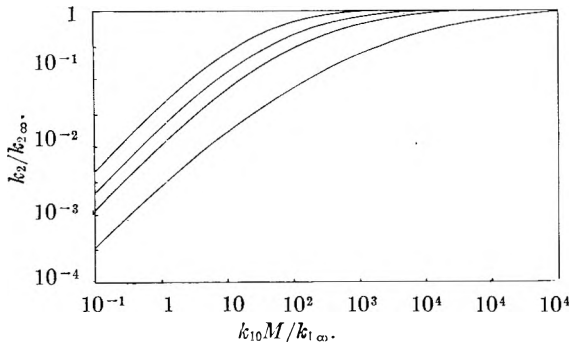

Fig. 4.—Rate constant of the reaction having the higher activation energy *versus* reduced pressure. Strong collision mechanism. From top to bottom $s = 5, 7, 9, 15$; $n_2^* - n_1^* = 5$; $e^{-\theta} = 0.6$; $\nu_2/\nu_1 = 1.13$.

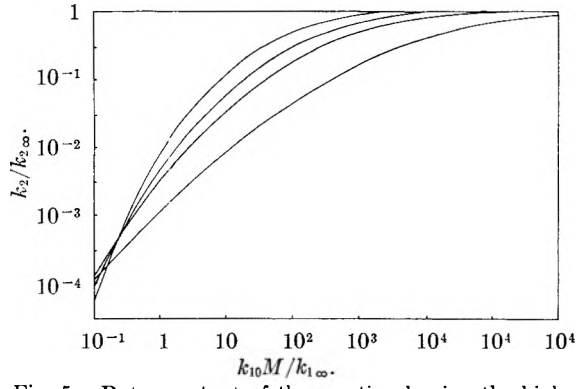

Fig. 5.—Rate constant of the reaction having the higher activation energy *versus* reduced pressure. Other data same as Fig. 2.

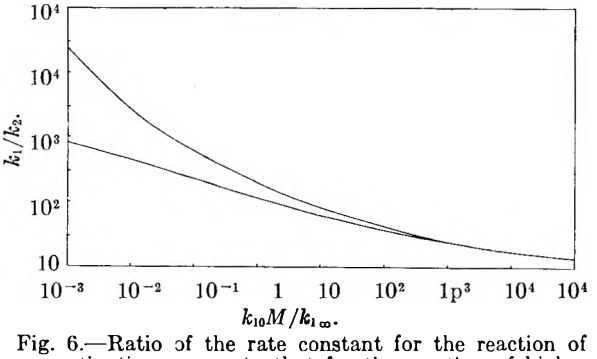

Fig. 6.—Ratio of the rate constant for the reaction of lower activation energy to that for the reaction of higher activation energy as a function of reduced pressure. Upper curve, stepwise mechanism, $s = 15$; lower curve, strong collision mechanism, $s = 17$. $n_2^* - n_1^* = 5$; $e^{-\theta} = 0.6$; $\nu_2/\nu_1 = 1.13$.

to completion and then just measure the ratio of products as a function of pressure, provided the products did not themselves react. This would permit one to work conveniently at pressures lower than are readily accessible when the rate constants themselves must be measured.

III. Photochemical Bireactions

A possible mechanism for certain photochemical reactions is

$$\begin{aligned} A_{ground} &\longrightarrow A_n^* \quad I \\ A_k^* + M &\longrightarrow A_i^* + M \quad a_{ik} \\ A_k^* &\longrightarrow (Products)_1 \quad c_i^1 \\ A_k^* &\longrightarrow A_{ground} \quad (+ h\nu_k) \quad d_k \end{aligned} \qquad (4)$$

A_{ground} represents a reactant molecule in its ground

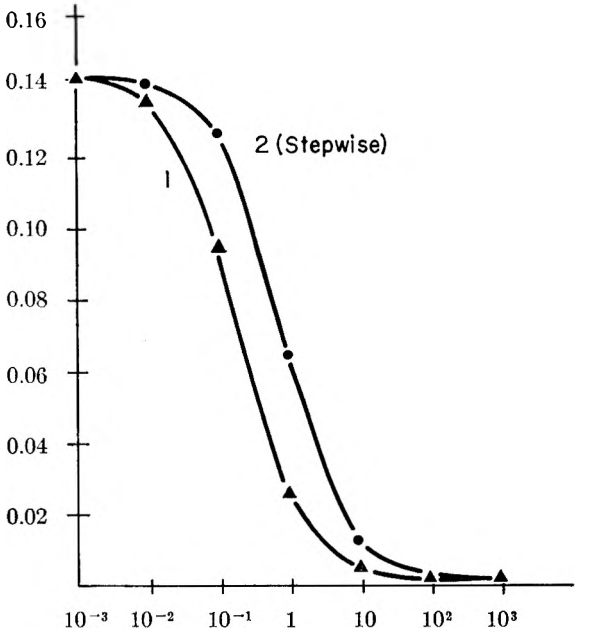

Fig. 7.—Quantum yield *versus* pressure. The model has 3 degrees of freedom, $\exp(-\theta) = 0.3$, photo-excitation is to the 8th state, the lowest reactive state is the 6th, and the ratio of the Kassel frequency factor to the rate constant for fluorescence (assumed independent of vibrational energy) was taken as 1.0.

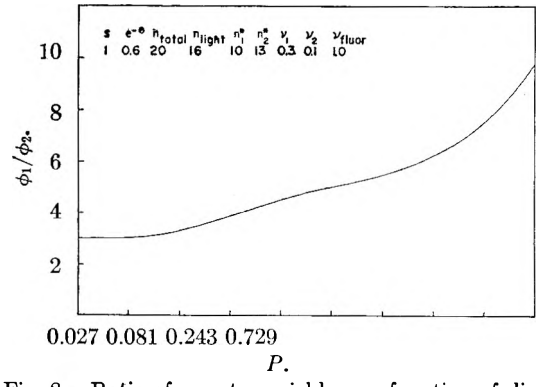

Fig. 8.—Ratio of quantum yields as a function of dimensionless pressure. n_{total} is the total number of levels considered in the calculation, n_{light} is the level to which photo-excitation occurs, n_1^* is the minimum number of quanta of vibrational energy required to produce $(Product)_1$, ν_1 is the frequency factor for reaction 1, and ν_{fluor} is the rate constant for fluorescence from any level.

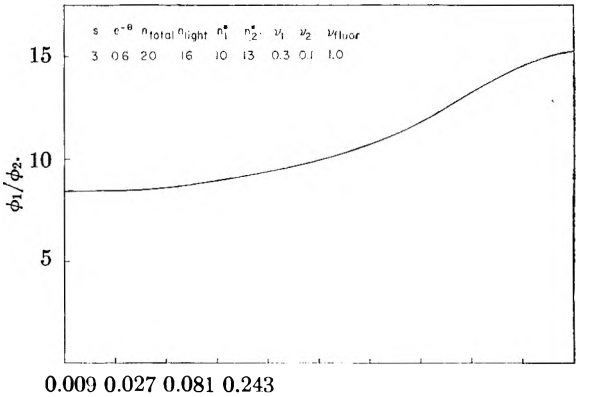

Fig. 9.—Ratio of quantum yields as a function of dimensionless pressure.

electronic state (we are not specifying the vibrational levels of this state explicitly); A_n^* is the vibrational level (or levels) of the electronic state to which reactant molecules are photo-excited; I is the intensity of light absorbed which induces this transition; and d_k is the probability of fluorescence and/or internal conversion from the kth vibrational level of the excited electronic state, assumed to be independent of pressure. The other symbols are essentially those previously defined. We set up the rate equations, invoked the steady-state assumption, solved the resulting system of linear inhomogeneous equations, and calculated quantum yields as functions of pressure for one stepwise and one strong collision model. The microscopic decomposition rate used was calculated by Kassel theory; the same formula was used as was employed in the unimolecular thermal reactions calculation discussed above. The stepwise model employed collisional transition rate constants identical to those described above. The strong collision model used rate constants $a_{ij} = a$, a constant, for transitions from higher to lower energy states. The "upward" transition rate constants then are defined by microscopic reversibility. The collision mechanisms in both cases met the requirements of microscopic reversibility, in contrast to some other models which have been treated recently.[3a,13] The neglect of the upward transition rates introduces little change in the general appearance of plots of quantum yield *vs.* pressure; however, in some cases this approximation appreciably changes the temperature dependence of the quantum yield. Figure 7 shows plots of quantum yield *vs.* a reduced pressure (on a log scale) for the strong (1) and stepwise (2) models. A simple shift of the pressure scale essentially superimposes the two curves, in agreement with Porter and Connelly's conclusion that measurements of quantum yields must be quite precise to distinguish between the two collision mechanisms.

Photochemical reactions in which one excited electronic state can decompose by two or more different modes to yield distinct products, however, may well be a much more profitable means to getting information about collisional energy transfer. For a strong collision mechanism and with photo-excitation to a range of levels over which the microscopic decomposition rates do not vary by much, it can be shown readily that the ratio of quantum yields is essentially independent of pressure. One must include the proviso that fluorescence or internal conversion occur to an extent which permits the ready return of electronically excited, vibrationally *de*activated molecules to the ground electronic state.

On the other hand, if a stepwise collisional vibrational energy process is operative, then, as is

(13) J. T. Dubois, *J. Chem. Phys.*, **33**, 229 (1960).

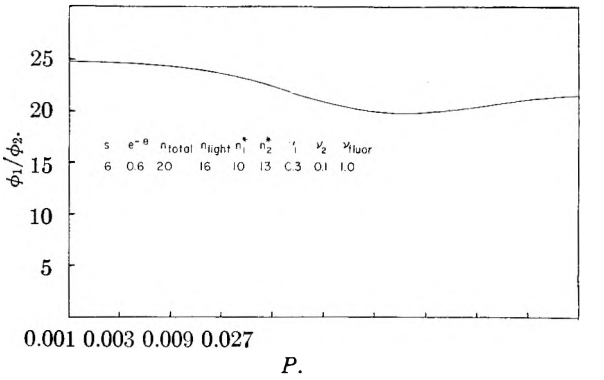

Fig. 10.—Ratio of quantum yields as a function of dimensionless pressure.

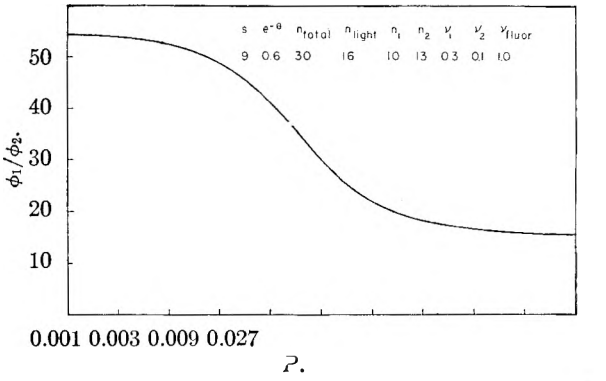

Fig. 11.—Ratio of quantum yields as a function of dimensionless pressure.

intuitively evident, the ratio of quantum yields is quite markedly dependent on pressure. The quantum yield of the reaction having the higher activation energy decreases the more rapidly as the pressure increases, *provided* that the vibrational energy of the state to which excitation occurs is large compared to skT. This effect is demonstrated in Fig. 8, 9, 10 and 11. The mechanism employed here is identical to the stepwise mechanism earlier described except that a second Kassel-type microscopic decomposition rate has been included, corresponding to the second mode of reaction. Similar plots for the strong collision mechanism would, of course, be essentially straight horizontal lines.

The fly in the ointment here, of course, is the difficulty of establishing beyond all reasonable doubt that reaction is occurring from only one excited electronic state. Studies of such reactions would, however, provide an interesting check on the results obtained by Rabinovitch and his coworkers,[14] in which the decomposition of "hot" secondary butyl radicals was found to lend support to the strong collision hypothesis.

(14) R. E. Harrington, B. S. Rabinovitch and M. R. Hoare, *ibid.*, **33**, 744 (1960).

INFRARED SPECTRA OF METAL CHELATE COMPOUNDS. V. EFFECT OF SUBSTITUENTS ON THE INFRARED SPECTRA OF METAL ACETYLACETONATES[1]

BY KAZUO NAKAMOTO,[2] YUKIYOSHI MORIMOTO,[2] AND ARTHUR E. MARTELL[2]

Department of Chemistry, Clark University, Worcester, Massachusetts

Received October 6, 1961

The infrared spectra of the metal chelate compounds of hexafluoro- and trifluoro-acetylacetone, benzoylacetone, and dibenzoylmethane with Cu(II) and Ni(II) have been measured in the range between 4000 and 300 cm.$^{-1}$. Vibrational frequencies of these compounds were calculated by the use of the perturbation method on the results of a previous normal coördinate treatment of bis-acetylacetono-Cu(II). The calculated force constants provide a quantitative measure of the electronic effect of the trifluoromethyl and phenyl groups on the chelate rings.

Introduction

In the previous papers,[3] the effect of changing the metal on the infrared spectra of metal acetylacetonates has been calculated by the use of the perturbation method. As a next step, this paper deals with the effect of replacement of the methyl groups of the metal acetylacetonates on the infrared spectra. The compounds studied are represented by the general formula

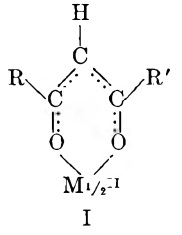

R, R′ = CF_3, CH_3 and C_6H_5
M = Cu and Ni

I

Changes of the electronic structures of the chelate rings resulting from substitution in the ligand can be detected from the infrared spectra, and more quantitative information can be deduced from calculations of the force constants by the use of the perturbation method.

It should be noted that these substituted compounds exhibit the absorptions characteristic of the chelate ring as well as of the substituents themselves. Therefore, caution must be taken in differentiating between these two kinds of absorption. The sorting out of the many infrared bands of these compounds is very difficult in the sodium chloride region, where overlapping of the bands is serious. On the other hand the spectra of the low frequency region are helpful in following substitution effects, since the organic substituents have very few strong absorptions below 600 cm.$^{-1}$.

Although the infrared spectra of some of the compounds described by formula I have been reported,[4-9] the previous papers have been concerned primarily with the carbonyl stretching frequencies and did not give spectra in the KBr and CsBr regions.

Experimental

Spectral Measurements.—A Perkin–Elmer Model 21 infrared spectrophotometer equipped with NaCl, KBr, and CsBr optics was used to obtain spectra in the range between 4000 and 300 cm.$^{-1}$. The KBr disk method was employed for the NaCl and KBr regions whereas the nujol mull technique was used for the CsBr region. Calibration of the frequency reading was made with polystyrene film (NaCl region), with 1,2,4-trichlorobenzene (KBr region), and with water vapor for all regions.

Preparation of Compounds.—All the compounds studied were prepared according to the methods described in the literature.[4-8,10] Purity of each compound was checked by measurement of the melting point and of the ultraviolet spectrum.

Results and Discussion

I. Trifluoromethyl Group.—Figures 1 and 2 show the infrared spectra of Cu(II) and Ni(II) complexes of substituted acetylacetonates indicated by formula I. The band assignments given for the acetylacetonates originate in the previous normal coördinate treatment.[11] In order to identify the CF_3 group absorptions, the infrared spectrum of gaseous CF_4[12] is shown by dotted curves on those of hexafluoroacetylacetonates. From the comparison of the spectrum of CF_4 with that of a hexafluoroacetylacetonato complex, the bands near 1200, 900, 700, and 500 cm.$^{-1}$ in the latter were empirically assigned as the bands characteristic of the CF_3 group. The bands characteristic of the chelate ring in the fluoro complex then were connected by dotted lines to those of the corresponding acetylacetonato complex. It is seen from Fig. 1 and 2 that CF_3 substitution causes marked shifts of the C=C(ν_8) and C=O(ν_1) stretching bands to higher frequencies, and of the M–O(ν_5) stretching band to lower frequency. Table I summarizes the frequencies of these bands together with the stability constants of the substituted compounds.

In order to confirm these empirical band assignments, perturbation calculations[2] were made for hexafluoroacetylacetonato complexes of Cu(II) and Ni(II) in which the CF_3 group was considered to be a single atom having the same mass as that of the group. The parameters used for the calcula-

(1) This work was supported by the U. S. Army Research Office (Durham) under Contract No. DA-19-020-ORD-5119 and grant No. DA-ORD-31-124-61-G61.

(2) Department of Chemistry, Illinois Institute of Technology, Technology Center, Chicago 16, Illinois.

(3) K. Nakamoto, P. J. McCarthy, A. Ruby and A. E. Martell, *J. Am. Chem. Soc.*, **83**, 1066, 1272 (1961).

(4) L. J. Bellamy and R. F. Branch, *J. Chem. Soc.*, 4487 (1954).

(5) R. L. Belford, A. E. Martell and M. Calvin, *J. Inorg. & Nuclear Chem.*, **2**, 11 (1956).

(6) H. F. Holtzclaw, Jr., and J. P. Collman, *J. Am. Chem. Soc.*, **79**, 3318 (1957).

(7) R. P. Dryden and A. Winston, *J. Phys. Chem.*, **62**, 635 (1958).

(8) G. A. Guter and G. S. Hammond, *J. Am. Chem. Soc.*, **81**, 4686 (1959).

(9) J. Charette and P. Teyssié, *Spectrochim. Acta*, **16**, 689 (1960).

(10) H. Schlesinger, H. Brown, J. Katz, S. Archer and R. Lad, *J. Am. Chem. Soc.*, **75**, 2448 (1953).

(11) K. Nakamoto and A. E. Martell, *J. Chem. Phys.*, **33**, 588 (1960).

(12) P. J. H. Woltz and A. H. Nielsen, *ibid.*, **20**, 307 (1952).

TABLE I

OBSERVED FREQUENCIES ($CM.^{-1}$) AND STABILITY CONSTANTS OF THE Cu(II) AND Ni(II) COMPLEXES WITH VARIOUS β-DIKETONES

Substituent R	Substituent R′	ν_8(C=C str.) Cu(II)	ν_8(C=C str.) Ni(II)	ν_1(C=O str.) Cu(II)	ν_1(C=O str.) Ni(II)	ν_5(M–O str.) Cu(II)	ν_5(M–O str.) Ni(II)	Stability const.[a] Cu(II)	Stability const.[a] Ni(II)
CF_3	CF_3	1644	1643	1614	1613	415	397	...	...
CF_3	CH_3	1611	1639	1600	1621	445	427	17.2	14.2
CH_3	CH_3	1580	1598	1548 1524	1598	455	452	23.66	17.08
C_6H_5	CH_3	1590	1591	1554	1591	458	455	23.01	18.00
C_6H_5	C_6H_5	1593	1595	1544	1595	462	458	24.94	20.72

[a] Log K_1K_2 in 75% dioxane–H_2O mixture at 30°. (L. G. Van Uitert, W. C. Fernelius, and B. E. Douglas, *J. Am. Chem. Soc.*, **75**, 457, 2736 (1953).)

TABLE II

MASS OF SUBSTITUENT, METAL–OXYGEN BOND DISTANCE AND FORCE CONSTANT

Metal	Substituent R	Substituent R′	Mass of substituent R (atomic weight)	Metal–oxygen distance, Å.	Force constant (10^5 dyne/cm.) K(C=O)	K(C=C)	K(C–R)	K(M–O)
Cu(II)	CF_3	CF_3	69	1.95	7.90	5.81	1.80	1.75
	CH_3	CH_3	15	1.95	6.90	5.35	3.60	2.20
	C_6H_5	C_6H_5	77	1.95	6.82	5.49	3.60	2.31
Ni(II)	CF_3	CF_3	69	2.05	7.72	5.88	1.80	1.35
	CH_3	CH_3	15	2.05	7.65	5.35	3.60	2.05
	C_6H_5	C_6H_5	77	2.05	7.55	5.36	3.60	2.25

tions are listed in Table II. Since no structural data are available for these substituted compounds, it was assumed that the bond distances in the chelate ring do not change appreciably by substitution. Although all the force constants are expected to be changed by substitution, only the relatively more important C=C, C=O, C–R, and M–O stretching force constants were adjusted to fit the observed frequencies. Evidently such an assumption does not give completely satisfactory results, especially for the vibrations which are neglected. For simplicity in the calculations and because the center of interest is in the C=C, C=O, and M–O stretching bands, only the force constants of these three bands plus that of the adjacent C–R group were employed for the perturbation calculation.

Table III compares the observed frequencies with the calculated values obtained by using the parameters given in Table II. The agreements are quite satisfactory for ν_8, ν_1, ν_3, ν_{11}, and ν_5 bands and less satisfactory for other bands, as expected, since their frequencies are functions of other force constants such as those involving angle deformation. It is to be noted that coupling between various vibrational modes also causes difficulty in adjusting some of these frequencies. Nevertheless, it is clear that the substitution of trifluoromethyl in place of a methyl group increases the C=C and C=O and decreases the C–R and M–O stretching force constants.

One would predict on the basis of electronic theory of bonding that the strong positive inductive effect of the CF_3 group strengthens the C=C and C=O bonds and weakens the M–O bonds. Therefore, the results of the present infrared study provide experimental evidence confirming this prediction. The weakening of the M–O bond by CF_3 substitution is also in agreement with the lower stability constants, shown in Table I, of the trifluoromethyl derivatives. Finally, it is seen that evidence is given in Table III indicating that the strength of the M–O bond in the trifluoroacetylacetonates is intermediate between those of the acetylacetonato and hexafluoroacetylacetonato complexes, since the spectra of the trifluoroacetylacetonates are intermediate between those of the latter two compounds.

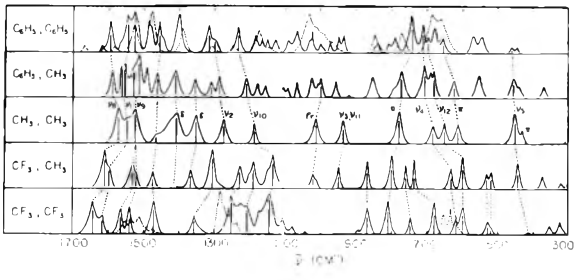

Fig. 1.—Infrared spectra of Cu(II) complexes of various β-diketones.

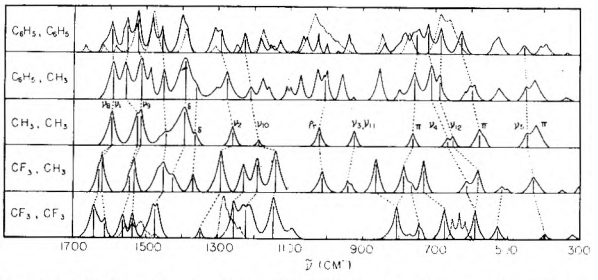

Fig. 2.—Infrared spectra of Ni(II) complexes of various β-diketones.

II. Phenyl Group.—Figures 1 and 2 show the infrared spectra of Cu(II) and Ni(II) complexes of benzoylacetone and dibenzoylmethane. The spectrum of benzene also is shown by dotted curves superimposed on the spectra of dibenzoylmethane complexes. It is seen that overlapping of the benzene bands with those of the chelate rings is serious in the whole range of the benzene spectrum, and empirical assignments therefore are virtually impossible. As is seen in Fig. 1 and 2, however, the C=C(ν_8), C=O(ν_1), and M–O(ν_5) stretching bands

TABLE III

COMPARISON OF CALCULATED AND OBSERVED FREQUENCIES IN SUBSTITUTED ACETYLACETONATES ($CM.^{-1}$)

CF_3, CF_3, Cu		CF_3, CF_3, Ni		C_6H_5, C_6H_5, Cu		C_6H_5, C_6H_5, Ni		
Obsd.	Calcd.	Obsd.	Calcd.	Obsd.	Calcd.	Obsd.	Calcd.	Assignments
1644	1647	1643	1644	1593	1592	1595	1595	C=C str. (ν_8)
1614	1614	1613	1612	1544	1543	1595	1595	C=O str. (ν_1)
1563	1505	1563	1498	1526	1486	1544	1515	CO str. + CH bend. (ν_9)
1537		1535				1522		
1357	1191	1349	1188	1295	1270	1293	1268	CC str. + CR str. (ν_2)
1145	1208	1145	1204	1233	1226	1230	1234	C–H in-plane bend. (ν_{10})
..	..	..	..	944	937	940	945	C–C_6H_5 str. (ν_3)
..	..	..	..	932	902	929	905	C–C_6H_5 str. (ν_{11})
869	874	805	873	..	..	..	..	C–CF_3 str. (ν_3)
746	730	746	730	..	..	..	..	C–CF_3 str. (ν_{11})
809	..	807	..	744	..	745	..	C–H out-of-plane bend.
618	608	588	593	707	663	719	659	Ring def. + M–O str. (ν_4)
597	602	588	580	694	634	686	632	C–R bend. + M–O str. (ν_{12})
415	416	397	397	462	462	458	460	M–O str. (ν_5)
355	371	320	371	337	373	337	373	Ring def. (ν_{13})

All the vibrations characteristic of the CF_3 and C_6H_5 groups are not listed.

are out of this range. Therefore the shifts of these bands resulting from phenyl substitution may be discussed without ambiguity.

Table I compares the frequencies of ν_8, ν_1, and ν_5 bands and the stability constant for the complexes of acetylacetone, benzoylacetone, and dibenzoylmethane. It is seen that phenyl substitution shifts the M–O stretching (ν_5) of the Cu(II) and Ni(II) complexes and the C=C stretching (ν_8) of the Cu(II) complex to higher frequencies. The shift of the C=O stretching (ν_1) band is somewhat irregular.

In order to confirm the foregoing empirical band assignments, perturbation calculations were carried out for the dibenzoylmethane complexes of Cu(II) and Ni(II), with the same assumptions as those made previously for CF_3 substitution. The results shown in Table III indicate that phenyl substitution slightly increases the C=C and M–O stretching force constants and slightly decreases the C=O stretching force constant. Neglecting the weak negative inductive effect of the aromatic ring, one may look for the principal electronic effects in the mesomeric interactions of the phenyl group with the semi-aromatic metal chelate ring. The result of resonance shift of π-electrons to the chelate ring can be visualized by assuming small contributions from resonance forms such as A, B, and C shown below

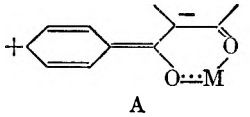

A

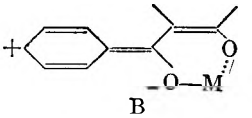

B

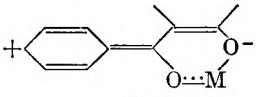

C

These structures indicate that the effect of the mesomeric electron release by the phenyl group could be a general strengthening of the M–O bonds by an increase of negative charge on the oxygen atoms. Superimposed on this effect, there would be an increased tendency toward π-bonding in the M–O linkages. It can be seen that both of these effects would strengthen the M–O and C–C bonds more than the C–O bonds of the chelate ring. It would be of interest to observe the effect with metal ions which do not form π-bonds. Thus one would expect a smaller shift of the M–O stretching bands of corresponding Mg and Ca complexes to higher frequencies (less bond strengthening) since these metal ions would not be able to participate in the conjugation effects described above.

Holtzclaw and Collman[6] suggested that phenyl substitution weakens the M–O bond since the neighboring C=O bond is weakened by conjugation with the phenyl ring. The present theoretical predictions, however, lead to a different conclusion. Also, the increase of the stability constant which occurs on phenyl substitution, shown in Table I, is in accord with the observed infrared shifts of the M–O bonds, as well as the results of the perturbation calculations described in this paper.

Acknowledgment.—The authors are indebted to the M.I.T. Computation Center for the use of an I.B.M. 709 computer for the calculations.

KINETIC STUDIES OF THE THIONINE–IRON SYSTEM. II[1]

BY R. HARDWICK

Department of Chemistry, University of California, Los Angeles, California

Received October 7, 1961 (Orginal Manuscript Received December 1, 1960)

The observed inhibitory effect of ferric ions on the bleaching of aqueous thionine–ferrous ion solutions formerly has been attributed to direct quenching of excited thionine. The results of the present experiments, reinforced by recent data of other authors, are used in an interpretation of the reaction mechanism which assigns a chemical, not quenching, role to ferric ions.

Introduction

The reversible, photochemical reaction of the purple dye thionine and ferrous ion has been repeatedly investigated during the last several years. A more complete discussion of the early work is given in the first paper of this series[1] (hereafter, I).

The equilibrium

$$T + Fe^{II} \underset{r}{\rightleftharpoons} Fe^{III} + S \qquad (1)$$

which normally lies far to the left, is shifted to the right with the absorption of visible light by thionine. Measurements of the position of the equilibrium are complicated by the further equilibria

$$S + Fe^{II} \underset{b'}{\overset{b}{\rightleftharpoons}} L + Fe^{III} \qquad (2)$$

and

$$2S \underset{c'}{\overset{c}{\rightleftharpoons}} L + T \qquad (3)$$

where T designates thionine (thio); S designates the singly reduced species, semithionine (semi); and L designates leucothionine (leuco).

At the present time, we do not find any of the currently proposed reaction schemes (including that of I) entirely satisfactory.[2] While we continue an investigation of the role of complexing of the dye, both with its own and with other ions, we report here results which concern the important role of ferric ions in the reaction system. We discuss also experimental evidence which does support the present view that the predominant dye species in photobleached solutions is the doubly reduced leuco.

Results and Discussion

I. Extent of Reduction.—Although it was proposed in I that semi comprised the major portion of reduced dye in photobleached solutions, the subsequent flash photolysis experiments of Parker[4] seem to show that the lifetime of semi may be too short to allow this species to predominate.

Parker's value for the semi dismutation rate constant, c, is $\sim 10^9$. A typical bleaching rate for an experiment like those of I and subsequent investigations by Ainsworth and others[5] would be about 10^{-6} moles/l. sec. In such a system the concentration of semi need rise only to $(S) \approx (10^{-6}/10^9)^{1/2} \approx 3 \times 10^{-8}$ for the rate of dismutation to equal the bleaching rate. Evidently, during bleaching, a small steady-state concentration of semi is established within the first fraction of a second; thereafter, all bleaching results in a net formation of leuco.

Although we are not satisfied that reduction of semi by ferrous ions may not be important, we can, for two reasons, add further support to the postulate of complete reduction.

(a) Semi is a free radical, thus should be measurable by electron spin resonance techniques. In several experiments, however, we have failed to detect its presence in photobleached solutions. While this is certainly not a definitive result, it indicates that semi may be present only in concentrations very much smaller than the total dye concentration.

(b) We propose below a new explanation of the role of ferric ions in retarding initial bleaching rates and depressing the amount of steady-state bleaching. This scheme, which is supported by experimental results, is compatible only with essentially complete reduction.

II. Role of Ferric Ions in the Reaction System.—The strong effects of (Fe^{III}) on the initial bleaching rate and the position of the photostationery state first were ascribed[1] to quenching of excited thio by ferric ions. Subsequent workers have used the resulting quantum yield (Fe^{III}) dependence

$$\gamma = \frac{a'(Fe^{II})}{a(Fe^{II}) + c + f(Fe^{III})}$$

where c is the rate constant for thermal quenching and f for quenching by Fe^{III}. Until recently, f has been assumed to have a fairly high value.

Further experiments in this Laboratory, however, have indicated that Fe^{III} does not act as a strong quencher but that its effect must be purely chemical.

We have found that certain other ions, quite similar to Fe^{III} in all respects save oxidizing power, show no quenching action on the photobleaching even when added in very large concentrations. These ions are Al^{III}, Co^{III}, Cr^{III}, Mn^{III} and Ce^{III}. This result, coupled with the negligible quenching action of Fe^{III} on the thionine fluorescence, suggests that Fe^{III} retards photobleaching through some mechanism by which its periodic table neighbors do not operate, or that the apparent quenching action is really a chemical reaction. There is no

(1) Paper I, R. Hardwick, *J. Am. Chem. Soc.*, **80**, 5667 (1958).

(2) Since submission of this work, a second paper by Hatchard and Parker[3] has proposed essentially the mechanism discussed in the present note. Our results from these somewhat different experiments support those of Parker, thus giving further verification to the proposed mechanism.

(3) C. G. Hatchard and C. A. Parker, *Trans. Faraday Soc.*, **57**, 1093 (1961).

(4) C. A. Parker, *J. Phys. Chem.*, **63**, 26 (1959).

(5) S. Ainsworth, *ibid.*, **64**, 715 (1960); J. Schlag, *Z. physik. Chem.* (Frankfurt), **20**, 53 (1959); R. Havemann and H. Pietsch, *Z. physik. Chem.* (Leipzig), **208**, 98 (1957).

way in which a chemical reaction may cause this effect in a system *that bleaches only to semi*, since the only reaction involving Fe^{III} *in such a system* is the reverse of 1, *viz.*, $S + Fe^{III} = T + Fe^{II}$, and this reaction, which then must be responsible also for the slow color restoration reaction, would be too slow to compete in the initial stages with the bleaching reaction. (As has been shown, this oxidation is fast, thus it cannot be rate controlling in the color restoration). A chemical "quenching" role for Fe^{III} exists, however, in a system which bleaches all the way to leuco. This is discussed below.

III. Reinterpretation of the Rate Data of I.—With this prologue, we attempt a reinterpretation of the earlier rate data. The attempt is not entirely successful, since in at least one case there is no simple analytical expression for the role of (Fe^{III}), but there is no case in which the earlier data are at serious variance with the new scheme.

(A) Initial Rate.—If the rate constant for dismutation is very large, semi immediately will establish a steady-state concentration, afterwards reacting with itself as rapidly as it is formed. In the absence of Fe^{III} this yields one molecule of leuco for every two thios which were reduced initially. The initial rate will not be second order in quanta absorbed, however, since the rate-determining reaction is the first-order creation of semi. The initial rate of disappearance of thio, $-(\dot{T}_i)$ (neglecting reduction of semi by Fe^{II}) is then

$$-(\dot{T}_i) = I_0\kappa\gamma(T_0) - c(S)^2 - r(S)(Fe^{III}) \qquad (4)$$

where I_0 represents initial light intensity, and κ the extinction coefficient of thio. In the absence of Fe^{III}, the quantum yield for semi, γ, may be calculated from the initial rate, since eq. 4 reduces merely to $-(\dot{T}_i) = I_0\,\kappa\,\gamma\,(T_0)/2$ after steady-state treatment for semi. At constant (Fe^{III}), the initial rate is linear in I_0, (T_0) and γ, in agreement with the data of I and subsequent data of others, although the maximum *net* quantum yield for bleaching is now 1/2 (this disagrees somewhat with our earlier experimental γ_{max} of about 0.75, but the difference may be due to experimental error or to some participation of reaction 2 in the reduction of semi). If the powerful retarding influence of ferric ion is to be ascribed to chemical action, the effect can take place only through the competition for semi between the dismutation reaction and the ferric reoxidation to thio. This process, leading as it does to a decreased steady-state concentration of semi, will result in a relative decrease of the rate of formation of leuco, thus of the apparent quantum yield.

After steady state treatment for semi, eq. 4 leads to

$$(\dot{T}_i) = \frac{I_0\kappa\gamma(T_0)}{2} - \frac{3r(Fe^{III})}{8}\sqrt{\left[\frac{r(Fe^{III})}{2c}\right]^2 + \frac{2I_0\kappa\gamma(T_0)}{c}} \qquad (5)$$

Although this expression is not amenable to simple plotting for (Fe^{III}) dependence, certain observations may be made from it.

(a) At $(Fe^{III}) = 0$, $-(\dot{T}_i) = I_0\,\kappa\gamma(T_0)/2$, as expected.

(b) If $[r(Fe^{III})/2c]^2 << 2I_0\,\kappa\gamma(T_0)/c$, the initial rate becomes linear in (Fe^{III}). Out of diffidence, we hesitate to present data to support this discussion, since, in truth, the ferric ion data are obliging enough to support nearly any mechanism, depending on the Fe^{III} concentration range used, the light intensity, etc. We have taken data, however, at quite low ferric ion concentrations (a maximum of ~25% of the lower values used in I) and find that the decrease in initial bleaching rate is fairly linear in (Fe^{III}) in the concentration range 0 to 5×10^{-4} moles/l. It may be seen that a non-linear dependence of $(\dot{T}_i)$ on I_0 is predicted by eq. 5. With a system having values for c, r, κ that seem to hold for our measurements, this non-linearity would be experimentally insignificant.

A rough calculation using Parker's estimated values of r and c and typical values for our experiments of Fig. 4 indicates that these rates ought to fall in the linear range; here the inequality of $[r(Fe^{III})/2c]^2 << 2I_0\kappa\gamma(T_0)/c$ is about $(10^{-4} \times 2 \times 10^{-4}/2)^2 < 2 \times 10^{-6}/10^{-9}$ or $10^{-16} < 2 \times 10^{-15}$, a factor of about 20. At $(Fe^{III}) \sim 10^{-3}$, the quantities are roughly even.

(c) If $[r(Fe^{III})/2c]^2 >> 2I_0\,\kappa\gamma(T_0)/c$, the initial rate becomes linear in $(Fe^{III})^2$. We have no reliable data in this range, $(Fe^{III}) \sim 10^{-2}$, because the initial rate becomes very small under these conditions.

(B) Steady State.—The effect of Fe^{III} in decreasing the steady-state degree of bleaching may be easily understood from the preceding discussion, although simple kinetic expressions are not available. Increasing Fe^{III} concentration reduces the steady-state concentration in two ways, by the reduction in the concentration of semi and by the increase in the rate of reoxidation of leuco. We have not yet found a way of using rate data to test this part of the mechanism quantitatively.

Acknowledgment.—The quenching experiments were done by Mr. Cannon Jensen. We are indebted to Dr. Tom Tuttle for assistance in the e.s.r. measurements. Part of this research was supported by the United States Air Force, Cambridge Research Center, Contract AF 19(604)-6643. This support is gratefully acknowledged.

THE PERMEABILITY OF NIOBIUM TO HYDROGEN

BY D. W. RUDD, D. W. VOSE AND S. JOHNSON

Research and Development Laboratories, Metal Hydrides Incorporated, Beverly, Massachusetts

Received October 11, 1961

The permeability (P) of niobium to hydrogen was investigated over a range of temperature between 950 to 1065° and pressure levels of 1.1 and 2.0 atmospheres. The resulting permeability was found to obey the relationship

$$P = 2.01 \times 10^3 \, e^{-5208+140/RT} \, \frac{\text{cm.}^3 \, H_2(0°, 1 \text{ atm.}) \, \text{hr.}^{-1}}{\text{cm.}^2 \, \text{mm.}^{-1} \, (\text{atm.})^{1/2}}$$

Introduction

The phenomenon of gases being transported through metal barriers has been studied by a large number of investigators and their results can be essentially divided into two categories: those studies involved in actual diffusion of gases in the metal itself, and those following the rate at which a gas will penetrate a metal barrier and be collected on the opposite face. The former category is referred to as diffusion, while the latter is called permeability. Diffusion is the more fundamental quantity, since it is related directly to the interactions of the gaseous particle with its metal environment while the gas is being transported within the metal. Permeation, on the other hand, is an over-all rate process which is believed to be composed of rates of adsorption, solution, diffusion, and desorption of a quantity of gas as it proceeds from one face of a metal barrier and is collected on the opposite face. Both diffusion and permeation are closely related by Fick's laws.

Although permeation is not as fundamental as diffusion, it is nevertheless a very useful quantity, since it is also a property of the gas–metal system involved and measures the total amount of gas that will penetrate the metal. Use of this phenomenon has been employed for a number of years in the purification of hydrogen, the metal acting as a superefficient filter.

A survey of the literature reveals that much of the early work has dealt with permeability studies while many of the more recent investigations have been concerned with diffusion. A very complete (1951) compilation and theoretical discussion of the entire field has been furnished by Barrer.[1]

The general mechanism of permeation was discussed in a previous investigation by the authors.[2] The results can be summarized: (1) Usually activated adsorption of the permeating gas is a prerequisite for subsequent solution and diffusion in the metal under consideration; (2) diatomic gases permeate metals as individual atoms; (3) the rate of permeation is inversely proportional to the thickness of the metal barrier; (4) hydrogen does not permeate along grain boundaries in metals but rather through the crystal lattice.

Material.—Niobium ingot, electron beam melted, was obtained from Pratt and Whitney Aircraft Corporation, CANEL Operations, Middletown, Connecticut. Spectrographic analysis detected < 10 p.p.m. of Fe, Al, Au, Mg, Si, Mn, Ag, Cu, Mo, the remainder being Nb.

Apparatus.—In general, apparatus for investigating the permeability of metals to hydrogen fall into two categories: those in which the metal barrier is cylindrical; and those in which the barrier is a flat disc, sometimes referred to as a membrane. An excellent illustrated summary is given by Flint.[3] The principal advantage of the disc over a cylinder is that it may be maintained more easily at a uniform temperature. Since permeability is very dependent on temperature, it is essential that the diffusing membrane be as free as possible from all thermal gradients. The great disadvantage of the disc is that it usually is held in position by welds, with the resulting possibility of leakage and diffusion of welding material into the membrane. The chief advantage of the cylinder is that it is somewhat easier to assemble and usually has no welds in the hot zone. The main disadvantage is concerned with the difficulty of maintaining a uniform temperature along the cylindrical axis. In this investigation, the disc was chosen.

To ensure against the above mentioned difficulties, the disc or membrane was fabricated from a cylinder of niobium stock about 15 cm. long. The cylindrical ingot was bored from both ends toward the center, stopping just before the center, leaving the flat disc fixed in position but with no welds. The wall thickness is quite large compared to the thickness of the membrane, being on the average in the ratio of 6:1. A basic cross sectional diagram is shown in Fig. 1. The membrane (A) can be maintained at a uniform temperature, and since there are no welds about the membrane, there can be no contamination from welding materials. There is the possibility of gas diffusing around the corner section where the membrane joins the wall. If this effect is present, it is of small magnitude, as evidenced from the reproducibility of values of specific rate and permeability. Three membranes were fabricated, the dimensions of which are given in Table I. A thermocouple well (B) was drilled at the vicinity of the membrane.

TABLE I

Membrane no.	1	2	3
Diameter, in.	0.6210	0.6235	0.6615
Thickness, in.	0.0940	0.1400	0.1710

After the membranes were machined, the finished ingot (hereafter referred to as the membrane assembly, which includes the finished ingot and the membrane) was fitted with caps at both ends, fabricated of the same material as the membrane assembly. Into the caps were fitted 25 cm. long 0.95 cm. o.d. tubes to allow for entrance and exit of the hydrogen. The tubes were constructed of niobium tubing. The interior of the tubes was clad with #446 stainless tubing. After the tubes were fitted into the caps, they were fastened to the caps by gold brazing on the interior face and niobium weld on the outer face. The purpose of such an elaborate tubing was to negate any detrimental effect of hydriding which developed in the tubing from the fact that part of the tubes were in the hot zone, while the other extremities were at room temperature. The caps and tubes were welded with a d.c. arc in an argon drybox. After welding, the entire apparatus was placed in an Inconel jacket (C). The interior of the jacket containing the membrane assembly was packed with niobium granules (D) to aid in heat conduction, and also connected to a vacuum system to prevent oxidation of the membrane assembly when at the temperatures being investigated. The outer extremity of the tubing which admitted hydrogen was connected to a bellows to allow for any thermal expan-

(1) R. M. Barrer, "Diffusion in and through Solids," Cambridge University Press, London, The Macmillan Co., New York, N. Y., 1951.

(2) D. W. Rudd, D. W. Vose and S. Johnson, *J. Phys. Chem.*, **65**, 1018 (1961).

(3) P. S. Flint, KAPL-659, General Electric Co., 1951.

TABLE II

SUMMARY OF RESULTS OF PERMEABILITY OF Nb TO HYDROGEN

Units: Rate = cc. H_2(0°, 1 atm.)hr.$^{-1}$ = v; specific rate = cc. H_2(0°, 1 atm.)hr.$^{-1}$/cm.^{2} mm.$^{-1}$ = S.R.; permeability = P = specific rate/$p^{1/2}$

		Membrane 1 Thickness 0.0940" Diameter 0.6210"			Membrane 2 Thickness 0.1400" Diameter 0.6235"			Membrane 3 Thickness 0.1710" Diameter 0.6615"		
t, °C.	p, atm.	v	S.R.	P	v	S.R.	P	v	S.R.	P
950	1.1	205	250	238	137	248	236	127	249	237
	1.5	239	292	234						
	2.0	277	339	239	186	335	237	171	335	237
1010	1.1	228	279	266	152	275	262	141	275	262
	2.0	306	374	265	206	372	263	188	368	260
1065	1.1	246	301	287				153	299	285
	2.0	333	406	287				204	400	283

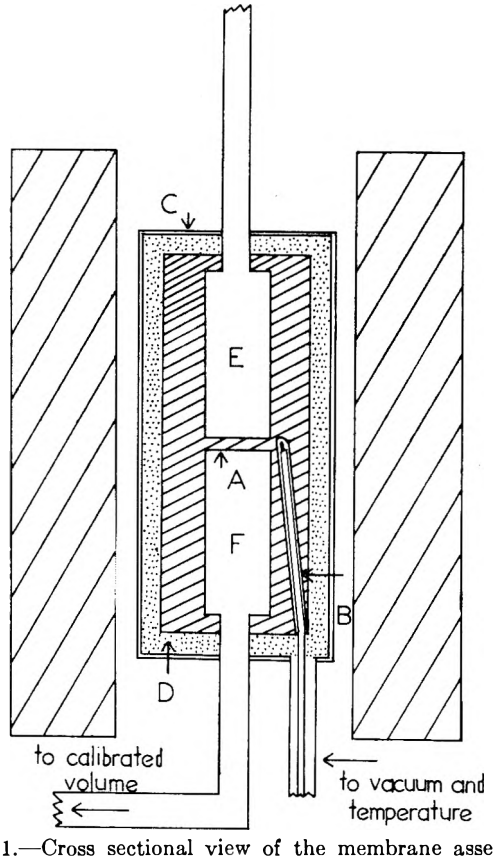

Fig. 1.—Cross sectional view of the membrane assembly including the caps, tubes, and Inconel jacket.

sion of the membrane assembly. The entire apparatus was placed in a resistance furnace. The temperature was controlled to ±1° by means of Wheelco "Capaciline" regulators and a recording potentiometer.

Tank hydrogen was fed successively through a catalytic getter, a 1-m. tower of calcium hydride, a 30-cm. tower of titanium hydride maintained at 1000°, and finally into the upstream section of the membrane assembly (E). The pressure of the gas in the upstream section was read by means of a Bourdon type gage and controlled by allowing a slight excess of hydrogen to enter the upstream section and then bleeding off this excess to a long column of mercury. On raising or lowering the mercury column, the pressure could be maintained to a very precise degree for an unlimited period. The gas leaving the downstream section (F) was pumped *via* a Toepler pump to a calibrated volume. The temperature about the calibrated volume was read to ±0.5°. Between the Toepler pump and the membrane assembly was placed a Dry Ice–acetone cold trap to prevent migration of mercury vapor to the downstream face of the membrane.

Experimental Accuracy.—Utilizing the above equipment, the over-all accuracy is generally in the range of ±1%. The precision of the individual readings often was better than this. Before any measurements were made, all three membranes were outgassed at 1100° for a period of 48 hours. The downstream section was evacuated by mercury diffusion pumps to a vacuum of 10^{-6} mm. After 48 hours, a blank run was initiated at 1065°, lasting 72 hours. At the end of this time period, no reading could be obtained at the calibrated volumes. This means that the error in readings, due to leaks in the system, is less than 0.000012 cm.^{3} (0°, 1 atm.) hr.$^{-1}$/cm.^{2}mm.$^{-1}$. Hydrogen pressure then was admitted to the membranes. The results are shown in Table II. Because of the danger of hydriding the membranes, the conditions of temperature and pressure were chosen so that the membranes would not form a hydride phase.[4] Data on membrane 2 are incomplete because the membrane inadvertently was cooled under hydrogen pressure as a result of a power failure.

Discussion

The permeability of a metal disc to a diatomic gas may be expressed by an equation of the form[2,5]

$$\alpha = (kDA/L)(p_1^{1/2} - p_2^{1/2})e^{-Ep/RT}t \qquad (1)$$

where

- α = the quantity of gas permeating the disc [cm.^{3} H_2-(0°, 1 atm.)]
- k = the solubility constant of atomic hydrogen in the metal
- D = the diffusion coefficient (cm.^{2}/sec.)
- A = the area of the disc (cm.^{2})
- p_1 = the pressure on one face of the disc (atm.)
- p_2 = the pressure on the other face
- Ep = the activation energy of permeation (cal./g. atom)
- L = the thickness of the disc (mm.)
- t = the time (hr.)

This investigation was so performed that several simplifications to (1) may be made. Since the downstream face is continuously evacuated to the calibrated volume so that $p_2 = 0$ essentially, the equation can be arranged to yield a rate expression at unit thickness and area (Specific Rate), the equation being

$$\text{Specific rate} = Cp_1^{1/2}e^{-Ep/RT}\ \frac{\text{cm.}^3\ H_2(0°, 1\ \text{atm.})\text{hr.}^{-1}}{\text{cm.}^2\ \text{mm.}^{-1}} \qquad (2)$$

where $C = kD$. This expression may be used for the evaluation of the pressure dependence, since, if the temperature is constant, the exponential term is essentially constant and (2) may be rewritten under these conditions as

$$\text{Specific rate} = C_1p^{1/2} \qquad (3)$$

where $C_1 = Ce^{-Ep/RT}$. The Specific Rate was plotted at each of the temperature levels shown in

(4) H. W. Paxton and J. M. Sheehan, AEC #AT(30-1)2041, Sept., 1957, Report from June 15–Sept. 15, 1957.

(5) C. J. Smithells, "Gases and Metals," John Wiley and Sons, New York, N. Y., 1937, p. 77.

Table II at the pressures of 1.1 and 2.0 atmospheres. The slopes of the subsequent lines were 0.5 ± 0.01, so that within the error of our apparatus, the pressure dependence is fixed at 1/2. Since equation (3) is independent of the dimensions of the membrane, the specific rate should be the same for all three membranes when they are at the same pressure and temperature. This expectation is confirmed by Table II. The permeability (P) may also be evaluated from the specific rate, since

$$\text{Permeability} = P \equiv \frac{\text{Specific rate}}{p_1^{1/2}} = Ce^{-Ep/RT} \frac{\text{cm.}^3\ H_2(0°,\ 1\ \text{atm.})\text{hr.}^{-1}}{\text{cm.}^2\text{mm.}^{-1}\ (\text{atm.})^{1/2}} \quad (4)$$

It can be seen from (4) that the permeability is dependent only on the temperature and should be the same for all the membranes regardless of pressure or dimensions. This also is confirmed by Table II. The activation energy for permeation was determined from (4) by the slope of the line resulting from a plot of log P *vs.* $1/T$. The average value of Ep was 5208 and the range ± 140.

Acknowledgment.—This investigation was sponsored by the Pratt and Whitney Aircraft Division of United Aircraft Corporation, CANEL Operations, Middletown, Connecticut, under prime contract AT(11-1)-229, subcontract AEC-13112.

NOTES

ABSORPTION MAXIMA OF SOME MOLECULAR COMPLEXES

By Mihir Chowdhury[1]

University College of Science & Technology, 92 Upper Circular Road, Calcutta, India

Received February 6, 1961

In a previous communication[2] the absorption maxima and equilibrium constants of hydrocarbon–tetrachlorophthalic anhydride complexes were reported. It was found that on changing the structure of the donor component slightly (*i.e.*, on replacing aromatics by aza-aromatics), no large shift in absorption maxima occurs. This led to the conclusion that probably the same type of level (which can only be π) was involved in both cases of charge-transfer absorption. We have varied the acceptor structure this time, and measured the absorption maxima of aromatic complexes of a number of similar acceptors such as phthalimide, phthalic anhydride, phthalic acid and maleic anhydride. The solvent used was chloroform and the spectrophotometer was a Beckman Model DU. The results are summarized in Table I.

Table I

Absorption Maxima of Complexes in mμ

	Phthalic anhydride	Phthal-imide	Malcic anhydride	Phthalic acid
Biphenyl	314	315	..	
Naphthalene	327	327	325	
Phenanthrene	348	352	354	No
Chrysene	363	362	367	absorption
Pyrene	378	377	384	
Anthracene	389	387	392	

As expected for a charge-transfer band λ_{max} increases with the decrease in ionization potential of the hydrocarbon. A plot of $h\nu$ against the ionization energy of the hydrocarbon gives a straight line with a slope near to unity. This is shown in Fig. 1 for phthalic anhydride complexes. Hydrocarbons evidently are behaving as donors, and phthalic anhydride as an acceptor. It may be pointed out here that phthalic anhydride is known to form a complex with $AlCl_3$,[3] where it presumably acts as a donor through the lone pair of the O-atom. It is evident from Table I that on replacing one acceptor by another, λ_{max} did not change much. This suggests that the energies of their lowest vacant π-levels should be approximately the same.

Phthalic acid has no tendency to form any complex with aromatic hydrocarbons. (This can be utilized in the detection of phthalic anhydride in phthalic acid.) Succinic anhydride also fails to form a complex.[4] What therefore seems to be important in imparting acceptor property to the molecule is the presence of two carbonyl groups in a cyclic conjugated system. Maleic anhydride

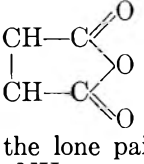

maintains cyclic conjugation through the lone pair of the anhydro-oxygen atom. The –NH– group possesses a lone pair and can replace the anhydro-oxygen atom. The oxygen atom also can be replaced by –CH=CH– when benzoquinone, a stronger acceptor, is formed.

It may be pointed out that λ_{max} of tetrachlorophthalic anhydride (T.C.P.) complexes[2] are higher than those of corresponding phthalic anhydride {$(PhCO)_2O$} complexes. The stronger acceptor property of T.C.P. presumably is due to electron-deficiency in the ring caused by the inductive effect of the Cl atoms.

Experimental

Phthalic and maleic anhydrides were purified by repeated sublimation. Small traces of acid in phthalic anhydride were removed by extraction of the anhydride with cold chloro-

(1) Chemistry Department, Pennsylvania State University, University Park, Pennsylvania, U. S. A.

(2) M. Chowdhury and S. Basu, *Trans. Faraday Soc.*, **56**, 335 (1960).

(3) Cooke, Susz and Herschmann, *Helv. Chim. Acta*, **37**, 1280 (1954); *Chem. Abstr.*, **48**, 12555i (1954).

(4) Keefer and Andrews, *J. Am. Chem. Soc.*, **75**, 3776 (1953).

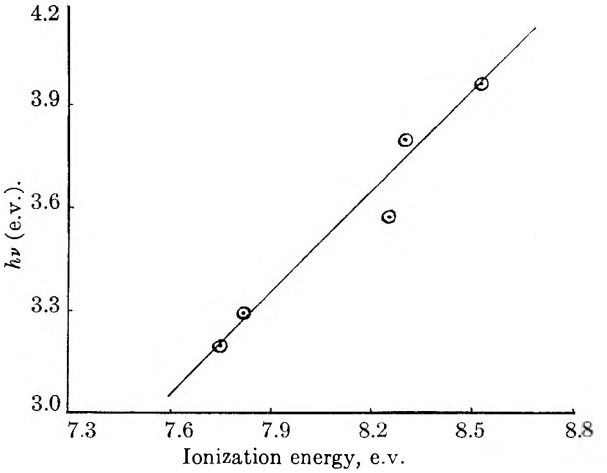

Fig. 1.

form and recrystallizing. Phthalimide was purified by recrystallizing from alcohol. Hydrocarbons were purified by methods described before.[5] Merck G. R. quality chloroform was used without further purification. Absorption measurements were made with a Beckman spectrophotometer Model DU. High concentrations of both acceptors and donors were used, and at that concentration the components had absorption at the wave length where the charge-transfer band was located. This was eliminated either by balancing the mixture against the component, or by subtracting the optical density of the components from the total optical density.

Thanks are due to Professor S. Basu for his helpful suggestions.

(5) Bhattacharya and Basu, *Trans. Faraday Soc.*, **54**, 1286 (1958).

A PHASE DIAGRAM STUDY OF THE SYSTEM AMMONIUM NITRATE-AMMONIUM PERCHLORATE[1a]

BY A. GREENVILLE WHITTAKER[1b] AND DAVID C. BARHAM

Sandia Laboratory, Albuquerque, New Mexico

Received June 9, 1961

In the course of some studies on the combustion of solid material, it became necessary to know something about phase behavior of the system ammonium nitrate–ammonium perchlorate. Since this was not an important part of the study, only a brief treatment of the system was carried out. Unfortunately, the complete diagram was not possible to obtain because the liquidus temperature at 12% ammonium perchlorate was high enough to cause rapid decomposition of ammonium nitrate.

Experimental

Reagent grade materials were used in this study without further purification. The samples were prepared by weighing out appropriate amounts on an analytical balance and mixing the components as dry powders. Most of the data were obtained by the conventional cooling curve method. Cooling rates were used that ranged between 0.12 to 0.25° per minute. Because of frequent super-cooling tendencies, the lower cooling rates were used most frequently. The accuracy of the points averaged about ±0.5°. X-Ray powder patterns were taken of both fused and unfused mixtures using a General Electric X-ray unit. Powder patterns were taken on compositions which cover the entire section of the phase diagram studied. Critical regions of the phase diagram were studied by watching the crystallization of small samples on a hot stage with a microscope using the technique described by McCrone.[2] This technique made it possible to determine the sequence with which the various phases crystallized as the sample cooled. A comparison method also was used in which four to eight five-g. samples of only slightly different composition were melted simultaneously in a forced air oven. The oven was allowed to cool slowly so that it was possible to determine the sequence in which crystallization started in the set of samples chosen. No temperatures were determined by this method. Only the relation between sample freezing point and composition was determined. This technique had the advantage over the hot stage fusion method in that evaporation of ammonium nitrate from the system was minimized; hence, the composition change was considerably less.

Results and Discussion

The results obtained from the cooling curves are shown in Tables I and II. The liquidus curves obtained from these data clearly indicated that the system did not have a simple eutectic; however, there was a small region lying between 6.8 and 8.2 mole % that was very difficult to resolve by the cooling curve techniques. This came about because the liquidus curve in this region remained within a temperature range of about 1°, which was approximately the accuracy of the measurements. Consequently, the resolution of this part of the liquidus curve was not good. The cooling curves indicated a short region of solid solution formation. It appeared that the solid solution boundary ran quite close to the liquidus curve up to approximately 0.5 mole % ammonium perchlorate and then dropped rather quickly to the eutectic line. This region was not investigated in detail. Table II

TABLE I

FREEZING AND MELTING POINTS OF THE SYSTEM AMMONIUM NITRATE-AMMONIUM PERCHLORATE

Mole % of NH_4ClO_4	No. of runs	A^a	Freezing point	No. of runs	A^a	Melting point
0.00	2	±0.1	169.7	2	±0.1	169.7
0.50	2	± .0	169.4	2	± .1	169.1
0.75	2	± .1	169.1	2	± .05	168.5
0.90	2	± .05	169.1	2	± .05	168.5
1.00	2	± .2	168.4	2	± .3	151.5
1.25	1	...	168.2	2	± .4	150.0
1.50	1	...	167.7	1	...	153.0
2.00	2	± .0	165.6	2	± .4	152.1
3.00	3	± .4	163.5	3	± .4	153.2
4.00	3	± .6	161.1	3	± .5	153.0
5.00	4	± .2	158.9	4	± .2	154.0
6.00	1	...	156.2	1	...	152.7
7.00	4	± .8	153.8	4	± .8	153.8
7.25	2	± .0	154.6	2	± .1	154.4
7.50	2	± .2	154.5	2	± .2	153.6
7.75	2	± .1	154.8	2	± .0	154.3
8.00	4	± .2	154.0	4	± .5	153.2
8.25	4	+ .7	155.6	4	± .4	154.5
8.50	2	± .2	155.9	2	± .2	153.4
9.00	7	±1.4	159.5	6	± .9	153.8
9.50	1	...	162.2	1	...	151.7
10.00	4	±3.0	165.4	4	± .4	153.8
10.50	2	±0.4	168.6	1	...	154.3
11.00	1	...	171.3	1	...	153.7
12.00	1	...	178.2	1	...	153.9

	M.p., °C.	Composition, mole %
Eutectic no. 1	153.5	6.8 NH_4ClO_4
Eutectic no. 2	154.0	8.1 NH_4ClO_4
New compound	154.5	7.6 NH_4ClO_4

[a] Average deviation in degrees for a group of runs of a given composition.

(1) (a) Work performed under the auspices of the U. S. Atomic Energy Commission; (b) Aerospace Corporation Laboratories Division 2400 East El Segundo Blvd., El Segundo, California.

(2) W. C. McCrone, Jr., "Fusion Methods in Chemical Microscopy," Interscience Publishers, Inc., New York, N. Y., 1957, p. 148.

TABLE II

TRANSITION POINTS OF AMMONIUM NITRATE–AMMONIUM PERCHLORATE SYSTEM

Mole % of NH_4ClO_4	Transition temp.	Mole % of NH_4ClO_4	Transition temp.
0.00	126.5	7.00	122.3
0.50	124.2	7.50	123.9
0.75	124.2	8.00	123.8
1.00	122.7	9.00	123.4
2.00	123.3		
5.00	123.7	10.00	123.8
6.00	123.3	11.00	124.0

shows the results obtained on the solid phase transition, which in ammonium nitrate corresponds to the transition from cubic to rhombohedral. This transition persisted across the entire part of the phase diagram studied. The transition temperature dropped rather sharply (about 2°) over the first half mole per cent. of ammonium perchlorate added. After this, it remained constant within the error of the measurements. This slight drop in the transition temperature corresponded to the region of solid solution formation. On the ammonium nitrate side of the diagram, the cooling curves remained at a constant temperature during the transition. As more ammonium perchlorate was added, the transition occurred over a temperature range rather than at a particular temperature. This temperature range increased with the ammonium perchlorate content. The temperatures given in Table II correspond to the highest temperature of the transition temperature range.

The X-ray diffraction apparatus was modified so that the samples could be held at approximately 135 ± 5° during the diffraction experiment. This put the samples above the transition temperature but below the melting point at any place on the diagram. The equilibrated samples showed new lines with *d*-spacings of 2.34, 2.80 and 3.60 Å. The first two lines were weak; the third was very strong. These lines did not occur in either of the pure components, nor did they occur in any of the mixtures that were not equilibrated by melting. In addition to these lines, the principal ammonium nitrate lines for *d*-spacings of 3.10 and 4.39 Å. were always strong even though the rest of the ammonium nitrate lines became weaker as the ammonium nitrate concentration decreased. Ammonium perchlorate lines also appeared in the patterns of the equilibrated samples. It was found, however, that these lines practically could be eliminated by cooling the samples very slowly. This behavior indicated that the compound must be rather highly dissociated at its melting point and that even rather slow cooling does not allow time for the equilibrium to reverse completely. Powder patterns were obtained for the pure components and for compositions containing 3, 6, 7.6 and 10 mole % ammonium perchlorate. Only the strongest new line appeared in the composition containing 3% ammonium perchlorate. All the lines appeared in the patterns for the rest of the samples, and their intensities increased as the concentration of ammonium perchlorate increased.

In an attempt to clarify the questionable region of the phase diagram, a hot stage microscope was employed to make a more careful study of the sequence with which the various phases appeared as a system crystallized. These observations indicated that a peritectic may exist in this region. Unfortunately, the results were of somewhat dubious value because cooling rates could not be controlled adequately and the ammonium nitrate vapor pressure was high enough to cause considerable evaporation of this component during the observations. This meant that samples of unknown composition were being observed. Because of this, a comparison method was developed using considerably larger samples. This minimized the effect of ammonium nitrate evaporation. Also, it was possible to get much lower cooling rates in the comparison method apparatus. The results obtained by this method indicated that there was a small hump in the phase diagram at about 7.6 mole % ammonium perchlorate with a eutectic quite close by on either side. Since the maximum height of this hump from the lowest eutectic to its top was only about 1°, and its width was only about 1 mole %, it was quite difficult to investigate this region and be sure of all the details.

If all the results are considered to have equal reliability it is difficult to decide the actual phase behavior of the system. The differential freezing point method seemed quite reliable and indicated a new compound at 7.6 mole % ammonium perchlorate, but this interpretation does not seem to be compatible with the fact that the ammonium nitrate solid phase transition extends past 7.6 mole % ammonium perchlorate. However, the persistence of the strong ammonium nitrate lines at 3.10 and 4.39 Å. may indicate that this compound may be ammonium nitrate-like in structure to the extent that some of its *d*-spacings are the same and a cubic to rhombohedral transition still is possible.

On the other hand, the X-ray data indicate the existence of a peritectic at about 8.2 mole % ammonium perchlorate. However, the cooling curves do not show holds at the expected temperature of about 155° for this composition and greater. The X-ray studies showed that the new compound is rather slow to form; therefore, it is possible that the cooling rates were too high to allow equilibrium conditions to be approached, thus causing the cooling curve holds to be missed. The increase in X-ray intensity of the new compound lines up to 10 mole % ammonium perchlorate is difficult to describe on any ground other than the formation of a peritectic. This may be the clinching argument for concluding that the system is best described as having a peritectic at about 8.2 mole % ammonium perchlorate.

There is not much possibility that the results are confused by decomposition products. Tests for chloride ion were always negative. It is doubtful that water from ammonium nitrate decomposition would accumulate significantly at the temperatures involved. All the rest of the possible decomposition products would leave the system rather quickly.

STUDIES ON THE SOL–GEL TRANSFORMATION OF THE FERRO- AND FERRICYANIDES OF SOME METALS. PART III. GELATION IN CHROMIC FERROCYANIDE

BY WAHID U. MALIK AND FASIH A. SIDDIQI

Chemical Laboratories, Muslim University, Aligarh, India

Received August 23, 1961

During the course of the work on heavy metal ferrocyanides we came across an unusual reaction, *viz.*, that between chromic chloride and potassium ferrocyanide, where unlike other metal ferrocyanides a soluble complex (reddish brown in color) of the composition[1,2] $KCr^{III}Fe^{II}Cy_6$ is formed. On carrying out the reaction at 80° an insoluble complex, highly viscous in nature and showing a tendency to gelatinize, is obtained. A study of some colloidal aspects of this compound was undertaken.

Experimental

The chromic ferrocyanide sol did not reveal vulnerability toward electrolytes as is generally the case with typical hydrophobic sols. However, interesting results were obtained on keeping it in the electrophoresis tube. Thus with a mixture of $CrCl_3$ and K_4FeCy_6 (concn. 0.075 and 0.025 *M*, respectively) of molar ratio $Cr^{3+}/FeCy_6^{4-}$ of 3:1, well-defined rings in the cathodic limb were formed; the liquid in the anodic limb depressed to about 1 cm. in about one hr. 15 min. (potential applied: 150 v.; current 2 to 5 mamp.). Mixtures of the molar ratio 1:3 (concn. $CrCl_3$ = 0.016 *M* and K_4FeCy_6 0.05 *M*) underwent movement toward the anode; with the equilibrium mixture (concn. 0.05 *M* of each reactant) there was no perceptible movement toward either of the electrodes.

The time of setting of chromic ferrocyanide gel as influenced by the $Cr^{3+}/FeCy_6^{4-}$ ratio was studied by Fleming's method[3] with the following four sets of mixtures. (i) 3.5 cc. of 0.78 *M* K_4FeCy_6 mixed with 1.0, 1.5, 2.0. . . . . .6.0, 6.5 cc. of 1.25 *M* $CrCl_3$. Total volume made up to 10 cc. (Molar ratio varied from 0.45:1 to 2.97:1.0); (ii) 5.0 cc. of 0.78 *M* K_4FeCy_6 mixed with 1.0, 1.2, ...4.2, 4.5 cc. of 1.25 *M* $CrCl_3$. Total volume made up to 15.0 cc. (Molar ratio varied from 0.32:1 to 1.8:1.0). (iii) 2.8 cc. of 0.78 *M* K_4FeCy_6 mixed with 0.96, 1.2,1.28,. . . . . 3.06, 3.2 cc. of 1.25 *M* $CrCl_3$. Total volume made up to 10 cc. (Molar ratio varied from 0.53:1.0 to 1.83:1.0); (iv) 1.8 cc. of 0.78 *M* K_4FeCy_6 mixed with 0.6, 0.8,. . . . . .2.0, 2.2 cc. of 1.25 *M* $CrCl_3$. Total volume made up to 10 cc. (Molar ratio varied from 0.534:1 to 2.0:1.0). The results are depicted in Figs. 1 and 2 (curves 1, 2, 3 and 4, respectively).

The time of gelation, besides being influenced by the $Cr^{3+}/FeCy_6^{4-}$ also was found to be dependent upon the concentration of the reactants. Thus the time of gelation of the mixture containing 3.5 cc. of 0.78 *M* K_4FeCy_6 and 2.5 cc. of 1.25 *M* $CrCl_3$ (molar ratio 1.1:1.0) increased from 12 min. to 15, 17, 28, 60, 155 min., respectively, on diluting the reactants to 4/5th, 3/5th, 2/5th, 1.5/5th and 1/5th of the original concentration.

Discussion

The results on the sol–gel transformation of chromic ferrocyanide reveal many points of dissimilarity with other metal ferrocyanides.[4] These are (i) lesser solubility of the complex with increasing temperature, optimum condition for gelation being reached in the vicinity of 80°; (ii) non-destructibility of the colloidal state by the addition of foreign ions; (iii) slow movement in the electrophoresis tube and indistinct separation of the phases at the interface; (iv) the tendency of the particles to assume a positive as well as negative charge (depending upon the excess of chromic or ferrocyanide ions). That the two types of gel-forming mixtures exist can be seen from the results on the time of gelation. Thus with the increasing concentration of the chromic ions a continuous decrease in the time of gelation is not realized. On the other hand, after reaching a minimum value for the equimolar mixture gradual increase in the time of gelation takes place (Figs. 1 and 2). However, in both cases the time of gelation is highly dependent upon the $Cr^{3+}/FeCy_6^{4-}$ ratio.

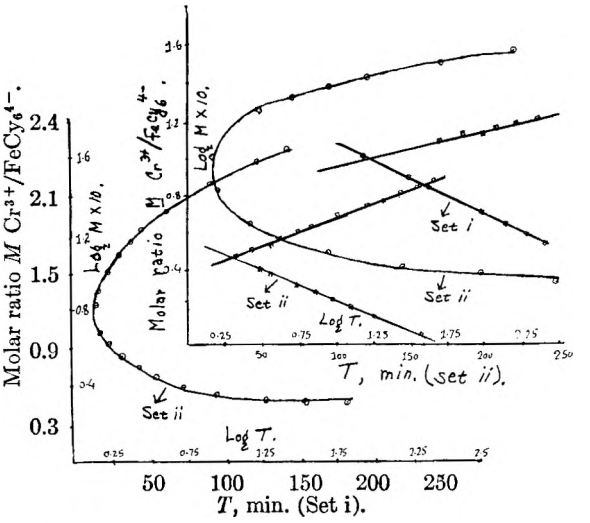

Fig. 1.—Set i and ii.

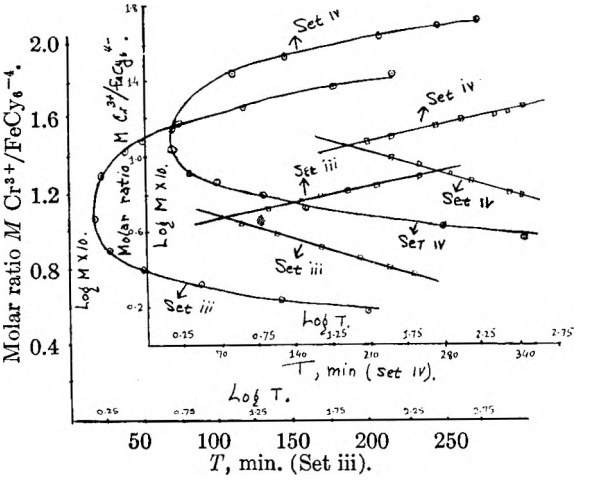

Fig. 2.—Set iii and iv.

The behavior, *viz.*, decrease in the time of gelation for mixtures of minimum gelation time (molar ratio 1.1:1.0) with increase in the concentration of the reactions is not unexpected since with concentrated solutions the degree of supersaturation increases and chances of gelation are enhanced.

A plot of log *M* against log *T* gives a pair of straight lines. The exponential nature of the curves can be represented by the empirical relationship

$$(T - \alpha M^n)(T - \beta M^{-m}) = 0$$

(1) W. U. Malik, *J. Sci. Ind. Research* (India), **18**, 463 (1959).
(2) W. U. Malik, *ibid.*, **20B.5**, 213 (1961).
(3) Fleming, *Z. Physik*, **41**, 427 (1902).
(4) K. Nasiruddin, W. U. Malik and A. K. Bhattacharya, *J. Phys. Chem.*, **59**, 488 (1955); W. U. Malik and A. K. Bhattacharya, *ibid.*, **59**, 490 (1955).

M being molar ratio and T the time of gelation, where α, β, n and m are constants. Their values for the four sets are α = 5.8, 19.9, 18.6, 10.0; β = 19.05, 14.2, 17.78, 36.14; n = 3.4, 5.0, 6.9, 6.25 and m = 2.91, 2.68, 4.16 and 4.68. The fact that the values of the constants are not the same may be due to the varying influence of factors like solubility, degree of supersaturation, extent of hydration and dilution during gelation.

Acknowledgment.—Thanks are due to Dr. A. R. Kidwai for providing facilities and to C.S.I.R. (India) for the award of a fellowship to F.A.S.

STUDIES ON THE SOL–GEL TRANSFORMATION OF THE FERRO- AND FERRICYANIDES OF SOME METALS. PART IV. VARIATIONS IN VISCOSITY AND HYDROGEN ION CONCENTRATION DURING THE GELATION OF CHROMIC FERROCYANIDE

BY WAHID U. MALIK AND FASIH A. SIDDIQI

Chemical Laboratories, Muslim University, Aligarh, India

Received August 23, 1961

The conductivity method, which was successfully employed[1] earlier in studying gelation of Prussian and Turnbull's blues, did not give any useful information here, and hence the methods based on the variations in viscosity and *p*H were adopted. The latter method was particularly chosen with a view to ascertain the hydrolytic effects operative during gel formation.

Experimental

Viscosity measurements were carried out at 80 ± 0.1° (Fisher Unitized constant temperature oil-bath) with the help of an Ostwald viscometer after applying a vacuum of 1 cm. (manometer tube supplied with koppeos viscometer unit was used for this purpose) at the head of the viscometer tube. Beckman *p*H meter (model H2) was used for *p*H measurements. Seven sets were studied, containing 0.25 M K_4FeCy_6 and varying concn. of $CrCl_3$ (0.083, 0.125, 0.18, 0.25, 0.375, 0.50 and 0.625 M) in the reaction mixture. The results are summarized in Table I.

TABLE I

Set	$Cr^{3+}/FeCy_6^{4-}$	Time interval for abrupt change in viscosity η (min.)	Change in η during this interval (centipoise)	Value of $(\eta_t - \eta_0)/\eta_0$ at abrupt change	*p*H change during gelation
I	0.33:1.0	218–250	0.70–2.4	0.75	4.0–7.25
II	0.5:1.0	120–140	0.95–2.7	0.90	3.8–6.8
III	0.75:1.0	72–80	1.15–4.8	1.10	3.6–4.0
IV	1:1	28–33	1.28–2.75	1.30	3.5–3.25
V	1.5:1.0	48–55	1.35–5.0	1.70	3.3–2.75
VI	2.0:1.0	120–150	1.45–3.6	2.10	3.12–2.02
VII	2.5:1.0	225–250	1.90–3.75	2.63	2.7–1.7

Discussion

The results on viscosity variations provide the following useful information regarding the gelation of chromic ferrocyanide: (1) the abrupt change in viscosity may be taken as a measure of the time of gelation since the values obtained by this and Fleming's method compare favorably (times of setting for the gelation mixtures of molar ratios 0.50:1.0, 1.0:1.0 and 2.0:1.0 being 25, 17, 85 minutes, respectively, by Fleming's method and 120, 28 and 120 minutes, respectively, by the viscosity method), provided due allowance is given to the disturbances experienced by the gel-forming mixture during its movement through the capillary; (2) similar types of curves are obtained by the two methods on plotting the time of setting against the molar ratio (Fig. 1), confirming thereby the existence of two types of gels in chromic ferrocyanide (Part III); (3) a straight line is obtained on plotting $\log (\eta_t - \eta_0)/\eta_0$ (for abrupt change) against the concentration of chromic chloride (Fig. 1, curve 2) (Cr^{3+} concn. for sets I to VII), which indicates a thixotropic behavior of chromic ferrocyanide gel (a linear relationship $\log \theta = A - Bc$, where θ is the time of setting and c is the concentration of the electrolyte and A and B are constants, was found by Freundlich,[2] Schalek and Szegvari[3] for the gelation of ferric oxide sol).

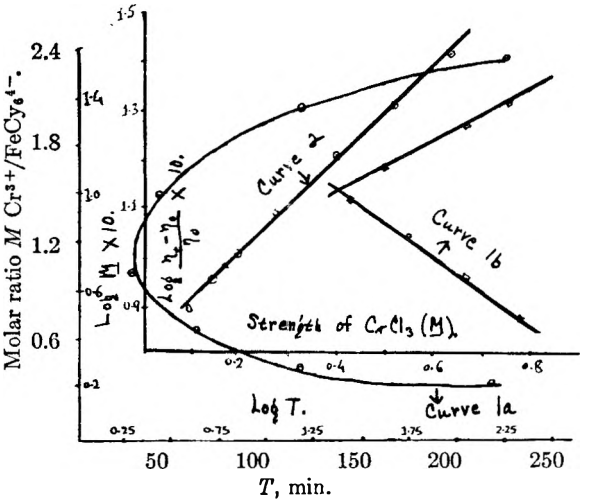

Fig. 1.—Curve 1a, T *vs.* M; curve 1b, $\log T$ *vs.* $\log M$; curve 2, strength of $CrCl_3$ *vs.* $\log (\eta_t - \eta_0)/\eta_0$.

The results on *p*H measurements, besides confirming the results on viscometry (the time when constancy in *p*H value is reached being taken as the time of setting), throw some light on the nature of the chromic ferrocyanide gel. As expected the mixtures containing excess of chromic ions have lower *p*H values and those containing excess of potassium ferrocyanide have higher *p*H values. But with lapse of time the *p*H of the mixtures having $Cr^{3+}/FeCy_6^{4-} > 1$ continuously decreases, while for those having $Cr^{3+}/FeCy_6^{4-} < 1$ the variations are of the reverse order. The behavior can be explained by assuming (a) the hydrolysis of chromic chloride, and (b) the hydrolytic decomposition of potassium ferrocyanide in the presence of chromic ions.[4,5] In the latter case the reaction takes the course

$$K_4FeCy_6 + H_2O \rightleftharpoons K_3(FeCy_6 \cdot H_2O) + KCN$$

$$KCN + H_2O \rightleftharpoons KOH + HCN$$

(1) W. U. Malik and A. K. Bhattacharya, *J. Phys. Chem.*, **59**, 490 (1955).

(2) H. Freundlich, "Thixotropy," Paris, 1935, pp. 7, 29.

(3) E. Schalek and A. Szegvari, *Kolloid-Z.*, **33**, 326 (1923).

(4) W. U. Malik, *J. Sci. Ind. Research* (India), **18**, 463 (1959).

(5) W. U. Malik, *ibid.*, **20B**, 5, 213 (1961).

thereby making the mixture less acidic. However, another significant point worth considering is that with mixtures having a molar ratio 1:1, the variations in *p*H with time are negligible (Table I).

Acknowledgment.—Thanks are due to Dr. A. R. Kidwai for providing facilities and C.S.I.R. (India) for the award of fellowship to F.A.S.

RETARDATION OF THE THERMAL DECOMPOSITION OF LITHIUM PERCHLORATE

BY MEYER M. MARKOWITZ AND DANIEL A. BORYTA

Foote Mineral Company, Research and Engineering Center, Chemical Division, P. O. Box 513, West Chester, Pennsylvania

Received November 20, 1961

The perchlorates frequently are regarded as prime examples of materials susceptible to catalytic thermal decomposition. Consistent with this viewpoint is the care usually taken to maintain high levels of purity when perchlorates are used or studied. Accordingly, it is of interest to report in this note some of the results from a continuing program aimed at resolving the decomposition processes of perchlorate salts. Specifically, a significant degree of retardation of the thermal breakdown of lithium perchlorate has been achieved by the use of certain silver salts as inhibitory additives.

An earlier paper[1] had presented evidence for an autocatalytic mechanism during the decomposition of lithium perchlorate; lithium chloride, the primary residual product, had been determined to be the autocatalytic agent. The top half of Fig. 1 shows the usual decomposition–time curves obtained for pure lithium perchlorate and for a 5 mole % lithium chloride–95 mole % lithium perchlorate mixture, each maintained at 417.8°. As these curves illustrate, decomposition is essentially complete after 2–4 hours. The lower half of Fig. 1 depicts the decomposition–time patterns for various mixtures of lithium perchlorate and silver nitrate, also kept at 417.8°. Clearly, there is a pronounced stabilization of the lithium perchlorate due to the presence of the silver nitrate and decomposition is almost complete only after about 39–45 hours. This stabilization is manifested by the prolongation of the induction period prior to the rapid, autocatalytic decomposition of the lithium perchlorate. Similar results have been obtained with silver perchlorate as the stabilizing additive.

The decomposition–time curves were obtained by means of an automatic recording thermobalance.[1,2] Though lithium and silver nitrates individually decompose slowly at 417.8°, it appears that in the reaction mixtures studied here the nitrate contents are conserved to a good degree. Decomposition residues from several lithium perchlorate–silver nitrate mixtures showed but very faint traces of nitrite and yielded more than 90%

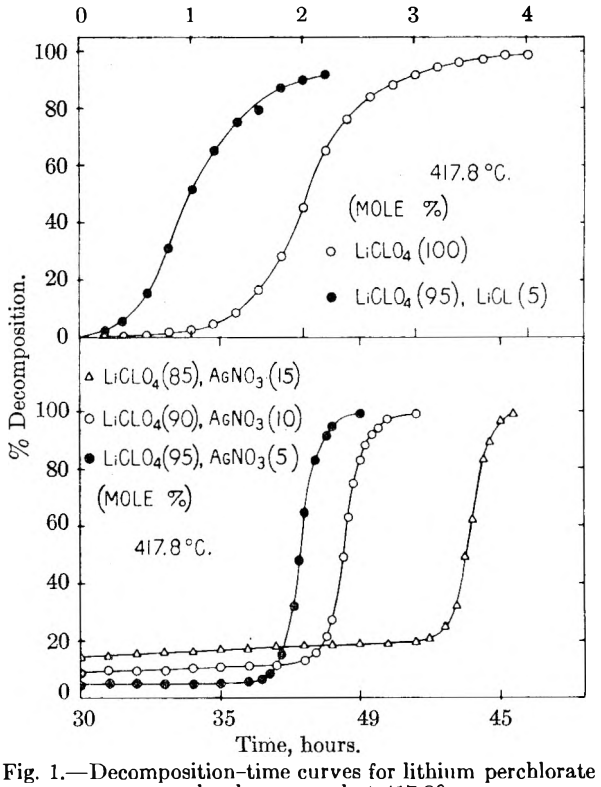

Fig. 1.—Decomposition–time curves for lithium perchlorate samples decomposed at 417.8°.

of the original nitrogen, recovered as ammonia after reduction with Devarda's alloy and distillation with sodium hydroxide solution. Accordingly, the percentage of lithium perchlorate decomposed was computed directly from the continuously recorded weight losses.

The mechanism of the stabilization effect appears to be related to the insolubility of silver chloride in mixtures rich in lithium perchlorate. As a consequence, the chloride-catalyzed decomposition is suppressed by immediate removal of the chloride ion because of formation of the insoluble silver chloride. Decomposition–time curves for mixtures of lithium perchlorate and silver chloride at 417.8° follow rather closely that characteristic of pure lithium perchlorate at the same temperature. Differential thermal analyses of mixtures of lithium perchlorate and silver chloride show the melting point of the lithium perchlorate (247°) to be virtually unaffected by the presence of the silver chloride; however, at the clearly defined melting point of silver chloride (455°) the decomposition of the lithium perchlorate becomes rapid, indicating that fusion of the silver chloride had permitted the introduction of chloride ions into the mass of molten lithium perchlorate.

It should be observed that as the proportion of silver nitrate to lithium perchlorate increases in the samples studied, the percentage of perchlorate decomposition increases for any given time prior to rapid decomposition. Apparently, though the silver ion does inhibit the autocatalytic reaction promoted by chloride ion, the silver ion also appears to catalyze to some small extent an alternate route of decomposition of lithium perchlorate.

(1) M. M. Markowitz and D. A. Boryta, *J. Phys. Chem.*, **65**, 1419 (1961).

(2) M. M. Markowitz and D. A. Boryta, *Anal. Chem.*, **32**, 1588 (1960).

THERMODYNAMICS OF PROTON DISSOCIATION IN DILUTE AQUEOUS SOLUTION. I. EQUILIBRIUM CONSTANTS FOR THE STEPWISE DISSOCIATION OF PROTONS FROM PROTONATED ADENINE, ADENOSINE, RIBOSE-5-PHOSPHATE AND ADENOSINEDIPHOSPHATE[1]

BY REED M. IZATT AND JAMES J. CHRISTENSEN

Department of Chemistry and Department of Chemical Engineering, Brigham Young University, Provo, Utah

Received July 14, 1961

Despite the vital importance of ribonucleotides in biological systems recent summaries[2,3] show that few pK_a data have been reported for proton dissociation from these or related substances. The available data have in nearly all cases been determined at high ionic strengths and at a single temperature. No pK_a data have been reported previously for ribose-5-phosphate (RP).

The present study is part of a program to determine equilibrium constants under identical experimental conditions for the stepwise dissociation of protons from ribonucleotides and related compounds as a function of ionic strength, μ, and temperature. pK_a data are reported here at 25° and as a function of μ for the dissociation of protons from protonated adenine, adenosine, adenosinediphosphate (ADP) and RP.

The higher of the two observed pK values of protonated adenine (I) generally is agreed to be associated with the removal of a proton from N_9 although tautomerism between N_7 and N_9 has been invoked[4] to explain the pH change observed upon formation of metal–adenine complex ions. Verification of the N_9–H bond is found in the fact that this dissociation is absent in adenosine, AMP, ADP and ATP, where the ribose group is attached to N_9. There are conflicting reports, however, concerning whether the lower pK value is associated with the N_1 or the amino group. Bock (ref. 2, p. 1) has pointed out that most workers assume the amino group to be the proton acceptor and so interpret their data. Nakajima and Pullman[5] and Zubay,[6] however, recently have presented data which indicate that the N_1 is the more basic.

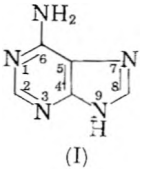

(I)

(1) Supported in Part by NIH Grant A-3021, and a Research Corp. Grant.

(2) R. M. Bock in "The Enzymes" Vol. 2, 2nd Edition, edited by P. D. Boyer, H. Lardy and K. Myrback, Academic Press, New York, N. Y., 1960, p. 15.

(3) D. O. Jordan, "The Chemistry of Nucleic Acids," Butterworths, Washington, 1960, p. 137.

(4) T. R. Harkins and H. Freiser, *J. Am. Chem. Soc.*, **80**, 1132 (1958).

(5) T. Nakajima and B. Pullman, *Bull. soc. chim. France*, **25**, 1502 (1958); *J. Am. Chem. Soc.*, **81**, 3876 (1959).

(6) D. Zubay *Biochim. et Biophys Acta.* **28** 644 (1958).

Experimental

Materials.—Reagent grade adenine hydrochloride (Schwarz Lab.), adenosine (Sigma Chem. Co.), ADP (Sigma Chem. Co.), RP (Sigma Chem. Co.), $HClO_4$ (Fisher), and $(CH_3)_4NOH$ (Eastman) were standardized by conventional means. The Na^+ originally present in the RP and ADP solutions was exchanged in a cation-exchange column for $(CH_3)_4N^+$ to prevent complexing of these substances by Na^+.

Procedure.—Solutions of protonated adenine, RP, adenosine and ADP were titrated with $(CH_3)_4NOH$ under a N_2 atmosphere at 25°. pH measurements were made at appropriate intervals with a Beckman Model GS pH meter using glass (Beckman E-2) and saturated calomel electrodes. The electrodes were calibrated throughout the titration range against appropriate buffer solutions. Reagents and instructions for the preparation of the buffer solutions were obtained from the National Bureau of Standards.[7]

Dissociation Constants.—Hydrogen ion activities were converted to concentrations by assuming the hydrogen ion activity coefficient to be identical with that in an HCl solution having the same μ value.[8] μ was calculated in the usual manner. In the case of ADP, however, it was assumed in the calculation of μ that the charge on the zwitterion species was equal to the total negative charge less the total positive charge. Molarity quotients, Q_n, were calculated from the experimental data,[9] and thermodynamic pK_n values obtained by plotting pQ_n *vs.* $\sqrt{\mu}$ and extrapolating to $\mu = 0$. The calculations were made with an IBM 650 computer.

Results

pQ_n values as a function of $\sqrt{\mu}$ are given in Table I together with previous work. pK_n values obtained by extrapolation of the present data are adenine, $pK_1 = 4.20$; RP, $pK_2 = 6.70$; ADP, $pK_1 = 4.20$, $pK_2 = 7.00$. A pK_3 value of 9.87 was calculated in the case of adenine using the activity coefficient[8] 0.87.

Discussion

Most previous work involving the substances studied here was carried out in solutions of high ionic strength (0.1–0.2); therefore, the data are not strictly comparable to those obtained in the present study. The present data are in good agreement with previous work where this was performed in solutions of low ionic strength. It is of interest that extrapolation of our pQ_2 values for ADP to $\mu = 0.2$ gives a value, 6.6, in good agreement with that obtained in other studies in which tetraalkylammonium rather than alkali metal ions were used. The pQ_2 value for ADP is considerably lower in the presence of Na^+ or K^+ due to complexing of these ions by the pyrophosphate group with resultant increased acidity of the phosphate proton.[10] RP and ADP have proton donor groups with pK values below 2. No pK data are available for these very acidic groups of RP, ADP or related compounds (AMP, ATP, etc.), nor could such data be obtained in the present study because of the high acidity in the pH region involved. It has been reported[11] that dissociation of a proton from the ribose group (pK approx 12.5) occurs with adenosine and related compounds, *e.g.*, guanosine, cyto-

(7) R. G. Bates, *Chimia*, **14**, 111 (1960).

(8) H. S. Harned and B. B. Owen, "The Physical Chemistry of Electrolytic Solutions," Reinhold Publ. Corp., New York, N. Y., 3rd Edition, 1958.

(9) R. M. Izatt, C. G. Haas, B. P. Block and W. C. Fernelius, *J. Phys. Chem.*, **58**, 1133 (1954).

(10) R. M. Smith and R. A. Alberty, *J. Am. Chem. Soc.*, **78**, 2376 (1956).

(11) "The Nucleic Acids," Vol. I, E. Chargaff and J. N. Davidson, editors, Academic Press, New York, N. Y., 1955, p. 156.

TABLE I

DISSOCIATION CONSTANTS OF SEVERAL RIBONUCLEOTIDES AND RELATED COMPOUNDS AT 25°

Previous work is given in parentheses.

Compound	$\sqrt{\mu_1} \times 10^2$	pQ_1 (N_1–H)	$\sqrt{\mu_2} \times 10^2$	pQ_2 (P–O–H)	$\sqrt{\mu_3} \times 10^2$	pQ_3 (N_6–H)
Adenine	2.48	4.21				
	3.51	4.16				
	4.96	4.15				
	7.00	4.14				
	7.90	4.10				
	11.2	4.09			14.0	9.66
	13.6	4.09			17.0	9.69
	15.8	4.07			19.8	9.88
		(4.1)[a]				(9.80)[b]
		(4.15)[b]				(9.75)[c]
		(4.12)[c]				
RP			6.32	6.60		
			8.92	6.50		
			9.96	6.60		
			14.0	6.34		
			17.2	6.31		
			19.8	6.46		
ADP	6.48	4.23	8.36	7.00		
	8.76	4.14	10.4	6.89		
	9.22	4.10	12.5	6.88		
	13.0	4.16	17.6	6.84		
	15.9	4.08	21.6	6.80		
	18.3	4.09	24.7	6.80		
		(3.95)[e]		(6.26)[e]		
		(3.99)[d]		(6.35)[d]		
		(3.9)[g]		(6.65)[e]		
				(6.68)[f]		
				(6.3)[g]		
Adenosine	11.3	3.52				
	13.8	3.51				
	15.9	3.47				
		(3.6)[a]				
		(3.63)[e]				
		(3.55)[d]				

[a] Results of A. G. Ogston, *J. Chem. Soc.*, 1713 (1936), μ not given. [b] Results of H. F. W. Taylor, *J. Chem. Soc.*, 765 (1948), μ = 0.001–0.007 *M*, no added salt. [c] Results of R. A. Alberty, R. M. Smith and R. M. Bock, *J. Biol. Chem.*, 193, 425 (1951), μ = 0.15 *M* NaCl. [d] Results of A. E. Martell and G. Schwarzenbach, *Helv. Chim. Acta*, 39, 653 (1956), μ = 0.1 *M* KCl. [e] Results of N. C. Melchior, *J. Biol. Chem.*, 208, 615 (1954), μ = 0.22 *M* $(C_2H_5)_4N^+$. [f] Results of Smith and Alberty, ref. 10, μ = 0.2 *M* $(n\text{-}C_3H_7)_4N^+$. [g] Results of R. M. Bock, *et al.*, *Arch. Biochem. Biophys.*, 62, 253 (1956), μ = 0.10 *M* NaCl.

sine and inosine. *p*H titration data in the present study indicate the probable dissociation of a proton with pK *ca.* 12 from RP, ADP and adenosine; however, glass electrode measurements in this *p*H region are quite unreliable. It would be of interest to study this dissociation further using methods capable of yielding quantitative results in this high *p*H region.

The increased acidities of adenosine and RP relative to that of adenine or $H_2PO_4^-$ (pK = 7.20) indicate that the ribose acts as an electron withdrawing group. It is interesting to note in this connection that pK_1 is the same in ADP as it is in adenine and pK_2 is appreciably larger in ADP than it is in RP. The increased pK_2 value probably is due to the increased negative charge on the ADP relative to that on RP. This is further substantiated by the increasing pK_2 values observed in the series adenosine mono-, di-, tri- and tetra-phosphate.[12]

(12) R. M. Smith and R. A. Alberty, *J. Phys. Chem.*, **60**, 180 (1956).

ULTRASONIC DETERMINATION OF REACTION RATES IN MAGNESIUM SULFATE AND MANGANOUS SULFATE SOLUTIONS

BY M. SURYANARAYANA

Department of Physics, Nizam College, Hyderabad, India

Received July 18, 1961

The rate constants of the dissociation of magnesium sulfate and manganous sulfate in aqueous solutions have been determined by ultrasonic methods by Bies[1] and by Kor and Verma,[2] respectively, using the theory of Bies (ref. 1). The theory of Bies, however, is based on the work of Manes[3] in liquids and is extended to include electrolyte solutions. Recently Tabuchi[4] has worked out a more detailed theory (applicable to electrolyte solutions also) and has shown that the work of Manes is only an approximation. Consequently, the rate constants obtained using the theory of Bies also will be approximate. Employing the same experimental data, the author has, therefore, determined the rate constants of the dissociation of magnesium and manganous sulfate in aqueous solutions with the help of Tabuchi's theory.

Because of absence of data Bies as well as Kor and Verma have taken the mean stoichiometric activity coefficients ($f_\pm\delta$) of zinc sulfate solutions recorded by Harned and Owen[5] as equivalent to the mean rational activity coefficients of magnesium and manganous sulfate solutions. The mean rational activity coefficient ($f_\pm$) and the degree of dissociation (δ) of these solutions are calculated by the author, without any reference to zinc sulfate solutions, by the usual method of successive approximations. Since dilute solutions are involved the author has used the approximate equation of Tabuchi's theory, namely, $\tau\omega_{max} = 1$. This approximation is justified by the earlier work by the author.[6]

Bies and Kor and Verma have found the rate constants to be invariant with concentration. However, employing the proper values of the activity coefficients and using either of the theories it is seen from Table I that the rate constants point to a decrease with increase of concentration. The decrease of k_b, the rate constant for the association of ions, with the increase of concentration and hence of ionic strength is in conformity with the theory as explained by Laidler.[7]

The molal volume changes, $(\Delta V)^2$, involved in these reactions are calculated for these solutions by using the formula given by Bies, where the concentration has to be expressed in moles per cc. The values obtained for magnesium and manganous

(1) D. Bies, *J. Chem. Phys.*, **23**, 428 (1955).
(2) S. K. Kor and G. S. Verma, *ibid.*, **29**, 9 (1958).
(3) M. Manes, *ibid.*, **21**, 428 (1953).
(4) D. Tabuchi, *ibid.*, **26**, 993 (1957).
(5) H. S. Harned and B. B. Owen, "Physical Chemistry of Electrolyte Solutions," Reinhold Publ. Corp., New York, N. Y., 1950, p. 190, 426.
(6) M. Krishnamurthi and M. Suryanarayana, *J. Phys. Soc. Japan*, **15**, 2318 (1960).
(7) K. Laidler, "Chemical Kinetics," McGraw-Hill Book Co., New York, N. Y., 1950, p. 132.

TABLE I

RATE CONSTANTS FOR IONIC DISSOCIATION IN AQUEOUS SOLUTIONS OF MAGNESIUM SULFATE AND MANGANOUS SULFATE (25°)

Salt	Concn. (mole/l.)	Degree of dissociation, δ	Mean rational activity coefficient $f_\pm$	Tabuchi's theory		Bies' theory	
				k_1, sec.$^{-1}$	k_b, l./mole-sec.	k_1, sec.$^{-1}$	k_b, l./mole-sec.
Magnesium sulfate	0.003	0.851	0.658	5.74×10^5	9.11×10^7	6.37×10^5	10.1×10^7
	.005	.809	.594	5.52	8.76	6.47	10.3
	.008	.776	.542	5.01	7.95	6.19	9.8
	.010	.760	.515	4.43	7.03	5.34	9.0
	.014	.734	.473	4.35	6.90	5.32	9.2
	.020	.707	.430	4.30	6.87	6.16	9.8
Manganous sulfate	.001	.902	.770	12.6×10^6	2.52×10^9	13.2×10^6	2.64×10^9
	.002	.851	.705	11.57	2.31	12.33	2.53
	.005	.779	.604	10.32	2.07	12.25	2.45
	.010	.717	.522	9.21	1.84	12.06	2.41
	.020	.662	.439	8.24	1.65	11.72	2.35

sulfate solutions are of the order of 7.7 and 120 (cc./mole)[2], respectively.

ON THE REACTIVITY OF HYDROGEN ATOMS IN AQUEOUS SOLUTIONS

BY JOSEPH RABANI

Department of Physical Chemistry, The Hebrew University, Jerusalem, Israel

Received July 19, 1961

Hart[1] measured the constants ratio k_1/k_2 for the reactions where HCO_2H denotes both formic acid

$$H + O_2 \longrightarrow HO_2 \qquad (1)$$

$$H + HCO_2H \longrightarrow H_2 + CO_2H \qquad (2)$$

and formate ion. Using various concentrations of formic acid and oxygen, it was shown that at low formic acid concentrations the ratio k_1/k_2 is about 500 at *p*H ~3. This value was used for the estimation of rate constants[2,3] at other *p*H values.

However, at the high formic acid concentration (1 *M*) this ratio is about 5000 (*p*H 1.7–1.8).[1] This discrepancy is due to the different reactivities of HCO_2H and HCO_2^- toward hydrogen atoms.[4]

Using various concentration ratios of formic acid and ferricyanide, the yield of the hydrogen produced by the action of X-rays was measured at the *p*H range of 1–3.[4] In this system, formate and ferricyanide compete for the hydrogen atoms according to reactions 2 and 3.

$$H + Fe(CN)_6^{3-} \longrightarrow H^+ + Fe(CN)_6^{4-} \qquad (3)$$

The ratio k_3/k_2 is *p*H dependent. At *p*H 1.3 this ratio is about 3500, falling to 800 at *p*H 2.05 and to 300 at *p*H 2.55. These results were obtained in solutions of constant (0.047 *M*) formic acid concentration, for direct comparison with Hart's experiments.

These results indicate that in the ferricyanide–formic acid system, only ferricyanide and formate ion (and not the undissociated acid itself) react with H atoms, at the *p*H range investigated. Reaction 2 has to be replaced by (2′).

$$H + HCO_2^- \longrightarrow H_2 + CO_2^- \qquad (2')$$

Kinetic evidence indicates that the oxidation of formic acid in solution by Cl_2,[5] permanganate,[6] some other inorganic ions[6] and SO_4^- radical[7] mainly proceeds by the oxidation of the formate ion.

The values of k_3/k_2' were found to be 12.5 at *p*H 1.3, 15.4 at *p*H 2.05 and 17.9 at *p*H 2.55. Thus, k_3/k_2' does not depend on the *p*H, within experimental errors, in agreement with the present interpretation.

In Table I, our results for the ferricyanide–formate system are compared with those for the oxygen–formate system.[1]

TABLE I

THE REACTIVITY OF H ATOMS IN FORMIC ACID SOLUTIONS

*p*H	k_1/k_2[1]	k_3/k_2[a]	k_1/k_3
1.71	3950	1700	2.3
1.83	5600	1300	4.3
2.32	1875	430	4.4
2.35	945	385	2.4
3.12	526	81	6.5

[a] Computed values.[4]

Taking into account the statistical weight of these data, a mean value of $k_1/k_3 = 5$ is obtained. Since k_3/k_2 is 3500 in 0.1 *N* H_2SO_4, it follows that $k_1/k_2 = 17{,}500$ at the same *p*H. Using the recent results of Riesz and Hart[3] for $k_{H+Fe^{3+}}$ (4.8×10^6 l. mole^{-1} sec.$^{-1}$) at *p*H 2.1, the following corrected values for the reactivity of H atoms are obtained (Table II). These "absolute" values are based on gaseous phase data. The numerical values in column 2 of this table represent relative rate constants with respect to O_2: k_{H+S}/k_{H+O_2} multiplied by 10^4.

The values taken from reference 4 were obtained from measurements of hydrogen yield in the ferricyanide–organic solute systems.

Much care should be taken in considering the reactivity of hydrogen atoms in aqueous irradiated

(1) E. J. Hart, *J. Am. Chem. Soc.*, **76**, 4312 (1954).

(2) J. H. Baxendale and D. H. Smithies, *Z. physik. Chem.* (Frankfurt), **7**, 242 (1956).

(3) P. Riesz and E. J. Hart, *J. Phys. Chem.*, **63**, 858 (1959).

(4) J. Rabani, Ph.D. Thesis, The Hebrew University, Jerusalem, Israel, 1961.

(5) J. Thamsen, *Acta Chem. Scand.*, **7**, 682 (1953).

(6) J. Halpern and S. M. Taylor, *Discussions Faraday Soc.*, 174 (1960).

(7) E. J. Hart, *J. Am. Chem. Soc.*, **83**, 567 (1961).

(8) W. G. Rothschild and A. O. Allen, *Radiation Research*, **8**, 101 (1958).

(9) J. H. Baxendale and G. Hughes, *Z. physik. Chem.* (Frankfurt), **14**, 306 (1958).

TABLE II

REACTIVITY OF H ATOMS

Substance	$k \times 10^{-8}$ (l. mole^{-1} sec.$^{-1}$)	pH of determination	Ref.
D_2	0.4	Gas	3
Fe^{3+}	48	2.1	3
Fe^{2+}	6.7	2.1	8
O_2	10000	2.1	8
$Fe(CN)_6^{3-}$	2000	1–3	4
HCO_3^-	130	1–3	4
HCO_2H	<0.57	0.1 N H_2SO_4	4
Cu^{2+}	32	.1 N H_2SO_4	2
C_2H_5OH	8.0	.1 N H_2SO_4	2
C_2H_5OH	8.8	.1 N H_2SO_4 and 3.05	4
DCO_2H (incl. DCO_2^-)	0.084	.1 N H_2SO_4	2
Glycerol	10	.1 N H_2SO_4	4
Glucose	20	.1 N H_2SO_4	4
Isopropyl alc.	26	.1 N H_2SO_4	4
HCHO	2.7	.1 N H_2SO_4	2
CH_3OH	0.85	.1 N H_2SO_4	2
Benzoquinone	1700	.1 N H_2SO_4	2
Benzoquinone	640	.1 N H_2SO_4	9

solutions, since H_2^+ and solvated electrons[10] also may take part in the radiation-induced specific reactions.

Hydrogen molecule ion probably is not involved in these reactions because of its relatively low rate of formation.[11] Specific reactions of solvated electrons were detected in systems containing relatively high concentrations of *electron scavengers* competing efficiently with electron capture by H^+ ions which leads to H atom formation.[10] In this case, the relative reactivities of the solutes competing for H atoms (or their precursors) will depend on the pH and on the scavenger concentrations. The rate constants ratio for the competition of ferricyanide and the formate anion[4] and of ferricyanide and ethanol for H atoms do not depend on pH in the region 1–3 and were found to be independent of the solute concentrations.

The systems containing inorganic ions, O_2 and benzoquinone, included in Table II were investigated at low scavenger concentrations, and no pH or concentration effects were detected which would indicate specific reactions of solvated electrons in these systems. In the solutions of organic compounds at low pH, the yield of molecular hydrogen is $G_H + G_{H_2}$[4,12] indicating complete dehydrogenation by atomic hydrogen as such. Thus these absolute rate constants obtained in acid solutions are due to elementary reactions of atomic hydrogen.

Acknowledgment.—The author wishes to thank Prof. G. Stein and Dr. J. Jortner for continuous encouragement and advice.

(10) J. T. Allan and G. Scholes, *Nature*, **187**, 218 (1960).

(11) G. Czapski, J. Jortner and G. Stein, *J. Phys. Chem.*, **63**, 1769 (1959).

(12) H. Fricke, E. J. Hart and H. P. Smith, *J. Chem. Phys.*, **6**, 229 (1938).

DECOMPOSITION PRESSURE OF UCd_{11}[1]

BY EWALD VELECKIS, HAROLD M. FEDER AND IRVING JOHNSON

Chemical Engineering Division, Argonne National Laboratory, 9700 S. Cass Avenue, Argonne, Illinois

Received July 19, 1961

The phase diagram of the uranium–cadmium system[2] shows only one intermediate phase, the compound UCd_{11}. The existence and formula of this compound were verified in the course of a study of the volatilization of cadmium from U–Cd alloys by means of a recording effusion balance. The pressure due to decomposition of UCd_{11} to cadmium vapor and α-uranium, measured in the course of that study and later, is the subject of this note.

The experimental arrangement of the recording effusion balance has been described elsewhere.[3] Cadmium was evaporated isothermally from approximately 250 mg. of powdered uranium–cadmium alloys contained in tantalum effusion cells until no further changes in sample weights were observed. The rates of vaporization in the heterogeneous region (U + UCd_{11}) were calculated from the weight loss *vs.* time records. Thirteen experiments were performed in the temperature range 305–378° with two effusion cells of different orifice areas. Decomposition pressures were calculated with the Knudsen equation and the assumption that the cadmium effusate was monatomic. Brewer[4] has estimated the heat of sublimation of Cd_2 to be 50.8 ± 1 kcal./mole. From this value and an estimate of the entropy of dimerization of cadmium, it can be shown that diatomic cadmium should be a minor constituent in the vapor.

The observed decomposition pressures of UCd_{11} are listed in column 3 of Table I. On the usual log P *vs.* $1/T$ plot three points (indicated in Table I) exhibited noticeable deviations from linearity and were discarded. These deviations probably are due to the occurrence of ratios of mean free path to orifice radius which are too small for exact conformance to the Knudsen equation. Similar departures from linearity have been observed for iodine[5a] and mercury[5b] when effusion pressure measurements are extended into the millimeter range.

TABLE I

DECOMPOSITION PRESSURE AND STANDARD FREE ENERGY OF FORMATION OF UCd_{11}

Effective orifice area, ka, cm.^{2}	Temp., °C.	P_{mm} (obsd.)	$-\Delta Ff^0$, cal./g.-atom
	378.1	0.448[a]	..
	367.8	.334	430
Cell B:	360.0	.247	494
1.718×10^{-3}	349.2	.172	533
	340.6	.122	574
	330.2	.0842	585
	320.4	.0570	630
	355.2	0.172[a]	..
	345.1	.127[a]	..
Cell C:	335.3	.0912	592
5.173×10^{-3}	324.9	.0626	604
	315.3	.0424	644
	304.9	.0273	693

[a] Measurements that show deviations from linearity.

(1) Work performed under the auspices of the U. S. Atomic Energy Commission.

(2) A. E. Martin, I. Johnson and H. M. Feder, *Trans. AIME*, **221**, 789 (1961).

(3) E. Veleckis, C. L. Rosen and H. M. Feder, *J. Phys. Chem.*, **65**, 2127 (1961).

(4) L. Brewer, Report No. UCRL-2854, University of California, Radiation Laboratory, Berkeley, Cal., 1955.

(5) (a) J. H. Stern and N. W. Gregory, *J. Phys. Chem.*, **61**, 1226 (1957); (b) K. D. Carlson, Ph.D. Thesis, University of Kansas, 1960.

The cell with the larger orifice (C) yielded observed decomposition pressures 9% lower than the cell with the smaller orifice (B). This behavior suggests that the evaporation coefficient, α, of cadmium from UCd_{11} is less than unity; the correction to zero orifice area has been made on this assumption. For the particular cell geometry involved the correction for low evaporation coefficient may be made by use of the relation[6] $P_{cor} = P_{obs}(1 + ka/\alpha A)$, where k is the Clausing short channel correction factor, a is the orifice area, and A the evaporating area of the condensed phase. The correction factors (P_{cor}/P_{obs}) for cells B and C were 1.051 and 1.154, respectively. The decomposition pressures, corrected as described, are shown in Fig. 1. The equation representing these data is

$$\log P_{mm} = 9.060 - 6105T^{-1} \quad (1)$$

The value of αA was estimated to be 0.0335 cm.^{2}. If the evaporating area is assumed to be the geometrical surface area of the sample (about 0.3 cm.^{2}), an evaporation coefficient for cadmium from UCd_{11} of about one-tenth may be inferred.

The standard free energy of formation per gram atom of UCd_{11}, *i.e.*, 1/12 of a mole, from solid α-uranium and liquid cadmium can be obtained from the relation $\Delta F_f^0 = x_{Cd} RT \ln (P/P^0)$, where x_{Cd} is the atom fraction of cadmium in the intermetallic compound (11/12), P the decomposition pressure of the alloy at temperature T, and P^0 the vapor pressure of pure liquid cadmium at the same temperature. For the latter we used the equation given by Kelley,[7] $\log P^0_{mm} = 11.655 - 1.086 \log T - 5706T^{-1}$. The free energies calculated from the corrected experimental data are listed in column 4 of Table I. These data may be represented by eq. 2

$$\Delta F_f^0 \text{ (cal./g.-atom)} = -2861 + 3.753T \ (\pm 14, \text{ std. dev.}) \quad (2)$$

The line representing eq. 1 intersects the vapor pressure curve for cadmium at 480°; this temperature corresponds to a hypothetical peritectic decomposition of the compound into pure uranium and cadmium. When a small correction for the solubility (2.5 wt. %) of uranium in liquid cadmium[2] is made the predicted peritectic temperature becomes 476°. Because of the long extrapolation (100°) of the effusion data, this value is in satisfactory agreement with the observed peritectic temperature,[2] 473°.

The standard free energy of formation of UCd_{11} also has been determined in a parallel e.m.f. study[8] at somewhat higher temperatures. The equivalent decomposition pressures are shown in Fig. 1. In the most unfavorable instance, the pressure calculated from the e.m.f. measurements is only 7% higher than our extrapolated value. This difference is within the combined expected experimental errors; however, the slope of the line through the e.m.f. data differs appreciably from the slope of the line through the pressure data. At 400° reliable estimates for the standard heat and entropy of formation of UCd_{11} are -2.48 ± 0.21 kcal./g.-atom and -3.38 ± 0.37 cal./deg. g.-atom.

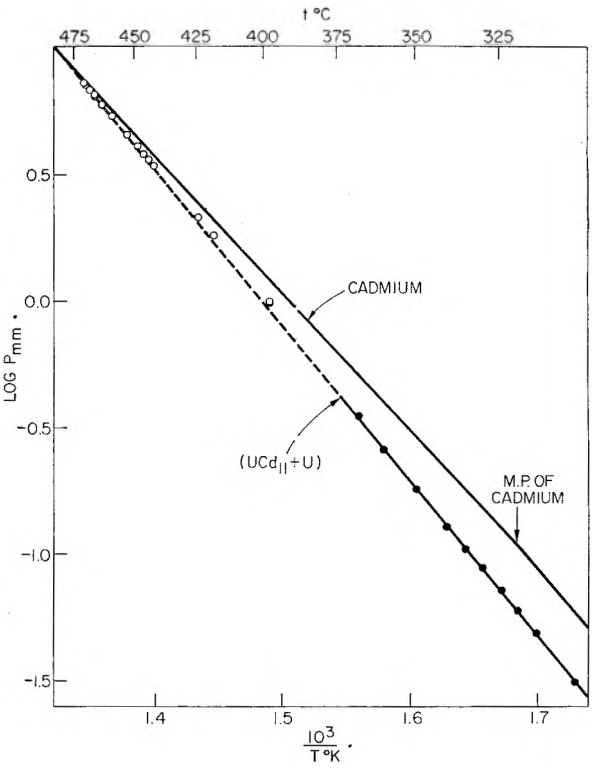

Fig. 1.—Decomposition pressure of UCd_{11}: ●, effusion measurements; ○, calcd. from e.m.f. measurements.[8]

We wish to thank Prof. T. F. Young for a helpful discussion.

(6) R. Speiser and H. L. Johnston, *Trans. Am. Soc. Metals*, **42**, 282 (1950).

(7) K. K. Kelley, "Contributions to the Data on Theoretical Metallurgy," U. S. Bureau of Mines, Bulletin 383, 1935, p. 28.

(8) I. Johnson and H. M. Feder, *Trans. AIME*, in press.

LIGHT SCATTERING STUDY OF SOLVENT EFFECT ON MICELLE FORMATION OF AEROSOL OT[1]

BY AYAO KITAHARA, TOKIKO KOBAYASHI AND TARO TACHIBANA[2]

Department of Chemistry, Toho University, Narashino, Chiba, Japan

Received July 25, 1961

It generally is recognized that a surface active substance shows characteristic properties such as micelle formation in an aqueous solution. It would be interesting in theory and practice to determine how these properties change in varying solvents. It is known that some surface active substances do form an inverted micelle in nonpolar solvents.[3] However, whether or not they would form micelles in polar organic solvents still is to be determined.

It was reported that copper laurate forms a large aggregate in toluene and a relatively smaller aggregate in isobutyl alcohol and pyridine.[4] Ralston, *et al.*, reported no micelle formation in alkylammonium chloride in methanol and ethanol with conductivity and solubility methods.[5] Kraus,

(1) Presented at the 14th Annual Meeting of the Chemical Society of Japan, Tokyo, April, 1961.

(2) Professor of Department of Chemistry, Ochanomizu University.

(3) C. R. Singleterry, *J. Am. Oil Chemists' Soc.*, **32**, 446 (1955).

(4) S. M. Nelson and R. C. Pink, *J. Chem. Soc.*, 1744 (1952).

(5) A. W. Ralston and C. W. Hoerr, *J. Am. Chem. Soc.*, **68**, 851 2460 (1946).

et al., showed no micelle formation of some octadecyl salts in nitrobenzene and dichloroethylene from conductivity data.[6] A conductivity method which is used for the determination of micelle formation is suitable for an aqueous solution of an ionic detergent, but inadequate for an electrolyte in non-aqueous solvents. A study by means of another method is desirable in order to examine the behavior of surface active substances in non-aqueous polar solvents.

A light scattering method is a relatively direct method of determining the particle weight, if suitable precaution is taken to remove dust from the solvent and solutions. The study of micelles by the light scattering method has been carried out in aqueous solutions since the original work of Debye,[7] but the method has been used in non-aqueous detergent systems in only a few instances.[8]

Di-(2-ethylhexyl) sodium sulfosuccinate (Aerosol OT), being soluble in various solvents, is suitable for a study of the effect of solvent on micelle formation. The particle weight of Aerosol OT in dodecane has been determined by means of an ultracentrifuge.[9]

In this paper the particle weight of Aerosol OT is determined by the light scattering method in various solvents, which differ in polarity, in order to study the solvent effect on the micelle formation, and to investigate whether or not micelle formation would take place in a polar organic solvent.

Experimental

Material.—Cyclohexane, benzene, ethanol, methanol and water were used as solvents. They were purified by the usual methods. Dehydration of cyclohexane and benzene was carried out with P_2O_5.

The Aerosol OT was a sample produced by Nippon Surfactant Co. which gave a purity of 96.6% by the Epton method, an acid value of 0.64, a saponification value of 247 (theoretical, 252), and an evaporation loss (water content) of 1.2% by vacuum drying. This vacuum-dried sample was designated as sample A. Portions of sample A then were purified according to one of the methods of Dixon, *et al.*[10] That is, it was dissolved in benzene, treated with activated carbon and filtered. The filtrate was freeze-dried. This sample was designated as sample B. Sample A gave a small quantity of cloudy precipitate on dissolving in methanol. The sample which was obtained by the evaporation of the filtrate of the methanol solution of sample A through a fine porosity glass filter was designated as sample C. The result of the analysis of sample C was: *Anal.* Calcd. for $C_{20}H_{37}O_7SNa$: C, 53.76; H, 8.82. Found: C, 54.17; H, 8.5.

Method and Apparatus.—Dust and other extraneous matter were excluded from a solvent through a fine porosity glass filter. Dissymmetry factors of the dust-free solvents were less than 1.01 in the cases of benzene and cyclohexane, less than 1.05 in methanol and ethanol, and less than 1.2 in water. A fine porosity glass filter also was used to remove dust in a stock solution. To test the effectiveness of this dust-removing procedure, the light scattering result for a solution of dodecylammonium benzoate clarified by a fine porosity glass filter was checked with that obtained using the stock solution clarified by a centrifuge (25,000 r.p.m., 30 minutes). The resulting particle weights, 5,000 through a fine porosity glass filter and 5,300 through a centrifuge, agree with that obtained by the vapor pressure depression[11] in the order of magnitude of the particle weight.

Each solution for which the scattered light was measured was prepared by adding a definite quantity of the stock solution into the cell containing the dust-free solvent through a pipet which was rinsed repeatedly with the dust-free solvent. It was suggested that the time dependence of micelle formation might affect the value of the particle weight.[12,13] Nevertheless, it seems that this effect need not be taken into consideration, because equilibrium of micelle formation must be established quickly in our method of preparing the solutions. The concentration of the stock solution was determined by evaporating the solvent.

The determination of the reduced scattering intensity (R_θ) and of the refractive index increment (dn/dc) were carried out by means of a Shimazu Photoelectric Light Scattering Instrument and a Differential Refractometer, respectively. The wave length was 436 mμ. All measurements were taken at room temperature (28 ± 4°).

Results and Discussion

Purity of Aerosol OT.—The measurement of surface tension of each aqueous solution of three samples A, B and C of Aerosol OT was carried out by a du Noüy tensiometer and a Traube stalagmometer in order to determine surface-chemical purity. Plots of surface tension against concentration appear in Fig. 1. A little difference was observable among the three samples. It is evident from Fig. 1 that sample C is the purest. The critical micelle concentration of Aerosol OT in an aqueous solution was found to be 2.4 mmoles/l. from the surface tension curve. This value is comparable to that obtained by Dixon, *et al.* (2.5 mmoles/l.).[10] Sample C was used throughout the following experiments.

Solvent Effect on Micelle Formation.—Since the values of the reduced scattering intensity at 90° (R_{90}) generally are low in these measurements, attention must be paid to their reproducibility. An example of the reproducibility appears in Fig. 2A for the ethanol solutions. It is seen from the figure that reproducibility in our measurement is satisfactory for this semi-quantitative examination of micelle formation. Some examples of plots of reduced intensities against concentration in benzene, cyclohexane, methanol and water are depicted in Fig. 2B for the benzene and cyclohexane solutions. The measurement in the aqueous solution was carried out in the absence of any inorganic salt. The correction for the micellar charge was neglected in the calculation of the particle weight.

If the intercept of the reduced intensity curve from the concentration axis is designated as C_0, it may be considered that formation of micelles or aggregates takes place at C_0. Therefore, it may be thought that C_0 should be a critical concentration for micelle formation (c.m.c.). The intercept was not sharply determined by the curve for an aqueous solution because of the bad reproducibility of reduced intensities at lower concentrations. The bad reproducibility probably is due to the slight occurrence of the hydrolysis of Aerosol OT in the aqueous solution. Tartar refers to the hydrolysis of sodium alkyl sulfate catalyzed by the ultrafine glass filter.[14] The C_0 value obtained by the surface tension method was used as C_c

(6) H. E. Weaver and C. A. Kraus, *J. Am. Chem. Soc.*, **70**, 1707 (1948); W. J. McDowell and C. A. Kraus, *ibid.*, **73**, 2173 (1951).

(7) P. Debye, *J. Phys. & Colloid Chem.*, **53**, 1 (1949).

(8) P. Debye and W. Prins, *J. Colloid Sci.*, **13**, 68 (1958); K. A. Allen, *J. Phys. Chem.*, **62**, 1119 (1958).

(9) M. B. Mathews and E. Hirschhorn, *J. Colloid Sci.*, **8**, 86 (1953).

(10) E. F. Williams, N. T. Woodberry and J. K. Dixon, *ibid.*, **12**, 452 (1957).

(11) A. Kitahara, *Bull. Chem. Soc. Japan*, **31**, 288 (1958).

(12) T. Nash, *J. Colloid Sci.*, **14**, 59 (1959).

(13) P. Becher and N. K. Clifton, *ibid.*, **14**, 519 (1959).

(14) H. V. Tartar, *ibid.*, **14**, 115 (1959).

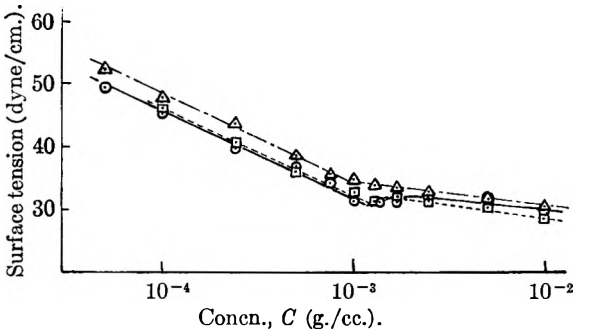

Fig. 1.—Plots of surface tension against concentration (logarithmic scale) of aqueous solutions of Aerosol OT: —⊙—, raw Aerosol OT dried; ---⊡---, Aerosol OT treated by charcoal; ---△---, Aerosol OT treated in methanol.

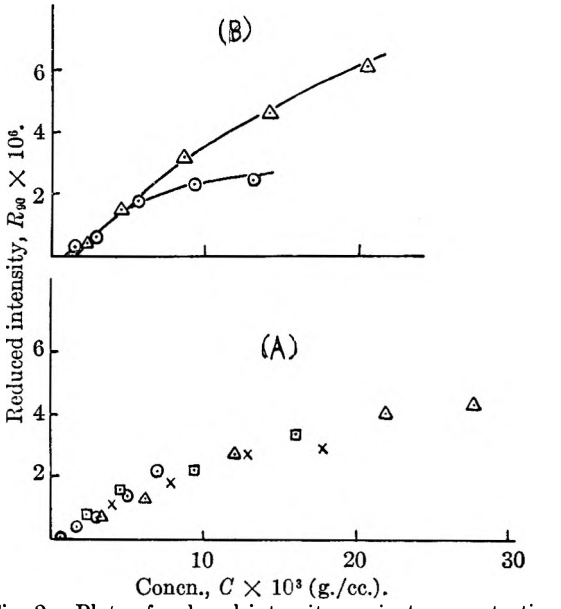

Fig. 2.—Plots of reduced intensity against concentration of Aerosol OT: A (bottom), in ethanol, each mark on the figure corresponds to each run; B (top), in cyclohexane (⊙) and benzene (△).

in the place of that obtained by the reduced intensity curve in the aqueous solution. Since the intercept on the abscissa was negligibly small in methanol and ethanol solutions, it was assumed that C'_0 was zero in both cases.

The particle weight (M) was determined by the use of the formula

$$K(C - C_0)/R_{90} = 1/M \cdot P(90) + 2B(C - C_0)$$

where K is the constant containing the refractive index increment, B the interaction constant, and $P(90)$ the particle scattering factor to correct for internal interference. Depolarization of the 90° scattering was small enough to be neglected. No appreciable dissymmetry was detected in the scattered light because of small particles in any case. Therefore, the calculation was carried out under the assumption that $P(90)$ was equal to unity.

Plots of $K(C - C_0)/R_{90}$ against $C - C_0$ gave the straight lines the above equation describes. The measured values of dn/dc and the particle weight obtained are shown in Table I. The table reveals that Aerosol OT forms a micelle in non-polar solvents such as cyclohexane and benzene, corresponding with the result in dodecane reported by Hirschhorn, *et al.*[9] It is considered that such a micelle is an inverted one due to the fact that water is solubilized in these non-polar solutions. On the other hand, the particle weight of Aerosol OT is too small to indicate micelle formation in ethanol and methanol. From the values of particle weights in Table I and with changing polarity of the solvent, this scheme is indicated

TABLE I

RESULTS OF LIGHT SCATTERING MEASUREMENTS ON AEROSOL OT SOLUTIONS

Solvent	dn/dc, cc./g.	$C_0 \times 10^2$, g./cc.	Particle weight	$K \times 10^6$
Cyclohexane	0.032	0.6	25,000 ± 4,000	1.9₅
Benzene	.052	1.2	10,500	4.9
Ethanol	.099	0.0	1,800 ± 700	16.6
Methanol	.124	0.0	750 ± 250	25.0
Water	.108	1.1	10,000	19.1

micellar dispersion ⟷ molecular dispersion ⟷ inverted micellar dispersion

(aqueous) ⟷ (polar) ⟷ (non-polar)

Acknowledgment.—The authors wish to express their sincere thanks to Dr. Akiyoshi Wada of Ochanomizu University for his helpful advice on the light scattering method. Thanks also are given to Nippon Surfactant Co. for providing the sample of Aerosol OT. The study in this paper was partly supported by grants from the Ministry of Education, to which the authors' thanks are due.

THE CHEMISORPTION OF NITRIC OXIDE BY ALUMINA GEL AT 0°[1]

BY AAGE SOLBAKKEN[2] AND LLOYD H. REYERSON

School of Chemistry, University of Minnesota, Minneapolis, Minnesota

Received August 3, 1961

In the earlier study, magnetic susceptibility measurements made during the sorption of NO on alumina gel[3] showed that slow chemisorption of the gas followed the first rapid physical adsorption. Rate studies indicated that the kinetics of this chemisorption gave a transmission coefficient of the order of magnitude of 10^{-8}. The authors suggested that this low transmission coefficient might be explained by the multiplicity change involved in such a reaction together with the low resonance energy of the system near or in the activated state. In the earlier work, when it became evident that the alumina gel chemisorbed the NO very slowly, no attempt was made to determine the final equilibrium for the chemisorbed state. The work here reported describes the results obtained by such an attempt.

Experimental

The alumina gel, prepared in the same manner as previously described, had a surface area of 287.3 m.²/g. as determined by the BET method The sorption system used in this work was essentially the same as previously reported,

(1) This investigation was supported by a grant from the National Science Foundation.

(2) Research Associate.

(3) A. Solbakken and L. H. Reyerson, *J. Phys. Chem.*, **64**, 1903 (1960).

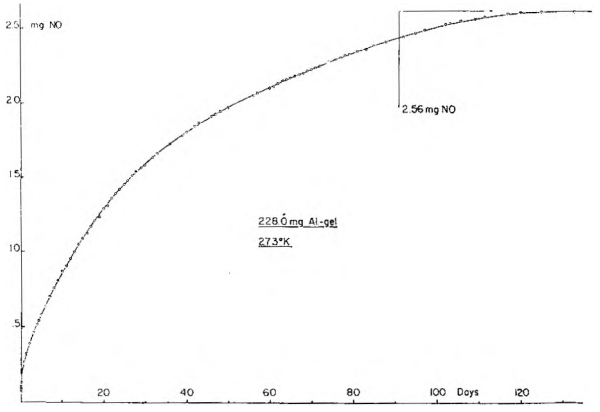

Fig. 1.—The chemisorption of NO by Al-gel *vs.* time.

except that it was not set up to obtain any magnetic data. The nitric oxide used came from the same source and was purified to the same degree as before.[4] Two hundred and twenty-eight mg. of alumina gel were weighed into the glass bucket which then was suspended from a calibrated sensitive quartz spiral balance. The sample was outgassed for days, up to a temperature of 300°, until a constant weight was reached at 10^{-6} m.m.p. The sample then was cooled to 0° for more than 24 hr. by surrounding this part of the sorption system with crushed ice in a large Dewar flask. This Dewar was kept filled with ice in water throughout the complete experiment. The system then was connected to a large enough flask containing gaseous NO at 40.1 mm. pressure so that the pressure change was negligible during the whole run. At the end of the experiment the NO was frozen and the color did not differ from that observed just prior to its use. The color of frozen NO is very sensitive to impurities such as other oxides of nitrogen or oxygen. The slow gain in weight of the sample due to chemisorption was determined at least twice a day during the four month period.

Results and Discussion

The chemisorption rate curve is shown in Fig. 1. One hundred twenty-eight days were required to reach equilibrium. The final chemisorbed NO amounted to 2.56 mg. on the 228-mg. sample of Al-gel. This is a value of 0.79×10^{14} molecules of NO per square centimeter of Al-gel surface. The curve is smoothly rounded indicating a change in the rate constant as chemisorption proceeds. In fact, calculations of the rate constant at different times during the experiment show a decrease in order from about 5 during the earlier part of the experiment to 1 in the later stages of the adsorption. The mechanisms assumed in the previous work were used in making the calculations. It is suggested that this change may be due to changes in the thermodynamic character of the complex, perhaps chiefly the entropy, on different sites or areas of the gel surface. Lateral interactions also may be involved as the surface becomes more highly covered.

Finally, since the chemisorption involves the uncoupling of a pair of electrons in the alumina gel followed by pairing with the odd electrons of two NO molecules, it seems possible that space limitations might well slow down the chemisorpt on process due to the fact that two physically adsorbed NO molecules should be adjacent to the site where the uncoupling of the pair of electrons in the alumina gel occurs. The magnetic data give no evidence for the existence of unpaired electrons in the alumina gel following pairing with one NO molecule.

As was pointed out earlier[3] the low transmission coefficient accounts for the slow chemisorption. The magnetic data showed that the NO lost its paramagnetism when it was chemisorbed, thus proving that its odd electron had paired with an electron on the alumina gel surface. Thus on one side of the activated state a doublet state exists while on the other side there is a singlet state. Between these two states the Hamiltonian takes a zero value. The only resonance energy is then spin–spin and spin–orbital interaction which at most will amount to only a few small calories of energy per mole. The cross-over point for the complex should be very sharp and statistically it seems quite probable that the reaction complex may jump to an upper surface where, as a doublet complex, it cannot exist because of its high energy. Splitting and desorption, as an unreacted molecule, then will occur. Such reasoning seems to explain the very low transmission coefficient for the reaction.

In conclusion, this study gives evidence for a true chemisorption process that is exceedingly slow. Earlier magnetic studies[3] elucidated the probable mechanism of such a sorption process.

(4) A. Solbakken and L. H. Reyerson, *J. Phys. Chem.*, **63**, 1622 (1959).

SHOCK TUBE STUDY OF HYDRAZINE DECOMPOSITION

BY WILLIAM H. MOBERLY

Rocketdyne, a Division of North American Aviation, Inc., Canoga Park, California

Received August 7, 1961

The homogeneous decomposition of hydrazine was studied in a shock tube using the single-pulse technique as described by Glick, Squire and Hertzberg.[1] This technique allows a sample of gas to be heated to a high temperature with a shock wave, held there for a few milliseconds, and then cooled rapidly with an expansion wave. Because of the short contact time, any reaction that occurs will be homogeneous.

Experimental

The shock tube used in this study was similar to that designed by the Cornell Aeronautical Laboratory.[2] The driven gas was a mixture of hydrazine and argon. A small amount of oxygen (0.11%) in the argon was removed by passing the argon through a heated stainless steel tube packed with copper. The hydrazine was obtained from the Olin Mathieson Corporation and was purified by distillation over barium oxide. The purity was greater than 99.5% with the principal impurity being water. The driver gas was a mixture of helium and nitrogen.

The velocity of the incident shock wave was measured with an optical system in which a collimated beam of light is reflected onto a photomultiplier tube connected to a microsecond timer upon passage of the shock wave. The first signal also triggers the sweep of an oscilloscope connected to an SLM pressure transducer located 2.5 in. from the end of the tube. The pressure–time trace was recorded with a Polaroid Land Camera.

The conditions behind the incident and reflected shock waves were calculated from the measured incident shock

(1) H. S. Glick, W. Squire and A. Hertzberg, "5th International Symposium on Combustion, New York," Reinhold Publ. Corp., New York, N. Y., 1955, pp. 393–402.

(2) H. S. Glick, J. J. Klein and W. Squire, *J. Chem. Phys.*, **27**, 850 (1957).

velocity using the usual conservation equations, the equation of state, and a knowledge of the enthalpy of hydrazine and argon as a function of temperature. The temperature rise due to reaction was not negligible in most runs and the calculated temperature was corrected for this effect.

Immediately after a run a solenoid valve at the end of the tube was opened for about a second and a sample withdrawn into an evacuated bulb. This sample was analyzed with a mass spectrometer. No driver gas was found in any of the samples. The amount of hydrazine decomposition was determined from the H_2/Ar ratio assuming the decomposition could be expressed by

$$2N_2H_4 \longrightarrow 2NH_3 + N_2 + H_2$$

This mode of homogeneous decomposition was found in flame studies.[3,4] At the low percentages used it was not possible to obtain a consistent N_2/H_2 ratio to check this assumption due to nitrogen background fluctuations.

Results and Discussion

The results of this study indicate that hydrazine decomposition follows the steady-state chain mechanism suggested by Adams and Stocks.[5] This mechanism is illustrated by the reactions

Initiation:

$$N_2H_4 \xrightarrow{k_1} 2NH_2 \quad (1) \qquad \Delta H = 60 \text{ kcal.}$$

Propagation:

$$N_2H_4 + NH_2 \xrightarrow{k_2} NH_3 + N_2H_3 \quad (2) \qquad \Delta H = -18 \text{ kcal.}$$

$$N_2H_3 \xrightarrow{k_3} N_2 + H_2 + H \quad (3) \qquad \Delta H = -8 \text{ kcal.}$$

$$H + N_2H_4 \xrightarrow{k_4} NH_3 + NH_2 \quad (4) \qquad \Delta H = -44 \text{ kcal.}$$

Termination:

$$H + N_2H_3 \xrightarrow{k_{5a}} N_2 + 2H_2 \quad (5a) \qquad \Delta H = -111 \text{ kcal.}$$

$$NH_2 + N_2H_3 \xrightarrow{k_{5b}} NH_3 + N_2 + H_2 \quad (5b) \qquad \Delta H = -112 \text{ kcal.}$$

$$H + NH_2 + X \xrightarrow{k_{5c}} NH_3 + X \quad (5c) \qquad \Delta H = -104 \text{ kcal.}$$

$$H + H + X \xrightarrow{k_{5d}} H_2 + X \quad (5d) \qquad \Delta H = -102 \text{ kcal.}$$

where X is a third body.

A steady-state concentration of each radical is assumed. Also the rate of disappearance of hydrazine by reactions 2 and 4 is assumed to be much greater than by reaction 1. With these assumptions, the rate expression for hydrazine decomposition can be expressed by one of four equations, depending on which termination step predominates. The four possibilities are

Step (5a)

$$-\frac{d(N_2H_4)}{dt} = 2\left(\frac{k_1k_3k_4}{k_{5a}}\right)^{1/2}(N_2H_4)$$

Step (5b)

$$-\frac{d(N_2H_4)}{dt} = 2\left(\frac{k_1k_2k_3}{k_{5b}}\right)^{1/2}(N_2H_4)$$

Step (5c)

$$-\frac{d(N_2H_4)}{dt} = 2\left(\frac{k_1k_2k_4}{k_{5c}}\right)^{1/2}\frac{(N_2H_4)^{3/2}}{(X)^{1/2}}$$

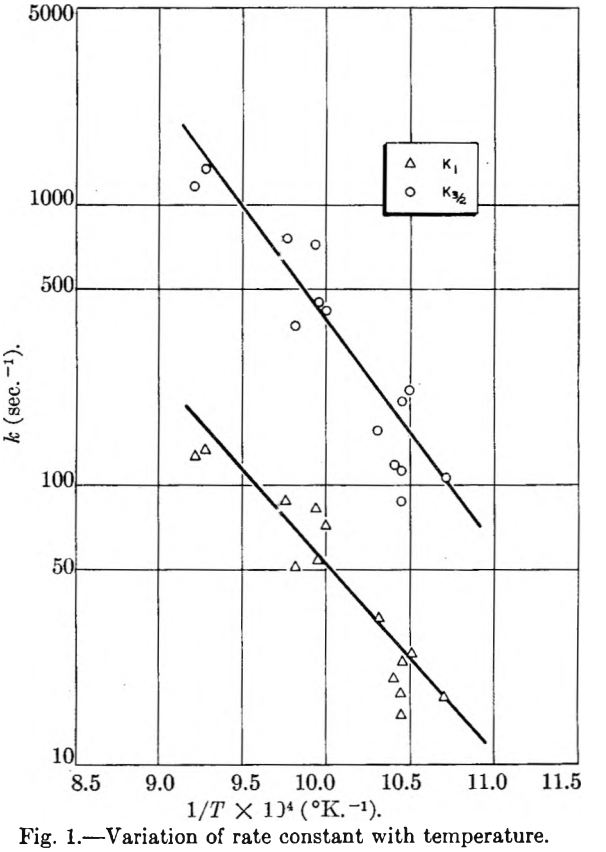

Fig. 1.—Variation of rate constant with temperature.

Step (5d)

$$-\frac{d(N_2H_4)}{dt} = 2\left(\frac{k_1k_4^2}{k_{5d}}\right)^{1/2}\frac{(N_2H_4)^{3/2}}{(X)^{1/2}}$$

These equations all assume the high pressure limit for k_1 and k_3 and are expected to be applicable in the present study. At low pressures k_1 and k_3 will have an implicit dependence on pressure and the rate will be a different function of total concentration. The assumed propagation steps are justified on energetic grounds and because they give the observed proportions of ammonia.

From the above equations it can be seen that only two different orders with respect to hydrazine and total gas concentration result from the four termination reactions. Since[6] $k_1 = 4 \times 10^{12}$ exp $(-60{,}000/RT)$ sec.$^{-1}$, it can be seen that the activation energy will be at least 30 kcal. in all cases with the exact value depending on the activation energies of k_2, k_3 and k_4. A value for k_4 of 10^{13} exp $(-7000/RT)$ cc./mole/sec. was estimated by Birse and Melville[7] from their study of the reaction between hydrogen atoms and hydrazine.

If pre-exponential factors of 10^{12} for k_2, k_3, k_{5a} and k_{5b} and 10^{16} for k_{5c} and k_{5d} are assumed, the pre-exponential factors for the over-all rate constants will be approximately 10^{13} and $10^{11.5}$ for the bimolecular and termolecular termination, respectively. These pre-exponential factors, of course, are very rough approximations and could be wrong by several orders of magnitude.

The shock tube data, shown in Table I, were fitted to both rate expressions and the pre-exponen-

(3) W. A. Rosser, Jr., J.P.L. Progress Report No. 20-305, Jan. 15, 1957.

(4) R. C. Murray and A. R. Hall, *Trans. Faraday Soc.*, **47**, 743 (1959).

(5) G. K. Adams and G. W. Stocks, "Fourth Symposium on Combustion," Williams and Wilkins, Baltimore, Md., 1953, pp. 239–248.

(6) M. Szwarc, *Proc. Roy. Soc.* (London), **A198**, 267 (1949).

(7) E. A. Birse and A. W. Melville, *ibid.*, **A175**, 164 (1940).

tial factors and activation energies determined by a least squares analysis of the plot of ln k *vs.* $1/T$ (Fig. 1). For bimolecular termination

$$k_1 = 10^{8.54} \exp(-31{,}400/RT) \text{ sec.}^{-1}$$

For termolecular termination

$$k_{3/2} = 10^{10.73} \exp(-37{,}500/RT) \text{ sec.}^{-1}$$

The subscripts refer to the order with respect to hydrazine. From the more reasonable pre-exponential factor for $k_{3/2}$, it is believed that a termolecular termination reaction predominates. This method of deciding the mechanism is admittedly very rough and can be taken only as a guess. Although the total pressure and hydrazine concentration were varied in this study, the scatter was too great to decide between the mechanisms from this variation. In any case the low experimental activation energy as compared to the energy required for the primary N–N bond rupture of hydrazine indicates a chain mechanism.

TABLE I

SHOCK TUBE DATA FOR HYDRAZINE DECOMPOSITION

Reaction temp., °K.	Reaction time, msec.	Initial N_2H_4 concn.,[a] g.-moles/cc. × 10^6	Final N_2H_4 concn., g.-moles/cc. × 10^6	Total concn., g.-moles/cc. × 10^4	k_1, sec.$^{-1}$	$k_{3/2}$, sec.$^{-1}$
935	5.7	2.16	1.95	0.72	17.9	105
952	6.0	1.96	1.69	1.36	25.0	214
957	6.0	2.07	1.80	1.36	23.4	198
958	6.0	2.34	2.14	0.70	15.0	86
958	6.0	1.96	1.76	.70	17.9	112
961	6.0	2.26	2.00	.70	20.4	117
969	5.1	1.60	1.35	.35	33.3	157
999	4.8	2.19	1.56	.62	71.1	413
1005	4.3	1.06	0.84	.62	54.6	446
1008	5.8	2.22	1.38	1.33	82.1	711
1019	5.2	0.77	0.59	0.34	51.4	367
1024	5.8	2.58	1.55	1.42	87.8	746
1077	6.0	2.04	0.91	1.30	134.5	1320
1085	5.6	2.18	1.08	1.28	125.5	1160

[a] Concentrations refer to conditions behind the reflected shock wave.

It is realized that more work needs to be done to define more precisely the decomposition mechanism. However, this investigation was one part of a larger program whose objectives were shifted after a six months' period. The new objectives did not include the homogeneous decomposition mechanism of hydrazine and therefore no further work is planned on this subject.

Acknowledgment.—This work was supported by Air Research and Development Command, U. S. Air Force. The author gratefully acknowledges many helpful discussions with Professor Harold S. Johnston.

A MOLECULAR ORBITAL STUDY OF THE EFFECT OF METHYL GROUPS ON IONIZATION POTENTIALS

BY A. STREITWIESER, JR.[1]

Department of Chemistry, University of California, Berkeley, California

Received August 8, 1961

Molecular orbital theory in its simplest form (Hückel Molecular Orbital or HMO method) has been shown to have only limited application to the calculation of ionization potentials of organic compounds.[2] The limitations are especially severe with hydrocarbon radicals and for methyl substituents. Although the simple theory is not suitable for the calculation of absolute ionization potentials, we have found that the change in potential caused by introduction of a methyl substituent can be represented satisfactorily with a particularly simple model of a methyl group. In this model, the methyl group itself is isolated from the π-system but its electron-donating effect is recognized by making the attached π-carbon more electropositive; *i.e.*, by assigning a negative h where h is defined by equation 1

$$\alpha_r = \alpha_0 + h\beta_0 \qquad (1)$$

In the simple HMO theory, the ionization potential is associated with the energy, ϵ_m, of the highest occupied molecular orbital. The effect of a change in α_r, $\delta\alpha_r$, on this energy is given to a first approximation by equation 3, in which the right-hand side is actually the first term of a power series.[3]

$$\epsilon_j = \alpha_0 + m_j\beta_0 \qquad (2)$$

$$\delta\epsilon_j = c^2_{jr}\,\delta\alpha_r = c^2_{jr}\,h\beta_0 \qquad (3)$$

According to this model for a methyl substituent, which has been called the "inductive model" and which has been used successfully in other molecular orbital applications,[2a,4] the change in ionization potential caused by methyl substitution at position r should be proportional to c^2_{mr}, the square of the coefficient of that position in the highest occupied MO.

The data available to test the relation are summarized in Table I. Because of the known differences between spectral and electron impact results, only data from the same method were used for parent and methyl-substituted systems. Furthermore, wherever possible, data from the same research group were used to determine the ionization potential differences. As shown in the table, these differences generally are reproducible and results from all three of the common methods, photoionization, ultraviolet spectra and electron impact, are represented.

Data for the *o*-xylyl radical are available but were not used because of the likelihood of an effect of steric hindrance. The perturbation of benzene to toluene requires comment because of the degeneracy of the two highest occupied orbitals in benzene. When the symmetry of the system is reduced to that for our model of toluene, one MO has a node through the methyl-substituted carbon and its energy is unaffected by the perturbation; the other MO has a node at right angles to the foregoing and its energy is *raised* by the per-

(1) Alfred P. Sloan Foundation Fellow.

(2) (a) A. Streitwieser, Jr., and P. M. Nair, *Tetrahedron*, **5**, 149 (1959); (b) A. Streitwieser, Jr., *J. Am. Chem. Soc.*, **82**, 4123 (1960); (c) earlier examples of such limitations are cited in W. C. Price, *Chem. Revs.*, **41**, 257 (1947), and R. S. Mulliken, *Phys. Rev.*, **74**, 736 (1948).

(3) C. A. Coulson and H. C. Longuet-Higgins, *Proc. Roy. Soc.* (London), **A191**, 39 (1947).

(4) For example, *cf.*, E. L. Mackor, G. D. Dallinga, H. J. Kruizing and A. Hofstra, *Rec. trav. chim.*, **75**, 836 (1956); E. L. Mackor, A. Hofstra and J. H. van der Waals, *Trans. Faraday Soc.*, **54**, 186 (1958).

TABLE I

EFFECT OF METHYL SUBSTITUENTS ON IONIZATION POTENTIALS

Parent system	I (e.v.)	Position of methyl substituent	I (e.v.) of methyl compd.	ΔI (e.v.)	Method[a]	c^2_{mr}[b]
Ethylene	10.516[c]	1	9.73[c]	0.786	PI	0.500
	10.80[d]		9.94[d]	.86	EI	
Butadiene	9.18[d]	1	8.68[e]	.50	EI	.362
	9.24[f]	2	9.08[f]	.16	EI	.138
	9.07[g]	2	8.86[g]	.21	UV	
	9.07[c]	2	8.845[c]	.225	PI	
Benzene	9.52[f]	1	9.23[f]	.29	EI	.333[h]
	9.52[i]		9.20[i]	.32	EI	
	9.24[j]		8.82[k]	.42	UV	
	9.245[c]		8.82[c]	.425	PI	
Naphthalene	8.12[c]	1	7.96[c]	.16	PI	.181
		2	7.95[c]	.17	PI	.069
Methyl	9.95[l]	1	8.78[m]	1.17	EI	1.000
Allyl	8.16[l]	1	7.71[n]	0.45	EI	0.500
		2	8.03[n]	.13	EI	.000
Benzyl	7.73[l]	2	7.65[o]	.08	EI	.000
		4	7.46[o]	.27	EI	.143

[a] PI = photoionization; EI = electron impact; UV = spectroscopic. [b] Values taken from C. A. Coulson and R. Daudel, "Dictionary of Values of Molecular Constants," Centre de Chimie Theorique de France, Paris, or from calculations by the author. [c] K. Watanabe, *J. Chem. Phys.*, 26, 542 (1957) and ASTIA Rept. No. AD 152 934. [d] J. Collin and F. P. Lossing, *J Am. Chem. Soc.*, 79, 5848 (1957). [e] J. Collin and F. P. Lossing, *ibid.*, 81, 2064 (1959). [f] J. D. Morrison and A. J. C. Nicholson, *J. Chem. Phys.*, 20, 1021 (1952). [g] W. C. Price and A. D. Walsh, *Proc. Roy. Soc.*, A174, 220 (1940). [h] See text. [i] I. Omura, K. Higasi and H. Baba, *Bull. Chem. Soc. Japan*, 29, 501 (1956); K. Higasi, I. Omura and H. Baba, *J. Chem. Phys.*, 24, 623 (1956). [j] W. C. Price and R. W. Wood, *ibid.*, 3, 439 (1935). [k] V. J. Hammond, W. C. Price, J. P. Teegan and A. D. Walsh, *Discussions Faraday Soc.*, 9, 53 (1950). [l] F. P. Lossing, K. U. Ingold and I. H. S. Henderson, *J. Chem. Phys.*, 22, 621 (1954). [m] J. B. Farmer and F. P. Lossing, *Can. J. Chem.*, 33, 861 (1955). [n] C. A. McDowell, F. P. Lossing, I. H. S. Henderson and J. B. Farmer, *ibid.*, 34, 345 (1956). [o] J. B. Farmer, F. P. Lossing, D. G. H. Marsden and C. A. McDowell, *J. Chem. Phys.*, 24, 52 (1956).

turbation. Hence, the latter MO is the one to be taken as the highest occupied MO and the appropriate coefficient is used accordingly.

A plot of the average value for ΔI *vs.* c_{mr}^2 gives a satisfactory straight line (Fig. 1). Only propylene and crotyl radical deviate seriously from the correlation line. α-Methylnaphthalene also deviates and, in particular, shows a smaller change than β-methylnaphthalene, contrary to prediction, but the photoionization potential of α-methylnaphthalene is somewhat doubtful.[5]

Some additional consequences of this treatment are interesting. The highest occupied MO of furan has a node through the oxygen; hence, this MO is the same as in butadiene. Substitution of a methyl group in the α-position causes a 0.50 v. decrease in I,[6] the same as that caused by methyl substitution in the 1-position of butadiene, in agreement with our predictions.

In odd alternant hydrocarbons, the charge density of a position also is given by c_{mr}; hence, according to the present treatment, the effect of a methyl substituent on the ionization potential

(5) K. Watanabe, *J. Chem. Phys.*, **26**, 542 (1957).
(6) K. Watanabe, ASTIA Rept. No. AD 152 934.

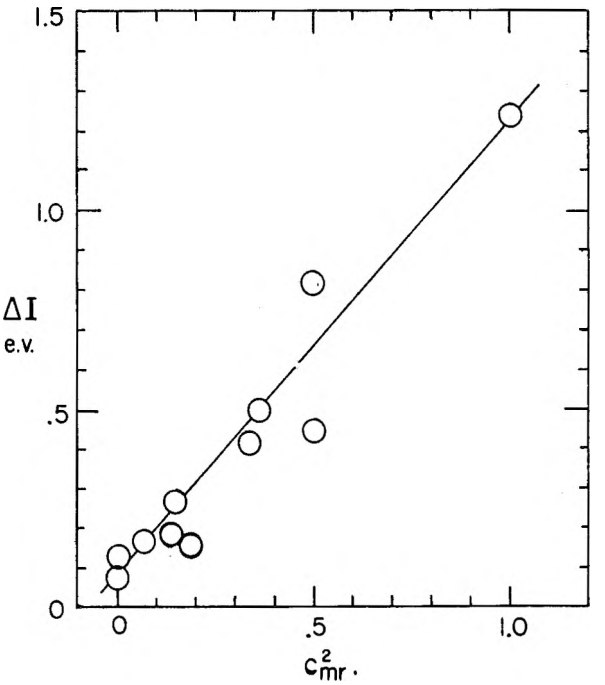

Fig. 1.—Effect on ionization potential of methyl substitution at position r compared with c^2_{mr}.

of the radical is a measure of the positive charge density at that position in the corresponding cation. The effect of methyl groups on the stability of benzylic cations intermediates in solvolytic reactions long has been associated with the charge distributions in such systems[7]; such application finds justification in the present treatment.

The slope of the correlation line, 1.2 e.v., is equal to $h\beta_0$. In a previous MO treatment of ionization potentials,[2a,b] β_0 was found to be -2.1 e.v. Use of this value for β_0 gives -0.54 for h; values of -0.3 to -0.5 have been used in previous applications with this model.[2a,4]

(7) C. G. Swain and W. P. Langsdorf, *J. Am. Chem. Soc.*, **73**, 2813 (1951); A. Streitwieser, Jr., *Chem. Revs.*, **56**, 647 (1956).

THE ACID DISSOCIATION OF γ-BUTYROLACTAM IN WATER AT 25°

BY RICHARD L. HANSEN

Central Research Dept., Minnesota Mining and Manufacturing Co., St. Paul, Minnesota

Received August 10, 1961

The conductometric method of Ballinger and Long[1] has been utilized for the determination of the acid dissociation constant of γ-butyrolactam. The equilibrium constant for the reaction $HA = H^+ + A^-$ is equal to the equilibrium constant, K_e, for $HA + OH^- = A^- + H_2O$ multiplied by the ion product of water whence eq. 1 results, where

$$K_eK_w = K_{HA} = (H^+)(A^-)f_{H^+}f_{A^-}/(HA)f_{HA} \quad (1)$$

the activity coefficients are referred to infinite dilution. At the concentrations of lactam required for this study it probably is not valid to assume that the activity coefficient ratio is unity even though

(1) P. Ballinger and F. A. Long, *J. Am. Chem. Soc.*, **81**, 1050, 2347 (1959); **82**, 795 (1960).

the activity coefficients of non-electrolytes are thought to remain close to one until comparatively high concentrations are reached.[2]

The electrical conductance of solutions of γ-butyrolactam in aqueous base may be treated by eq. 2 to yield K_e. In eq. 2

$$K_e = \alpha/(1 - \alpha)\ [(\text{lactam}) - \alpha(OH^-)] \qquad (2)$$

where

$$\alpha = \frac{R_0\lambda_c^{NaOH} - R_{(cor)}\,\lambda_c^{Na^+} - R_{(cor)}\,\lambda_c^{OH^-}}{R_{(cor)}(\lambda_c^{A^-} - \lambda_c^{OH^-})}$$

the concentrations refer to initial values. R_0 and λ_c^{NaOH} are the resistance and equivalent conductance of the aqueous base in the absence of lactam. $R_{(cor)}$ is the resistance of aqueous solutions of base plus lactam corrected for viscosity changes and the λ_c's are ionic conductances at the base concentration employed.

Experimental

The γ-butyrolactam was a product of General Aniline and Film Corp. and was fractionally distilled prior to use. The material had a b.p. of 138°(20 mm.) and $n^{21}D$ 1.4873. Vapor phase chromatography failed to detect any significant impurity content. A 5 *M* solution in water had a specific conductance of 2.4×10^{-6} ohm.$^{-1}$. The sodium hydroxide was prepared from a saturated aqueous solution and standardized against HCl. All of the water used was distilled, deionized and then bubbled for several days with carbon dioxide-free air. The material obtained in this way had a specific conductance less than 10^{-6} ohm.$^{-1}$.

A conductivity cell of the Washburn type[3] with very lightly platinized electrodes was used. The cell had a capacity of about 15 ml. The cell constant as determined with carefully prepared KCl solutions was 2.206 cm.$^{-1}$. An Industrial Instruments Model RC 16B2 conductivity bridge equipped with a 1 K.C. oscillator and a vacuum tube null point indicator was employed. A Cannon–Fenske viscometer was used to determine relative viscosities.

All measurements were made in a conventional water thermostat maintained at 25.0 ± 0.005° with a mercury-in-glass regulator and an electronic relay.

Preliminary experiments showed that the hydrolysis of the lactam at 25° would not complicate the study. That is, a solution 0.2 *M* in lactam and 0.1 *M* in sodium hydroxide underwent 6% hydrolysis in 24 hr. at 25°. Conductances of the solutions of lactam in dilute sodium hydroxide were measured not more than 15 min. after preparation. The conductance of these solutions became constant after about five min. in the thermostat and only after an hour or so did the conductance noticeably decrease indicating hydrolysis.

The experimental data required for the solution of eq. 2 were obtained by measuring the conductance of solutions containing 0.004348 *M* sodium hydroxide and varying amounts of the lactam. Part of the change in conductance observed when lactam was introduced was found to be due to the increased viscosity of the solution. Therefore, the effect of the lactam on the conductance and viscosity of 0.00400 *M* potassium chloride was measured and it then was assumed that the lactam would affect the conductance of sodium hydroxide in the same way.

The value $\lambda_c^{Na^+} = 47.9$ was employed based on the reported value for $\lambda_0^{Na^+}$ and the variation of the equivalent conductance of sodium chloride with concentration.[4] The equivalent conductance of sodium hydroxide, λ_c^{NaOH}, was calculated from the conductance of the 0.004 *M* sodium hydroxide containing no lactam and was found to be 231.7, which is 4% lower than the best literature value. This is due probably to slight, unavoidable contamination by CO_2. The difference between λ_c^{NaOH} and $\lambda_0^{Na^+}$ yielded $\lambda_c^{OH^-} = 183.8$. $\lambda_c^{A^-}$ was determined by choosing a series of values between 10 and 80 and plotting $1/K_e$ as a function of $\lambda_c^{A^-}$ at each lactam concentration. A family of straight lines was obtained which intersected at or near $\lambda_c^{A^+} = 41$.

(2) F. A. Long and W. F. McDevit, *Chem. Revs.*, **51**, 119 (1952).

(3) E. W. Washburn, *J. Am. Chem. Soc.*, **38**, 2431 (1916).

(4) All conductivity data were taken from H. S. Harned and B. B. Owen, "The Physical Chemistry of Electrolytic Solutions," 3rd Ed., Reinhold Publ. Corp., New York, N. Y., 1958.

Results and Discussion

The conductance and viscosity data as well as calculated values of K_e at each lactam concentration are given in Table I.

TABLE I

THE CONDUCTANCE OF 0.004348 *M* NaOH[5] AND THE VISCOSITY OF 0.00400 *M* KCl CONTAINING γ-BUTYROLACTAM AT 25°

(Lactam), *M*	R,[a] ohm × 10^{-3}	$\eta^{a,c}$ relative	R,[b] ohm × 10^{-3}	R^b(cor.), ohm × 10^{-3}	α	K_e
0.00	35.9	1.000	2.19	2.19		
.2			2.32	2.26	0.0503	0.265
.25	36.8	1.049				
.5	38.8	1.100	2.44	2.29	.0709	.153
1.0	41.2	1.211	2.75	2.41	.1481	.173
1.5			3.09	2.51	.2069	.174
2.0	48.1	1.479	3.50	2.62	.2663	.181
2.5			3.93	2.71	.3113	.180
3.0	56.0	1.820	4.53	2.89	.3930	.216
3.5			5.17	3.06	.4613	.245
4.0	65.9	2.254				

Av. $K_e = 0.198 \pm 0.032$

[a] Refers to 0.00400 *M* KCl. [b] Refers to 0.004348 *M* NaOH. [c] Corrected for density. Kinetic energy corrections were not applied since they change the relative viscosity by less than 0.1%.

The conductance of aqueous potassium chloride containing γ-butyrolactam is not a linear function of the viscosity of the solution. It is clear that simple multiplication of the observed conductance by the relative viscosity would considerably overcorrect for this effect.

Multiplication of K_e by 1.02×10^{-14}, the ion product of water at 25°, leads to $K_{HA} = 2 \pm 1 \times 10^{-15}$ mole/liter. Acid dissociation constants for this and other lactams do not appear to have been reported previously. However, acid dissociation constants of a number of amides and several alcohols have been determined in isopropyl alcohol.[6] Comparison of the constants obtained for methanol, ethanol and allyl alcohol in isopropyl alcohol with those obtained in water[1] indicates that the dissociation constants in water differ from those defined for isopropyl alcohol by a factor of about 10^{-16}. If this same factor is applied to the amide dissociation constants, values in the range 10^{-14} to 10^{-17} result. It is hoped that the effects of ring size and substituents on the acidity of other lactams can be made the subject of further study.

(5) Additional experiments were conducted with 0.001087 *M* NaOH. However, at this concentration CO_2 became a bigger problem and much scatter was observed. The average K_{HA} at this base concentration was 3×10^{-11}.

(6) J. Hine and M. Hine, *J. Am. Chem. Soc.*, **74**, 5266 (1952).

THE CRYSTAL STRUCTURE OF $NiZrH_3$

BY WILLIAM L. KORST

Atomics International, A Division of North American Aviation, Inc., Canoga Park, California

Received August 14, 1961

The interaction of the intermetallic compound NiZr with hydrogen has been investigated previously by Libowitz, Hayes and Gibb,[1] who reported a hydride phase with a composition ap-

proaching $NiZrH_3$. X-Ray diffraction powder patterns for the hydride and for NiZr itself were reported to be essentially similar, except that the lines for the hydride pattern were displaced toward smaller diffraction angles, indicating that the alloy and the hydride probably have similar structures, but that the hydride lattice is expanded over that of the alloy itself. The patterns were tentatively indexed on the basis of a "distorted cubic" lattice.

The crystal structure of NiZr since has been reported by Smith, Kirkpatrick, Bailey and Williams.[2] It is described as having an orthorhombic unit cell, with cell constants $a = 3.26$ Å., $b = 9.97$ Å. and $c = 4.08$ Å. More precise cell constants since have been reported by Larsen and Kirkpatrick[3] as follows: $a = 3.268$ Å., $b = 9.937$ Å. and $c = 4.101$ Å. The space group is given as Cmcm, with 4 Ni and 4 Zr located in the positions: (000; $^1/_2,^1/_2,0$) $\pm$ ($0,y,^1/_4$), with $y = 0.082$ for Ni and 0.361 for Zr. This structure is similar to that reported for CoTh,[4] and for ζ-BCr,[5] which has been designated the B_f structure type. The positional parameters given for NiZr indicate that the origin of the unit cell is shifted by an amount $(b+c)/2$ from that used in CoTh and ζ-BCr; if an adjustment is made to give NiZr the same origin the y-parameters of the Ni and Zr atoms become 0.418 and 0.139, respectively.

It is the purpose of this paper to present evidence showing that the crystal structure of the hydride, $NiZrH_3$, is an expanded version of that of the parent compound, NiZr. In so doing evidence also is presented confirming the crystal structure reported for NiZr.

Experimental

The compound NiZr was prepared from high-purity electrolytic nickel and crystal-bar zirconium. The nickel, in the form of spheres, was annealed at 1000° in a stream of hydrogen in an effort to remove dissolved oxygen. Suitably-sized pieces of zirconium were etched in a mixture of nitric and hydrofluoric acids. The two metals in the proper proportion to give a 1:1 atomic ratio were melted together under about one-half atmospheric pressure of argon in an arc-melter, using a water-cooled copper hearth and a tungsten electrode tip. Each sample was remelted several times.

Alloy buttons were cleaned with the etching solution described above, and cut into suitably-sized pieces for hydride preparations using a Carborundum wheel. Filings or fragments were removed for preparation of Debye–Scherrer photographs to make certain the compound had been obtained.

The hydride was prepared on a vacuum line, using hydrogen evolved from uranium hydride, with the amount of hydrogen absorption measured volumetrically. After an initial outgassing at temperatures as low as 450° while the system was being evacuated, some samples reacted with hydrogen at room temperature. In other preparations heating of the sample in the presence of hydrogen was necessary to initiate the reaction.

Two particular samples are of interest here, a hydride sample having a composition of $NiZrH_{2.7}$, which resulted from three cycles of heating the sample to 700° and cooling to room temperature in a hydrogen atmosphere, and a deuteride sample having a composition of $NiZrD_{2.93}$, which was prepared at temperatures below 150°. X-Ray data from these samples were used in the calculations described below.

Powdered alloy or hydride samples were placed in thin-walled Pyrex capillaries. X-Ray powder photographs were prepared using Ni-filtered Cu radiation (λ for Cu $K\alpha$ = 1.5418 A.). A 114.6 mm. diameter Straumanis-type camera was used, and corrections made for film shrinkage. Line intensities were estimated visually. Intensities from a diffractometer pattern were found to be of value in adjusting the parameters of the atomic positions in the hydride.

Results and Discussion

NiZr.—The positions and intensities of the lines in the powder pattern for NiZr have been calculated using the cell constants and the atomic parameters given above. Measurements of X-ray powder patterns give data which are in good agreement with the calculated data. The indexing of the lines in the observed powder patterns makes possible a recomputation of the cell constants, which has been carried out according to the method described by Mueller, Heaton and Miller,[6] using the Nelson–Riley correction function. In this computation seventeen unambiguously-indexed lines were used, corresponding to values of 2θ between 68 and 100°, approximately. The values of the cell constants arrived at as a result of this computation are: $a = 3.2581 \pm 0.0003$ Å., $b = 9.941 \pm 0.001$ Å., and $c = 4.0937 \pm 0.0005$ Å. The values given for the precision are the standard errors.[6] These cell constants agree fairly well with the values given by Larsen and Kirkpatrick.

Hydride Phase.—Powder patterns for the samples of the hydride phase were found to be similar to the pattern for the alloy, as had been reported previously. After a preliminary indexing of the pattern, the intensities of all possible diffraction maxima were calculated, using the expression

$$I = k|F|^2 p \left(\frac{1 + \cos^2 2\theta}{\sin^2\theta \cos\theta}\right)$$

where k is a proportionality constant, F is the structure factor of the individual reflection, p is the multiplicity and the term in parentheses is the Lorentz-polarization factor. The Ni and Zr atoms initially were assumed to have the same positions in the unit cell as reported for the alloy. However, several significant discrepancies between the observed and calculated intensities were found to exist, and the y-parameters of the atoms were adjusted to eliminate these discrepancies. Intensities obtained by diffractometer as well as by film methods were used in making these adjustments. The parameters which were found to give the best values of the calculated intensities are: $y_{Ni} = 0.431 \pm 0.003$, $y_{Zr} = 0.140 \pm 0.003$.

Cell constants for both the hydride and the deuteride phases were obtained by least-squares calculations, using twelve unambiguously-indexed lines up to a value of 2θ of approximately 84°. From a comparison of the calculated and observed $1/d^2$ values it is apparent that there is a slight systematic error, doubtless due primarily to absorption. However, the application of a systematic correc-

(1) G. G. Libowitz, H. F. Hayes and T. R. P. Gibb, Jr., *J. Phys. Chem.*, **62**, 76 (1958).

(2) J. F. Smith, M. E. Kirkpatrick, D. M. Bailey and D. E. Williams, U. S. Atomic Energy Comm. Report ISC-1050, March 1, 1959, pp. 55–58.

(3) W. L. Larsen and M. E. Kirkpatrick, U. S. Atomic Energy Comm. Report IS-193, Dec., 1960. p. 66.

(4) J. V. Florio, N. C. Baenziger and R. E. Rundle, *Acta Cryst.*, **9**, 367 (1956).

(5) Structure Reports for 1949. Utrecht: Oosthoek, Vol. 12, p. 30.

(6) M. H. Mueller, L. Heaton and K. T. Miller, *Acta Cryst.*, **13**, 828 (1960).

TABLE I

DIFFRACTION DATA FOR $NiZrH_3$

hkl	$1/d^2$ (calcd.)[a]	$1/d^2$ (obsd.)	I (obsd.)	I (calcd.)
020	0.0364	0.0376	vvw	8.8
110	.0895	...	..	<0.1
021	.0905	.0920	w	18.7
111	.1436	.1463	vvs	100.0
040	.1457			23.4
130	.1624	.1642	m	42.5
041	.1998	.2021	w	28.8
002	.2162	.2181	vs	34.6
131	.2165			61.4
022	.2526	...	..	1.1
112	.3057	...	..	<0.1
150	.3082	...	..	<0.1
200	.3216	.3231	m	17.6
060	.3280	...	..	<0.1
220	.3581	...	..	0.6
042	.3620	.3636	m-	11.1
151	.3623			3.3
132	.3786	.3810	s	21.1
061	.3821			12.9
221	.4122	.4118	vw	3.7
240	.4674	.4669	w	7.0
241	.5215			11.2
023	.5229	.5262	s	1.2
152	.5244			<0.1
170	.5269			14.1
202	.5378	.5364	m	14.1
062	.5442	...	..	<0.1
222	.5743	...	..	0.5
113	.5759	.5761	m	10.1
171	.5809	...	..	<0.1
080	.5831	...	..	<0.1
043	.6322	.6357	w	4.2
081	.6372			3.0
133	.6488	.6489	w	9.4
260	.6497	...	..	<0.1
242	.6836	.6848	w	7.4
261	.7037	.7032	w	7.6
310	.7328	...	..	<0.1
172	.7431	.7421	m	16.5

[a] Calcd. using least-squares cell constants before rounding-off: $a = 3.5264$, $b = 10.476$, $c = 4.3015$. [b] s = strong, m = moderate, w = weak, v = very.

tion function, such as is described above for the least-squares calculation of the cell constants of NiZr, was not feasible as there are only a half-dozen unambiguously-indexed lines above $2\theta = 60°$, the approximate lower limit of application of the Nelson–Riley function. The cell constants obtained are listed below. The errors given here are the estimated limits of accuracy.

	a, Å.	b, Å.	c, Å.
Hydride phase	3.53 ± 0.01	10.48 ± 0.02	4.30 ± 0.01
Deuteride phase	3.51 ± 0.01	10.44 ± 0.02	4.30 ± 0.01

Though the deuteride phase would be expected to have smaller cell constants than the hydride phase, the differences here probably are not too significant, since the hydride phase contained considerably less hydrogen than did the deuteride phase, and the cell constants no doubt vary with composition.

In Table I a comparison is made of the observed and calculated X-ray diffraction data for the hydride phase. The agreement between the observed and calculated lines appears to be sufficiently good to warrant the conclusion that the structure of the hydride is indeed an expanded version of that of the alloy.

It certainly would be of great interest to establish the location of the deuterium atoms in the deuteride phase by means of neutron diffraction. Certainly the large amount of hydrogen absorbed by NiZr is not something that would have been expected, since the zirconium hydride phase richest in hydrogen is ZrH_2, and nickel dissolves hydrogen to only a small extent, endothermically.[7] It is possible that spatial configuration plays a significant role in the formation of $NiZrH_3$. The alloy compound CoTh, which is isostructural with NiZr, has been found to absorb hydrogen to a maximum composition in excess of that indicated by the formula $CoThH_{4.2}$.[8] This is somewhat analogous to the NiZr reaction with hydrogen, since the thorium hydride phase richest in hydrogen has the composition $ThH_{3.75}$,[9] and the behavior of cobalt is much like that of nickel.[7]

Acknowledgment.—The hydride sample, $NiZrH_{2.7}$, was prepared by I. R. Tannenbaum, and one X-ray diffraction pattern of the alloy used was prepared by S. B. Austerman. This research was supported by the U. S. Atomic Energy Commission.

(7) D. P. Smith, "Hydrogen in Metals," University of Chicago Press, Chicago, Ill., 1948.
(8) W. L. Korst, unpublished work.
(9) W. H. Zachariasen, *Acta Cryst.*, 6, 393 (1953).

LOW ENERGY ELECTRON IRRADIATION OF METHANE[1,2]

BY RUSSELL R. WILLIAMS, JR.[3]

Haverford College, Haverford, Pa.

Received August 29, 1961

The yields of total condensable product from the low energy electron bombardment of methane have been reported previously.[4] The variation of the yield with electron energy was such as to indicate a large contribution from excitation (as opposed to ionization) as a primary process. The composition of the condensable products now has been examined as a function of electron energy and other conditions.

Experimental

Irradiation of gaseous methane with low energy electrons has been accomplished by the technique of internal electron acceleration as previously described,[4] except that an improved reaction chamber, shown in Fig. 1, has been used. As before, photoelectrons are ejected from the silver cathode by 2537 Å. light. These electrons then are accelerated in the gas by application of a d.c. potential between the cathode and the screen anode.

Samples of methane gas at 8–100 mm. pressure were irradiated at various applied voltages and the (electron

(1) Presented at the 139th National Meeting of the American Chemical Society, St. Louis, Mo., March 27, 1961.
(2) Work supported by the U. S. Atomic Energy Commission under Contract AT(30-1)-2357.
(3) Deceased.
(4) R. R. Williams, Jr., *J. Phys. Chem.*, 63, 776 (1959).

current) × (time) product measured. Condensable products were trapped at liquid nitrogen temperature and collected in a small volume for measurement and analysis.

The collected products (C_2 and higher) were analyzed by vapor chromatography using, in most instances, a column consisting of 2.4 m. of β,β'-oxydipropionitrile plus 3.0 m. of di-*n*-octyl phthalate. This column, operated at room temperature, could not distinguish between C_2H_6, C_2H_4 and C_2H_2, but other olefins were separated from the corresponding alkanes. In some experiments a 60-cm. column of activated silica gel was used, which permitted separation of C_2H_6, C_2H_4 and C_2H_2. In all cases the detection method was the argon ionization chamber, which permitted analysis of samples as small as one micromole total.

Results

A priori, the most interesting variable was considered to be the applied electron accelerating voltage, since this should determine the electron energy. Table I shows a selection of results in the irradiation of methane at 30 mm. pressure. These data show that there is practically no variation in product composition over the range 700–1300 v.

TABLE I

PRODUCT COMPOSITION IN ELECTRON IRRADIATION OF METHANE

CH_4 pressure = 30 mm.; temp. = 30°; H_2 not measured.

Run no.	M-29	M-18	M-20	M-28
Applied voltage	700	900	1100	1300
Product composition (%)				
C_2H_6	83.8	84.9	81.8	79.8
C_3H_8	13.0	12.9	15.0	16.6
i-C_4H_{10}	1.2	0.8	1.3	1.8
n-C_4H_{10}	1.2	.9	1.0	1.0
i-C_5H_{12}	0.4	.4	0.4	0.4
n-C_5H_{12}	0.3	< .1	<0.1	0.1

Several other variables also were explored. The pressure P of methane was varied from 8 to 100 mm. with corresponding changes in voltage V to keep V/P constant. At fixed voltage and pressure, the extent of decomposition was varied from 0.4 to 1.5%. The ultraviolet light was operated from an alternating current source, as well as from the usual direct current source, to test for any intermittency effect. None of these variations produced any significant change in the composition of the products.

In separate analyses, using the silica gel column, it was established that no significant amounts of ethylene or acetylene were produced in these experiments.

Discussion

The lack of significant variations in product composition with electron energy, as determined by the applied voltage, indicates that a single primary process probably is responsible for the whole spectrum of products observed. The ratio of secondary electrons (with accompanying positive ions) to primary photoelectrons varies from <0.3 at 700 volts to >10 at 1300 volts. This attests to the change in the electron energy distribution and in spite of the large change in positive ion population no corresponding change in product composition was observed. However, even at the highest voltages the excitation yield still may be large, around 9.0 molecules per electron, whereas the ion yield undoubtedly would be small, near 1.0 molecule per ion, and the contribution of ionic processes might go unobserved. Thus the present data probably give no information about ionic processes.

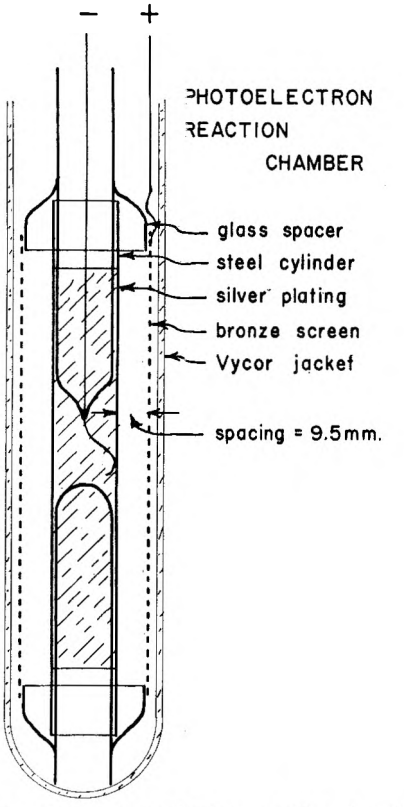

Fig. 1.—Low energy electron reaction chamber.

TABLE II

COMPARISON OF METHODS OF IRRADIATION OF METHANE

(Hydrogen omitted in all cases)

Method	2 Mev. e^-	4 Mev. e^-	X-rays in Ar	e^-
Ref.	5	6	7	This work
Product dist. (%)				
C_2H_6	91	73	81	80–84
C_3H_8	6	14	13	17–13
i-C_4H_{10}		2		1
n-C_4H_{10}	2	2	6	1
i-C_5H_{12}		1		0.4

It is interesting to compare the product spectrum obtained here with that observed in conventional radiolysis of methane. This has been done in Table II and it is seen that considerable correspondence is obtained. This suggests that the effect of high energy electrons may involve, in large part, the same primary process: namely, excitation rather than ionization. This also has been suggested by Mains and Newton[6] after a comparison of radiolysis with mercury-photosensitized photolysis of methane.

(5) F. Lampe, *J. Am. Chem. Soc.*, **79**, 1055 (1957).

(6) G. Mains and A. Newton, *J. Phys. Chem.*, **64**, 511 (1960).

(7) G. Meisels, W. H. Hamill and R. R. Williams, Jr., *ibid.*, **61**, 1458 (1957).

NON-IONIC SURFACE-ACTIVE COMPOUNDS. VI. DETERMINATION OF CRITICAL MICELLE CONCENTRATION BY A SPECTRAL DYE METHOD

By Paul Becher

Chemical Research Department, Atlas Chemical Industries, Inc., Wilmington, Del.

Received August 30, 1961

The convenient determination of the critical micelle concentrations of non-ionic surface-active agents long has been something of a problem. As recently as ten years ago Moilliet and Collie[1] could state, of the spectral dye method, "no suitable dyestuffs have as yet been found which show sufficient alteration in spectrum by non-ionogenic surface-active agents to render them suitable indicators."

More recently, Ross and Olivier[2] have shown that changes in the absorption spectrum of iodine in the presence of non-ionic agents were suitable for this purpose. The method of Ross and Olivier has the additional advantage of being usable in both aqueous and non-aqueous media. On the other hand, in aqueous systems, it is somewhat inconvenient, owing to the difficulty of preparation and poor stability of the aqueous iodine solutions. A substitute for this technique, for aqueous solutions at least, thus would appear to be desirable.

Some years ago Martin and Standing[3] reported that the presence of non-ionic surface-active agents caused a change in the absorption spectrum of the azo dye Benzopurpurin 4B. This effect was ascribed to the formation of a complex between the dye and the surface-active agent, but the possibility that the effect might be related to micelle formation was recognized. However, the measurements reported in this paper all were made at concentrations much higher than the critical micelle concentration.

In view of the possibility that this effect might be usable for the determination of the c.m.c., it was decided to re-examine these data at concentrations at which the effect of micelle formation could be determined.

Experimental

Benzopurpurin 4B of biological stain grade, manufactured by the National Aniline Division of Allied Chemical Corp., was used as received. The dye was made up as a 0.005% solution in distilled water. For the study of the effect of added surface-active agents, commercial non-ionic materials whose properties have been reported[4] previously were used at a range of concentrations less than 0.10 g./dl.

The measurement of the total visible absorption spectrum was done on a Beckman Model DK-2 spectrophotometer. Subsequent measurements were made on a Beckman Model B spectrophotometer at a wave length of 530 mμ, using a one-centimeter cell.

Discussion

Addition of a non-ionic surface-active agent to an aqueous solution of Benzopurpurin 4B causes the color to change from deep red to a reddish orange. However, examination of the total absorption spectrum in the visible shows that, although there is a change in the spectrum, it is too small to be suitable for a measure of critical micelle concentration. If, however, the spectrum of the solution of surface-active agent is determined using the aqueous dye solution as the reference liquid (rather than distilled water), this differential absorption spectrum shows marked differences as a function of the concentration of non-ionic, as indicated in Fig. 1, for polyoxyethylene (23) lauryl alcohol, at four different concentrations.

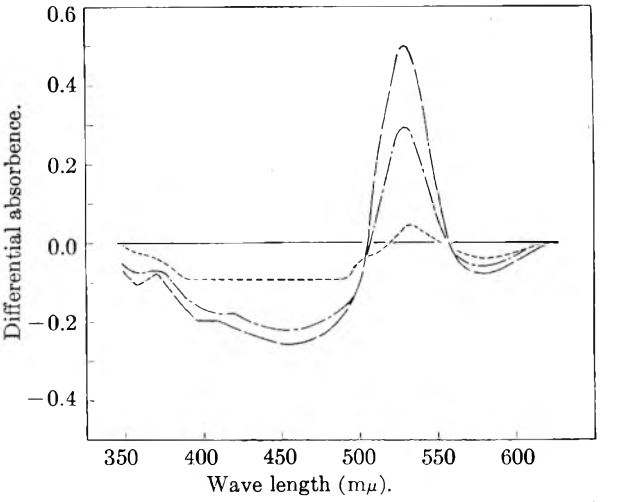

Fig. 1.—Differential absorbence of 0.005% solutions of benzopurpurin 4B containing various amounts of polyoxyethylene (23) lauryl alcohol: — — —, 0.10 g./dl.; - — - —, 0.04 g./dl.; - - - -, 0.01 g./dl.; ———, 0.002 g./dl.

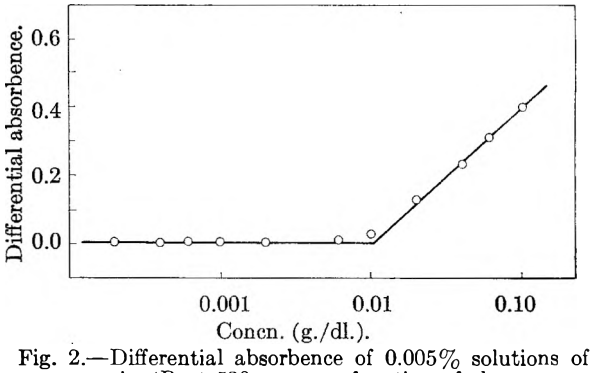

Fig. 2.—Differential absorbence of 0.005% solutions of benzopurpurin 4B at 530 mμ as a function of the concentration of polyoxyethylene (23) lauryl alcohol.

As can be seen, as little as 0.01 g./dl. of non-ionic causes a marked increase in absorbance at 530 mμ, and a somewhat less striking decrease in absorbance in the region of 460 mμ. At concentrations below about 0.002 g./dl., on the other hand, there is scarcely any difference in the absorption curves, and the resulting differential absorption curve is a straight line, parallel to the wave length axis, and at a differential absorbance of zero.

If one now plots the differential absorbance at 530 mμ as a function of the logarithm of the concentration, a curve of the form of Fig. 2 is obtained,

(1) J. L. Moilliet and B. Collie, "Surface Activity," D. Van Nostrand Co., Inc., New York, N. Y., 1951, p. 50.

(2) S. Ross and J. P. Olivier, *J. Phys. Chem.*, **63**, 1671 (1959).

(3) J. T. Martin and H. A. Standing, *J. Textile Inst.*, **40**, T689 (1949).

(4) P. Becher, *J. Phys. Chem.*, **63**, 1675 (1959); *J. Colloid Sci.*, **16**, 49 (1961).

with a pronounced break at the critical micelle concentration.

It is of interest to compare the results of measurements by this technique with others. The critical micelle concentration of polyoxyethylene (23) lauryl alcohol has been found to be 0.011 g./dl. by measurement of the break in the surface tension curve, by the iodine method, and by the present technique. Less perfect agreement has been found with a sample of polyoxyethylene (15) nonylphenol, whose c.m.c. was determined to be 0.0081 g./dl. by surface tension, 0.0077 g./dl. by the iodine method, and 0.0074 g./dl. by the present method. Since the mean square deviation of these latter results is 2.5% the agreement still may be regarded as quite satisfactory.

In view of the data on the lauryl alcohol derivative, and other results obtained in additional measurements, it is questionable whether any significance can be attached to the fact that the c.m.c. obtained for the nonylphenol derivative by methods involving interaction of another molecule with the micelle is lower than that obtained from the surface tension–concentration curve.

Acknowledgment.—The absorption spectra were obtained by Mr. Richard G. Smith, while the Model B determinations were carried out by Mrs. N. Goodyear. The author wishes to thank Mr. John Roll of Purdue University for calling his attention to the paper of Martin and Standing.

EFFECT OF MONOMERIC REAGENTS ON THE MELTING (CONTRACTION) AND RECRYSTALLIZATION OF FIBROUS PROTEINS

BY L. MANDELKERN, W. T. MEYER AND A. F. DIORIO

Polymer Structure Section, National Bureau of Standards, Washington 25, D. C.

Received August 30, 1961

The concomitant processes of contraction with melting and re-elongation with recrystallization now have been demonstrated for a variety of fibrous macromolecules including the fibrous proteins.[1–7] The dimensional changes that occur are manifestations of the same molecular phenomena observed during the so-called helix–coil transition in dilute solution[8,9] and are reflections of the conformational differences of the individual polymer molecules in the crystalline and amorphous states.[10,11] In the absence of an external stress, reversion to the original oriented crystalline state from the molten state requires the presence of intermolecular cross-links which were imposed in the oriented state and which survive the melting process.[2]

Contraction in the fibrous proteins can be brought about by a diversity of chemical reagents,[2,12] with the same basic molecular mechanism being involved. The equilibrium between the crystalline and liquid phases thus is governed by chemical processes, and the concept of melting being controlled by chemical reactions becomes apparent. The action of the various reagents could be purely physical and involve only a change in the solvent power of the supernatant phase. On the other hand, complexes could be formed which would be characterized by definite stoichiometric relations. In either case, the underlying principles involved in contraction will remain the same. In this context, for the process to be reversible in the absence of any external force, not only must appropriately introduced cross-links be present but the chemical reaction also must be reversed. Instances wherein these conditions are not fulfilled, though contraction has been demonstrated to occur as a consequence of melting, already have been indicated.[5–7] The effects of some of the more common reagents, whose aqueous solutions are known to induce contraction in the fibrous proteins, were investigated from this point of view.

Experimental

The reagents utilized, KCNS, $CaCl_2$, KI, LiBr and urea, were all of reagent grade. Elastoidin fibers were chosen as a model system for study because of their relatively low melting temperatures in pure water and their ease of procurement. Individual fibers were extracted from the dorsal fins of the dogfish (*Squalus acanthias*). Any adhering tissue was carefully removed, and the fibers were stored in distilled water at 4°. Fiber diameters were approximately 0.4 mm. Elastoidin fibers are structurally very similar to collagen and differ only slightly in amino acid content. Though they possess some intermolecular cross-links by virtue of their cystine content, additional cross-links were introduced by reaction with formaldehyde. This procedure raised the shrinkage temperature from 56–57° to 60–61° and allowed for reversible shrinkage and re-elongation, as has been previously reported by Champetier and Fauré-Fremet.[13,14]

The fibers were mounted in a tube containing a large excess of the aqueous solution, and the tube was inserted in a thermostat controlled to within 0.1°.[6] Small weights of approximately 50 mg. were fixed to the bottom of each specimen to prevent curling and to facilitate the length measurement. It can be shown that this load has no significant effect on either the melting temperature or subsequent recrystallization. Fiber lengths were approximately 30 mm. and were measured by means of a cathetometer accurate to 0.001 mm. The temperature of the bath was increased at the rate of approximately 1°/30 min. and the length was determined after the establishment of thermal equilibrium. Subsequent to melting, the length of the fiber was measured in the solution at 25°. The fiber then was transferred to a succession of tubes of pure water and the length redetermined at this temperature. Wide-angle X-ray diffraction patterns, utilizing methods and conditions previously described,[6] were obtained for the native fiber, the transformed (shrunken) fiber, and the fiber after cooling both in the solution and in pure water.

Results and Discussion

The length measurements, at a fixed composition

(1) J. F. M. Oth and P. J. Flory, *J. Am. Chem. Soc.*, **80**, 1297 (1958).

(2) L. Mandelkern, D. E. Roberts, A. F. Diorio and A. S. Posner, *ibid.*, **81**, 4148 (1959).

(3) P. J. Flory and R. R. Garrett, *ibid.*, **80**, 4836 (1958).

(4) P. J. Flory and O. K. Spurr, Jr., *ibid.*, **83**, 1308 (1961).

(5) L. Mandelkern, A. S. Posner, A. F. Diorio and K. Laki, *Proc. Natl. Acad. Sci. U. S.*, **45**, 814 (1959).

(6) L. Mandelkern, J. C. Halpin, A. F. Diorio and A. S. Posner, *J. Am. Chem. Soc.*, in press.

(7) L. Mandelkern, J. C. Halpin and A. F. Diorio, *J. Polymer Sci.*, in press.

(8) P. Doty, *Rev. Mod. Phys.*, **31**, 107 (1959).

(9) P. J. Flory, *J. Polymer Sci.*, **49**, 105 (1961).

(10) P. J. Flory, *Science*, **124**, 53 (1956).

(11) P. J. Flory, *J. Am. Chem. Soc.*, **78**, 5222 (1956).

(12) J. C. Kendrew in "The Proteins," Vol. II, P. B ed. by H. Neurath and K. Bailey, Academic Press, Inc., New York, N. Y., 1954, p. 862.

(13) E. Fauré-Fremet, *J. chim. phys.*, **34**, 126 (1937).

(14) G. Champetier and E. Fauré-Fremet, *ibid.*, **34**, 197 (1937).

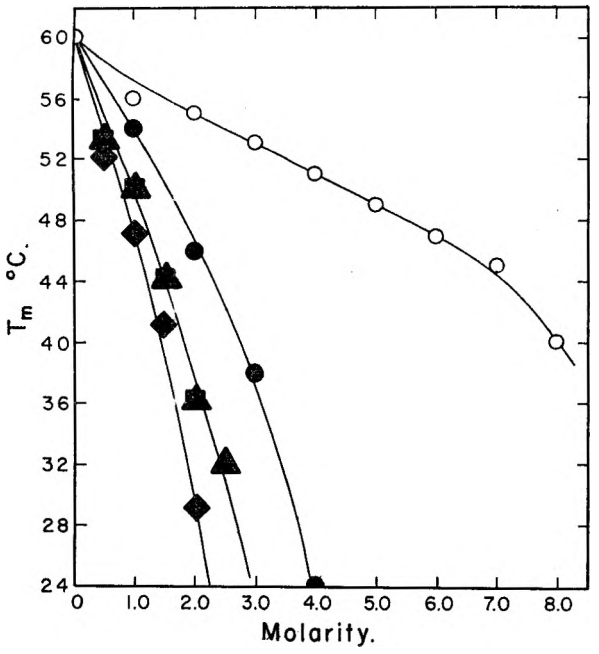

Fig. 1.—Plot of melting temperature T_m of elastoidin fibers against concentration of reagent in supernatant aqueous phase: ○, urea; ■, $CaCl_2$; ◆, KCNS; ▲, KI; ●, LiBr.

of the supernatant phase, displayed the characteristics of a first-order phase transition[2,10,11] in that a large axial contraction was observed over a narrow temperature interval. The shrinkage factor ranged from about 2.5 to 5, depending on the nature and composition of the surrounding medium. Wide-angle X-ray patterns demonstrated that the characteristic axially-ordered collagen-type crystal structure had disappeared, as only an amorphous halo is observed following contraction. The melting temperature was taken as the point at which the transition had terminated.

The melting temperature plotted as a function of the concentration of the various reagents is given in Fig. 1. Among the diverse reagents that induce melting, the effectiveness of the neutral salts appears to be quite similar. On a molar basis, however, the melting-point depression caused by urea is not nearly so great. Thus, for example, for a 3 M $CaCl_2$ solution the melting temperature is reduced to below room temperature; for the same concentration of urea only a 7° depression of T_m is observed. Though melting is in general caused by chemical reactions, distinctly different processes appear to be involved. For each series, the ratio of the shrunken length at the melting temperature to the initial length increases with increasing concentration of reagent added. This indicates that the swelling ratio in the amorphous phase is increasing with a necessarily concomitant decrease in the relative polymer concentration in this phase. A decrease in the isotropic melting temperature would be expected from this cause in addition to any specific effects of the chemical reaction.

The distinction in the chemical processes involved is further enhanced by consideration of the behavior of the specimens after cooling. Though increases in length are observed after cooling of the fiber in solution in all instances, it is not necessarily implied that recrystallization has occurred. X-Ray diffraction patterns indicate that only in solutions of 4–5 M urea or less does regeneration of the native crystalline structure occur in the solution at temperatures below the transformation temperature. In all other cases an amorphous X-ray pattern is obtained when the fiber is immersed in the transforming solution even at room temperature. The increase in length observed on cooling in these cases can be attributed to swelling of the molten polymer phase. However, if the fibers are transferred to pure water, an additional increase in length is observed and X-ray diffraction patterns indicate the regeneration of the native ordered structure. Hence, in the case of the neutral salts a cyclic process involving the melting and crystallization of the fiber can be established but it involves changing the composition of the supernatant phase after the transformation. A similar behavior has been reported for α-keratin and β-keratin fibers immersed in aqueous LiBr solutions.[6,7]

The action of urea in lowering the transformation temperature of both the fibrous and globular proteins has been treated from the point of view of binding theory.[15–17] The chemical potential of the structural repeating unit in the amorphous phase is lowered as a result of binding of urea to the peptide group, and consequently at fixed polymer composition the melting temperature T_m is reduced from that in the pure supernatant.[18] At this temperature, therefore, the free energy change representing that for fusion plus binding vanishes. Below this temperature, if the binding is less favored, the ordered state is more stable and recrystallization should ensue. This hypothesis is in accord with the results reported.

The results for the other reagents cannot be explained on this simple basis since reversion does not occur merely by cooling. The possibility exists that the conformational properties of the molten polypeptide chains have been altered as a consequence of the interaction with the neutral salts preventing the recrystallization of the native state.[6,7] The redevelopment of the native ordered state upon removal of the transforming reagent is indicative of the transitory nature of these alterations.

Though substantial additional evidence has been offered for the coupling of anisotropic dimensional changes in the fibrous proteins with the crystal–liquid equilibrium through utilization of a diversity of reagents, the chemical processes involved can be placed in distinctly different categories. Further detailed studies of the interactions of the peptide linkages with these reagents are required. It becomes important, however, to distinguish clearly between the basic molecular mechanism involved in contraction and the chemical reactions governing melting.

(15) J. A. Schellman, *Compt. rend. trav. lab. Carlsberg. Ser. Chim.*, **29**, 230 (1955).

(16) L. Peller, *J. Phys. Chem.*, **63**, 1199 (1959).

(17) A. Nakajima and H. A. Scheraga, *J. Am. Chem. Soc.*, **83**, 1575 (1961).

(18) P. J. Flory, *J. Cellular Comp. Physiol.*, **49**, Suppl. 1, 175 (1957).

MOLAR REFRACTIONS OF AQUEOUS SOLUTIONS OF SOME CONDENSED PHOSPHATES[1]

BY ROBERT C. BRASTED AND ARTHUR K. NELSON

The School of Chemistry, University of Minnesota, Minneapolis, Minnesota

Received September 11, 1961

It is well known that the molar refraction is an additive function of the atoms or groups of atoms within a molecule. Exact additivity is not always realized since the property also is constitutive. Since the condensed phosphates are formed by the sharing of oxygen atoms at the corners of PO_4 tetrahedra, the molar refraction of a condensed phosphate may be expected to be a function of the number and kind of PO_4 tetrahedra present. This study involves the determination of the apparent molar refractions of aqueous solutions of the crystalline condensed phosphates of sodium. These include the pyrophosphate $Na_4P_2O_7$, the tripolyphosphate $Na_5P_3O_{10}$, the trimetaphosphate $Na_3P_3O_9$, and the tetrametaphosphate $Na_4P_4O_{12}$.

Experimental

Compounds.—Samples of sodium tripolyphosphate, sodium trimetaphosphate and sodium tetrametaphosphate were obtained from the Victor Chemical Works and the Monsanto Chemical Company. These phosphates were purified by repeated recrystallization from water by methods essentially the same as those given in the literature.[2] In addition, anhydrous sodium pyrophosphate was prepared by ignition of reagent $Na_4P_2O_7 \cdot 10H_2O$ at 1000°.

Preparation of Solutions.—A series of several solutions of each phosphate was made up by weight from conductivity water using ground-glass stoppered bottles. All weighings were made with calibrated weights and tares and buoyancy corrections were applied using the density of air from the recorded temperature, barometric pressure and relative humidity for each weighing.

Density Measurements.—A modified Sprengel (bicapillary type) pycnometer with a capacity of approximately 10 ml. was used for all density measurements. Solutions to be measured were transferred to the pycnometer by means of suction and then held at 25.00 ± 0.02° for 20 to 30 min. The pycnometer then was removed from the constant-temperature bath, wiped dry and weighed after equilibration with the air in the balance. This process was repeated and the density obtained as an average of two or three fillings and weighings. Vacuum corrections were applied to all weighings.

Refractive Index Measurements.—The refractive index was determined for a separate portion of each solution using a Bausch and Lomb Dipping Refractometer. White light was used as a source. Measurements were taken in a trough designed for use with the instrument held at 25.00 ± 0.02° with a constant temperature circulating system purchased from Precision Scientific Company.

Results

Apparent molar refractions, R_{app}, were calculated using the equation given by Kohner[3]

$$R_{app} = \left(\frac{n^2 - 1}{n^2 + 2} \times \frac{1}{d}\right)\left(\frac{1000}{m} + M\right) - \left(\frac{n_0^2 - 1}{n_0^2 + 2} \times \frac{1}{d_0}\right)\left(\frac{1000}{m}\right)$$

where n and d refer to the solution and n_0 and d_0 refer to the solvent while m is the molality of the solute of molecular weight M. For the solvent, water, values of the refractive index n_0 and the density d_0 were defined as

$$n_0 = n^{25}D = 1.33252$$

$$d_0 = d^{25}_4 = 0.99708 \text{ g. ml.}^{-1}$$

The associated error in each value of R_{app} was estimated by means of the approximate equation of Kohner.[3] The results are listed in Table I.

TABLE I

APPARENT MOLAR REFRACTIONS OF AQUEOUS SOLUTIONS OF SODIUM PHOSPHATES

Phosphate	Molality	d^{25}_4	$n^{25}D$	R_{app}, ml. mole^{-1}
$Na_4P_2O_7$	0.21931	1.05125	1.34245	29.03 ± 0.11
	.16772	1.03895	1.34023	28.93 ± .14
	.10177	1.02286	1.33734	29.01 ± .24
	.048348	1.00959	1.33486	28.49 ± .50[a]
			Av.	29.0 ± 0.1
$Na_5P_3O_{10}$	0.31623	1.09585	1.34941	40.58 ± 0.08
	.26330	1.08007	1.34681	40.61 ± .09
	.17631	1.05366	1.34240	40.63 ± .14
	.10052	1.03005	1.33834	40.37 ± .24
	.040446	1.01067	1.33495	40.08 ± .60[a]
			Av.	40.6 ± 0.1
$Na_3P_3O_9$	0.46393	1.09594	1.34657	34.90 ± 0.04
	.37815	1.07876	1.34420	34.85 ± .06
	.26837	1.05609	1.34102	34.76 ± .09
	.15006	1.03078	1.33743	34.67 ± .16
	.091918	1.01786	1.33560	34.94 ± .26
			Av.	34.8 ± 0.1
$Na_4P_4O_{12}$	0.26576	1.07661	1.34442	46.31 ± 0.09
	.21940	1.06326	1.34248	46.35 ± .11
	.16071	1.04610	1.33997	46.43 ± .15
	.11458	1.03245	1.33793	46.35 ± .21
	.056595	1.01488	1.33528	46.23 ± .42[a]
			Av.	46.4 ± 0.1

[a] Values not used in computing average R_{app}.

From Table I it can be seen that the apparent molar refraction is constant within the limits of experimental error over the concentration range available. Any extrapolation to infinite dilution here would yield a straight-line relationship within experimental error. The average value can be considered equal to the value at infinite dilution. Certain values indicated by *a* in Table I were not used in computing the average because of unfavorable experimental error at higher dilutions.

At infinite dilution the molar refraction of an electrolyte may be considered as the sum of individual ionic refractions. The accepted value of R_{Na^+} at 25° and for the D-line of sodium is 0.200 ml. mole^{-1}.[4,5] Using this value and neglecting the possible existence of $NaP_3O_9^{-2}$ and $NaP_4O_{12}^{-3}$ the ionic refractions may be determined for each phosphate anion

Phosphate	R_{app}	Anion	R_{anion}
$Na_4P_2O_7$	29.0	$P_2O_7^{-4}$	28.2
$Na_5P_3O_{10}$	40.6	$P_3O_{10}^{-5}$	39.6
$Na_3P_3O_9$	34.8	$P_3O_9^{-3}$	34.2
$Na_4P_4O_{12}$	46.4	$P_4O_{12}^{-4}$	45.6

(1) Taken from the Ph.D. thesis of Arthur K. Nelson, 1959.

(2) (a) O. T. Quimby, *J. Phys. Chem.*, **58**, 603 (1954); (b) L. F. Audrieth, "Inorganic Syntheses," Vol. III, McGraw-Hill Book Co., New York, N. Y., 1950, p. 104.

(3) H. Kohner, *Z. physik. Chem.*, **B1**, 427 (1928).

(4) W. Geffcken, *ibid.*, **B5**, 81 (1929).

(5) R. Lubdemann, *ibid.*, **B29**, 133 (1935).

Discussion

The condensed phosphates are formed by the sharing of oxygen atoms at the corners of PO_4 tetrahedra. Since the two known ring phosphates, trimetaphosphate and tetrametaphosphate, contain only middle groups of PO_4 tetrahedra, the refraction due to a middle group may be calculated

$$R_{P_3O_9^{-3}} = 34.2;\ R_{middle} = \frac{34.2}{3} = 11.4$$

$$R_{P_4O_{12}^{-4}} = 45.6;\ R_{middle} = \frac{45.6}{4} = 11.4$$

The pyrophosphate and tripolyphosphate are the first two members of a family of chain phosphates. Pyrophosphate contains two end groups

$$R_{P_2O_7^{-4}} = 28.2;\ R_{end} = \frac{28.2}{2} = 14.1$$

Tripolyphosphate contains two end groups and one middle group. Hence, the expected ionic refraction of tripolyphosphate may be calculated

$$R_{P_3O_{10}^{-5}} = 2R_{end} + R_{middle} = 2 \times 14.1 + 11.4 = 39.6$$

This is exactly equal to the experimentally-determined ionic refraction.

The ionic refraction of condensed phosphate anions is an additive function of the number of end and middle groups present. This result further demonstrates the equivalence of middle groups in rings and chains. A nuclear magnetic resonance study of phosphorus compounds[6] also has shown this equivalence. An extension of the present work would involve the ionic refractions of the long-chain glassy phosphates.

An end group contributes more to the ionic refraction than a middle group. If the shared oxygen atoms are considered, an end group "owns" 3.5 oxygen atoms while a middle group "owns" 3 oxygen atoms. The environment of an end group obviously differs from that of a middle group. In the corresponding acids, middle group hydrogens are invariably strongly ionized while end group hydrogens are only weakly ionized.

Griffith[7] previously has reported values of R_{app} at 25° and for the D-line for these same condensed phosphates at two chosen concentrations, 50.0 and 100.0 g./l. The results of Griffith differ markedly from those quoted here. Griffith provides sufficient data for a recalculation of R_{app}. This was done for $Na_5P_3O_{10}$ at 100.0 g./l. and a value of 39.1 was obtained, compared with his reported value of 71.49 and the value 40.6 reported here as an average R_{app}. The value 71.49 apparently was obtained by the incorrect use of the equation

$$R_{app} = \left(\frac{n^2 - 1}{n^2 + 2}\right)\left(\frac{M_1 + W_0}{d}\right) - r_0W_0$$

where n and d refer to the solution, M_1 is the molecular weight of the solute, r_0 the specific refraction of water and w_0 the weight of solvent containing one mole of solute. The definition of W_0 according to Kohner is not that used by Griffith, who apparently substituted the weight of solvent taken rather than the weight of solvent containing one mole of solute. In order to obtain a value of 71.49 W_0 must be taken as approximately 101 g. Actually, using Griffith's data, 3,623.1 g. of water would contain one mole or 367.9 g. of $Na_5P_3O_{10}$.

The apparent molar refraction of a solute generally changes very little with concentration. Because R_{app} changes only slightly with concentration and because the accuracy in R_{app} is greatly decreased in very dilute solutions, apparent molar refractions have largely been obtained for concentrated solutions. Common practice has involved extrapolation of R_{app} values obtained at solute concentrations above 1 N to infinite dilution.[4,5] The limited solubilities of the crystalline sodium phosphates negate this procedure.

Hence, when considered in terms of R_{app}, the concentration interval used by Griffith is very small. Yet, many conclusions concerning polarizabilities of crystalline and glassy phosphates were drawn on the basis of the change in R_{app}, ΔR_{app}, observed. In this work, R_{app} has been shown to be practically constant in this concentration range. The conclusions of Griffith based on his calculations would seem to have no credence. In order to detect any change in R_{app} over this concentration interval, more precise measurements would be necessary.

Acknowledgment.—An academic-year fellowship extended to Arthur K. Nelson by the Dow Chemical Company is gratefully acknowledged.

(6) J. R. Van Wazer, C. F. Callis and J. N. Shoolery, *J. Am. Chem. Soc.*, **77**, 4945 (1955); J. R. Van Wazer, C. F. Callis, J. N. Shoolery and R. C. Jones, *ibid.*, **78**, 5715 (1956).

(7) E. J. Griffith, *ibid.*, **79**, 509 (1957).

COMMUNICATIONS TO THE EDITOR

RATIO OF SELF-DIFFUSION COEFFICIENTS IN LIQUID ARGON–KRYPTON MIXTURES[1]

Sir:

We have developed a statistical mechanical theory of diffusion in binary liquid solutions.[2] This theory predicts that the ratio of the self-diffusion coefficients of the two species should be in the inverse ratio of their molar volumes, providing that the intermolecular potentials are spherically symmetric and similar, the volumes are additive, and the sizes of the molecules are sufficiently close that radial distribution functions are independent of composition. Recently, Cini-Castagnoli and Ricci[3] have published self-diffusion data for argon and krypton in pure argon. Over a temperature range extending from 84–90°K., they found $D(\text{Ar–Ar}) = 61 \exp[-312/T] \times 10^{-5}$ cm.²/sec. and $D(\text{Kr–Ar}) = 52.5 \exp[-312/T] \times 10^{-5}$ cm.²/sec. with an estimated experimental error of about six per cent. Since krypton and argon are similar, these measurements should provide a test of our theory. In a paper otherwise devoted to molten salts, Lundén[4] has compared the results of the theory with those of the experiment and has concluded that the ratio of diffusion coefficients is more nearly equal to the inverse cube root of the ratio of volumes than to the inverse ratio itself. This latter result would be expected if predictions based on the simple Stokes–Einstein equation were correct. In order to test our theory, molar volumes in the liquid phase are required. Lundén[5] estimated these from ratios of atomic radii quoted from Pauling[6] in the "Handbook of Chemistry and Physics."[7] It is by no means obvious that these adequately represent the liquid state. We have decided therefore to analyze the available data more carefully. We shall evaluate the molar volume ratios from thermodynamic data in the liquid phase for comparison with our theory and also re-estimate the atomic radii for comparison with predictions from the Stokes–Einstein equation. Density data for liquid argon exist in the neighborhood of the temperatures utilized in the diffusion experiments.[8] Data exist[8] for krypton only in the temperature range 130–208°K. (the triple point[8] is at 116°K.), but these may be extrapolated (neglecting small compressibility effects) with an accuracy of about three per cent. if the curve continues to show no extrema or anomalous behavior. Thus we find at 90.0°K. the density of liquid argon is 1.37 g./cc. and of liquid krypton is 2.61 g./cc. The ratio of molar volumes v is virtually temperature independent over the range of temperatures of the diffusion experiments. Some uncertainty exists in the choice of atomic radii for use in testing predictions of the Stokes–Einstein equation. The values listed by Pauling[6] and used by Lundén[5] are the so-called "univalent radii." It appears that these are theoretical, although it is not entirely clear how they were obtained for the rare gases. Certainly, their significance is not clear in the present context. We therefore use instead estimates based on three kinds of data: (i) We use the atomic radius values r of 1.91 Å. for argon and 2.01 Å. for krypton obtained by Neuberger from empirical crystal structure data.[9] (ii) We use the diameters σ calculated from gas phase properties.[8,10] For argon all data appear to be consistent.[10] We select the value 3.41 Å. from Whalley and Schneider.[10b] For krypton the diameter depends on whether second virial data or gas phase transport data are used to calculate the Lennard–Jones 6–12 potential parameters.[10c] In the first case Whalley and Schneider find 3.68 Å. whereas in the second case Mason finds 3.50 Å. Since there appears to be no basis for choosing either of these arbitrarily, we shall simply average them and use 3.59 Å. in our calculations. (iii) For a third measure of the ratio of the radii we use the cube root of the ratio of the molar volumes in the liquid phase. In Table I we collect the results of the calculations. It appears that the inverse ratio of the molar volumes agrees with the ratio of diffusion coefficients within experimental error. The three reasonable estimates of the inverse ratio of the atomic radii are in substantial agreement and differ from the ratio of the diffusion coefficients by an amount which seems to be slightly beyond experimental error. We conclude that the data of Cini-Castagnoli and Ricci do provide a verification of our theory.[11]

TABLE I

D_{Ar}/D_{Kr}	v_{Kr}/v_{Ar}	r_{Kr}/r_{Ar}	σ_{Kr}/σ_{Ar}	$(v_{Kr}/v_{Ar})^{1/3}$
1.16	1.10	1.05	1.05	1.03

DEPARTMENT OF CHEMISTRY
UNIVERSITY OF KANSAS
LAWRENCE, KANSAS
RICHARD J. BEARMAN

RECEIVED DECEMBER 4, 1961

(1) This research was supported by a grant from the U. S. Air Force to the University of Kansas.

(2) (a) R. J. Bearman, *J. Chem. Phys.*, **32**, 1308 (1960); (b) *J. Phys. Chem.*, **65**, 1961 (1961).

(3) G. Cini-Castagnoli and F. P. Ricci, *Nuovo Cimento*, **15**, 795 (1960).

(4) A. Lundén, *Trans. Chalmers Univ. of Tech.*, No. 241 (1961).

(5) The author is indebted to Dr. Lundén for this information.

(6) L. Pauling, "The Nature of the Chemical Bond," Cornell University Press, Ithaca, N. Y., 3rd ed., 1960.

(7) Chem. Rubber Pub. Co., 41st ed., Cleveland, 1959.

(8) "Argon, Helium, and the Rare Gases," Vol. 1, Ed. G. A. Cook, Interscience Publishers, New York, N. Y., 1961, pp. 359–360.

(9) M. C. Neuberger, *Z. Krist.*, **93**, 1 (1936).

(10) (a) J. O. Hirschfelder, C. F. Curtiss and R. B. Bird, "Molecular Theory of Gases and Liquids," John Wiley and Sons, Inc., New York, N. Y., 1954, p. 22 and Appendix I-A; (b) E. Whalley and W. G. Schneider, *J. Chem. Phys.*, **23**, 1644 (1955); (c) E. A. Mason, *ibid.*, **32**, 1832 (1960).

(11) Our conclusion does rest upon the adoption of the estimate of experimental error provided by Cini Castagnoli and Ricci and our estimate of the error in extrapolating the density of krypton. A more pessimistic view of the errors still would lead to the conclusion that our theory fits the results at least as well as the proposed alternatives.

THE STABILITY OF SILICA

Sir:

Chipman[1] recently reviewed five lines of evidence that indicate that the presently accepted heat of formation of silica (−209.9 kcal./mole)[2] calculated from the heat of combustion of silicon in an oxygen bomb may be as much as 5 kcal./mole too positive. Still more recently, Good[3] measured the heat of formation of aqueous fluosilicic acid and calculated a value of −217.5 ± 0.5 kcal./mole for $\Delta H_f^0{}_{298}$ (*c*, quartz) which is 7.6 kcal./mole more negative than the literature value. Some recent effusion measurements that the authors have made of the reactions between gallium and quartz and gallium and magnesium oxide in an alumina cell[4] provide an independent basis for calculating this value.

The heats listed for reactions I and II in the table were obtained by third law treatment of the effusion results. These two heats are combined with other thermochemical data in the table to derive the heat of formation for crystalline quartz. (The heat for reaction I has been decreased by 0.3 kcal. to correct for the fact that vitreous quartz was employed in the effusion experiments whereas thermodynamic functions for crystalline quartz were used in deriving the former heat for reaction I from the effusion data. Values from JANAF Thermochemical Tables[5] were employed in making this correction.)

TABLE I

	Reaction	$\Delta H^0{}_{298}$
I	$2Ga(l) + SiO_2(vitreous) \rightleftarrows SiO(v) + Ga_2O(v)$	+170.8 ± 0.7
II	$2Ga(l) + MgO(c) \rightleftarrows Mg(v) + Ga_2O(v)$	+159.3 ± 0.7
III	$SiO_2(d, quartz) \rightleftarrows SiO_2$-(vitreous)	+0.54[6] ± 0.1[9]
IV	$\frac{1}{2}Si(c) + \frac{1}{2}SiO_2(c, tridymite) \rightleftarrows SiO(v)$	+82.98 ± 0.23[6,7]
V	$\frac{1}{2}SiO_2(c, quartz) \rightleftarrows \frac{1}{2}SiO_2$-(c, tridymite)	+0.25[8] ± 0.1[9]
VI	$Mg(c) + \frac{1}{2}O_2(v) \rightleftarrows MgO(c)$	−143.7 ± 0.3[5]
VII	$Mg(c) \rightleftarrows Mg(v)$	+35.38[5] ± 0.3[9]
VIII	= I − II + III − IV − V − VI + VII $\frac{1}{2}SiO_2(c, quartz) \rightleftarrows \frac{1}{2}Si(c) + \frac{1}{2}O_2(v)$	+107.9 ± 1.1
	$Si(c) + O_2(v) \rightleftarrows SiO_2(c, quartz)$	−215.8 ± 2.2

The heat of formation of silicon monoxide from tridymite and silicon in reaction IV was calculated from data given by Brewer and Edwards[6] in their analysis of the effusion data of Schäfer and Hörnle.[7] The heat of formation of silicon monoxide that is listed in most of the recent thermodynamic compilations could not be employed because it was derived using the heat of formation of silica that is in question.

The heats for reactions V, VI, and VII were taken in each case from the most recent thermodynamic compilations in which they appeared.

The derived value of −215.8 kcal./mole for $\Delta H_f^0{}_{298}$(c, quartz) indicates that quartz is about 6 kcal. more stable than previously thought, in good agreement with the values given by Chipman and Good.

ALUMINUM COMPANY OF AMERICA
ALCOA RESEARCH LABORATORIES
PHYSICAL CHEMISTRY DIVISION
NEW KENSINGTON, PENNSYLVANIA
C. N. COCHRAN
L. M. FOSTER

RECEIVED NOVEMBER 22, 1961

(1) J. Chipman, *J. Am. Chem. Soc.*, **83**, 1762 (1961).

(2) J. P. Coughlin, U. S. Bureau of Mines Bull. 542 (1954); G. L. Humphrey and E. G. King, *J. Am. Chem. Soc.*, **74**, 2041 (1952).

(3) W. D. Good, presented at the International Calorimetry Conference, Ottawa, Ontario, Canada, August 14–18, 1961.

(4) Accepted for publication in *J. Electrochem. Soc.*

(5) Joint Army-Navy-Air Force Interim Thermochemical Tables, Thermal Laboratory, Dow Chemical Co., Midland, Michigan.

(6) L. Brewer and R. K. Edwards, *J. Phys. Chem.*, **58**, 351 (1954).

(7) H. Schäfer and R. Hörnle, *Z. anorg. u. allgem. Chem.*, **263**, 261 (1950).

(8) J. P. Coughlin, U. S. Bureau of Mines Bull. 542 (1954).

(9) Estimated by the authors.

THE HEAT OF FORMATION OF SILICA[1]

Sir:

The free energy of formation of silica is a subject of current interest. Chipman[2] has discussed evidence that the free energy of formation of silica (in any of its various forms) is about 5 kcal. mole^{-1} more negative than the presently accepted value. Recent work in this Laboratory has shown that the thermochemical discrepancies noted by Chipman are the result of an error in the reported heat of formation data.[3] The earlier heat of formation value was based on measurements of the heat of combustion of silicon in an oxygen bomb. The value reported here was obtained by a different thermochemical process, which avoided uncertainties that are inherent in the earlier method.[3]

In the present experiments, the heat of formation of aqueous fluosilicic acid was determined in a rotating-bomb calorimeter. Mixtures of silicon and vinylidene fluoride polymer were burned in oxygen in the presence of aqueous HF, the product of combustion being fluosilicic acid in excess HF solution. Experimental procedures were similar to those already described.[4] A sample of high purity silicon (99.96% Si, 0.04% SiO_2; 50 to 75 micron particle size) was obtained through the courtesy of Dr. J. E. Kunzler, Bell Telephone Laboratories, Murray Hill, N. J. The combustion samples were prepared by mixing the silicon and powdered vinylidene fluoride polymer in sealed polyester bags, which then were rolled and pelleted. The samples burned completely, and all of the silicon was converted to aqueous fluosilicic acid.

The result for the heat of formation of fluosilicic acid and those for the heat of solution of silica in aqueous HF reported by King[5] permit calculation of the heat of formation of silica. The thermochemical equations are

$$Si(c) + O_2(g) + 47HF\cdot172H_2O(liq.) = H_2SiF_6\cdot41HF\cdot174H_2O(liq.) \quad \Delta H = -250.3 \pm 0.3 \quad (I)$$

(1) Presented at the International Calorimetry Conference, Ottawa, Ontario, Canada, August 14–18, 1961.

(2) J. Chipman, *J. Am. Chem. Soc.*, **83**, 1762 (1961).

(3) J. P. Coughlin, U. S. Bur. Mines Bull. 542 (1954); G. L. Humphrey and E. G. King, *J. Am. Chem. Soc.*, **74**, 2041 (1952).

(4) W. D. Good, D. R. Douslin, D. W. Scott, A. George, J. L. Lacina, J. P. Dawson and G. Waddington, *J. Phys. Chem.*, **63**, 1133 (1959); W. D. Good, D. W. Scott and G. Waddington, *ibid.*, **60**, 1080 (1956).

(5) E. G. King, *J. Am. Chem. Soc.*, **73**, 656 (1951).

$H_2SiF_6 \cdot 759HF \cdot 3378H_2O(liq.) = SiO_2(c, quartz) + 765HF \cdot 3376H_2O(liq.)$ $\Delta H = 32.3 \pm 0.1$ (II)

$H_2SiF_6 \cdot 41HF \cdot 174H_2O(liq.) + 718HF \cdot 3204H_2O(liq.) = H_2SiF_6 \cdot 759HF \cdot 3378H_2O(liq.)$ $\Delta H = 0.0 \pm 0.3$ (III)

$765HF \cdot 3376H_2O(liq.) = 718HF \cdot 3204H_2O(liq.) + 47HF \cdot 172H_2O(liq.)$ $\Delta H = 0.5 \pm 0.2$ (IV)

$Si(c) + O_2(g) = SiO_2(c, quartz)$ $\Delta H = -217.5 \pm 0.5$ (V)

The heats of reaction are expressed in kilocalories at 25°. Equation I gives the result of the measurements of this laboratory. Equation II gives the result of the heat of solution measurements of King,[5] extrapolated to 25° and corrected for the change in the atomic weight of silicon from 28.06 to 28.09. Equation III represents a dilution reaction studied in this Laboratory by a somewhat crude method already described.[6] The heat of eq. III was found to be very small and probably is thermally insignificant, but this result should be verified by more sensitive dilution calorimetry. The heat of dilution for eq. IV was computed from values in Circular 500.[7] Addition of eq. I, II, III and IV results in eq. V, the equation for the formation of quartz from the elements and the heat of formation.

The previously accepted value for the heat of formation of quartz[3] is -209.9 ± 1.0 kcal., about 8 kcal. mole^{-1} less negative than the present value. Thus, the free energy of formation of silica at 25° is about 8 kcal. mole^{-1} more negative than the earlier value,[3] in agreement with Chipman's conclusion.[2]

Full details of this investigation will be given in a paper in preparation. The results presented here are confirmed by those in the accompanying letters, which were determined by entirely different thermochemical methods.

CONTRIBUTION NO. 112 FROM THE
THERMODYNAMICS LABORATORY
BARTLESVILLE PETROLEUM RESEARCH CENTER W. D. GOOD
BUREAU OF MINES, U. S. DEPARTMENT OF
INTERIOR, BARTLESVILLE, OKLAHOMA

RECEIVED DECEMBER 2, 1961

(6) W. D. Good, D. W. Scott, J. L. Lacina and J. P. McCullough, *J. Phys. Chem.*, **63**, 1139 (1959).

(7) F. D. Rossini, D. D. Wagman, W. H. Evans, S. Levine and I. Jaffe, "Selected Values of Chemical Thermodynamic Properties," Natl. Bur. Standards Circular 500 (1952).

THE HEAT OF FORMATION OF SILICA AND SILICON TETRAFLUORIDE[1,2]

Sir:

Chipman[3] has presented evidence, based on a number of observed equilibria, that the standard free energy of formation of silica is about 5 kcal. mole^{-1} more negative than the currently accepted value.[4] Unless all the observed equilibria coincidentally err in the same sense and amount, Chipman's observation implies either that the standard heat of formation of quartz at 25° is about 5 kcal. mole^{-1} more negative than the currently accepted value[4] of -209.9 ± 1.0 kcal. mole^{-1} or that the accepted entropies of crystalline silicon or quartz at 25° are in error by absurdly large amounts. In a paper which apparently has gone unnoticed in this country, a Russian thermochemist, Golutvin,[5] has presented evidence that Humphrey and King[4] erred in their analytical determination of the quantity of unburned silicon remaining after oxygen-bomb combustions, and that the true value of the standard heat of formation of silica lies between -215 and -219 kcal. mole^{-1}. To resolve this problem we sought the simplest combination of reactions that would yield an unequivocal value for the heat of formation of silica. The method we chose is based on fluorine-bomb calorimetry[6]; it consists of combining the thermochemical equations

$$Si(c) + 2F_2(g) = SiF_4(g); \qquad \Delta H_1 \quad (1)$$

and

$$SiO_2(\alpha,c) + 2F_2(g) - SiF_4(g) + O_2; \quad \Delta H_2 \quad (2)$$

to give

$$Si(c) + O_2(g) = SiO_2(\alpha,c); \qquad \Delta Hf = \Delta H_1 - \Delta H_2 \quad (3)$$

For the measurement of ΔH_1 and ΔH_2 weighed amounts of crushed crystals of the high purity materials, silicon or alpha quartz, were mixed with a small known amount of powdered silicon and placed on a nickel support dish. On exposure to four atmospheres of fluorine in a two-chamber nickel bomb and tank system (described elsewhere[7]), the powdered silicon ignited spontaneously and fired the entire sample. Because the products of combustion were solely the gases indicated in (1) and (2), the extent of the reactions was determined by weighing the residues. ΔH_1 and ΔH_2, at 25°, were found to be -386.02 ± 0.24[8] and -168.27 ± 0.24 kcal. mole^{-1}, respectively. Hence, for α-quartz $\Delta Hf^0_{298.15} = -217.75 \pm 0.34$ kcal. mole^{-1}. The agreement between this determination and that of Good[9] (preceding communication) is excellent; the conclusions of Chipman[3] and Golutvin[5] are substantiated.

Full details of this investigation and of its extension to other forms of silica will be presented later.

UNIVERSITY OF WISCONSIN S. S. WISE
MADISON, WISCONSIN J. L. MARGRAVE
ARGONNE NATIONAL LABORATORY H. M. FEDER
ARGONNE, ILLINOIS W. N. HUBBARD

RECEIVED DECEMBER 2, 1961

(1) This work was performed under the auspices of the U. S. Atomic Energy Commission.

(2) Abstracted from a thesis submitted by S. S. Wise to the faculty of the University of Wisconsin in partial fulfillment of the requirements for the Ph.D. degree.

(3) J. Chipman, *J. Am. Chem. Soc.*, **83**, 1762 (1961).

(4) J. P. Coughlin, U. S. Bur. Mines Bull. 542 (1954), based on the work of G. L. Humphrey and E. G. King, *J. Am. Chem. Soc.*, **74**, 2041 (1952).

(5) Yu. M. Golutvin, *Zhur. Fiz. Khim.*, **30**, 2251 (1956).

(6) Previous papers dealing with this subject are (a) E. Greenberg, J. L. Settle, H. M. Feder and W. N. Hubbard, *J. Phys. Chem.*, **65**, 1168 (1961); (b) J. L. Settle, H. M. Feder and W. N. Hubbard, *ibid.*, **65**, 1337 (1961); (c) S. S. Wise, J. L. Margrave, H. M. Feder and W. N. Hubbard, *ibid.*, **65**, 2157 (1961).

(7) R. L. Nuttall, S. S. Wise and W. N. Hubbard, *Rev. Sci. Instr.*, in press.

(8) This value for the heat of formation of $SiF_4(g)$ differs considerably from literature values; the latter, however, either are based on ΔHf (SiO_2) or depend on unreliable experimental methods.

(9) W. D. Good, *J. Phys. Chem.*, **66**, 380 (1962).

DETERMINATION OF INTERFACIAL TENSIONS, CONTACT ANGLES, AND DISPERSION FORCES IN SURFACES BY ASSUMING ADDITIVITY OF INTERMOLECULAR INTERACTIONS IN SURFACES

Sir:

If we consider surface tensions (γ) to be a measure of the attractive force between surface layers and liquid phase, and that such forces and their contribution to the free energy are additive, we may expect surface tensions of liquid metals or polar liquids (having at least two independent types of intermolecular force) to be made up of independent additive terms. For water (1), in which hydrogen-bonding (h) and dispersion forces (w) are the main intermolecular forces

$$\gamma_1 = \gamma_1^h + \gamma_1^w \qquad (1)$$

This is in contrast to saturated hydrocarbons (2) in which $\gamma_2 = \gamma_2^w$.

At an interface between saturated hydrocarbons and water the attractive forces between unlike molecules are mainly the dispersion forces; this leads to an interfacial tension expression[1]

$$\gamma_{12} = \gamma_1 + \gamma_2 - 2\sqrt{\gamma_1^w \gamma_2} \qquad (2)$$

Evaluation of γ_1^w with γ_2 and γ_{12} values for saturated hydrocarbons at 20°[1,2] gives $\gamma_{H_2O}^w = 21.8 \pm 0.7$ dynes/cm. and $\gamma_{Hg}^w = 198 \pm 11$ dynes/cm. Since the main intermolecular force between water and mercury is the dispersion force, the above equation was used to calculate the interfacial tension between these liquids also: $\gamma_{12} = \gamma_1 + \gamma_2 - 2\sqrt{21.8 \times 198} = 425.6 \pm 2$ dynes/cm. The experimental findings (426–427 dynes/cm.)[3] are in excellent agreement.

If we apply the same methods to contact angle equilibria, using the Young equation, but assuming $\pi_e = 0$ when $\theta > 0$, we obtain

$$\gamma_L(1 + \cos\theta) = 2\sqrt{\gamma_L^w \gamma_S^w} \qquad (3)$$

This assumption has been questioned before[4] on the basis of a π_e calculated for water on graphite by the Bangham integration of the Gibbs adsorption equation. However, this technique assumes a uniform monolayer on graphite, now known to be highly non-uniform[5]; therefore, it appears reasonable to assume that π_e values for liquids on non-wetted solids are zero, just as is known to be the case for hydrocarbons on water.

To use equation 3 we may rearrange it to

$$\cos\theta = 2\sqrt{\gamma_S^w}\left(\frac{\sqrt{\gamma_L^w}}{\gamma_L}\right) - 1 \qquad (4)$$

and plot cos θ *vs.* $\sqrt{\gamma_L^w/\gamma_L}$. Data for various liquids on a given low-energy solid should give a straight line intercepting the cos θ axis at -1, and the cos $\theta = +1$ line at $\gamma_L/\sqrt{\gamma_L^w} = \sqrt{\gamma_S^w}$. For liquids having only dispersion force interactions the intercept at cos $\theta = +1$ occurs when $\gamma_L = \gamma_S^w$. This is essentially Zisman's γ_c, the critical surface tension for spreading, which has been evaluated for a variety of low-energy solids and adsorbed monolayers.[6] A plot of some of these data is shown in Fig. 1, showing very reasonable agreement with the proposed contact angle equation. The γ_L scale at the top of the figure is for liquids having only dispersion force interactions (aromatics and some esters are included).

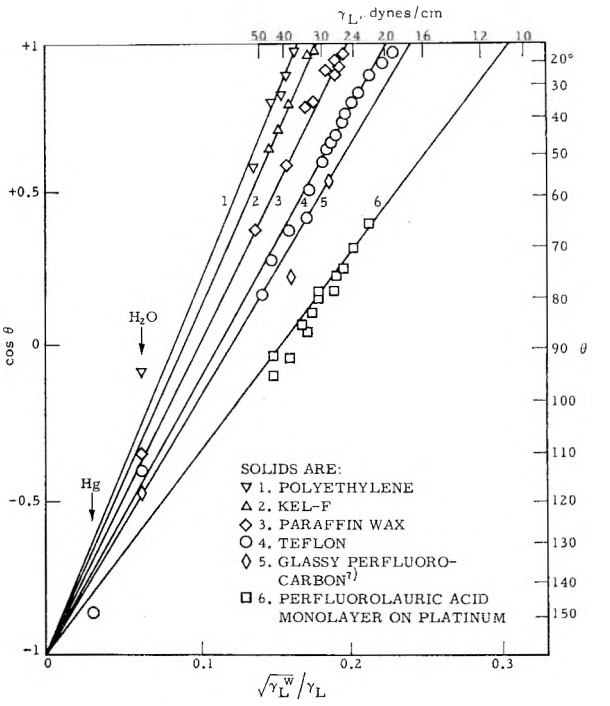

Fig. 1.—Relation of contact angle θ to surface tension of liquids γ_L.

It should be noted that γ_S^w is not the surface tension of the solid, but only its dispersion force term, which is not influenced by crystallinity or mechanical strains. Furthermore, while hydrocarbons appear to have only dispersion forces, fluorocarbons do not, as shown by the value of $\gamma_S^w = 17$ dynes/cm. (or perhaps lower) for a glassy fluorocarbon having $\gamma_S = 22$ dynes/cm.[7]

The straight lines of Fig. 1 all start from the same origin ($\theta = 180°$ when γ_L^w or $\gamma_S^w = 0$), and consequently a single point is enough to predict the contact angles of any liquids of known γ_L^w and γ_L values on the chosen solid. Thus contact angles of hydrocarbons on paraffin wax predict $\theta = 111°$ for water and 135° for mercury; values for water are generally 108–112°,[8] but no measurements for mercury on wax have been found.

The agreement of experiment with equation 3 is good evidence in favor of the assumption that π_e is negligible when $\theta > 0$.

SHELL DEVELOPMENT COMPANY F. M. FOWKES
EMERYVILLE, CALIFORNIA

RECEIVED DECEMBER 8, 1961

(1) F. A. Girifalco and R. J. Good, *J. Phys. Chem.*, **61**, 904 (1957).
(2) M. E. Nicholas, *et al.*, *ibid.*, **65**, 1373 (1961).
(3) C. A. Smolders, *Rec. trav. chim.*, **80**, 635–658 (1961).
(4) W. D. Harkins, "Physical Chemistry of Surface Films," Reinhold Publishing Corp., New York, N. Y., 1952, pp. 286–291.
(5) G. J. Young, J. J. Chessick, F. H. Healey and A. C. Zettlemoyer, *J. Phys. Chem.*, **58**, 313 (1954).
(6) E. G. Shafrin and W. A. Zisman, *ibid.*, **64**, 519 (1960).
(7) F. M. Fowkes and W. M. Sawyer, *J. Chem. Phys.*, **20**, 1650 (1952).
(8) F. M. Fowkes and W. D. Harkins, *J. Am. Chem. Soc.*, **62**, 3377 (1940).

THE DIELECTRIC CONSTANT OF WATER BETWEEN 0° AND 40°

Sir:

In recent reviews on dielectrics[1,2] it has been pointed out that considerable disagreement exists as to the dielectric constant of water and its temperature coefficient. On the basis of the careful investigation that was made of possible bridge and cell errors, the data of Malmberg and Maryott[3] seem to be preferred to the earlier work of Wyman and Ingalls[4] who used a resonator method. These two sets of data differ in absolute value by as much as 0.5% and have quite different temperature coefficients. Recently, Owen and co-workers,[5] using a resonance technique, have reported dielectric constants of water from 0 to 70°. Their results are in fair agreement with those of Malmberg and Maryott except for the temperature coefficient. The absolute value and the temperature coefficient of Owen agree almost exactly with the unpublished data of Lees.[6] Our results, obtained by a bridge method involving a new design of dielectric cell, agree well with those of Owen and of Lees at all temperatures but only approach those of Malmberg and Maryott at the higher temperature.

The measurements were carried out on an improved Cole–Gross capacitance–conductance bridge[7] equipped with a calibrated General Radio Type 1422-CC variable capacitor. The cell was designed for absolute measurements and consisted of concentric Pyrex cylinders with electrodes formed by fusing a platinum film onto the surface of the glass. The inside electrode contained an extended guard ring on each side of the working electrode with a gap of less than 0.2 mm. The outside surface of the cell was completely shielded by a silver coating. The cell constant of 4.594 pf. was determined with the cell filled with dry nitrogen and corrected to vacuum. Water of specific conductivity 6–8 $\times$ 10^{-8} ohms^{-1} cm.$^{-1}$ was obtained by passing distilled water through a mixed bed ion-exchange resin. Since a scrupulously clean cell was found essential for reproducible results, the cell was cleaned with chromic acid solution and thoroughly leached.

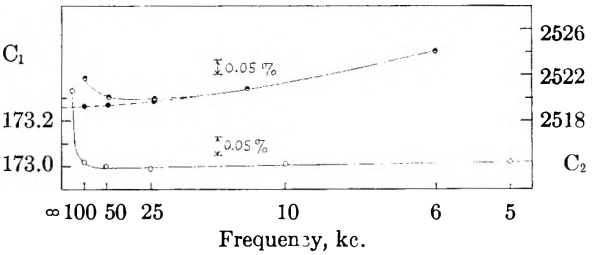

Fig. 1.—Capacitance in pf. (C_1, this research; C_2, ref. 3) *vs.* reciprocal frequency; ○ this research, ◓ Malmberg and Maryott, measured values; ● Malmberg and Maryott, corrected values.

The results are compared in Table I with the data of other workers.

TABLE I

DIELECTRIC CONSTANTS OF WATER

Temp., °C.	This research	Ref. 5	Ref. 3	Ref. 4
0	87.90	87.90	87.74	88.15
20	80.20	80.18	80.10	80.36
25	78.37	78.36	78.30	78.54
40	73.19	73.15	73.15	73.35

We estimate that the error in our results is no more than ±0.04 unit in the dielectric constant and can be attributed to the uncertainty in determining the cell constant. In Fig. 1 is shown the frequency dependence of a typical measurement as compared to that reported by Malmberg and Maryott. Because of the use of water of such low conductivity and wider spacing between electrodes (4 mm.), our frequency curve is essentially flat up to about 100 kc./sec. An extrapolation of the slight curvature to infinite frequency to eliminate electrode polarization effects is not necessary in our case in view of the accuracy claimed. At 500 cps., C_1 is higher than the value at 10 kc./sec. by only 0.06%.

A detailed report of this work will be published when cells of varying cell constant have been investigated thoroughly.

Acknowledgment.—The authors are indebted to Professor R. H. Cole for the use of his equipment and for many invaluable discussions and suggestions. This work was supported by the U. S. Atomic Energy Commission under Contract AT-(30-1)2727.

METCALF RESEARCH LABORATORY
BROWN UNIVERSITY GEORGE A. VIDULICH
PROVIDENCE 12, RHODE ISLAND ROBERT L. KAY

RECEIVED DECEMBER 21, 1961

(1) R. H. Cole, *Ann. Rev. Phys. Chem.*, **11**, 149 (1960).

(2) J. B. Hasted, "Progress in Dielectrics," Vol. 3, Heywood and Co., Ltd., London, 1961, p. 103.

(3) C. G. Malmberg and A. A. Maryott, *J. Research Natl. Bur. Standards.*, **56**, 1 (1956).

(4) J. Wyman, Jr., and E. N. Ingalls, *J. Am. Chem. Soc.*, **60**, 1182 (1938).

(5) B. B. Owen, R. C. Miller, C. E. Milner and H. L. Cogan, *J. Phys. Chem.*, **65**, 2065 (1961).

(6) W. L. Lees, Dissertation, Department of Physics, Harvard University, 1949.

(7) R. H. Cole and P. M. Gross, Jr., *Rev. Sci. Instr.*, **20**, 252 (1949).

16881